frontiers | Research Topics

Community series in antiviral innate immune sensing, regulation, and viral immune evasion, volume II

Edited by
Chenhe Su, Rongtuan Lin, Junji Xing and Huifang Zhu

Published in
Frontiers in Immunology

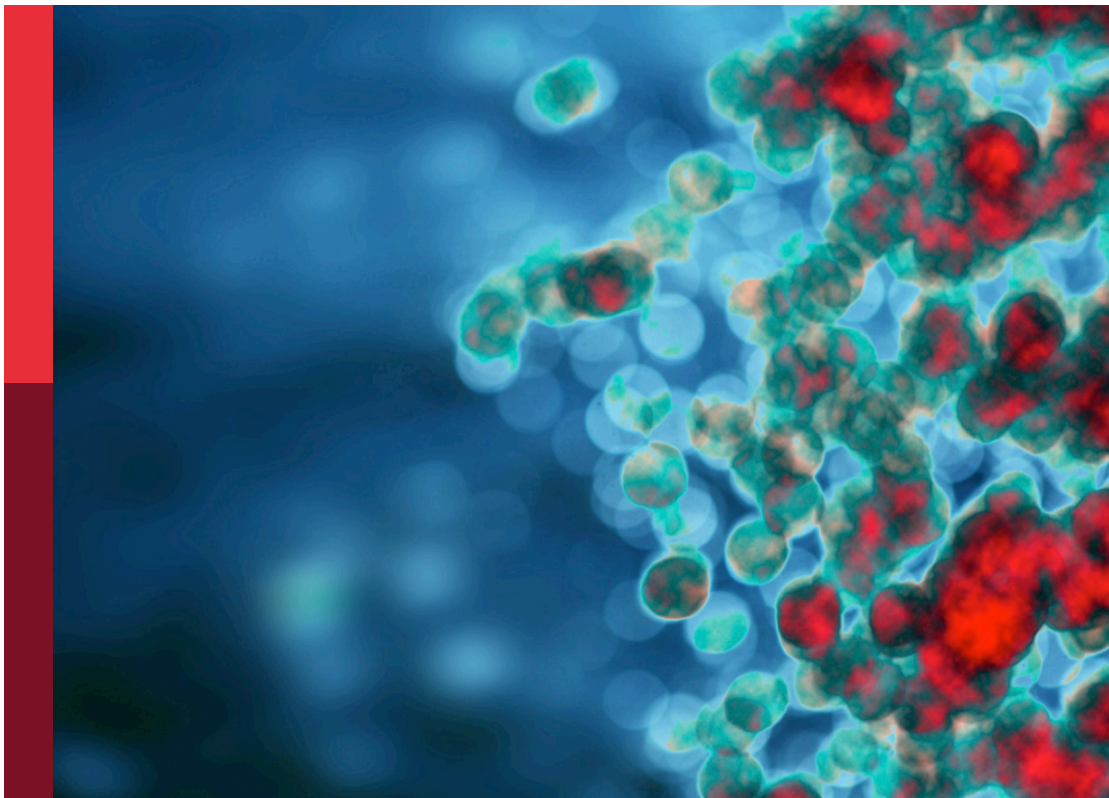

ISSN 1664-8714
ISBN 978-2-8325-4140-1
DOI 10.3389/978-2-8325-4140-1

About Frontiers

Frontiers is more than just an open access publisher of scholarly articles: it is a pioneering approach to the world of academia, radically improving the way scholarly research is managed. The grand vision of Frontiers is a world where all people have an equal opportunity to seek, share and generate knowledge. Frontiers provides immediate and permanent online open access to all its publications, but this alone is not enough to realize our grand goals.

Frontiers journal series

The Frontiers journal series is a multi-tier and interdisciplinary set of open-access, online journals, promising a paradigm shift from the current review, selection and dissemination processes in academic publishing. All Frontiers journals are driven by researchers for researchers; therefore, they constitute a service to the scholarly community. At the same time, the *Frontiers journal series* operates on a revolutionary invention, the tiered publishing system, initially addressing specific communities of scholars, and gradually climbing up to broader public understanding, thus serving the interests of the lay society, too.

Dedication to quality

Each Frontiers article is a landmark of the highest quality, thanks to genuinely collaborative interactions between authors and review editors, who include some of the world's best academicians. Research must be certified by peers before entering a stream of knowledge that may eventually reach the public - and shape society; therefore, Frontiers only applies the most rigorous and unbiased reviews. Frontiers revolutionizes research publishing by freely delivering the most outstanding research, evaluated with no bias from both the academic and social point of view. By applying the most advanced information technologies, Frontiers is catapulting scholarly publishing into a new generation.

What are Frontiers Research Topics?

Frontiers Research Topics are very popular trademarks of the *Frontiers journals series*: they are collections of at least ten articles, all centered on a particular subject. With their unique mix of varied contributions from Original Research to Review Articles, Frontiers Research Topics unify the most influential researchers, the latest key findings and historical advances in a hot research area.

Find out more on how to host your own Frontiers Research Topic or contribute to one as an author by contacting the Frontiers editorial office: frontiersin.org/about/contact

Community series in antiviral innate immune sensing, regulation, and viral immune evasion, volume II

Topic editors

Chenhe Su — Henan Normal University, China
Rongtuan Lin — McGill University, Canada
Junji Xing — Houston Methodist Research Institute, United States
Huifang Zhu — First Affiliated Hospital of Gannan Medical University, China

Citation

Su, C., Lin, R., Xing, J., Zhu, H., eds. (2024). *Community series in antiviral innate immune sensing, regulation, and viral immune evasion, volume II*.
Lausanne: Frontiers Media SA. doi: 10.3389/978-2-8325-4140-1

Table of contents

frontiers | Frontiers in Immunology

TYPE Editorial
PUBLISHED 01 December 2023
DOI 10.3389/fimmu.2023.1341193

OPEN ACCESS

EDITED AND REVIEWED BY
Pei-Hui Wang,
Shandong University, China

*CORRESPONDENCE
Junji Xing
jxing@houstonmethodist.org

RECEIVED 20 November 2023
ACCEPTED 27 November 2023
PUBLISHED 01 December 2023

CITATION
Wang L and Xing J (2023) Editorial: Community series in antiviral innate immune sensing, regulation, and viral immune evasion: volume II.
Front. Immunol. 14:1341193.
doi: 10.3389/fimmu.2023.1341193

Editorial: Community series in antiviral innate immune sensing, regulation, and viral immune evasion: volume II

Ling Wang[1,2] and Junji Xing[1,3]*

[1]Department of Surgery and Immunobiology and Transplant Science Center, Houston Methodist Research Institute, Houston Methodist, Houston, TX, United States, [2]Department of Obstetrics and Gynecology, The Second Hospital of Jilin University, Changchun, China, [3]Department of Cardiovascular Sciences, Houston Methodist Research Institute, Houston Methodist, Houston, TX, United States

KEYWORDS

innate immunity, antiviral immunity, innate immune sensing, immune regulation, viral immune evasion

Editorial on the Research Topic
Community series in antiviral innate immune sensing, regulation, and viral immune evasion: volume II

Innate immunity is the cellular host's frontline defense against viral infections. It employs pattern recognition receptors (PRRs) to detect viral nucleotides recognized as 'pathogen-associated molecular patterns' (PAMPs) (1, 2). Key RNA-sensing PRRs include Toll-like receptors (TLRs), Retinoic Acid Inducible Gene-I (RIG-I)-like receptors (RLRs), NOD-like receptors (NLRs), C-type lectin receptors (CLRs), Protein Kinase R (PKR), and 2'-5'-Oligoadenylate Synthetases (OAS) and many others (3, 4). Moreover, DNA-sensing PRRs include cyclic GMP-AMP synthase (cGAS), interferon gamma-inducible protein 16 (IFI16), DDX41 and others (5, 6). Following the detection of specific viral PAMPs, PRRs trigger the activation of intracellular signaling cascades, ultimately leading to the induction of type I interferons (IFNs), pro-inflammatory cytokines, and antiviral genes through the activation of interferon regulatory factor 3 (IRF3) and nuclear factor kappa B (NF-κB) (2). These processes not only inhibit viral propagation but also activate the adaptive immune system (2). However, viruses have developed numerous strategies to circumvent the host's innate immune defense, enabling them to persist and establish ongoing infections. Therefore, understanding the mechanisms of antiviral innate immunity and viral immune evasion strategies remains a focal point of research within the field of innate immunity.

This Research Topic "*Antiviral Innate Immune Sensing, Regulation, and Viral Immune Evasion: Volume II*" highlights 14 recent studies that investigate the mechanisms about antiviral innate immune sensing and regulation in the host, and summarize the innate immune evasion strategies employed by viruses.

The innate immune system plays a vital role in defending against viruses and other pathogens by detecting viral PAMPs and activating various antiviral signaling pathways. These pathways must be precisely regulated to achieve effective antiviral responses while

preventing dysregulated immune signaling. The COVID-19 pandemic underscores the importance of comprehending the mechanisms of antiviral innate immune sensing and regulation. Zheng et al. explored the link between COVID-19, rheumatoid arthritis (RA), and the cell death process known as pyroptosis, identifying common biomarkers and potential drug targets. Using comprehensive bioinformatics and network pharmacology analyses, they identified caspase-1 as a key gene involved in the inflammatory responses of both diseases. They also found that the drug minocycline could interact with caspase-1, potentially reducing inflammation in COVID-19 and RA patients. Gu et al. identified A20 as a key regulator in mitigating the inflammation caused by Influenza A virus (IAV) infection. They demonstrated that chronic exposure to low-dose lipopolysaccharide (LPS) reduced inflammation by increasing A20 expression, which then enhanced the activity of peroxisome proliferator-activated receptor alpha (PPAR-α) and PPAR-γ, leading to the suppression of the NF-κB signaling pathway and NLRP3 inflammasome. Huang et al. showed the role of the Ect4 protein in the immune response against viral infections in Drosophila. They found that Ect4, an adaptor protein in the Toll pathway, controlled viral load post-Drosophila C virus (DCV) infection by interacting with Stat92E to regulate the induction of STAT-responsive genes. Mahish et al. investigated the role of Toll-like receptor 4 (TLR4) in Chikungunya virus (CHIKV) infection and the host immune response. They revealed that TLR4 facilitated CHIKV attachment and entry into host macrophages, with TLR4 inhibition significantly reducing viral load, pro-inflammatory responses, and improving survival rates in mouse models. Wu et al. explored the relationship between echovirus infection and autophagy, a key component of the host's defense mechanisms. They found that echovirus infection triggered autophagy, as evidenced by increased expression of LC3-II and autophagosome formation, and altered signaling pathways involved in autophagosome formation, including decreased phosphorylation of mTOR and ULK1 and increased VPS34 and Beclin-1 levels. Sun et al. investigated how toll-like receptors (TLRs), particularly TLR2 and its heterodimers, affected enterovirus 71 (EV71) replication and innate immune activation. They demonstrated that overexpressing human or mouse TLR monomers and TLR2 heterodimers significantly hindered EV71 replication by stimulating interleukin-8 production via activation of the phosphoinositide 3-kinase/protein kinase B (PI3K/AKT) and mitogen-activated protein kinase (MAPK) pathways. The findings highlight that these membrane-bound TLRs play a critical role in antiviral innate immune sensing and regulation of EV71 infection.

Viruses deploy complex tactics to circumvent the host's innate defenses and sustain infections. Understanding these evasion techniques will advance our knowledge of viral behavior and inform the development of treatments and vaccines. Weerawardhana et al. showed that the 2B protein of Foot-and-mouth disease virus (FMDV) disrupted the IFN-β production by degrading RIG-I and MDA5, two critical sensors in the type I IFN signaling pathway. They found that FMDV 2B induced ubiquitination and proteasomal degradation of RIG-I via E3 ubiquitin ligase RNF125 and led to MDA5 degradation through caspase-3 and caspase-8, thereby reducing IFN-β production. Wang et al. summarized the antiviral innate immune mechanisms triggered by IFN signal transduction pathways in host cells and the immune evasion mechanisms employed by Rift Valley fever virus (RVFV), particularly through its nonstructural proteins (NSs), providing insight into potential drug targets and strategies to combat Rift Valley fever outbreaks. Zhou et al. reviewed the research progress of the conserved herpesvirus protein kinase UL13 in immune escape and viral replication, providing insights into the pathogenic mechanisms of herpesviruses and potential strategies for their immune escape and replication. Zhao et al. reviewed mechanisms employed by senecavirus A (SVA) to circumvent host defenses, including evading pattern recognition receptor signaling, IFN-α/β receptor pathways, interferon-stimulated genes, autophagy, and stress granules, thereby enhancing our understanding of SVA's pathogenesis and informing the development of antiviral strategies and vaccines. Zhang et al. highlighted the need for further research into the interplay between herpes simplex encephalitis and innate immunity. Wen et al. reviewed how pestiviruses, significant pathogens in livestock, evaded IFN-mediated immune responses, particularly highlighting the roles of their unique glycoproteins Erns, which inhibits IFN production by cleaving viral RNAs, and Npro, which targets the transcription factor IRF-3 for degradation. Hao et al. identified the African swine fever virus (ASFV) protein QP383R as an inhibitor of the cyclic GMP-AMP synthase (cGAS) pathway, a crucial part of the antiviral innate immune response. They found that QP383R suppressed type I IFN production by interfering with cGAS functions including DNA binding, dimerization, and enzymatic activity, thereby enabling ASFV to evade the cGAS-mediated antiviral innate immune response. Liu et al., investigated patients with hepatitis B (HBsAg-negative but HBV DNA-positive) and found that their cellular immune function, indicated by T-lymphocyte subsets and serum cytokines, was superior to that of HBsAg-positive patients, suggesting reduced liver inflammation. Sequencing of the HBV S region in these patients revealed high-frequency amino acid substitutions and immune escape mutations, potentially leading to undetectable HBsAg levels and changes in its antigenicity and secretion.

Finally, we would like to thank all the authors for entrusting us with their discoveries, and all the referees for their careful and insightful reviews. We are confident that the collection of articles in this Research Topic will captivate researchers focused on antiviral innate immunity and viral immune evasion. Insights into the mechanisms of antiviral immune sensing and evasion are poised to inform the creation of vaccines and antiviral therapies, potentially shaping the response to the COVID-19 pandemic and other infectious diseases in the future.

Author contributions

JX: Conceptualization, Funding acquisition, Writing – original draft, Writing – review & editing. LW: Writing – original draft.

Funding

The author(s) declare financial support was received for the research, authorship, and/or publication of this article. This work was supported by the American Heart Association Career Development Award 20CDA35260116 and Transformational Project Award 23TPA1055437 (https://doi.org/10.58275/AHA.23TPA1055437.pc.gr.172259) (JX).

Acknowledgments

We would like to thank the authors, reviewers, and editors for their essential contribution to this exciting and unexplored Research Topic, as well as of the members of the Frontiers in Immunology Editorial Office.

Conflict of interest

The authors declare that the research was conducted in the absence of any commercial or financial relationships that could be construed as a potential conflict of interest.

The author(s) declared that they were an editorial board member of Frontiers, at the time of submission. This had no impact on the peer review process and the final decision.

Publisher's note

References

1. Takeuchi O, Akira S. Pattern recognition receptors and inflammation. *Cell* (2010) 140:805–20. doi: 10.1016/j.cell.2010.01.022

2. Wu J, Chen ZJ. Innate immune sensing and signaling of cytosolic nucleic acids. *Annu Rev Immunol* (2014) 32:461–88. doi: 10.1146/annurev-immunol-032713-120156

3. Hur S. Double-stranded RNA sensors and modulators in innate immunity. *Annu Rev Immunol* (2019) 37:349–75. doi: 10.1146/annurev-immunol-042718-041356

4. Zhang E, Fang M, Jones C, Minze LJ, Xing J, Zhang Z. Mechanisms involved in controlling RNA virus-induced intestinal inflammation. *Cell Mol Life Sci* (2022) 79:313. doi: 10.1007/s00018-022-04332-z

5. Paludan SR, Bowie AG. Immune sensing of DNA. *Immunity* (2013) 38:870–80. doi: 10.1016/j.immuni.2013.05.004

6. Lin R, Xing J, Zheng C. Editorial: sensing DNA in antiviral innate immunity. *Front Immunol* (2021) 12:644310. doi: 10.3389/fimmu.2021.644310

frontiers | Frontiers in Immunology

TYPE Original Research
PUBLISHED 29 September 2022
DOI 10.3389/fimmu.2022.1020262

OPEN ACCESS

EDITED BY
Rongtuan Lin,
McGill University, Canada

REVIEWED BY
Liang-Guo Xu,
Jiangxi Normal University, China
Dan Li,
Lanzhou Veterinary Research Institute, Chinese Academy of Agricultural Sciences, China

*CORRESPONDENCE
Jong-Hyeon Park
parkjhvet@korea.kr
Jong-Soo Lee
jongsool@cnu.ac.kr

†These authors have contributed equally to this work and share first authorship

SPECIALTY SECTION
This article was submitted to Viral Immunology, a section of the journal Frontiers in Immunology

RECEIVED 16 August 2022
ACCEPTED 13 September 2022
PUBLISHED 29 September 2022

CITATION
Weerawardhana A, Uddin MB, Choi J-H, Pathinayake P, Shin SH, Chathuranga K, Park J-H and Lee J-S (2022) Foot-and-mouth disease virus non-structural protein 2B downregulates the RLR signaling pathway *via* degradation of RIG-I and MDA5. *Front. Immunol.* 13:1020262. doi: 10.3389/fimmu.2022.1020262

Foot-and-mouth disease virus non-structural protein 2B downregulates the RLR signaling pathway *via* degradation of RIG-I and MDA5

Asela Weerawardhana[1†], Md Bashir Uddin[1,2,3†], Joo-Hyung Choi[4,5], Prabuddha Pathinayake[1,6], Sung Ho Shin[4], Kiramage Chathuranga[1], Jong-Hyeon Park[4*] and Jong-Soo Lee[1*]

[1]College of Veterinary Medicine, Chungnam National University, Daejeon, South Korea, [2]Department of Medicine, Sylhet Agricultural University, Sylhet, Bangladesh, [3]Department of Microbiology and Immunology, University of Texas Medical Branch, Galveston, TX, United States, [4]Foot and Mouth Disease Division, Animal Quarantine and Inspection Agency, Anyang, South Korea, [5]Wildlife Disease Response Team, National Institute of Wildlife Disease Control and Prevention (NIWDC), Gwangju, South Korea, [6]Immune Health Program, Hunter Medical Research Institute, University of Newcastle, Newcastle, NSW, Australia

Foot-and-mouth disease virus (FMDV) is a single-stranded, positive-sense RNA virus containing at least 13 proteins. Many of these proteins show immune modulation capabilities. As a non-structural protein of the FMDV, 2B is involved in the rearrangement of the host cell membranes and the disruption of the host secretory pathway as a viroporin. Previous studies have also shown that FMDV 2B plays a role in the modulation of host type-I interferon (IFN) responses through the inhibition of expression of RIG-I and MDA5, key cytosolic sensors of the type-I IFN signaling. However, the exact molecular mechanism is poorly understood. Here, we demonstrated that FMDV 2B modulates host IFN signal pathway by the degradation of RIG-I and MDA5. FMDV 2B targeted the RIG-I for ubiquitination and proteasomal degradation by recruiting E3 ubiquitin ligase ring finger protein 125 (RNF125) and also targeted MDA5 for apoptosis-induced caspase-3- and caspase-8-dependent degradation. Ultimately, FMDV 2B significantly inhibited RNA virus-induced IFN-β production. Importantly, we identified that the C-terminal amino acids 126-154 of FMDV 2B are essential for 2B-mediated degradation of the RIG-I and MDA5. Collectively, these results provide a clearer understanding of the specific molecular mechanisms used by FMDV 2B to inhibit the IFN responses and a rational approach to virus attenuation for future vaccine development.

KEYWORDS

foot and mouth disease virus (FMDV), 2B, RIG-I, MDA5, RNF125

Introduction

The innate immune signaling cascade plays a crucial role in the antiviral immune responses elicited by various viruses, resulting in the induction of type-I interferons (IFN), inflammatory cytokines, and IFN-stimulated genes (ISGs) (1–3). Pattern recognition receptors (PRRs), including toll-like receptors (TLRs), retinoic acid-inducible gene-I (RIG-I)-like receptors (RLRs), and Nucleotide-binding and oligomerization domain (NOD)-like receptors (NLRs), recognize pathogen-associated molecular patterns (PAMPs) (1, 4, 5). Among the PRRs, the significant members of the RLRs family, RIG-I and melanoma differentiation-associated gene 5 (MDA5) play a pivotal role in sensing cytosolic viral RNAs (1, 4, 6, 7), a critical role in the recognition of picornaviruses (1, 8, 9). After sensing the viral RNA in the cytoplasm by RIG-I or MDA5, they interact with the downstream mitochondrial antiviral signaling protein (MAVS) (10–13) through their tandem N-terminal caspase recruitment domains (CARDs) and activate type-I IFN responses and proinflammatory responses *via* downstream molecules such as TANK-binding kinase 1 (TBK1)/Inhibitor of nuclear factor kappa-B kinase subunit epsilon (IKKϵ), Interferon regulatory factor 3 (IRF3), Nuclear factor-kappa B (NF-κB), etc. (14, 15).

RIG-I plays a significant role in maintaining antiviral immunity by preventing the spread of the virus and is involved in host immune homeostasis due to the presence of several regulatory molecules (16). In addition, post-translational modifications (PTMs), including ubiquitination, phosphorylation, and acetylation, are fundamental regulatory mechanisms involved in the activation or the inactivation of RIG-I (17). Also, MDA5 is another major intracellular sensor for viral dsRNA, and several positive and negative regulatory molecules are involved in the activation or the inactivation of MDA5 to maintain the host immune homeostasis after a viral infection (16). Among the various regulatory mechanisms, one of the less-studied facts related to the regulation of MDA5 is the caspase-3- and caspase-8-dependent cleavage of MDA5 (18). These important sensing molecules are a major target for immune evasion of viruses.

Foot-and-mouth disease (FMD) is a highly contagious vesicular disease in cloven-hoofed animals. It is one of the most economically devastating diseases that are considered to be a significant concern in animal health (19, 20). The etiologic agent of FMD is foot-and-mouth disease virus (FMDV), the prototype member of the *Aphthovirus* genus in the *Picornaviridae* family. FMDV has seven known serotypes (A, O, Asia, C, SAT1, SAT2, and SAT3) (21). The FMDV virion consists of a single-stranded, positive-sense RNA genome of about 8.5 kb in length and enclosed by four structural proteins to form an icosahedral capsid (9). The genomic RNA is translated into a single, long open reading frame for a polyprotein, and subsequently, the polyprotein is cleaved by various proteases, resulting in several intermediate or structural proteins (VP1-VP4) and non-structural proteins (L^{pro}, 2A, 2B, 2C, 3A, 3B, $3C^{pro}$ and 3D) (22).

Among FMDV non-structural proteins, 2B is involved in the interaction with the endoplasmic reticulum (ER) membrane through the predicted two hydrophobic domains for the viral replication (23) and is also related to the permeability of the host cell membrane and the disruption of the cellular secretory pathway (24–27). Studies on the 2B proteins of other family members of *Picornaviridae* show different functions of the 2B protein. Poliovirus 2B protein blocks cellular protein secretion (28), and coxsackievirus 2B protein facilitates virus release by modifying membrane permeability (29). Moreover, recent studies have shown that FMDV 2B protein plays the role of a negative regulator of RLR-mediated type-I IFN signaling by targeting RIG-I, LGP2, and MDA5 (23, 27, 30). However, the exact molecular mechanism through which FMDV 2B targets these molecules is not yet clear. In this study, we demonstrated the precise molecular mechanism by which FMDV 2B mediates the degradation of RIG-I and MDA5.

Results

FMDV 2B negatively regulates antiviral immune responses

To evade and suppress the host innate immune system, viruses must regulate the type-I IFN signal transduction. Previous studies have shown that FMDV 2B plays an important role in regulating IFN-dependent immune responses (23, 27). However, the molecular mechanisms underlying FMDV 2B-mediated inhibition of the host antiviral innate immune responses remain unclear. To reconfirm that FMDV 2B is involved in the downregulation of IFN-β signaling, we screened FMDV proteins for IFN-β luciferase activity. When human embryonic kidney (HEK293T) cells were co-transfected with the indicated plasmids, we found that FMDV 2B and FMDV 3C significantly inhibited RIG-I-induced IFN-β reporter activity (Supplementary Figure 1A). For a specific study on FMDV 2B, we evaluated IFN antagonism mediated by FMDV 2B in different serotypes of FMDV and observed that the 2B proteins of all FMDV serotypes downregulated IFN-β promoter activity in a dose-dependent manner. In particular, compared with other serotypes, SAT1, SAT2, and SAT3 showed noticeable reductions in the luciferase activity (Supplementary Figure 1B). These results suggest that FMDV 2B inhibits IFN-β promoter activity.

Next, we investigated whether FMDV 2B affects the replication of other viruses. FMDV 2B expression plasmids were transiently transfected into porcine kidney epithelial cells

(PK-15) and HEK293T cells (Supplementary Figures 2A, B) and were infected with GFP-tagged vesicular stomatitis virus (VSV-GFP) (Figures 1A, C), influenza A virus PR8 strain (PR8-GFP) (Supplementary Figure 2D), EV-71 (Supplementary Figure 2H), and coxsackievirus H3-GFP (Supplementary Figure 2I). Interestingly, we found that the virus replication in FMDV 2B-overexpressed cells was significantly higher than that in the control cells in different cell lines (Figures 1A, C). Next, we measured the amount of IFN-β and IL-6 secreted from the virus-infected cells using enzyme-linked immunosorbent assay (ELISA). Consistent with the results of the virus replication, we found that the FMDV 2B-overexpressed cells secreted fewer cytokines than the control cells (Figures 1B, D; Supplementary Figure 2E). Additionally, RAW264.7 cells stably expressing FMDV 2B were prepared (Supplementary Figure 2C) and infected with VSV-GFP (Figure 1E) and PR8-GFP (Figure 1G). As expected, a higher level of virus replication and lower levels of IL-6, IFN-β, IFN-α, TNF-α, and IL-1β secretions (Figures 1E–H, Supplementary Figures 2F, G) were observed in RAW264.7 cells stably expressing FMDV 2B. These results suggest that FMDV 2B negatively regulates the production of type-I IFNs and proinflammatory cytokines and enhances the RNA virus replication in the macrophage and the epithelial cell lines. These results suggest that FMDV 2B negatively regulates the type-I IFN pathway and weakens the antiviral status of the host cells by reducing the IFN secretion in response to a viral infection, thereby facilitating the RNA virus replication in the macrophage and the epithelial cell lines.

FMDV 2B targets RIG-I and MDA5 to inhibit type-I IFN signaling

To further confirm the effects of FMDV 2B on antiviral signaling cascades, we investigated RNA virus-mediated phosphorylation of TBK1, IRF3, and p65 in RAW264.7 cells stably expressing FMDV 2B. As shown in Figure 2A, phosphorylation levels of TBK1, IRF3, and p65 were significantly lower in FMDV 2B-overexpressed RAW264.7 cells than in the control cells at the indicated time points after

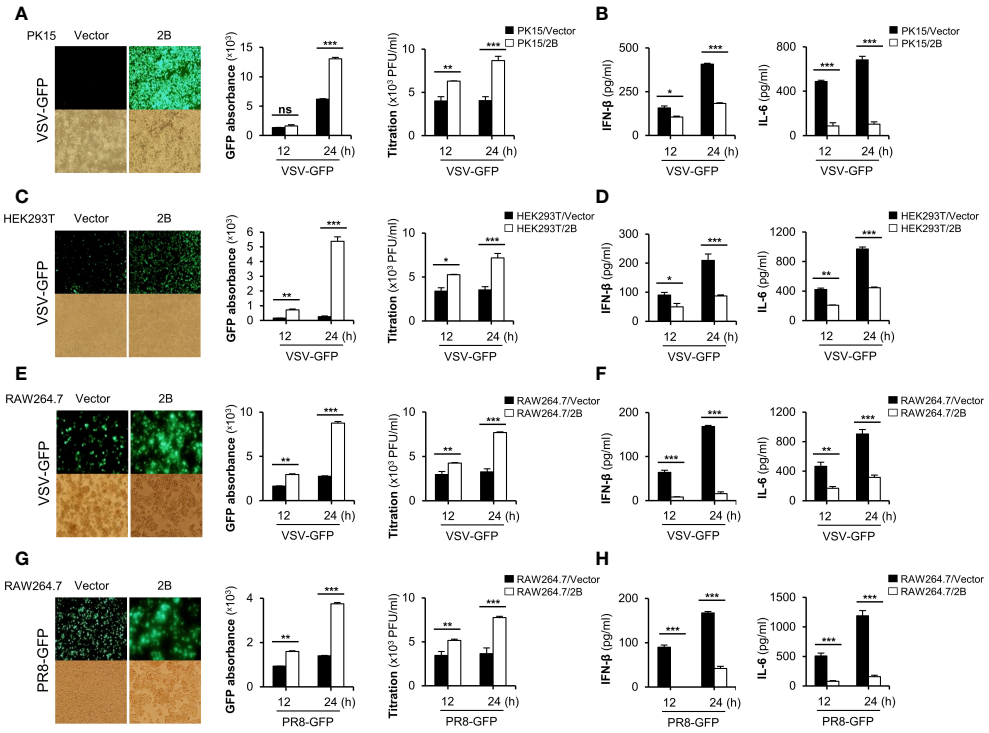

FIGURE 1
FMDV 2B negatively regulate RNA virus-mediated innate immune responses. PK-15 cells **(A, B)** and HEK293T cells **(C, D)** were transiently transfected with the control vector or FMDV 2B and infected with VSV-GFP. GFP expression, GFP absorbance, and virus titer was taken at 12 and 24 hpi **(A, C)**. The concentration of secreted IFN-β and IL-6 in supernatants was determined at 12 and 24 hpi by ELISA **(B, D)**. Control vector and FMDV 2B stably expressing RAW264.7 cells were infected with VSV-GFP **(E, F)** and PR8-GFP **(G, H)**. GFP expression, GFP absorbance, and virus titer was taken at 12 and 24 hpi **(E, G)**. The concentration of IFN-β and IL-6 secreted in supernatants were determined at 12 and 24 hpi by ELISA **(F, H)**. Results representative of at least two independent experiments, each with similar results, and the values are expressed as mean ± SD of three biological replicates. Student's t-test; *p < 0.05; **p < 0.01; ***p < 0.001; ns, not significant.

the infection. Additionally, we also analyzed the effect of FMDV 2B on the transcription of IFNs and IFN-inducible genes in FMDV 2B-overexpressed RAW264.7 cells. For this experiment, we infected FMDV 2B-overexpressed RAW264.7 cells with VSV-GFP and performed real-time qPCR using specific primers. As a result, the expressions of mRNA encoding IFNs and other antiviral genes were significantly lower in FMDV 2B-overexpressed cells (Figure 2B) than they were in the control cells. These data support the notion that FMDV 2B negatively regulates the type-I IFN signaling pathway and expression of antiviral genes in response to a virus infection.

Next, to identify the potential target of FMDV 2B in the type-I IFN cascade, we performed a luciferase promoter assay by co-expressing both genes with several IFN-related genes as indicated in Figures 2C, D. We found that FMDV 2B markedly inhibited H1N1, NDV-GFP, poly(I:C), MDA5, and RIG-I-mediated activation of the IFN-β promoter in a dose-dependent manner (Figures 2C, D). However, no detectable changes occurred in MAVS, TRIF, and TBK1-mediated promoter activity with increased expression of FMDV 2B. These results suggested that FMDV 2B regulates type-I IFN signaling at the level of RIG-I and MDA5.

FMDV 2B interacts with RIG-I and mediates the degradation of RIG-I

Many viruses express proteins that target RIG-I to suppress the host defense mechanisms. A lot of the interactions between viral proteins and RIG-I result in the cleavage, degradation, suspension, or inhibition of RIG-I (16). Based on our luciferase results, FMDV 2B targets RIG-I, and previous reports have also shown that FMDV 2B inhibits RIG-I expression (23, 27). In this study, we first investigated the degradation of RIG-I by FMDV 2B. HEK293T cells were co-transfected with RIG-I expression plasmids and increasing doses of FMDV 2B expression plasmids, followed by an immunoblot analysis of whole-cell lysates. Interestingly, we found that the overexpression of FMDV 2B resulted in a significant decrease in RIG-I levels, which was FMDV 2B dose-dependent (Figure 3A). Concurrently, we confirmed that FMDV 2B reduced the expression of the endogenous porcine RIG-I (pRIG-I) in PK-15 cells in a dose-dependent manner (Figure 3B).

Next, to determine whether FMDV 2B affects the expression or the degradation of RIG-I, we co-transfected RIG-I and FMDV 2B expression plasmids into cells treated with different inhibitors

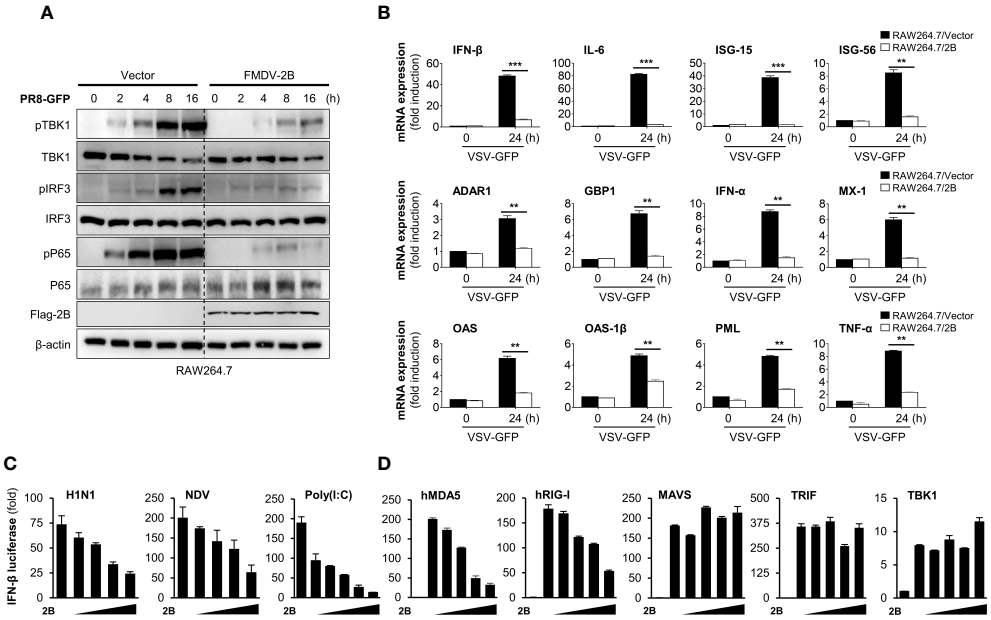

FIGURE 2
FMDV 2B inhibit the transcription of antiviral genes and type-I IFN signaling. Control vector and FMDV 2B stably expressing RAW264.7 cells were infected with PR8-GFP. Cells were harvested at indicated time points after the infection of PR8-GFP. Total and phosphorylated TBK1, IRF3, and p65 were measured by immunoblotting. β-actin was used as the loading control **(A)**. Control vector and FMDV 2B stably expressing RAW264.7 cells were infected with VSV-GFP. At 0 and 24 hpi, cells were harvested, and quantitative real-time PCR was performed to analyze the levels of antiviral genes **(B)**. HEK293T cells were transfected with interferon-β promoter encoding firefly luciferase plasmid, TK-Renilla plasmid, increasing dose of Flag-FMDV 2B plasmid and stimulated with H1N1, NDV infection, Poly(I:C) treatment **(C)** or transfected with MDA5, RIG-I, MAVS, TRIF, and TBK1 encoding plasmids **(D)** for 24 hours. Results are expressed relative to those of Renilla luciferase alone (internal control). Results representative of at least two independent experiments, each with similar results, and the values are expressed as mean ± SD of three biological replicates. Student's t-test; **p < 0.01; ***p < 0.001.

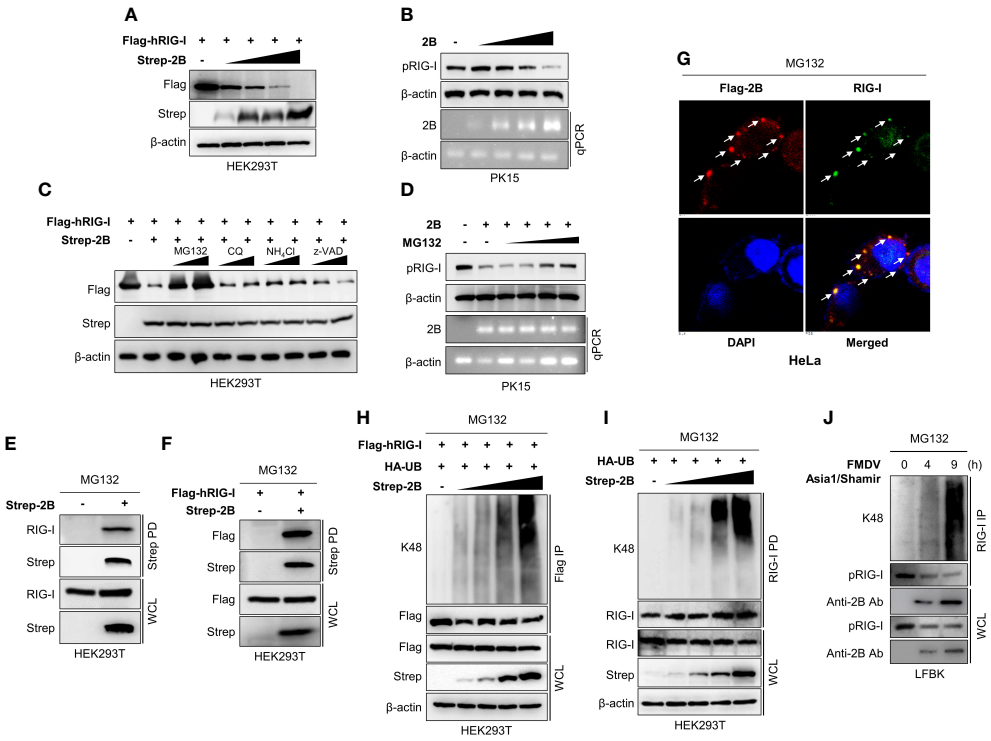

FIGURE 3
FMDV 2B targets RIG-I and mediates degradation of RIG-I *via* K48-linked polyubiquitination. HEK293T cells were transfected with Flag-hRIG-I plasmid, and increasing doses of Strep-FMDV 2B plasmids **(A)**, PK-15 cells were transfected with increasing amounts of FMDV 2B and 24 hrs post-transfection cells were infected with SeV [1 multiplicity of infection (MOI)] **(B)**. Cells were harvested at 24 hrs post-infection, and RIG-I expression level was measured by immunoblotting. HEK293T cells were transfected with Flag-hRIG-I together with Strep-FMDV 2B and treated with two doses of MG132, chloroquine, NH_4Cl, or z-VAD for 6 hours before harvesting the cells. Whole-cell lysates were subjected to immunoblotting with indicated antibodies **(C)**. PK-15 cells were transfected with Strep-FMDV 2B, and 24 hrs post-transfection cells were infected with SeV (1MOI). Cells were treated with increasing doses of MG132 at 18 hours hrs post-infection and harvested at 24 hrs post-infection. The RIG-I expression level was measured by immunoblotting **(D)**. HEK293T cells were transfected with Strep-FMDV 2B **(E)** or Flag-RIG-I together with Strep-FMDV 2B **(F)** and treated with MG132 for 6 hours before harvesting the cells. Cell lysates were subjected to Strep pull-down and immunoblotted with the indicated antibodies. HeLa cells were transfected with Flag-FMDV 2B and treated with MG132 for 6 hours before fixing the plate, followed by confocal microscopy with anti-Flag (red) and anti-RIG-I (green) antibodies. Nuclei were stained with DAPI (blue) **(G)**. HEK293T cells were transfected with Flag-RIG-I, HA-ubiquitin together with increasing doses of Strep-FMDV 2B plasmids and treated with MG132 for 6 hours before harvesting the cells. Whole-cell lysates were subjected to Flag immunoprecipitation and immunoblotted with indicated antibodies **(H)**. HEK293T cells were transfected with HA-ubiquitin together with increasing doses of Strep-2B plasmids and treated with MG132 for 6 hours before harvesting the cells. Whole-cell lysates were subjected to immunoprecipitation with RIG-I antibody and immunoblotted with indicated antibodies **(I)**. LFBK cells were infected with FMDV Asia1/Shamir strain and treated with MG132 for 6 hours before harvesting the cells. Cells were harvested at indicated time after infection and whole-cell lysates were immunoprecipitated with anti-RIG-I antibody and immunoblotted with indicated antibodies **(J)**. Results representative of at least two independent experiments, each with similar results. (pRIG-I: porcine RIG-I, hRIG-I: human RIG-I).

to determine the type of degradation caused by FMDV 2B. As shown in Figure 3C, D, the expression of RIG-I was restored upon treatment with a proteasomal inhibitor MG132 but not upon treatment with lysosomal inhibitors (chloroquine and NH_4Cl) or a caspase inhibitor (z-VAD). These results suggest that RIG-I undergoes FMDV 2B-mediated proteasomal degradation. Similarly, FMDV 2B also degrades RIG-I 2CARD (1-186 aa fragment of RIG-I containing CARD1 and CARD2 domains) (Supplementary Figure 3B) but does not induce RIG-I or RIG-I 2CARD degradation in the presence of MG132 (Supplementary Figures 3A, C). Next, we performed an immunoprecipitation assay to assess whether FMDV 2B physically interacts with RIG-I and induces degradation. As shown in Figures 3E, F, FMDV 2B strongly interacted with RIG-I in the presence of MG132, and additionally, we confirmed the co-localization of FMDV 2B and RIG-I with MG132 treatment (Figure 3G). Thus, we next asked whether RIG-I degradation is mediated by ubiquitination. As shown in Figure 3H, HEK293T cells were co-transfected with the indicated plasmids in the presence of MG132, followed by immunoprecipitation and immunoblotting with a K48-specific antibody. Interestingly, the RIG-I underwent K48-linked ubiquitination in the presence of FMDV 2B, and its ubiquitination activity was enhanced by increasing doses of FMDV 2B. K48

ubiquitination of the endogenous RIG-I by FMDV 2B was also examined (Figure 3I). Next, to further validate whether RIG-I undergo ubiquitination upon FMDV infection, we infected the fetal porcine kidney (LFBK) cells with FMDV in the presence of MG132. Results of Figure 3J shows K48 ubiquitination of RIG-I and ubiquitination enhanced with time after virus infection. These findings indicate that FMDV 2B mediates ubiquitin-dependent proteasomal degradation of RIG-I by conjugating K48-linked polyubiquitin chains.

FMDV 2B recruits RNF125 to mediate degradation of RIG-I by K48 ubiquitination

While some viruses have non-canonical E3 ligases (31), others use alternative strategies to maintain E3 ligase activity by recruiting and redirecting host E3 ligases for the ubiquitination of the host proteins. For example, the E6 oncoproteins of human papillomavirus (HPV) induce p53 degradation by recruiting host E3 ligase E6-associated protein (E6AP) (32–34). Since FMDV 2B does not have E3 ligase activity on its own, we hypothesized that FMDV 2B recruits host E3 ligase for the ubiquitination and degradation of RIG-I. Hence, we searched for a potential E3 ligase that mediates the proteasomal degradation of RIG-I and selected RNF125. RNF125 is the first identified E3 ligase that conjugates K48-linked ubiquitination and mediates the degradation of RIG-I *via* the proteasome pathway (35). To determine whether FMDV 2B interacts with RNF125, HEK293T cells were transfected with the indicated plasmids and a co-IP assay was performed. Interestingly, we found that the RNF125 was precipitated from the lysate of cells transfected with the FMDV 2B expression plasmids (Figure 4A and Supplementary Figure 4A). Consistent with the above results, we confirmed the co-localization of the RNF125 and FMDV 2B by confocal microscopy (Figure 4B).

Next, to identify the mechanism underlying the RNF125-mediated degradation of RIG-I, we set out to investigate whether RNF125 degrades RIG-I in the presence of increasing doses of an FMDV 2B expression plasmid. As expected, the expression of RIG-I was reduced by RNF125 (Figure 4C). Interestingly, RNF125 increased the degradation of RIG-I in an FMDV 2B dose-dependent manner under endogenous (Figure 4C) and overexpressed conditions (Supplementary Figure 4B).

Next, to investigate RIG-I status during FMDV infections, LFBK cells were infected with FMD O1 Manisa virus, and RIG-I levels were measured over time. Cell lysates were inactivated and immunoprecipitated with an anti-FMDV 2B antibody, then immunoblotted with anti-RIG-I and anti-RNF125 antibodies. As shown in Figure 4D, the FMDV 2B interacted with the RIG-I and the RNF125. Interestingly, at 6 hours post-infection (hpi), the overall amounts of the RIG-I began to decrease, and at 8 hpi, the interaction between the RIG-I almost disappeared. These results indicate that FMDV induces marked degradation of RIG-I in an RNF125-mediated manner as the infection progresses.

To further evaluate whether RNF125 is essential for FMDV 2B-mediated degradation of RIG-I, we designed siRNA targeting RNF125 and performed an immunoblotting to detect the RIG-I expression after the overexpression of the indicated plasmids in the RNF125 knockdown cells or the control HEK293T cells. As shown in Figure 4E, the knockdown of RNF125 did not promote RIG-I degradation. These results suggest that the degradation of RIG-I by FMDV 2B is dependent on RNF125. To confirm these results, we performed virus replication experiments in which RAW264.7 cells were treated with control or RNF125 siRNA, then transfected with the indicated plasmids, and lastly, infected with VSV-GFP. As shown in Figures 4F, G, the knockdown of RNF125 did not induce an enhancement of viral replication and inhibition of IFN-β secretion. Furthermore, to reassess whether RNF125 is essential for K48-linked polyubiquitination of RIG-I, the RNF125 knockdown or the control HEK293T cells were transfected with the indicated plasmids, and whole cell lysates were immunoprecipitated with Flag-tagged RIG-I. As shown in Figure 4H, the knockdown of RNF125 failed to promote K48-linked ubiquitination of RIG-I. Previous studies suggest that the lysine residue at position 181 of RIG-I is essential for RNF125-mediated ubiquitination and degradation of RIG-I (35). Hence, we constructed the RIG-I K181R mutant to confirm the hypothesis that FMDV 2B degrades RIG-I by recruiting RNF125. As shown in Figure 4I and Supplementary Figure 4C the RIG-I undergoes ubiquitination in the presence of RNF125 and FMDV 2B, whereas the RIG-I K181R mutant does not. Taken together, these results indicate that FMDV 2B hijacks the host RIG-I degradation mechanism mediated by RNF125 to suppress the host immune response to FMDV infection.

C-terminal region of FMDV 2B is essential for the interaction and proteasomal degradation of RIG-I

While our experiments confirmed an interaction between RIG-I and FMDV 2B, the specific domains mediating this association were still unclear. To identify the domain within RIG-I that interacts with FMDV 2B, we constructed GST-fused CARD1, CARD2, or 2CARD of RIG-I expression plasmids (Figure 5A) and performed an immunoprecipitation assay. As shown in Figure 5B, the FMDV 2B bound strongly to the CARD1 (aa 1-92) of RIG-I. Similarly, a series of truncated mutants of FMDV 2B were constructed, and a GST pull-down assay using these mutants was performed. As shown in Figures 5C, D, RIG-I interacted with C-terminal amino acids (aa) 126-154 of FMDV 2B. Next, we investigated which region of FMDV 2B was required for the interaction with RNF125. As shown in Figures 5E, F, aa 99-113 of FMDV 2B is involve in the interaction between FMDV 2B and RNF125. We also

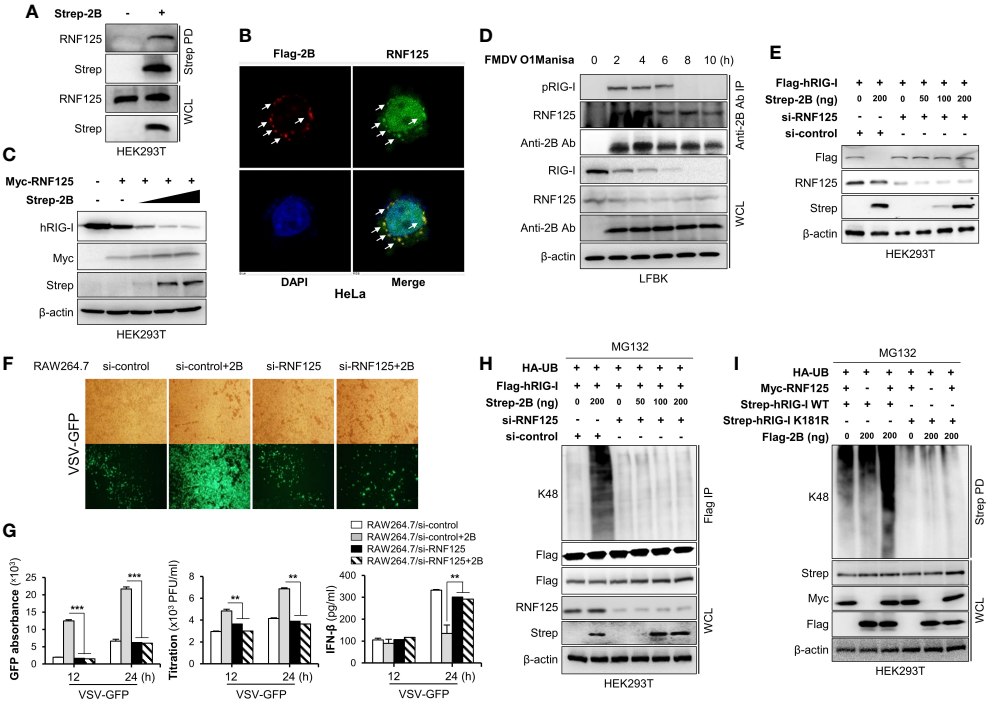

FIGURE 4
FMDV 2B recruit RNF125 to mediate K48-linked polyubiquitination and degradation of RIG-I. HEK293T cells were transfected with Strep-FMDV 2B. Cell lysates were subjected to Strep pull-down assay and immunoblotted with indicated antibodies **(A)**. HeLa cells were transfected with Flag-FMDV 2B, followed by confocal microscopy assay with anti-Flag (red) and anti-RNF125 (green) antibodies. Nuclei were stained with DAPI (blue) **(B)**. HEK293T cells were transfected with Myc-RNF125 together with increasing doses of Strep-FMDV 2B. The whole-cell lysate was immunoblotted with indicated antibodies **(C)**. LFBK cells were infected with FMDV O1Manisa strain, and cells were harvested after indicated time period post-infection. The whole-cell lysate was immunoprecipitated with FMDV 2B rabbit polyclonal antibody and immunoblotted with indicated antibodies **(D)**. HEK293T cells were transfected with si-control or si-RNF125 together with Flag-RIG-I and different doses of Strep-2B plasmids. The whole-cell lysate was immunoblotted with indicated antibodies **(E)**. **(F, G)** RAW264.7 cells were transfected with si-control or si-RNF125 together with Flag-FMDV 2B and infected with VSV-GFP. Viral replication was measured by fluorescence microscopy, GFP absorbance, and plaque assay at indicated time points. The concentration of secreted IFN-β in supernatants was determined at 12 and 24 hpi by ELISA. HEK293T cells were transfected with si-control or si-RNF125 together with Flag-RIG-I, HA-ubiquitin, indicated doses of Strep-FMDV 2B and treated with MG132 6 hours before harvesting the cells. Whole-cell lysates were subjected to Flag-immunoprecipitation and immunoblotted with indicated antibodies **(H)**. HEK293T cells were transfected with Strep-RIG-I wild-type or RIG-I K181R mutant together with HA-ubiquitin, Myc-RNF-125, indicated doses of Flag-FMDV 2B and treated with MG132 6 hours before harvesting the cells. Whole-cell lysates were subjected to Strep pull-down and immunoblotted with indicated antibodies **(I)**. Results representative of at least two independent experiments, each with similar results, and the values are expressed as mean ± SD of three biological replicates. Student's t-test; **p < 0.01; ***p < 0.001.

reconfirmed the interaction between CARD2 (aa 93-186) of RIG-I and RNF125 as in previous studies (35) (Figure 5G). These results suggest that the aa 99-113 region of FMDV 2B recruits RNF125 and the aa 126-154 region interacts with RIG-I for RNF125-mediated ubiquitination and degradation of RIG-I. Based on these findings, to investigate whether the C-terminal deletion of FMDV 2B affects the RIG-I-mediated type-I IFN cascade, we generated two FMDV deletion mutants containing aa 115-154 deleted FMDV△2B (1–114) and aa 126-154 deleted FMDV△2B (1–125). As shown in Figures 5H, I, each indicating plasmid was transiently transfected into HEK293T cells, and each cell was infected with VSV-GFP. Interestingly, we found that the deletion mutants of FMDV 2B did not show higher levels of virus replication and lower levels of IFN-β secretion as in FMDV 2B. Altogether, these results indicated that the aa 126-154 region of FMDV 2B was essential for interaction with RIG-I, and this interaction was crucial for FMDV 2B-mediated inhibition of type-I IFN cascade *via* the ubiquitination and proteasomal degradation of RIG-I.

FMDV 2B induces apoptosis and mediates caspase-3- and caspase-8-dependent degradation of MDA5

Cytosolic RNA sensor MDA5 is known to be essential for the recognition of FMDV (36). Hence we checked the effect of FMDV infection on MDA5 protein expression. Results of Figure 6A shows that FMDV infection in to LFBK cells reduced the MDA5 protein expression similar to RIG-I

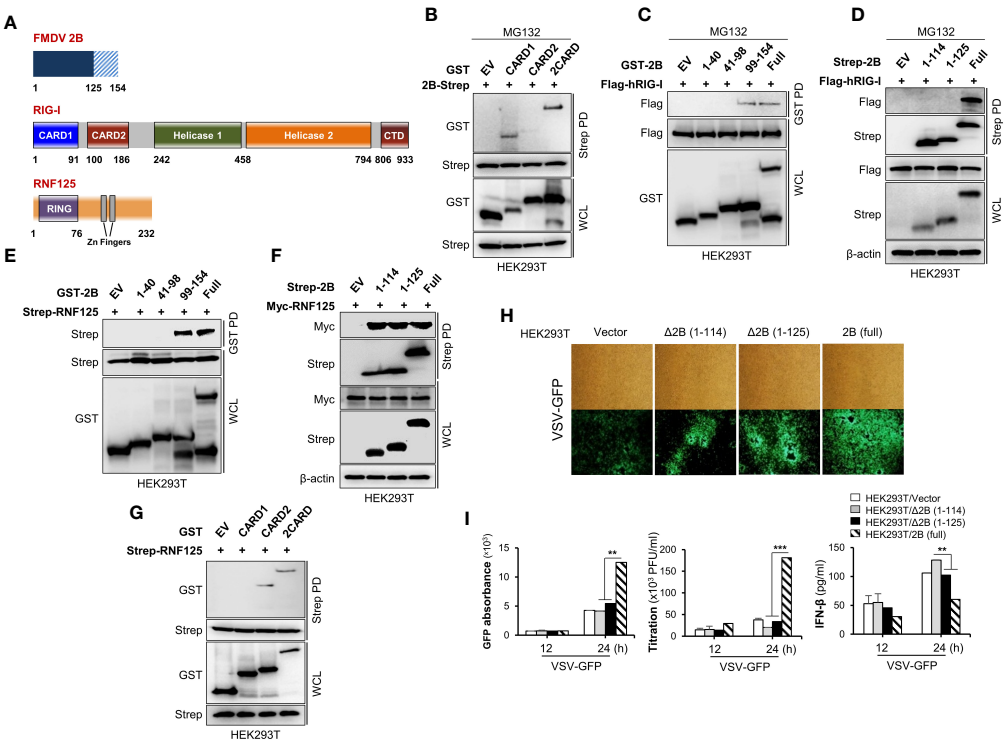

FIGURE 5
C-terminal region of FMDV 2B is important for the interaction and proteasomal degradation of RIG-I. Schematic representation of the domain construction of FMDV 2B, RIG-I, and RNF125 **(A)**. HEK293T cells were transfected with GST-RIG-I domain constructs together with Strep-FMDV 2B plasmids and treated with MG132 for 6 hours before harvesting the cells. Whole-cell lysates were subjected to the Strep pull-down assay, followed by immunoblotting with indicated antibodies **(B)**. HEK293T cells were transfected with Flag-RIG-I together with GST-FMDV 2B domain constructs containing plasmids and treated with MG132 for 6 hours before harvesting the cells. Whole-cell lysates were subjected to GST pull-down and immunoblotted with indicated antibodies **(C)**. HEK293T cells were transfected with Strep-FMDV 2B domain constructs together with Flag-RIG-I plasmids and treated with MG132 for 6 hours before harvesting the cells. Whole-cell lysates were subjected to the Strep pull-down assay, followed by immunoblotting with indicated antibodies **(D)**. HEK293T cells were transfected with Strep-RNF125 together with GST-FMDV 2B domain constructs containing plasmids. Whole-cell lysates were subjected to GST pull own and immunoblotted with indicated antibodies **(E)**. HEK293T cells were transfected with Myc-RNF125 together with Strep-FMDV 2B deletion mutant constructs containing plasmids. Whole-cell lysates were subjected to Strep pull own and immunoblotted with indicated antibodies **(F)**. HEK293T cells were transfected with Strep-RNF125 together with GST-RIG-I domain constructs containing plasmids. Whole-cell lysates were subjected to strep pull down and immunoblotted with indicated antibodies **(G)**. **(H, I)** HEK293T cells were transfected with control vector, FMDV Δ2B (1-114) mutant, FMDV Δ2B (1-125) mutant, and FMDV 2B wild-type plasmids and infected with VSV-GFP. Viral replication was measured by fluorescence microscopy, GFP absorbance, and plaque assay at indicated time points. The concentration of secreted IFN-β in supernatants was determined at 12 and 24 hpi by ELISA. Results representative of at least two independent experiments, each with similar results, and the values are expressed as mean ± SD of three biological replicates. Student's t-test; **p < 0.01; ***p < 0.001.

(Figure 6A; Supplementary Figure 5A). Based on the IFN-β reporter assay (Figure 2D) and the results of previous studies (27), we also investigated whether FMDV 2B affects MDA5. First, HEK293T cells were co-transfected with MDA5 expression plasmids and increasing doses of FMDV 2B expression plasmids, followed by an immunoblot analysis. As shown in Supplementary Figure 5B, we found that the overexpression of FMDV 2B resulted in a significant decrease in the MDA5 levels in a dose-dependent manner. Concurrently, we confirmed that FMDV 2B also reduced the expression of the endogenous porcine MDA5 (pMDA5) in PK-15 cells in a dose-dependent manner (Figure 6B). Next, to confirm whether FMDV 2B affects the expression or the degradation of MDA5, we co-transfected FMDV 2B and MDA5 expression plasmids into cells treated with different inhibitors. As shown in Figure 6C, the expression of MDA5 was restored upon treatment with a z-VAD. In addition, the degradation of the endogenous MDA5 in PK-15 cells was recovered in a dose-dependent manner by treatment with z-VAD (Figure 6D).

In the previous studies, mouse MDA5 undergoes caspase-3- and caspase-8-dependent cleavage upon apoptosis stimulation (18). To investigate whether the FMDV 2B-mediated degradation of MDA5 is caspase-3- or caspase-8-dependent, HEK293T cells were co-transfected with MDA5 and FMDV 2B expression plasmids in the presence of increasing doses of a caspase-3 inhibitor (zDEVD-FMK) or a caspase-8 inhibitor

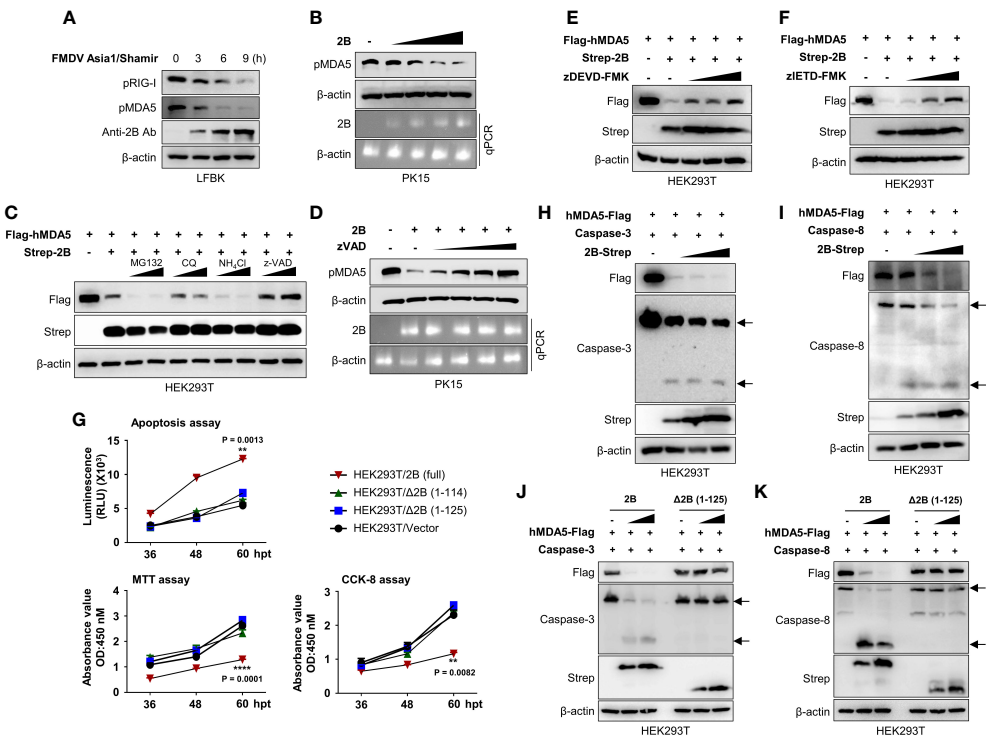

FIGURE 6
FMDV 2B induces apoptosis and apoptosis-mediated caspase-3 and caspase-8 dependent degradation of MDA5. LFBK cells were infected with 0.1MOI of FMDV Asia1/Shamir for 0, 3, 6, 9 hours and whole-cell lysates were immunoblotted with indicated antibodies **(A)**. PK-15 cells were transfected with increasing doses of FMDV 2B, and 24 hrs post-transfection cells were infected with SeV (1MOI). Cells were harvested at 24 hrs post-infection, and the MDA5 expression level was measured by immunoblotting **(B)**. HEK293T cells were transfected with Flag-MDA5 together with Strep-FMDV 2B and treated with two doses of MG132, chloroquine, NH_4Cl, or zVAD for 6 hours before harvesting the cells. Whole-cell lysates were subjected to immunoblotting with indicated antibodies **(C)**. PK-15 cells were transfected with FMDV 2B, and 24 hrs post-transfection, cells were infected with SeV (1MOI). Cells were treated with increasing doses of zVED for 6 hours before harvesting cells. Whole-cell lysates were subjected to immunoblotting with indicated antibodies **(D)**. **(E, F)** HEK293T cells were treated with Flag-hMDA5, Strep-FMDV 2B plasmids, and treated with increasing doses of zDEVD-FMK **(E)**, or zIETD-FMK **(F)**, 6 hours before harvesting the cells. Whole-cell lysates were subjected to immunoblotting with indicated antibodies. HEK293T cells were transfected with Strep-FMDV 2B wild-type, FMDV Δ2B (1-114) mutant, FMDV Δ2B (1-125) mutant, and control vector. Annexin V apoptosis assay, CCK-8 assay, and MTT assay were conducted at indicated time points post-transfection **(G)**. **(H, I)** HEK293T cells were transfected with Flag-MDA5, caspase-3 **(G)**, or caspase-8 **(H)** plasmids together with increasing doses of Strep-FMDV 2B plasmids. Whole-cell lysates were subjected to immunoblotting with indicated antibodies. **(J, K)** HEK293T cells were transfected with Flag-MDA5, caspase-3 **(J)**, or caspase-8 **(K)** plasmids together with increasing doses of Strep-FMDV 2B wild-type or FMDV Δ2B (1-125) mutant. Whole-cell lysates were subjected to immunoblotting with indicated antibodies. Results representative of at least two independent experiments, each with similar results. Student's t-test; **p < 0.01; ****p < 0.0001.

(zIETD-FMK). As shown in Figures 6E, F, the MDA5 was not degraded in the presence of both inhibitors.

Picornaviruses induce cellular apoptosis after infection (37). Among the various viral proteins of picornaviruses, viroporins modify membrane permeability and disrupt the Ca^{2+} balance, leading to apoptosis (26, 38, 39). In particular, viroporin is known to induce caspase-dependent apoptosis (39). Since FMDV 2B shows viroporin activity (26), we investigated the apoptotic activity of FMDV 2B using an Annexin V apoptosis assay, a cell counting kit-8 (CCK-8) assay, and 3-[4,5-dimethylthiazol-2-yl]-2,5-diphenyltetrazolium bromide (MTT) assay. As shown in Figure 6G and Supplementary Figure 5C, FMDV 2B induces significant apoptosis in HEK293T cells and PK-15 cells after transfection with FMDV 2B expression plasmids. However, surprisingly, FMDV△2B (1-114) and FMDV△2B (1-125) did not show apoptosis. Next, we checked the activation of caspase-3 and caspase-8 in the presence of increasing doses of FMDV 2B. As shown in Figure 6H, I, the FMDV 2B activated both caspase-3 and caspase-8, and activation of these caspases was consistent with the degradation of the MDA5. However, FMDV△2B (1-114) and FMDV△2B (1-125) neither activated the caspases nor degraded the MDA5 (Figures 6J, K; Supplementary Figures 5D, E). Taken together, these results suggest that the C-terminal region of FMDV 2B is critical for the induction of caspase-dependent apoptosis and the degradation of MDA5 in a dose-dependent manner. Consequently, FMDV 2B affects the MDA5-mediated type-I IFN cascade.

Discussion

The RLR-mediated Type-I IFN response is a critical defense mechanism against RNA viruses, including FMDV (16). Therefore, FMDV is highly sensitive to the IFN response. To avoid this, FMDV has evolved various immune evasion strategies to ensure effective replication in host cells (40). FMDV proteases, L^{pro}, and $3C^{pro}$ play a crucial role in interfering with host protein translation to induce FMDV replication within host cells. Specifically, FMDV L^{pro} is associated with cleavage of translation initiation factor eIF4G to inhibit cellular protein synthesis (41), mediate the degradation of NF-κB subunit, p65/RelA (42), inhibition of NF-κB dependent gene expression (43), reduced expression of IFN-β mRNA levels by direct cleavage of LGP2 (44), acting as a viral deubiquitinase to deubiquitinate RIG-I, TBK1, TRAF3, and TRAF6 (45), to enhance FMDV replication by suppressing host immune response. $3C^{pro}$ has mainly involved in the inhibition of NF-κB and IRF signaling, followed by direct cleavage of NEMO (46), cleavage of nuclear protein Sam68 (47), cleavage of G3BP1 and inhibit stress granule formation (48), degradation of KPNA1 nuclear translocation signal receptor to inhibit STAT1/STAT2 nuclear translocation (49), degradation of cellular viral RNA sensors, RIG-I, MDA5 (50), and LGP2 (30). Apart from proteases, other FMDV non-structural proteins also play a significant role in modulating host immune response. FMDV 2C is associated with inhibition of autophagy and enhanced viral replication by interacting with Beclin-1 (51). FMDV 3A is the largest 3A protein among all picornavirus family members. It is also associated with disruption of RLR-mediated IFN-β signaling by downregulating RIG-I, MDA5 transcript levels (52), DDX56 dependent inhibition of IRF3 phosphorylation (53), upregulation of LRRC25 to inhibit G3BP1 mediated RLH signaling pathway (9). FMDV VP3 mediates the degradation of JAK1 (54), decreases the expression of RIG-I and MDA5 (55) and inhibits MAVS aggregation (56). Furthermore, FMDV VP1 interacts with sorcin to inhibit IFN signaling (57). Moreover, a recent study shows that FMDV VP1 inhibits MAVS-TRAF3 binding to downregulate interferon signaling and VP1 E83K mutated virus shows attenuation in pigs (58).

In this study, we demonstrated two novel molecular mechanisms of FMDV 2B-mediated RIG-I and MDA5 degradation to evade host IFN responses. First, we showed that the overexpression of FMDV 2B in epithelial cells induces enhancement of RNA virus replication and also downregulates RNA virus-induced IFN-β and proinflammatory cytokine-signaling cascades. Second, FMDV 2B interacted with RIG-I and induced K48 ubiquitination and proteasomal degradation of the RIG-I by recruiting E3 ubiquitin ligase, RNF125. Third, FMDV 2B protein was involved in inducing apoptosis and apoptosis-mediated caspase-3- and caspase-8-dependent cleavage of MDA5. Fourth, aa 126-154 of FMDV 2B are essential for 2B-mediated degradation of RIG-I and MDA5. Taken together, these findings indicate a specific molecular mechanism of FMDV 2B that negatively regulates host type-I IFN signaling by degradation of RIG-I and caspase-dependent degradation of MDA5.

FMDV 2B is known to be primarily associated with host cell membrane rearrangement and the inhibition of the cellular secretory pathway (ER-to-Golgi transport) (24, 40). Sequence and structural analysis of FMDV 2B showed that the 2B protein consists of two hydrophobic regions and is mainly localized in ER (26, 40). Previous studies have shown that FMDV 2B increases Ca^{2+} ion content in host cells and also increases membrane permeability in both bacteria and mammalian cells (26). Consequently, researchers suggest that FMDV 2B acts as a viroporin during viral infections, and it is also known that the viroporin activity of FMDV 2B mediates NLRP3 inflammasome activation (59). Notably, it has already been suggested that FMDV 2B is involved in the impairment of RIG-I or LGP2-mediated antiviral signaling (23, 30), and Zhu and colleagues suggested that FMDV 2B inhibits the expression of RIG-I and MDA5 to antagonize RIG-I-mediated type-I IFN response (23). However, the precise molecular mechanisms of FMDV 2B targeting RIG-I and MDA5 for negative regulation of type-I IFN signaling is still unknown. In this study, we showed an IFN inhibition phenotype after the overexpression of FMDV 2B as in previous reports and confirmed that FMDV 2B targets RIG-I by an IFN-β luciferase reporter assay. However, we evaluated the effect of MG132 on HEK293T cell overexpression system (Figure 3C and Supplementary Figure 3A), as well as in PK15 cell endogenous system (Figure 3D), showing a clear inhibition of 2B-mediated RIG-I degradation by MG132, which differs from the previous report. Ultimately, we found an interaction between FMDV 2B and RIG-I and demonstrated the degradation of RIG-I rather than the inhibition of protein expression.

The overexpression of FMDV 2B significantly induced the degradation of RIG-I in a dose-dependent manner, and its degradation was found to be proteasomal by K48 ubiquitination. Although FMDV 2B can induce K48 ubiquitination of RIG-I, it does not have E3 ligase activity. Therefore, we hypothesized that 2B enhances ubiquitination and degradation of RIG-I by recruiting a host E3 ligase such as a latent membrane protein 1 (LMP1) of Epstein-Barr virus (EBV), which mediates the proteasomal degradation of RIG-I by recruiting E3 ligase CHIP (60). So far, RNF125, CHIP, RNF122, and MARCH5 have been reported to mediate the K48 ubiquitination and the degradation of RIG-I for the downregulation of RIG-I-mediated IFN signaling (35, 61–63). Among them, we found that FMDV 2B specifically interacted with RNF125 and strongly co-localized in HeLa cells, and this interaction increases proteasomal degradation followed by K48

ubiquitination of RIG-I (Figures 4B, C, H). Previous studies have reported that the K181 residue of the RIG-I is responsible for the ubiquitination and degradation by RNF125 (35). Therefore, for more reliable evidence, we tested the effect of a (RIG-I) (K181R) mutant on FMDV 2B-mediated RIG-I ubiquitination, and showed that the FMDV 2B was unable to induce the ubiquitination and degradation of RIG-I (K181R) by RNF125 (Figure 4I). Furthermore, we also found that the overexpression of FMDV 2B significantly induced the degradation of MDA5 in a dose-dependent manner. We further investigated the mechanism of the MDA5 degradation by FMDV 2B and found that it is a caspase-dependent degradation. However, we could not see an interaction between FMDV 2B and MDA5 in the presence of the caspase inhibitors. Therefore, we hypothesized that this degradation of MDA5 was a binding-independent degradation. Previously, Kovacsovics and colleagues demonstrated that the MDA5 undergoes caspase-dependent cleavage upon stimulation of apoptosis and that this cleavage of MDA5 is a caspase-3- or caspase-8-dependent cleavage that can be inhibited by specific inhibitors (DEVD, IETD) (18). Furthermore, previous findings have shown that infections of picornaviruses, such as Enterovirus 71 (EV71) and Poliovirus (PV), sequentially induce apoptosis and the cleavage of MDA5 without proteinases ($2A^{pro}$, $3C^{pro}$) activity (64). In this study, together with previous findings, we showed that the overexpression of FMDV 2B activates the apoptotic pathway. The apoptotic stimulation converted procaspase-3 and procaspase-8 into an activated form, and as a result, caspase-3- or caspase-8-dependent degradation of MDA5 was confirmed (Figures 6H, I).

Based on the mapping study, we identified that the C-terminal fragment (aa 126-154) of 2B is essential for the interaction between CARD1 domain of RIG-I and FMDV 2B (Figures 5B, C). For the impact of the interaction domain of 2B, we constructed 2B mutant △126-154 and found that the mutant was unable to induce the ubiquitination and the degradation of RIG-I and ultimately lost the ability to modulate the IFN response (Figures 5D, H, I). Interestingly, the mutant was also unable to induce apoptosis leading to caspase-dependent cleavage of MDA5 (Figures 6G–K). Additionally, we confirmed that the C-terminal domain (aa 99-114) of 2B interacts with RNF125, and RNF125 interacts with CARD2 domain of RIG-I individually without interfering with complex formations (Figures 5E–G).

Currently, there are commercially available vaccines against FMDV. Nevertheless, the research and necessity for attenuated FMDV strains are required in various aspects including safety. The development of the attenuated FMDV strain by genetic manipulation is a reasonable approach and, perhaps, a safer methodology. To confirm the role and the molecular mechanism of FMDV 2B identified in the FMDV itself, a construction of a recombinant FMD virus harboring 2B mutation (△126-154) and an evaluation of virulence in swine are needed in the future.

In summary, ongoing studies of the immune evasion mechanisms used by FMDV are critical to better understanding the pathogenesis of FMDV. Our results demonstrate that FMDV 2B is a negative regulator of type-I IFN-signaling cascade for virus replication. To inhibit type-I IFN-signaling, FMDV 2B recruits the E3 ubiquitin ligase RNF125 to induce proteasomal degradation of RIG-I by K48 ubiquitination and also targets MDA5 for caspase-3- and caspase-8-dependent cleavage of the MDA5 by apoptosis induction. These findings may provide a new understanding of molecular mechanisms used by the FMDV 2B to counteract the type-I IFN responses and expand our knowledge on immune evasion strategies used by FMDV. Furthermore, our study may provide a rational approach to virus attenuation for future FMDV vaccine development.

Materials and methods

Cells and antibodies

RAW264.7 (ATCC TIB-71), HEK293T (ATCC-11268), HeLa (ATCC CCL-2), PK-15 (ATCC CCL-33), LFBK (RRID: CVCL_RX26), cells were cultured in Dulbecco's Modified Eagle Medium (DMEM) (HyClone) supplemented with 10% fetal bovine serum (FBS) (Gibco) and 1% antibiotic/antimycotic (Gibco). Cells were maintained in a humidified 5% CO2 incubator at 37°C. Antibodies used for the immunoblot and immunoprecipitation analysis are as follows, anti-Flag (Cell Signaling, 8146), anti-Strep (Qiagen, 34850), anti-GST (Santa Cruz, sc-138), anti-IRF3 (Abcam, ab25950), anti-phospho IRF3 (Ser396) (Cell Signaling, 4947), anti-p65 (Cell Signaling, 4764S), anti-phospho p65 (Cell Signaling, 3031S), anti-TBK1 (Cell Signaling, 3504S), anti-phospho-TBK1 (Cell Signaling, 5483S), anti-β-actin (Santa Cruz,SC 47778), RIG-I (D14G6; 3743), MDA-5 (D74E4; 5321), Anti-FMDV 2B (homemade), anti-Caspase8 (Cell Signaling, 9746S), anti-Caspase3 (Cell Signaling, 9662S) and anti-β-actin (Santa Cruz,SC 47778)

Preparation of stable cell lines

To prepare FMDV 2B overexpressing stable cell line, RAW264.7 cells were seeded in 6-well culture plates 12 hours after seeding (60% cell confluence), pIRES-Flag-2B plasmid was transfected into the cells by incubating with Lipofectamine 2000 (Invitrogen) and for 6 hours. Next, culture media was changed into complete DMEM and incubated for 12 hours before transferring the cells into a 100 mm culture dish. Cells were incubated with complete DMEM media, and after cells were attached, media was replaced with complete DMEM with 2 μg/ml puromycin. Replace media with fresh puromycin containing 10% DMEM every 2 days

until resistant colonies appear. Expression of Flag-tagged 2B was confirmed by immunoblotting.

Virus propagation, infection, and stimulant transfection

Recombinant Green Fluorescent Protein (GFP) expressing viruses such as H1N1 influenza A virus (A/PR8/8/34; PR8-GFP) and Newcastle disease virus (NDV-GFP) were propagated in allantoic fluid of 10-day old embryonated chicken eggs. And GFP-expressing vesicular stomatitis virus (VSV-GFP), GFP-expressing coxsackievirus (H3-GFP), and EV-71 were propagated in the monolayer of *Ceropithecus aethiops* epithelial kidney (Vero; ATCC® CCL-81™) cells, and virus titer was determined by the plaque assay. During virus infection, we changed the culture media to 1% FBS containing DMEM, and viruses were added to the medium with the indicated multiplicity of infection (MOI). After 2 hours of infection, the media was changed to complete DMEM. Poly (I·C) was transfected with Lipofectamine 2000 into HEK293T cells or used to treat RAW264.7 cells. 5'- triphosphate double-stranded RNA (5'ppp-dsRNA, Invivogen) was transfected into both cell lines with Lipofectamine RNAiMAX (Invitrogen) to stimulate immune response pathways. According to the manufacturer's instructions, cell lysates were harvested at the indicated time, and GFP expression was measured with the Glomax multi-detection system (Promega, Wisconsin, USA).

Virus infection and stimulant transfection

GFP-expressing H1N1 influenza A virus (A/PR8/8/34; PR8-GFP) and GFP-expressing Newcastle disease virus (NDV-GFP) were propagated in the allantoic fluid of 10-day-old specific-pathogen-free embryonated chicken eggs GFP-expressing vesicular stomatitis virus (VSV-GFP), GFP-expressing Coxsackievirus (H3-GFP), and EV-71 were propagated on a monolayer of Vero cells. Cultured cells medium was replaced with DMEM or RPMI containing 1% FBS before virus infection, and the viruses were added into the medium with the indicated MOI. After 2 h of incubation, the extracellular virus was removed and replaced with 10% FBS DMEM or RPMI. Poly(I:C) (Invivogen) was transfected to HEK293T cells with Lipofectamine 2000 (Invitrogen) and treated to RAW264.7 cells, respectively. 5'ppp-dsRNA (Invivogen, tlrl-3prna) was transfected to both cell lines with Lipofectamine RNA iMAX (Invitrogen) to stimulate immune response pathways. According to the manufacturer's instructions, cell lysates were harvested at the indicated time, and GFP expression was measured with the Glomax multi-detection system (Promega, Wisconsin, USA).

FMDV infection into cell culture

Fetal porcine kidney (LFBK) cells were used to perform the FMDV infection experiment. The cell monolayer was prepared in cell culture plates (90x20mm) and incubated overnight, followed by infection with FMDV Asia1/Shamir at 0.1MOI for 2 hours before replacing with complete DMEM culture media. For the RIG-I ubiquitination assay, cells were treated with MG132 (10μM) for 6 hours before collecting the cells. Cells were collected at indicated time points after infection, RIG-I and MDA5 expression levels, RIG-I ubiquitination and RIG-I interaction with RNF125 and FMDV 2B were examined by immunoblotting.

Determination of virus titer

To evaluate the virus titer of cell culture supernatants, plaque assays or TCID50 was performed. Cell culture supernatants of growing cells or freeze-thawed cells were used to titrate VSV-GFP, H3-GFP, or PR8-GFP, respectively. The supernatants were serially 10-fold diluted and inoculated into Vero cells in 1% FBS containing DMEM. Following 2 h incubation at 37°C, the inoculums were removed and replaced with DMEM containing 0.1% agarose (Sigma-Aldrich). Plates were then incubated for another 36 hr at 37°C and examined for plaque formation at 200× magnification. The virus titer was calculated using the number of plaque-forming units and the dilution factor. TCID50 was carried out for EV-71 virus titration. Briefly, 100 μL of Vero cells cultured were prepared at 96 well flat-bottomed cell culture plates, and 100 μL of 10-fold serial dilutions of virus suspensions were added to plates, with each dilution being repeated in eight wells and incubated at 37°C for 3-4 days. CPE was observed in each well under a light microscope, and TCID50 was calculated using the method described by Reed and Muench (65).

mRNA expression analysis by qRT-PCR

FMDV 2B or pIRES empty vector stably expressing RAW264.7 cells or HEK293T cells were infected with VSV-GFP or PR8-GFP virus, and cells were collected in different time courses. Total mRNA was obtained from cells using RNeasy Mini Kit (Qiagen), and cDNA synthesis was performed using a ReverTra Ace kit (Toyobo). qRT-PCR analysis was performed using QuantiTect SYBR Green PCR kit (Qiagen) on a Rotor-Gene Q (Qiagen). The target gene expression was normalized to the expression of the glyceraldehyde-3-phosphate dehydrogenase (GAPDH) reference gene. The primer sequences for genes used for real-time PCR are listed in Table 1.

TABLE 1 The primer sequences for the genes used in real-time PCR.

Target gene	Forward primer	Reverse primer
IFN-β	TCCAAGAAAGGACGAACATTCG	TGCGGACATCTCCCACGTCAA
IL-6	GACAACTTTGGCATTGTGG	ATGCAGGGATGATGTTCTG
ISG-15	CAATGGCCTGGGACCTAAA	CTTCTTCAGTTCTGACACCGTCAT
ISG-56	AGAGAACAGCTACCACCTTT	TGGACCTGCTCTGAGATTCT
GBP1	AAAAACTTCGGGGACAGCTT	CTGAGTCACCTCATAAGCCAAA
IFN-α	ATAACCTCAGGAACAACAG	TCATTGCAGAATGAGTCTAGGAG
Mx1	ACAAGCACAGGAAACCGTATCAG	AGGCAGTTTGGACCATCTTAGTG
OAS-1β	AGGTGGTAAAGGGTGGCT	TGCTTGACTAGGCGGATG
TNF-α	AGCAAACCACCAAGTGGAGGA	GCTGGCACCACTAGTTGGTGGT
GAPDH Mouse	AGCAAACCACCAAGTGGAGGA	GACGGACACATTGGGGGTAG

Immunoprecipitation

Cells were co-transfected with indicated plasmids, and 36 h post-transfection cells were harvested. Whole-cell lysates (WCL) were obtained after lysis with protease inhibitor cocktail- and phosphatase inhibitor cocktail (Sigma)-containing radioimmunoprecipitation assay (RIPA) lysis buffer (50 mM Tris-HCl, 150 mM NaCl, 0.5% sodium deoxycholate, 1% IGEPAL, 1 mM NaF, 1 mM Na3VO4) and sonication with a sonicator (Sonics). The WCLs were pre-cleared with Sepharose 6B (GE Life Sciences) at 4°C for 2 h. The pre-cleared whole cell lysates were incubated overnight with 2 μg target protein antibodies, 50% slurry of glutathione-conjugated Sepharose (GST) beads (Amersham Biosciences) or Strep beads (IBA Life Sciences) with agitation at 4°C. Only for the whole cell lysate incubated with antibodies, 20 μl protein, A/G PLUS-agarose was added to precipitate proteins attached with antibodies. The immunoprecipitated beads were collected after centrifugation and were washed with lysis buffer under different washing conditions. Precipitates were subjected to SDS-PAGE, and immunoblotting was performed with the appropriate antibody.

Immunoblot analysis

Cell lysates or immunoprecipitated beads were mixed with 2× sample buffer (Sigma), samples were loaded onto SDS-PAGE, and proteins were separated by molecular weight. Samples were separated by SDS-PAGE and transferred onto a PVDF membrane (Bio-rad) in a buffer containing 30 mM Tris, 200 mM glycine, and 20% methanol for 2 hr. The membranes were blocked with Tris-buffered saline containing 0.05% Tween 20 (TBST) and 5% bovine serum albumin (BSA) for 1 h and incubated with target antibodies overnight at 4°C. To detect target proteins, the membranes were washed with phosphate-buffered saline containing 0.05% Tween 20 (PBST) or TBST and incubated with a 1:3,000 dilution of horseradish peroxidase (HRP)-conjugated secondary antibodies for 1 h, and the HRP on the membranes were developed with Western blotting detection reagents (GE Healthcare; ECL Select Western blotting detection reagent) and visualized using an ImageQuant LAS 4000 (GE Life Sciences).

Luciferase reporter assay

HEK293T cells were transfected with 400ng of firefly luciferase reporter plasmid (pGL-3), 100ng of pRL-TK (Renilla luciferase- as an internal control) (Promega), increasing amounts of FMDV 2B-Flag (0-1600ng) expression plasmid and pIRES empty vector to equalize the transfection amounts using Polyethylenimine (PEI) transfection reagent. To stimulate the IFN-β promoter, plasmids carrying the RIG-I, MAVS, TRIF, and TBK1 gene were co-transfected together with luciferase reporter plasmids or PR8-GFP, NDV-GFP viruses infection, poly(I·C) transfection were conducted at 12 h post-transfection. At 12 h after stimulation, the cells were washed with PBS and lysed with 1X Passive Lysis buffer (Promega) for 20 minutes. Following the manufacturer's instruction, luciferase activity was measured using the Dual-Luciferase Reporter Assay System (Promega; E1980). Luciferase activity in cells expressing only IFN-β reporter and Renilla plasmids was measured as a control. Data are expressed in accordance with relative firefly luciferase activity normalized against Renilla luciferase activities.

Immunofluorescence and confocal analysis

The HeLa cells were seeded in collagen-coated chamber slides (LabTek, Nunc). 12 hours later, cells were transfected with the indicated plasmids and incubated for 36 hours (MG132 treatment was done 28 hours after transfection). After 36 hours of incubation, the cultured cells were washed with phosphate buffer saline (PBS) and fixed with 4% paraformaldehyde for

20 min, then permeabilized through incubation for 20 min with 100% methanol at -20°C. The fixed cells were first incubated with 2% FBS diluted in PBS for 1 hour to block the non-specific binding of antibodies. Next, cells were incubated with indicated antibodies for 12 hours in 4°C.

After three times washing with PBS, cells were incubated with the 1:100 diluted secondary antibodies for 1 hr at room temperature. After three times PBS washing, the nuclei were visualized following incubation for 10 min with 1:50000 diluted DAPI (Sigma) adding 1 mg/ml RNase A, and the slides were mounted with the mounting solution (VECTOR). Images were captured using a Nikon C2 Plus confocal microscope (Nikon), consisting of a Nikon Eclipse Ti inverted microscope with a confocal scanning system (Nikon) in conjunction with a C-HGFIE precentered fiber illuminator (Nikon). Fluorescein isothiocyanate (FITC) and tetramethylrhodamine isocyanate (TRITC) fluorescence were detected using the 488-nm and 561-nm laser lines of a Sapphire driver unit (Coherent), respectively, and DAPI fluorescence was detected using the 405-nm laser line of a Cube laser system (Coherent). The image data were analyzed using NIS Elements microscope imaging software (Nikon).

Cell apoptosis assay

HEK293T and PK-15 cells were seeded in 6 well plates and incubated for 12 hours. After incubation, for 12 hours, cells were transfected with indicated plasmids. 12 hours after transfection, cells were removed and seeded in 96 well plates. Cell apoptosis and proliferation were measured in given time points using RealTime-Glo™ Annexin V Apoptosis and Necrosis Assay (Promega, JA1000), CellTiter 96® Non-Radioactive Cell Proliferation Assay-MTT (Promega, G4000), and Cell Counting Kit-8 (Dojindo Molecular Technologies) according to manufacturer's instructions.

RNA interference

For RNF125 knockdown, we transfected HEK293T cells with 50 nM of RNF125-specific siRNA oligos or non-targeting control siRNA (Bioneer, Korea) using Lipofectamine 2000 (Invitrogen) for 48 h. The sequence targeting human RNF125 was: 5'-CCGUGUGCCUUGAGGUGUU-3'.

Statistical analysis

Data are presented as the means and standard deviations (SD) and represent at least two independent experiments. Statistical analysis was performed with Student's t-test in GraphPad Prism 6 software. P values are indicated in the legends. *P < 0.05, **P < 0.01, ***P < 0.001, ****P < 0.0001.

Data availability statement

The original contributions presented in the study are included in the article/Supplementary Material. Further inquiries can be directed to the corresponding authors.

Author contributions

AW and MBU performed most of the experiments. J-HC, PP, SS, and KC helped with the experiments and contributed to the discussions. AW, MBU, J-HP, and J-SL designed the study. AW, MBU, and J-SL wrote the manuscript. J-HP and J-SL supervised the study. All the authors helped with data analysis. All authors contributed to the article and approved the submitted version.

Funding

This work was supported by the National Research Foundation (Grant No. 2018M3A9H4079660, 2019R1A2C2008283, 2021R1A6A1A03045495) and Korea Research Institute of Bioscience and Biotechnology Research Initiative Program (KGM9942011), Republic of Korea.

Conflict of interest

The authors declare that the research was conducted in the absence of any commercial or financial relationships that could be construed as a potential conflict of interest.

Publisher's note

Supplementary material

The Supplementary Material for this article can be found online at: https://www.frontiersin.org/articles/10.3389/fimmu.2022.1020262/full#supplementary-material

References

1. Rehwinkel J, Gack MU. Rig-I-Like receptors: Their regulation and roles in rna sensing. *Nat Rev Immunol* (2020) 20(9):537–51. doi: 10.1038/s41577-020-0288-3

2. Takeuchi O, Akira S. Pattern recognition receptors and inflammation. *Cell* (2010) 140(6):805–20. doi: 10.1016/j.cell.2010.01.022

3. Kawai T, Akira S. Innate immune recognition of viral infection. *Nat Immunol* (2006) 7(2):131–7. doi: 10.1038/ni1303

4. Fitzgerald KA, Kagan JC. Toll-like receptors and the control of immunity. *Cell* (2020) 180(6):1044–66. doi: 10.1016/j.cell.2020.02.041

5. Liu Y, Olagnier D, Lin R. Host and viral modulation of rig-I-Mediated antiviral immunity. *Front Immunol* (2017) 7:662. doi: 10.3389/fimmu.2016.00662

6. Luo L, Lucas RM, Liu L, Stow JL. Signalling, sorting and scaffolding adaptors for toll-like receptors. *J Cell Sci* (2020) 133(5):jcs239194. doi: 10.1242/jcs.239194

7. Schulz KS, Mossman KL. Viral evasion strategies in type I ifn signaling–a summary of recent developments. *Front Immunol* (2016) 7:498. doi: 10.3389/fimmu.2016.00498

8. Wang Y, Ma L, Stipkovits L, Szathmary S, Li X, Liu Y. The strategy of picornavirus evading host antiviral responses: Non-structural proteins suppress the production of ifns. *Front Microbiol* (2018) 9:2943. doi: 10.3389/fmicb.2018.02943

9. Yang W, Li D, Ru Y, Bai J, Ren J, Zhang J, et al. Foot-and-Mouth disease virus 3a protein causes upregulation of autophagy-related protein Lrrc25 to inhibit the G3bp1-mediated rig-like helicase-signaling pathway. *J Virol* (2020) 94(8):e02086–19. doi: 10.1128/JVI.02086-19

10. Matsuda A, Suzuki Y, Honda G, Muramatsu S, Matsuzaki O, Nagano Y, et al. Large-Scale identification and characterization of human genes that activate nf-kappab and mapk signaling pathways. *Oncogene* (2003) 22(21):3307–18. doi: 10.1038/sj.onc.1206406

11. Kawai T, Takahashi K, Sato S, Coban C, Kumar H, Kato H, et al. Ips-1, an adaptor triggering rig-i- and Mda5-mediated type I interferon induction. *Nat Immunol* (2005) 6(10):981–8. doi: 10.1038/ni1243

12. Meylan E, Curran J, Hofmann K, Moradpour D, Binder M, Bartenschlager R, et al. Cardif is an adaptor protein in the rig-I antiviral pathway and is targeted by hepatitis c virus. *Nature* (2005) 437(7062):1167–72. doi: 10.1038/nature04193

13. Seth RB, Sun L, Ea CK, Chen ZJ. Identification and characterization of mavs, a mitochondrial antiviral signaling protein that activates nf-kappab and irf 3. *Cell* (2005) 122(5):669–82. doi: 10.1016/j.cell.2005.08.012

14. Cui S, Eisenächer K, Kirchhofer A, Brzózka K, Lammens A, Lammens K, et al. The c-terminal regulatory domain is the rna 5′-triphosphate sensor of rig-I. *Mol Cell* (2008) 29(2):169–79. doi: 10.1016/j.molcel.2007.10.032

15. Wan Q, Yang C, Rao Y, Liao Z, Su J. Mda5 induces a stronger interferon response than rig-I to gcrv infection through a mechanism involving the phosphorylation and dimerization of Irf3 and Irf7 in cik cells. *Front Immunol* (2017) 8:189. doi: 10.3389/fimmu.2017.00189

16. Lee H-C, Chathuranga K, Lee J-S. Intracellular sensing of viral genomes and viral evasion. *Exp Mol Med* (2019) 51(12):1–13. doi: 10.1038/s12276-019-0299-y

17. Chan YK, Gack MU. Viral evasion of intracellular DNA and rna sensing. *Nat Rev Microbiol* (2016) 14(6):360–73. doi: 10.1038/nrmicro.2016.45

18. Kovacsovics M, Martinon F, Micheau O, Bodmer J-L, Hofmann K, Tschopp J. Overexpression of helicard, a card-containing helicase cleaved during apoptosis, accelerates DNA degradation. *Curr Biol* (2002) 12(10):838–43. doi: 10.1016/S0960-9822(02)00842-4

19. Mason PW, Grubman MJ, Baxt B. Molecular basis of pathogenesis of fmdv. *Virus Res* (2003) 91(1):9–32. doi: 10.1016/S0168-1702(02)00257-5

20. Knight-Jones TJ, Robinson L, Charleston B, Rodriguez L, Gay C, Sumption KJ, et al. Global foot-and-Mouth disease research update and gap analysis: 4-diagnostics. *Transboundary Emerg Dis* (2016) 63:42–8. doi: 10.1111/tbed.12523

21. Belsham G. Distinctive features of fmdv, a member of the picorna virus family, aspects of virus protein synthesis, protein processing and structure. *Prog Biophysics Mol Biol* (1993) 60:241–60. doi: 10.1016/0079-6107(93)90016-D

22. Li C, Zhu Z, Du X, Cao W, Yang F, Zhang X, et al. Foot-and-Mouth disease virus induces lysosomal degradation of host protein kinase pkr by 3c proteinase to facilitate virus replication. *Virology* (2017) 509:222–31. doi: 10.1016/j.virol.2017.06.023

23. Zhu Z, Wang G, Yang F, Cao W, Mao R, Du X, et al. Foot-and-Mouth disease virus viroporin 2b antagonizes rig-I-Mediated antiviral effects by inhibition of its protein expression. *J Virol* (2016) 90(24):11106–21. doi: 10.1128/JVI.01310-16

24. Moffat K, Howell G, Knox C, Belsham GJ, Monaghan P, Ryan MD, et al. Effects of foot-and-Mouth disease virus nonstructural proteins on the structure and function of the early secretory pathway: 2bc but not 3a blocks endoplasmic reticulum-to-Golgi transport. *J Virol* (2005) 79(7):4382–95. doi: 10.1128/JVI.79.7.4382-4395.2005

25. Moffat K, Knox C, Howell G, Clark SJ, Yang H, Belsham GJ, et al. Inhibition of the secretory pathway by foot-and-Mouth disease virus 2bc protein is reproduced by coexpression of 2b with 2c, and the site of inhibition is determined by the subcellular location of 2c. *J Virol* (2007) 81(3):1129–39. doi: 10.1128/JVI.00393-06

26. Ao D, Guo H-C, Sun S-Q, Sun D-H, Fung TS, Wei Y-Q, et al. Viroporin activity of the foot-and-Mouth disease virus non-structural 2b protein. *PloS One* (2015) 10(5):e0125828. doi: 10.1371/journal.pone.0125828

27. Li M, Xin T, Gao X, Wu J, Wang X, Fang L, et al. Foot-and-Mouth disease virus non-structural protein 2b negatively regulates the rlr-mediated ifn-β induction. *Biochem Biophys Res Commun* (2018) 504(1):238–44. doi: 10.1016/j.bbrc.2018.08.161

28. Doedens JR, Kirkegaard K. Inhibition of cellular protein secretion by poliovirus proteins 2b and 3a. *EMBO J* (1995) 14(5):894–907. doi: 10.1002/j.1460-2075.1995.tb07071.x

29. van Kuppeveld FJ, Hoenderop JG, Smeets RL, Willems PH, Dijkman HB, Galama JM, et al. Coxsackievirus protein 2b modifies endoplasmic reticulum membrane and plasma membrane permeability and facilitates virus release. *EMBO J* (1997) 16(12):3519–32. doi: 10.1093/emboj/16.12.3519

30. Zhu Z, Li C, Du X, Wang G, Cao W, Yang F, et al. Foot-and-Mouth disease virus infection inhibits Lgp2 protein expression to exaggerate inflammatory response and promote viral replication. *Cell Death Dis* (2017) 8(4):e2747–e. doi: 10.1038/cddis.2017.170

31. Yu Y, Wang SE, Hayward GS. The kshv immediate-early transcription factor rta encodes ubiquitin E3 ligase activity that targets Irf7 for proteosome-mediated degradation. *Immunity* (2005) 22(1):59–70. doi: 10.1016/j.immuni.2004.11.011

32. Huibregtse JM, Scheffner M, Howley PM. A cellular protein mediates association of P53 with the E6 oncoprotein of human papillomavirus types 16 or 18. *EMBO J* (1991) 10(13):4129–35. doi: 10.1002/j.1460-2075.1991.tb04990.x

33. Scheffner M, Huibregtse JM, Vierstra RD, Howley PM. The hpv-16 E6 and E6-ap complex functions as a ubiquitin-protein ligase in the ubiquitination of P53. *Cell* (1993) 75(3):495–505. doi: 10.1016/0092-8674(93)90384-3

34. Scheffner M, Werness BA, Huibregtse JM, Levine AJ, Howley PM. The E6 oncoprotein encoded by human papillomavirus types 16 and 18 promotes the degradation of P53. *cell* (1990) 63(6):1129–36. doi: 10.1016/0092-8674(90)90409-8

35. Arimoto K-i, Takahashi H, Hishiki T, Konishi H, Fujita T, Shimotohno K. Negative regulation of the rig-I signaling by the ubiquitin ligase Rnf125. *Proc Natl Acad Sci* (2007) 104(18):7500–5. doi: 10.1073/pnas.0611551104

36. Hüsser L, Alves MP, Ruggli N, Summerfield A. Identification of the role of rig-I, mda-5 and Tlr3 in sensing rna viruses in porcine epithelial cells using lentivirus-driven rna interference. *Virus Res* (2011) 159(1):9–16. doi: 10.1016/j.virusres.2011.04.005

37. Sun D, Wen X, Wang M, Mao S, Cheng A, Yang X, et al. Apoptosis and autophagy in picornavirus infection. *Front Microbiol* (2019) 10:2032. doi: 10.3389/fmicb.2019.02032

38. Gonzalez ME, Carrasco L. Viroporins. *FEBS Lett* (2003) 552(1):28–34. doi: 10.1016/s0014-5793(03)00780-4

39. Madan V, Castelló A, Carrasco L. Viroporins from rna viruses induce caspase-dependent apoptosis. *Cell Microbiol* (2008) 10(2):437–51. doi: 10.1111/j.1462-5822.2007.01057.x

40. Medina GN, Segundo FD-S, Stenfeldt C, Arzt J, de Los Santos T. The different tactics of foot-and-Mouth disease virus to evade innate immunity. *Front Microbiol* (2018) 9:2644. doi: 10.3389/fmicb.2018.02644

41. Kirchweger R, Ziegler E, Lamphear BJ, Waters D, Liebig HD, Sommergruber W, et al. Foot-and-Mouth disease virus leader proteinase: Purification of the lb form and determination of its cleavage site on eif-4 gamma. *J Virol* (1994) 68(9):5677–84. doi: 10.1128/jvi.68.9.5677-5684.1994

42. de Los Santos T, Diaz-San Segundo F, Grubman MJ. Degradation of nuclear factor kappa b during foot-and-Mouth disease virus infection. *J Virol* (2007) 81(23):12803–15. doi: 10.1128/jvi.01467-07

43. Zhu J, Weiss M, Grubman MJ, de los Santos T. Differential gene expression in bovine cells infected with wild type and leaderless foot-and-Mouth disease virus. *Virology* (2010) 404(1):32–40. doi: 10.1016/j.virol.2010.04.021

44. Rodríguez Pulido M, Sánchez-Aparicio MT, Martínez-Salas E, García-Sastre A, Sobrino F, Sáiz M. Innate immune sensor Lgp2 is cleaved by the leader protease of foot-and-Mouth disease virus. *PloS Pathog* (2018) 14(6):e1007135. doi: 10.1371/journal.ppat.1007135

45. Wang D, Fang L, Li P, Sun L, Fan J, Zhang Q, et al. The leader proteinase of foot-and-Mouth disease virus negatively regulates the type I interferon pathway by acting as a viral deubiquitinase. *J Virol* (2011) 85(8):3758–66. doi: 10.1128/jvi.02589-10

46. Wang D, Fang L, Li K, Zhong H, Fan J, Ouyang C, et al. Foot-and-Mouth disease virus 3c protease cleaves nemo to impair innate immune signaling. *J Virol* (2012) 86 (17):9311–22. doi: 10.1128/jvi.00722-12

47. Lawrence P, Schafer EA, Rieder E. The nuclear protein Sam68 is cleaved by the fmdv 3c protease redistributing Sam68 to the cytoplasm during fmdv infection of host cells. *Virology* (2012) 425(1):40–52. doi: 10.1016/j.virol.2011.12.019

48. Ye X, Pan T, Wang D, Fang L, Ma J, Zhu X, et al. Corrigendum: Foot-and-Mouth disease virus counteracts on internal ribosome entry site suppression by G3bp1 and inhibits G3bp1-mediated stress granule assembly *via* post-translational mechanisms. *Front Immunol* (2021) 12:702530. doi: 10.3389/fimmu.2021.702530

49. Du Y, Bi J, Liu J, Liu X, Wu X, Jiang P, et al. 3cpro of foot-and-Mouth disease virus antagonizes the interferon signaling pathway by blocking Stat1/Stat2 nuclear translocation. *J Virol* (2014) 88(9):4908–20. doi: 10.1128/jvi.03668-13

50. Ekanayaka P, Shin SH, Weeratunga P, Lee H, Kim T-H, Chathuranga K, et al. Foot-and-Mouth disease virus 3c protease antagonizes interferon signaling and C142t substitution attenuates the fmd virus. *Front Microbiol* (2021) 12. doi: 10.3389/fmicb.2021.737031

51. Gladue DP, O'Donnell V, Baker-Branstetter R, Holinka LG, Pacheco JM, Fernandez-Sainz I, et al. Foot-and-Mouth disease virus nonstructural protein 2c interacts with Beclin1, modulating virus replication. *J Virol* (2012) 86(22):12080–90. doi: 10.1128/jvi.01610-12

52. Li D, Lei C, Xu Z, Yang F, Liu H, Zhu Z, et al. Foot-and-Mouth disease virus non-structural protein 3a inhibits the interferon-β signaling pathway. *Sci Rep* (2016) 6:21888. doi: 10.1038/srep21888

53. Fu SZ, Yang WP, Ru Y, Zhang KS, Wang Y, Liu XT, et al. Ddx56 cooperates with fmdv 3a to enhance fmdv replication by inhibiting the phosphorylation of Irf3. *Cell Signal* (2019) 64:109393. doi: 10.1016/j.cellsig.2019.109393

54. Li D, Wei J, Yang F, Liu HN, Zhu ZX, Cao WJ, et al. Foot-and-Mouth disease virus structural protein Vp3 degrades janus kinase 1 to inhibit ifn-Γ signal transduction pathways. *Cell Cycle (Georgetown Tex)* (2016) 15(6):850–60. doi: 10.1080/15384101.2016.1151584

55. Li D, Yang W, Yang F, Liu H, Zhu Z, Lian K, et al. The Vp3 structural protein of foot-and-Mouth disease virus inhibits the ifn-β signaling pathway. *FASEB J Off Publ Fed Am Societies Exp Biol* (2016) 30(5):1757–66. doi: 10.1096/fj.15-281410

56. Ekanayaka P, Lee BH, Weerawardhana A, Chathuranga K, Park JH, Lee JS. Inhibition of mavs aggregation-mediated type-I interferon signaling by foot-and-Mouth disease virus Vp3. *Viruses* (2021) 13(9):1776. doi: 10.3390/v13091776

57. Li X, Wang J, Liu J, Li Z, Wang Y, Xue Y, et al. Engagement of soluble resistance-related calcium binding protein (Sorcin) with foot-and-Mouth disease virus (Fmdv) Vp1 inhibits type I interferon response in cells. *Veterinary Microbiol* (2013) 166(1-2):35–46. doi: 10.1016/j.vetmic.2013.04.028

58. Ekanayaka P, Lee SY, Herath TUB, Kim JH, Kim TH, Lee H, et al. Foot-and-Mouth disease virus Vp1 target the mavs to inhibit type-I interferon signaling and Vp1 E83k mutation results in virus attenuation. *PloS Pathog* (2020) 16(11): e1009057. doi: 10.1371/journal.ppat.1009057

59. Zhi X, Zhang Y, Sun S, Zhang Z, Dong H, Luo X, et al. Nlrp3 inflammasome activation by foot-and-Mouth disease virus infection mainly induced by viral rna and non-structural protein 2b. *RNA Biol* (2020) 17(3):335–49. doi: 10.1080/15476286.2019.1700058

60. Xu C, Sun L, Liu W, Duan Z. Latent membrane protein 1 of Epstein–Barr virus promotes rig-I degradation mediated by proteasome pathway. *Front Immunol* (2018) 9:1446. doi: 10.3389/fimmu.2018.01446

61. Park Y-J, Oanh NTK, Heo J, Kim S-G, Lee H-S, Lee H, et al. Dual targeting of rig-I and mavs by March5 mitochondria ubiquitin ligase in innate immunity. *Cell Signalling* (2020) 67:109520. doi: 10.1016/j.cellsig.2019.109520

62. Wang W, Jiang M, Liu S, Zhang S, Liu W, Ma Y, et al. Rnf122 suppresses antiviral type I interferon production by targeting rig-I cards to mediate rig-I degradation. *Proc Natl Acad Sci* (2016) 113(34):9581–6. doi: 10.1073/pnas.1604277113

63. Zhao K, Zhang Q, Li X, Zhao D, Liu Y, Shen Q, et al. Cytoplasmic Stat4 promotes antiviral type I ifn production by blocking chip-mediated degradation of rig-I. *J Immunol* (2016) 196(3):1209–17. doi: 10.4049/jimmunol.1501224

64. Barral PM, Morrison JM, Drahos J, Gupta P, Sarkar D, Fisher PB, et al. Mda-5 is cleaved in poliovirus-infected cells. *J Virol* (2007) 81(8):3677–84. doi: 10.1128/JVI.01360-06

65. Reed LJ, Muench H. A simple method of estimating fifty per cent endpoints. *Am J Epidemiol* (1938) 27(3):493–7. doi: 10.1093/oxfordjournals.aje.a118408

frontiers | Frontiers in Immunology

TYPE Review
PUBLISHED 30 November 2022
DOI 10.3389/fimmu.2022.1088690

OPEN ACCESS

EDITED BY
Junji Xing,
Houston Methodist Research Institute,
United States

REVIEWED BY
Yuexiu Zhang,
The Ohio State University,
United States
Xiaochuan Liu,
University of California, Riverside,
United States

*CORRESPONDENCE
Mingshu Wang
mshwang@163.com

†These authors have contributed equally to this work

SPECIALTY SECTION
This article was submitted to Viral Immunology, a section of the journal Frontiers in Immunology

RECEIVED 03 November 2022
ACCEPTED 15 November 2022
PUBLISHED 30 November 2022

CITATION
Zhou L, Cheng A, Wang M, Wu Y, Yang Q, Tian B, Ou X, Sun D, Zhang S, Mao S, Zhao X-X, Huang J, Gao Q, Zhu D, Jia R, Liu M and Chen S (2022) Mechanism of herpesvirus protein kinase UL13 in immune escape and viral replication. *Front. Immunol.* 13:1088690. doi: 10.3389/fimmu.2022.1088690

Mechanism of herpesvirus protein kinase UL13 in immune escape and viral replication

Lin Zhou[1,2,3†], Anchun Cheng[1,2,3†], Mingshu Wang[1,2,3*], Ying Wu[1,2,3], Qiao Yang[1,3], Bin Tian[1,2,3], Xumin Ou[1,2,3], Di Sun[1,2,3], Shaqiu Zhang[1,2,3], Sai Mao[1,2,3], Xin-Xin Zhao[1,2,3], Juan Huang[1,2,3], Qun Gao[1,2,3], Dekang Zhu[2,3], Renyong Jia[1,2,3], Mafeng Liu[1,2,3] and Shun Chen[1,2,3]

[1]Institute of Preventive Veterinary Medicine, Sichuan Agricultural University, Chengdu, Sichuan, China, [2]Key Laboratory of Animal Disease and Human Health of Sichuan Province, Sichuan Agricultural University, Chengdu, Sichuan, China, [3]Avian Disease Research Center, College of Veterinary Medicine, Sichuan Agricultural University, Chengdu, Sichuan, China

Upon infection, the herpes viruses create a cellular environment suitable for survival, but innate immunity plays a vital role in cellular resistance to viral infection. The UL13 protein of herpesviruses is conserved among all herpesviruses and is a serine/threonine protein kinase, which plays a vital role in escaping innate immunity and promoting viral replication. On the one hand, it can target various immune signaling pathways *in vivo*, such as the cGAS-STING pathway and the NF-κB pathway. On the other hand, it phosphorylates regulatory many cellular and viral proteins for promoting the lytic cycle. This paper reviews the research progress of the conserved herpesvirus protein kinase UL13 in immune escape and viral replication to provide a basis for elucidating the pathogenic mechanism of herpesviruses, as well as providing insights into the potential means of immune escape and viral replication of other herpesviruses that have not yet resolved the function of it.

KEYWORDS

UL13, serine/threonine protein kinase, immune escape, viral replication, cGAS-STING, NF-κB

Introduction

Herpes virus is a virus of double-stranded DNA that can be divided into three subfamilies: α-, β-, and γ-herpesvirus. For instance, Herpes simplex virus type 1/2 (HSV1/2), Varicella-zoster virus (VZV), Pseudorabies virus (PRV), Epstein-Barr virus (EBV), Human cytomegalovirus (HCMV), Kaposi's sarcoma-associated herpesvirus (KSHV), Murine gamma-herpesvirus 68(MHV-68), Marek's disease virus (MDV) and Duck plague virus (DPV) (1–3). Herpes virus infections severely impact the health of

humans and animals. The host's innate immune system is the first line of defense against invading pathogens, it relies on the mutual recognition of various pathogen recognition receptors (PRR) and pathogen-associated molecular patterns (PAMP) on the surface of the pathogenic organism. The interaction between PRR and PAMP on the surface of pathogenic organisms induces the production of Type I interferon (IFN-I) and other antiviral factors, promoting cellular antiviral immunity and activating the corresponding immune system (4). cyclic GMP-AMP synthase (cGAS) is a nucleotidyltransferase, as a member of the PRR family, which is activated by binding viral double-stranded DNA to induce the production of IFN-ß (5, 6). The nuclear factor kappa-B (NF-κB) regulates the production of inflammatory and immune responses to protect the host from pathogens (7, 8). Similarly, the JAK-STAT signaling pathway, the PKR-eIF2α signaling pathway, the Sterile alpha motif and HD domain-containing protein 1 (SAMHD1), and the CD8+ T cell play a critical role in antiviral response.

The HSV pUL13 and its homologs (e.g., EBV pBGLF4, HCMV pUL97, KSHV pORF36, MHV-68 pORF36, and VZV pORF47) are serine/threonine protein kinase belonging to the conserved herpesvirus protein kinase family (CHPK), which is a tegument protein of herpes virions (9–11). Their catalytic core consists of 12 conserved subdomains (12–15) (Table 1), which can catalyze the transfer of the γ-phosphate of a nucleoside triphosphate to amino acid residues of protein substrates to affect their function. CHPK from different herpesvirus subfamilies has considerable amino acid variation, and there is no consensus phosphorylation sequence for all CHPKs (16–18). Moreover, the herpesvirus protein kinases have very low homology with known cell kinases.

With the continuous discovery of UL13 protein kinase substrates (Table 2), pUL13 has been shown to play an important role in the physiological activity of the herpes virus. For example, VZV pORF47 and KSHV pORF36 are essential for virus proliferation in T and B cells (19–21); PRV pUL13 affects IFN- β by inhibiting zinc finger CCHC-type containing protein 3 (ZCCHC3) expression (22); EBV pBGLF4 is a regulator of the EBV immune genes BCRF1 and BPLF1 (23). Moreover, HSV-2 pUL13 Ser18 was significantly crucial for the HSV-2 capacity of replication and cell-to-cell spread in U2OS cells (24); the deletion of pUL13 reduced the size and number of Viral plaques of DPV (25); CHPK of β and γ herpes viruses promotes DNA virus replication by mimicking cyclin-dependent kinases1/2 (CDK1/2) phosphorylation of cyclin (26, 27). These suggest that pUL13 plays an essential role in immune escape and viral replication of herpes viruses.

The role of pUL13 in viral evasion of innate immunity

Inhibition of the cGAS/STING pathway

The type I interferon pathway is a significant component of innate immunity and plays an essential role in the control and clearance of pathogens. Upon infection, inhibition of interferon regulatory factor 3 (IRF3) by viral infection is a critical link for the termination of the type I interferon pathway. Here, IRF3 is an essential target for pUL13 action during herpes virus infection because many studies have shown that they can phosphorylate IRF3 and inhibit IRF3 dimerization, binding to the positive regulatory domains III-I (PRDIII-I), and interaction with the CREB-binding protein and P300 protein (CBP/P300) (28–32). Meanwhile, Lin Lv et al. showed that PRV UL13 relies on its kinase active sites of Lys49 and Lys387 to target IRF3 and promote its ubiquitination for degradation by the proteasome (33) (Figure 1).

TABLE 1 The Protein kinase catalytic subdomain.

Conserved subdomain	Conserved amino acid	Function
I	Gly-X-Gly-X-X-GLy-X-Va1	Anchor the ATP
II	Lys	proton transfer
III	Glu	Stabilizing the interaction between the functional subdomain II Lys and the α and β phosphate groups of ATP
IV	/	/
V	/	/
VIA	/	Supporting action
VIB	Asp,Asn	Asn interacts with Asp to stabilize ATP and bind Mg2+ to form a salt bridge
VII	Asp, Gly	Orientation of ATP
VIII	Ala,Pro,Glu	Identification of substrate
IX	Asp, Gly	Hydrogen-bonded with Arg of subdomain VIB to stabilize the catalytic ring.
X	/	/
XI	Arg	Stabilization

There are no conserved amino acids among the subdomains IV, V, VIA and X. "/" indicates that there is no Conserved amino acid site in "conserved amino acid" and that the Function is not clear in "function".

10.3389/fimmu.2022.1088690

TABLE 2 The substrates of herpes virus UL13 protein kinase.

Protein	Substrates	
	Cellular proteins	Viral proteins
UL13	STING	BRMF1/4
	IRF-3	EBNA-LP
	PRDX1	PP65
	UXT	U69
	SAMDH1	UL41
	PKR	UL44
	Rb	UL49
	CKIIβ	ICP22
	EF-1δ	ICP0
	H2AX	gE/gI
	H2B	US3
	LaminA/C	IE62/IE63
	RNA pol II	VP13/14
	AKT	K-bZIP
	JNK	BZLF1
	p60	EBNA2
	HADC1/2	EA-D
	Tip60	ORF9
	LANA	ORF36

UL13: represents the conserved herpesvirus protein kinase of all herpesviruses, such as EBV BGLF4 and KSHV ORF36.
pUL13, dependent or independent of its kinase activity, regulates Cellular and Viral proteins that affect innate immunity and the cell cycle to promote viral replication.

In addition, pUL13 promotes the ubiquitinated degradation of immunomodulatory proteins as a necessary action affecting innate immunity. For example, PRV pUL13 recruits the E3 ligase RING-finger protein 5 (RNF5) to degrade the stimulator of interferon genes protein (STING) indirectly and also participates in ubiquitination degradation of the host protein peroxidase 1 (PRDX1) to inhibit innate immunity (34, 35) (Figure 1). Tripartite motif (TRIM) proteins play a critical role in the antiviral host response. Based on E3 ubiquitin ligases RNF5, TRIM29 and TRIM30α are responsible for the ubiquitination degradation of STING protein; TRIM18 recruit protein phosphatase 1A (PPM1A) to dephosphorylate TANK binding kinase 1 (TBK1) to suppress the innate immune response (36, 37). We believe that the TRIM family members (such as TRIM29 and TRIM18) may be essential partners of herpesvirus pUL13 in promoting the ubiquitination degradation of host immune proteins. However, there are no reports about the interaction between TRIM family members and pUL13.

Inhibition of NF-κB pathway

After virus infection, NF-κB is activated and translocated into the nucleus, which induces an inflammatory and immune response to protect the host from the pathogen (38, 39). As a vital component of the immune system, which can be regulated by the ubiquitously expressed transcript (UXT). In 2012, Chang et al. found that EBV pBGLF4 phosphorylated UXT at the Thr3, weakening interaction with p65 to inhibit NF-κB activity (40) (Figure 1). Not only did it reveal the role of the conserved herpesvirus protein kinases in evading immune clearance by NF-κB, but it also revealed its essential for promoting the lytic cycle.

Furthermore, short interspersed elements (SINEs) are non-coding retrotransposons transcribed by RNA polymerase III (RNA Pol III), which activate antiviral NF-κB signaling through a mitochondrial antiviral signaling protein (MAVS)-dependent and independent mechanism pathways (41). However, MHV-68 infection can sustainably induce transcription of SINE ncRNA, which is explained by Xiaonan Dong et al.: Inducing phosphorylation degradation of the RelA/p65 subunit of NF-κB in the pre-MHV-68 infection period to blunt the NF-κB transcription response, it is associated with IKKβ kinase (42). In 2020, Aaron M Schaller et al. reported that CHPKs-mediated chromatin modification changes contribute to activating B2 SINEs during MHV68 infection; hijacking uses B2 SINE RNA signal to activate IKKβ kinase and phosphorylates transcription initiation factor Rta to promote viral replication (43) (Figure 1). Much more interesting is that the activated SINE ncRNA can directly interact with RNA pol II to participate in the transcriptional suppression of genes (44, 45). By and large, the B2 SINEs seem to do more harm than good for viral replication. Nevertheless, the herpes virus pUL13 chose it, demonstrating that B2 SINEs have many potential mechanisms to be developed in the life cycle of herpes viruses.

Inhibition of the JAK/STAT signaling pathway

JAK/STAT acts as an inflammatory signaling pathway for stress and has immunomodulatory effects, receiving multiple cytokine signals from cells, such as IFN-α and IFN-γ (46, 47). In 2017, Yuka Sato et al. reported that pUL13 could phosphorylate the associated constitutive transcription factor SP1 (SP1) to induce suppressor of cytokine signaling 3(SOCS3) production, which regulates the JAK/STAT signaling pathway negatively (48) (Figure 2). That is SP1 can combine with GC-rich regions of the SOCS3 promoter to facilitate transcription and translation of SOCS3 (49, 50), and then curb the JAK/STAT signal pathway (51–53). Moreover, the phosphorylation of Sp1 by pUL13 could specifically induce the transcription of the immediate-early and early genes expression of the herpes virus (54–57), which reveals the importance of pUL13 for transcriptional regulation of herpesvirus genes.

SOCS3 plays a significant role in modulating the outcome of infections and autoimmune diseases. And many viruses, such as HSV- 1, EBV, and VZV (58–61), can activate the expression of SOCS3 because of the close relationship between SOCS3 and

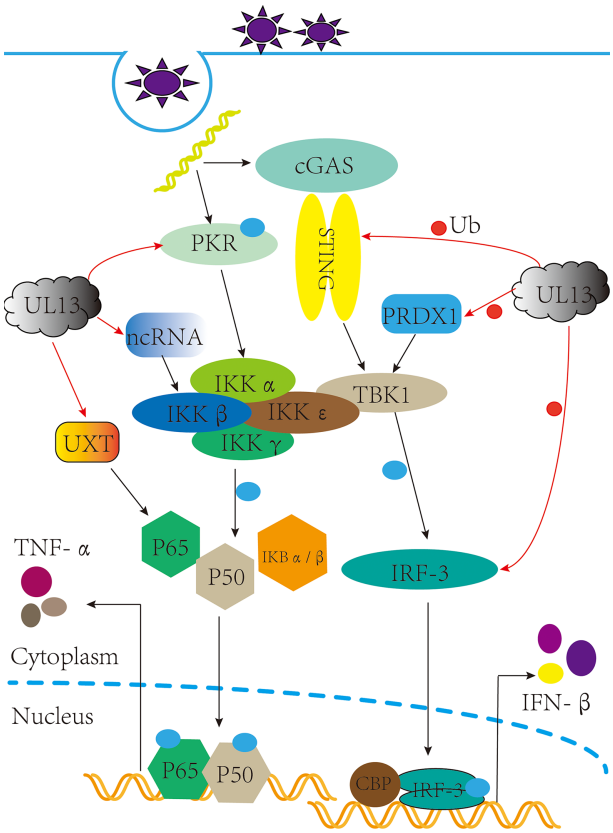

FIGURE 1
pUL13 inhibits the cGAS-STING signaling pathway and the NF-κB signaling pathway. pUL13 can inhibit the dimerization, nuclear translocation, CBP binding, and binding to IFN-β promoter elements of interferon regulatory factor 3 (IRF3); meanwhile, it can ubiquitinally degrade stimulator of interferon genes (STING), IRF-3, and peroxidase 1 (PRDX1) to inhibit the production of IFN-β. pUL13 indirectly inhibits the NF-κB pathway by regulating ubiquitously expressed transcript (UXT), Protein kinase R (PKR), and B2 SINE ncRNA.

JAK kinase with STAT signaling factors (62–65). It was suggested that SOCS3 is induced that not only inhibits the antiviral response of the JAK-STAT signal pathway but also maintains immune homeostasis in the body under pathological conditions and physiological conditions (66), such as the expression of SOCS3 inhibits several NF-κB-regulated proapoptotic pathways to protect β-cells from IL- 1 β-mediated apoptosis (67). Perhaps this is more important for the production of SOCS3 induced by pUL13 during herpesvirus infection.

Effect on PKR-eIF2α-mediated antiviral effects

Protein kinase R (PKR) in host cells exerts antiviral effects by inhibiting viral mRNA translation and inducing apoptosis. Many data indicate PKR promotes NF-κB activation (68–73), promotes mRNA stability of IFN-β (74), and is involved in the tumor suppressor function of p53 protein (75–77). When dsRNA binds to the Conserved double-stranded RNA binding motif (dsRBMs) of PKR, it is activated by autophosphorylation at Thr446 (78). Next, it phosphorylates Ser 51 of eukaryotic initiation factor 2α (eIF2α) and inhibits the translation initiation activity of mRNAs which encode antiviral factors and mediate stress responses (79, 80). In the PKR-eIF2a pathway, PKR inhibition and eIF2a dephosphorylation must be used to achieve massive replication of the virus, so the virus has evolved a variety of strategies in regulating the PKR-eIF2a pathway: controlling dsRNA masking and degradation (81–84), PKR degradation (85), inhibiting PKR dimerization and autophosphorylation (86–89), dephosphorylation of eIF2α (90–92), and PKR desensitization (93, 94). In 2020, Rosamaria Pennisi et al. demonstrated that HSV-1 pUL13 inhibits the phosphorylation of cellular PKR. Although the specific pathway by which pUL13 inhibits PKR phosphorylation cannot be demonstrated (95) (Figure 2). These suggest that pUL13 inhibition of PKR can not only evade innate immunity and prevent PKR-mediated apoptosis but also use eIF2α to promote viral mRNA translation.

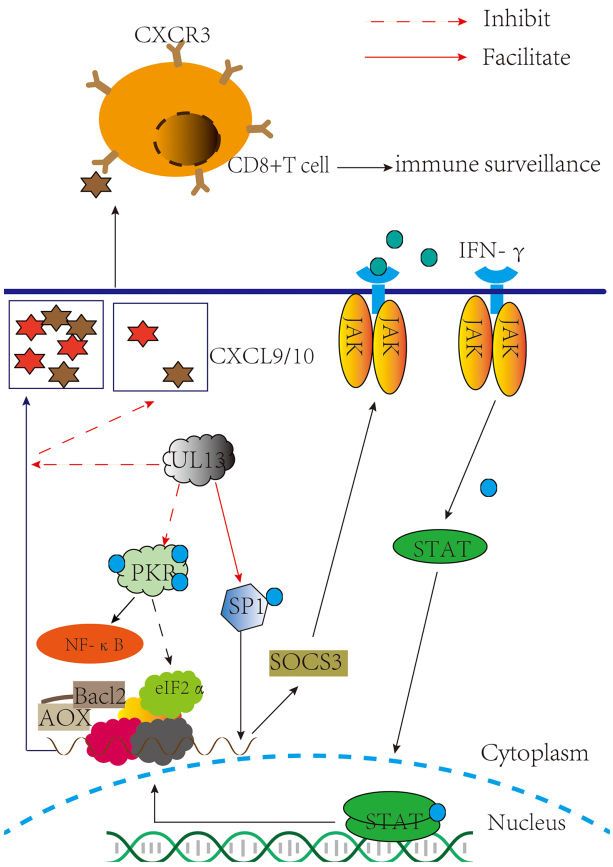

FIGURE 2
pUL13 inhibits PKR, CD8+ T cells, and the JAK-STAT signaling pathway to evade innate immunity. pUL13 inhibits PKR phosphorylation to evade innate immunity and promotes viral protein translation with eukaryotic initiation factor 2α (eIF2α); pUL13 phosphorylates the associated constitutive transcription factor SP1 (SP1), which induces suppressor of cytokine signaling 3 (SOCS3) expression to inhibit the JAK-STAT signaling pathway; and pUL13 can down-regulate the C-X-C motif chemokine ligand 9 (CXCL9) signaling molecules to prevent cd8+ T cell molecules from clustering at the site of infection.

Especially, PKR is one of four kinases that integrate stress responses. It regulates the protein homeostasis of the cell to maintain the body's homeostasis; conversely, its abnormal activation can cause severe damage to the body, such as systemic lupus erythematosus (96, 97). Based on these results, whether the molecular mechanism of pUL13 inhibition of PKR can inspire treating diseases associated with abnormal activation of PKR remains to be further studied.

Effect on CD8+ T cells mediated antiviral effects

Compared with pICP47 and pUS3 recognizing the main histocompatibility complex (MHC I) that are distributed on the cell surface and presentation of antigen peptides to T cells to exert cellular immune clearance regulation, the effect of pUL13 on it is not apparent (98–101). However, HSV- 1 pUL13 triggered viral encephalitis in mice by downregulating CXCL-9 and inhibiting the infiltration of CD8+ T cell molecules at the site of infection (102) (Figure 2). The author also points out that the HSV-1 pUL13- mediated immune evasion mechanism might be specific to the CNS. Maybe it associated with CXCL-9/10 and CD8+ T cells inhibiting the reactivation of HSV within nerve cells, further suggesting the role of pUL13 in the latent reactivation of the herpes virus (103–106). Although the molecular mechanisms underlying the downregulation of CXCL-9 by pUL13 are unclear, it is suggested that inhibition of pUL13 has a potential effect in treating encephalitis of the central nervous system caused by HSV-1 infection (107–110).

Inhibition of SAMHD1

SAMHD1 is an antiviral host limiting factor (111–116), and the virus has adopted a variety of strategies to inhibit its dNTP

enzyme activity, such as HIV-2 and SIV virus-encoded Vpx proteins, to induce SAMHD1 degradation and promote self-replication (117–120); Ribonucleotide reductase (RNR) (121) and thymidine kinase (TK) (122, 123) encoded by DNA viruses can antagonize SAMHD1's dNTP enzyme activity, providing the necessary substrate for viral DNA polymerase; The intracellular CyclinA2/CDK1/CDK2 complex regulates phosphorylation of SAMHD1 Thr592 (124), and phosphorylation of Thr592 has been shown to reduce SAMHD1 antiviral activity (125), echoing IFN-I-induced dephosphorylation of SAMHD1 Thr592 (126). It has been also reported that pUL13 of the β and γ herpes virus participates in phosphorylation of SAMHD1 T592, inhibiting the dNTP enzyme activity of SAMHD1 from ensuring adequate intracellular levels of dNTPs for viral replication (127, 128) (Figure 3).

SAMHD1 can inhibit the excessive immune and inflammatory response, possibly proving why VZV and KSHV proliferate in lymphocytes requiring pORF47 and pORF36 (129). However, whether and how pUL13 can phosphorylate SMADH1 to coordinate the immune and inflammatory response remains to be studied.

It is revealed here that pUL13 plays an essential role in inhibiting various antiviral factors from escaping innate immunity. Additionally, pUL13 also plays an important role in viral replication, latent infection, and other critical physiological activities.

The role of pUL13 in promoting viral replication

pUL13 phosphorylates H2AX to promote viral replication

DNA-damage response (DDR) is a mechanism by which cells protect themselves through DNA damage repair and apoptosis to resist DNA damage induced by various factors (130, 131). Micah A. Luftig has discussed the interrelationship between viruses and DDR, noting that DNA viruses require DDR activation for replication (132). The research shows that the viral infection process acts on the different nodes of the DNA damage response pathway. For example, HSV-1 infections activate ataxia telangiectasia mutated (ATM) kinase activity but inhibit the role of ataxia telangiectasia- and Rad3-related protein (ATR); EBV virus infection activates upstream regulators of the DDR pathway in the DDR pathway-histone acetyltransferase TIP60 (133–135).

H2A histone family member X (H2AX) is a substrate of ATM, ATR, and DNA-dependent protein kinase catalytic subunits in phosphatidylinositol 3-kinase-like protein kinase family (PIKKs) (136–140); it is also a substrate for pUL13 (141, 142). In H2AX knockdown cells, the replication capacity of MHV-68 and KSHV are significantly abating (143, 144), and the date of EBV pBGLF4, PRV pUL13 what suggesting that pUL13 phosphorylate H2AX to activate DDR for viral replication (145, 146). Still, VZV pORF47 cannot phosphorylate H2AX and indicates the difference in the members of the CHPKs (147). An attractive hypothesis is that replication of viral DNA requires or is enhanced by the cellular DNA damage machinery (133, 148–150) (Figure 4). Generally, more evidence is needed to support whether pUL13 of the herpes virus plays a vital role in this matter.

pUL13 phosphorylates EF-1δ to promote viral replication

Herpesvirus pUL13 can promote host cell synthesis of proteins, such as the KSHV pORF36 mimicking cellular protein S6 kinase (S6KB1) to promote cell proliferation (151). Similarly, as a substrate of pUL13, the translation extension factor -1δ (EF-1δ) exists in two forms in the normal state of hypophosphorylation and hyperphosphorylation, involved in the process of mRNA translation into peptide chain extension. EF-1δ is mainly present in the hyperphosphorylated form in HSV-1-infected cells. Because HSV-1 pUL13, HCMV pUL97, EBV pBGLF4, and intracellular cycle-dependent kinase cdc2 are involved in EF-1δ's hyperphosphorylation and work together on its Ser 133 (152–154). It shows that UL13 can synthesize its viral protein using EF-1δ.

pUL13 works with SUMO proteins to promote viral replication

Small Ubiquitin-related Modifier (SUMO) is a post-translational modifier protein. The SUMO system is essential in herpes virus replication, such as KSHV replication and transcription activator (K-Rta) and HSV-1 ICP0 degrade SUMO-modified promyelocytic leukemia-nuclear bodies (PML-NBs) (155, 156), inhibition of the NF-κB signaling pathway (157) and participation in degradation of IRF-3 and IRF-7 (158–160). KSHV basic region-leucine zipper (K-bZIP) is a potent transcriptional repressor that binds directly to K-Rta and attenuates K-Rta-mediated trans-activation activity, relying on SUMO modifications to regulate viral and host gene expression (161, 162). Studies have shown that KSHV ORF36 phosphorylates Thr111 of K-bZIP and inhibits the SUMO level of bZIP, causing a decrease in transcriptional inhibition activity (163) (Figure 5), and appears to cooperate with K-Rta inhibition of K-bZIP to promote viral transcriptional expression (164);

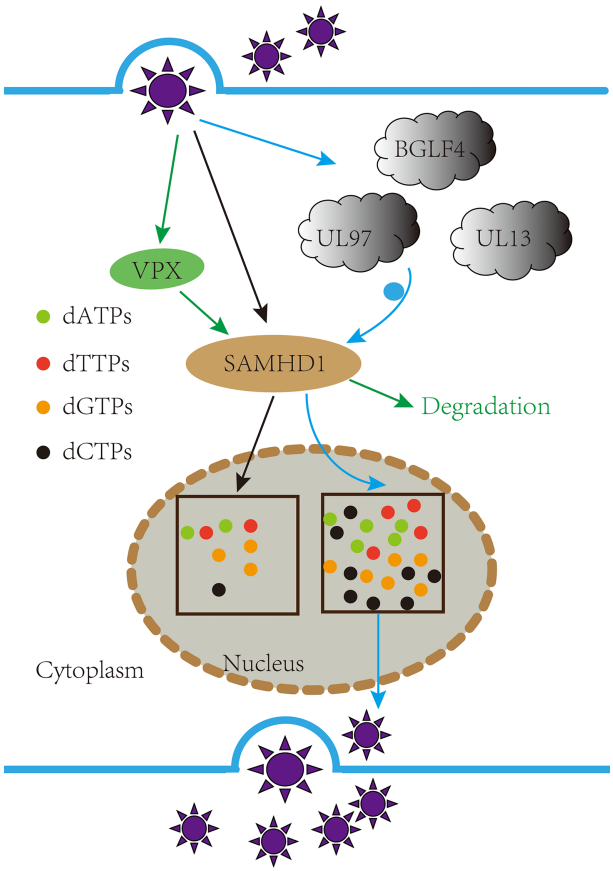

FIGURE 3
pUL13 phosphorylated the antiviral factor SAMDH1 Thr592 to promote viral replication. Inhibiting the dNTP enzyme activity of the sterile alpha motif and HD domain-containing protein 1 (SAMHD1) from ensuring adequate intracellular levels of dNTPs for viral replication.

Also involved in the phosphorylation of the cell chromatin remodeling molecule KAP-1 inhibits SUMO level and thus inhibits chromosomal remodeling capacity (165). It is also reflected in the EBV pBGLF4 negatively regulating SUMO-modified Zta to promote the establishment of viral latency (166, 167). It suggests that although the protein kinase of the γ-herpes virus cannot be modified by SUMO, its phosphorylation and SUMO can cooperate to promote viral replication.

pUL13 promotes viral replication in conjunction with ICP22 and VP22

The interaction between herpesvirus protein kinase and viral proteins to promote its replication is a complex network, such as the interaction of KSHV pORF36 and pORF45 (168), HSV-1 pUL13 and pUL41 (169). As early as 1993, Purves reported that pUL13 phosphorylation modulated ICP22 to stabilize to increase transcription of specific subpopulations of viral RNA and accumulate corresponding viral proteins (170). Subsequently, it was found that ICP22 and pUL13 were jointly involved in phosphorylation of RNA Pol II, mediating the degradation of cyclins A and B1 and activating cdc2, in which activated cdc2 and viral DNA synthesis factor pUL42 formed a complex to recruit topoisomerase II to promote the expression of advanced genes (171–179), indicating that ICP22 and pUL13 were necessary for early gene expression of herpes virus.

In HSV-1-infected cells, UL13 protein kinase promotes the dissociation of VP22 from virions and phosphorylate VP22 (169, 180). VP22 released into cells can interact with Template-activating factor I (TAF-1) proteins and histone H4 (Histone H4), inhibit the assembly of nucleosomes on DNA and H4 histone acetylation and participate in chromatin recombination,

10.3389/fimmu.2022.1088690

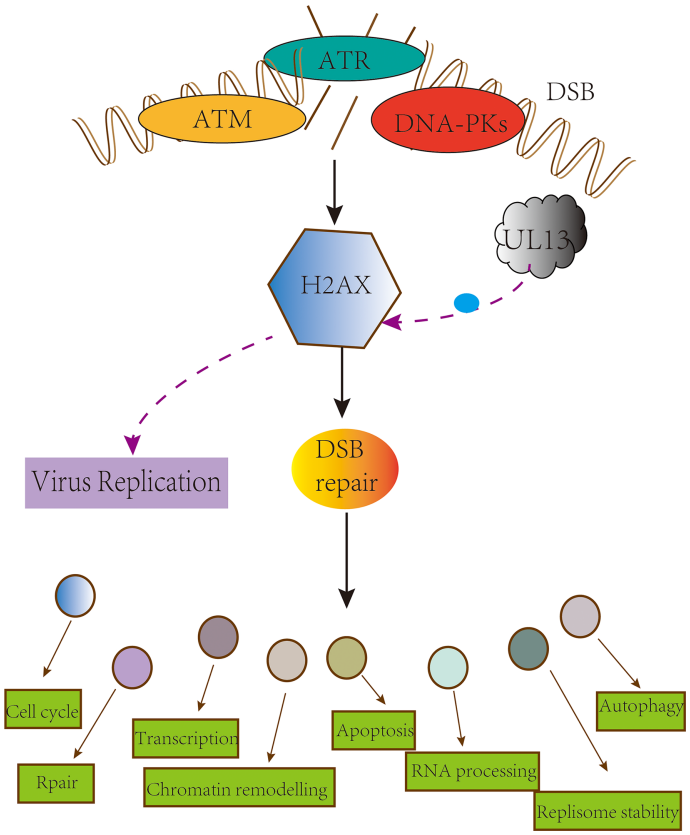

FIGURE 4
pUL13 phosphorylates H2AX to promote viral replication. The conserved herpesvirus Protein kinase pUL13 regulates DNA damage marker H2A histone family member X (H2AX), and pUL13-mediated H2AX phosphorylation plays a pivotal role in efficient virus replication and progeny production.

cell cycle control, and gene regulation (181, 182). The expression of VP22 can also inhibit cGAS activity and affect natural immunity (183). It can be seen that pUL13 can promote viral replication by regulating the ICP22 and VP22 proteins and collaborating.

pUL13 is involved in multiple processes of herpes virus replication, including gene replication, transcription, and translation of viruses (184); pUL13 in herpesvirus can destroy LaminA/C to promote capsid exodus from the nucleus (185–187); assembly, maturation, and release of virions (188). It is meaningful to construct pUL13 protein interaction networks to understand better the function of UL13 protein kinases in the life cycle of the herpes virus.

The role of pUL13 in latent infection

Induction and escape of herpesvirus genomic silencing is a biological marker of the herpes virus. Many reports suggest that pUL13 may play an essential role in the latent infection of the herpes virus. Firstly, Jolien Van Cleemput's study found that pUL13 may be indirectly involved in the latent infection reactivation of α herpesvirus by phosphorylating other cortical proteins (189); Secondly, in γ herpes virus, EBV pBGLF4 and KSHV pORF36 are closely associated with latent infection-related proteins as such Rta, Zta, the latency-associated nuclear antigen (LANA), and TAT interacting protein 60 kD (TIP60) (190–195); Lastly, MHV-68 pORF36 inhibits the antiviral effects of bone marrow-specific STAT1 expression and promotes the establishment of latent infection of MHV-68 in spleen B cells (196). In addition, herpesvirus CHPKs can also use CD8+ T cells and many host proteins (UXT, H2AX, small ubiquitin-related modification regulatory proteins) to promote the establishment of latent infections (197–199). Although the complex mechanism of establishment and reactivation of herpes virus latent infection is unknown, UL13 protein kinase will be an essential breakthrough for the follow-up study of latent infection of herpes virus.

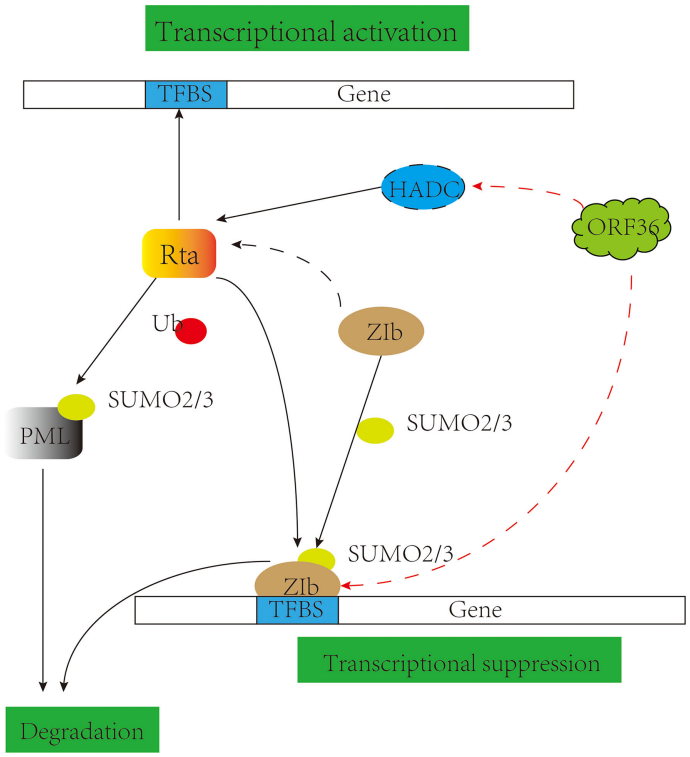

FIGURE 5
pUL13 works with SUMO proteins to promote viral replication. Gammaherpesvirus protein kinase pORF36 interacts with histone deacetylase 1 and 2 (HADC1/2) and prevents the association of these HDACs with the viral promoter driving expression of KSHV replication and transcription activator (K-Rta). pORF36 phosphorylates Thr111 of KSHV basic region-leucine zipper (K-bZIP) and inhibits the SUMO level of K-bZIP to repress the transcriptional inhibition activity.

Summary and prospect

pUL13 acts as a serine/threonine kinase encoded by the herpes virus. It is retained in the continuous natural screening of the virus and plays a vital role in the physiological activity of the herpes virus.

In terms of immune escape, to evade innate immune defense line and persist in host cells, pUL13 and its homologs directly or indirectly play a role in signaling pathways, which acts on different immunoregulatory proteins and many antiviral factors. Then pUL13 use varieties transcription factors and translation factors in host cells to assist the lytic cycle, such as EF-16, H2AX, SP1, embodied in lacking pUL13 will lead to the weakening of the replication ability and virulence of the virus. At the same time, herpesvirus can use pUL13 to assist in the establishment and reactivation of its latent infection.

pUL13 can phosphorylate many protein targets and participate in the activation and inhibition of related protein functions. It is similar to a switch in the life cycle of the herpes virus. It is committed to building a systematic protein interaction network diagram of pUL13, which is conducive to unveiling pUL13 in the life cycle of the herpes virus.

Herpesvirus pUL13 is an important target for developing anti-herpesvirus drugs. With the initial clinical application of GCV (200), followed by the anti-herpesvirus trials of compounds such as Maribavir (201), K252A (202), ISIS 1082 (203, 204), and 17-DMAG (205), as well as the continuous innovation of UL13 gene deletion vaccine (206, 207) and immunotherapy (208–210). However, given that low homology among different CHPK members complicates the development of compounds targeting an entire group, further development of more broad-spectrum, efficient and safe herpesvirus protein kinase inhibitors for the treatment of herpesvirus is needed.

pUL13 undertakes a variety of functions in the life cycle of herpes virus, and exploring the mechanism of action of pUL13 can not only solve the problem of infection, transmission, and immune escape mechanism of herpes virus but also provide a theoretical basis for the research and development of clinical drugs for the anti-herpes virus.

Author contributions

LZ and AC contributed to the design of the manuscript. XO, DS, SM, JH, QY, YW, SC, SZ, and DZ provided ideas contributing to the conception of this manuscript. RJ, ML, X-XZ, QG, and BT helped to create the figures. MW modified the manuscript. All the authors reviewed the manuscript. All authors contributed to the article and approved the submitted version.

Funding

This work was supported by the China Agricultural Research System of MOF and MARA and Sichuan Veterinary Medicine and Drug Innovation Group of China Agricultural Research System (SCCXTD-2020-18).

Conflict of interest

The authors declare that the research was conducted in the absence of any commercial or financial relationships that could be construed as a potential conflict of interest.

Publisher's note

References

1. Qi X, Yang X, Cheng A, Wang M, Zhu D, Jia R. Quantitative analysis of virulent duck enteritis virus loads in experimentally infected ducklings. *Avian Dis* (2008) 52(2):338–44. doi: 10.1637/8120-100207-ResNote.1

2. Wu Y, Cheng A, Wang M, Yang Q, Zhu D, Jia R, et al. Complete genomic sequence of Chinese virulent duck enteritis virus. *J Virol* (2012) 86(10):5965. doi: 10.1128/jvi.00529-12

3. Jia R, Cheng A, Wang M, Qi X, Zhu D, Ge H, et al. Development and evaluation of an antigen-capture Elisa for detection of the Ul24 antigen of the duck enteritis virus, based on a polyclonal antibody against the Ul24 expression protein. *J Virol Methods* (2009) 161(1):38–43. doi: 10.1016/j.jviromet.2009.05.011

4. Gong T, Liu L, Jiang W, Zhou R. Damp-sensing receptors in sterile inflammation and inflammatory diseases. *Nat Rev Immunol* (2020) 20(2):95–112. doi: 10.1038/s41577-019-0215-7

5. Sun L, Wu J, Du F, Chen X, Chen ZJ. Cyclic gmp-amp synthase is a cytosolic DNA sensor that activates the type I interferon pathway. *Science* (2013) 339 (6121):786–91. doi: 10.1126/science.1232458

6. Wu J, Sun L, Chen X, Du F, Shi H, Chen C, et al. Cyclic gmp-amp is an endogenous second messenger in innate immune signaling by cytosolic DNA. *Science* (2013) 339(6121):826–30. doi: 10.1126/science.1229963

7. Hayden MS, Ghosh S. Nf-Kb in immunobiology. *Cell Res* (2011) 21(2):223–44. doi: 10.1038/cr.2011.13

8. Lawrence T. The nuclear factor nf-kappab pathway in inflammation. *Cold Spring Harb Perspect Biol* (2009) 1(6):a001651. doi: 10.1101/cshperspect.a001651

9. Asai R, Kato A, Kato K, Kanamori-Koyama M, Sugimoto K, Sairenji T, et al. Epstein-Barr Virus protein kinase Bglf4 is a virion tegument protein that dissociates from virions in a phosphorylation-dependent process and phosphorylates the viral immediate-early protein Bzlf1. *J Virol* (2006) 80 (11):5125–34. doi: 10.1128/jvi.02674-05

10. Overton HA, McMillan DJ, Klavinskis LS, Hope L, Ritchie AJ, Wong-kai-in P. Herpes simplex virus type 1 gene Ul13 encodes a phosphoprotein that is a component of the virion. *Virology* (1992) 190(1):184–92. doi: 10.1016/0042-6822(92)91204-8

11. van Zeijl M, Fairhurst J, Baum EZ, Sun L, Jones TR. The human cytomegalovirus Ul97 protein is phosphorylated and a component of virions. *Virology* (1997) 231(1):72–80. doi: 10.1006/viro.1997.8523

12. Hanks SK, Quinn AM, Hunter T. The protein kinase family: Conserved features and deduced phylogeny of the catalytic domains. *Science* (1988) 241 (4861):42–52. doi: 10.1126/science.3291115

13. Hanks SK, Quinn AM. Protein kinase catalytic domain sequence database: Identification of conserved features of primary structure and classification of family members. *Methods Enzymol* (1991) 200:38–62. doi: 10.1016/0076-6879(91)00126-h

14. Hanks SK, Hunter T. Protein kinases 6. the eukaryotic protein kinase superfamily: Kinase (Catalytic) domain structure and classification. *FASEB J* (1995) 9(8):576–96. doi: 10.1096/fasebj.9.8.7768349

15. Leader DP. Viral protein kinases and protein phosphatases. *Pharmacol Ther* (1993) 59(3):343–89. doi: 10.1016/0163-7258(93)90075-o

16. Cano-Monreal GL, Tavis JE, Morrison LA. Substrate specificity of the herpes simplex virus type 2 Ul13 protein kinase. *Virology* (2008) 374(1):1–10. doi: 10.1016/j.virol.2007.11.023

17. Baek MC, Krosky PM, Coen DM. Relationship between autophosphorylation and phosphorylation of exogenous substrates by the human cytomegalovirus Ul97 protein kinase. *J Virol* (2002) 76(23):11943–52. doi: 10.1128/jvi.76.23.11943-11952.2002

18. Kenyon TK, Grose C. Vzv Orf47 serine protein kinase and its viral substrates. *Curr Top Microbiol Immunol* (2010) 342:99–111. doi: 10.1007/82_2009_5

19. Soong W, Schultz JC, Patera AC, Sommer MH, Cohen JI. Infection of human T lymphocytes with varicella-zoster virus: An analysis with viral mutants and clinical isolates. *J Virol* (2000) 74(4):1864–70. doi: 10.1128/jvi.74.4.1864-1870.2000

20. Besser J, Sommer MH, Zerboni L, Bagowski CP, Ito H, Moffat J, et al. Differentiation of varicella-zoster virus Orf47 protein kinase and Ie62 protein binding domains and their contributions to replication in human skin xenografts in the scid-hu mouse. *J Virol* (2003) 77(10):5964–74. doi: 10.1128/jvi.77.10.5964-5974.2003

21. Anders PM, Montgomery ND, Montgomery SA, Bhatt AP, Dittmer DP, Damania B. Human herpesvirus-encoded kinase induces b cell lymphomas in vivo. *J Clin Invest* (2018) 128(6):2519–34. doi: 10.1172/jci97053

22. Chen X, Shan T, Sun D, Zhai H, Dong S, Kong N, et al. Host zinc-finger cchc-type containing protein 3 inhibits pseudorabies virus proliferation by regulating type I interferon signaling. *Gene* (2022) 827:146480. doi: 10.1016/j.gene.2022.146480

23. McKenzie J, Lopez-Giraldez F, Delecluse HJ, Walsh A, El-Guindy A. The Epstein-Barr virus immunoevasins Bcrf1 and Bplf1 are expressed by a mechanism independent of the canonical late pre-initiation complex. *PloS Pathog* (2016) 12 (11):e1006008. doi: 10.1371/journal.ppat.1006008

24. Koyanagi N, Kato A, Takeshima K, Maruzuru Y, Kozuka-Hata H, Oyama M, et al. Regulation of herpes simplex virus 2 protein kinase Ul13 by phosphorylation and its role in viral pathogenesis. *J Virol* (2018) 92(17):e00807-18. doi: 10.1128/jvi.00807-18

25. Hu X, Wang M, Chen S, Jia R, Zhu D, Liu M, et al. The duck enteritis virus early protein, Ul13, found in both nucleus and cytoplasm, influences viral replication in cell culture. *Poult Sci* (2017) 96(8):2899–907. doi: 10.3382/ps/pex043

26. Kuny CV, Chinchilla K, Culbertson MR, Kalejta RF. Cyclin-dependent kinase-like function is shared by the beta- and gamma- subset of the conserved herpesvirus protein kinases. *PloS Pathog* (2010) 6(9):e1001092. doi: 10.1371/journal.ppat.1001092

27. Iwahori S, Hakki M, Chou S, Kalejta RF. Molecular determinants for the inactivation of the retinoblastoma tumor suppressor by the viral cyclin-dependent kinase Ul97. *J Biol Chem* (2015) 290(32):19666–80. doi: 10.1074/jbc.M115.660043

28. Wang JT, Doong SL, Teng SC, Lee CP, Tsai CH, Chen MR. Epstein-Barr Virus Bglf4 kinase suppresses the interferon regulatory factor 3 signaling pathway. *J Virol* (2009) 83(4):1856–69. doi: 10.1128/jvi.01099-08

29. Vandevenne P, Lebrun M, El Mjiyad N, Ote I, Di Valentin E, Habraken Y, et al. The varicella-zoster virus Orf47 kinase interferes with host innate immune response by inhibiting the activation of Irf3. *PloS One* (2011) 6(2):e16870. doi: 10.1371/journal.pone.0016870

30. Hwang S, Kim KS, Flano E, Wu TT, Tong LM, Park AN, et al. Conserved herpesviral kinase promotes viral persistence by inhibiting the irf-3-Mediated type I interferon response. *Cell Host Microbe* (2009) 5(2):166–78. doi: 10.1016/j.chom.2008.12.013

31. Bo Z, Miao Y, Xi R, Zhong Q, Bao C, Chen H, et al. Prv Ul13 inhibits cgas-Sting-Mediated ifn-B production by phosphorylating Irf3. *Vet Res* (2020) 51 (1):118. doi: 10.1186/s13567-020-00843-4

32. Escalante CR, Nistal-Villán E, Shen L, García-Sastre A, Aggarwal AK. Structure of irf-3 bound to the prdiii-I regulatory element of the human interferon-beta enhancer. *Mol Cell* (2007) 26(5):703–16. doi: 10.1016/j.molcel.2007.04.022

33. Lv L, Cao M, Bai J, Jin L, Wang X, Gao Y, et al. Prv-encoded Ul13 protein kinase acts as an antagonist of innate immunity by targeting Irf3-signaling pathways. *Vet Microbiol* (2020) 250:108860. doi: 10.1016/j.vetmic.2020.108860

34. Kong Z, Yin H, Wang F, Liu Z, Luan X, Sun L, et al. Pseudorabies virus tegument protein Ul13 recruits Rnf5 to inhibit sting-mediated antiviral immunity. *PloS Pathog* (2022) 18(5):e1010544. doi: 10.1371/journal.ppat.1010544

35. Lv L, Bai J, Gao Y, Jin L, Wang X, Cao M, et al. Peroxiredoxin 1 interacts with Tbk1/Ikkε and negatively regulates pseudorabies virus propagation by promoting innate immunity. *J Virol* (2021) 95(19):e0092321. doi: 10.1128/jvi.00923-21

36. Fang M, Zhang A, Du Y, Lu W, Wang J, Minze LJ, et al. Trim18 is a critical regulator of viral myocarditis and organ inflammation. *J BioMed Sci* (2022) 29 (1):55. doi: 10.1186/s12929-022-00840-z

37. Li Q, Lin L, Tong Y, Liu Y, Mou J, Wang X, et al. Trim29 negatively controls antiviral immune response through targeting sting for degradation. *Cell Discovery* (2018) 4:13. doi: 10.1038/s41421-018-0010-9

38. Alexopoulou L, Holt AC, Medzhitov R, Flavell RA. Recognition of double-stranded rna and activation of nf-kappab by toll-like receptor 3. *Nature* (2001) 413 (6857):732–8. doi: 10.1038/35099560

39. Kawai T, Akira S. Signaling to nf-kappab by toll-like receptors. *Trends Mol Med* (2007) 13(11):460–9. doi: 10.1016/j.molmed.2007.09.002

40. Chang LS, Wang JT, Doong SL, Lee CP, Chang CW, Tsai CH, et al. Epstein-Barr Virus Bglf4 kinase downregulates nf-Kb transactivation through phosphorylation of coactivator uxt. *J Virol* (2012) 86(22):12176–86. doi: 10.1128/jvi.01918-12

41. Mounce BC, Mboko WP, Bigley TM, Terhune SS, Tarakanova VL. A conserved gammaherpesvirus protein kinase targets histone deacetylases 1 and 2 to facilitate viral replication in primary macrophages. *J Virol* (2013) 87(13):7314–25. doi: 10.1128/jvi.02713-12

42. Dong X, Feng P. Murine gamma herpesvirus 68 hijacks mavs and ikkβ to abrogate nfκb activation and antiviral cytokine production. *PloS Pathog* (2011) 7 (11):e1002336. doi: 10.1371/journal.ppat.1002336

43. Schaller AM, Tucker J, Willis I, Glaunsinger BA. Conserved herpesvirus kinase Orf36 activates B2 retrotransposons during murine gammaherpesvirus infection. *J Virol* (2020) 94(14):e00262-20. doi: 10.1128/jvi.00262-20

44. Kassube SA, Fang J, Grob P, Yakovchuk P, Goodrich JA, Nogales E. Structural insights into transcriptional repression by noncoding rnas that bind to human pol ii. *J Mol Biol* (2013) 425(19):3639–48. doi: 10.1016/j.jmb.2012.08.024

45. Ponicsan SL, Houel S, Old WM, Ahn NG, Goodrich JA, Kugel JF. The non-coding B2 rna binds to the DNA cleft and active-site region of rna polymerase ii. *J Mol Biol* (2013) 425(19):3625–38. doi: 10.1016/j.jmb.2013.01.035

46. Darnell JEJr., Kerr IM, Stark GR. Jak-stat pathways and transcriptional activation in response to ifns and other extracellular signaling proteins. *Science* (1994) 264(5164):1415–21. doi: 10.1126/science.8197455

47. Stark GR, Darnell JEJr. The jak-stat pathway at twenty. *Immunity* (2012) 36 (4):503–14. doi: 10.1016/j.immuni.2012.03.013

48. Sato Y, Koshizuka T, Ishibashi K, Hashimoto K, Ishioka K, Ikuta K, et al. Involvement of herpes simplex virus type 1 Ul13 protein kinase in induction of socs genes, the negative regulators of cytokine signaling. *Microbiol Immunol* (2017) 61 (5):159–67. doi: 10.1111/1348-0421.12483

49. Vizcaíno C, Mansilla S, Portugal J. Sp1 transcription factor: A long-standing target in cancer chemotherapy. *Pharmacol Ther* (2015) 152:111–24. doi: 10.1016/j.pharmthera.2015.05.008

50. Barclay JL, Anderson ST, Waters MJ, Curlewis JD. Socs3 as a tumor suppressor in breast cancer cells, and its regulation by prl. *Int J Cancer* (2009) 124(8):1756–66. doi: 10.1002/ijc.24172

51. Yokota S, Yokosawa N, Okabayashi T, Suzutani T, Miura S, Jimbow K, et al. Induction of suppressor of cytokine signaling-3 by herpes simplex virus type 1 contributes to inhibition of the interferon signaling pathway. *J Virol* (2004) 78 (12):6282–6. doi: 10.1128/jvi.78.12.6282-6286.2004

52. Yokota S, Yokosawa N, Okabayashi T, Suzutani T, Fujii N. Induction of suppressor of cytokine signaling-3 by herpes simplex virus type 1 confers efficient viral replication. *Virology* (2005) 338(1):173–81. doi: 10.1016/j.virol.2005.04.028

53. Shen X, Hong F, Nguyen VA, Gao B. Il-10 attenuates ifn-Alpha-Activated Stat1 in the liver: Involvement of Socs2 and Socs3. *FEBS Lett* (2000) 480(2-3):132–6. doi: 10.1016/s0014-5793(00)01905-0

54. Jones KA, Tjian R. Sp1 binds to promoter sequences and activates herpes simplex virus 'Immediate-early' gene transcription in vitro. *Nature* (1985) 317 (6033):179–82. doi: 10.1038/317179a0

55. Ostler JB, Thunuguntla P, Hendrickson BY, Jones C. Transactivation of herpes simplex virus 1 (Hsv-1) infected cell protein 4 enhancer by glucocorticoid receptor and stress-induced transcription factors requires overlapping krüppel-like transcription factor 4/Sp1 binding sites. *J Virol* (2021) 95(4):e01776-20. doi: 10.1128/jvi.01776-20

56. Gu B, Rivera-Gonzalez R, Smith CA, DeLuca NA. Herpes simplex virus infected cell polypeptide 4 preferentially represses Sp1-activated over basal transcription from its own promoter. *Proc Natl Acad Sci U.S.A.* (1993) 90 (20):9528–32. doi: 10.1073/pnas.90.20.9528

57. Kim DB, DeLuca NA. Phosphorylation of transcription factor Sp1 during herpes simplex virus type 1 infection. *J Virol* (2002) 76(13):6473–9. doi: 10.1128/jvi.76.13.6473-6479.2002

58. Akhtar LN, Benveniste EN. Viral exploitation of host socs protein functions. *J Virol* (2011) 85(5):1912–21. doi: 10.1128/jvi.01857-10

59. Choi EJ, Lee CH, Shin OS. Suppressor of cytokine signaling 3 expression induced by varicella-zoster virus infection results in the modulation of virus replication. *Scand J Immunol* (2015) 82(4):337–44. doi: 10.1111/sji.12323

60. Frey KG, Ahmed CM, Dabelic R, Jager LD, Noon-Song EN, Haider SM, et al. Hsv-1-Induced socs-1 expression in keratinocytes: Use of a socs-1 antagonist to block a novel mechanism of viral immune evasion. *J Immunol* (2009) 183 (2):1253–62. doi: 10.4049/jimmunol.0900570

61. Michaud F, Coulombe F, Gaudreault E, Paquet-Bouchard C, Rola-Pleszczynski M, Gosselin J. Epstein-Barr Virus interferes with the amplification of ifnalpha secretion by activating suppressor of cytokine signaling 3 in primary human monocytes. *PloS One* (2010) 5(7):e11908. doi: 10.1371/journal.pone.0011908

62. Sasaki A, Yasukawa H, Suzuki A, Kamizono S, Syoda T, Kinjyo I, et al. Cytokine-inducible Sh2 protein-3 (Cis3/Socs3) inhibits janus tyrosine kinase by binding through the n-terminal kinase inhibitory region as well as Sh2 domain. *Genes Cells* (1999) 4(6):339–51. doi: 10.1046/j.1365-2443.1999.00263.x

63. Yasukawa H, Misawa H, Sakamoto H, Masuhara M, Sasaki A, Wakioka T, et al. The jak-binding protein jab inhibits janus tyrosine kinase activity through binding in the activation loop. *EMBO J* (1999) 18(5):1309–20. doi: 10.1093/emboj/18.5.1309

64. Wormald S, Zhang JG, Krebs DL, Mielke LA, Silver J, Alexander WS, et al. The comparative roles of suppressor of cytokine signaling-1 and -3 in the inhibition and desensitization of cytokine signaling. *J Biol Chem* (2006) 281(16):11135–43. doi: 10.1074/jbc.M509595200

65. Wang Y, van Boxel-Dezaire AH, Cheon H, Yang J, Stark GR. Stat3 activation in response to il-6 is prolonged by the binding of il-6 receptor to egf receptor. *Proc Natl Acad Sci U.S.A.* (2013) 110(42):16975–80. doi: 10.1073/pnas.1315862110

66. Carow B, Rottenberg ME. Socs3, a major regulator of infection and inflammation. *Front Immunol* (2014) 5:58. doi: 10.3389/fimmu.2014.00058

67. Karlsen AE, Heding PE, Frobøse H, Rønn SG, Kruhøffer M, Orntoft TF, et al. Suppressor of cytokine signalling (Socs)-3 protects beta cells against il-1beta-Mediated toxicity through inhibition of multiple nuclear factor-Kappab-Regulated proapoptotic pathways. *Diabetologia* (2004) 47(11):1998–2011. doi: 10.1007/s00125-004-1568-3

68. Zamanian-Daryoush M, Mogensen TH, DiDonato JA, Williams BR. Nf-kappab activation by double-Stranded-Rna-Activated protein kinase (Pkr) is mediated through nf-Kappab-Inducing kinase and ikappab kinase. *Mol Cell Biol* (2000) 20(4):1278–90. doi: 10.1128/mcb.20.4.1278-1290.2000

69. Gu L, Ge Z, Wang Y, Shen M, Zhao P, Chen W. Double-stranded rna-dependent kinase pkr activates nf-Kb pathway in acute pancreatitis. *Biochem Biophys Res Commun* (2018) 503(3):1563–9. doi: 10.1016/j.bbrc.2018.07.080

70. Paludan SR, Mogensen SC. Virus-cell interactions regulating induction of tumor necrosis factor alpha production in macrophages infected with herpes

simplex virus. *J Virol* (2001) 75(21):10170–8. doi: 10.1128/jvi.75.21.10170-10178.2001

71. Hu Z, Du H, Lin G, Han K, Cheng X, Feng Z, et al. Grass carp (Ctenopharyngodon idella) pact induces cell apoptosis and activates nf-Kb *Via* pkr. *Fish Shellfish Immunol* (2020) 103:377–84. doi: 10.1016/j.fsi.2020.05.036

72. Li X, Wu Z, An X, Mei Q, Bai M, Hanski L, et al. Blockade of the Lrp16-Pkr-Nf-Kb signaling axis sensitizes colorectal carcinoma cells to DNA-damaging cytotoxic therapy. *Elife* (2017) 6:e27301. doi: 10.7554/eLife.27301

73. Gil J, Alcamí J, Esteban M. Activation of nf-kappa b by the dsrna-dependent protein kinase, pkr involves the I kappa b kinase complex. *Oncogene* (2000) 19 (11):1369–78. doi: 10.1038/sj.onc.1203448

74. Schulz O, Pichlmair A, Rehwinkel J, Rogers NC, Scheuner D, Kato H, et al. Protein kinase r contributes to immunity against specific viruses by regulating interferon mrna integrity. *Cell Host Microbe* (2010) 7(5):354–61. doi: 10.1016/j.chom.2010.04.007

75. Yoon CH, Lee ES, Lim DS, Bae YS. Pkr, a P53 target gene, plays a crucial role in the tumor-suppressor function of P53. *Proc Natl Acad Sci U.S.A.* (2009) 106 (19):7852–7. doi: 10.1073/pnas.0812148106

76. Cuddihy AR, Wong AH, Tam NW, Li S, Koromilas AE. The double-stranded rna activated protein kinase pkr physically associates with the tumor suppressor P53 protein and phosphorylates human P53 on serine 392 in vitro. *Oncogene* (1999) 18(17):2690–702. doi: 10.1038/sj.onc.1202620

77. Huang Q, Xie D, Mao H, Wang H, Wu Z, Huang K, et al. Ctenopharyngodon idella P53 mediates between nf-Kb and pkr at the transcriptional level. *Fish Shellfish Immunol* (2017) 69:258–64. doi: 10.1016/j.fsi.2017.08.012

78. Dey M, Cao C, Dar AC, Tamura T, Ozato K, Sicheri F, et al. Mechanistic link between pkr dimerization, autophosphorylation, and Eif2alpha substrate recognition. *Cell* (2005) 122(6):901–13. doi: 10.1016/j.cell.2005.06.041

79. Dar AC, Dever TE, Sicheri F. Higher-order substrate recognition of Eif2alpha by the rna-dependent protein kinase pkr. *Cell* (2005) 122(6):887–900. doi: 10.1016/j.cell.2005.06.044

80. Su Q, Wang S, Baltzis D, Qu LK, Wong AH, Koromilas AE. Tyrosine phosphorylation acts as a molecular switch to full-scale activation of the Eif2alpha rna-dependent protein kinase. *Proc Natl Acad Sci U.S.A.* (2006) 103(1):63–8. doi: 10.1073/pnas.0508207103

81. Rabouw HH, Langereis MA, Knaap RC, Dalebout TJ, Canton J, Sola I, et al. Middle East respiratory coronavirus accessory protein 4a inhibits pkr-mediated antiviral stress responses. *PloS Pathog* (2016) 12(10):e1005982. doi: 10.1371/journal.ppat.1005982

82. Sharma NR, Majerciak V, Kruhlak MJ, Zheng ZM. Kshv inhibits stress granule formation by viral Orf57 blocking pkr activation. *PloS Pathog* (2017) 13 (10):e1006677. doi: 10.1371/journal.ppat.1006677

83. Dauber B, Pelletier J, Smiley JR. The herpes simplex virus 1 vhs protein enhances translation of viral true late mrnas and virus production in a cell type-dependent manner. *J Virol* (2011) 85(11):5363–73. doi: 10.1128/jvi.00115-11

84. Dauber B, Poon D, Dos Santos T, Duguay BA, Mehta N, Saffran HA, et al. The herpes simplex virus virion host shutoff protein enhances translation of viral true late mrnas independently of suppressing protein kinase r and stress granule formation. *J Virol* (2016) 90(13):6049–57. doi: 10.1128/jvi.03180-15

85. Li C, Zhu Z, Du X, Cao W, Yang F, Zhang X, et al. Foot-and-Mouth disease virus induces lysosomal degradation of host protein kinase pkr by 3c proteinase to facilitate virus replication. *Virology* (2017) 509:222–31. doi: 10.1016/j.virol.2017.06.023

86. Valchanova RS, Picard-Maureau M, Budt M, Brune W. Murine cytomegalovirus M142 and M143 are both required to block protein kinase r-mediated shutdown of protein synthesis. *J Virol* (2006) 80(20):10181–90. doi: 10.1128/jvi.00908-06

87. McKenna SA, Lindhout DA, Shimoike T, Aitken CE, Puglisi JD. Viral dsrna inhibitors prevent self-association and autophosphorylation of pkr. *J Mol Biol* (2007) 372(1):103–13. doi: 10.1016/j.jmb.2007.06.028

88. Poppers J, Mulvey M, Perez C, Khoo D, Mohr I. Identification of a lytic-cycle Epstein-Barr virus gene product that can regulate pkr activation. *J Virol* (2003) 77(1):228–36. doi: 10.1128/jvi.77.1.228-236.2003

89. Lussignol M, Queval C, Bernet-Camard MF, Cotte-Laffitte J, Beau I, Codogno P, et al. The herpes simplex virus 1 Us11 protein inhibits autophagy through its interaction with the protein kinase pkr. *J Virol* (2013) 87(2):859–71. doi: 10.1128/jvi.01158-12

90. He B, Gross M, Roizman B. The Gamma134.5 protein of herpes simplex virus 1 has the structural and functional attributes of a protein phosphatase 1 regulatory subunit and is present in a high molecular weight complex with the enzyme in infected cells. *J Biol Chem* (1998) 273(33):20737–43. doi: 10.1074/jbc.273.33.20737

91. Esteban M, García MA, Domingo-Gil E, Arroyo J, Nombela C, Rivas C. The latency protein Lana2 from kaposi's sarcoma-associated herpesvirus inhibits apoptosis induced by dsrna-activated protein kinase but not rnase l activation. *J Gen Virol* (2003) 84(Pt 6):1463–70. doi: 10.1099/vir.0.19014-0

92. He B, Gross M, Roizman B. The Gamma(1)34.5 protein of herpes simplex virus 1 complexes with protein phosphatase 1alpha to dephosphorylate the alpha subunit of the eukaryotic translation initiation factor 2 and preclude the shutoff of protein synthesis by double-stranded rna-activated protein kinase. *Proc Natl Acad Sci U.S.A.* (1997) 94(3):843–8. doi: 10.1073/pnas.94.3.843

93. Borghese F, Michiels T. The leader protein of cardioviruses inhibits stress granule assembly. *J Virol* (2011) 85(18):9614–22. doi: 10.1128/jvi.00480-11

94. Borghese F, Sorgeloos F, Cesaro T, Michiels T. The leader protein of theiler's virus prevents the activation of pkr. *J Virol* (2019) 93(19):e01010-19. doi: 10.1128/jvi.01010-19

95. Pennisi R, Musarra-Pizzo M, Lei Z, Zhou GG, Sciortino MT. Vhs, Us3 and Ul13 viral tegument proteins are required for herpes simplex virus-induced modification of protein kinase r. *Sci Rep* (2020) 10(1):5580. doi: 10.1038/s41598-020-62619-2

96. Costa-Mattioli M, Walter P. The integrated stress response: From mechanism to disease. *Science* (2020) 368(6489):eaat5314. doi: 10.1126/science.aat5314

97. Watanabe T, Imamura T, Hiasa Y. Roles of protein kinase r in cancer: Potential as a therapeutic target. *Cancer Sci* (2018) 109(4):919–25. doi: 10.1111/cas.13551

98. Raafat N, Sadowski-Cron C, Mengus C, Heberer M, Spagnoli GC, Zajac P. Preventing vaccinia virus class-I epitopes presentation by hsv-Icp47 enhances the immunogenicity of a tap-independent cancer vaccine epitope. *Int J Cancer* (2012) 131(5):E659–69. doi: 10.1002/ijc.27362

99. Aisenbrey C, Sizun C, Koch J, Herget M, Abele R, Bechinger B, et al. Structure and dynamics of membrane-associated Icp47, a viral inhibitor of the mhc I antigen-processing machinery. *J Biol Chem* (2006) 281(41):30365–72. doi: 10.1074/jbc.M603000200

100. Deruelle MJ, Van den Broeke C, Nauwynck HJ, Mettenleiter TC, Favoreel HW. Pseudorabies virus Us3- and Ul49.5-dependent and -independent downregulation of mhc I cell surface expression in different cell types. *Virology* (2009) 395(2):172–81. doi: 10.1016/j.virol.2009.09.019

101. Imai T, Koyanagi N, Ogawa R, Shindo K, Suenaga T, Sato A, et al. Us3 kinase encoded by herpes simplex virus 1 mediates downregulation of cell surface major histocompatibility complex class I and evasion of Cd8+ T cells. *PloS One* (2013) 8(8):e72050. doi: 10.1371/journal.pone.0072050

102. Koyanagi N, Imai T, Shindo K, Sato A, Fujii W, Ichinohe T, et al. Herpes simplex virus-1 evasion of Cd8+ T cell accumulation contributes to viral encephalitis. *J Clin Invest* (2017) 127(10):3784–95. doi: 10.1172/jci92931

103. Spranger S, Dai D, Horton B, Gajewski TF. Tumor-residing Batf3 dendritic cells are required for effector T cell trafficking and adoptive T cell therapy. *Cancer Cell* (2017) 31(5):711–23.e4. doi: 10.1016/j.ccell.2017.04.003

104. Canny SP, Goel G, Reese TA, Zhang X, Xavier R, Virgin HW. Latent gammaherpesvirus 68 infection induces distinct transcriptional changes in different organs. *J Virol* (2014) 88(1):730–8. doi: 10.1128/jvi.02708-13

105. Prabhakaran K, Sheridan BS, Kinchington PR, Khanna KM, Decman V, Lathrop K, et al. Sensory neurons regulate the effector functions of Cd8+ T cells in controlling hsv-1 latency ex vivo. *Immunity* (2005) 23(5):515–25. doi: 10.1016/j.immuni.2005.09.017

106. Knickelbein JE, Khanna KM, Yee MB, Baty CJ, Kinchington PR, Hendricks RL. Noncytotoxic lytic granule-mediated Cd8+ T cell inhibition of hsv-1 reactivation from neuronal latency. *Science* (2008) 322(5899):268–71. doi: 10.1126/science.1164164

107. Nair A, Hunzeker J, Bonneau RH. Modulation of microglia and Cd8(+) T cell activation during the development of stress-induced herpes simplex virus type-1 encephalitis. *Brain Behav Immun* (2007) 21(6):791–806. doi: 10.1016/j.bbi.2007.01.005

108. Menendez CM, Carr DJJ. Herpes simplex virus-1 infects the olfactory bulb shortly following ocular infection and exhibits a long-term inflammatory profile in the form of effector and hsv-1-Specific T cells. *J Neuroinflamm* (2017) 14(1):124. doi: 10.1186/s12974-017-0903-9

109. Lang A, Nikolich-Zugich J. Development and migration of protective Cd8+ T cells into the nervous system following ocular herpes simplex virus-1 infection. *J Immunol* (2005) 174(5):2919–25. doi: 10.4049/jimmunol.174.5.2919

110. Banerjee K, Biswas PS, Kumaraguru U, Schoenberger SP, Rouse BT. Protective and pathological roles of virus-specific and bystander Cd8+ T cells in herpetic stromal keratitis. *J Immunol* (2004) 173(12):7575–83. doi: 10.4049/jimmunol.173.12.7575

111. Coquel F, Silva MJ, Técher H, Zadorozhny K, Sharma S, Nieminuszczy J, et al. Samhd1 acts at stalled replication forks to prevent interferon induction. *Nature* (2018) 557(7703):57–61. doi: 10.1038/s41586-018-0050-1

112. Cabello-Lobato MJ, Wang S, Schmidt CK. Samhd1 sheds moonlight on DNA double-strand break repair. *Trends Genet* (2017) 33(12):895–7. doi: 10.1016/j.tig.2017.09.007

113. Hollenbaugh JA, Gee P, Baker J, Daly MB, Amie SM, Tate J, et al. Host factor Samhd1 restricts DNA viruses in non-dividing myeloid cells. *PloS Pathog* (2013) 9(6):e1003481. doi: 10.1371/journal.ppat.1003481

114. Kim ET, White TE, Brandariz-Núñez A, Diaz-Griffero F, Weitzman MD. Samhd1 restricts herpes simplex virus 1 in macrophages by limiting DNA replication. *J Virol* (2013) 87(23):12949–56. doi: 10.1128/jvi.02291-13

115. Sze A, Belgnaoui SM, Olagnier D, Lin R, Hiscott J, van Grevenynghe J. Host restriction factor Samhd1 limits human T cell leukemia virus type 1 infection of monocytes *Via* sting-mediated apoptosis. *Cell Host Microbe* (2013) 14(4):422–34. doi: 10.1016/j.chom.2013.09.009

116. Chen Z, Zhu M, Pan X, Zhu Y, Yan H, Jiang T, et al. Inhibition of hepatitis b virus replication by Samhd1. *Biochem Biophys Res Commun* (2014) 450(4):1462–8. doi: 10.1016/j.bbrc.2014.07.023

117. Laguette N, Sobhian B, Casartelli N, Ringeard M, Chable-Bessia C, Ségéral E, et al. Samhd1 is the dendritic- and myeloid-Cell-Specific hiv-1 restriction factor counteracted by vpx. *Nature* (2011) 474(7353):654–7. doi: 10.1038/nature10117

118. Chougui G, Munir-Matloob S, Matkovic R, Martin MM, Morel M, Lahouassa H, et al. Hiv-2/Siv viral protein X counteracts hush repressor complex. *Nat Microbiol* (2018) 3(8):891–7. doi: 10.1038/s41564-018-0179-6

119. Hrecka K, Hao C, Gierszewska M, Swanson SK, Kesik-Brodacka M, Srivastava S, et al. Vpx relieves inhibition of hiv-1 infection of macrophages mediated by the Samhd1 protein. *Nature* (2011) 474(7353):658–61. doi: 10.1038/nature10195

120. Goujon C, Rivière L, Jarrosson-Wuilleme L, Bernaud J, Rigal D, Darlix JL, et al. Sivsm/Hiv-2 vpx proteins promote retroviral escape from a proteasome-dependent restriction pathway present in human dendritic cells. *Retrovirology* (2007) 4:2. doi: 10.1186/1742-4690-4-2

121. Rudd SG, Tsesmetzis N, Sanjiv K, Paulin CB, Sandhow L, Kutzner J, et al. Ribonucleotide reductase inhibitors suppress Samhd1 ara-ctpase activity enhancing cytarabine efficacy. *EMBO Mol Med* (2020) 12(3):e10419. doi: 10.15252/emmm.201910419

122. Iwasawa C, Tamura R, Sugiura Y, Suzuki S, Kuzumaki N, Narita M, et al. Increased cytotoxicity of herpes simplex virus thymidine kinase expression in human induced pluripotent stem cells. *Int J Mol Sci* (2019) 20(4):810. doi: 10.3390/ijms20040810

123. Valle-Casuso JC, Allouch A, David A, Lenzi GM, Studdard L, Barré-Sinoussi F, et al. P21 restricts hiv-1 in monocyte-derived dendritic cells through the reduction of deoxynucleoside triphosphate biosynthesis and regulation of Samhd1 antiviral activity. *J Virol* (2017) 91(23):e01324-17. doi: 10.1128/jvi.01324-17

124. Yan J, Hao C, DeLucia M, Swanson S, Florens L, Washburn MP, et al. Cyclina2-Cyclin-Dependent kinase regulates Samhd1 protein phosphohydrolase domain. *J Biol Chem* (2015) 290(21):13279–92. doi: 10.1074/jbc.M115.646588

125. White TE, Brandariz-Nuñez A, Valle-Casuso JC, Amie S, Nguyen LA, Kim B, et al. The retroviral restriction ability of Samhd1, but not its deoxynucleotide triphosphohydrolase activity, is regulated by phosphorylation. *Cell Host Microbe* (2013) 13(4):441–51. doi: 10.1016/j.chom.2013.03.005

126. Szaniawski MA, Spivak AM, Cox JE, Catrow JL, Hanley T, Williams E, et al. Samhd1 phosphorylation coordinates the anti-Hiv-1 response by diverse interferons and tyrosine kinase inhibition. *mBio* (2018) 9(3):e00819-18. doi: 10.1128/mBio.00819-18

127. Businger R, Deutschmann J, Gruska I, Milbradt J, Wiebusch L, Gramberg T, et al. Human cytomegalovirus overcomes Samhd1 restriction in macrophages *Via* Pul97. *Nat Microbiol* (2019) 4(12):2260–72. doi: 10.1038/s41564-019-0557-8

128. Zhang K, Lv DW, Li R. Conserved herpesvirus protein kinases target Samhd1 to facilitate virus replication. *Cell Rep* (2019) 28(2):449–59.e5. doi: 10.1016/j.celrep.2019.04.020

129. Chen S, Bonifati S, Qin Z, St Gelais C, Kodigepalli KM, Barrett BS, et al. Samhd1 suppresses innate immune responses to viral infections and inflammatory stimuli by inhibiting the nf-Kb and interferon pathways. *Proc Natl Acad Sci U.S.A.* (2018) 115(16):E3798–e807. doi: 10.1073/pnas.1801213115

130. Reuvers TGA, Kanaar R, Nonnekens J. DNA Damage-inducing anticancer therapies: From global to precision damage. *Cancers (Basel)* (2020) 12(8):2098. doi: 10.3390/cancers12082098

131. Jackson SP, Bartek J. The DNA-damage response in human biology and disease. *Nature* (2009) 461(7267):1071–8. doi: 10.1038/nature08467

132. Luftig MA. Viruses and the DNA damage response: Activation and antagonism. *Annu Rev Virol* (2014) 1(1):605–25. doi: 10.1146/annurev-virology-031413-085548

133. Lilley CE, Carson CT, Muotri AR, Gage FH, Weitzman MD. DNA Repair proteins affect the lifecycle of herpes simplex virus 1. *Proc Natl Acad Sci U.S.A.* (2005) 102(16):5844–9. doi: 10.1073/pnas.0501916102

134. Wilkinson DE, Weller SK. Herpes simplex virus type I disrupts the atr-dependent DNA-damage response during lytic infection. *J Cell Sci* (2006) 119(Pt 13):2695–703. doi: 10.1242/jcs.02981

135. Li R, Zhu J, Xie Z, Liao G, Liu J, Chen MR, et al. Conserved herpesvirus kinases target the DNA damage response pathway and Tip60 histone acetyltransferase to promote virus replication. *Cell Host Microbe* (2011) 10(4):390–400. doi: 10.1016/j.chom.2011.08.013

136. Yedjou CG, Tchounwou HM, Tchounwou PB. DNA Damage, cell cycle arrest, and apoptosis induction caused by lead in human leukemia cells. *Int J Environ Res Public Health* (2015) 13(1):ijerph13010056. doi: 10.3390/ijerph13010056

137. van Attikum H, Gasser SM. Crosstalk between histone modifications during the DNA damage response. *Trends Cell Biol* (2009) 19(5):207–17. doi: 10.1016/j.tcb.2009.03.001

138. Bogliolo M, Lyakhovich A, Callén E, Castellà M, Cappelli E, Ramírez MJ, et al. Histone H2ax and fanconi anemia Fancd2 function in the same pathway to maintain chromosome stability. *EMBO J* (2007) 26(5):1340–51. doi: 10.1038/sj.emboj.7601574

139. Saldivar JC, Cortez D, Cimprich KA. The essential kinase atr: Ensuring faithful duplication of a challenging genome. *Nat Rev Mol Cell Biol* (2017) 18(10):622–36. doi: 10.1038/nrm.2017.67

140. Banerjee S, Smallwood A, Hultén M. Atp-dependent reorganization of human sperm nuclear chromatin. *J Cell Sci* (1995) 108(Pt 2):755–65. doi: 10.1242/jcs.108.2.755

141. Tarakanova VL, Leung-Pineda V, Hwang S, Yang CW, Matatall K, Basson M, et al. Gamma-herpesvirus kinase actively initiates a DNA damage response by inducing phosphorylation of H2ax to foster viral replication. *Cell Host Microbe* (2007) 1(4):275–86. doi: 10.1016/j.chom.2007.05.008

142. Chen MR, Chang SJ, Huang H, Chen JY. A protein kinase activity associated with Epstein-Barr virus Bglf4 phosphorylates the viral early antigen ea-d in vitro. *J Virol* (2000) 74(7):3093–104. doi: 10.1128/jvi.74.7.3093-3104.2000

143. Mounce BC, Tsan FC, Droit L, Kohler S, Reitsma JM, Cirillo LA, et al. Gammaherpesvirus gene expression and DNA synthesis are facilitated by viral protein kinase and histone variant H2ax. *Virology* (2011) 420(2):73–81. doi: 10.1016/j.virol.2011.08.019

144. Jha HC, Upadhyay SK, M AJP, Lu J, Cai Q, Saha A, et al. H2ax phosphorylation is important for Lana-mediated kaposi's sarcoma-associated herpesvirus episome persistence. *J Virol* (2013) 87(9):5255–69. doi: 10.1128/jvi.03575-12

145. Li R, Wang L, Liao G, Guzzo CM, Matunis MJ, Zhu H, et al. Sumo binding by the Epstein-Barr virus protein kinase Bglf4 is crucial for Bglf4 function. *J Virol* (2012) 86(10):5412–21. doi: 10.1128/jvi.00314-12

146. Ming X, Bo Z, Miao Y, Chen H, Bao C, Sun L, et al. Pseudorabies virus kinase Ul13 phosphorylates H2ax to foster viral replication. *FASEB J* (2022) 36(3):e22221. doi: 10.1096/fj.202101360RR

147. Yamamoto T, Ali MA, Liu X, Cohen JI. Activation of H2ax and atm in varicella-zoster virus (Vzv)-infected cells is associated with expression of specific vzv genes. *Virology* (2014) 452-453:52–8. doi: 10.1016/j.virol.2013.12.039

148. Daikoku T, Kudoh A, Sugaya Y, Iwahori S, Shirata N, Isomura H, et al. Postreplicative mismatch repair factors are recruited to Epstein-Barr virus replication compartments. *J Biol Chem* (2006) 281(16):11422–30. doi: 10.1074/jbc.M510314200

149. Wilkinson DE, Weller SK. Recruitment of cellular recombination and repair proteins to sites of herpes simplex virus type 1 DNA replication is dependent on the composition of viral proteins within prereplicative sites and correlates with the induction of the DNA damage response. *J Virol* (2004) 78(9):4783–96. doi: 10.1128/jvi.78.9.4783-4796.2004

150. Taylor TJ, Knipe DM. Proteomics of herpes simplex virus replication compartments: Association of cellular DNA replication, repair, recombination, and chromatin remodeling proteins with Icp8. *J Virol* (2004) 78(11):5856–66. doi: 10.1128/jvi.78.11.5856-5866.2004

151. Bhatt AP, Wong JP, Weinberg MS, Host KM, Giffin LC, Buijnink J, et al. A viral kinase mimics S6 kinase to enhance cell proliferation. *Proc Natl Acad Sci U.S.A.* (2016) 113(28):7876–81. doi: 10.1073/pnas.1600587113

152. Kawaguchi Y, Matsumura T, Roizman B, Hirai K. Cellular elongation factor 1delta is modified in cells infected with representative alpha-, beta-, or gammaherpesviruses. *J Virol* (1999) 73(5):4456–60. doi: 10.1128/jvi.73.5.4456-4460.1999

153. Kato K, Kawaguchi Y, Tanaka M, Igarashi M, Yokoyama A, Matsuda G, et al. Epstein-Barr Virus-encoded protein kinase Bglf4 mediates hyperphosphorylation of cellular elongation factor 1delta (Ef-1delta): Ef-1delta is universally modified by conserved protein kinases of herpesviruses in mammalian cells. *J Gen Virol* (2001) 82(Pt 6):1457–63. doi: 10.1099/0022-1317-82-6-1457

154. Kawaguchi Y, Van Sant C, Roizman B. Eukaryotic elongation factor 1delta is hyperphosphorylated by the protein kinase encoded by the U(L)13 gene of

herpes simplex virus 1. *J Virol* (1998) 72(3):1731–6. doi: 10.1128/jvi.72.3.1731-1736.1998

155. Boutell C, Cuchet-Lourenço D, Vanni E, Orr A, Glass M, McFarlane S, et al. A viral ubiquitin ligase has substrate preferential sumo targeted ubiquitin ligase activity that counteracts intrinsic antiviral defence. *PloS Pathog* (2011) 7(9): e1002245. doi: 10.1371/journal.ppat.1002245

156. Tatham MH, Geoffroy MC, Shen L, Plechanovova A, Hattersley N, Jaffray EG, et al. Rnf4 is a poly-Sumo-Specific E3 ubiquitin ligase required for arsenic-induced pml degradation. *Nat Cell Biol* (2008) 10(5):538–46. doi: 10.1038/ncb1716

157. Liu J, Wu Z, Han D, Wei C, Liang Y, Jiang T, et al. Mesencephalic astrocyte-derived neurotrophic factor inhibits liver cancer through small ubiquitin-related modifier (Sumo)Ylation-related suppression of nf-Kb/Snail signaling pathway and epithelial-mesenchymal transition. *Hepatology* (2020) 71(4):1262–78. doi: 10.1002/hep.30917

158. Kubota T, Matsuoka M, Chang TH, Tailor P, Sasaki T, Tashiro M, et al. Virus infection triggers sumoylation of Irf3 and Irf7, leading to the negative regulation of type I interferon gene expression. *J Biol Chem* (2008) 283(37):25660–70. doi: 10.1074/jbc.M804479200

159. Bentz GL, Shackelford J, Pagano JS. Epstein-Barr Virus latent membrane protein 1 regulates the function of interferon regulatory factor 7 by inducing its sumoylation. *J Virol* (2012) 86(22):12251–61. doi: 10.1128/jvi.01407-12

160. Chang TH, Kubota T, Matsuoka M, Jones S, Bradfute SB, Bray M, et al. Ebola Zaire Virus blocks type I interferon production by exploiting the host sumo modification machinery. *PloS Pathog* (2009) 5(6):e1000493. doi: 10.1371/journal.ppat.1000493

161. Izumiya Y, Ellison TJ, Yeh ET, Jung JU, Luciw PA, Kung HJ. Kaposi's sarcoma-associated herpesvirus K-bzip represses gene transcription *Via* sumo modification. *J Virol* (2005) 79(15):9912–25. doi: 10.1128/jvi.79.15.9912-9925.2005

162. Izumiya Y, Lin SF, Ellison T, Chen LY, Izumiya C, Luciw P, et al. Kaposi's sarcoma-associated herpesvirus K-bzip is a coregulator of K-rta: Physical association and promoter-dependent transcriptional repression. *J Virol* (2003) 77 (2):1441–51. doi: 10.1128/jvi.77.2.1441-1451.2003

163. Izumiya Y, Izumiya C, Van Geelen A, Wang DH, Lam KS, Luciw PA, et al. Kaposi's sarcoma-associated herpesvirus-encoded protein kinase and its interaction with K-bzip. *J Virol* (2007) 81(3):1072–82. doi: 10.1128/jvi.01473-06

164. Izumiya Y, Kobayashi K, Kim KY, Pochampalli M, Izumiya C, Shevchenko B, et al. Kaposi's sarcoma-associated herpesvirus K-rta exhibits sumo-targeting ubiquitin ligase (Stubl) like activity and is essential for viral reactivation. *PloS Pathog* (2013) 9(8):e1003506. doi: 10.1371/journal.ppat.1003506

165. Chang PC, Fitzgerald LD, Van Geelen A, Izumiya Y, Ellison TJ, Wang DH, et al. Kruppel-associated box domain-associated protein-1 as a latency regulator for kaposi's sarcoma-associated herpesvirus and its modulation by the viral protein kinase. *Cancer Res* (2009) 69(14):5681–9. doi: 10.1158/0008-5472.Can-08-4570

166. Hagemeier SR, Dickerson SJ, Meng Q, Yu X, Mertz JE, Kenney SC. Sumoylation of the Epstein-Barr virus Bzlf1 protein inhibits its transcriptional activity and is regulated by the virus-encoded protein kinase. *J Virol* (2010) 84 (9):4383–94. doi: 10.1128/jvi.02369-09

167. Adamson AL, Kenney S. Epstein-Barr Virus immediate-early protein Bzlf1 is sumo-1 modified and disrupts promyelocytic leukemia bodies. *J Virol* (2001) 75 (5):2388–99. doi: 10.1128/jvi.75.5.2388-2399.2001

168. Avey D, Tepper S, Pifer B, Bahga A, Williams H, Gillen J, et al. Discovery of a coregulatory interaction between kaposi's sarcoma-associated herpesvirus Orf45 and the viral protein kinase Orf36. *J Virol* (2016) 90(13):5953–64. doi: 10.1128/jvi.00516-16

169. Asai R, Ohno T, Kato A, Kawaguchi Y. Identification of proteins directly phosphorylated by Ul13 protein kinase from herpes simplex virus 1. *Microbes Infect* (2007) 9(12-13):1434–8. doi: 10.1016/j.micinf.2007.07.008

170. Purves FC, Ogle WO, Roizman B. Processing of the herpes simplex virus regulatory protein alpha 22 mediated by the Ul13 protein kinase determines the accumulation of a subset of alpha and gamma mrnas and proteins in infected cells. *Proc Natl Acad Sci U.S.A.* (1993) 90(14):6701–5. doi: 10.1073/pnas.90.14.6701

171. Baek MC, Krosky PM, Pearson A, Coen DM. Phosphorylation of the rna polymerase ii carboxyl-terminal domain in human cytomegalovirus-infected cells and in vitro by the viral Ul97 protein kinase. *Virology* (2004) 324(1):184–93. doi: 10.1016/j.virol.2004.03.015

172. Long MC, Leong V, Schaffer PA, Spencer CA, Rice SA. Icp22 and the Ul13 protein kinase are both required for herpes simplex virus-induced modification of the Large subunit of rna polymerase ii. *J Virol* (1999) 73(7):5593–604. doi: 10.1128/jvi.73.7.5593-5604.1999

173. Jenkins HL, Spencer CA. Rna polymerase ii holoenzyme modifications accompany transcription reprogramming in herpes simplex virus type 1-infected cells. *J Virol* (2001) 75(20):9872–84. doi: 10.1128/jvi.75.20.9872-9884.2001

174. Advani SJ, Brandimarti R, Weichselbaum RR, Roizman B. The disappearance of cyclins a and b and the increase in activity of the G(2)/M-phase cellular kinase Cdc2 in herpes simplex virus 1-infected cells require expression of the Alpha22/U(S)1.5 and U(L)13 viral genes. *J Virol* (2000) 74 (1):8–15. doi: 10.1128/JVI.74.1.8-15.2000

175. Advani SJ, Weichselbaum RR, Roizman B. Cdc2 cyclin-dependent kinase binds and phosphorylates herpes simplex virus 1 U(L)42 DNA synthesis processivity factor. *J Virol* (2001) 75(21):10326–33. doi: 10.1128/jvi.75.21.10326-10333.2001

176. Advani SJ, Weichselbaum RR, Roizman B. Herpes simplex virus 1 activates Cdc2 to recruit topoisomerase ii alpha for post-DNA synthesis expression of late genes. *Proc Natl Acad Sci U.S.A.* (2003) 100(8):4825–30. doi: 10.1073/pnas.0730735100

177. Jacob RJ, Roizman B. Anatomy of herpes simplex virus DNA viii. properties of the replicating DNA. *J Virol* (1977) 23(2):394–411. doi: 10.1128/jvi.23.2.394-411.1977

178. Fraser KA, Rice SA. Herpes simplex virus immediate-early protein Icp22 triggers loss of serine 2-phosphorylated rna polymerase ii. *J Virol* (2007) 81 (10):5091–101. doi: 10.1128/jvi.00184-07

179. Durand LO, Advani SJ, Poon AP, Roizman B. The carboxyl-terminal domain of rna polymerase ii is phosphorylated by a complex containing Cdk9 and infected-cell protein 22 of herpes simplex virus 1. *J Virol* (2005) 79(11):6757–62. doi: 10.1128/jvi.79.11.6757-6762.2005

180. Morrison EE, Wang YF, Meredith DM. Phosphorylation of structural components promotes dissociation of the herpes simplex virus type 1 tegument. *J Virol* (1998) 72(9):7108–14. doi: 10.1128/jvi.72.9.7108-7114.1998

181. Ren X, Harms JS, Splitter GA. Bovine herpesvirus 1 tegument protein Vp22 interacts with histones, and the carboxyl terminus of Vp22 is required for nuclear localization. *J Virol* (2001) 75(17):8251–8. doi: 10.1128/jvi.75.17.8251-8258.2001

182. van Leeuwen H, Okuwaki M, Hong R, Chakravarti D, Nagata K, O'Hare P. Herpes simplex virus type 1 tegument protein Vp22 interacts with taf-I proteins and inhibits nucleosome assembly but not regulation of histone acetylation by inhat. *J Gen Virol* (2003) 84(Pt 9):2501–10. doi: 10.1099/vir.0.19326-0

183. Huang J, You H, Su C, Li Y, Chen S, Zheng C. Herpes simplex virus 1 tegument protein Vp22 abrogates Cgas/Sting-mediated antiviral innate immunity. *J Virol* (2018) 92(15):e00841-18. doi: 10.1128/jvi.00841-18

184. Hamza MS, Reyes RA, Izumiya Y, Wisdom R, Kung HJ, Luciw PA. Orf36 protein kinase of kaposi's sarcoma herpesvirus activates the c-jun n-terminal kinase signaling pathway. *J Biol Chem* (2004) 279(37):38325–30. doi: 10.1074/jbc.M400964200

185. Lee CP, Huang YH, Lin SF, Chang Y, Chang YH, Takada K, et al. Epstein-Barr Virus Bglf4 kinase induces disassembly of the nuclear lamina to facilitate virion production. *J Virol* (2008) 82(23):11913–26. doi: 10.1128/jvi.01100-08

186. Cano-Monreal GL, Wylie KM, Cao F, Tavis JE, Morrison LA. Herpes simplex virus 2 Ul13 protein kinase disrupts nuclear lamins. *Virology* (2009) 392 (1):137–47. doi: 10.1016/j.virol.2009.06.051

187. Kato A, Yamamoto M, Ohno T, Tanaka M, Sata T, Nishiyama Y, et al. Herpes simplex virus 1-encoded protein kinase Ul13 phosphorylates viral Us3 protein kinase and regulates nuclear localization of viral envelopment factors Ul34 and Ul31. *J Virol* (2006) 80(3):1476–86. doi: 10.1128/jvi.80.3.1476-1486.2006

188. Ng TI, Ogle WO, Roizman B. Ul13 protein kinase of herpes simplex virus 1 complexes with glycoprotein e and mediates the phosphorylation of the viral fc receptor: Glycoproteins e and I. *Virology* (1998) 241(1):37–48. doi: 10.1006/viro.1997.8963

189. Van Cleemput J, Koyuncu OO, Laval K, Engel EA, Enquist LW. Crispr/Cas9-constructed pseudorabies virus mutants reveal the importance of Ul13 in alphaherpesvirus escape from genome silencing. *J Virol* (2021) 95(6):e02286-20. doi: 10.1128/jvi.02286-20

190. Lukac DM, Renne R, Kirshner JR, Ganem D. Reactivation of kaposi's sarcoma-associated herpesvirus infection from latency by expression of the orf 50 transactivator, a homolog of the ebv r protein. *Virology* (1998) 252(2):304–12. doi: 10.1006/viro.1998.9486

191. Guito J, Lukac DM. Kshv rta promoter specification and viral reactivation. *Front Microbiol* (2012) 3:30. doi: 10.3389/fmicb.2012.00030

192. Damania B, Jeong JH, Bowser BS, DeWire SM, Staudt MR, Dittmer DP. Comparison of the Rta/Orf50 transactivator proteins of gamma-2-Herpesviruses. *J Virol* (2004) 78(10):5491–9. doi: 10.1128/jvi.78.10.5491-5499.2004

193. Simpson S, Fiches G, Jean MJ, Dieringer M, McGuinness J, John SP, et al. Inhibition of Tip60 reduces lytic and latent gene expression of kaposi's sarcoma-associated herpes virus (Kshv) and proliferation of kshv-infected tumor cells. *Front Microbiol* (2018) 9:788. doi: 10.3389/fmicb.2018.00788

194. Kedes DH, Lagunoff M, Renne R, Ganem D. Identification of the gene encoding the major latency-associated nuclear antigen of the kaposi's sarcoma-associated herpesvirus. *J Clin Invest* (1997) 100(10):2606–10. doi: 10.1172/jci119804

195. Shamay M, Liu J, Li R, Liao G, Shen L, Greenway M, et al. A protein array screen for kaposi's sarcoma-associated herpesvirus Lana interactors links Lana to

Tip60, Pp2a activity, and telomere shortening. *J Virol* (2012) 86(9):5179–91. doi: 10.1128/jvi.00169-12

196. Sylvester PA, Jondle CN, Stoltz KP, Lanham J, Dittel BN, Tarakanova VL. Conserved gammaherpesvirus protein kinase counters the antiviral effects of myeloid cell-specific Stat1 expression to promote the establishment of splenic b cell latency. *J Virol* (2021) 95(17):e0085921. doi: 10.1128/jvi.00859-21

197. Liu T, Khanna KM, Chen X, Fink DJ, Hendricks RL. Cd8(+) T cells can block herpes simplex virus type 1 (Hsv-1) reactivation from latency in sensory neurons. *J Exp Med* (2000) 191(9):1459–66. doi: 10.1084/jem.191.9.1459

198. Doherty PC, Christensen JP, Belz GT, Stevenson PG, Sangster MY. Dissecting the host response to a gamma-herpesvirus. *Philos Trans R Soc Lond B Biol Sci* (2001) 356(1408):581–93. doi: 10.1098/rstb.2000.0786

199. Hollingworth R, Horniblow RD, Forrest C, Stewart GS, Grand RJ. Localization of double-strand break repair proteins to viral replication compartments following lytic reactivation of kaposi's sarcoma-associated herpesvirus. *J Virol* (2017) 91(22):e00930-17. doi: 10.1128/jvi.00930-17

200. Zimmermann A, Wilts H, Lenhardt M, Hahn M, Mertens T. Indolocarbazoles exhibit strong antiviral activity against human cytomegalovirus and are potent inhibitors of the Pul97 protein kinase. *Antiviral Res* (2000) 48 (1):49–60. doi: 10.1016/s0166-3542(00)00118-2

201. Gershburg E, Hong K, Pagano JS. Effects of maribavir and selected indolocarbazoles on Epstein-Barr virus protein kinase Bglf4 and on viral lytic replication. *Antimicrob Agents Chemother* (2004) 48(5):1900–3. doi: 10.1128/aac.48.5.1900-1903.2004

202. Goswami R, Gershburg S, Satorius A, Gershburg E. Protein kinase inhibitors that inhibit induction of lytic program and replication of Epstein-Barr virus. *Antiviral Res* (2012) 96(3):296–304. doi: 10.1016/j.antiviral.2012.09.021

203. Hoke GD, Draper K, Freier SM, Gonzalez C, Driver VB, Zounes MC, et al. Effects of phosphorothioate capping on antisense oligonucleotide stability, hybridization and antiviral efficacy versus herpes simplex virus infection. *Nucleic Acids Res* (1991) 19(20):5743–8. doi: 10.1093/nar/19.20.5743

204. Crooke RM, Hoke GD, Shoemaker JE. *In vitro* toxicological evaluation of Isis 1082, a phosphorothioate oligonucleotide inhibitor of herpes simplex virus. *Antimicrob Agents Chemother* (1992) 36(3):527–32. doi: 10.1128/aac.36.3.527

205. Sun X, Bristol JA, Iwahori S, Hagemeier SR, Meng Q, Barlow EA, et al. Hsp90 inhibitor 17-dmag decreases expression of conserved herpesvirus protein kinases and reduces virus production in Epstein-Barr virus-infected cells. *J Virol* (2013) 87(18):10126–38. doi: 10.1128/jvi.01671-13

206. Lv L, Liu X, Jiang C, Wang X, Cao M, Bai J, et al. Pathogenicity and immunogenicity of a Gi/Ge/Tk/Ul13-Gene-Deleted variant pseudorabies virus strain in swine. *Vet Microbiol* (2021) 258:109104. doi: 10.1016/j.vetmic.2021.109104

207. Olotu FA, Soliman MES. Immunoinformatics prediction of potential b-cell and T-cell epitopes as effective vaccine candidates for eliciting immunogenic responses against Epstein-Barr virus. *BioMed J* (2021) 44(3):317–37. doi: 10.1016/j.bj.2020.01.002

208. Uldrick TS, Polizzotto MN, Aleman K, O'Mahony D, Wyvill KM, Wang V, et al. High-dose zidovudine plus valganciclovir for kaposi sarcoma herpesvirus-associated multicentric castleman disease: A pilot study of virus-activated cytotoxic therapy. *Blood* (2011) 117(26):6977–86. doi: 10.1182/blood-2010-11-317610

209. Wang QJ, Jenkins FJ, Jacobson LP, Kingsley LA, Day RD, Zhang ZW, et al. Primary human herpesvirus 8 infection generates a broadly specific Cd8(+) T-cell response to viral lytic cycle proteins. *Blood* (2001) 97(8):2366–73. doi: 10.1182/blood.v97.8.2366

210. Robey RC, Lagos D, Gratrix F, Henderson S, Matthews NC, Vart RJ, et al. The Cd8 and Cd4 T-cell response against kaposi's sarcoma-associated herpesvirus is skewed towards early and late lytic antigens. *PloS One* (2009) 4(6):e5890. doi: 10.1371/journal.pone.0005890

frontiers | Frontiers in Immunology

TYPE Original Research
PUBLISHED 01 December 2022
DOI 10.3389/fimmu.2022.1058884

OPEN ACCESS

EDITED BY
Chenhe Su,
Wistar Institute, United States

REVIEWED BY
Sharah Jabeen,
Bangladesh Agricultural University, Bangladesh
Yuexiu Zhang,
The Ohio State University, United States
Weizheng Liang,
First Affiliated Hospital of Hebei North University, China

*CORRESPONDENCE
Weihong Xu
xuweihong815@126.com
Wanming Wang
wangwm93@126.com

†These authors have contributed equally to this work

SPECIALTY SECTION
This article was submitted to Viral Immunology, a section of the journal Frontiers in Immunology

RECEIVED 30 September 2022
ACCEPTED 15 November 2022
PUBLISHED 01 December 2022

CITATION
Zheng Q, Lin R, Chen Y, Lv Q, Zhang J, Zhai J, Xu W and Wang W (2022) SARS-CoV-2 induces "cytokine storm" hyperinflammatory responses in RA patients through pyroptosis. *Front. Immunol.* 13:1058884. doi: 10.3389/fimmu.2022.1058884

SARS-CoV-2 induces "cytokine storm" hyperinflammatory responses in RA patients through pyroptosis

Qingcong Zheng[1†], Rongjie Lin[1†], Yuchao Chen[2†], Qi Lv[1], Jin Zhang[3], Jingbo Zhai[4], Weihong Xu[5*] and Wanming Wang[1*]

[1]Department of Orthopedics, 900th Hospital of Joint Logistics Support Force, Fuzhou, China, [2]Department of Paediatrics, Fujian Provincial Hospital South Branch, Fuzhou, China, [3]Department of Pharmacology and Toxicology, University of Mississippi Medical Center, Jackson, MS, United States, [4]Key Laboratory of Zoonose Prevention and Control at Universities of Inner Mongolia Autonomous Region, Medical College, Inner Mongolia Minzu University, Tongliao, China, [5]Department of Orthopedics, First Affiliated Hospital of Fujian Medical University, Fuzhou, China

Background: The coronavirus disease (COVID-19) is a pandemic disease that threatens worldwide public health, and rheumatoid arthritis (RA) is the most common autoimmune disease. COVID-19 and RA are each strong risk factors for the other, but their molecular mechanisms are unclear. This study aims to investigate the biomarkers between COVID-19 and RA from the mechanism of pyroptosis and find effective disease-targeting drugs.

Methods: We obtained the common gene shared by COVID-19, RA (GSE55235), and pyroptosis using bioinformatics analysis and then did the principal component analysis(PCA). The Co-genes were evaluated by Gene Ontology (GO), Kyoto Encyclopedia of Genes and Genomes (KEGG), and ClueGO for functional enrichment, the protein-protein interaction (PPI) network was built by STRING, and the k-means machine learning algorithm was employed for cluster analysis. Modular analysis utilizing Cytoscape to identify hub genes, functional enrichment analysis with Metascape and GeneMANIA, and NetworkAnalyst for gene-drug prediction. Network pharmacology analysis was performed to identify target drug-related genes intersecting with COVID-19, RA, and pyroptosis to acquire Co-hub genes and construct transcription factor (TF)-hub genes and miRNA-hub genes networks by NetworkAnalyst. The Co-hub genes were validated using GSE55457 and GSE93272 to acquire the Key gene, and their efficacy was assessed using receiver operating curves (ROC); SPEED2 was then used to determine the upstream pathway. Immune cell infiltration was analyzed using CIBERSORT and validated by the HPA database. Molecular docking, molecular dynamics simulation, and molecular mechanics-generalized born surface area (MM-GBSA) were used to explore and validate drug-gene relationships through computer-aided drug design.

Results: COVID-19, RA, and pyroptosis-related genes were enriched in pyroptosis and pro-inflammatory pathways(the NOD-like receptor family

pyrin domain containing 3 (NLRP3) inflammasome complex, death-inducing signaling complex, regulation of interleukin production), natural immune pathways (Network map of SARS-CoV-2 signaling pathway, activation of NLRP3 inflammasome by SARS-CoV-2) and COVID-19-and RA-related cytokine storm pathways (IL, nuclear factor-kappa B (NF-κB), TNF signaling pathway and regulation of cytokine-mediated signaling). Of these, CASP1 is the most involved pathway and is closely related to minocycline. YY1, hsa-mir-429, and hsa-mir-34a-5p play an important role in the expression of CASP1. Monocytes are high-caspase-1-expressing sentinel cells. Minocycline can generate a highly stable state for biochemical activity by docking closely with the active region of caspase-1.

Conclusions: Caspase-1 is a common biomarker for COVID-19, RA, and pyroptosis, and it may be an important mediator of the excessive inflammatory response induced by SARS-CoV-2 in RA patients through pyroptosis. Minocycline may counteract cytokine storm inflammation in patients with COVID-19 combined with RA by inhibiting caspase-1 expression.

KEYWORDS

SARS-CoV-2, COVID-19, rheumatoid arthritis, pyroptosis, caspase-1, minocycline

Introduction

In 2019, SARS-CoV-2-caused COVID-19 was recognized as a public health emergency of international concern (PHIEC) and subsequently identified as a pandemic by the World Health Organization (WHO) (1–6). SARS-CoV-2 is the third widespread coronavirus outbreak after SARS CoV in 2003 (7, 8) and MERS CoV in 2012 (9, 10). Droplets and aerosols mostly transmit SARS-CoV-2 at close range (11–13). From the COVID-19 dashboard of the Johns Hopkins Coronavirus Resource Center: As of 2022.8.28, more than 200 countries/regions worldwide have recorded over 600 million confirmed cases and over 6.48 million deaths, with a total of 12.124 billion vaccine doses administered (14). Coronaviruses (CoVs) are a group of enveloped viruses with a single-stranded RNA genome (+ssRNA) that exhibits a high mutation rate and variable recombination rates (15–17). SARS-CoV-2 is the ninth coronavirus threatening human health (18, 19) and has a high degree of host genetic variation (20–23). SARS-CoV-2 can encode 29 proteins (24, 25), consisting of 16 non-structural proteins (NSP) (26), 4 structural proteins (spike [S], envelope [E], membrane [M], and nucleocapsid [N]) (27), and 9 auxiliary proteins (28). COVID-19 is not just a respiratory disease but also a systemic disease that affects many of the body's systems and organs (29, 30). SARS-CoV-2 infection frequently disrupts the immune system (31), resulting in increased expression of autoantigens during infection and the development of autoantibodies due to the organism's potential antigenic cross-reactivity (32–34). SARS-CoV-2 is not only predisposed to the onset and progression of autoimmune diseases (35–37), but even SARS-CoV-2 vaccination can trigger autoimmune phenomena (38, 39). Consequently, patients with autoimmune illnesses have a higher risk of contracting COVID-19 (40, 41).

The COVID-19 Global Rheumatology Alliance Global Registry records: As of 2022.08.31, the most common autoimmune/rheumatic disease among COVID-19 patients is RA (40.92%) (42). RA is one of the most prevalent autoimmune diseases, with a prevalence of up to 1 percent (43–46), and its expanding population coverage has posed a significant threat to global public health (47). The three primary causes of RA development are genetic, environmental, and immunological factors (48, 49), with viruses, as part of the environmental factors, playing a significant role in the development of RA (50, 51). Correspondingly, the immunological dysregulation in RA patients favors the invasion of SARS-CoV-2 (52, 53). Additionally, the traditional use of DMARDs and glucocorticoids in RA enhances viral replication *via* immunosuppression, and the use of biological agents (e.g., TNF-α-inhibitors) also raises the likelihood of viral infection in RA (54–57). Therefore, there may be a potential mutual pathogenic factor between COVID-19 and RA that contributes to disease progression, and we need to find appropriate therapeutic agents to combat it.

Pyroptosis is an emerging form of regulated cell death (RCD) and an active area of research (58). It is caused by innate immune dysregulation and disruption of organism/cellular homeostasis due to pathogen invasion (59), as shown

by increased plasma membrane permeability, cell swelling, and rupture (60, 61). caspase-1 is one of the first pro-pyroptosis inflammatory cystathiases identified (62–65), creating NLRP3 inflammasome by binding to NLRP3, apoptosis-associated speck-like Protein (ASC), which establishes the canonical route of pyroptosis leading to cell lysis and the release of IL-1β and IL-18 (66–70). Firstly, active NLRP3 inflammasome and caspase-1 are detected in the peripheral blood and tissues of COVID-19 patients and are positively correlated with severity markers for COVID-19 (e.g., IL-6) (71). In SARS-CoV-2 infected cells, NLRP3 inflammasome and caspase-1 activity increase and promote pyroptosis and cytokine storm (72–74). Secondly, the overactivation of NLRP3 inflammasome and caspase-1 in individuals with RA's serum, synovium, and synovial fluid induces pyroptosis and inflammatory responses and is positively linked with disease activity (75–79). Thus, the caspase-1-mediated classical pyroptosis pathway may be an important cause of the vicious cycle of cytokine storm caused by the interaction between COVID-19 and RA disease. This study investigates the pathogenesis and disease targets of COVID-19 associated with RA through bioinformatics and network pharmacology analysis as well as computer-aided drug design methods and explores the drug and pharmacology of this target.

Methods

Data collection and processing

Three RA datasets (GSE55235, GSE55457, GSE93272) were screened using the National Center for Biotechnology Information (NCBI) Gene Expression Omnibus (GEO) (https://www.ncbi.nlm.nih.gov/geo/) (Table 1). GSE55235 contains synovial tissue samples from 10 RA cases and 10 healthy people. GSE55457 contains synovial tissue samples from 13 RA cases and 10 healthy people, and GSE93272 contains 232 whole blood samples from RA patients and 43 healthy people. The GeneCards database (https://www.genecards.org/) (80) platform searched for the keywords "SARS-CoV-2" and "COVID-19" and found 4055 and 4778 related genes. Xiong et al., 2020 (81), Ziegler et al., 2020 (82), and Jain et al., 2020 (83), respectively, contributed an additional 25, 17, and 28 COVID-19-related genes (Supplementary Table 1). A total of 5103 COVID-19-related genes were obtained by pooling and de-duplicating these genes. Similarly, a search of the GeneCards database using the keyword "pyroptosis" yielded 254 related genes.

Identification of co-genes

The empirical Bayesian method in the limma package (http://www.bioconductor.org/packages/release/bioc/html/limma.html) (84) was used to analyze the RA and healthy controls (HC) groups of the GSE55235 dataset in different gene expression analyses. |log2 FC| >0.5 and $P< 0.05$ as the cutoff. Further mapping of volcanoes using the ggplot2 package to reflect RA-differentially expressed genes (DEGs). Co-genes were obtained from the intersection of COVID-19, RA-DEGs (GSE55235), and pyroptosis-related genes using the Venn-diagram package in R software and subjected to PCA.

GO, KEGG, and ClueGO enrichment analyses of co-genes

For the investigation of the pathway and function of the Co-genes, the R package "clusterProfiler" (85) was used to conduct GO and KEGG enrichment analyses. Co-genes are visualized through ClueGO (a plug-in for Cytoscape, using kappa's statistical analysis method) to differentiate between up-and down-regulated genes to construct interactive gene network maps and analyze the function of target gene sets.

PPI network analysis and machine learning for the identification of hub genes

The STRING database (https://string-db.org/) (86) was utilized to analyze the Co-genes and build a PPI network with a confidence score > 0.40 as the threshold. The k-means algorithm is an effective unsupervised machine learning technique (87). It enables the prediction of protein-protein interactions without explicit data labeling. We used the k-means algorithm (the network was clustered to a specified number of clusters, the number clusters: 3) Clustering analysis of Co-genes. The Cytoscape platform (88) is utilized to visualize PPI network data, while the MCODE (a Cytoscape plug-in) is

TABLE 1 Basic information of selected datasets.

Dataset ID	Platform	Tissue(Homo sapiens)	Experimental group	Normal control	Experiment type
GSE55235	GPL96	Synovium	10	10	Array
GSE55457	GPL96	Synovium	13	10	Array
GSE93272	GPL570	Whole blood	232	43	Array

utilized for modular analysis of PPI networks. The cytoHubba uses the Degree algorithm to identify Hub genes from Co-genes.

Metascape, geneMANIA and network analyst analyses of hub genes

Metascape (https://metascape.org/gp/index.html#/main/step1) (89) is a gene function analysis website that aggregates over 40 databases and groups genes into clusters based on Terms with a $P< 0.01$, a minimum count of 3, and an enrichment factor >1.5 to group genes into clusters and find pathways for the enrichment of Hub genes and associated functional annotations. Cytoscape connected terms with similarity > 0.30 to further build a network graphic to capture the linkages between gene clusters. GeneMANIA (http://www.genemania.org) (90) is a website that integrates different databases and technologies, including Gene Expression Omnibus (GEO) and the Biological General Repository for Interaction Datasets (BioGRID), for predicting the functions of Hub genes and identifying gene priority and interconnections. NetworkAnalyst (https://www.networkanalyst.ca/) (91) is a website for visual analysis of gene expression profiling and meta-analysis. The hub genes were analyzed for associations with potentially relevant medications (DrugBank Version 5.0) by the site's Protein-drug interactions function (minimum network).

Screening for minocycline-related target genes and co-hub genes

CASP1, CASP3, and ILB in the hub genes were closely related to minocycline from NetworkAnalyst analysis. Therefore, minocycline was hypothesized to be an effective drug against this mechanism, and relevant validation was carried out. We used SwissTargetPrediction (http://www.swisstargetprediction.ch/) (92), CTD (http://ctdbase.org/) (93), Drugbank (https://go.drugbank.com/drugs/DB01017) (94) and STITCH (http://stitch.embl.de/cgi/input.pl) which are four databases to search for potentially related genes of minocycline. The STITCH database unifies drug-gene connections between more than 68,000 distinct compounds and 1.5 million genes; we utilize STITCH to visualize minocycline and target genes. COVID-19, RA-DEGs (GSE55235), pyroptosis-related genes, and minocycline-related target genes were intersected to determine the set of Co-targets. Subsequently, the Hub genes were intersected with the Co-targets to obtain Co-hub genes.

Establishment of the TF-hub genes and miRNA-hub genes network

Co-hub genes were submitted to the NetworkAnalyst platform, TFs were obtained from the ENCODE database, and miRNAs were obtained from miRTarBase and TarBase. Visualization of TF-hub genes and miRNA-hub genes network using Cytoscape.

Validation of co-hub genes and identification of key gene

To increase the reliability of the results as well as comprehensiveness, we included GSE55457 and GSE93272 as validation sets in this study. The intersection of the co-hub genes, RA-DEGs (GSE55457) and RA-DEGs (GSE93272), was identified as a key gene. Boxplot analyzed the expression of the key gene, and ROC (95) was used to determine the sensitivity and specificity of the key gene. The area under the curve (AUC) > 0.8 is considered to have a significant diagnostic value.

Upstream pathway activity

SPEED2 (https://speed2.sys-bio.net/) (96) is an upstream signaling pathway enrichment analysis platform that evaluates the significance of 16 classical signaling pathways based on *P*-values using gene set data from human cell biology research. We used the bates test in SPEED2 to predict the upstream signaling pathways of the co-hub genes and the Key gene.

Analysis of immune cell infiltration

The CIBERSORT algorithm (http://CIBERSORT.stanford.edu/) is a linear support vector regression-based methodology (97) applied to assess the makeup and number of immune cells in RA and HC. The relationship between the expression of the key gene and the abundance of immune cells in RA was revealed using person correlation coefficient analysis to find the immune cells closely related to it. The Human Protein Atlas (https://www.proteinatlas.org/) contains data on the tissue and cellular distribution and expression abundance of nearly all human proteins. The HPA database was utilized to validate the key gene-immune cell associations to guarantee the accuracy of the results.

Molecular docking

Molecular docking techniques were used to verify the affinity of minocycline to the crystal structure of the protein expressed by the Key gene. First, a two-dimensional (2D) structure of minocycline was obtained in sdf format from the Drugbank database or the PubChem database (https://pubchem.ncbi.nih.gov/) (98) for use as a ligand. Entry for Key gene obtained from Uniport database (https://www.uniprot.org/) (99) (CASP1:

P29466). Enter the entry into the RCSB PDB database (https://www.rcsb.org/) (100) and download the protein structure in pdb format to use as a receptor. Second, using ChemBio 3D Ultra 12.0 software, the 2D structure of the ligand (minocycline) was transformed to a 3D structure, optimized, and saved in mol2 format. The receptor (caspase-1) was processed using PyMOL 2.4.0 software to remove solvent molecules and ligands and then saved in pdb format. Third, After processing the ligands and receptors in Autodock 1.5.6 software and saving the results in pdbqt format, molecular docking was used to identify the activity pockets of candidate loci and export the results in gpf format. Finally, the AutoDock Vina software was used to carry out the molecular docking commands, and PyMOL 2.4.0 was used to visualize and analyze the results.

Molecular dynamics simulation and molecular mechanics-generalized born solvent accessibility

Further investigation of the dynamic properties, stability, and structural flexibility of protein-drug complexes can be done by molecular dynamics simulations. It permits the examination of the interaction between the drug and the amino acid residues of the target protein and acts as an in-depth validation of molecular docking. MD to MDS and MM-GBSA calculations are a series of workflows for computer-aided drug design to study the properties of ligand-receptor interactions.

AMBER 18 was used to examine the stability of the complexes by simulating the molecular docking of ligands and receptors using all-atom MDS of ligands and receptors. Before the simulation, the charge of the minocycline was determined using the HF-SCF (6-31G**) computation with the antechamber module and gauss 09 software. The GAFF2 small molecule force field and the ff14SB protein force field were utilized to describe, respectively, the ligand (minocycline) and the receptor (caspase-1) (101, 102). The LEaP module was utilized to introduce hydrogen atoms, and a TIP3P solvent cartridge was added at 10Å. The system's charge is then balanced by adding Na^+/Cl^-, and the topology and parameter files required for the molecular simulation are then output. Optimization of system energy *via* a 2500-step steepest descent method and a 2500-step conjugate gradient method. The system was warmed up at 200 ps and stabilized from 0 K to 298.15 K, followed by a 500 ps NVT ensemble simulation and a 500 ps equilibrium simulation. The system was warmed up at 200 ps, from 0 K to 298.15 K, followed by an NVT system simulation (isothermal isomer) at 500 ps, followed by an equilibrium simulation (isothermal isobaric) at 500 ps. The final NVT system simulation (isothermal isobaric) was carried out for 100 ns. Other parameters: truncation distance set to 10 Å, collision frequency γ set to 2 ps^{-1}, system pressure 1 atm, integration step 2 fs, trajectory saved at 10 ps intervals.

The free energy of binding between receptor and ligand is calculated by the MM/GBSA method (103, 104). The specific formula is as follows:

$$\Delta G_{bind} = \Delta G_{complex} - \left(\Delta G_{receptor} + \Delta G_{ligand}\right)$$

$$= \Delta E_{internal} + \Delta E_{VDW} + \Delta E_{elec} + \Delta G_{GB} + \Delta G_{SA}$$

$\Delta E_{internal}$: Internal energy, ΔE_{VDW} : Van der Waals interactions, ΔE_{elec} : Electrostatic interactions, ΔG_{GB} and ΔG_{SA} : solvation-free energy.

The flowchart shows all of our study's key and important procedures (Figure 1). The GitHub page for this study is HTTPS (https://github.com/zheng5862/COVID-19-RA.git).

Results

Identification of co-genes

2230 RA-DEGs were obtained from the GSE55235 dataset and visualized using volcano maps and clustered heat maps (Figures 2, 3). Co-genes are intersecting genes for COVID-19, RA-DEGs (GSE55235), and pyroptosis and include 35 genes, of which 23 are upregulated and 12 are down-regulated (Figure 4A). PCA analysis of the Co-genes in the GSE55235 dataset revealed that PC1 (54.84%) and PC2 (7.91%) confirmed the Co-genes' significant reliability and between-group variability (Figure 4B).

Functional enrichment analyses of co-genes

GO analysis showed that the biological process (BP) was mainly enriched in the immune system process (Figure 5A). Cellular component (CC) was mainly enriched in the cytoplasm, inflammasome complex, death-inducing signaling complex, NLRP3, and NLRP1 inflammasome complex (Figure 5B). Molecular function (MF) was mainly enriched in signaling receptor binding, protein domain-specific binding, cytokine receptor binding, tumor necrosis factor receptor superfamily binding, and death receptor binding (Figure 5C). The ClueGO analysis showed visually that the upregulated genes of Co-genes were mainly enriched in NLRP3 inflammasome complex, positive response to cytokine stimulus, cytokine production involved in immune response, and regulation of interleukin (IL-1β, IL-6, IL-8, IL-17) production (Figure 5D). KEGG analysis was mainly enriched in the NOD-like receptor (NLR) signaling pathway, the IL-17 signaling pathway, and the Toll-like receptor (TLR) signaling pathway (Figure 5E).

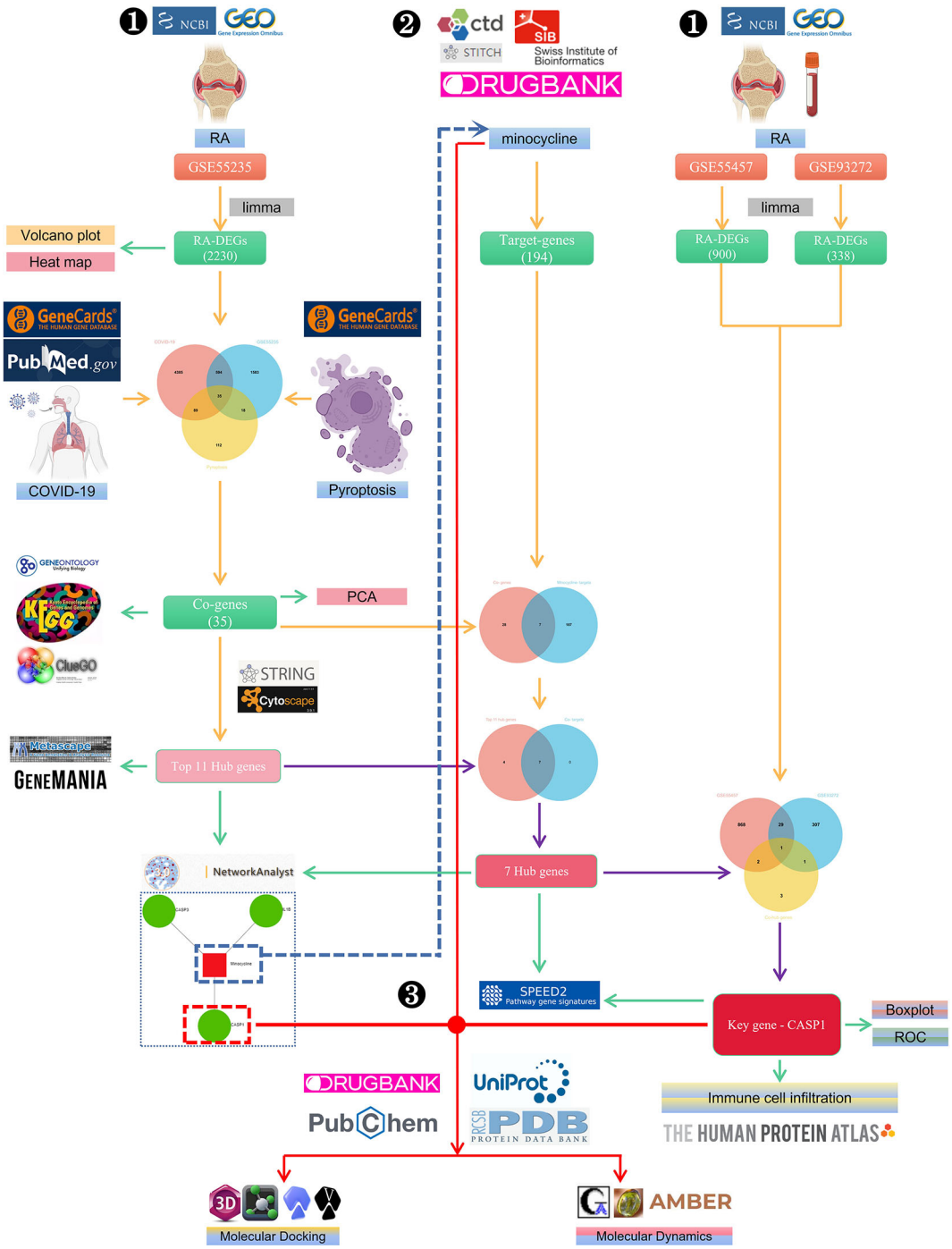

FIGURE 1
The schematic block diagram of the entire workflow of this study. ❶ Bioinformatics analysis. ❷ Network pharmacology. ❸ Computer-aided drug design.

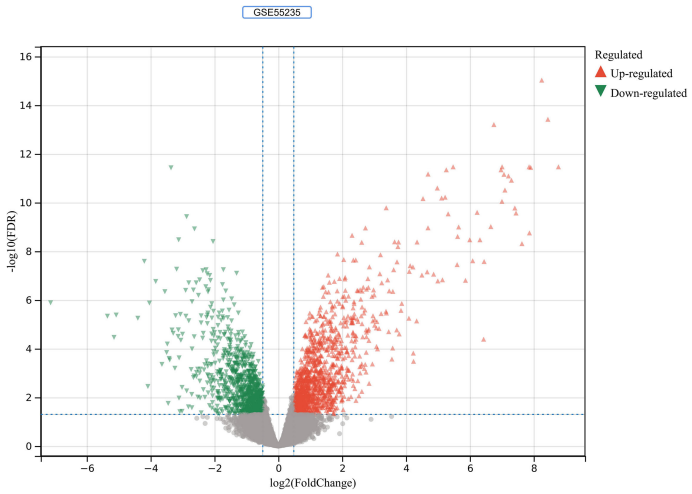

FIGURE 2
RA-DEGs identification. In the GSE55235 dataset, red triangles represent upregulated genes ($P < 0.05$), green triangles represent downregulated genes ($P < 0.05$), and gray dots represent genes not significantly differentially expressed across the RA and HC groups ($P > 0.05$).

PPI network analysis and machine learning for hub genes

This PPI network has 35 nodes, 202 edges, an average node degree of 11.5, and an average local clustering coefficient of 0.632 (Figure 6A). Using a machine learning algorithm, the k-means clustering analysis of the PPI data predicted the four genes in the lower right corner of the amplified content to be CASP1, NLRP3, IL1B, and IL18 (Figure 6B). These are the genes for the four most important proteins in the caspase-1-driven classical pyroptosis pathway. By using the degree algorithm of the CytoHubba program to the PPI data, the distribution of genes becomes specific and hierarchical, and it can be seen that the top 11 hub genes in the center of the ring were: IL1B, CASP1, CASP3, JUN, MYD88, CASP8, NLRP3, HSP90AA1, CXCL8, IL18, EGFR (where the Degree algorithm values for IL18 and EGFR were equal) (Figure 6C).

Functional network analysis of the top 11 hub genes

The results of the Metascape analysis were as follows. In pathway and process enrichment analysis, the main enrichments were in the network map of the SARS-CoV-2 signaling pathway; Nucleotide-binding oligomerization domain (NOD) pathway; and Signaling by Interleukins (Table 2) (Figure 7A). Network diagrams will allow visualization of the associations between the pathways (Figure 7B). In the PPI enrichment analysis, the main enrichments were in the NOD pathway, the activation of the NLRP3 inflammasome by SARS-CoV-2 (Figure 7C), and the NLR signaling pathway (Figure 7D). Inflammasome complex, positive regulation of cysteine-type endopeptidase activity, production of IL(LI-1β, IL-6), NF-κB signaling, TNF-mediated signaling pathway, and regulation of cytokine-mediated signaling pathway were all enriched in GeneMANIA analysis of the top 11 hub genes (Figure 8A). Of these, CASP1 is the most involved in the pathway. The protein-drug interactions function on NetworkAnalyst (DrugBank database 5.0) found minocycline to be closely related to CASP1, CASP3, and IL1B (Figure 8B).

Identification of minocycline-related target genes and co-hub genes

Top 100, 92, 12, and 10 minocycline-related target genes from SwissTargetPrediction, CTD, Drugbank, and STITCH databases, respectively (Supplementary Table 2). We can visualize the connection between minocycline, each target gene, and gene to gene in the STITCH interaction network diagram (Figure 9A). A total of 194 minocycline-related Targets were obtained by pooling the total genes and removing duplicates. Co-targets were 194 genes intersecting with COVID-19, RA-DEGs (GSE55235), and pyroptosis-related genes, including 7 genes: CASP1, CASP8, IL1B, CASP3, JUN, EGFR, CXCL8 (Figure 9B). Co-targets were intersected with the top 11 hub genes to obtain the Co-hub genes (Figure 9C). All 7 genes in the Co- Targets were contained in the top 11 hub genes, suggesting that the targets of minocycline action may be proteins of core genes involved in the pyroptosis mechanism of COVID-19 and RA.

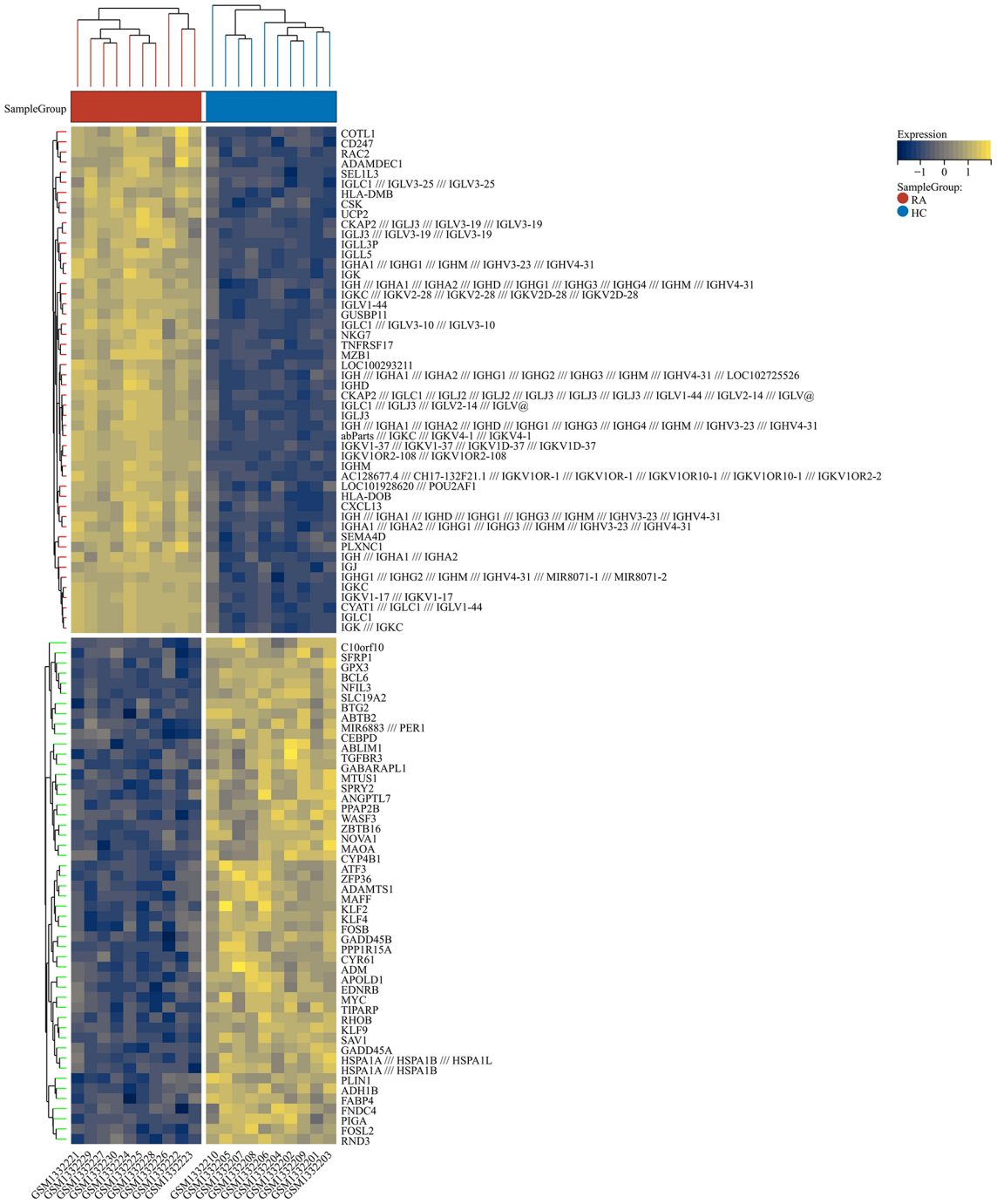

FIGURE 3
RA-DEGs distribution. The Clustering heat map displays the top one hundred DEGs from the GSE55235 dataset. The samples from the RA group were colored red, while those from the HC group were colored blue. Yellow rectangles represent highly expressed genes ($P < 0.05$), while blue rectangles represent lowly expressed genes ($P < 0.05$).

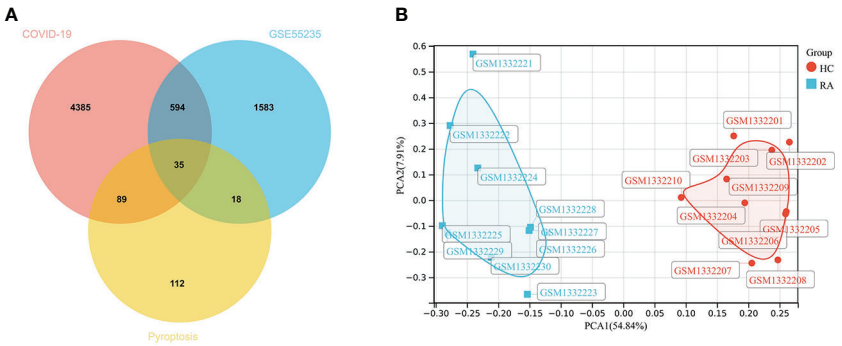

FIGURE 4
Screening Co-genes. **(A)** Venn-diagram on COVID-19, RA-DEGs (GSE55235), pyroptosis-related genes. Co-genes include 35 genes. **(B)** PCA analysis of Co-genes in the GSE55235 dataset: PC1 (54.84%) and PC2 (7.91%).

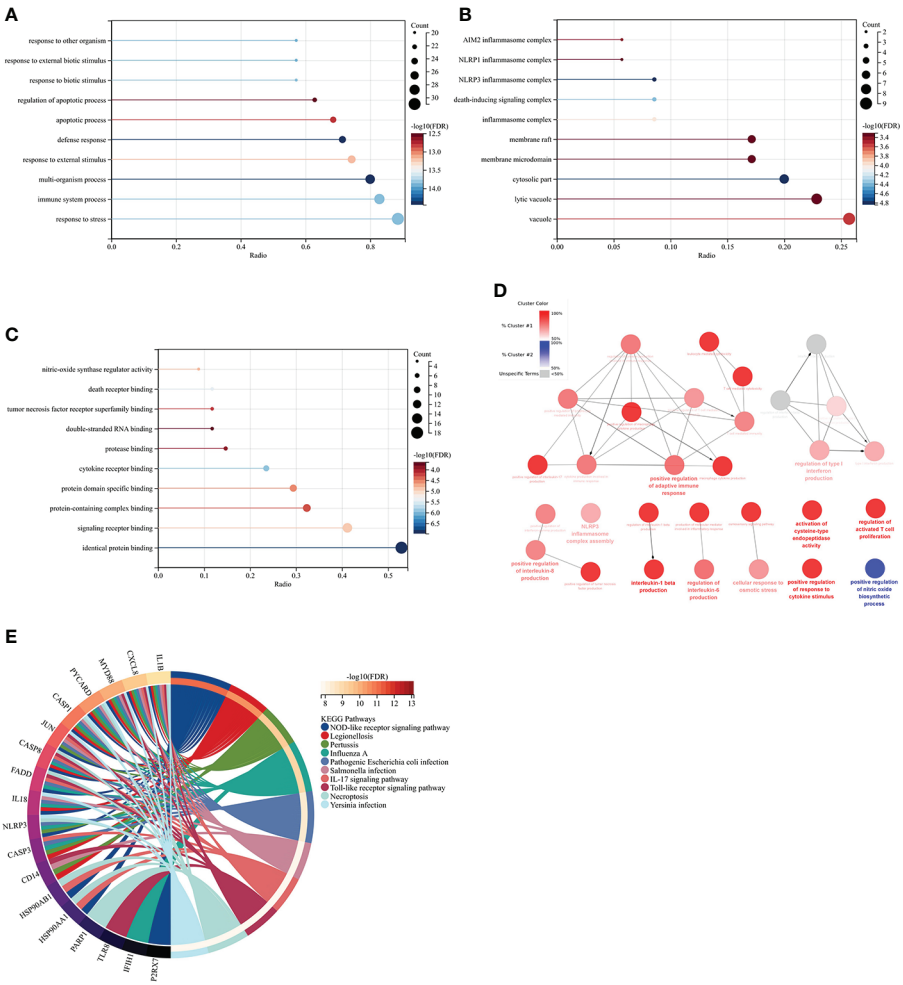

FIGURE 5
Co-genes functional enrichment analysis using GO, ClueGO, and KEGG. **(A)** Enrichment of Co-genes in BP. **(B)** Enrichment of Co-genes in CC. **(C)** Enrichment of Co-genes in MF. **(D)** Co-genes Analysis Using ClueGO. Red-denoted pathways for upregulated genes, while blue-denoted pathways for downregulated genes. **(E)** Co-genes Analysis Using KEGG.

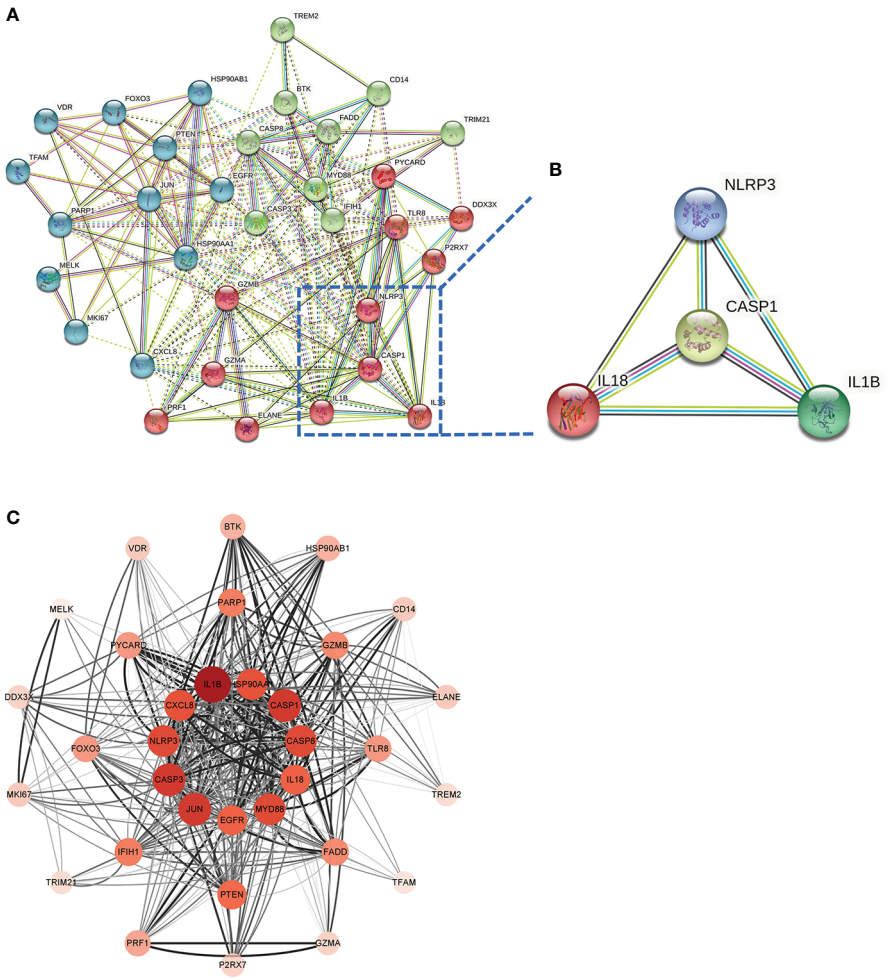

FIGURE 6
Screening Hub genes. **(A)** PPI network diagram obtained after applying the k-means algorithm based on machine learning to the Co-genes. The four genes in the lower right-hand corner of the enlarged diagram are CASP1, NLRP3, IL1B, and IL18. **(B)** PPI network diagram after processing with Cytoscape software. **(C)** The Top 11 hub genes are filtered using the Degree algorithm under the CytoHubba package condition.

TF-hub genes and miRNA-hub genes network for co-hub genes

The TF-hub genes network consists of 7 seeds, 51 edges, and 40 nodes (Figure 10A), and the simplified minimum network consists of 7 seeds, 19 edges, and 14 nodes (Figure 10B). YY1 has the potential to regulate CASP1, CASP8, and CXCL8. The miRNA-hub genes analyzed using the TarBase package consisted of 7 seeds, 407 edges, and 267 nodes (Figure 10C), and the simplified minimum network consisted of 7 seeds, 40 edges, and 17 nodes (Figure 10D). CASP1, CASP3, IL1B, CXCL8, and JUN were all closely related to hsa-mir-429. The miRNA-hub genes analyzed using the miRTarBase package consisted of 7 seeds, 210 edges, and 189 nodes (Figure 10E), and the simplified minimum network consisted of 7 seeds, 19 edges, and 14 nodes (Figure 10F). CASP1, CASP3, and CASP8 were all closely related to hsa-mir-34a-5p. In conclusion, YY1, hsa-mir-429, and hsa-mir-34a-5p may play an important role in the expression of CASP1.

Validation of co-hub genes and identification of key gene

900 DEGs were obtained from the GSE55457 validation set, of which 470 were upregulated genes and 430 were down-regulated genes (Figure 11A). 338 DEGs were obtained from the GSE93272 validation set, 322 upregulated genes, and 16 down-regulated genes (Figure 11B). The distribution of these two RA-DEGs was visualized separately using volcano plots. The only Key gene in the Venn-diagram intersection of the Co-hub genes with these two RA-DEGs is CASP1

TABLE 2 Pathway and Process Enrichment Analysis in metascape.

GO	Category	Description	Count	%	Log10(P)	Log10(q)
hsa05417	KEGG Pathway	Lipid and atherosclerosis	10	90.91	-20.53	-16.18
hsa05133	KEGG Pathway	Pertussis	7	63.64	-15.8	-12.3
WP5115	WikiPathways	Network map of SARS-CoV-2 signaling pathway	8	72.73	-14.93	-11.49
WP1433	WikiPathways	Nucleotide-binding oligomerization domain (NOD) pathway	6	54.55	-14.71	-11.31
hsa04657	KEGG Pathway	IL-17 signaling pathway	6	54.55	-12.45	-9.28
R-HSA-449147	Reactome Gene Sets	Signaling by Interleukins	8	72.73	-12.35	-9.22
WP2324	WikiPathways	AGE/RAGE pathway	5	45.45	-10.71	-7.68
hsa04625	KEGG Pathway	C-type lectin receptor signaling pathway	5	45.45	-9.7	-6.91
M110	Canonical Pathways	PID IL1 PATHWAY	4	36.36	-9.36	-6.59
WP2873	WikiPathways	Aryl hydrocarbon receptor pathway	4	36.36	-8.74	-6.09
GO:0062197	GO Biological Processes	cellular response to chemical stress	5	45.45	-7.64	-5.13
GO:0000165	GO Biological Processes	MAPK cascade	4	36.36	-6.41	-4.08
GO:0046677	GO Biological Processes	response to antibiotic	3	27.27	-6.27	-3.96
GO:1902107	GO Biological Processes	positive regulation of leukocyte differentiation	3	27.27	-4.5	-2.49

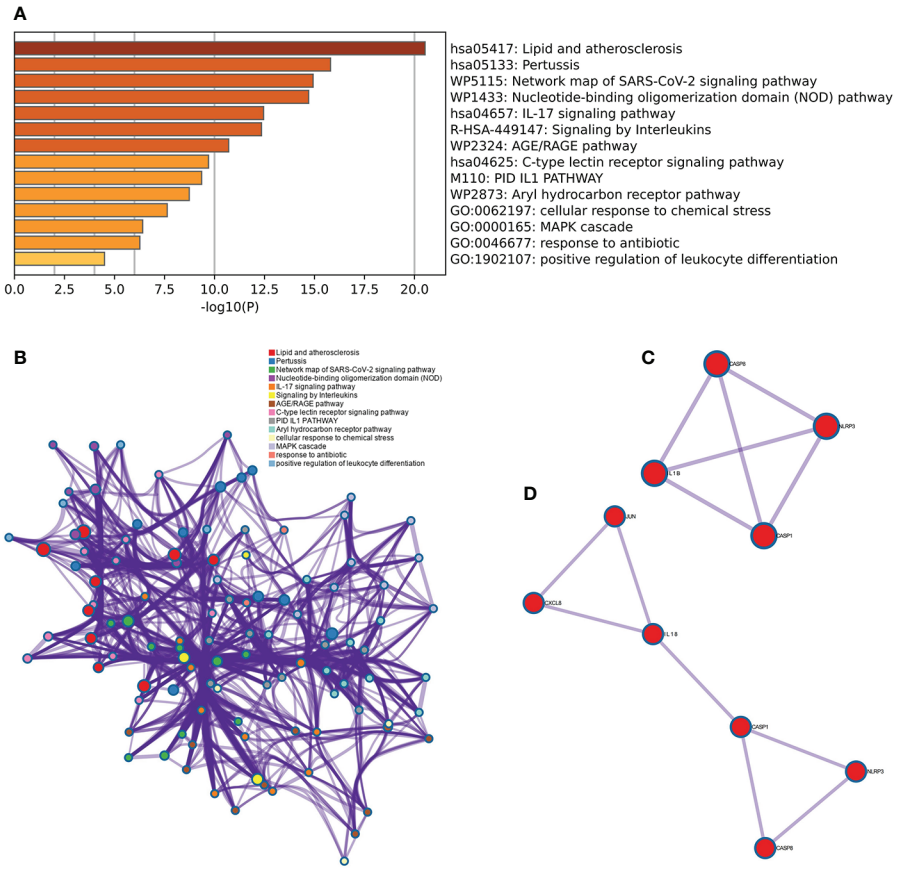

FIGURE 7
Metascape analysis of Hub genes. **(A)** Pathway and process richness analysis. **(B)** The network is shown using Cytoscape[5], with nodes with the same cluster ID typically located close to one another. **(C, D)** Protein-protein Interaction Enrichment Analysis.

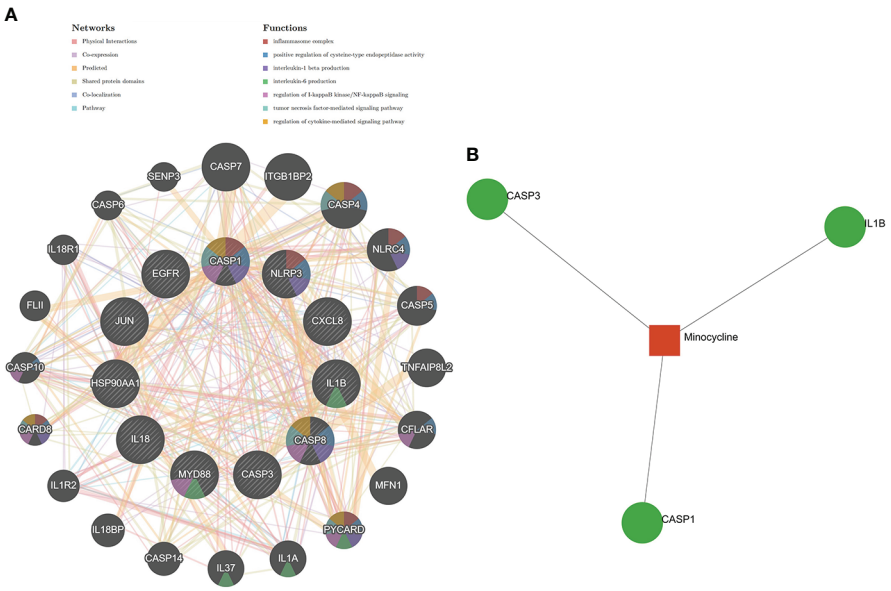

FIGURE 8
GeneMANIA and NetworkAnalyst analysis of Hub genes. **(A)** The GeneMANIA database examined the gene-gene interaction network of the top 11 hub genes and the 20 most nearby genes. Each node represents a gene. The color of the node links shows the relationship between the relevant genes. **(B)** Results for the top 11 Hub genes by NetworkAnalyst's Protein-Drug Interaction Function (DrugBank database 5.0). Drugs were in red and target genes were in green.

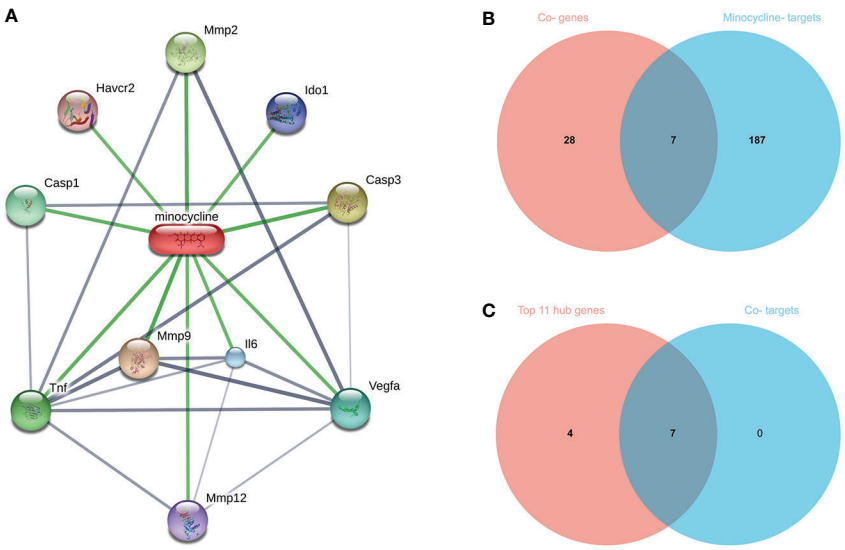

FIGURE 9
(A) Network diagram of minocycline and related target genes on the STITCH platform, with minocycline in capsules and related target genes in circles. **(B)** Venn-diagram of Co-genes versus minocycline-targets. **(C)** Venn diagram of the top 11 hub genes versus Co-targets, with Co-targets all contained in the top 11 hub genes.

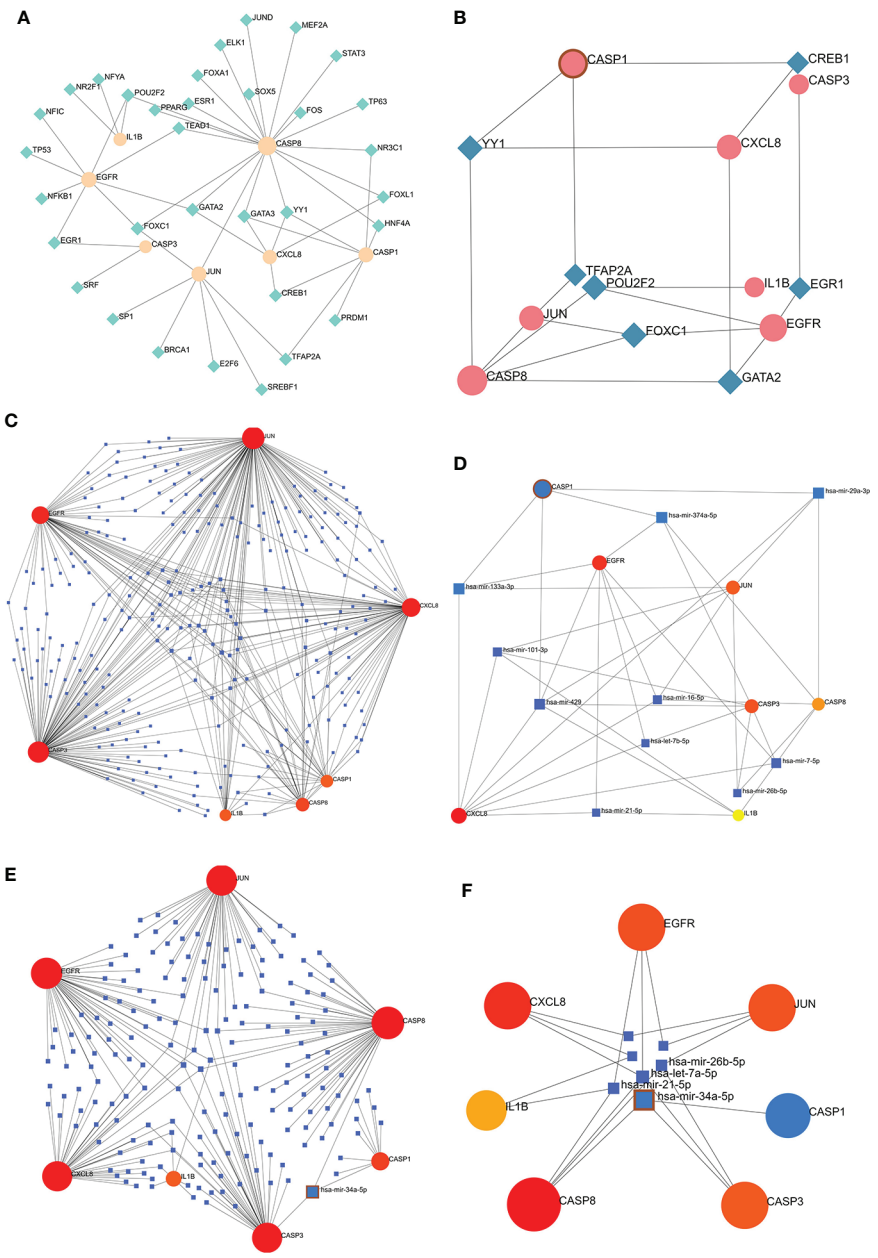

FIGURE 10
TF-hub genes and miRNA-hub genes network construction using NetworkAnalyst. **(A, B)** TF-hub genes network and simplified diagram. Circles were genes, while squares were TFs. **(C, D)** miRNA-hub genes network and simplified diagram (TarBase version 8.0). Circles represent genes, while squares are miRNAs. **(E, F)** miRNA-hub genes network and simplified diagram (miRTarBase v8.0). Circles represent genes, while squares are miRNAs.

(Figure 11C). CASP1 was highly expressed in the RA group in all three datasets ($P<0.01$) (Figures 11D–F). The AUC values of CASP1 in the GSE55235, GSE55457, and GSE93272 datasets were 0.97 (0.91-1.00), 0.88 (0.72-1.00), and 0.85 (0.79-0.90), respectively, all of which were greater than 0.8, using ROC curves to verify the diagnostic validity of CASP1 as a biomarker with good specificity and sensitivity (Figures 11G–I).

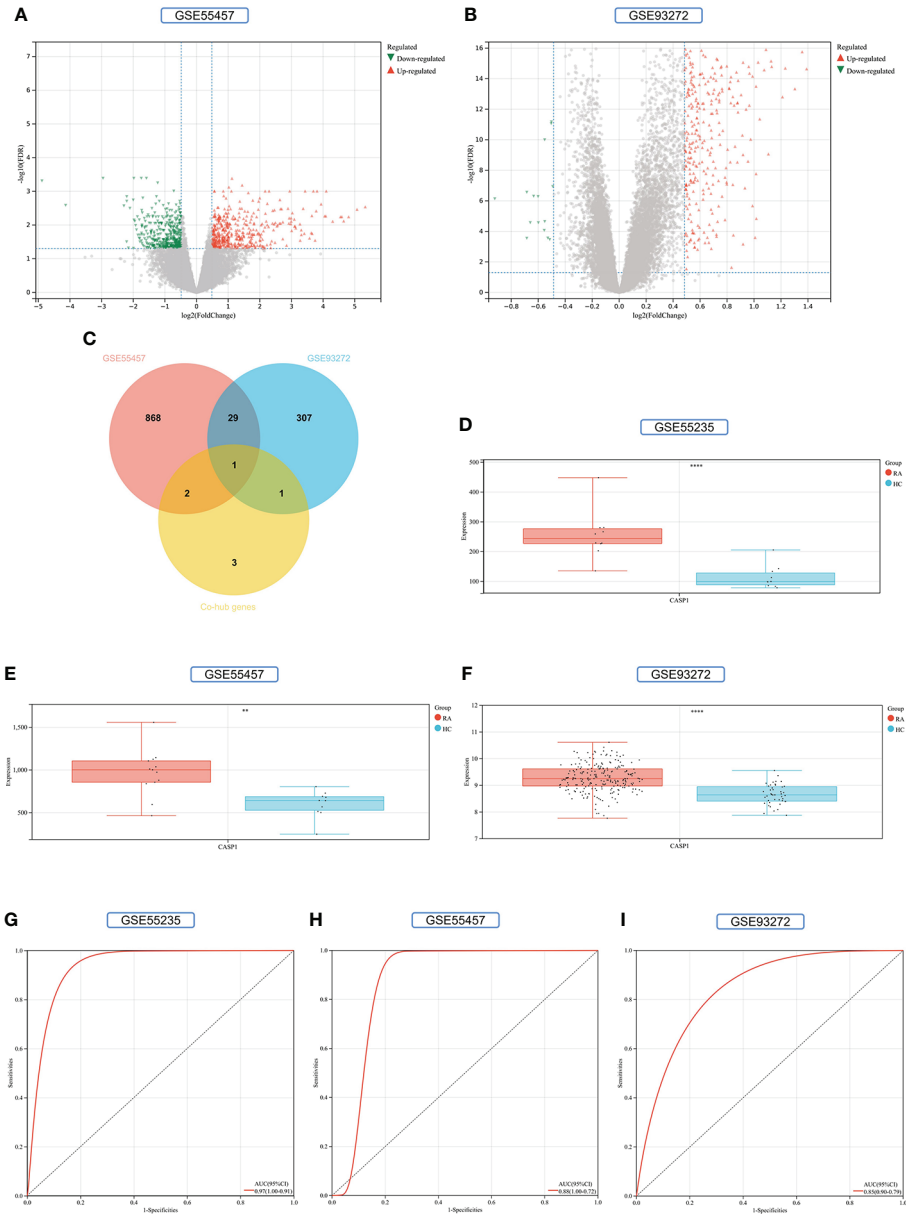

FIGURE 11
Screening and validation of key gene. **(A)** Volcano map of the GSE55457 dataset. **(B)** Volcano map of the GSE93272 dataset. Red triangles represent upregulated genes ($P < 0.05$), green triangles represent downregulated genes ($P < 0.05$), and gray dots represent genes not significantly differentially expressed across the RA and HC groups ($P > 0.05$). **(C)** Venn-diagram of RA-DEGs of GSE55457 and GSE93272 with Co-hub genes. **(D–F)** Expression of CASP1 in the GSE55235, GSE5457, and GSE93272 datasets, Red for the RA group and cyan for the HC group (**$P < 0.01$ and ****$P < 0.0001$). **(G–I)** The AUC of the ROC curve verifies the diagnostic validity of CASP1 in GSE55235, GSE55457和GSE93272 ($P < 0.05$).

Upstream pathway activity

SPEED2 analysis in the context of all human gene sets showed that Co-Hub Genes were associated with the IL-1 signaling pathway (Figure 12A), and the Key gene (CASP1) was associated with the Janus kinase/signal transducer and activator of transcription (JAK-STAT) signaling pathway (Figure 12B).

Immune infiltration analysis

In this study, LM22 immune cell infiltration data in RA (GSE93272) was obtained by the CIBERSORT algorithm. CASP1 was positively correlated with monocytes, dendritic cells activated, and neutrophils by Pearson correlation coefficient analysis (Figure 13A–C). Both the HPA and

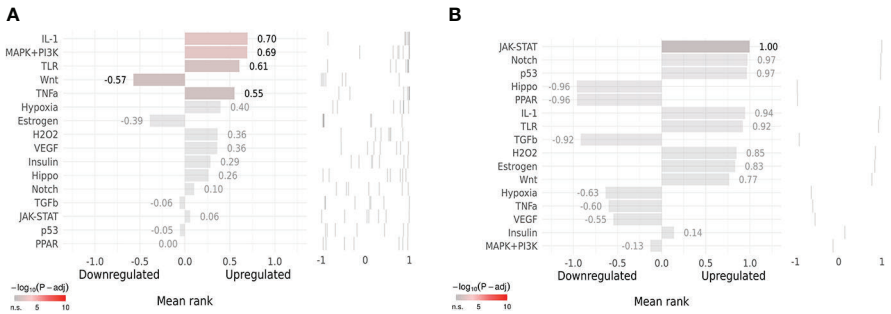

FIGURE 12
Upstream Pathway Activity. **(A, B)** SPEED2 platform analysis for Co-Hub Genes and key gene.

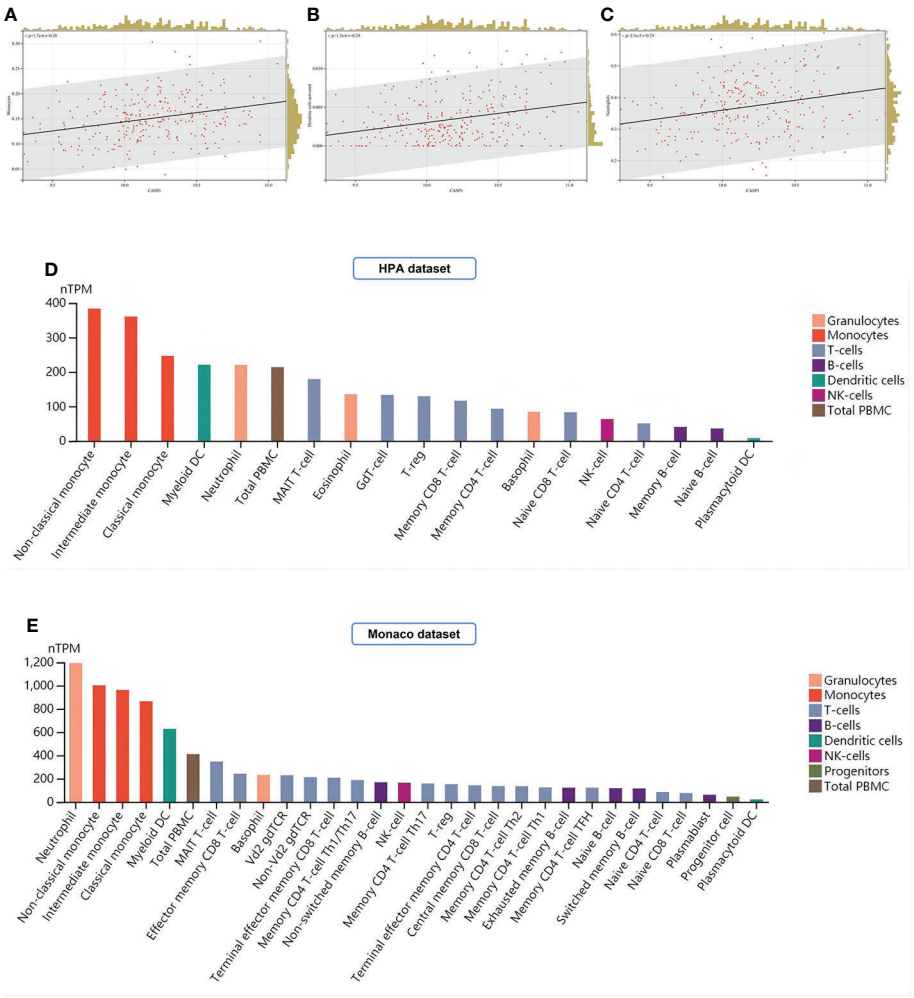

FIGURE 13
Analysis of immune cell infiltration. **(A–C)** Immune infiltrating cells positively associated with high CASP1 expression in LM22: Monocytes, Dendritic cells activated, and Neutrophils. **(D, E)** Distribution of CASP1 expression in immune cells from HPA datasets and Monaco datasets.

Monaco datasets in the HPA platform showed that the top three immune cells with high CASP1 expression were monocytes, dendritic cells (DCs), and neutrophils (Figures 13D, E), thus validating our results for immune infiltration analysis.

Molecular docking

A drug's conformation within a protein target binding site can be predicted by molecular docking, which can also predict the binding affinity. We obtained the 2D and 3D structures of minocycline (Figures 14A, B) and showed by MD analysis that minocycline forms four hydrogen bonds with the four amino acid residues ASP-157, LYS-158, SER-159, and HIS-404 of caspase-1, allowing minocycline to bind tightly to the active pocket of caspase-1 to form a stable complex (Figure 14C).

Molecular dynamics simulation and MM-GBSA

The MDS's root-mean-square deviation (RMSD) depicts the movement of caspase-1 and minocycline; a greater value and amplitude of the RMSD suggests an intense movement and vice versa for a smooth movement. In Figure 15A, caspase-1 (red line) swings widely in the early portion of the simulation, begins to converge at 40 ns and plateaus later in the simulation, and caspase-1 fluctuates within 5Å overall, indicating that there has been no major disintegration. Minocycline's (black line) value and amplitude were minor, fluctuating steadily around 1 Å and not reaching 1.5 Å. Typically, the RMSD of small molecules does not exceed 2 Å, indicating a weak conformational change. In conclusion, caspase-1 binds stably to the minocycline, almost tightly bound to the active site docked with caspase-1. The root-mean-square fluctuation (RMSF) indicates the flexibility of caspase-1 during the MDS process. When the drug attaches to the protein's active site, its flexibility diminishes, stabilizing the protein and allowing the drug to have its biochemically active action. In Figure 15B, caspase-1 is composed of Chain A and Chain B. Overall, Chain A has a lower RMSF than Chain B, indicating that Chain A is less flexible. Minocycline interacts with Chain The start sequence of caspase-1 (the yellow background highlights the binding site) and the fact that the RMSF value for this region is less than 2 Å, indicating low protein flexibility, indicates that the binding of minocycline to caspase-1 is in a highly stable state.

Based on MDS, the binding energy of minocycline to caspase-1 was determined using MM-GBSA. It can reflect the binding pattern of the medication to the protein more precisely. A negative binding energy value (ΔG_{bind}) implies that the

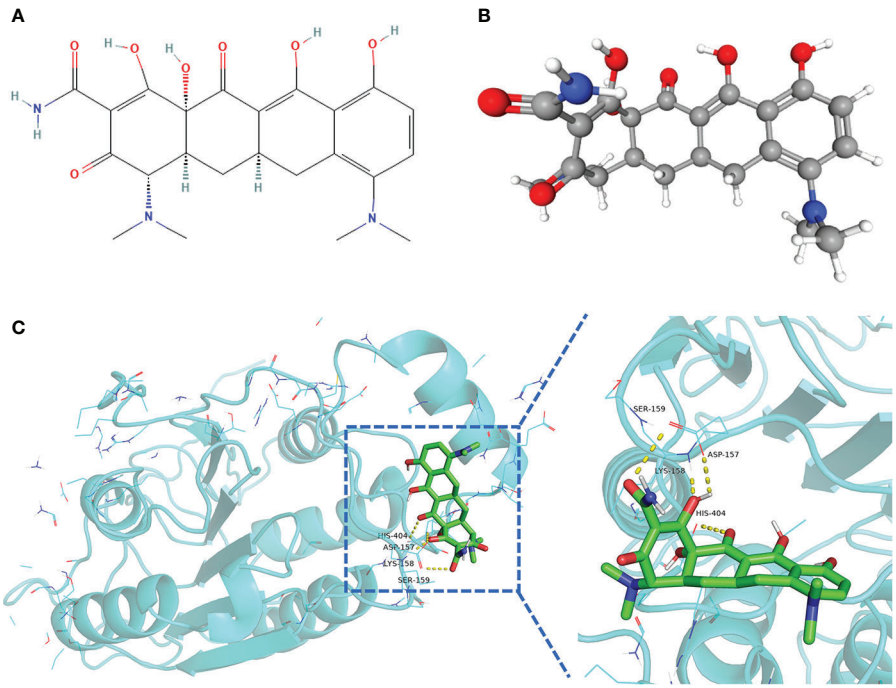

FIGURE 14
Structure of minocycline and molecular docking. **(A, B)** 2D and 3D structures of minocycline. **(C)** Results of molecular docking of minocycline with caspase-1 protein.

medication binds to the protein with affinity, whereas a smaller value indicates a greater binding capability. The binding energy of minocycline/caspase-1 was -21.43 ± 3.89 kcal/mol, showing that minocycline has a strong binding affinity for caspase-1. The energy decomposition reveals that van der Waals and electrostatic forces are the primary contributors to their binding (Table 3). The amino acid residue decomposition results of MM-GBSA can be more accurate than the active amino acid residues obtained by molecular docking. In Figure 15C, The top 10 amino acids that play a key role in minocycline/caspase-1 were: ILE-155, TRP-145, ASP-157, LEU-154, ALA-141, MET-156, GLN-142, SER-159, ARG-161. The ILE-155 ΔG_{bind} is -2.625 kcal/mol, TRP-145 is -1.513 kcal/mol, and ASP-157 is -0.967 kcal/mol (Table 4). Thus ILE-155, TRP-145, and ASP-157 are the major and maintained by hydrogen bonding minocycline/caspase-1 tightly bound amino acids. Hydrogen bonding is one of the greatest forces for the non-covalent binding of medicines and proteins, and an investigation of the number of hydrogen bonds is required to comprehend the relationship between minocycline and caspase-1. Based on MDS trajectory monitoring, we acquired the coordinates of the number of hydrogen bond formations between minocycline and caspase-1 over time. In Figure 15D, In the early part of the simulation (0-20 ns), the number of hydrogen bonds fluctuated in the range of 1-5, and in the middle and late part of the simulation (20-100 ns), the number of hydrogen bonds was mainly concentrated in 1-2. Thus, minocycline interaction with caspase-1 relies heavily on 1-2 hydrogen bonding forces.

Discussion

35 Co-genes were obtained by the intersection of COVID-19, RA (GSE55235), and pyroptosis-related genes enriched in NLR/TLR signaling pathway, NLRP3 inflammasome complex, death-inducing signaling complex, regulation of interleukin production and cytokine production involved in immune responses. The top 11 hub genes in Metascape were enriched in the network map of the SARS-CoV-2 signaling pathway, activation of the NLRP3 inflammasome by SARS-CoV-2, NLR signaling pathway, and interleukins signaling pathway. While they were enriched in GeneMANIA in inflammasome complex, IL production pathway, NF-κB signaling, TNF signaling, and regulation of cytokine-mediated signaling pathway. CASP1 was

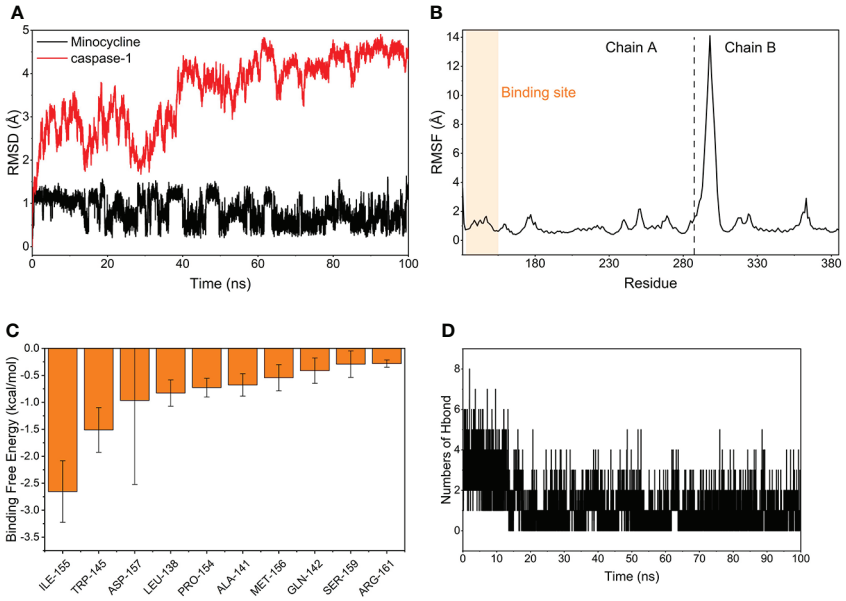

FIGURE 15
Molecular Dynamics Simulation and MM-GBSA. **(A)** Variation of the root means square deviation (RMSD) difference with time for small molecule compounds (black line) and proteins (red line) during molecular dynamics simulations. **(B)** Root mean square fluctuations (RMSF) are calculated based on molecular dynamics simulation trajectories. **(C)** The top 10 amino acids that contribute to small molecule and protein binding. **(D)** Changes in the number of hydrogen bonds between small molecules and proteins result from molecular dynamics simulations.

TABLE 3 The prediction of binding free energies and energy components by MM/GBSA.

System name	Minocycline/caspase-1(kcal/mol)
ΔE_{vdw}	-31.73±1.15
ΔE_{elec}	-33.22 ±9.62
ΔG_{GB}	47.07±5.66
ΔG_{surf}	-3.55 ±0.11
ΔG_{bind}	-21.43 ±3.89

ΔE_{vdW}: van der Waals energy.
ΔE_{elec}: electrostatic energy.
ΔG_{GB}: electrostatic contribution to solvation.
ΔG_{SA}: non-polar contribution to solvation.
ΔG_{bind}: binding free energy.

most involved in these enrichment pathways. Minocycline was found to be closely associated with CASP1 by NetworkAnalyst analysis. Therefore, based on bioinformatics analysis and further network pharmacology analysis, it was surprising to find that the 7 Co-hub genes obtained from the intersection of minocycline with COVID-19, RA (GSE55235), and pyroptosis were all contained in the top 11 hub genes of COVID-19, RA (GSE55235), and pyroptosis. One important TF (YY1) and two important miRNAs (hsa-mir-429 and hsa-mir-34a-5p) associated with CASP1 were obtained by TF-hub genes and miRNA-hub genes network. The key gene was validated by the GSE55457 and GSE93272 validation sets and obtained as CASP1, which was highly expressed in the RA group in all three datasets and validated with ROC for significantly good test performance. This gene coincided with the results of previous pathway analysis. SPEED2 analysis indicates that CASP1 is associated with the JAK-STAT signaling pathway. Immune cell infiltration analysis revealed that monocytes, dendritic cells activated, and neutrophils were able to express CASP1 at high levels, and the reliability of the results was verified by using the HPA dataset and Monaco dataset databases. Finally, the relationship between minocycline and caspase-1 was investigated and verified by MD, MDS, and MM-GBSA:

TABLE 4 The binding energy of top10 amino acids contributes to minocycline/caspase-1 binding.

Residue	ΔG_{bind}(kcal/mol)	STD
ILE-155	-2.6540984	0.571406151
TRP-145	-1.512980667	0.413772826
ASP-157	-0.966774667	1.55565844
LEU-138	-0.828761067	0.244439787
PRO-154	-0.727401867	0.173517763
ALA-141	-0.677654667	0.207741157
MET-156	-0.544312933	0.242333531
GLN-142	-0.412951867	0.235780676
SER-159	-0.292502533	0.244958839
ARG-161	-0.282	0.068203128

minocycline can dock close to the active site of caspase-1 to form a highly stable state and exert the biochemical activity of the drug.

Caspase-1 induces the classical pathway of pyroptosis

In this study, COVID-19, the crossover genes between RA and pyroptosis were enriched in the NLR/TLR signaling pathway, NLRP3 inflammasome complex, death-inducing signaling complex, regulation of interleukin production, NF-κB signaling, and TNF signaling. These pathways are all closely related to the caspase-1-induced pyroptosis pathway.

It is known that the innate immune system can recognize the viral pathogen-associated molecular pattern (PAMP) and host cell-derived damage-associated molecular pattern (DAMP) using the pathogen recognition receptor (PRR) (105–107). PRRs are divided into 2 main categories of 4 sensors: transmembrane proteins (TLRs, C-type lectin-receptors (CLRs)) and cytoplasmic proteins (RIG-I-like receptors (RLRs), NLRs) (108–110). NLRs, also known as versatile cytosolic sentinels (111, 112), play a significant role in the molecular processes (antigen presentation, inflammatory response, and cell death) linked to viral infectious diseases and autoimmune diseases (111, 113, 114). Five isoforms of NLRs, NLRA, NLRB, NLRC, NLRP, and NLRX1, activate two downstream signaling pathways: NOD1/NOD2 signaling and inflammasome signaling pathways (115), which recruit immune cells to produce pro-inflammatory cytokines (116). Caspases are a class of conserved cysteinyl proteases that activate themselves and other caspases by aspartate-specific cleavage (117) and can also cleave vast quantities of cellular substrates to drive cell death (e.g., apoptosis, pyroptosis) and inflammation (118). Caspases are classified as either apoptotic or inflammatory (119), with caspase-1 being the first member of the protease family of cysteases to be found (120) and the apical caspase of the inflammasome (121). caspase-1, one of the most typical inflammatory caspases, plays a crucial function in the regulation of pyroptosis and pro-inflammatory activities (122, 123). Since inflammatory caspases are inactive zymogens, they must be activated by the inflammasome to become proteolytically active (124). Inflammasomes are multiprotein complexes activated in response to endogenous and microbiological stimuli (125). The NLRP3 inflammasome is one of the most thoroughly researched and best-characterized inflammasomes in recent years (126), and it is the canonical activation platform for caspase-1 (127). The NLRP3 inflammasome is made up of a sensor (NLRP3), an adaptor (ASC), and an effector (caspase-1) (128). NLRP3 has a C-terminal Leucine rich repeat (LRR), a central nucleotide-binding and oligomerization domain (NACHT), and an N-terminal pyrin domain (PYD) (129, 130), whereas ASC has an

N-terminal PYD and a C-terminal caspase recruitment domain (CARD) (131). full-length caspase-1 is composed of an N-terminal CARD, a main big catalytic domain (p20), and a C-terminal small catalytic subunit domain (p10) (132). PYD and CARD structural domains belong to the death domain (DD) fold superfamily (133).

NLRP3 inflammasome requires an initiation and activation pathway. The beginning step is the NF-κB-NLRP3 axis, in which the detection of PAMP/DAMP by a particular PRR (e.g., TLR) activates the NF-κB pathway, increasing NLRP3 expression (134, 135). During the initiation phase, phosphorylation and ubiquitination are further post-translational modifications of NLRP3 (136). The activation phase is the NLRP3/ASC/pro-caspase-1/caspase-1 axis, with NLRP3 recruiting the adaptor ASC through PYD-PYD interactions (137, 138), then ASC recruiting pro-Caspase-1 through CARD-CARD interactions (139, 140). Since autocatalytic activity permits autoconversion into p33 (both CARD and p20) and p10, removing CARD from the inflammasome after secondary autoconversion of caspase-1 p33/p10 releases an enzymatically active caspase-1 tetramer comprising p20/p10 subunits (141–143). There are two primary caspase-1 effector routes. One is the cleavage of pro-IL-1β and pro-IL-18 by the p20/p10 subunit of active caspase-1, which results in the release of IL-1β and IL-18 and the initiation of an inflammatory response (144–147). The second is for active caspase-1 to cleave and activate the executioner gasdermin D (GSDMD), cleave and remove its inhibitory GSDMD-C domain, and release the GSDMD-N domain (GSDMD-NT), allowing it to generate pores in the cell membrane and initiate pyroptosis (148–150).

Therefore, pyroptosis is a classical cytolytic type of PCD induced by caspase-1 (151). The pyroptosis pathway can be activated by various viral infections (64, 152–154) and can also be induced by autoantibodies to autoimmune diseases (AID) (155, 156). COVID-19 and RA share a tight relationship with the pyroptosis mechanism, which may be one of the pathogenic mechanisms by which COVID-19 interacts with RA to induce deterioration.

Caspase-1 in COVID-19

In this study, the top 11 hub genes pathways of COVID-19, RA, and pyroptosis were enriched in the Network map of the SARS-CoV-2 signaling pathway, Activation of the NLRP3 inflammasome by SARS-CoV-2, IL, NF-κB, TNF signaling pathway and regulation of cytokine-mediated signaling pathway. Caspase-1 activation is not only a critical effector molecule in the development of acute respiratory distress syndrome (ARDS) (157, 158), but it is also a major contributor to the development of ALI (159, 160). In peripheral blood immune cells and tissues of COVID-19 patients, activated NLRP3 inflammasome, caspase-1, and high levels of GSDMD-NT were found, as well as elevated expression of IL-1β and IL-18 in serum (161–166). In animal investigations, high caspase-1 expression was also detected in the peripheral immune cells of SARS-CoV-2-infected rhesus monkeys (167). With the in-depth study of the mechanism of pyroptosis triggered by SARS-CoV-2, it was found that NSP6 in non-structural proteins (74, 168), N-protein (169), and S-protein (170) in structural proteins, and ORF3a protein (171) in auxiliary proteins all lead to overexpression and activation of NLRP3 inflammasome and caspase-1 and are positively correlated with the severity of COVID-19 (164). SARS-CoV-2 ultimately leads to an excessive inflammatory response in the form of a "cytokine storm" (172–174) and severe host cell pyroptosis (175). Cytokine storm is an uncontrolled, lethal immune disease characterized by the excessive release of pro-inflammatory cytokines and chemical mediators from immune cells (176, 177), capable of causing damage to multiple organs, including the respiratory system (165, 178), and it is believed to be a major cause of deterioration and death in COVID-19 patients (179).

In this study, immune cell infiltration analysis of COVID-19, RA, and the key gene for pyroptosis (CASP1) was found to be positively correlated with Monocytes, and the reliability of the results was verified by the HPA dataset and Monaco dataset databases. Among the numerous immune cells, monocytes play a vital part in the cytokine storm of COVID-19 patients (180). It was demonstrated that monocytes in COVID-19 patients are the outposts of SARS-CoV-2 invasion *via* TLR sensing and can release inflammatory cytokines by assembling NLRP3, activating caspase-1 to generate a "cytokine storm," and synthesizing GSDMD-NT to induce cellular pyroptosis (72, 168). Monocytes from COVID-19 patients not only overexpress IL-1β and IL-18 but also show pyroptosis morphology, suggesting that pyroptosis is a possible key mechanism for cytokine storm in COVID-19 (123, 166).

Caspase-1 in RA

The peripheral blood and synovial tissue of RA patients have been reported to contain a high level of expression and activation of the NLRP3 inflammasome and caspase-1, as well as a high level of expression of IL-1β and IL-18 (181–183). In animal investigations, inhibition of NLRP3 and caspase-1 was also found to be useful in alleviating the symptoms of arthritis in RA (CIA mouse model) (79). A cytokine network in the form of a cytokine storm, similar to that in COVID-19, is also present in RA and is a major factor in the disease's onset, persistence, and progression (184, 185). The most important pro-inflammatory cytokines in RA are IL-1β and IL-18, and the expression of these cytokines is positively correlated with active disease status (186–188). In recent years the mechanism of pyroptosis has been shown to play a key role in the development of autoimmune

diseases. In the course of the pro-inflammatory process, activation of the pyroptosis pathway causes host cells to release large amounts of pro-inflammatory cytokines and directs innate immune cells to the site of injury (119), which ultimately results in an overreactive immune response akin to a "cytokine storm" that sustains an ongoing autoimmune disease (189, 190).

In this study, immune cell infiltration analysis of the CASP1 in the RA dataset revealed that its expression was positively correlated with monocytes, dendritic cells activated, and neutrophils. It was found that high expression of NLRP3 and activated caspase-1 was detected in monocytes, dendritic cells, and neutrophils in the peripheral blood of RA patients, most notably in monocytes (181, 191, 192). Blood that circulates in the periphery Monocytes from RA patients can cleave GSDMD *via* the TLR4-NLRP3-caspase-1 pathway, resulting in pyroptosis and the production of a significant variety of cytokines, including IL-1β and IL-18, and are positively linked with disease activity (75, 193).

In conclusion, COVID-19 and RA are both capable of high expression of activated caspase-1 in peripheral blood and tissues. The invasion of SARS-CoV-2 in RA patients may enhance the caspase-1-induced pyroptosis mechanism, creating a vicious cycle of common outbreaks of "cytokine storm" and cell death, leading to increased hospitalization, morbidity, and mortality (194–197).

The JAK-STAT pathway upstream of caspase-1

In this study, the functional enrichment of the collection of Co-genes and the Top 11 Hub Genes included the regulation of IL-6 production, and the Upstream Pathway of the key gene (CASP1) was closely related to the JAK-STAT signaling pathway. The JAK/STAT pathway, also called the IL-6 signaling pathway, can be activated by IL-6 (198, 199), which is also a significant indication of COVID-19 severity (1, 200). Activation of the JAK/STAT pathway, which produces pro-inflammatory cytokines, also a significant role in the development of rheumatoid arthritis (RA) (201). Thus the JAK/STAT pathway is also one of the crosstalk pathways of COVID-19 and RA (202, 203). JAK inhibitors, represented by Tofacitinib, have been approved by the FDA to treat moderately and severely active RA (204, 205). However, it increases the risk of viral infection (206, 207). Since IFN can trigger the JAK/STAT pathway to launch a cascade response against viral infection (208), JAK inhibitors would interfere with the natural IFN/ISG antiviral immune system in the context of SARS-CoV-2 infection. Currently, the WHO only advises baricitinib for the treatment of severe COVID-19 (209), and the evidence for the use of JAK inhibitors in the treatment of COVID-19 is weak and requires additional investigation (210–212). Since the JAK/STAT pathway can promote caspase-1 expression and activation *via* cytokines (e.g., GM-CSF) and interferons (e.g., IFN-γ) (213–216), this study, in conjunction with other evidence, suggests that the NLRP3/caspase-1 pathway is a key mechanism by which COVID-19 and RA disease exacerbate each other.

Therefore, we can look for drug targets downstream of the JAK/STAT pathway to avoid interfering with the IFN/ISG system by inhibiting the JAK/STAT pathway, but also to effectively inhibit the pyroptosis link, interrupting the "cytokine storm" that erupts from each other and thus interrupting the vicious cycle. Interestingly, caspase-1 is one of the common crosstalk targets between JAK/STAT and pyroptosis pathways.

Minocycline and caspase-1

In the present COVID-19 pandemic, the discovery of new medications is challenging, time-consuming, risky, and less successful, and drug repurposing is a good option (217, 218). Minocycline is a second-generation semi-synthetic tetracycline derivative with a good safety profile (219). In addition to being a broad-spectrum antibiotic (220), it is also a broad-spectrum antiviral agent (e.g., HIV, WNV, DENV) (221–223) and possesses anti-inflammatory, antioxidant, anti-cell death (e.g., pyroptosis), immunomodulatory effects in terms of non-anti-microbial action (224–226). Fundamental investigations have demonstrated that minocycline inhibits caspase-1 activity in mice suffering from traumatic brain injury (TBI) (227); reduces the expression of caspase-1 to alleviate stress-induced depression in mice (228); acts as a caspase-1 inhibitor to delay the death of mice with Huntington's disease (229); reduces caspase-1 activity in the retina of diabetic mice (230) and suppresses caspase-1 activation in mice with acute lung injury to reduce inflammation (231). Retrospective multicentre cohort studies have shown that minocycline inhibits caspase-1 to reduce the incidence of acute renal failure (232). In conclusion, minocycline can reduce IL-1β and IL-18 levels by selectively inhibiting caspase-1 expression and activation, and it can have anti-inflammatory and anti-pyroptosis effects in the lung and throughout the body. Minocycline could play an important potential role in treating patients with COVID-19 through these properties (233) and exert a powerful antimicrobial effect against co-infections/secondary bacterial infections in patients with COVID-19 (234, 235). A current clinical study indicates that the combination of minocycline and favipiravir has significant efficacy and safety in treating COVID-19 inpatients (236). Minocycline has also demonstrated efficacy in treating COVID-19 individuals who are secluded at home (237). In addition, minocycline has been known to be clearly and effectively used in treating RA for many years (238–240).

Thus, minocycline can counteract the "cytokine storm" inflammatory response and resist pyroptosis in patients with

COVID-19 combined with RA by inhibiting the expression and activation of caspase-1. This process also indirectly demonstrates a potential caspase-1-directed pyroptosis and a shared pro-inflammatory mechanism between COVID-19 and RA, which requires further basic and clinical research.

Conclusions

Bioinformatic analysis revealed that COVID-19, RA, and pyroptosis-related genes were enriched in pyroptosis and pro-inflammatory pathways (NLR/TLR signaling pathway, NLRP3 inflammasome complex, death-inducing signaling complex, regulation of interleukin production), natural immune pathways (activation of the NLRP3 inflammasome by SARS-CoV-2) and COVID-19-and RA-related cytokine storm pathways (IL, NF-κB, TNF signaling pathway and regulation of cytokine-mediated signaling). Of these, CASP1 is involved in most pathways. The genes related to minocycline were then obtained by network pharmacology analysis and intersected with COVID-19, RA, and pyroptosis to obtain the common hub gene, and then the key gene was verified as CASP1 by two validation sets. Caspase-1 may be an important mediator of the excessive inflammatory response induced by SARS-CoV-2 in RA patients through pyroptosis. Finally, minocycline was analyzed by computer-aided drug design as an effective drug against the mechanism of caspase-1-induced pyroptosis. Our study provides insight into the causes of the high hospitalization and mortality rates of COVID-19 combined with RA from a new perspective of pyroptosis and offers potentially effective drugs that could provide new directions for further analysis of its pathogenesis and the development of targeted clinical treatments.

Data availability statement

The datasets presented in this study can be found in online repositories. The names of the repository/repositories and accession number(s) can be found in the article/Supplementary Material.

Author contributions

QZ, RL and YC: Consulted the literature and prepared materials. QZ, RL, YC, QL, JZ and JBZ: Experimented and analyzed the data. QZ, RL and YC: Drawn up the manuscript. WW and WX devised the concept and supervised the study. All authors contributed to the article and approved the submitted version.

Acknowledgments

We acknowledge the GEO and Genecards databases for providing their platforms and contributors for uploading meaningful datasets.

Conflict of interest

The authors declare that the research was conducted in the absence of any commercial or financial relationships that could be construed as a potential conflict of interest.

Publisher's note

All claims expressed in this article are solely those of the authors and do not necessarily represent those of their affiliated organizations, or those of the publisher, the editors and the reviewers. Any product that may be evaluated in this article, or claim that may be made by its manufacturer, is not guaranteed or endorsed by the publisher.

Supplementary material

The Supplementary Material for this article can be found online at: https://www.frontiersin.org/articles/10.3389/fimmu.2022.1058884/full#supplementary-material

References

1. Huang C, Wang Y, Li X, Ren L, Zhao J, Hu Y, et al. Clinical features of patients infected with 2019 novel coronavirus in wuhan, China. *Lancet* (2020) 395 (10223):497–506. doi: 10.1016/S0140-6736(20)30183-5

2. Chen N, Zhou M, Dong X, Qu J, Gong F, Han Y, et al. Epidemiological and clinical characteristics of 99 cases of 2019 novel coronavirus pneumonia in wuhan, China: a descriptive study. *Lancet* (2020) 395(10223):507–13. doi: 10.1016/S0140-6736(20)30211-7

3. Lu R, Zhao X, Li J, Niu P, Yang B, Wu H, et al. Genomic characterisation and epidemiology of 2019 novel coronavirus: implications for virus origins and receptor binding. *Lancet* (2020) 395(10224):565–74. doi: 10.1016/S0140-6736(20)30251-8

4. Poon LLM, Peiris M. Emergence of a novel human coronavirus threatening human health. *Nat Med* (2020) 26(3):317–9. doi: 10.1038/s41591-020-0796-5

5. Jiang S, Xia S, Ying T, Lu L. A novel coronavirus (2019-nCoV) causing pneumonia-associated respiratory syndrome. *Cell Mol Immunol* (2020) 17(5):554. doi: 10.1038/s41423-020-0372-4

6. Zhou P, Yang XL, Wang XG, Hu B, Zhang L, Zhang W, et al. A pneumonia outbreak associated with a new coronavirus of probable bat origin. *Nature* (2020) 579(7798):270–3. doi: 10.1038/s41586-020-2012-7

7. Parry J. WHO issues guidelines to manage any future SARS outbreak. *BMJ* (2003) 327(7412):411. doi: 10.1136/bmj.327.7412.411-a

8. Drazen JM. SARS–looking back over the first 100 days. *N Engl J Med* (2003) 349(4):319–20. doi: 10.1056/NEJMp038118

9. Assiri A, McGeer A, Perl TM, Price CS, Al Rabeeah AA, Cummings DA, et al. Hospital outbreak of middle East respiratory syndrome coronavirus. *N Engl J Med* (2013) 369(5):407–16. doi: 10.1056/NEJMoa1306742

10. de Groot RJ, Baker SC, Baric RS, Brown CS, Drosten C, Enjuanes L, et al. Middle East respiratory syndrome coronavirus (MERS-CoV): announcement of the coronavirus study group. *J Virol* (2013) 87(14):7790–2. doi: 10.1128/JVI.01244-13

11. Wiersinga WJ, Rhodes A, Cheng AC, Peacock SJ, Prescott HC. Pathophysiology, transmission, diagnosis, and treatment of coronavirus disease 2019 (COVID-19): A review. *JAMA* (2020) 324(8):782–93. doi: 10.1001/jama.2020.12839

12. Guan WJ, Ni ZY, Hu Y, Liang WH, Ou CQ, He JX, et al. China Medical treatment expert group for covid-19. clinical characteristics of coronavirus disease 2019 in China. *N Engl J Med* (2020) 382(18):1708–20. doi: 10.1056/NEJMoa2002032

13. Riou J, Althaus CL. Pattern of early human-to-human transmission of wuhan 2019 novel coronavirus (2019-nCoV), December 2019 to January 2020. *Euro Surveill.* (2020) 25(4):2000058. doi: 10.2807/1560-7917.ES.2020.25.4.2000058

14. Johns Hopkins Coronavirus Resource Center. *COVID-19 dashboard* (2021). Available at: https://coronavirus.jhu.edu/map.html.

15. Masters PS. The molecular biology of coronaviruses. *Adv Virus Res* (2006) 66:193–292. doi: 10.1016/S0065-3527(06)66005-3

16. Xu Z, Shi L, Wang Y, Zhang J, Huang L, Zhang C, et al. Pathological findings of COVID-19 associated with acute respiratory distress syndrome. *Lancet Respir Med* (2020) 8(4):420–2. doi: 10.1016/S2213-2600(20)30076-X

17. Cui J, Li F, Shi ZL. Origin and evolution of pathogenic coronaviruses. *Nat Rev Microbiol* (2019) 17(3):181–92. doi: 10.1038/s41579-018-0118-9

18. Holmes EC, Goldstein SA, Rasmussen AL, Robertson DL, Crits-Christoph A, Wertheim JO, et al. The origins of SARS-CoV-2: A critical review. *Cell* (2021) 184(19):4848–56. doi: 10.1016/j.cell.2021.08.017

19. Ye ZW, Yuan S, Yuen KS, Fung SY, Chan CP, Jin DY. Zoonotic origins of human coronaviruses. *Int J Biol Sci* (2020) 16(10):1686–97. doi: 10.7150/ijbs.45472

20. Bai C, Zhong Q, Gao GF. Overview of SARS-CoV-2 genome-encoded proteins. *Sci China Life Sci* (2022) 65(2):280–94. doi: 10.1007/s11427-021-1964-4

21. Brant AC, Tian W, Majerciak V, Yang W, Zheng ZM. SARS-CoV-2: from its discovery to genome structure, transcription, and replication. *Cell Biosci* (2021) 11(1):136. doi: 10.1186/s13578-021-00643-z

22. Tonkin-Hill G, Martincorena I, Amato R, Lawson ARJ, Gerstung M, Johnston I, et al. Wellcome Sanger institute COVID-19 surveillance team. patterns of within-host genetic diversity in SARS-CoV-2. *Elife* (2021) 10:e66857. doi: 10.7554/eLife.66857

23. Focosi D, Maggi F. Recombination in coronaviruses, with a focus on SARS-CoV-2. *Viruses* (2022) 14(6):1239. doi: 10.3390/v14061239

24. Yadav R, Chaudhary JK, Jain N, Chaudhary PK, Khanra S, Dhamija P, et al. Role of structural and non-structural proteins and therapeutic targets of SARS-CoV-2 for COVID-19. *Cells* (2021) 10(4):821. doi: 10.3390/cells10040821

25. Wong NA, Saier MHJr. The SARS-coronavirus infection cycle: A survey of viral membrane proteins, their functional interactions and pathogenesis. *Int J Mol Sci* (2021) 22(3):1308. doi: 10.3390/ijms22031308

26. Rohaim MA, El Naggar RF, Clayton E, Munir M. Structural and functional insights into non-structural proteins of coronaviruses. *Microb Pathog* (2021) 150:104641. doi: 10.1016/j.micpath.2020.104641

27. Yang H, Rao Z. Structural biology of SARS-CoV-2 and implications for therapeutic development. *Nat Rev Microbiol* (2021) 19(11):685–700. doi: 10.1038/s41579-021-00630-8

28. Naqvi AAT, Fatima K, Mohammad T, Fatima U, Singh IK, Singh A, et al. Insights into SARS-CoV-2 genome, structure, evolution, pathogenesis and therapies: Structural genomics approach. *Biochim Biophys Acta Mol Basis Dis* (2020) 1866(10):165878. doi: 10.1016/j.bbadis.2020.165878

29. Ashraf UM, Abokor AA, Edwards JM, Waigi EW, Royfman RS, Hasan SA, et al. SARS-CoV-2, ACE2 expression, and systemic organ invasion. *Physiol Genomics* (2021) 53(2):51–60. doi: 10.1152/physiolgenomics.00087.2020

30. Flaumenhaft R, Enjyoji K, Schmaier AA. Vasculopathy in COVID-19. *Blood* (2022) 140(3):222–35. doi: 10.1182/blood.2021012250

31. Kim H, Byun JE, Yoon SR, Koohy H, Jung H, Choi I. SARS-CoV-2 peptides bind to NKG2D and increase NK cell activity. *Cell Immunol* (2022) 371:104454. doi: 10.1016/j.cellimm.2021.104454

32. Saheb Sharif-Askari N, Saheb Sharif-Askari F, Ahmed SBM, Hannawi S, Hamoudi R, Hamid Q, et al. Enhanced expression of autoantigens during SARS-CoV-2 viral infection. *Front Immunol* (2021) 12:686462. doi: 10.3389/fimmu.2021.686462

33. Vojdani A, Kharrazian D. Potential antigenic cross-reactivity between SARS-CoV-2 and human tissue with a possible link to an increase in autoimmune diseases. *Clin Immunol* (2020) 217:108480. doi: 10.1016/j.clim.2020.108480

34. Dotan A, Muller S, Kanduc D, David P, Halpert G, Shoenfeld Y. The SARS-CoV-2 as an instrumental trigger of autoimmunity. *Autoimmun Rev* (2021) 20(4):102792. doi: 10.1016/j.autrev.2021.102792

35. Liu Y, Sawalha AH, Lu Q. COVID-19 and autoimmune diseases. *Curr Opin Rheumatol* (2021) 33(2):155–62. doi: 10.1097/BOR.0000000000000776

36. Zhong J, Shen G, Yang H, Huang A, Chen X, Dong L, et al. COVID-19 in patients with rheumatic disease in hubei province, China: a multicentre retrospective observational study. *Lancet Rheumatol* (2020) 2(9):e557–64. doi: 10.1016/S2665-9913(20)30227-7

37. Tang KT, Hsu BC, Chen DY. Autoimmune and rheumatic manifestations associated with COVID-19 in adults: An updated systematic review. *Front Immunol* (2021) 12:645013. doi: 10.3389/fimmu.2021.645013

38. Ishay Y, Kenig A, Tsemach-Toren T, Amer R, Rubin L, Hershkovitz Y, et al. Autoimmune phenomena following SARS-CoV-2 vaccination. *Int Immunopharmacol.* (2021) 99:107970. doi: 10.1016/j.intimp.2021.107970

39. Bartels LE, Ammitzbøll C, Andersen JB, Vils SR, Mistegaard CE, Johannsen AD, et al. Local and systemic reactogenicity of COVID-19 vaccine BNT162b2 in patients with systemic lupus erythematosus and rheumatoid arthritis. *Rheumatol Int* (2021) 41(11):1925–31. doi: 10.1007/s00296-021-04972-7

40. Ferri C, Giuggioli D, Raimondo V, L'Andolina M, Tavoni A, Cecchetti R, et al. COVID-19 & ASD Italian study group. COVID-19 and rheumatic autoimmune systemic diseases: report of a large Italian patients series. *Clin Rheumatol* (2020) 39(11):3195–204. doi: 10.1007/s10067-020-05334-7

41. Freites Nuñez DD, Leon L, Mucientes A, Rodriguez-Rodriguez L, Font Urgelles J, Madrid García A, et al. Risk factors for hospital admissions related to COVID-19 in patients with autoimmune inflammatory rheumatic diseases. *Ann Rheum Dis* (2020) 79(11):1393–9. doi: 10.1136/annrheumdis-2020-217984

42. *The COVID-19 global rheumatology alliance global registry* (2020). Available at: https://rheum-covid.org/updates/combined-data.html (Accessed 17 Aug).

43. Scott DL, Wolfe F, Huizinga TW. Rheumatoid arthritis. *Lancet* (2010) 376(9746):1094–108. doi: 10.1016/S0140-6736(10)60826-4

44. Smolen JS, Aletaha D, McInnes IB. Rheumatoid arthritis. *Lancet* (2016) 388(10055):2023–38. doi: 10.1016/S0140-6736(16)30173-8

45. McInnes IB, Schett G. The pathogenesis of rheumatoid arthritis. *N Engl J Med* (2011) 365(23):2205–19. doi: 10.1056/NEJMra1004965

46. van der Woude D, van der Helm-van Mil AHM. Update on the epidemiology, risk factors, and disease outcomes of rheumatoid arthritis. *Best Pract Res Clin Rheumatol* (2018) 32:174–87. doi: 10.1016/j.berh.2018.10.005

47. Safiri S, Kolahi AA, Hoy D, Smith E, Bettampadi D, Mansournia MA, et al. Global, regional and national burden of rheumatoid arthritis 1990-2017: A systematic analysis of the global burden of disease study 2017. *Ann Rheum Dis* (2019) 78(11):1463–71. doi: 10.1136/annrheumdis-2019-215920

48. Karami J, Aslani S, Jamshidi A, Garshasbi M, Mahmoudi M. Genetic implications in the pathogenesis of rheumatoid arthritis; an updated review. *Gene* (2019) 702:8–16. doi: 10.1016/j.gene.2019.03.033

49. Firestein GS, McInnes IB. Immunopathogenesis of rheumatoid arthritis. *Immunity* (2017) 46(2):183–96. doi: 10.1016/j.immuni.2017.02.006

50. Joo YB, Lim YH, Kim KJ, Park KS, Park YJ. Respiratory viral infections and the risk of rheumatoid arthritis. *Arthritis Res Ther* (2019) 21(1):199. doi: 10.1186/s13075-019-1977-9

51. Klatt T, Ouyang Q, Flad T, Koetter I, Bühring HJ, Kalbacher H, et al. Expansion of peripheral CD8+ CD28- T cells in response to Epstein-Barr virus in patients with rheumatoid arthritis. *J Rheumatol* (2005) 32(2):239–51.

52. van Delft MAM, Huizinga TWJ. An overview of autoantibodies in rheumatoid arthritis. *J Autoimmun* (2020) 110:102392. doi: 10.1016/j.jaut.2019.102392

53. Scherer HU, Häupl T, Burmester GR. The etiology of rheumatoid arthritis. *J Autoimmun* (2020) 110:102400. doi: 10.1016/j.jaut.2019.102400

54. Furst DE. The risk of infections with biologic therapies for rheumatoid arthritis. *Semin Arthritis Rheumatol* (2010) 39(5):327–46. doi: 10.1016/j.semarthrit.2008.10.002

55. Roongta R, Ghosh A. Managing rheumatoid arthritis during COVID-19. *Clin Rheumatol* (2020) 39(11):3237–44. doi: 10.1007/s10067-020-05358-z

56. Dixon WG. Rheumatoid arthritis: biological drugs and risk of infection. *Lancet* (2015) 386(9990):224–5. doi: 10.1016/S0140-6736(14)61907-3

57. Bongartz T, Sutton AJ, Sweeting MJ, Buchan I, Matteson EL, Montori V. Anti-TNF antibody therapy in rheumatoid arthritis and the risk of serious infections and malignancies: systematic review and meta-analysis of rare harmful

effects in randomized controlled trials. *JAMA* (2006) 295(19):2275–85. doi: 10.1001/jama.295.19.2275

58. Galluzzi L, Vitale I, Aaronson SA, Abrams JM, Adam D, Agostinis P, et al. Molecular mechanisms of cell death: recommendations of the nomenclature committee on cell death 2018. *Cell Death Differ* (2018) 25(3):486–541. doi: 10.1038/s41418-017-0012-4

59. Jorgensen I, Miao EA. Pyroptotic cell death defends against intracellular pathogens. *Immunol Rev* (2015) 265(1):130–42. doi: 10.1111/imr.12287

60. Fink SL, Cookson BT. Caspase-1-dependent pore formation during pyroptosis leads to osmotic lysis of infected host macrophages. *Cell Microbiol* (2006) 8(11):1812–25. doi: 10.1111/j.1462-5822.2006.00751.x

61. Kovacs SB, Miao EA. Gasdermins: Effectors of pyroptosis. *Trends Cell Biol* (2017) 27(9):673–84. doi: 10.1016/j.tcb.2017.05.005

62. Cookson BT, Brennan MA. Pro-inflammatory programmed cell death. *Trends Microbiol* (2001) 9(3):113–4. doi: 10.1016/s0966-842x(00)01936-3

63. Black RA, Kronheim SR, Merriam JE, March CJ, Hopp TP. A pre-aspartate-specific protease from human leukocytes that cleaves pro-interleukin-1 beta. *J Biol Chem* (1989) 264:5323–6. doi: 10.1016/S0021-9258(18)83546-3

64. Bergsbaken T, Fink SL, Cookson BT. Pyroptosis: host cell death and inflammation. *Nat Rev Microbiol* (2009) 7(2):99–109. doi: 10.1038/nrmicro2070

65. Zychlinsky A, Prevost MC, Sansonetti PJ. Shigella flexneri induces apoptosis in infected macrophages. *Nature* (1992) 358(6382):167–9. doi: 10.1038/358167a0

66. Kayagaki N, Stowe IB, Lee BL, O'Rourke K, Anderson K, Warming S, et al. Caspase-11 cleaves gasdermin d for non-canonical inflammasome signalling. *Nature* (2015) 526(7575):666–71. doi: 10.1038/nature15541

67. Qiu S, Liu J, Xing F. 'Hints' in the killer protein gasdermin d: unveiling the secrets of gasdermins driving cell death. *Cell Death Differ* (2017) 24(4):588–96. doi: 10.1038/cdd.2017.24

68. Shi J, Zhao Y, Wang K, Shi X, Wang Y, Huang H, et al. Cleavage of GSDMD by inflammatory caspases determines pyroptotic cell death. *Nature* (2015) 526 (7575):660–5. doi: 10.1038/nature15514

69. He WT, Wan H, Hu L, Chen P, Wang X, Huang Z, et al. Gasdermin d is an executor of pyroptosis and required for interleukin-1β secretion. *Cell Res* (2015) 25 (12):1285–98. doi: 10.1038/cr.2015.139

70. Liu X, Zhang Z, Ruan J, Pan Y, Magupalli VG, Wu H, et al. Inflammasome-activated gasdermin d causes pyroptosis by forming membrane pores. *Nature* (2016) 535(7610):153–8. doi: 10.1038/nature18629

71. Rodrigues TS, de Sá KSG, Ishimoto AY, Becerra A, Oliveira S, Almeida L, et al. Inflammasomes are activated in response to SARS-CoV-2 infection and are associated with COVID-19 severity in patients. *J Exp Med* (2021) 218(3): e20201707. doi: 10.1084/jem.20201707

72. Junqueira C, Crespo Â, Ranjbar S, de Lacerda LB, Lewandrowski M, Ingber J, et al. FcγR-mediated SARS-CoV-2 infection of monocytes activates inflammation. *Nature* (2022) 606(7914):576–84. doi: 10.1038/s41586-022-04702-4

73. Lara PC, Macías-Verde D, Burgos-Burgos J. Age-induced NLRP3 inflammasome over-activation increases lethality of SARS-CoV-2 pneumonia in elderly patients. *Aging Dis* (2020) 11(4):756–62. doi: 10.14336/AD.2020.0601

74. Sun X, Liu Y, Huang Z, Xu W, Hu W, Yi L, et al. SARS-CoV-2 non-structural protein 6 triggers NLRP3-dependent pyroptosis by targeting ATP6AP1. *Cell Death Differ* (2022) 29(6):1240–54. doi: 10.1038/s41418-021-00916-7

75. Wu XY, Li KT, Yang HX, Yang B, Lu X, Zhao LD, et al. Complement C1q synergizes with PTX3 in promoting NLRP3 inflammasome over-activation and pyroptosis in rheumatoid arthritis. *J Autoimmun* (2020) 106:102336. doi: 10.1016/j.jaut.2019.102336

76. Spel L, Martinon F. Inflammasomes contributing to inflammation in arthritis. *Immunol Rev* (2020) 294(1):48–62. doi: 10.1111/imr.12839

77. Zhang Y, Yang W, Li W, Zhao Y. NLRP3 inflammasome: Checkpoint connecting innate and adaptive immunity in autoimmune diseases. *Front Immunol* (2021) 12:732933. doi: 10.3389/fimmu.2021.732933

78. Shen HH, Yang YX, Meng X, Luo XY, Li XM, Shuai ZW, et al. NLRP3: A promising therapeutic target for autoimmune diseases. *Autoimmun Rev* (2018) 17(7):694–702. doi: 10.1016/j.autrev.2018.01.020

79. Guo C, Fu R, Wang S, Huang Y, Li X, Zhou M, et al. NLRP3 inflammasome activation contributes to the pathogenesis of rheumatoid arthritis. *Clin Exp Immunol* (2018) 194(2):231–43. doi: 10.1111/cei.13167

80. Safran M, Dalah I, Alexander J, Rosen N, Iny Stein T, Shmoish M, et al. GeneCards version 3: the human gene integrator. *Database (Oxford).* (2010) 2010: baq020. doi: 10.1093/database/baq020

81. Xiong Y, Liu Y, Cao L, Wang D, Guo M, Jiang A, et al. Transcriptomic characteristics of bronchoalveolar lavage fluid and peripheral blood mononuclear cells in COVID-19 patients. *Emerg Microbes Infect* (2020) 9(1):761–70. doi: 10.1080/22221751.2020.1747363

82. Ziegler CGK, Allon SJ, Nyquist SK, Mbano IM, Miao VN, Tzouanas CN, et al. HCA lung biological network. electronic address: lung-network@humancellatlas.org; HCA lung biological network. SARS-CoV-2 receptor ACE2 is an interferon-stimulated gene in human airway epithelial cells and is detected in specific cell subsets across tissues. *Cell* (2020) 181(5):1016–1035.e19. doi: 10.1016/j.cell.2020.04.035

83. Jain R, Ramaswamy S, Harilal D, Uddin M, Loney T, Nowotny N, et al. Host transcriptomic profiling of COVID-19 patients with mild, moderate, and severe clinical outcomes. *Comput Struct Biotechnol J* (2020) 19:153–60. doi: 10.1016/j.csbj.2020.12.016

84. Ritchie ME, Phipson B, Wu D, Hu Y, Law CW, Shi W, et al. Limma powers differential expression analyses for RNA-sequencing and microarray studies. *Nucleic Acids Res* (2015) 43(7):e47. doi: 10.1093/nar/gkv007

85. Yu G, Wang LG, Han Y, He QY. clusterProfiler: an r package for comparing biological themes among gene clusters. *OMICS* (2012) 16(5):284–7. doi: 10.1089/omi.2011.0118

86. Szklarczyk D, Gable AL, Lyon D, Junge A, Wyder S, Huerta-Cepas J, et al. STRING v11: protein-protein association networks with increased coverage, supporting functional discovery in genome-wide experimental datasets. *Nucleic Acids Res* (2019) 47(D1):D607–13. doi: 10.1093/nar/gky1131

87. Sarkar D, Saha S. Machine-learning techniques for the prediction of protein-protein interactions. *J Biosci* (2019) 44(4):104. doi: 10.1007/s12038-019-9909-z

88. Shannon P, Markiel A, Ozier O, Baliga NS, Wang JT, Ramage D, et al. Cytoscape: a software environment for integrated models of biomolecular interaction networks. *Genome Res* (2003) 13(11):2498–504. doi: 10.1101/gr.1239303

89. Zhou Y, Zhou B, Pache L, Chang M, Khodabakhshi AH, Tanaseichuk O, et al. Metascape provides a biologist-oriented resource for the analysis of systems-level datasets. *Nat Commun* (2019) 10(1):1523. doi: 10.1038/s41467-019-09234-6

90. Warde-Farley D, Donaldson SL, Comes O, Zuberi K, Badrawi R, Chao P, et al. The GeneMANIA prediction server: biological network integration for gene prioritization and predicting gene function. *Nucleic Acids Res* (2010) 38(Web Server issue):W214–2. doi: 10.1093/nar/gkq537

91. Zhou G, Soufan O, Ewald J, Hancock REW, Basu N, Xia J. NetworkAnalyst 3.0: a visual analytics platform for comprehensive gene expression profiling and meta-analysis. *Nucleic Acids Res* (2019) 47(W1):W234–41. doi: 10.1093/nar/gkz240

92. Gfeller D, Grosdidier A, Wirth M, Daina A, Michielin O, Zoete V. SwissTargetPrediction: a web server for target prediction of bioactive small molecules. *Nucleic Acids Res* (2014) 42(Web Server issue):W32–8. doi: 10.1093/nar/gku293

93. Davis AP, Grondin CJ, Johnson RJ, Sciaky D, Wiegers J, Wiegers TC, et al. Comparative toxicogenomics database (CTD): update 2021. *Nucleic Acids Res* (2021) 49(D1):D1138–43. doi: 10.1093/nar/gkaa891

94. Wishart DS, Feunang YD, Guo AC, Lo EJ, Marcu A, Grant JR, et al. DrugBank 5.0: a major update to the DrugBank database for 2018. *Nucleic Acids Res* (2018) 46(D1):D1074–82. doi: 10.1093/nar/gkx1037

95. Robin X, Turck N, Hainard A, Tiberti N, Lisacek F, Sanchez JC, et al. pROC: an open-source package for r and s+ to analyze and compare ROC curves. *BMC Bioinf* (2011) 12:77. doi: 10.1186/1471-2105-12-77

96. Rydenfelt M, Klinger B, Klünemann M, Blüthgen N. SPEED2: inferring upstream pathway activity from differential gene expression. *Nucleic Acids Res* (2020) 48(W1):W307–12. doi: 10.1093/nar/gkaa236

97. Chen B, Khodadoust MS, Liu CL, Newman AM, Alizadeh AA. Profiling tumor infiltrating immune cells with CIBERSORT. *Methods Mol Biol* (2018) 1711:243–59. doi: 10.1007/978-1-4939-7493-1_12

98. Kim S, Chen J, Cheng T, Gindulyte A, He J, He S, et al. PubChem in 2021: new data content and improved web interfaces. *Nucleic Acids Res* (2021) 49(D1): D1388–95. doi: 10.1093/nar/gkaa971

99. UniProt Consortium. UniProt: the universal protein knowledgebase in 2021. *Nucleic Acids Res* (2021) 49(D1):D480–9. doi: 10.1093/nar/gkaa1100

100. Berman HM, Westbrook J, Feng Z, Gilliland G, Bhat TN, Weissig H, et al. The protein data bank. *Nucleic Acids Res* (2000) 28(1):235–42. doi: 10.1093/nar/28.1.235

101. Wang J, Wolf RM, Caldwell JW, Kollman PA, Case DA. Development and testing of a general amber force field. *J Comput Chem* (2004) 25(9):1157–74. doi: 10.1002/jcc.20035

102. Maier JA, Martinez C, Kasavajhala K, Wickstrom L, Hauser KE, Simmerling C. ff14SB: Improving the accuracy of protein side chain and backbone parameters from ff99SB. *J Chem Theory Comput* (2015) 11(8):3696–713. doi: 10.1021/acs.jctc.5b00255

103. Genheden S, Ryde U. The MM/PBSA and MM/GBSA methods to estimate ligand-binding affinities. *Expert Opin Drug Discovery* (2015) 10(5):449–61. doi: 10.1517/17460441.2015.1032936

104. Rastelli G, Del Rio A, Degliesposti G, Sgobba M. Fast and accurate predictions of binding free energies using MM-PBSA and MM-GBSA. *J Comput Chem* (2010) 31(4):797–810. doi: 10.1002/jcc.21372

105. Sellge G, Kufer TA. PRR-signaling pathways: Learning from microbial tactics. *Semin Immunol* (2015) 27(2):75–84. doi: 10.1016/j.smim.2015.03.009

106. Carty M, Guy C, Bowie AG. Detection of viral infections by innate immunity. *Biochem Pharmacol* (2021) 183:114316. doi: 10.1016/j.bcp.2020.114316

107. Iwasaki A, Medzhitov R. Control of adaptive immunity by the innate immune system. *Nat Immunol* (2015) 16(4):343–53. doi: 10.1038/ni.3123

108. Takeuchi O, Akira S. Pattern recognition receptors and inflammation. *Cell* (2010) 140(6):805–20. doi: 10.1016/j.cell.2010.01.022

109. Broz P, Monack DM. Newly described pattern recognition receptors team up against intracellular pathogens. *Nat Rev Immunol* (2013) 13(8):551–65. doi: 10.1038/nri3479

110. Kumagai Y, Akira S. Identification and functions of pattern-recognition receptors. *J Allergy Clin Immunol* (2010) 125(5):985–92. doi: 10.1016/j.jaci.2010.01.058

111. Barbé F, Douglas T, Saleh M. Advances in nod-like receptors (NLR) biology. *Cytokine Growth Factor Rev* (2014) 25(6):681–97. doi: 10.1016/j.cytogfr.2014.07.001

112. Motta V, Soares F, Sun T, Philpott DJ. NOD-like receptors: versatile cytosolic sentinels. *Physiol Rev* (2015) 95(1):149–78. doi: 10.1152/physrev.00009.2014

113. Neerincx A, Castro W, Guarda G, Kufer TA. NLRC5, at the heart of antigen presentation. *Front Immunol* (2013) 4:397. doi: 10.3389/fimmu.2013.00397

114. Wang L, Hauenstein AV. The NLRP3 inflammasome: Mechanism of action, role in disease and therapies. *Mol Aspects Med* (2020) 76:100889. doi: 10.1016/j.mam.2020.100889

115. Chen L, Cao SQ, Lin ZM, He SJ, Zuo JP. NOD-like receptors in autoimmune diseases. *Acta Pharmacol Sin* (2021) 42(11):1742–56. doi: 10.1038/s41401-020-00603-2

116. Zhang Y, Liang C. Innate recognition of microbial-derived signals in immunity and inflammation. *Sci China Life Sci* (2016) 59(12):1210–7. doi: 10.1007/s11427-016-0325-6

117. Lamkanfi M, Declercq W, Kalai M, Saelens X, Vandenabeele P. Alice In caspase land. a phylogenetic analysis of caspases from worm to man. *Cell Death Differ* (2002) 9(4):358–61. doi: 10.1038/sj.cdd.4400989

118. Lamkanfi M, Festjens N, Declercq W, Vanden Berghe T, Vandenabeele P. Caspases in cell survival, proliferation and differentiation. *Cell Death Differ* (2007) 14(1):44–55. doi: 10.1038/sj.cdd.4402047

119. Kesavardhana S, Malireddi RKS, Kanneganti TD. Caspases in cell death, inflammation, and pyroptosis. *Annu Rev Immunol* (2020) 38:567–95. doi: 10.1146/annurev-immunol-073119-095439

120. Martinon F, Tschopp J. Inflammatory caspases and inflammasomes: master switches of inflammation. *Cell Death Differ* (2007) 14(1):10–22. doi: 10.1038/sj.cdd.4402038

121. Sagulenko V, Vitak N, Vajjhala PR, Vince JE, Stacey KJ. Caspase-1 is an apical caspase leading to caspase-3 cleavage in the AIM2 inflammasome response, independent of caspase-8. *J Mol Biol* (2018) 430(2):238–47. doi: 10.1016/j.jmb.2017.10.028

122. Martinon F, Tschopp J. Inflammatory caspases: linking an intracellular innate immune system to autoinflammatory diseases. *Cell* (2004) 117(5):561–74. doi: 10.1016/j.cell.2004.05.004

123. Shi J, Gao W, Shao F. Pyroptosis: Gasdermin-mediated programmed necrotic cell death. *Trends Biochem Sci* (2017) 42(4):245–54. doi: 10.1016/j.tibs.2016.10.004

124. Yazdi AS, Guarda G, D'Ombrain MC, Drexler SK. Inflammatory caspases in innate immunity and inflammation. *J Innate Immun* (2010) 2(3):228–37. doi: 10.1159/000283688

125. Bryant C, Fitzgerald KA. Molecular mechanisms involved in inflammasome activation. *Trends Cell Biol* (2009) 19(9):455–64. doi: 10.1016/j.tcb.2009.06.002

126. Schroder K, Tschopp J. The inflammasomes. *Cell* (2010) 140(6):821–32. doi: 10.1016/j.cell.2010.01.040

127. Kelley N, Jeltema D, Duan Y, He Y. The NLRP3 inflammasome: An overview of mechanisms of activation and regulation. *Int J Mol Sci* (2019) 20(13):3328. doi: 10.3390/ijms20133328

128. Swanson KV, Deng M, Ting JP. The NLRP3 inflammasome: molecular activation and regulation to therapeutics. *Nat Rev Immunol* (2019) 19(8):477–89. doi: 10.1038/s41577-019-0165-0

129. Weber ANR, Bittner ZA, Shankar S, Liu X, Chang TH, Jin T, et al. Recent insights into the regulatory networks of NLRP3 inflammasome activation. *J Cell Sci* (2020) 133(23):jcs248344. doi: 10.1242/jcs.248344

130. Broderick L, De Nardo D, Franklin BS, Hoffman HM, Latz E. The inflammasomes and autoinflammatory syndromes. *Annu Rev Pathol* (2015) 10:395–424. doi: 10.1146/annurev-pathol-012414-040431

131. Nambayan RJT, Sandin SI, Quint DA, Satyadi DM, de Alba E. The inflammasome adapter ASC assembles into filaments with integral participation of its two death domains, PYD and CARD. *J Biol Chem* (2019) 294(2):439–52. doi: 10.1074/jbc.RA118.004407

132. Guey B, Bodnar M, Manié SN, Tardivel A, Petrilli V. Caspase-1 autoproteolysis is differentially required for NLRP1b and NLRP3 inflammasome function. *Proc Natl Acad Sci U S A.* (2014) 111(48):17254–9. doi: 10.1073/pnas.1415756111

133. Ferrao R, Wu H. Helical assembly in the death domain (DD) superfamily. *Curr Opin Struct Biol* (2012) 22(2):241–7. doi: 10.1016/j.sbi.2012.02.006

134. Chen MY, Ye XJ, He XH, Ouyang DY. The signaling pathways regulating NLRP3 inflammasome activation. *Inflammation* (2021) 44(4):1229–45. doi: 10.1007/s10753-021-01439-6

135. Bauernfeind FG, Horvath G, Stutz A, Alnemri ES, MacDonald K, Speert D, et al. Cutting edge: NF-kappaB activating pattern recognition and cytokine receptors license NLRP3 inflammasome activation by regulating NLRP3 expression. *J Immunol* (2009) 183(2):787–91. doi: 10.4049/jimmunol.0901363

136. Yang J, Liu Z, Xiao TS. Post-translational regulation of inflammasomes. *Cell Mol Immunol* (2017) 14(1):65–79. doi: 10.1038/cmi.2016.29

137. Vajjhala PR, Mirams RE, Hill JM. Multiple binding sites on the pyrin domain of ASC protein allow self-association and interaction with NLRP3 protein. *J Biol Chem* (2012) 287(50):41732–43. doi: 10.1074/jbc.M112.381228

138. Franklin BS, Bossaller L, De Nardo D, Ratter JM, Stutz A, Engels G, et al. The adaptor ASC has extracellular and 'prionoid' activities that propagate inflammation. *Nat Immunol* (2014) 15(8):727–37. doi: 10.1038/ni.2913

139. Lu A, Magupalli VG, Ruan J, Yin Q, Atianand MK, Vos MR, et al. Unified polymerization mechanism for the assembly of ASC-dependent inflammasomes. *Cell* (2014) 156(6):1193–206. doi: 10.1016/j.cell.2014.02.008

140. Lu A, Wu H. Structural mechanisms of inflammasome assembly. *FEBS J* (2015) 282(3):435–44. doi: 10.1111/febs.13133

141. Malik A, Kanneganti TD. Inflammasome activation and assembly at a glance. *J Cell Sci* (2017) 130(23):3955–63. doi: 10.1242/jcs.207365

142. Davis BK, Wen H, Ting JP. The inflammasome NLRs in immunity, inflammation, and associated diseases. *Annu Rev Immunol* (2011) 29:707–35. doi: 10.1146/annurev-immunol-031210-101405

143. Boucher D, Monteleone M, Coll RC, Chen KW, Ross CM, Teo JL, et al. Caspase-1 self-cleavage is an intrinsic mechanism to terminate inflammasome activity. *J Exp Med* (2018) 215(3):827–40. doi: 10.1084/jem.20172222

144. He Y, Hara H, Núñez G. Mechanism and regulation of NLRP3 inflammasome activation. *Trends Biochem Sci* (2016) 41(12):1012–21. doi: 10.1016/j.tibs.2016.09.002

145. Yang CA, Chiang BL. Inflammasomes and human autoimmunity: A comprehensive review. *J Autoimmun* (2015) 61:1–8. doi: 10.1016/j.jaut.2015.05.001

146. Rathinam VA, Vanaja SK, Fitzgerald KA. Regulation of inflammasome signaling. *Nat Immunol* (2012) 13(4):333–42. doi: 10.1038/ni.2237

147. Segovia JA, Tsai SY, Chang TH, Shil NK, Weintraub ST, Short JD, et al. Nedd8 regulates inflammasome-dependent caspase-1 activation. *Mol Cell Biol* (2015) 35(3):582–97. doi: 10.1128/MCB.00775-14

148. Wang K, Sun Q, Zhong X, Zeng M, Zeng H, Shi X, et al. Structural mechanism for GSDMD targeting by autoprocessed caspases in pyroptosis. *Cell* (2020) 180(5):941–955.e20. doi: 10.1016/j.cell.2020.02.002

149. Ding J, Wang K, Liu W, She Y, Sun Q, Shi J, et al. Pore-forming activity and structural autoinhibition of the gasdermin family. *Nature* (2016) 535(7610):111–6. doi: 10.1038/nature18590

150. Sborgi L, Rühl S, Mulvihill E, Pipercevic J, Heilig R, Stahlberg H, et al. GSDMD membrane pore formation constitutes the mechanism of pyroptotic cell death. *EMBO J* (2016) 35(16):1766–78. doi: 10.15252/embj.201694696

151. Frank D, Vince JE. Pyroptosis versus necroptosis: similarities, differences, and crosstalk. *Cell Death Differ* (2019) 26(1):99–114. doi: 10.1038/s41418-018-0212-6

152. Kuriakose T, Man SM, Malireddi RK, Karki R, Kesavardhana S, Place DE, et al. ZBP1/DAI is an innate sensor of influenza virus triggering the NLRP3 inflammasome and programmed cell death pathways. *Sci Immunol* (2016) 1(2):aag2045. doi: 10.1126/sciimmunol.aag2045

153. Man SM, Karki R, Kanneganti TD. Molecular mechanisms and functions of pyroptosis, inflammatory caspases and inflammasomes in infectious diseases. *Immunol Rev* (2017) 277(1):61–75. doi: 10.1111/imr.12534

154. Vande Walle L, Lamkanfi M. Pyroptosis. *Curr Biol* (2016) 26(13):R568–72. doi: 10.1016/j.cub.2016.02.019

155. Li Z, Guo J, Bi L. Role of the NLRP3 inflammasome in autoimmune diseases. *BioMed Pharmacother.* (2020) 130:110542. doi: 10.1016/j.biopha.2020.110542

156. Shin JI, Lee KH, Joo YH, Lee JM, Jeon J, Jung HJ, et al. Inflammasomes and autoimmune and rheumatic diseases: A comprehensive review. *J Autoimmun* (2019) 103:102299. doi: 10.1016/j.jaut.2019.06.010

157. Dolinay T, Kim YS, Howrylak J, Hunninghake GM, An CH, Fredenburgh L, et al. Inflammasome-regulated cytokines are critical mediators of acute lung injury. *Am J Respir Crit Care Med* (2012) 185(11):1225–34. doi: 10.1164/rccm.201201-0003OC

158. Grailer JJ, Canning BA, Kalbitz M, Haggadone MD, Dhond RM, Andjelkovic AV, et al. Critical role for the NLRP3 inflammasome during acute lung injury. *J Immunol* (2014) 192(12):5974–83. doi: 10.4049/jimmunol.1400368

159. Hoshino T, Okamoto M, Sakazaki Y, Kato S, Young HA, Aizawa H. Role of proinflammatory cytokines IL-18 and IL-1beta in bleomycin-induced lung injury in humans and mice. *Am J Respir Cell Mol Biol* (2009) 41(6):661–70. doi: 10.1165/rcmb.2008-0182OC

160. Jones HD, Crother TR, Gonzalez-Villalobos RA, Jupelli M, Chen S, Dagvadorj J, et al. The NLRP3 inflammasome is required for the development of hypoxemia in LPS/mechanical ventilation acute lung injury. *Am J Respir Cell Mol Biol* (2014) 50(2):270–80. doi: 10.1165/rcmb.2013-0087OC

161. Plassmeyer M, Alpan O, Corley MJ, Premeaux TA, Lillard K, Coatney P, et al. Caspases and therapeutic potential of caspase inhibitors in moderate-severe SARS-CoV-2 infection and long COVID. *Allergy* (2022) 77(1):118–29. doi: 10.1111/all.14907

162. Kroemer A, Khan K, Plassmeyer M, Alpan O, Haseeb MA, Gupta R, et al. Inflammasome activation and pyroptosis in lymphopenic liver patients with COVID-19. *J Hepatol* (2020) 73(5):1258–62. doi: 10.1016/j.jhep.2020.06.034

163. Conti P, Caraffa A, Gallenga CE, Ross R, Kritas SK, Frydas I, et al. Coronavirus-19 (SARS-CoV-2) induces acute severe lung inflammation. *via IL-1 causing Cytokine storm COVID-19: promising inhibitory strategy. J Biol Regul Homeost Agents.* (2020) 34(6):1971–5. doi: 10.23812/20-1-E

164. Toldo S, Bussani R, Nuzzi V, Bonaventura A, Mauro AG, Cannatà A, et al. Inflammasome formation in the lungs of patients with fatal COVID-19. *Inflammation Res* (2021) 70(1):7–10. doi: 10.1007/s00011-020-01413-2

165. Costela-Ruiz VJ, Illescas-Montes R, Puerta-Puerta JM, Ruiz C, Melguizo-Rodríguez L. SARS-CoV-2 infection: The role of cytokines in COVID-19 disease. *Cytokine Growth Factor Rev* (2020) 54:62–75. doi: 10.1016/j.cytogfr.2020.06.001

166. Zhang J, Wu H, Yao X, Zhang D, Zhou Y, Fu B, et al. Pyroptotic macrophages stimulate the SARS-CoV-2-associated cytokine storm. *Cell Mol Immunol* (2021) 18(5):1305–7. doi: 10.1038/s41423-021-00665-0

167. Aid M, Busman-Sahay K, Vidal SJ, Maliga Z, Bondoc S, Starke C, et al. Vascular disease and thrombosis in SARS-CoV-2-Infected rhesus macaques. *Cell* (2020) 183(5):1354–1366.e13. doi: 10.1016/j.cell.2020.10.005

168. Naqvi I, Giroux N, Olson L, Morrison SA, Llanga T, Akinade TO, et al. DAMPs/PAMPs induce monocytic TLR activation and tolerance in COVID-19 patients; nucleic acid binding scavengers can counteract such TLR agonists. *Biomaterials* (2022) 283:121393. doi: 10.1016/j.biomaterials.2022.121393

169. Pan P, Shen M, Yu Z, Ge W, Chen K, Tian M, et al. SARS-CoV-2 n protein promotes NLRP3 inflammasome activation to induce hyperinflammation. *Nat Commun* (2021) 12(1):4664. doi: 10.1038/s41467-021-25015-6

170. Theobald SJ, Simonis A, Georgomanolis T, Kreer C, Zehner M, Eisfeld HS, et al. Long-lived macrophage reprogramming drives spike protein-mediated inflammasome activation in COVID-19. *EMBO Mol Med* (2021) 13(8):e14150. doi: 10.15252/emmm.202114150

171. Zhang J, Ejikemeuwa A, Gerzanich V, Nasr M, Tang Q, Simard JM, et al. Understanding the role of SARS-CoV-2 ORF3a in viral pathogenesis and COVID-19. *Front Microbiol* (2022) 13:854567. doi: 10.3389/fmicb.2022.854567

172. Vardhana SA, Wolchok JD. The many faces of the anti-COVID immune response. *J Exp Med* (2020) 217(6):e20200678. doi: 10.1084/jem.20200678

173. Hu B, Huang S, Yin L. The cytokine storm and COVID-19. *J Med Virol* (2021) 93(1):250–6. doi: 10.1002/jmv.26232

174. Ye Q, Wang B, Mao J. The pathogenesis and treatment of the `Cytokine storm' in COVID-19. *J Infect* (2020) 80(6):607–13. doi: 10.1016/j.jinf.2020.03.037

175. Ferreira AC, Soares VC, de Azevedo-Quintanilha IG, Dias SDSG, Fintelman-Rodrigues N, Sacramento CQ, et al. SARS-CoV-2 engages inflammasome and pyroptosis in human primary monocytes. *Cell Death Discovery* (2021) 7(1):43. doi: 10.1038/s41420-021-00428-w

176. Teijaro JR, Walsh KB, Rice S, Rosen H, Oldstone MB. Mapping the innate signaling cascade essential for cytokine storm during influenza virus infection. *Proc Natl Acad Sci U S A.* (2014) 111(10):3799–804. doi: 10.1073/pnas.1400593111

177. Li X, Geng M, Peng Y, Meng L, Lu S. Molecular immune pathogenesis and diagnosis of COVID-19. *J Pharm Anal* (2020) 10(2):102–8. doi: 10.1016/j.jpha.2020.03.001

178. Pedersen SF, Ho YC. SARS-CoV-2: a storm is raging. *J Clin Invest.* (2020) 130(5):2202–5. doi: 10.1172/JCI137647

179. Mehta P, McAuley DF, Brown M, Sanchez E, Tattersall RS, Manson JJ. HLH across speciality collaboration, UK. *COVID-19: consider Cytokine storm syndromes immunosuppression. Lancet* (2020) 395(10229):1033–4. doi: 10.1016/S0140-6736(20)30628-0

180. Zhou Y, Fu B, Zheng X, Wang D, Zhao C, Qi Y, et al. Pathogenic T-cells and inflammatory monocytes incite inflammatory storms in severe COVID-19 patients. *Natl Sci Rev* (2020) 7(6):998–1002. doi: 10.1093/nsr/nwaa041

181. Cheng L, Liang X, Qian L, Luo C, Li D. NLRP3 gene polymorphisms and expression in rheumatoid arthritis. *Exp Ther Med* (2021) 22(4):1110. doi: 10.3892/etm.2021.10544

182. Jäger E, Murthy S, Schmidt C, Hahn M, Strobel S, Peters A, et al. Calcium-sensing receptor-mediated NLRP3 inflammasome response to calciprotein particles drives inflammation in rheumatoid arthritis. *Nat Commun* (2020) 11 (1):4243. doi: 10.1038/s41467-020-17749-6

183. Mathews RJ, Robinson JI, Battellino M, Wong C, Taylor JCBiologics in Rheumatoid Arthritis Genetics and Genomics Study Syndicate (BRAGGSS), et al. Evidence of NLRP3-inflammasome activation in rheumatoid arthritis (RA); genetic variants within the NLRP3-inflammasome complex in relation to susceptibility to RA and response to anti-TNF treatment. *Ann Rheum Dis* (2014) 73(6):1202–10. doi: 10.1136/annrheumdis-2013-203276

184. Kondo N, Kuroda T, Kobayashi D. Cytokine networks in the pathogenesis of rheumatoid arthritis. *Int J Mol Sci* (2021) 22(20):10922. doi: 10.3390/ijms222010922

185. Burska A, Boissinot M, Ponchel F. Cytokines as biomarkers in rheumatoid arthritis. *Mediators Inflamm* (2014) 2014:545493. doi: 10.1155/2014/545493

186. Dai SM, Shan ZZ, Xu H, Nishioka K. Cellular targets of interleukin-18 in rheumatoid arthritis. *Ann Rheum Dis* (2007) 66(11):1411–8. doi: 10.1136/ard.2006.067793

187. Vervoordeldonk MJ, Tak PP. Cytokines in rheumatoid arthritis. *J Curr Rheumatol Rep* (2002) 4(3):208–17. doi: 10.1007/s11926-002-0067-0

188. Song P, Yang C, Thomsen JS, Dagnæs-Hansen F, Jakobsen M, Brüel A, et al. Lipidoid-siRNA nanoparticle-mediated IL-1β gene silencing for systemic arthritis therapy in a mouse model. *Mol Ther* (2019) 27(8):1424–35. doi: 10.1016/j.ymthe.2019.05.002

189. Deets KA, Vance RE. Inflammasomes and adaptive immune responses. *Nat Immunol* (2021) 22(4):412–22. doi: 10.1038/s41590-021-00869-6

190. You R, He X, Zeng Z, Zhan Y, Xiao Y, Xiao R. Pyroptosis and its role in autoimmune disease: A potential therapeutic target. *Front Immunol* (2022) 13:841732. doi: 10.3389/fimmu.2022.841732

191. McInnes IB, Schett G. Cytokines in the pathogenesis of rheumatoid arthritis. *Nat Rev Immunol* (2007) 7(6):429–42. doi: 10.1038/nri2094

192. Choulaki C, Papadaki G, Repa A, Kampouraki E, Kambas K, Ritis K, et al. Enhanced activity of NLRP3 inflammasome in peripheral blood cells of patients with active rheumatoid arthritis. *Arthritis Res Ther* (2015) 17(1):257. doi: 10.1186/s13075-015-0775-2

193. Ruscitti P, Cipriani P, Di Benedetto P, Liakouli V, Berardicurti O, Carubbi F, et al. Monocytes from patients with rheumatoid arthritis and type 2 diabetes mellitus display an increased production of interleukin (IL)-1β via the nucleotide-binding domain and leucine-rich repeat containing family pyrin 3(NLRP3)-inflammasome activation: a possible implication for therapeutic decision in these patients. *Clin Exp Immunol* (2015) 182(1):35–44. doi: 10.1111/cei.12667

194. Elemam NM, Maghazachi AA, Hannawi S. COVID-19 infection and rheumatoid arthritis: mutual outburst cytokines and remedies. *Curr Med Res Opin* (2021) 37(6):929–38. doi: 10.1080/03007995.2021.1906637

195. Raiker R, DeYoung C, Pakhchanian H, Ahmed S, Kavadichanda C, Gupta L, et al. Outcomes of COVID-19 in patients with rheumatoid arthritis: A multicenter research network study in the united states. *Semin Arthritis Rheumatol* (2021) 51(5):1057–66. doi: 10.1016/j.semarthrit.2021.08.010

196. England BR, Roul P, Yang Y, Kalil AC, Michaud K, Thiele GM, et al. Risk of COVID-19 in rheumatoid arthritis: A national veterans affairs matched cohort study in At-risk individuals. *Arthritis Rheumatol* (2021) 73(12):2179–88. doi: 10.1002/art.41800

197. Favalli EG, Ingegnoli F, De Lucia O, Cincinelli G, Cimaz R, Caporali R. COVID-19 infection and rheumatoid arthritis: Faraway, so close! *Autoimmun Rev* (2020) 19(5):102523. doi: 10.1016/j.autrev.2020.102523

198. Mihara M, Hashizume M, Yoshida H, Suzuki M, Shiina M. IL-6/IL-6 receptor system and its role in physiological and pathological conditions. *Clin Sci (Lond).* (2012) 122(4):143–59. doi: 10.1042/CS20110340

199. Huang YP, Chen DR, Lin WJ, Lin YH, Chen JY, Kuo YH, et al. Ergosta-7,9 (11),22-trien-3β-ol attenuates inflammatory responses via inhibiting MAPK/AP-1 induced IL-6/JAK/STAT pathways and activating Nrf2/HO-1 signaling in LPS-

stimulated macrophage-like cells. *Antioxidants (Basel).* (2021) 10(9):1430. doi: 10.3390/antiox10091430

200. Chen G, Wu D, Guo W, Cao Y, Huang D, Wang H, et al. Clinical and immunological features of severe and moderate coronavirus disease 2019. *J Clin Invest.* (2020) 130(5):2620–9. doi: 10.1172/JCI137244

201. Malemud CJ. The role of the JAK/STAT signal pathway in rheumatoid arthritis. *Ther Adv Musculoskelet Dis* (2018) 10(5-6):117–27. doi: 10.1177/1759720X18776224

202. Simon LS, Taylor PC, Choy EH, Sebba A, Quebe A, Knopp KL, et al. The Jak/STAT pathway: A focus on pain in rheumatoid arthritis. *Semin Arthritis Rheumatol* (2021) 51(1):278–84. doi: 10.1016/j.semarthrit.2020.10.008

203. Luo W, Li YX, Jiang LJ, Chen Q, Wang T, Ye DW. Targeting JAK-STAT signaling to control cytokine release syndrome in COVID-19. *Trends Pharmacol Sci* (2020) 41(8):531–43. doi: 10.1016/j.tips.2020.06.007

204. Smolen JS, Landewé R, Bijlsma J, Burmester G, Chatzidionysiou K, Dougados M, et al. EULAR recommendations for the management of rheumatoid arthritis with synthetic and biological disease-modifying antirheumatic drugs: 2016 update. *Ann Rheum Dis* (2017) 76(6):960–77. doi: 10.1136/annrheumdis-2016-210715

205. You H, Xu D, Zhao J, Li J, Wang Q, Tian X, et al. JAK inhibitors: Prospects in connective tissue diseases. *Clin Rev Allergy Immunol* (2020) 59(3):334–51. doi: 10.1007/s12016-020-08786-6

206. Winthrop KL. The emerging safety profile of JAK inhibitors in rheumatic disease. *Nat Rev Rheumatol* (2017) 13(5):320. doi: 10.1038/nrrheum.2017.51

207. Curtis JR, Xie F, Yang S, Bernatsky S, Chen L, Yun H, et al. Risk for herpes zoster in tofacitinib-treated rheumatoid arthritis patients with and without concomitant methotrexate and glucocorticoids. *Arthritis Care Res (Hoboken).* (2019) 71(9):1249–54. doi: 10.1002/acr.23769

208. Schneider WM, Chevillotte MD, Rice CM. Interferon-stimulated genes: a complex web of host defenses. *Annu Rev Immunol* (2014) 32:513–45. doi: 10.1146/annurev-immunol-032713-120231

209. Agarwal A, Rochwerg B, Lamontagne F, Siemieniuk RA, Agoritsas T, Askie L, et al. A living WHO guideline on drugs for covid-19. *BMJ* (2020) 370:m3379. doi: 10.1136/bmj.m3379

210. Reuken PA, Teich N, Stallmach A. Safety of tofacitinib in the COVID-19 pandemic-enough is not enough. *Inflammation Bowel Dis* (2021) 27(8):e89. doi: 10.1093/ibd/izab051

211. Levy G, Guglielmelli P, Langmuir P, Constantinescu SN. JAK inhibitors and COVID-19. *J Immunother Cancer.* (2022) 10(4):e002838. doi: 10.1136/jitc-2021-002838

212. Kramer A, Prinz C, Fichtner F, Fischer AL, Thieme V, Grundeis F, et al. Janus kinase inhibitors for the treatment of COVID-19. *Cochrane Database Syst Rev* (2022) 6(6):CD015209. doi: 10.1002/14651858.CD015209

213. Yang X, Zhan N, Jin Y, Ling H, Xiao C, Xie Z, et al. Tofacitinib restores the balance of γδTreg/γδT17 cells in rheumatoid arthritis by inhibiting the NLRP3 inflammasome. *Theranostics* (2021) 11(3):1446–57. doi: 10.7150/thno.47860

214. Furuya MY, Asano T, Sumichika Y, Sato S, Kobayashi H, Watanabe H, et al. Tofacitinib inhibits granulocyte-macrophage colony-stimulating factor-induced NLRP3 inflammasome activation in human neutrophils. *Arthritis Res Ther* (2018) 20(1):196. doi: 10.1186/s13075-018-1685-x

215. Chin YE, Kitagawa M, Kuida K, Flavell RA, Fu XY. Activation of the STAT signaling pathway can cause expression of caspase 1 and apoptosis. *Mol Cell Biol* (1997) 17(9):5328–37. doi: 10.1128/MCB.17.9.5328

216. Voutsadakis IA. Interferon-alpha and the pathogenesis of myeloproliferative disorders. *Med Oncol* (2000) 17(4):249–57. doi: 10.1007/BF02782189

217. Jiang S. Don't rush to deploy COVID-19 vaccines and drugs without sufficient safety guarantees. *Nature* (2020) 579(7799):321. doi: 10.1038/d41586-020-00751-9

218. Singh H, Kakkar AK, Chauhan P. Repurposing minocycline for COVID-19 management: mechanisms, opportunities, and challenges. *Expert Rev Anti Infect Ther* (2020) 18(10):997–1003. doi: 10.1080/14787210.2020.1782190

219. FDA. *Minocycline label* . Available at: https://www.accessdata.fda.gov/drugsatfda_docs/label/2010/050649023lbl.pdf.

220. Bishburg E, Bishburg K. Minocycline–an old drug for a new century: emphasis on methicillin-resistant staphylococcus aureus (MRSA) and acinetobacter baumannii. *Int J Antimicrob Agents.* (2009) 34(5):395–401. doi: 10.1016/j.ijantimicag.2009.06.021

221. Quick ED, Seitz S, Clarke P, Tyler KL. Minocycline has anti-inflammatory effects and reduces cytotoxicity in an. *Ex Vivo Spinal Cord Slice Culture Model West Nile Virus Infection. J Virol* (2017) 91(22):e00569-17. doi: 10.1128/JVI.00569-17

222. Leela SL, Srisawat C, Sreekanth GP, Noisakran S, Yenchitsomanus PT, Limjindaporn T. Drug repurposing of minocycline against dengue virus infection. *Biochem Biophys Res Commun* (2016) 478(1):410–6. doi: 10.1016/j.bbrc.2016.07.029

223. Singh M, Singh P, Vaira D, Amand M, Rahmouni S, Moutschen M. Minocycline attenuates HIV-1 infection and suppresses chronic immune activation in humanized NOD/LtsZ-scidIL-2Rγ(null) mice. *Immunology* (2014) 142(4):562–72. doi: 10.1111/imm.12246

224. Yang F, Zhu W, Cai X, Zhang W, Yu Z, Li X, et al. Minocycline alleviates NLRP3 inflammasome-dependent pyroptosis in monosodium glutamate-induced depressive rats. *Biochem Biophys Res Commun* (2020) 526(3):553–9. doi: 10.1016/j.bbrc.2020.02.149

225. Garrido-Mesa N, Zarzuelo A, Gálvez J. Minocycline: far beyond an antibiotic. *Br J Pharmacol* (2013) 169(2):337–52. doi: 10.1111/bph.12139

226. Garrido-Mesa N, Zarzuelo A, Gálvez J. What is behind the non-antibiotic properties of minocycline? *Pharmacol Res* (2013) 67(1):18–30. doi: 10.1016/j.phrs.2012.10.006

227. Sanchez Mejia RO, Ona VO, Li M, Friedlander RM. Minocycline reduces traumatic brain injury-mediated caspase-1 activation, tissue damage, and neurological dysfunction. *Neurosurgery* (2001) 48(6):1393–9; discussion 1399-401. doi: 10.1097/00006123-200106000-00051

228. Wong ML, Inserra A, Lewis MD, Mastronardi CA, Leong L, Choo J, et al. Inflammasome signaling affects anxiety- and depressive-like behavior and gut microbiome composition. *Mol Psychiatry* (2016) 21(6):797–805. doi: 10.1038/mp.2016.46

229. Chen M, Ona VO, Li M, Ferrante RJ, Fink KB, Zhu S, et al. Minocycline inhibits caspase-1 and caspase-3 expression and delays mortality in a transgenic mouse model of huntington disease. *Nat Med* (2000) 6(7):797–801. doi: 10.1038/77528

230. Vincent JA, Mohr S. Inhibition of caspase-1/interleukin-1beta signaling prevents degeneration of retinal capillaries in diabetes and galactosemia. *Diabetes* (2007) 56(1):224–30. doi: 10.2337/db06-0427

231. Peukert K, Fox M, Schulz S, Feuerborn C, Frede S, Putensen C, et al. Inhibition of caspase-1 with tetracycline ameliorates acute lung injury. *Am J Respir Crit Care Med* (2021) 204(1):53–63. doi: 10.1164/rccm.202005-1916OC

232. Lodise TP, Fan W, Griffith DC, Dudley MN. Sulham KA. a retrospective cohort analysis shows that coadministration of minocycline with colistin in critically ill patients is associated with reduced frequency of acute renal failure. *Antimicrob Agents Chemother* (2017) 62(1):e01165-17. doi: 10.1128/AAC.01165-17

233. Gautam SS, Gautam CS, Garg VK, Singh H. Combining hydroxychloroquine and minocycline: potential role in moderate to severe COVID-19 infection. *Expert Rev Clin Pharmacol* (2020) 13(11):1183–90. doi: 10.1080/17512433.2020.1832889

234. Garcia-Vidal C, Sanjuan G, Moreno-García E, Puerta-Alcalde P, Garcia-Pouton N, Chumbita M, et al. COVID-19 researchers group. incidence of co-infections and superinfections in hospitalized patients with COVID-19: a retrospective cohort study. *Clin Microbiol Infect* (2021) 27(1):83–8. doi: 10.1016/j.cmi.2020.07.041

235. Hughes S, Troise O, Donaldson H, Mughal N, Moore LSP. Bacterial and fungal coinfection among hospitalized patients with COVID-19: a retrospective cohort study in a UK secondary-care setting. *Clin Microbiol Infect* (2020) 26(10):1395–9. doi: 10.1016/j.cmi.2020.06.025

236. Itoh K, Sakamaki I, Hirota T, Iwasaki H. Evaluation of minocycline combined with favipiravir therapy in coronavirus disease 2019 patients: A case-series study. *J Infect Chemother* (2022) 28(1):124–7. doi: 10.1016/j.jiac.2021.09.016

237. Gironi LC, Damiani G, Zavattaro E, Pacifico A, Santus P, Pigatto PDM, et al. Tetracyclines in COVID-19 patients quarantined at home: Literature evidence supporting real-world data from a multicenter observational study targeting inflammatory and infectious dermatoses. *Dermatol Ther* (2021) 34(1):e14694. doi: 10.1111/dth.14694

238. Kloppenburg M, Mattie H, Douwes N, Dijkmans BA, Breedveld FC. Minocycline in the treatment of rheumatoid arthritis: relationship of serum concentrations to efficacy. *J Rheumatol* (1995) 22(4):611–6.

239. Greenwald RA. The road forward: the scientific basis for tetracycline treatment of arthritic disorders. *Pharmacol Res* (2011) 64(6):610–3. doi: 10.1016/j.phrs.2011.06.010

240. Janakiraman K, Krishnaswami V, Sethuraman V, Natesan S, Rajendran V, Kandasamy R. Development of methotrexate and minocycline loaded nanoparticles for the effective treatment of rheumatoid arthritis. *AAPS PharmSciTech.* (2019) 21(2):34. doi: 10.1208/s12249-019-1581-y

10.3389/fimmu.2022.1058884

Glossary

Go	Gene Ontology
KEGG	Kyoto Encyclopedia of Genes and Genomes
PPI	Protein-Protein Interaction
TF	Transcription Factor
PCA	Principal Component Analysis
ROC	Receiver Operating Curve
MM-GBSA	Molecular Mechanics/Generalized Born Surface Area
DEG	Differentially Expressed Genes
GEO	Gene Expression Omnibus
BioGRID	the Biological General Repository for Interaction Datasets
BP	Biological Process
CC	Cellular Component
MF	Molecular Function
PRR	Pathogen Recognition Receptor
NLR	NOD-Like Receptor
TLR	Toll-Like Receptor
CLR	C-Type Lectin-Receptor
RLR	RIG-I-Like Receptor
NLRP3	The NOD-Like Receptor Family Pyrin Domain Containing 3
ASC	Apoptosis-Associated Speck-Like Protein
DD	Death Domain
PAMP	Pathogen-Associated Molecular Pattern
DAMP	Damage-Associated Molecular Pattern
RCD	Regulated Cell Death
ISG	Interferon-stimulated Gene
HC	Healthy Controls
NOD	Nucleotide-Binding Oligomerization Domain
AUC	Area Under the Curve
JAK	Janus Kinase
STAT	Signal Transducer and Activator of Transcription
DCs	Dendritic cells
RMSD	Root-Mean-Square Deviation
RMSF	Root-Mean-Square Fluctuation
NF-Kb	Nuclear Factor-kappa B
AID	Autoimmune Disease
NSP6	Non-Structural Protein 6
N-protein	Nucleocapsid protein
S-protein	Spike protein
E-protein	Envelope protein
M-protein	Membrane protein
LRR	Leucine Rich Repeat
NACHT	Nucleotide-Binding and Oligomerization Domain
PYD	Pyrin Domain
CARD	Caspase Recruitment Domain
ARDS	Acute Respiratory Distress Syndrome

frontiers | Frontiers in Immunology

TYPE Mini Review
PUBLISHED 22 December 2022
DOI 10.3389/fimmu.2022.1084230

OPEN ACCESS

EDITED BY
Chenhe Su,
Wistar Institute, United States

REVIEWED BY
Chuanmin Zhou,
Wuhan University, China
Yuexiu Zhang,
The Ohio State University, United States
Aarthi Narayanan,
George Mason University, United States

*CORRESPONDENCE
Leiliang Zhang
armzhang@hotmail.com

SPECIALTY SECTION
This article was submitted to Viral Immunology, a section of the journal Frontiers in Immunology

RECEIVED 30 October 2022
ACCEPTED 12 December 2022
PUBLISHED 22 December 2022

CITATION
Wang X, Yuan Y, Liu Y and Zhang L (2022) Arm race between Rift Valley fever virus and host. *Front. Immunol.* 13:1084230. doi: 10.3389/fimmu.2022.1084230

Arm race between Rift Valley fever virus and host

Xiao Wang[1,2,3], Yupei Yuan[2], Yihan Liu[2,3] and Leiliang Zhang[1,2,3]*

[1]Department of Infectious Diseases, Shandong Provincial Hospital Affiliated to Shandong First Medical University, Jinan, Shandong, China, [2]Department of Pathogen Biology, School of Clinical and Basic Medical Sciences, Shandong First Medical University and Shandong Academy of Medical Sciences, Jinan, Shandong, China, [3]Medical Science and Technology Innovation Center, Shandong First Medical University and Shandong Academy of Medical Sciences, Jinan, Shandong, China

Rift Valley fever (RVF) is a zoonotic disease caused by Rift Valley fever virus (RVFV), an emerging arbovirus within the *Phenuiviridae* family of *Bunyavirales* that has potential to cause severe diseases in both humans and livestock. It increases the incidence of abortion or foetal malformation in ruminants and leads to clinical manifestations like encephalitis or haemorrhagic fever in humans. Upon virus invasion, the innate immune system from the cell or the organism is activated to produce interferon (IFN) and prevent virus proliferation. Meanwhile, RVFV initiates countermeasures to limit antiviral responses at transcriptional and protein levels. RVFV nonstructural proteins (NSs) are the key virulent factors that not only perform immune evasion but also impact the cell replication cycle and has cytopathic effects. In this review, we summarize the innate immunity host cells employ depending on IFN signal transduction pathways, as well as the immune evasion mechanisms developed by RVFV primarily with the inhibitory activity of NSs protein. Clarifying the arms race between host innate immunity and RVFV immune evasion provides new avenues for drug target screening and offers possible solutions to current and future epidemics.

KEYWORDS

Rift Valley fever virus, innate immunity, interferon, immune evasion, nonstructural proteins

1 Introduction

Rift Valley fever virus (RVFV), belonging to the *Phlebovirus* genus of the *Phenuiviridae* family from *Bunyavirales* (1), is an arthropod-borne virus that affects people and livestock. It was first discovered in 1930 when a fatal infectious disease broke out among sheep in the Rift Valley, Kenya (2). Since the 1950s, the RVF pandemic had regularly occurred throughout Africa (3). The infected area expanded to Yemen and Saudi Arabia in the Arabian Peninsula after 2000 (4, 5). Transmitted by *Aedes* and *Culex* mosquitoes, RVFV spreads in larger geographic ranges due to climate change, making its propagation a possible hazard to non-

epidemic countries (6, 7). Instead of mosquito bites, most human cases are caused by contact with infected animal fluids or tissues (8). RVFV causes human diseases including mild flu-like symptoms, hepatitis, retinitis, lethal encephalitis, and hemorrhagic fever, and the overall mortality rate is 0.5 to 1% (9). Pregnant livestock, especially sheep, are highly susceptible to RVFV infection. It generates abortion storms in which almost all pregnant infected animals have miscarriages (10). It also incurs a high mortality rate among newborn lambs (11). Therefore, RVFV infection has severe economic and human health costs. RVFV is now classified as a Category A disease by the National Institute of Allergy and Infectious Diseases (NIAID) and the National Institutes of Health (NIH) because of its potential for purposeful aerosol transmission and the absence of FDA-approved antiviral therapies or licensed vaccinations for humans. RVFV is also a select agent by the Centers for Disease Control and Prevention (CDC) and the U.S. Department of Agriculture (USDA).

RVFV genome consists of tripartite negative-sense single-stranded RNA segments. The RNA-dependent RNA polymerase is encoded by the large (L) segment (Figure 1). The medium (M) segment encodes the nonstructural protein NSm and envelope glycoproteins Gn and Gc. NSm-1 and NSm-2 are expressed from alternative start codons (Figure 1) (12). The nucleocapsid protein (N) and the nonstructural proteins (NSs) are both encoded by the small (S) segment (Figure 1). These two proteins are expressed in an ambisense manner, which means the N gene is encoded in the negative-sense genome, and NSs gene is encoded in the positive-sense genome (13, 14).

When host cells detect an RNA virus, a series of complicated innate immune responses are initiated to eliminate the virus, alert cells nearby, and assemble more specialized immune cells to the site of infection. Retinoic acid-inducible gene I (RIG-I), melanoma differentiation factor 5 (MDA5), and Toll-like-receptors (TLRs) are cytosol pattern recognition receptors (PRRs) capable of detecting RNA viruses (15). RIG-I can be recruited to the mitochondria where it associates with the mitochondrial antiviral signaling protein (MAVS) (16). This activated RIG-I/MAVS complex serves as the intersection of multiple innate immune pathways stimulated immediately, particularly the interferon (IFN) and nuclear factor κB (NF-κB) signals (17). However, RNA viruses have advanced procedures to avoid, exploit, or dysregulate these innate immune pathways, which can be seen in chikungunya virus (CHIKV) infection (18). The E1, E2, and nsP2 proteins of CHIKV potently inhibit the activity of MDA5/RIG-I, and nsP2 also suppresses the downstream phosphorylation of signal transducer and activator of transcription 1 (STAT1), blocking the IFN-induced JAK-STAT pathway (18). In this review, we summarize host innate immune responses to RVFV and how they are dysregulated by viral interference, which will offer possible insights into the vaccine and antiviral developments against RVFV.

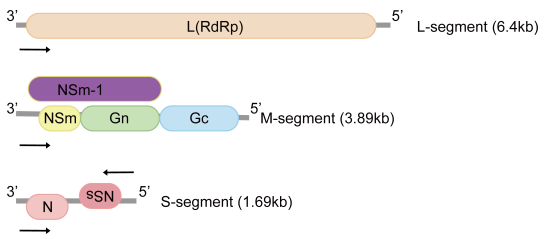

FIGURE 1
Genomic structure of Rift Valley fever virus. The tripartite negative-sense single-stranded RNA segments are named according to sizes: small (S), medium (M) and large (L), and proteins encoded by each segment are illustrated. The M-segment encodes at least four types of proteins: Gn, Gc, NSm and NSm-1. N and NSs are expressed in an ambisense manner. L, L protein; RdRp, RNA-dependent RNA polymerase; Gn, Gc: glycoproteins; NSm, non-structural protein M; N, nucleocapsid protein; NSs, non-structural protein S.

2 Innate antiviral host defense: Interferon response as the crucial step

Interferon is a potent cytokine and a key component of the first line of defense against viral infection (19), which has immunological effects mainly through the direct induction of anti-pathogen molecules that inhibit viral replication (20). There are three types of IFNs involved in antiviral immunity, including IFN-I, IFN-II, and IFN-III. IFN-I and IFN-III share important antiviral properties and are expressed by cells with immunologic and tissue specificity (20, 21).

RNA-triggered intrinsic immunity of RVFV is initiated predominantly by recognition of RIG-I (22). RIG-I consists of a C-terminal domain, a DECH helicase, and N-terminal caspase activation and recruitment domains (CARDs). When cytoplasmic RIG-I is bound with viral RNA, its recruitment to MAVS is activated through the liberated CARDs (23). RIG-I/MAVS complex then catalyzes the combination of TANK-binding kinase 1(TBK1) and inhibitor of κB kinase ϵ (IKKϵ) to phosphorylate and dimerize interferon regulatory factor 3 (IRF3). The phosphorylated dimeric IRF3 could be transported into the nucleus to directly promote IFN-I transcription (24). IFN-I aims primarily to activate the JAK/STAT immune signals in autocrine and paracrine manners, which results in IFN-stimulated genes (ISGs) expression, eliciting subsequent adaptive immune responses (25).

2.1 MAVS is crucial for mounting IFN-I response

RIG-I is critical for IFN generation in a TLR-independent way by primary immune cells like macrophages and dendritic

cells. That signaling through MAVS protects cells against mortality and mild morbidity during live RVFV mucosal infection (22). RVFV has been emerging as a noticeable neuropathogen (26, 27) and airborne transmission causes severe encephalitis. To understand the precise molecular mechanisms by which RVFV infection is controlled in the brain, a recent study found that microglia, the resident immune cell in the central nervous system acting as macrophages, strongly upregulated transcriptional levels of antiviral immune genes and increased levels of activation markers as well as cytokine secretion. This process was dependent on MAVS rather than TLR3 or TLR7 (28). MAVS-/- mice displayed IFN-I defects and lymphocyte infiltration dysregulation, leading to enhanced susceptibility to RVFV and higher mortality. This study defines a protective role for MAVS in propagating antiviral responses in the brain and suggests that signaling through MAVS may also be required for cerebral functional T and NK cell responses.

2.2 Intrinsic antiviral effect of exosomes

Exosomes belong to extracellular vesicles (EVs) and make contributions to cell–cell communication, immunomodulation, as well as infectivity enhancement during viral infections (29). The content of exosomes depends on the cellular origin and the type of infection (30, 31). They are thought to originate from late endosomes and then are secreted into the extracellular environment (32).

Although studies have shown the role of exosomes in viral infections (33), little is known about the mechanisms by which exosome exchanges control the immune response and impact the pathogenesis of RVFV. Researchers generated RVFV-resistant latent clones whose exosomes contain not only normal marker CD63 but also viral RNA and proteins like N and NSs (34). Some of the neighboring recipient cells showed drastically increased apoptosis *via* PARP cleavage and caspase 3 activation. Later, one study revealed how exosomes affect viral production and protect recipient cells in an innate immune manner (35). Exosomes that are purified from RVFV-infected cells carry RNA genome segments, which activate RIG-I to induce IFN-dependent activation of autophagy in naïve recipient cells like monocytes to suppress viral replication and dissemination.

2.3 Host cell metabolites and immune response

2.3.1 Polyamine depletion stimulates innate immune signal

To successfully infect a host cell, viruses need cellular metabolites, and there are different ways they can take over these molecules. One of the critical members of these metabolites is polyamines. They are small, positively charged host-derived molecules that play diverse roles in human cells (36), and polyamine-depleted mammalian cells maintain viability without significant toxicity (37). RNA viruses rely on polyamines for replication (38) and a recent study showed that diverse bunyaviruses, especially RVFV, La Crosse virus (LACV), and Keystone virus (KEYV), require polyamines for productive infection (39). Viral noninfectious particles can interfere with productive infection *via* binding cellular receptors or usurping cellular and viral machinery from infectious viruses (40). In polyamine-depleted cells, bunyaviruses produce a large number of noninfectious virions that are indistinguishable from infectious particles, but these particles could disrupt productive infection and stimulate antiviral signaling pathways like the IFN-I pathway. To conclude, polyamine depletion results in the accumulation of noninfectious particles that interfere with viral replication and stimulate innate immune signaling to limit infectivity. Later, researchers investigated how polyamines precisely function in RVFV infection and found that spermidine, a specific type of polyamine, is required for RVFV replication (41). Furthermore, RVFV also relies on polyamines for cholesterol synthesis to complete replication and form progeny virions, including the incorporation of cholesterol in virions (42). It will emphasize a promising method of targeting host polyamines to reduce virus replication.

2.3.2 AMPK inhibits fatty acid synthesis to restrict viral infection

Viruses also manipulate cellular lipids to form complex structures required for viral replication, many of which are dependent on *de novo* fatty acid synthesis (43). For example, envelope formation during viral assembly involves membrane lipid modifications (44). The energy regulator AMP-activated protein kinase (AMPK), which strongly inhibits fatty acid synthesis (45), could restrict infection of RVFV, and it relies on the upstream activator LKB1 (46). AMPK is activated during RVFV infection, leading to the phosphorylation and inhibition of acetyl-CoA carboxylase, the first rate-limiting enzyme in fatty acid synthesis. Therefore, the activation of AMPK both restricts infection and reduces lipid levels. Also, this pathway plays a broad role in the antiviral defense of various arboviruses. Taken together, AMPK is an important component of the host cell innate immune response that provides a novel antiviral therapeutic target associated with the suppression of fatty acid metabolism.

2.4 TCF/β-catenin regulates virus-induced IFN-β expression

Production of IFN-β plays a key role in the innate antiviral response. Using genome-wide RNA interference (RNAi)

screening, canonical Wnt/β-catenin signaling was found to be an important host pathway during RVFV infection. It can regulate optimal cell cycle conditions and mediate the formation of the TCF/β-catenin complex to promote efficient viral replication (47). β-catenin can be found within a degradation complex associated with GSK-3, the Wnt/β-catenin pathway kinase. Inhibiting GSK-3 increases the amount of β-catenin and promotes its nuclear accumulation. β-catenin interacts with T-cell factor (TCF), rather than IRF3, to form the TCF/β-catenin complex, which can be recruited over the IFN-β promoter and increase the degree of constitutive IFN-β expression in uninfected cells (48). Additionally, raising the level of constitutive IFN-β is capable of conferring an effective antiviral state to naïve cells in order to promote subsequent virus-induced IFN-β expression. In RVFV infection, active TCF/β-catenin complexes are formed and the host Wnt/β-catenin pathway is targeted at the transcriptional and protein levels. NS protein is the major virulent factor to inhibit Wnt/β-catenin signaling by regulating relevant gene expression. Removal of NS protein from RVFV activates the Wnt/β-catenin pathway, forming a TCF/β-catenin complex, and TCF directly upregulates IFN-β expression.

3 Viral countermeasure and innate immune evasion

Host cells tend to take immediate measures to limit viral replication and propagation right after being infected, and simultaneously the virus initiates countermeasures to limit the cell's antiviral responses. This includes suppressing the host innate immune pathway, and directly disrupting host gene expression.

3.1 Alternative splicing of RIOK3 during RVFV infection reverses its antiviral and anti-inflammatory effects

Transcriptome studies have revealed that viral invasion could change host splicing patterns (49). A significant post- and co-transcriptional regulatory mechanism known as alternative splicing (AS) affects the expression of more than 95% of the genes in the human genome and increases genetic coding capacity (50). Through its functional relationship with nonsense-mediated decay (NMD) to degrade premature termination selectively, AS enables the creation of structurally varied protein isoforms from a single gene and can help regulate gene expression (51, 52).

Atypical RIO Kinase 3 (RIOK3) has been demonstrated to play a significant role in promoting IFN-I production *via* PRR signaling mediated by RIG-I-like receptors to inhibit RVFV propagation (53). However, RIOK3 mRNA expression is distorted shortly after RVFV infection to produce alternatively spliced variants, RIOK3 X2, the truncated protein encoding premature termination codons to act as NMD substrate (54). This alternative splicing of the RIOK3 transcript reduces interferon expression conversely. Splicing factor TRA2-β is the key to regulating RIOK3 splicing isoforms (55). TRA2-β interaction with specific regions of RIOK3 pre-mRNA is essential for constitutive splicing of RIOK3 mRNA and RIOK3's antiviral effect while lacking TRA2-β increases alternative splicing. TRA2-β mRNA is also alternatively spliced during RVFV infection, leading to a decrease in cellular TRA2-β levels. The roles of RIOK3 and its spliced isoform in both IFN and NF-κB pathways are intriguing (56). RIOK3 negatively regulates the inflammatory response, but RIOK3 X2 reverses the effects, mitigating the IFN response and increasing the inflammatory NF-κB response. Therefore, both RIOK3 and its X2 isoform have particular functions in separate RVFV-induced innate immune pathways (Figure 2).

3.2 NSs protein: primary virulence factor inducing immune escape

3.2.1 Main functions of RVFV NSs protein

RVFV NSs accumulates in the nucleus and cytoplasm, while nuclear NSs forms a filamentous structure (57). Encoded on the S-segment of the RVFV genome, it is an important virulence factor which could potently suppress the innate immune response (58). NSs binds to Sin3A Associated Protein 30 (SAP30), and through interactions with the transcription factor Yin Yang 1(YY1) protein, the NSs-SAP30-YY1 complex blocks the activation of the IFN-β promoter (59). Viral evasion can occur with the contribution of NSs protein since RVFV lacking NSs is shown to induce abundant IFN-I in mice and no viremia is present (60).

Also, NSs generally inhibits host transcription and facilitates viral translation. Eukaryotic transcription factor IIH (TFIIH) is a general transcription factor for transcriptional initiation by eukaryotic RNA polymerase II and plays an important role in nucleotide excision DNA repair. TFIIH is comprised of ten subunits, including the core complex XPD, XPB, p44, p62, p8, p34 and p52. RVFV NSs could competitively bind to p44 and sequester it from binding with XPD (61). p62 is degraded by NSs in a post-translational way. Under the ubiquitin-proteasome pathway, NSs works as an adaptor protein in the cullin 1-Skp1-FBXO3 E3 ligase complex for p62 degradation (62, 63). These two methods disrupt the recruitment of the TFIIH complex in the nucleus, thus leading to the host transcriptional shutoff (Figure 2).

Similarly, RVFV NSs protein enhances the post-translational degradation of dsRNA-dependent protein kinase R(PKR) (64).

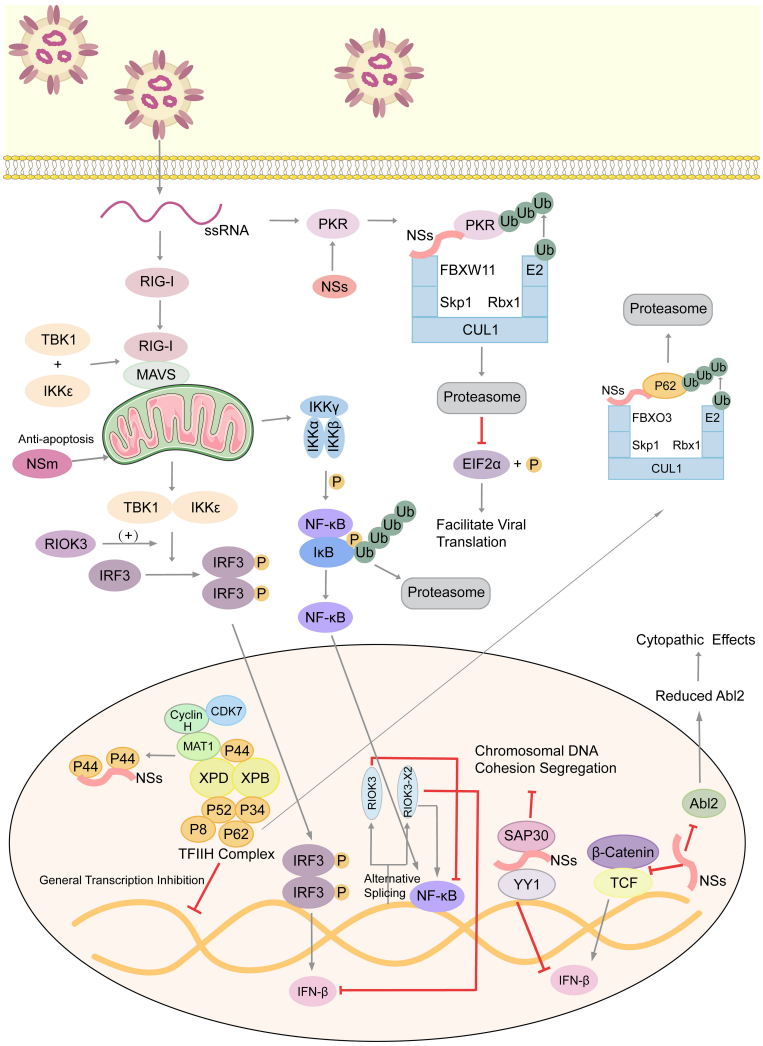

FIGURE 2
Arm race between RVFV and host, with emphasis on immune evasion by RVFV. RVFV ssRNA is recognized by cytosolic RIG-I. RIG-I associates with mitochondrial MAVS to activate multiple innate immune pathways. The kinase RIOK3 facilitates IFN expression and inhibits the inflammatory response pathway mediated by NF-κB, while the alternative splicing isoform RIOK3 X2 antagonizes these effects. RVFV infection also stimulates the Wnt pathway to produce IFNβ, but the NSs protein inhibits this process. NSs conduct the immune escape from several aspects. Those include inhibiting the aggregation of TFIIH complex to extensively inhibit host transcription, degrading kinase PKR to decrease eIF2α phosphorylation and promote the translation of viral proteins, and forming SAP30-NSs-YY1 co-repressor complex at the IFN promoter to block its transcription. Moreover, NSs affect the formation of cytoskeleton *via* suppressing Abl2 expression, which changes cell morphology and movement. Also, NSs could damage the host chromosomal DNA and disrupt mitosis. NSm, however, plays an anti-apoptotic role in mitochondria. ssRNA, single-stranded RNA; RIG-I, retinoic acid-inducible gene I; MAVS, mitochondrial antiviral signaling protein; TBK1, TANK-binding kinase 1; IKK, inhibitor of κB kinase; IκB, inhibitor of NF-κB; IRF3, interferon regulatory factor 3; TCF, T-cell factor; RIOK3, RIO Kinase 3; TFIIH, transcription factor IIH; CUL1, cullin 1; FBXO3, F-box protein 3; Skp1, S-phase kinase associated protein 1; FBXW11, F-box and WD repeat domain containing 11; Rbx-1, ring-box 1; PKR, protein kinase R; eIF2α, eukaryotic initiation factor 2α; SAP30, Sin3A associated protein 30; YY1, transcription factor Yin Yang 1; Abl2, Abelson murine leukemia viral oncogene 2; P, phosphate group; Ub, ubiquitin.

PKR is a translation-inhibiting protein kinase. It can phosphorylate Eukaryotic initiation factor 2α (eIF2α), and then phosphorylated eIF2α inhibits the translation process. NSs participates in the formation of the E3 ligase complex, which consists of CUL1, Skp1, and FBXW11 (65, 66). This E3 ligase complex promotes the degradation of PKR *via* the ubiquitin-proteasome system as well. In consequence, PKR-mediated eIF2α phosphorylation is blocked and viral translation is facilitated effectively (Figure 2) (67).

Because of the genetic similarity of viruses within the *Phenuiviridae* family, NSs is also a key virulence factor of other phenuiviruses and its antiviral immune suppression in those phenuiviruses is worth investing in. NSs of *Dabie bandavirus* (severe fever with thrombocytopenia syndrome

virus, SFTSV) has an intriguing mechanism to form granules in the cytoplasm, the inclusion bodies, to entrap factors involved in IFN-induced antiviral responses, like TBK1 and the E3 ubiquitin ligase TRIM25 that is essential for RIG-I activation (68). TBK1 is a critical regulator of not only IFN responses but also the NF-κB inflammatory pathway because it hinders the form of the IKK complex to limit the release and nuclear translocation of NF-κB. The inhibition of TBK1 during SFTSV infection leads to hyper-activation of NF-κB and inflammatory response (69). NSs of SFTSV could induce the cytokine storm, which leads to a high fatality rate of SFTS. Therefore, the different regulatory mechanisms of NS proteins in the innate immune system between RVFV and SFTSV have strong correspondence with their divergent pathogenicity and clinical manifestations.

3.2.2 NSs affects host cell replication

Nuclear abnormalities and a decreased mitotic rate observed in RVFV-infected cells, like micronuclei and lobulated nuclei, are largely because of the chromosomal cohesion and segregation defects (70). NSs filaments accumulating in the nucleus induce canonical DNA damage signaling, including checkpoint kinase 2 (Chk2), ataxia-telangiectasia mutated (ATM), and p53 (Figure 2). They also induce cell cycle arrest at the S phase or the G0/G1 phase (71). The SAP30-YY1 complex formed by NSs protein could affect not only IFN-β expression but also the cohesion and segregation of chromatin DNA. Through the SAP30-binding domain, RVFV NSs filaments interact with the pericentromeric major γ-satellite sequence, but not the centromeric minor α-satellite sequence. Also, YY1 could mediate the interaction between the NSs-SAP30 complex and the γ-satellite sequence DNA (70). It is assumed that through NSs-mediated DNA damage, erroneous host cell replication impairs normal tissue development and may contribute to fetal deformity in infected ruminants.

3.2.3 NSs and cytopathic effects

Besides functioning as the main virulence factor counteracting the host innate antiviral response to facilitate viral replication and spread, the role of NSs in RVFV-induced cytopathic effects was investigated (72). Abelson murine leukemia viral oncogene homolog 2 (Abl2) is a key regulator of the actin cytoskeleton, regulating cell morphology and mobility as well as cell-cell and cell-matrix adhesion (73, 74) *via* its tyrosine kinase domain and two filamentous actin binding domains (75). The impact of NSs expression on the actin cytoskeleton was examined when carrying out infections with the NSs-expressing virulent (ZH548) strain, the attenuated (MP12) strain, and the non-NSs-expressing (ZH548ΔNSs) strain, as well as following the ectopic expression of NSs. The upregulation of Abl2 expression in macrophages, fibroblasts, and hepatocytes, which would be identified as a component of antiviral responses, was blocked by NSs expression. In addition, ZH548-infected cells had increased mobility compared to ZH548ΔNSs-infected fibroblasts with substantial alterations in cell morphology, including the loss of lamellipodia, cell spreading, and distortion of adherens junctions. All these phenomena are similar to the ZH548-induced cytopathic effects seen *in vivo*. Taken together, NSs protein affects the actin cytoskeleton of host cells at the transcriptional and cellular levels, and the upregulation of Abl2 expression is proposed to be part of the host strategy to restrict virulence (Figure 2).

3.3 Anti-apoptotic role of NSm proteins

Like NSs protein, NSm is not essential for viral replication in cell cultures (76). A recent study screened and identified 9 host proteins that putatively interact with RVFV NSm, and three of them (Cpsf2, Ppil2, SNAP-25) are the most promising targets during viral infection (77). RVFV NSm was identified as the first *Phlebovirus* protein that has an anti-apoptotic function (78). The C-terminal region of NSm, which contains a basic amino acid cluster and a putative transmembrane domain, targets itself to the mitochondrial outer membrane to resist apoptosis (Figure 2) (79).

In comparison to RVFV arMP-12-infected cells, RVFV arMP-12-del21/384-infected cells which lacked NSm expression caused widespread cell death because of the cleavage of Caspase-3 and its downstream substrate poly (ADP-ribose) polymerase. And the initiator caspases, caspase-8 and -9, were all activated earlier. Further, NSm does not require other viral proteins to prevent cell apoptosis because NSm production prevents the staurosporine(STP)-induced activation of caspase-8 and-9. The P38-MAPK pathway is essential for cell survival, and RVFV NSm could also regulate the p38-MAPK response in mammalian cells (80). The specific host factors involved in the NSm-mediated anti-apoptosis are worth investigating, and whether NSm contributes to reaching a balance with the pro-apoptotic NSs protein is an interesting problem requiring further comparison of various environmental factors and mutual molecular mechanisms.

4 Conclusion and perspectives

As one of the most important bunyaviruses, RVFV has been responsible for significant human and ruminant outbreaks that have devastated local economies with increasing mortality and morbidity. Upon viral infection, the innate immune system is activated as the first line of defense. IFN response is induced by intricate upstream pathways. The MDA5 and RIG-I are RIG-I-like receptors (RLRs) sensing foreign RNA in the cytoplasm, which transduce a signaling cascade to induce downstream IFN

production and subsequent antiviral responses. Lack of metabolites essential for the viral replication cycle and production of noninfectious particles are also methods against RVFV infection. RVFV evolves to evade immune attacks and in turn impairs cellular functions, which is mainly achieved by the powerful virulent NSs protein. These studies are critical to the development of RVFV attenuated vaccines that have been created so far, as well as the research on novel targets for effective viral inhibitors.

According to the effects of exosomes, it is verified that antiviral autophagy can be induced by IFN signals in RVFV infection. ERK1/2 Akt/mTOR signaling pathway might participate in the antiviral immunity since they have been in anti-tumor immunity (81). Meanwhile, IFN-β also activates caspase-dependent apoptosis, and autophagy could in turn decrease apoptosis to promote cell growth (81). Although IFN-induced innate immunity is TLR-independent, there still exists a Toll receptor-autophagy axis in RVFV infection with Toll-7 and Toll-like receptor adaptor MyD88 (82). Since NSs presents potent suppression of IFN-β transcription and induces the p53 signaling pathway to increase cell apoptosis (83), it is of great significance to discover other independent autophagy-activated systems to restrict viral replication in time. Further research on the precise mechanism in which autophagy is initiated by anti-RVFV innate immune responses and on the intrinsic correlation between IFN-induced autophagy and IFN-related apoptosis during RVFV infection is still needed.

TCF/β-catenin complexes can upregulate the level of IFN-β expression in response to RVFV infection, which is antagonized by the virulence factor NSs. In addition, Wnt/β-catenin signals are shown to regulate the polyamine metabolic pathway in aggressive prostate cancer, reducing the concentrations of citrate and spermine (84). β-catenin signals also promote fatty acid β-oxidation as energy resources for osteoblast metabolism (85). Given that polyamine depletion and fatty acid synthesis inhibition could shut off viral replication and stimulate IFN-induced innate immune responses, it is a promising strategy to target the Wnt/β-catenin pathway and produce a combined action to limit the progress of RVFV infection.

NSs is a key virulence factor of phenuiviruses as an antiviral immune antagonist, but NSs in these viruses have slight differences in anti-immune mechanisms and corresponding cellular effects. Unlike RVFV filamentous NSs in the nucleus, SFTSV, Toscana virus (TOSV) and Uukuniemi virus (UUKV) NSs proteins localize only in the cytoplasm, so they could not directly inhibit host transcription. Besides the unique cytoplasmic granules generated by SFTSV NSs to sequester numerous host factors, TOSV NSs degrades PKR to facilitate viral translation similarly with RVFV, but TOSV NSs could also degrade RIG-I to suppress IFN-β signal activation with its E3 ubiquitin ligase activity (86, 87). NSs of the Punta Toro virus (PTV) can inhibit host transcription, but the nuclear NSs does not form a filamentous structure (88). Sandfly fever virus (SFV) NSs blocks downstream IFN-I signals by inhibiting Jak1 phosphorylation (89). In general, despite the genetic diversity of NSs among different phenuiviruses, it is of great significance to find out their highly conserved IFN-inhibitory activity in immune evasion to drive the development of broad-spectrum drugs and effective vaccines.

From what has been discussed above, most studies have concentrated on how the virus works to counteract the innate immune response, which is the body's initial and first line of defense. However, RVFV has also developed additional means of attacking various cellular processes, like the cytopathic effects and pro-apoptosis. These methods contribute to viral pathogenicity and should be further investigated in the future.

Author contributions

LZ conceived the study. XW wrote the first draft. YY and LZ revised the manuscript. XW and YL generated the Figures. All authors read and approved the final manuscript.

Funding

This work was supported by grants from National College Students innovation and entrepreneurship training program [202210439003], Taishan Scholars Program, and Academic promotion programme of Shandong First Medical University [2019LJ001].

Conflict of interest

The authors declare that the research was conducted in the absence of any commercial or financial relationships that could be construed as a potential conflict of interest.

Publisher's note

References

1. Adams MJ, Lefkowitz EJ, King AMQ, Harrach B, Harrison RL, Knowles NJ, et al. Changes to taxonomy and the international code of virus classification and nomenclature ratified by the international committee on taxonomy of viruses (2017). *Arch Virol* (2017) 162:2505–38. doi: 10.1007/s00705-017-3358-5

2. Daubney R, Hudson JR, Garnham PCC. Enzootic hepatitis or rift valley fever. an undescribed virus disease of sheep cattle and man from east africa. *J Pathol Bacteriol* (1931) 34:545–79. doi: 10.1002/path.1700340418

3. McMillen CM, Hartman AL. Rift valley fever in animals and humans: Current perspectives. *Antiviral Res* (2018) 156:29–37. doi: 10.1016/j.antiviral.2018.05.009

4. Madani TA, Al-Mazrou YY, Al-Jeffri MH, Mishkhas AA, Al-Rabeah AM, Turkistani AM, et al. Rift valley fever epidemic in Saudi Arabia: epidemiological, clinical, and laboratory characteristics. *Clin Infect Dis* (2003) 37:1084–92. doi: 10.1086/378747

5. Nasher AAW, Shiban AK, Al-Eriyani M, Aly-Bourgy A, Al-Kohlani AH, Benbrake M, et al. Outbreak of rift valley fever–Yemen, august-October 2000. *MMWR Morb Mortal Wkly Rep* (2000) 49:1065–6.

6. Samy AM, Elaagip AH, Kenawy MA, Ayres CFJ, Peterson AT, Soliman DE. Climate change influences on the global potential distribution of the mosquito culex quinquefasciatus, vector of West Nile virus and lymphatic filariasis. *PloS One* (2016) 11:e0163863. doi: 10.1371/journal.pone.0163863

7. Iwamura T, Guzman-Holst A, Murray KA. Accelerating invasion potential of disease vector aedes aegypti under climate change. *Nat Commun* (2020) 11:2130. doi: 10.1038/s41467-020-16010-4

8. Nicholas DE, Jacobsen KH, Waters NM. Risk factors associated with human rift valley fever infection: systematic review and meta-analysis. *Trop Med Int Health* (2014) 19:1420–9. doi: 10.1111/tmi.12385

9. Ikegami T, Makino S. The pathogenesis of rift valley fever. *Viruses* (2011) 3:493–519. doi: 10.3390/v3050493

10. Coetzer JA. The pathology of rift valley fever. II. lesions occurring in field cases in adult cattle, calves and aborted foetuses. *Onderstepoort J Vet Res* (1982) 49:11–7.

11. Bird BH, Githinji JWK, Macharia JM, Kasiiti JL, Muriithi RM, Gacheru SG, et al. Multiple virus lineages sharing recent common ancestry were associated with a large rift valley fever outbreak among livestock in Kenya during 2006-2007. *J Virol* (2008) 82:11152–66. doi: 10.1128/JVI.01519-08

12. Kreher F, Tamietti C, Gommet C, Guillemot L, Ermonval M, Failloux A-B, et al. The rift valley fever accessory proteins NSm and P78/NSm-GN are distinct determinants of virus propagation in vertebrate and invertebrate hosts. *Emerg Microbes Infect* (2014) 3:e71. doi: 10.1038/emi.2014.71

13. Bouloy M, Weber F. Molecular biology of rift valley fever virus. *Open Virol J* (2010) 4:8–14. doi: 10.2174/1874357901004010008

14. Ikegami T. Molecular biology and genetic diversity of rift valley fever virus. *Antiviral Res* (2012) 95:293–310. doi: 10.1016/j.antiviral.2012.06.001

15. Brisse M, Ly H. Comparative structure and function analysis of the RIG-I-Like receptors: RIG-I and MDA5. *Front In Immunol* (2019) 10:1586. doi: 10.3389/fimmu.2019.01586

16. Sun Q, Sun L, Liu H-H, Chen X, Seth RB, Forman J, et al. The specific and essential role of MAVS in antiviral innate immune responses. *Immunity* (2006) 24:633–42. doi: 10.1016/j.immuni.2006.04.004

17. Seth RB, Sun L, Ea C-K, Chen ZJ. Identification and characterization of MAVS, a mitochondrial antiviral signaling protein that activates NF-kappaB and IRF 3. *Cell* (2005) 122:669–82. doi: 10.1016/j.cell.2005.08.012

18. Liu Y, Yuan Y, Zhang L. Innate immune evasion by alphaviruses. *Front Immunol* (2022) 13:1005586. doi: 10.3389/fimmu.2022.1005586

19. Sadler AJ, Williams BRG. Interferon-inducible antiviral effectors. *Nat Rev Immunol* (2008) 8:559–68. doi: 10.1038/nri2314

20. Stanifer ML, Pervolaraki K, Boulant S. Differential regulation of type I and type III interferon signaling. *Int J Mol Sci* (2019) 20:1445. doi: 10.3390/ijms20061445

21. Hervas-Stubbs S, Perez-Gracia JL, Rouzaut A, Sanmamed MF, Le Bon A, Melero I. Direct effects of type I interferons on cells of the immune system. *Clin Cancer Res* (2011) 17:2619–27. doi: 10.1158/1078-0432.CCR-10-1114

22. Ermler ME, Yerukhim E, Schriewer J, Schattgen S, Traylor Z, Wespiser AR, et al. RNA Helicase signaling is critical for type i interferon production and protection against rift valley fever virus during mucosal challenge. *J Virol* (2013) 87:4846–60. doi: 10.1128/JVI.01997-12

23. Kowalinski E, Lunardi T, McCarthy AA, Louber J, Brunel J, Grigorov B, et al. Structural basis for the activation of innate immune pattern-recognition receptor RIG-I by viral RNA. *Cell* (2011) 147:423–35. doi: 10.1016/j.cell.2011.09.039

24. Honda K, Takaoka A, Taniguchi T. Type I interferon [corrected] gene induction by the interferon regulatory factor family of transcription factors. *Immunity* (2006) 25:349–60. doi: 10.1016/j.immuni.2006.08.009

25. Nan Y, Wu C, Zhang Y-J. Interplay between janus Kinase/Signal transducer and activator of transcription signaling activated by type I interferons and viral antagonism. *Front In Immunol* (2017) 8:1758. doi: 10.3389/fimmu.2017.01758

26. Wiley CA. Emergent viral infections of the CNS. *J Neuropathol Exp Neurol* (2020) 79:823–42. doi: 10.1093/jnen/nlaa054

27. Connors KA, Hartman AL. Advances in understanding neuropathogenesis of rift valley fever virus. *Annu Rev Virol* (2022) 9:437–50. doi: 10.1146/annurev-virology-091919-065806

28. Hum NR, Bourguet FA, Sebastian A, Lam D, Phillips AM, Sanchez KR, et al. MAVS mediates a protective immune response in the brain to rift valley fever virus. *PloS Pathog* (2022) 18:e1010231. doi: 10.1371/journal.ppat.1010231

29. Sampey GC, Meyering SS, Zadeh MA, Saifuddin M, Hakami RM, Kashanchi F. Exosomes and their role in CNS viral infections. *J Neurovirol* (2014) 20:199–208. doi: 10.1007/s13365-014-0238-6

30. Hui WW, Hercik K, Belsare S, Alugubelly N, Clapp B, Rinaldi C, et al. Salmonella enterica serovar typhimurium alters the extracellular proteome of macrophages and leads to the production of proinflammatory exosomes. *Infect Immun* (2018) 86:e00386-17. doi: 10.1128/IAI.00386-17

31. Tucher C, Bode K, Schiller P, Claßen L, Birr C, Souto-Carneiro MM, et al. Extracellular vesicle subtypes released from activated or apoptotic T-lymphocytes carry a specific and stimulus-dependent protein cargo. *Front In Immunol* (2018) 9:534. doi: 10.3389/fimmu.2018.00534

32. Hessvik NP, Llorente A. Current knowledge on exosome biogenesis and release. *Cell Mol Life Sci* (2018) 75:193–208. doi: 10.1007/s00018-017-2595-9

33. Fleming A, Sampey G, Chung M-C, Bailey C, van Hoek ML, Kashanchi F, et al. The carrying pigeons of the cell: exosomes and their role in infectious diseases caused by human pathogens. *Pathog Dis* (2014) 71:109–20. doi: 10.1111/2049-632X.12135

34. Ahsan NA, Sampey GC, Lepene B, Akpamagbo Y, Barclay RA, Iordanskiy S, et al. Presence of viral RNA and proteins in exosomes from cellular clones resistant to rift valley fever virus infection. *Front In Microbiol* (2016) 7:139. doi: 10.3389/fmicb.2016.00139

35. Alem F, Olanrewaju AA, Omole S, Hobbs HE, Ahsan N, Matulis G, et al. Exosomes originating from infection with the cytoplasmic single-stranded RNA virus rift valley fever virus (RVFV) protect recipient cells by inducing RIG-I mediated IFN-b response that leads to activation of autophagy. *Cell Biosci* (2021) 11:220. doi: 10.1186/s13578-021-00732-z

36. Mandal S, Mandal A, Johansson HE, Orjalo AV, Park MH. Depletion of cellular polyamines, spermidine and spermine, causes a total arrest in translation and growth in mammalian cells. *Proc Natl Acad Sci U.S.A.* (2013) 110:2169–74. doi: 10.1073/pnas.1219002110

37. Simoneau AR, Gerner EW, Nagle R, Ziogas A, Fujikawa-Brooks S, Yerushalmi H, et al. The effect of difluoromethylornithine on decreasing prostate size and polyamines in men: results of a year-long phase IIb randomized placebo-controlled chemoprevention trial. *Cancer Epidemiol Biomarkers Prev* (2008) 17:292–9. doi: 10.1158/1055-9965.EPI-07-0658

38. Mounce BC, Cesaro T, Moratorio G, Hooikaas PJ, Yakovleva A, Werneke SW, et al. Inhibition of polyamine biosynthesis is a broad-spectrum strategy against RNA viruses. *J Virol* (2016) 90:9683–92. doi: 10.1128/JVI.01347-16

39. Mastrodomenico V, Esin JJ, Graham ML, Tate PM, Hawkins GM, Sandler ZJ, et al. Polyamine depletion inhibits bunyavirus infection *via* generation of noninfectious interfering virions. *J Virol* (2019) 93:e00530-19. doi: 10.1128/JVI.00530-19

40. Rezelj VV, Levi LI, Vignuzzi M. The defective component of viral populations. *Curr Opin Virol* (2018) 33:74–80. doi: 10.1016/j.coviro.2018.07.014

41. Mastrodomenico V, Esin JJ, Qazi S, Khomutov MA, Ivanov AV, Mukhopadhyay S, et al. Virion-associated polyamines transmit with bunyaviruses to maintain infectivity and promote entry. *ACS Infect Dis* (2020) 6:2490–501. doi: 10.1021/acsinfecdis.0c00402

42. Mastrodomenico V, LoMascolo NJ, Cruz-Pulido YE, Cunha CR, Mounce BC. Polyamine-linked cholesterol incorporation in rift valley fever virus particles promotes infectivity. *ACS Infect Dis* (2022) 8:1439–48. doi: 10.1021/acsinfecdis.2c00071

43. Miller S, Krijnse-Locker J. Modification of intracellular membrane structures for virus replication. *Nat Rev Microbiol* (2008) 6:363–74. doi: 10.1038/nrmicro1890

44. Welsch S, Müller B, Kräusslich H-G. More than one door - budding of enveloped viruses through cellular membranes. *FEBS Lett* (2007) 581:2089–97. doi: 10.1016/j.febslet.2007.03.060

45. Hardie DG, Pan DA. Regulation of fatty acid synthesis and oxidation by the AMP-activated protein kinase. *Biochem Soc Trans* (2002) 30:1064–70. doi: 10.1042/bst0301064

46. Moser TS, Schieffer D, Cherry S. AMP-activated kinase restricts rift valley fever virus infection by inhibiting fatty acid synthesis. *PloS Pathog* (2012) 8: e1002661. doi: 10.1371/journal.ppat.1002661

47. Harmon B, Bird SW, Schudel BR, Hatch AV, Rasley A, Negrete OA. A genome-wide RNA interference screen identifies a role for wnt/β-catenin signaling during rift valley fever virus infection. *J Virol* (2016) 90:7084–97. doi: 10.1128/JVI.00543-16

48. Marcato V, Luron L, Laqueuvre LM, Simon D, Mansuroglu Z, Flamand M, et al. Beta-catenin upregulates the constitutive and virus-induced transcriptional capacity of the interferon beta promoter through T-cell factor binding sites. *Mol Cell Biol* (2016) 36:13–29. doi: 10.1128/MCB.00641-15

49. Havranek KE, White LA, Lanchy J-M, Lodmell JS. Transcriptome profiling in rift valley fever virus infected cells reveals modified transcriptional and alternative splicing programs. *PloS One* (2019) 14:e0217497. doi: 10.1371/journal.pone.0217497

50. Wang ET, Sandberg R, Luo S, Khrebtukova I, Zhang L, Mayr C, et al. Alternative isoform regulation in human tissue transcriptomes. *Nature* (2008) 456:470–6. doi: 10.1038/nature07509

51. Lewis BP, Green RE, Brenner SE. Evidence for the widespread coupling of alternative splicing and nonsense-mediated mRNA decay in humans. *Proc Natl Acad Sci U.S.A.* (2003) 100:189–92. doi: 10.1073/pnas.0136770100

52. Chang Y-F, Imam JS, Wilkinson MF. The nonsense-mediated decay RNA surveillance pathway. *Annu Rev Biochem* (2007) 76:51–74. doi: 10.1146/annurev.biochem.76.050106.093909

53. Feng J, De Jesus PD, Su V, Han S, Gong D, Wu NC, et al. RIOK3 is an adaptor protein required for IRF3-mediated antiviral type I interferon production. *J Virol* (2014) 88:7987–97. doi: 10.1128/JVI.00643-14

54. Havranek KE, White LA, Bisom TC, Lanchy JM, Lodmell JS. The atypical kinase RIOK3 limits RVFV propagation and is regulated by alternative splicing. *Viruses* (2021) 13:367. doi: 10.3390/v13030367

55. White LA, Bisom TC, Grimes HL, Hayashi M, Lanchy JM, Lodmell JS. Tra2beta-dependent regulation of RIO kinase 3 splicing during rift valley fever virus infection underscores the links between alternative splicing and innate antiviral immunity. *Front Cell Infect Microbiol* (2021) 11:799024. doi: 10.3389/fcimb.2021.799024

56. Bisom TC, White LA, Lanchy JM, Lodmell JS. RIOK3 and its alternatively spliced isoform have disparate roles in the innate immune response to rift valley fever virus (MP12) infection. *Viruses* (2022) 14:2064. doi: 10.3390/v14092064

57. Flick R, Bouloy M. Rift valley fever virus. *Curr Mol Med* (2005) 5:827–34. doi: 10.2174/156652405774962263

58. Ly HJ, Ikegami T. Rift valley fever virus NSs protein functions and the similarity to other bunyavirus NSs proteins. *Virol J* (2016) 13:118. doi: 10.1186/s12985-016-0573-8

59. Le May N, Mansuroglu Z, Léger P, Josse T, Blot G, Billecocq A, et al. A SAP30 complex inhibits IFN-beta expression in rift valley fever virus infected cells. *PloS Pathog* (2008) 4:e13. doi: 10.1371/journal.ppat.0040013

60. Bouloy M, Janzen C, Vialat P, Khun H, Pavlovic J, Huerre M, et al. Genetic evidence for an interferon-antagonistic function of rift valley fever virus nonstructural protein NSs. *J Virol* (2001) 75:1371–7. doi: 10.1128/JVI.75.3.1371-1377.2001

61. Le May N, Dubaele S, Proietti De Santis L, Billecocq A, Bouloy M, Egly J-M. TFIIH transcription factor, a target for the rift valley hemorrhagic fever virus. *Cell* (2004) 116:541–50. doi: 10.1016/S0092-8674(04)00132-1

62. Kalveram B, Lihoradova O, Ikegami T. NSs protein of rift valley fever virus promotes posttranslational downregulation of the TFIIH subunit p62. *J Virol* (2011) 85:6234–43. doi: 10.1128/JVI.02255-10

63. Kainulainen M, Habjan M, Hubel P, Busch L, Lau S, Colinge J, et al. Virulence factor NSs of rift valley fever virus recruits the f-box protein FBXO3 to degrade subunit p62 of general transcription factor TFIIH. *J Virol* (2014) 88:3464–73. doi: 10.1128/JVI.02914-13

64. Habjan M, Pichlmair A, Elliott RM, Overby AK, Glatter T, Gstaiger M, et al. NSs protein of rift valley fever virus induces the specific degradation of the double-stranded RNA-dependent protein kinase. *J Virol* (2009) 83:4365–75. doi: 10.1128/JVI.02148-08

65. Mudhasani R, Tran JP, Retterer C, Kota KP, Whitehouse CA, Bavari S. Protein kinase r degradation is essential for rift valley fever virus infection and is regulated by SKP1-CUL1-F-box (SCF)FBXW11-NSs E3 ligase. *PloS Pathog* (2016) 12:e1005437. doi: 10.1371/journal.ppat.1005437

66. Kainulainen M, Lau S, Samuel CE, Hornung V, Weber F. NSs virulence factor of rift valley fever virus engages the f-box proteins FBXW11 and β-TRCP1 to degrade the antiviral protein kinase PKR. *J Virol* (2016) 90:6140–7. doi: 10.1128/JVI.00016-16

67. Ikegami T, Narayanan K, Won S, Kamitani W, Peters CJ, Makino S. Rift valley fever virus NSs protein promotes post-transcriptional downregulation of protein kinase PKR and inhibits eIF2alpha phosphorylation. *PloS Pathog* (2009) 5: e1000287. doi: 10.1371/journal.ppat.1000287

68. Wu X, Qi X, Qu B, Zhang Z, Liang M, Li C, et al. Evasion of antiviral immunity through sequestering of TBK1/IKKε/IRF3 into viral inclusion bodies. *JVirol* (2014) 88:3067–76. doi: 10.1128/JVI.03510-13

69. Khalil J, Yamada S, Tsukamoto Y, Abe H, Shimojima M, Kato H, et al. The non-structural protein NSs of SFTSV causes cytokine storm through the hyper-activation of NF-κB. *Mol Cell Biol* (2020) 41:e00542-20. doi: 10.1128/MCB.00542-20

70. Mansuroglu Z, Josse T, Gilleron J, Billecocq A, Leger P, Bouloy M, et al. Nonstructural NSs protein of rift valley fever virus interacts with pericentromeric DNA sequences of the host cell, inducing chromosome cohesion and segregation defects. *J Virol* (2010) 84:928–39. doi: 10.1128/JVI.01165-09

71. Baer A, Austin D, Narayanan A, Popova T, Kainulainen M, Bailey C, et al. Induction of DNA damage signaling upon rift valley fever virus infection results in cell cycle arrest and increased viral replication. *J Biol Chem* (2012) 287:7399–410. doi: 10.1074/jbc.M111.296608

72. Bamia A, Marcato V, Boissière M, Mansuroglu Z, Tamietti C, Romani M, et al. The NSs protein encoded by the virulent strain of rift valley fever virus targets the expression of Abl2 and the actin cytoskeleton of the host, affecting cell mobility, cell shape, and cell-cell adhesion. *J Virol* (2020) 95:e01768-20. doi: 10.1128/JVI.01768-20

73. Zandy NL, Playford M, Pendergast AM. Abl tyrosine kinases regulate cell-cell adhesion through rho GTPases. *Proc Natl Acad Sci U.S.A.* (2007) 104:17686–91. doi: 10.1073/pnas.0703077104

74. Bradley WD, Koleske AJ. Regulation of cell migration and morphogenesis by abl-family kinases: emerging mechanisms and physiological contexts. *J Cell Sci* (2009) 122:3441–54. doi: 10.1242/jcs.039859

75. Khatri A, Wang J, Pendergast AM. Multifunctional abl kinases in health and disease. *J Cell Sci* (2016) 129:9–16. doi: 10.1242/jcs.175521

76. Won S, Ikegami T, Peters CJ, Makino S. NSm and 78-kilodalton proteins of rift valley fever virus are nonessential for viral replication in cell culture. *J Virol* (2006) 80:8274–8. doi: 10.1128/JVI.00476-06

77. Engdahl C, Näslund J, Lindgren L, Ahlm C, Bucht G. The rift valley fever virus protein NSm and putative cellular protein interactions. *Virol J* (2012) 9:139. doi: 10.1186/1743-422X-9-139

78. Won S, Ikegami T, Peters CJ, Makino S. NSm protein of rift valley fever virus suppresses virus-induced apoptosis. *J Virol* (2007) 81:13335–45. doi: 10.1128/JVI.01238-07

79. Terasaki K, Won S, Makino S. The c-terminal region of rift valley fever virus NSm protein targets the protein to the mitochondrial outer membrane and exerts antiapoptotic function. *J Virol* (2013) 87:676–82. doi: 10.1128/JVI.02192-12

80. Narayanan A, Popova T, Turell M, Kidd J, Chertow J, Popov SG, et al. Alteration in superoxide dismutase 1 causes oxidative stress and p38 MAPK activation following RVFV infection. *PloS One* (2011) 6:e20354. doi: 10.1371/journal.pone.0020354

81. Li Y, Zhu H, Zeng X, Fan J, Qian X, Wang S, et al. Suppression of autophagy enhanced growth inhibition and apoptosis of interferon-beta in human glioma cells. *Mol Neurobiol* (2013) 47:1000–10. doi: 10.1007/s12035-013-8403-0

82. Moy RH, Gold B, Molleston JM, Schad V, Yanger K, Salzano M-V, et al. Antiviral autophagy restrictsRift valley fever virus infection and is conserved from flies to mammals. *Immunity* (2014) 40:51–65. doi: 10.1016/j.immuni.2013.10.020

83. Narayanan A, Amaya M, Voss K, Chung M, Benedict A, Sampey G, et al. Reactive oxygen species activate NFkappaB (p65) and p53 and induce apoptosis in RVFV infected liver cells. *Virology* (2014) 449:270–86. doi: 10.1016/j.virol.2013.11.023

84. Casero RAJr., Murray Stewart T, Pegg AE. Polyamine metabolism and cancer: treatments, challenges and opportunities. *Nat Rev Cancer* (2018) 18:681–95. doi: 10.1038/s41568-018-0050-3

85. Moorer MC, Riddle RC. Regulation of osteoblast metabolism by wnt signaling. *Endocrinol Metab (Seoul)* (2018) 33:318–30. doi: 10.3803/EnM.2018.33.3.318

86. Kalveram B, Ikegami T. Toscana virus NSs protein promotes degradation of double-stranded RNA-dependent protein kinase. *J Virol* (2013) 87:3710–8. doi: 10.1128/JVI.02506-12

87. Gori Savellini G, Anichini G, Gandolfo C, Prathyumnan S, Cusi MG. Toscana virus non-structural protein NSs acts as E3 ubiquitin ligase promoting RIG-I degradation. *PloS Pathog* (2019) 15:e1008186. doi: 10.1371/journal.ppat.1008186

88. Lihoradova OA, Indran SV, Kalveram B, Lokugamage N, Head JA, Gong B, et al. Characterization of rift valley fever virus MP-12 strain encoding NSs of punta toro virus or sandfly fever Sicilian virus. *PloS Negl Trop Dis* (2013) 7:e2181. doi: 10.1371/journal.pntd.0002181

89. Moalem Y, Malis Y, Voloshin K, Dukhovny A, Hirschberg K, Sklan EH. Sandfly fever viruses attenuate the type I interferon response by targeting the phosphorylation of JAK-STAT components. *Front Immunol* (2022) 13:865797. doi: 10.3389/fimmu.2022.865797

frontiers | Frontiers in Immunology

TYPE Review
PUBLISHED 22 December 2022
DOI 10.3389/fimmu.2022.1107173

OPEN ACCESS

EDITED BY
Chenhe Su,
Wistar Institute, United States

REVIEWED BY
Xiaochuan Liu,
University of California, Riverside, United States
Yanzhu Zhu,
Chinese Academy of Agricultural Sciences (CAAS), China

*CORRESPONDENCE
Wanzhe Yuan
yuanwanzhe@126.com
Xiaozhan Zhang
zhangxz@hnuahe.edu.cn

SPECIALTY SECTION
This article was submitted to Viral Immunology, a section of the journal Frontiers in Immunology

RECEIVED 24 November 2022
ACCEPTED 12 December 2022
PUBLISHED 22 December 2022

CITATION
Zhao K, Zhang S, Liu X, Guo X, Guo Z, Zhang X and Yuan W (2022) The game between host antiviral innate immunity and immune evasion strategies of senecavirus A - A cell biological perspective.
Front. Immunol. 13:1107173.
doi: 10.3389/fimmu.2022.1107173

The game between host antiviral innate immunity and immune evasion strategies of senecavirus A - A cell biological perspective

Kuan Zhao[1,2], Shixia Zhang[1], Xiaona Liu[1], Xiaoran Guo[1], Zhaomeng Guo[1], Xiaozhan Zhang[3]* and Wanzhe Yuan[1,2]*

[1]College of Veterinary Medicine, Hebei Agricultural University, Baoding, China, [2]Hebei Veterinary Biotechnology Innovation Center, Hebei Agricultural University, Baoding, China, [3]College of Veterinary Medicine, Henan University of Animal Husbandry and Economy, Zhengzhou, China

Innate immunity is the first line of the cellular host to defend against viral infection. Upon infection, viruses can be sensed by the cellular host's pattern recognition receptors (PRRs), leading to the activation of the signaling cascade and the robust production of interferons (IFNs) to restrict the infection and replication of the viruses. However, numerous cunning viruses have evolved strategies to evade host innate immunity. The senecavirus A (SVA) is a newly identified member of the *Picornaviridae* family, causing severe vesicular or ulcerative lesions on the oral mucosa, snout, coronary bands, and hooves of pigs of different ages. During SVA infection, the cellular host will launch the innate immune response and various physiological processes to restrict SVA. In contrast, SVA has evolved several strategies to evade the porcine innate immune responses. This review focus on the underlying mechanisms employed by SVA to evade pattern recognition receptor signaling pathways, type I interferon (IFN-α/β) receptor (IFNAR) signaling pathway, interferon-stimulated genes (ISGs) and autophagy, and stress granules. Deciphering the antiviral immune evasion mechanisms by SVA will enhance our understanding of SVA's pathogenesis and provide insights into developing antiviral strategies and improving vaccines.

KEYWORDS

senecavirus A (SVA), antiviral innate immunity, ISGs, immune evasion, autophagy, stress granules

Introduction

Senecavirus A (SVA) is a single-strand positive-sense RNA virus belonging to the genus *Senecavirus* of the family *Picornaviridae* and contains only one serotype (1). It was first discovered incidentally in the cell culture medium as a contaminant in 2002 (2). It is not pathogenic in human and does not infect human cells (3), but it has been verified as an oncolytic virus that can propagate in tumor cells of human, so after the first isolation of SVA, it has been used as an oncolytic virotherapy candidate in humans (4–7). Since its first identification in 2002, SVA has been reported as a causative agent associated with sporadic cases of vesicular disease in pigs in the USA (8) and Canada (9). However, several continuous outbreaks of vesicular disease associated with SVA in swine farms were then reported in Canada (10), Thailand (11), Colombia (12), Vietnam (13), India (14), Brazil (15–17), China (18, 19) and USA (20) since 2014. The diseased swine are characterized by severe vesicular and/or ulcerative lesions on the oral mucosa, snout, coronary bands, and hooves, which are indistinguishable from the clinical symptoms caused by foot-and-mouth disease virus (FMDV), vesicular stomatitis virus (VSV) (21). Until now, the outbreaks of SVA caused considerable economic losses to the pig industry worldwide.

The genome of SVA is about 7.2 kb in length and contains a unique open reading frame (ORF) flanked by a 5' untranslated region (UTR) and 3' UTR, with a viral protein (VPg) covalently linked to 5' end of the genome, and with a 3' poly(A) tail. The SVA 5' UTR also contains a hepatitis C virus (HCV)-like internal ribosome entry site (IRES), which recruits ribosomal subunits using a process independent of the cap-binding protein eukaryotic initiation factor (eIF) 4E. (22). The IRES of SVA was predicted to harbor domain II and domain III with pseudoknots which is essential for SVA translation (23, 24). Under the guidance of IRES, the ORF is translated into a single polyprotein and then processed by virus-encoded proteases into Leader protein and P1, P2, and P3 protein intermediate. P1 is further cleaved into four structural proteins, VP4, VP2, VP3, and VP1, responsible for binding to proteins such as the receptor antx-1 and inducing the neutralizing antibodies. The P2 and P3 are cleaved into nonstructural proteins 2A, 2B, 2C and 3A, 3B, 3C, and 3D, respectively (2), which are critical for the replication of SVA in the cells.

Innate immunity is the first line of host defense against invading pathogens that plays a vital role in restricting viral spread and replication. Upon viral infection, the released viral nucleotides are sensed by the host pattern recognition receptors (PRRs) in the cytoplasm or the nucleus and subsequently lead to the activation of a signaling cascade that ultimately results in the robust production of IFN, including IFN-α, IFN-β, and IFN-γ. IFNs bind to IFN receptors and then activate the Janus kinase (JAK)-signal transducer and activator of transcription (STAT) pathway leading to the transcriptional regulation of numerous IFN-regulated genes (ISGs), which exert numerous antiviral functions directly or indirectly (25–27). Although the hosts have developed highly efficient strategies to detect and control invading viruses to resist viral infection and spread, lots of viruses have evolved strategies to evade host defenses and thus effectively infect and replicate in host cells (28). As a cunning virus, increasing evidence suggests that SVA can evade the host's antiviral effect in several ways for better infection and replication.

Evasion of PRR signaling pathways

Pathogen-associated molecular patterns (PAMPs) are unique features in viruses that are recognized by PRRs to activate the innate immune response and proinflammatory cytokine responses during viral infection (25, 29). Upon viral infection, viral PAMPs are sensed by PRRs. Toll-like receptors (TLRs), RIG-I-like receptors (RLRs), and DNA sensors are mammals' main PRRs that sense viral infection. TLRs are transmembrane proteins to recognize PAMPs derived from various microbes and initiate the transcription of inflammatory cytokines and IFNs. Among these TLRs, TLR3 recognizes the double-strand RNA, and TLR7 and TLR8 recognize the single-strand RNA during RNA viral infection (30–32). RLR9 recognizes DNA containing unmethylated CpG motifs in numerous viral and non-viral pathogens (33). Toll-interleukin 1 receptor domain-containing adapter inducing interferon-β (TRIF) is recruited by TLR3, and the myeloid differentiation factor 88 (MyD88) is recruited by TLR7 when they bind to the dsRNA and ssRNA respectively (34). However, the TLRs are limited in sensing viruses as they are only expressed in certain cell types (29). In contrast, RLRs, retinoic acid-inducible gene I (RIG-I), and melanoma differentiation-associated protein 5 (MDA5) were expressed in almost all of the cell types which can recognize the non-self RNA motif (29, 35). RIG-I recognizes short double-stranded (ds) RNA of viruses with 5′-phosphorylated blunt ends, whereas MDA5 binds long dsRNA molecules with no end specificity (36, 37). After RIG-I and MDA5 bind to RNA, it leads to the activation of a signaling cascade and recruits downstream ligand, mitochondrial antiviral signaling protein (MAVS, also known as IPS-1/VISA/Cardif), to activate IRF3 and NF-κB. RIG-I, MDA5 of porcine, two important sensors, interact with MAVS, the downstream adaptor, to activate the innate immune antiviral response during infection (38, 39). Of course, other different adaptors were also recruited. Still, the final result is to stimulate the two downstream kinases, tank-binding kinase 1 (TBK1) and inhibitor of κB kinase ϵ (IKKϵ), resulting in the

phosphorylation and activation of transcription factors, including IFN regulatory factor 3 (IRF3), NF-κB, and AP-1 (40). These transcription factors combine to form transcription factor complexes and enter the nucleus, producing type I IFN. Type I IFN have a broad and diverse impact on the priming of expansion and maturation of adaptive immunity (41, 42). SVA has evolved complex strategies to evade type I IFN restriction, as illustrated in Figure 1, which is discussed in detail.

Targeting RIG-I

RIG-I preferentially recognizes the short dsRNA characterized by blunt ends and a 5′ triphosphate moiety distinguishing host and viral dsRNA (35). RIG-I is under an auto-repressed state without dsRNA ligands. While upon the presentation of a viral dsRNA, the conformation of RIG-I is rearrangement to allow ATP binding to it, a necessary step for activating RIG-I (43). Once it is activated, the downstream adapter can be recruited and activated to induce the production of IFN. So, as a sensor, RIG-I can directly function as an effector in antiviral immunity. To complete viral replication and infection, picornaviruses have evolved strategies to antagonize the antiviral immunity of RIG-I by different methods, such as degrading and cleaving of RIG-I.

The L, 3C, and 2B proteins of the FMDV can degrade the RIG-I (44). EV71 3C protein targets RIG-I to block subsequent recruitment of adaptor molecule MAVS and inhibit consequent

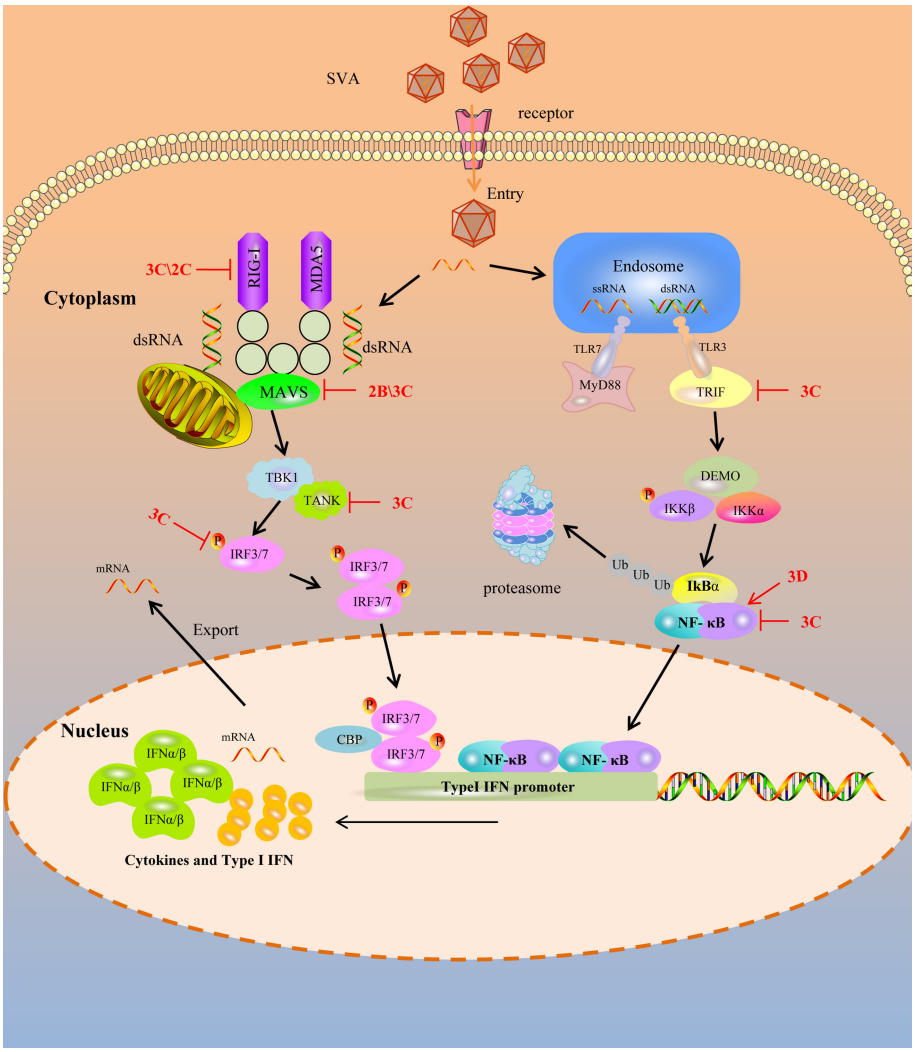

FIGURE 1
SVA escapes PRR mediated IFN-I signaling pathway. Cytoplasmic RNA sensors, such as TLR3, TLR7, RIG-1 and MDA-5, recognize SVA RNA in the cytosol and trigger the generation of IFN-I by transmitting a series of signals. SVA protein can target multiple steps in RLR-mediated IFN-I signaling pathway. The solid line represents the defined interaction between the adaptor and the SVA protein. The red arrow represents the promoting effect, and the red T-shaped symbol represents the inhibiting effect.

nuclear translocation of IRF3, and it also inhibits the ubiquitination of RIG-I to block IFN production (45, 46). Besides, the 3C protein of poliovirus and encephalomyocarditis virus (EMCV) is responsible for the cleavage of RIG-I (47). SVA, as a picornavirus, can evade the host's innate immunity. Overexpressing RIG-I can significantly restrict the replication of SVA, while RIG-I was degraded in SVA-infected cells, with 2C and 3C playing essential roles in this process. Although 3C can interact with RIG-I, 2C cannot. They both significantly reduced Sev or RIG-I-induced IFN-β production. Moreover, 2C and 3C-induced RIG-I degradation depends on the caspase signaling pathway (48). So, the antiviral immunity induced by RIG-I against SVA is weakened by the 2C and 3C of SVA.

Targeting MAVS

The mitochondrial antiviral signaling protein (MAVS) is an important adaptor protein in host anti-RNA virus immunity. It contains an N-terminal CARD domain that interacts with the tandem CARD domains of RIG-I and the C-terminal transmembrane domain that localizes itself to the mitochondrial outer membrane. It mediates the activation of NF-κB and IRFs and induces the production of IFN (49). During viral infection, weakening or blocking the MAVS function will play a multiplier effect in resisting the host's antiviral immunity.

SVA has evolved the ability to suppress the host's innate immune responses to benefit its replication by blocking type I IFN production and ISG expression. Previous studies showed that the 2B protein of SVA can decrease the expression of both exogenous and endogenous MAVS in dose-dependent manners. In contrast, the decrease of MAVS was not associated with the formation of insoluble fractions and the cleaved process. 2B protien of SVA degraded the MAVS by colocalized and interacting with MAVS depending on caspase-9 and caspase-3. In addition, the 1-48 and 100-128aa regions of 2B were essential for inhibiting the type I IFN production (50). Besides, the 3C protein of SVA can interact with MAVS, and the cleavage of the MAVS depends on its protease activity. The cellular apoptosis and degradation process impairs the cleavage of MAVS by the 3C protein. The fragments of MAVS cleavaged by 3C protein lost their activity to induce IFN production (51). So, for MAVS, an important adapter protein, the cunning SVA blocks the host antiviral innate immunity by weakening MAVS biological functions through its 2B and 3C protein.

Targeting IFN regulatory factor

IRF3 and IRF7 are important molecules in virus-mediated induction of type I IFN production. Normally, they remain in the cytoplasm without phosphorylation. During viral infection, the activation of innate immunity could induce IRF3 and IRF7 to undergo phosphorylation, dimerization, and translocation into the nucleus, leading to the expression of IFN which then induce the production of ISGs (52, 53). For this important effect of innate immunity, SVA has evolved strategies to antagonize this antiviral process. Previous researchers found that the 3C protein of SVA inhibited the expression of IRF3 and IRF7 depending on its protease activity. If the catalytic box of the 3C protein was mutated, it failed to mediate the reduction of IRF3 and IRF7. Moreover, it can interact with IRF3 and IRF7 and induce a reduction in the phosphorylation of IRF3 and IRF7 by the protease activity to suppress the production of IFN (54). While for FMDV, another member of picornavirus, reduces the expression of IRF3 and IRF7 by the L protein depending on the protease activity (55). So the 3C protein of SVA functions similarly to the FMDV L protein in antagonizing the innate immune response.

Targeting TRIF and TANK

Toll-like receptors, including TLR3, TLR7, TLR8, TLR9, RIG-I, and MDA5, are the main PRRs to recognize the virus RNA and induce the production of IFN. In the TLR3 signaling pathway, TRIF regulates TLR3-mediated IRF3 and NF-κB activation (56). Besides, tumor necrosis factor receptor-associated factor (TRAF) family member-associated NF-κB activator (TANK) is critical in regulating RLR- and TLR-mediated interferon production. TANK regulates the TBK1-IKK-mediated IFN antiviral response by interacting with several signal molecules, such as MAVS, TRIF, TBK1, and IRF3 (57). Although the host has evolved various antiviral strategies to defend against viral infection, the virus can still complete its replication and infection naturally, so there must be ways to antagonize the antiviral effect of the host. For SVA, during its infection, it failed to trigger host IFN production and the 3C protein showed an extremely inhibitory effect. Further investigation showed that the inhibition of IFN production by 3C depends on the cleavage of TRIF, TANK, and MAVS (51). Furthermore, the cleavage of TRIF and TANK depends on the activity of 3C by interacting with them. TRIF and TANK cleavage fragments lost their functions to induce IFN production. So the SVA antagonizes the host antiviral innate immunity by cleaving TRIF, MAVS and TANK molecular which are crucial for the TLR3 mediated and RLR mediated signaling pathway (51).

Targeting NF-κB

NF-κB is a ubiquitous transcription factor that regulates innate immunity and inflammatory responses. The NF-κB signaling pathway plays an important role in the virus life cycle. The NF-κB pathway is usually activated by RIG-I/

MAVS or cGAS/STING signaling cascades, begins with the cellular PRRs recognizing the PAMPs, especially virus RNA, and then delivers the signaling cascade, which induces the transcription of interferon related genes and then restricting the replication of viruses (58). The NF-κB signaling module consists of five NF-κB monomers (RelA/p65, RelB, cRel, NF-κB1 p50, and NF-κB2 p52), which can dimerize to form up to 15 unique transcription factors (59). NF-κB-p65 is a key NF-κB subunits directly responsible for transactivating NF-κB target genes. In the early stage of SVA infection, the host activates NF-κB by recognizing SVA RNA and then induces a signaling cascade that causes transcriptional expression of downstream molecules to exert antiviral effects (60). However, at the late stage of infection, the NF-κB-p65 could be cleaved by the 3C protein of SVA. While, further studies indicated that the cleavage of NF-κB-p65 is not the direct action of the 3C protein but mediated by caspases. Besides, SVA infection can induce the apoptosis of host cells to promote the replication of itself. Interestingly, NF-κB-p65 prevents the apoptosis induced by SVA, so at the late-stage infection, the cleavage of NF-κB-p65 and induction of host cell apoptosis may be critical for SVA replication and release from infected cells (61, 62). Moreover, the 3D protein of SVA could promote the activation of NF-κB by binding IKKα and IKKβ, which further upregulates the NLRP3 and pro-IL-1β transcription. Then, the N-terminal of 3D promotes the assembly of the NLRP3 inflammatory complex to induce IL-1β production by binding to the NACHT domain of NLRP3 (63), which may be another way for the cunning SVA to evade the innate immunity strategy.

The game between the intrinsic antiviral proteins and SVA

Many intrinsic antiviral proteins can inhibit the replication of SVA, and at the same time, SVA has evolved multiple ways to antagonize thegse proteins. The evasion of ISGs and intrinsic antiviral proteins by SVA is illustrated in Figure 2.

DDX21

DEAD (Asp-Glu-Ala-Asp)-box RNA helicases (DDXs) are the largest family of evolutionarily conserved RNA helicases that are involved in a broad array of host processes, especially in antiviral immunity (64, 65). DDX21, a member of the DDX family, possesses all the signature motifs required for DEAD-helicase function and contains atypical FRGQR repeats in its C-terminus. Furthermore, growing evidences suggest that DDX21 plays an important role in regulating host antiviral immunity against picornaviruses. DDX21 regulated the replication of FMDV by increasing IFN-β and IL-8 production in FMDV infected cells. It also co-precipitates with FMDV IRES and restricts viral IRES-dependent translation and replication (66). Our previous study suggested that DDX21 restricted the replication of SVA in PK15 and BHK-21 cells. Overexpression of DDX21 in the cells suppressed the replication of SVA and knocking down the expression of DDX21 promoted the replication of SVA. In contrast, SVA can effectively replicate in the natural infection condition. Therefore, SVA inevitable could evade the antiviral effect of DDX21. Our further investigation revealed that the expression level of DDX21 gradually decreased with the prolongation of infection time. So, SVA evades the antiviral activity of DDX21 mainly dependent on decreasing its expression. 2B and 3C proteins of SVA were critical for the degradation of DDX21, which depends on the caspase pathway. Moreover, when the activity sites of the 3C protein were mutated, the protease activity was lost. The mutated 3C failed to induce the degradation of DDX21. All of these suggested that the protease activity of 3C protein was necessary for the degradation of DDX21, which contributed to SVA evading the antiviral effect of DDX21 (67).

DHX30

Another RNA helicase, DExH-box helicases (DExH), can act as a sensor molecule to regulate antiviral innate immunity and exert direct antiviral effects by targeting viral proteins or RNA (68). DHX30, a multi-role member of DExH, is involved in the biosynthesis of mitochondrial ribosomes (69) and can be recruited by Zinc-finger antiviral protein (ZAP) through interacting with each other and then increase the antiviral effects of ZAP (70). It can inhibit the replication of numerous viruses, such as HIV-1 and influenza A virus, through different molecular mechanisms (71, 72). Researchers have shown that overexpression of DHX30 inhibits the replication of SVA, and downregulated DHX30 promotes the replication of SVA at the early stage of the life cycle, depending on its helicase activity. For SVA, to antagonize the anti-SVA effects of DHX30, during the infection of SVA, the 3C protein of SVA interacts with DHX30 and cleaves DHX30 at the Q220 site. The SVA 3C protein cleaves DHX30 through its protease activity and independent cellular caspases. Though 3C-mediated DHX30 cleavage products still bound SVA RNA, they lost the ability to inhibit virus replication. The researchers speculated that the cleavage products lost the helicase activity, so they could not exert an antiviral effect. Nevertheless, the reason for this need further investigation (73).

CH25H

Cholesterol-25-hydroxylase (CH25H) is an ISG induced by IFN. As a member of ISG protein, it can convert cholesterol to

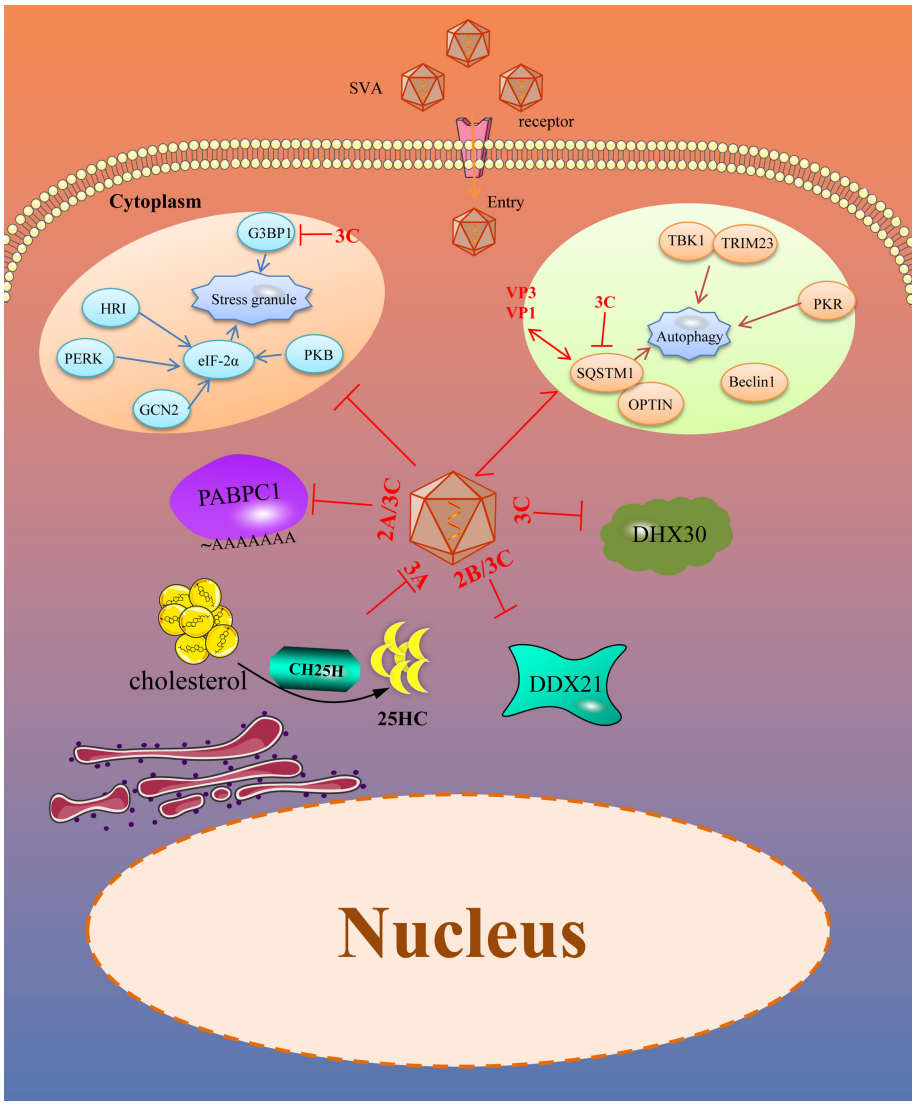

FIGURE 2
SVA evades intrinsic antiviral proteins as well as autophagy and stress granules (SGs). Viral proteins of SVA engage multiple strategies to evade the restriction of intrinsic antiviral proteins. In addition, SVA infection can trigger some other immune responses, such as SGs and autophagy, which helps to limit viral infection. However, these immune responses are also controlled by viral proteins. The solid line represents the defined interaction between the adapter and the SVA protein. The red two-way arrow represents interaction, and the red T-shaped symbol represents the inhibiting effect.

25-hydroxy cholesterol (25HC) (74). 25HC is a soluble factor that suppresses sterol synthesis by regulating sterol-responsive element binding proteins (SREBP) and nuclear receptors, which is reported to inhibit the stage of viral abortion and entry (75, 76). Researchers have demonstrated that CH25H and 25HC can suppress many viruses infection progresses, such as Zika virus (ZIKV), Porcine epidemic diarrhea virus (PEDV), Pseudorabies virus (PRV), EMCV, Porcine reproductive and respiratory syndrome virus (PRRSV) and Herpes simplex virus type 1 (HSV-1) (77–82). In addition, CH25H and 25HC can also inhibit SVA. Overexpression of CH25H inhibits SVA replication. On the contrary, knockdown or knockout of the endogenous CH25H promotes SVA infection. Further, 25HC exerts its antiviral effect by inhibiting virus replication and attachment. Interestingly, the CH25H-M (CH25H mutant) lacking hydroxylase activity still retains its antiviral properties through selectively interaction and degrade SVA 3A protein *via* the ubiquitin-proteasome manner. The antiviral effect of CH25H was dependent and independent of its enzymatic activity (83). For 25HC, it exerts its antiviral effect in the entire life cycle of SVA, especially in the adsorption process of SVA (84). Different viruses have developed strategies to

antagonize the antiviral effect of CH25H and 25HC. PRRSV nsp1β and nsp11 can degrade the CH25H by lysosomal pathway. Moreover, the E protein of PRRSV degrades the CH25H by the ubiquitin-proteasome pathway (85, 86). For SVA, CH25H expression was downregulated during SVA infection and the degradation of CH25H becomes more serious with the prolongation of infection, which maybe a strategy for SVA to antagonize the antiviral effect of CH25H (83). In addtion to, from the results of previous study we found that after CH25H-M was co-transfected with SVA protein, CH25H-M could be degraded by VP4, 2B and 3C protein of SVA to a certain extent (84). All of these revealed that the SVA maybe escape the antiviral effects of CH25H by degraded it with some viral proteins, but it needs further investigation.

PABPC1

The poly(A) binding protein cytoplasmic 1 (PABPC1) is a poly(A) binding protein which consists of a globular domain, four non-identical RNA-recognition motifs (RRMs) and a proline-rich C-terminal domain (87, 88). In the cells, the poly (A) binding protein, mRNA, and eukaryotic translation initiation factor 4 gamma (eIF4G) interacted with each other to constitute a complex that initiating the translation and mRNA circularization (89). Studies have confirmed that PABPC1 is an antiviral protein against SVA. During SVA infection, the PABPC1 was cleaved at residue 437 mediated by the 3C protein through its protease activity which was similar to the EMCV (90). As PABPC1 is critical for protein synthesis and the PABPC1 cleaved by 3C protein will decrease the protein synthesis rates. SVA infection can inhibit the cellular protein synthesis rates over time and interfer with the cell defense system. Besides SVA, the NSP3A protein of rotavirus can bind to eIF4G to transfer PABPC1 from the translation complex (91). The 2A and 3C proteases of picornavirus can inactivate PABPC1 by cleaving the N-terminal of PABPC1 resulting in it cannot bind to eIF4G, thus affecting the normal translation of the host (90, 92). Poliovirus 3C protease cleaves poly(A) binding protein and eIF4G to inhibit host cell translation (93). So, clearing poly (A) binding protein may be a common method for picornavirus to antagonize the antiviral effect of PABPC1.

SVA evades autophagy and stress granules

Viruses are acellular organisms whose life cycle must depend on the host cell enzyme and translation system. The virus is only composed of proteins and nucleic acids. During the viral infection process, the proteins or nucleic acids act as foreign substances that may stimulate the stress responses of the host cells, including autophagy, stress granules, apoptosis, and pyroptosis. While we only discuss autophagy and stress granules antagonized by SVA (Figure 2).

Autophagy

Autophagy is a conserved cellular process important for cell survival and homeostasis. Autophagy enables cells to recycle nutrients and remodel and dispose of unwanted cytoplasmic constituents, critical for protecting the host cells from pathogenic infections (94). Recently, many studies have focused on the antiviral effect of autophagy and found that autophagy is an effective defense strategy against a wide variety of invading viruses (95, 96). However, viruses including Newcastle disease virus (NDV), PRRSV, EMCV, FMDV, PEDV have developed multiple strategies to antagonize the host autophagy process for their benefit (97–101). SVA infection can induce autophagy in different cells by detecting autophagosome formation, GFP-LC3 puncta, and accumulation of LC3-II proteins. However, autophagy suppresses or promotes SVA replication in a species-specific manner, restricting SVA replication in human cells and promoting SVA replication in pig cells (102, 103). Sequestosome 1 (SQSTM1), a selective autophagy receptor, interacts with VP1 and VP3 of SVA and targets them to phagophores for degradation to inhibit viral replication. To counteract this, the 3C protein of SVA targets the receptor SQSTM1 for cleavage at glutamic acid 355, glutamine 392, and glutamine 395 and abolishes its capacity to mediate selective autophagy. Besides, the cleavage products of SQSTM1 mediated by 3C protein lost the ability to inhibit viral propagation (103). In addition, the 2AB protein of SVA interacts with MARCHF8/MARCH8 and LC3 to antagonize the antiviral effect of autophagy. MARCHF8 can combine with MAVS to form a complex and stimulate the IFN-I signaling. The interaction of MARCHF8 and 2AB prevents this combination to deactivate IFN-I signaling. LC3 is also degraded by 2AB and inhibits autophagy (104). So, SVA can evade the autophagy to promote viral replication, mainly dependent on viral 3C and 2AB protein.

Stress granules

Stress granules (SG) are mRNA storage sites that regulate mRNA translation, localization, and degradation. SG responds to various environmental stress and viral infection and is one of the pathways by which host cells respond to pathogenic infection. Viral infection can cause cellular stress and regulate gene expression by influencing mRNA translation, localization, and degradation (105). There is a close relationship between SG and viral infection replication. Four different SG formation

patterns exist during viral infection, including no SG formation, stable SG formation, transient SG formation, and alternate SG formation. Several studies have confirmed that many viruses can induce stable SG formation, such as the PRRSV and NDV (106, 107). As the inhibitory effect of SGs on numerous virus replication, different viruses have evolved unique strategies to prevent SG formation and promote efficient viral propagation. SVA infection induces transient SG formation *via* a PKR-eIF2a-dependent manner at the early stage of infection, and this transient SG is not related to the replication effect of SVA. Besides, Ras-GTPase-activating protein (SH3 domain) binding protein 1 (G3BP1) is a stress granule-resident protein and G3BP1 induced SGs are related to the activation of innate immune responses through NF-κB and JNK. Researchers have found that SVA infection inhibits the SG formation by 3C protein depending on its protease activity at the late stage of infection. In addition to, the 3C protein also disrupts eIF4GI-G3BP1 interaction, which blocks the SG formation (108). However, the significance of SVA blocking SG formation needs further studies.

Conclusions and discussions

The host's innate immune response is the first line of defense against infection by pathogenic microorganisms. Viruses have evolved various strategies to evade the antiviral effect of the host for better proliferation. SVA causes swine vesicular disease, which is clinically indistinguishable from Foot-and-mouth disease and Vesicular stomatitis. It is associated with an increased number of outbreaks in pigs in several countries. This review summarizes the strategies of SVA to counteract the antiviral innate immune responses. Many proteins of SVA are involved in this process, especially the nonstructural protein, including 3C and 2C. 3C or 2C protein can cleave and degrade the key components of PRR signaling pathways to suppress the production of IFN, including RIG-I, MAVS, IRF3, IRF7, TRIF, and TANK. Besides, some ISGs and antiviral proteins are cleaved by nonstructural proteins, especially 2B, 2C, and 3C proteins. Most of the cleavages by 3C or 2C proteins depend on their protease activity. These nonstructural proteins might be an excellent target for developing antiviral drugs.

Currently, there is no research on SVA antagonizing the JAK-STAT signaling pathway, which is the main signaling pathway for ISG production. Therefore, it is not explained in the review. However, other picornaviruses, such as FMDV, and EMCV, could utilize VP3 and 3C proteins targeting JAK1, JAK2, IRF9, and STAT to evade the antiviral effect (109). It is necessary to be clarified how SVA antagonizes the JAK-STAT signaling pathway and the VP3 and 3C proteins of SVA might be the focus of the research in the future. Besides, for pyroptosis and apoptosis, SVA induces but does not inhibit these responses. And, SVA-induced apoptosis and pyroptosis contribute to the replication of SVA in tumor cells and promote an oncolytic effect (110, 111).

A detailed understanding and careful examination of the mechanisms of how SVA evades the host immune system will help develop new antiviral drugs for the treatment of SVA, as well as highly efficient vaccines for the prevention of related diseases.

Author contributions

KZ conceptualized the idea and wrote the manuscript. SXZ, XNL, XRG and ZMG generated the figures. WZY and XZZ made constructive comments to the review. All authors contributed to the article and approved the submitted version.

Funding

This work was supported by the Talents Introduction Projects of Hebei Agricultural University (Grant No. YJ201945); the Key Research and Development Projects of Hebei (Grant No. 20326625D); the National Natural Science Foundation of China (Grant No. 32102644 and 32002264).

Acknowledgments

We thank all of the members of the Veterinary Biologics Team for their suggestions and excellent technical assistance.

Conflict of interest

The authors declare that the research was conducted without any commercial or financial relationships that could be construed as a potential conflict of interest.

Publisher's note

References

1. Zhang X, Zhu Z, Yang F, Cao W, Tian H, Zhang K, et al. Review of Seneca valley virus: A call for increased surveillance and research. *Front Microbiol* (2018) 9:940. doi: 10.3389/fmicb.2018.00940

2. Hales LM, Knowles NJ, Reddy PS, Xu L, Hay C, Hallenbeck PL. Complete genome sequence analysis of Seneca valley virus-001, a novel oncolytic picornavirus. *J Gen Virol* (2008) 89:1265–75. doi: 10.1099/vir.0.83570-0

3. Zhang H, Chen P, Hao G, Liu W, Chen H, Qian P, et al. Comparison of the pathogenicity of two different branches of senecavirus a strain in China. *Pathogens* (2020) 9:39. doi: 10.3390/pathogens9010039

4. Friedman GK, Cassady KA, Beierle EA, Markert JM, Gillespie GY. Targeting pediatric cancer stem cells with oncolytic virotherapy. *Pediatr Res* (2012) 71:500–10. doi: 10.1038/pr.2011.58

5. Kennedy EM, Denslow A, Hewett J, Kong L, De Almeida A, Bryant JD, et al. Development of intravenously administered synthetic RNA virus immunotherapy for the treatment of cancer. *Nat Commun* (2022) 13:1–13. doi: 10.1038/s41467-022-33599-w

6. Luo D, Wang H, Wang Q, Liang W, Liu B, Xue D, et al. Senecavirus a as an oncolytic virus: Prospects, challenges and development directions. *Front Oncol* (2022) 12. doi: 10.3389/fonc.2022.839536

7. Rudin CM, Poirier JT, Senzer NN, Stephenson JJr., Loesch D, Burroughs KD, et al. Phase I clinical study of Seneca valley virus (SVV-001), a replication-competent picornavirus, in advanced solid tumors with neuroendocrine features. *Clin Cancer Res an Off J Am Assoc Cancer Res* (2011) 17:888–95. doi: 10.1158/1078-0432.CCR-10-1706

8. Singh K, Corner S, Clark S, Scherba G, Fredrickson R. Seneca Valley virus and vesicular lesions in a pig with idiopathic vesicular disease. *J Vet Sci Technol* (2012) 3:1–3. doi: doi.10.4172/2157-7579.1000123

9. Pasma T, Davidson S, Shaw SL. Idiopathic vesicular disease in swine in Manitoba. *Can Veterinary J* (2008) 49:84. doi: 10.2376/0005-9366-121-78

10. Xu W, Hole K, Goolia M, Pickering B, Salo T, Lung O, et al. Genome wide analysis of the evolution of senecavirus a from swine clinical material and assembly yard environmental samples. *PloS One* (2017) 12:e0176964. doi: 10.1371/journal.pone.0176964

11. Saeng-Chuto K, Rodtian P, Temeeyasen G, Wegner M, Nilubol D. The first detection of senecavirus a in pigs in Thailand 2016. *Transboundary Emerging Dis* (2018) 65:285–8. doi: 10.1111/tbed.12654

12. Sun D, Vannucci F, Knutson T, Corzo C, Marthaler D. Emergence and whole-genome sequence of senecavirus a in Colombia. *Transboundary Emerging Dis* (2017) 64:1346–9. doi: 10.1111/tbed.12669

13. Arzt J, Bertram MR, Vu LT, Pauszek SJ, Hartwig EJ, Smoliga GR, et al. First detection and genome sequence of senecavirus a in Vietnam. *Microbiol Resource Announcements* (2019) 8:e01247–01218. doi: 10.1128/MRA.01247-18

14. Maan S, Batra K, Chaudhary D, Punia M, Kadian V, Joshi V, et al. Detection and genomic characterization of senecavirus from Indian pigs. *Indian J Anim Res* (2021) B-4722:1–7. doi: 10.18805/IJAR.B-4722

15. Joshi LR, Mohr KA, Clement T, Hain KS, Myers B, Yaros J, et al. Detection of the emerging picornavirus senecavirus a in pigs, mice, and houseflies. *J Clin Microbiol* (2016) 54:1536–45. doi: 10.1128/JCM.03390-15

16. Leme R, Zotti E, Alcântara B, Oliveira M, Freitas L, Alfieri A, et al. Senecavirus a: An emerging vesicular infection in Brazilian pig herds. *Transboundary Emerging Dis* (2015) 62:603–11. doi: 10.1111/tbed.12430

17. Vannucci FA, Linhares D, Barcellos D, Lam H, Collins J, Marthaler D. Identification and complete genome of Seneca valley virus in vesicular fluid and sera of pigs affected with idiopathic vesicular disease, Brazil. *Transboundary Emerging Dis* (2015) 62:589–93. doi: 10.1111/tbed.12410

18. Wang H, Li C, Zhao B, Yuan T, Yang D, Zhou G, et al. Complete genome sequence and phylogenetic analysis of senecavirus a isolated in northeast China in 2016. *Arch Virol* (2017) 162:3173–6. doi: 10.1007/s00705-017-3480-4

19. Wu Q, Zhao X, Bai Y, Sun B, Xie Q, Ma J. The first identification and complete genome of senecavirus a affecting pig with idiopathic vesicular disease in China. *Transboundary Emerging Dis* (2017) 64:1633–40. doi: 10.1111/tbed.12557

20. Canning P, Canon A, Bates J, Gerardy K, Linhares D, Piñeyro P, et al. Neonatal mortality, vesicular lesions and lameness associated with senecavirus a in a US sow farm. *Transboundary Emerging Dis* (2016) 63:373–8. doi: 10.1111/tbed.12516

21. Joshi LR, Fernandes MHV, Clement T, Lawson S, Pillatzki A, Resende TP, et al. Pathogenesis of senecavirus a infection in finishing pigs. *J Gen Virol* (2016) 97:3267–79. doi: 10.1099/jgv.0.000631

22. Martínez-Salas E, Francisco-Velilla R, Fernandez-Chamorro J, Lozano G, Diaz-Toledano R. Picornavirus IRES elements: RNA structure and host protein interactions. *Virus Res* (2015) 206:62–73. doi: 10.1016/j.virusres.2015.01.012

23. Liu F, Wang N, Wang Q, Shan H. Motif mutations in pseudoknot stem I upstream of start codon in senecavirus a genome: Impacts on activity of viral IRES and on rescue of recombinant virus. *Vet Microbiol* (2021) 262:109223. doi: 10.1016/j.vetmic.2021.109223

24. Wang N, Wang H, Shi J, Li C, Liu X, Fan J, et al. The stem-loop I of senecavirus a IRES is essential for cap-independent translation activity and virus recovery. *Viruses* (2021) 13:2159. doi: 10.3390/v13112159

25. Beachboard DC, Horner SM. Innate immune evasion strategies of DNA and RNA viruses. *Curr Opin Microbiol* (2016) 32:113–9. doi: 10.1016/j.mib.2016.05.015

26. Schneider WM, Chevillotte MD, Rice CM. Interferon-stimulated genes: A complex web of host defenses. *Annu Rev Immunol* (2014) 32:513. doi: 10.1146/annurev-immunol-032713-120231

27. Schoggins JW, Rice CM. Interferon-stimulated genes and their antiviral effector functions. *Curr Opin Virol* (2011) 1:519–25. doi: 10.1016/j.coviro.2011.10.008

28. Zhu H, Zheng C. The race between host antiviral innate immunity and the immune evasion strategies of herpes simplex virus 1. *Microbiol Mol Biol Rev* (2020) 84:e00099–00020. doi: 10.1128/MMBR.00099-20

29. Chow J, Franz KM, Kagan JC. PRRs are watching you: Localization of innate sensing and signaling regulators. *Virology* (2015) 479:104–9. doi: 10.1016/j.virol.2015.02.051

30. Alexopoulou L, Holt AC, Medzhitov R, Flavell RA. Recognition of double-stranded RNA and activation of NF-κB by toll-like receptor 3. *Nature* (2001) 413:732–8. doi: 10.1038/35099560

31. Diebold SS, Kaisho T, Hemmi H, Akira S, Reis e Sousa C. Innate antiviral responses by means of TLR7-mediated recognition of single-stranded RNA. *Science* (2004) 303:1529–31. doi: 10.1126/science.1093616

32. Heil F, Hemmi H, Hochrein H, Ampenberger F, Kirschning C, Akira S, et al. Species-specific recognition of single-stranded RNA *via* toll-like receptor 7 and 8. *Science* (2004) 303:1526–9. doi: 10.1126/science.1093620

33. Bauer S, Kirschning CJ, Häcker H, Redecke V, Hausmann S, Akira S, et al. Human TLR9 confers responsiveness to bacterial DNA *via* species-specific CpG motif recognition. *Proc Natl Acad Sci* (2001) 98:9237–42. doi: 10.1073/pnas.161293498

34. Yamamoto M, Sato S, Hemmi H, Hoshino K, Kaisho T, Sanjo H, et al. Role of adaptor TRIF in the MyD88-independent toll-like receptor signaling pathway. *Science* (2003) 301:640–3. doi: 10.1126/science.1087262

35. Kato H, Takeuchi O, Sato S, Yoneyama M, Yamamoto M, Matsui K, et al. Differential roles of MDA5 and RIG-I helicases in the recognition of RNA viruses. *Nature* (2006) 441:101. doi: 10.1038/nature04734

36. Kato H, Takeuchi O, Mikamo-Satoh E, Hirai R, Kawai T, Matsushita K, et al. Length-dependent recognition of double-stranded ribonucleic acids by retinoic acid–inducible gene-I and melanoma differentiation–associated gene 5. *J Exp Med* (2008) 205:1601–10. doi: 10.1084/jem.20080091

37. Pichlmair A, Schulz O, Tan CP, Naslund TI, Liljestrom P, Weber F, et al. RIG-i-mediated antiviral responses to single-stranded RNA bearing 5'-phosphates. *Science* (2006) 314:997–1001. doi: 10.1126/science.1132998

38. Dong XY, Liu WJ, Zhao MQ, Wang JY, Pei JJ, Luo YW, et al. Classical swine fever virus triggers RIG-I and MDA5-dependent signaling pathway to IRF-3 and NF-κB activation to promote secretion of interferon and inflammatory cytokines in porcine alveolar macrophages. *Virol J* (2013) 10:1–11. doi: 10.1186/1743-422X-10-286

39. Wang TY, Sun MX, Zhang HL, Wang G, Zhan G, Tian ZJ, et al. Evasion of antiviral innate immunity by porcine reproductive and respiratory syndrome virus. *Front Microbiol* (2021) 12:693799. doi: 10.3389/fmicb.2021.693799

40. Kawai T, Akira S. Innate immune recognition of viral infection. *Nat Immunol* (2006) 7:131–7. doi: 10.1038/ni1303

41. Bogdan C. The function of type I interferons in antimicrobial immunity. *Curr Opin Immunol* (2000) 12:419–24. doi: 10.1016/S0952-7915(00)00111-4

42. Theofilopoulos AN, Baccala R, Beutler B, Kono DH. Type I interferons (alpha/beta) in immunity and autoimmunity. *Annu Rev Immunol* (2005) 23:307. doi: 10.1146/annurev.immunol.23.021704.115843

43. Brisse M, Ly H. Comparative structure and function analysis of the RIG-i-like receptors: RIG-I and MDA5. *Front Immunol* (2019) 10:1586. doi: 10.3389/fimmu.2019.01586

44. Zhu Z, Wang G, Yang F, Cao W, Mao R, Du X, et al. Foot-and-mouth disease virus viroporin 2B antagonizes RIG-i-mediated antiviral effects by inhibition of its protein expression. *J Virol* (2016) 90:11106–21. doi: 10.1128/JVI.01310-16

45. Chen N, Li X, Li P, Pan Z, Ding Y, Zou D, et al. Enterovirus 71 inhibits cellular type I interferon signaling by inhibiting host RIG-I ubiquitination. *Microbial Pathogenesis* (2016) 100:84–9. doi: 10.1016/j.micpath.2016.09.001

46. Lei X, Liu X, Ma Y, Sun Z, Yang Y, Jin Q, et al. The 3C protein of enterovirus 71 inhibits retinoid acid-inducible gene I-mediated interferon regulatory factor 3 activation and type I interferon responses. *J Virol* (2010) 84:8051–61. doi: 10.1128/JVI.02491-09

47. Barral PM, Sarkar D, Fisher PB, Racaniello VR. RIG-I is cleaved during picornavirus infection. *Virology* (2009) 391:171–6. doi: 10.1016/j.virol.2009.06.045

48. Wen W, Yin M, Zhang H, Liu T, Chen H, Qian P, et al. Seneca Valley virus 2C and 3C inhibit type I interferon production by inducing the degradation of RIG-I. *Virology* (2019) 535:122–9. doi: 10.1016/j.virol.2019.06.017

49. Seth RB, Sun L, Ea CK, Chen ZJ. Identification and characterization of MAVS, a mitochondrial antiviral signaling protein that activates NF-κB and IRF3. *Cell* (2005) 122:669–82. doi: 10.1016/j.cell.2005.08.012

50. Liu H, Li K, Chen W, Yang F, Cao W, Zhang K, et al. Senecavirus a 2B protein suppresses type I interferon production by inducing the degradation of MAVS. *Mol Immunol* (2022) 142:11–21. doi: 10.1016/j.molimm.2021.12.015

51. Qian S, Fan W, Liu T, Wu M, Zhang H, Cui X, et al. Seneca Valley virus suppresses host type I interferon production by targeting adaptor proteins MAVS, TRIF, and TANK for cleavage. *J Virol* (2017) 91:e00823–17. doi: 10.1128/JVI.00823-17

52. Ning S, Huye LE, Pagano JS. Regulation of the transcriptional activity of the IRF7 promoter by a pathway independent of interferon signaling. *J Biol Chem.* (2005) 280:12262–70. doi: 10.1074/jbc.M404260200

53. Yoneyama M, Suhara W, Fujita T. Control of IRF-3 activation by phosphorylation. *J Interferon Cytokine Res* (2002) 22:73–6. doi: 10.1089/107999002753452674

54. Xue Q, Liu H, Zhu Z, Yang F, Ma L, Cai X, et al. Seneca Valley virus 3C(pro) abrogates the IRF3- and IRF7-mediated innate immune response by degrading IRF3 and IRF7. *Virology* (2018) 518:1–7. doi: 10.1016/j.virol.2018.01.028

55. Wang D, Fang L, Li P, Sun L, Fan J, Zhang Q, et al. The leader proteinase of foot-and-mouth disease virus negatively regulates the type I interferon pathway by acting as a viral deubiquitinase. *J Virol* (2011) 85:3758–66. doi: 10.1128/JVI.02589-10

56. Oshiumi H, Matsumoto M, Funami K, Akazawa T, Seya T. TICAM-1, an adaptor molecule that participates in toll-like receptor 3–mediated interferon-β induction. *Nat Immunol* (2003) 4:161–7. doi: 10.1038/ni886

57. Guo B, Cheng G. Modulation of the interferon antiviral response by the TBK1/IKKi adaptor protein TANK. *J Biol Chem* (2007) 282:11817–26. doi: 10.1074/jbc.M700017200

58. Dorrington MG, Fraser IDC. NF-kappaB signaling in macrophages: Dynamics, crosstalk, and signal integration. *Front Immunol* (2019) 10:705. doi: 10.3389/fimmu.2019.00705

59. Gonzalez-Crespo S, Levine M. Related target enhancers for dorsal and NF-κB signaling pathways. *Science* (1994) 264:255–8. doi: 10.1126/science.8146656

60. Wang J, Mou C, Wang M, Pan S, Chen Z. Transcriptome analysis of senecavirus a-infected cells: Type I interferon is a critical anti-viral factor. *Microbial Pathogenesis* (2020) 147:104432. doi: 10.1016/j.micpath.2020.104432

61. Fernandes MH, Maggioli MF, Otta J, Joshi LR, Lawson S, Diel DG. Senecavirus a 3C protease mediates host cell apoptosis late in infection. *Front Immunol* (2019) 10:363. doi: 10.3389/fimmu.2019.00363

62. Hoch Vieira Fernandes M. Senecavirus a: Pathogenicity and interactions with host cell death pathway. *Electronic Theses and Dissertations* (2019) 3372. Available at: https://openprairie.sdstate.edu/etd/3372.

63. Choudhury SM, Ma X, Zeng Z, Luo Z, Li Y, Nian X, et al. Senecavirus a 3D interacts with NLRP3 to induce IL-1β production by activating NF-κB and ion channel signals. *Microbiol Spectr* (2022) 10:e02097–02021. doi: 10.1128/spectrum.02097-21

64. Linder P, Jankowsky E. From unwinding to clamping–the DEAD box RNA helicase family. *Nat Rev Mol Cell Biol* (2011) 12:505–16. doi: 10.1038/nrm3154

65. Ullah R, Li J, Fang P, Shaobo X, Fang L. DEAD/H-box helicases: Anti-viral and pro-viral roles during infections. *Virus Res* (2021) 309:198658. doi: 10.1016/j.virusres.2021.198658

66. Abdullah SW, Wu J, Zhang Y, Bai M, Guan J, Liu X, et al. DDX21, a host restriction factor of FMDV IRES-dependent translation and replication. *Viruses* (2021) 13:1765. doi: 10.3390/v13091765

67. Zhao K, Guo XR, Liu SF, Liu XN, Han Y, Wang LL, et al. 2B and 3C proteins of senecavirus a antagonize the antiviral activity of DDX21 *via* the caspase-dependent degradation of DDX21. *Front Immunol* (2022) 13. doi: 10.3389/fimmu.2022.951984

68. Su C, Tang YD, Zheng C. DExD/H-box helicases: Multifunctional regulators in antiviral innate immunity. *Cell Mol Life Sci* (2022) 79:1–12. doi: 10.1007/s00018-021-04072-6

69. Lessel D, Schob C, Küry S, Reijnders MR, Harel T, Eldomery MK, et al. *De novo* missense mutations in DHX30 impair global translation and cause a neurodevelopmental disorder. *Am J Hum Genet* (2017) 101:716–24. doi: 10.1016/j.ajhg.2017.09.014

70. Ye P, Liu S, Zhu Y, Chen G, Gao G. DEXH-box protein DHX30 is required for optimal function of the zinc-finger antiviral protein. *Protein Cell* (2010) 1:956–64. doi: 10.1007/s13238-010-0117-8

71. Chen G, Ma LC, Wang S, Woltz RL, Grasso EM, Montelione GT, et al. A double-stranded RNA platform is required for the interaction between a host restriction factor and the NS1 protein of influenza a virus. *Nucleic Acids Res* (2020) 48:304–15. doi: 10.1093/nar/gkz1094

72. Zhou Y, Ma J, Roy BB, Wu JYY, Pan Q, Rong L, et al. The packaging of human immunodeficiency virus type 1 RNA is restricted by overexpression of an RNA helicase DHX30. *Virology* (2008) 372:97–106. doi: 10.1016/j.virol.2007.10.027

73. Wen W, Zheng Z, Wang H, Zhao Q, Yin M, Chen H, et al. Seneca Valley virus induces DHX30 cleavage to antagonize its antiviral effects. *J Virol* (2022) 96 (17):e01121–01122. doi: 10.1128/jvi.01121-22

74. Lund EG, Kerr TA, Sakai J, Li W-P, Russell DW. cDNA cloning of mouse and human cholesterol 25-hydroxylases, polytopic membrane proteins that synthesize a potent oxysterol regulator of lipid metabolism. *J Biol Chem* (1998) 273:34316–27. doi: 10.1074/jbc.273.51.34316

75. Janowski BA, Grogan MJ, Jones SA, Wisely GB, Kliewer SA, Corey EJ, et al. Structural requirements of ligands for the oxysterol liver X receptors LXRα and LXRβ. *Proc Natl Acad Sci* (1999) 96:266–71. doi: 10.1073/pnas.96.1.266

76. Wang J, Zeng L, Zhang L, Guo Z-Z, Lu S-F, Ming S-L, et al. Cholesterol 25-hydroxylase acts as a host restriction factor on pseudorabies virus replication. *J Gen Virol* (2017) 98:1467–76. doi: 10.1099/jgv.0.000797

77. Ke W, Fang L, Jing H, Tao R, Wang T, Li Y, et al. Cholesterol 25-hydroxylase inhibits porcine reproductive and respiratory syndrome virus replication through enzyme activity-dependent and-independent mechanisms. *J Virol* (2017) 91: e00827–00817. doi: 10.1128/JVI.00827-17

78. Li C, Deng YQ, Wang S, Ma F, Aliyari R, Huang X-Y, et al. 25-hydroxycholesterol protects host against zika virus infection and its associated microcephaly in a mouse model. *Immunity* (2017) 46:446–56. doi: 10.1016/j.immuni.2017.02.012

79. Li S, Li L, Zhu H, Shi M, Fan H, Gao Y, et al. Cholesterol 25-hydroxylase inhibits encephalomyocarditis virus replication through enzyme activity-dependent and independent mechanisms. *Veterinary Microbiol* (2020) 245:108658. doi: 10.1016/j.vetmic.2020.108658

80. Song Z, Zhang Q, Liu X, Bai J, Zhao Y, Wang X, et al. Cholesterol 25-hydroxylase is an interferon-inducible factor that protects against porcine reproductive and respiratory syndrome virus infection. *Veterinary Microbiol* (2017) 210:153–61. doi: 10.1016/j.vetmic.2017.09.011

81. You H, Yuan H, Fu W, Su C, Wang W, Cheng T, et al. Herpes simplex virus type 1 abrogates the antiviral activity of Ch25h *via* its virion host shutoff protein. *Antiviral Res* (2017) 143:69–73. doi: 10.1016/j.antiviral.2017.04.004

82. Zhang Y, Song Z, Wang M, Lan M, Zhang K, Jiang P, et al. Cholesterol 25-hydroxylase negatively regulates porcine intestinal coronavirus replication by the production of 25-hydroxycholesterol. *Veterinary Microbiol* (2019) 231:129–38. doi: 10.1016/j.vetmic.2019.03.004

83. Li H, Zhao Z, Li X, Qin L, Wen W, Chen H, et al. Cholesterol-25-Hydroxylase suppresses Seneca valley virus infection *via* producing 25-hydroxycholesterol to block adsorption procedure. *Virol Sin* (2021) 36:1210–9. doi: 10.1007/s12250-021-00377-9

84. Zhu H, Yan J, Liu X, Li L, Liu W, Wang X, et al. Cholesterol 25-hydroxylase inhibits senecavirus a replication by enzyme activity-dependent and independent mechanisms. *Veterinary Microbiol* (2021) 256:109038. doi: 10.1016/j.vetmic.2021.109038

85. Dong H, Zhou L, Ge X, Guo X, Han J, Yang H. Porcine reproductive and respiratory syndrome virus nsp1β and nsp11 antagonize the antiviral activity of cholesterol-25-hydroxylase *via* lysosomal degradation. *Veterinary Microbiol* (2018) 223:134–43. doi: 10.1016/j.vetmic.2018.08.012

86. Ke W, Fang L, Tao R, Li Y, Jing H, Wang D, et al. Porcine reproductive and respiratory syndrome virus e protein degrades porcine cholesterol 25-hydroxylase *via* the ubiquitin-proteasome pathway. *J Virol* (2019) 93:e00767–00719. doi: 10.1128/JVI.00767-19

87. Gao J, Tang YD. When Poly(A) binding proteins meet viral infections, including SARS-CoV-2. *J Virol* (2022) 96(7):e00136–22. doi: 10.1128/jvi.00136-22

88. Smith RWP, Gray NK. Poly(A)-binding protein (PABP): A common viral target. *Biochem J* (2010) 426:1–12. doi: 10.1042/BJ20091571

89. Barbara G, Gray NK. The roles of cytoplasmic poly(A)-binding proteins in regulating gene expression: A developmental perspective. *Briefings Funct Genomics Proteomics* (2004) 3(2):125–41. doi: 10.1093/bfgp/3.2.125.

90. Kobayashi M, Arias C, Garabedian A, Palmenberg AC, Mohr I. Site-specific cleavage of the host poly(A) binding protein by the encephalomyocarditis virus 3C proteinase stimulates viral replication. *J Virol* (2012) 86:10686–94. doi: 10.1128/JVI.00896-12

91. Harb M, Becker MM, Vitour D, Baron CH, Vende P, Brown SC, et al. Nuclear localization of cytoplasmic poly(a)-binding protein upon rotavirus infection involves the interaction of nsp3 with eif4g and roxan. *J Virol* (2008) 82 (22):11283–93. doi: 10.1128/JVI.00872-08

92. Belsham GJ, Mcinerney GM, Ross-Smith N. Foot-and-Mouth disease virus 3C protease induces cleavage of translation initiation factors eIF4A and eIF4G within infected cells. *J Virol* (2000) 74:272–80. doi: 10.1128/JVI.74.1.272-280.2000

93. Kuyumcu-Martinez NM, Van Eden ME, Younan P, Lloyd RE. Cleavage of Poly(A)-binding protein by poliovirus 3C protease inhibits host cell translation: A novel mechanism for host translation shutoff. *Mol Cell Biol* (2004) 24:1779–90. doi: 10.1128/MCB.24.4.1779-1790.2004

94. Klionsky D, Emr SD. Autophagy as a regulated pathway of cellular degradation. *Science* (2001) 290:1717–21. doi: 10.1126/science.290.5497.1717

95. Alexander DE, Ward SL, Mizushima N, Levine B, Leib DA. Analysis of the role of autophagy in replication of herpes simplex virus in cell culture. *J Virol* (2007) 81:12128–34. doi: 10.1128/JVI.01356-07

96. Yoshimori T. How autophagy saves mice: A cell-autonomous defense system against sindbis virus infection. *Cell Host Microbe* (2010) 7:83–4. doi: 10.1016/j.chom.2010.02.003

97. Meng C, Zhou Z, Jiang K, Yu S, Jia L. Newcastle Disease virus triggers autophagy in U251 glioma cells to enhance virus replication. *Arch virol* (2012) 157 (6):1011–8. doi: 10.1007/s00705-012-1270-6

98. Fan X, Han S, Yan D, Gao Y, Wei Y, Liu X, et al. Foot-and-mouth disease virus infection suppresses autophagy and NF-κB antiviral responses *via* degradation of ATG5-ATG12 by 3Cpro. *Nat Publishing Group* (2018) 8(1): e2561. doi: 10.1038/cddis.2016.489

99. Kong N, Shan T, Wang H, Jiao Y, Zuo Y, Li L, et al. BST2 suppresses porcine epidemic diarrhea virus replication by targeting and degrading virus nucleocapsid protein with selective autophagy. *Autophagy* (2020) 16:1737–52. doi: 10.1080/15548627.2019.1707487

100. Liu Q, Qin Y, Lei Z, Kou Q, Xin G, Ge X, et al. Autophagy sustains the replication of porcine reproductive and respiratory virus in host cells. *Virology* (2012) 429:136–47. doi: 10.1016/j.virol.2012.03.022

101. Sun MX, Huang L, Wang R, Yu YL, Li C, Li PP, et al. Porcine reproductive and respiratory syndrome virus induces autophagy to promote virus replication. *Autophagy* (2012) 8:1434–47. doi: 10.4161/auto.21159

102. Hou L, Dong J, Zhu S, Yuan F, Liu J. Seneca Valley virus activates autophagy through the PERK and ATF6 UPR pathways. *Virology* (2019) 537:254–63. doi: 10.1016/j.virol.2019.08.029

103. Wen W, Li X, Yin M, Wang H, Qin L, Li H, et al. Selective autophagy receptor SQSTM1/ p62 inhibits Seneca valley virus replication by targeting viral VP1 and VP3. *Autophagy* (2021) 17:3763–75. doi: 10.1080/15548627.2021.1897223

104. Sun D, Kong N, Dong S, Chen X, Qin W, Wang H, et al. 2AB protein of senecavirus a antagonizes selective autophagy and type I interferon production by degrading LC3 and MARCHF8. *Autophagy* (2022) 18:1969–81. doi: 10.1080/15548627.2021.2015740

105. Piotrowska J, S. J, Hansen N, Park K, Jamka P. Stable formation of compositionally unique stress granules in virus-infected cells. *J Virol* (2010) 84 (7):3654–65. doi: 10.1128/JVI.01320-09

106. Catanzaro N, Meng X-J. Porcine reproductive and respiratory syndrome virus (PRRSV)-induced stress granules are associated with viral replication complexes and suppression of host translation. *Virus Res* (2019) 265:47–56. doi: 10.1016/j.virusres.2019.02.016

107. Sun Y, Dong L, Yu S, Wang X, Zheng H, Zhang P, et al. Newcastle Disease virus induces stable formation of bona fide stress granules to facilitate viral replication through manipulating host protein translation. *FASEB J* (2017) 31:1337. doi: 10.1096/fj.201600980R

108. Wen W, Zhao Q, Yin M, Qin L, Hu J, Chen H, et al. Seneca Valley virus 3C protease inhibits stress granule formation by disrupting eIF4GI-G3BP1 interaction. *Front Immunol* (2020) 11:577838. doi: 10.3389/fimmu.2020.577838

109. Zhang X, Paget M, Wang C, Zhu Z, Zheng H. Innate immune evasion by picornaviruses. *Eur J Immunol* (2020) 50:1268–82. doi: 10.1002/eji.202048785

110. Liu T, Li X, Wu M, Qin L, Chen H, Qian P. Seneca Valley virus 2C and 3C (pro) induce apoptosis *via* mitochondrion-mediated intrinsic pathway. *Front Microbiol* (2019) 10:1202. doi: 10.3389/fmicb.2019.01202

111. Wen W, Li X, Wang H, Zhao Q, Yin M, Liu W, et al. Seneca Valley virus 3C protease induces pyroptosis by directly cleaving porcine gasdermin d. *J Immunol* (2021) 207:189–99. doi: 10.4049/jimmunol.2001030

frontiers | Frontiers in Immunology

TYPE Original Research
PUBLISHED 16 January 2023
DOI 10.3389/fimmu.2023.1119473

OPEN ACCESS

EDITED BY
Junji Xing,
Houston Methodist Research Institute,
United States

REVIEWED BY
Yaling Dou,
Texas A&M Health Science Center,
United States
Guangchuan Wang,
Jinzhou Medical University, China

*CORRESPONDENCE
Fang Wang
wf@jlu.edu.cn

SPECIALTY SECTION
This article was submitted to
Viral Immunology,
a section of the journal
Frontiers in Immunology

RECEIVED 08 December 2022
ACCEPTED 02 January 2023
PUBLISHED 16 January 2023

CITATION
Gu Y, Hsu AC-Y, Zuo X, Guo X, Zhou Z, Jiang S, Ouyang Z and Wang F (2023) Chronic exposure to low-level lipopolysaccharide dampens influenza-mediated inflammatory response *via* A20 and PPAR network.
Front. Immunol. 14:1119473.
doi: 10.3389/fimmu.2023.1119473

Chronic exposure to low-level lipopolysaccharide dampens influenza-mediated inflammatory response *via* A20 and PPAR network

Yinuo Gu[1], Alan Chen-Yu Hsu[2,3,4], Xu Zuo[1], Xiaoping Guo[1], Zhengjie Zhou[1], Shengyu Jiang[1], Zhuoer Ouyang[1] and Fang Wang[1]*

[1]Department of Pathogeny Biology, College of Basic Medical Sciences, Jilin University, Changchun, China, [2]Signature Research Program in Emerging Infectious Diseases, Duke - National University of Singapore (NUS) Graduate Medical School, Singapore, Singapore, [3]School of Medicine and Public Health, The University of Newcastle, Newcastle, NSW, Australia, [4]Viruses, Infections/Immunity, Vaccines and Asthma, Hunter Medical Research Institute, Newcastle, NSW, Australia

Influenza A virus (IAV) infection leads to severe inflammation, and while epithelial-driven inflammatory responses occur *via* activation of NF-κB, the factors that modulate inflammation, particularly the negative regulators are less well-defined. In this study we show that A20 is a crucial molecular switch that dampens IAV-induced inflammatory responses. Chronic exposure to low-dose LPS environment can restrict this excessive inflammation. The mechanisms that this environment provides to suppress inflammation remain elusive. Here, our evidences show that chronic exposure to low-dose LPS suppressed IAV infection or LPS stimulation-induced inflammation *in vitro* and *in vivo*. Chronic low-dose LPS environment increases A20 expression, which in turn positively regulates PPAR-α and -γ, thus dampens the NF-κB signaling pathway and NLRP3 inflammasome activation. Knockout of A20 abolished the inhibitory effect on inflammation. Thus, A20 and its induced PPAR-α and -γ play a key role in suppressing excessive inflammatory responses in the chronic low-dose LPS environment.

KEYWORDS

A20 (TNFAIP3), IAV, PPAR, NF-κB, NLRP3 inflammasome

Introduction

IAV frequently causes severe infection with heightened inflammation that drives disease pathogenesis. While inflammation is essential in virus clearance, excessive inflammatory responses cause epithelial tissue destruction, acute lung injury and pneumonia (1, 2). Upon infection in airway epithelial cells, the primary site of IAV infection, IAV viral RNAs are recognized by the host pattern recognition receptors including retinoic acid inducible gene

(RIG)-I and toll-like receptor (TLR)3. RIG-I binding to viral RNAs leads to activation of interferon regulatory factor (IRF)3 that facilitate the production of antiviral cytokines type I interferon (IFN). TLR3 promotes the activation of nuclear factor kappa-lightchain-enhancer of activated B cells (NF-κB), leading to the induction of pro-inflammatory cytokines such as interleukin (IL)-6 and tumour-necrosis-factor (TNF)α. Upon infection or stimulation, NLRP3, ASC, and pro-caspase-1 assembles to form an inflammasome complex, which activates pro-caspase-1 by cleavage. IL-1β is a potent inflammatory cytokine that is produced as a pro-protein that is then cleaved by caspase-1 (3).

It has been suggested that the host inflammatory response to IAV is more likely to have serious consequences than viral load (1).

The mechanisms that drive NF-κB pathway are well characterized, however the negative control factors that dampen NF-κB activation is less well studied. A recent study showed that chronic exposure of low-dose lipopolysaccharide (LPS) protected against the development of allergy and asthma (4, 5).

The molecular mechanisms underpinning this observation is unclear. We recently showed that A20 (also known as TNFα-induced protein 3) was crucial in limiting IAV-mediated NF-κB activation and IAV diseases *in vitro* and *in vivo*. The mechanisms by which low-grade LPS and A20 protect the host from heightened inflammation is unknown. In this study we determined that human airway epithelial cells and mice that were chronically exposed to low-dose LPS reduced subsequent IAV- and high-dose LPS-mediated NF-κB and NLRP3 activation, and this low-grade LPS tolerance was mediated by increased A20 and PPAR-α and PPAR-γ expression, the latter of which were also negative regulators of NF-κB.

Materials and methods

Cell culture and IAV

Human lung adenocarcinoma epithelial (A549) cells and Madin-Darby canine kidney (MDCK) cells were purchased from the Chinese Academy of Sciences Cell Bank (Shanghai, China). A549 cells were cultured in Ham's F-12 K medium supplemented with 10% fetal bovine serum (FBS). MDCK cells were cultured in DMEM medium supplemented with 10% FBS. All cells were cultured with 5% CO_2 at 37°C.

H1N1 influenza virus, A/Fort Monmouth/1/1947 virus (FM1), was propagated in the allantoic cavities of 9-11 day-old embryonated specific pathogen-free chicken eggs cultured at 37°C. After 48 h allantoic fluids of infected eggs were collected. Various dilutions of allantoic fluids were incubated with MDCK cells to determine the 50% tissue culture infectious dose ($TCID_{50}$) calculated by the Reed-Muench method. $TCID_{50}$ is $10^{-4.1}$. To determine the 50% lethal dose (LD_{50}), the allantoic fluids were serially 10-fold diluted. The number of deaths and survivals in each dilution was used to calculate the LD_{50} by the Reed–Muench method. Based on the titrations, 1 LD_{50} of the allantoic fluids was determined to be $10^{-5.5}$.

Animals and animal experiments

Female BALB/c mice (6–8 weeks old) were purchased from the Yisi Laboratory Animal Technology Co., Ltd. (Changchun, China), and maintained in micro-isolator cages under specific pathogen-free conditions. The experimental manipulation of the mice was undertaken in accordance with the National Institute of Health Guide for the Care and Use of Laboratory Animals, with the approval of the Scientific Investigation Board of Science & Technology of Jilin Province, China. All mice received human care in compliance with the 2011 Guide for the Care and Use of Laboratory Animals published by the National Institutes of Health. The mouse experiments were approved by the ethics committee of The College of Basic Medical Sciences of Jilin University with the number 2022-467.

We intranasally administered with 100 ng LPS for chronic-LPS^{lo} group or PBS for control group every other day. After 2 weeks, both groups of mice were treated with non-infectious allantoic fluid, H1N1 (10 LD_{50}), and high-dose (10 μg/mL) LPS. Both H1N1 and high-dose LPS were inoculated intranasally after mice were anesthetized with 10% chloral hydrate intraperitoneally. Mice were sacrificed 24 h post infection points for sampling.

Histological analysis and haematoxykin & eosin staining

The lungs of the infected mice were fixed in 4% (weight/vol.) paraformaldehyde, embedded into paraffin and cut into 4-μm-thick sections. The sections were stained with haematoxylin & eosin, and observed under the microscope. Pathological scores of the lungs were determined based on the criteria: 0, normal lung tissue structure with no inflammatory cell infiltration; 1, normal alveolar structure, mild lung injury (< 25% of the lung) with little inflammatory cell infiltration; 2, alveolar collapse, moderate injury (25– 50% of the lung) with some inflammatory cell infiltration; 3, no alveolar structure, severe injury (> 50% of the lung) with massive inflammatory cell infiltration.

Chronic low-dose LPS stimulation, H1N1 infection and high-dose LPS stimulation in A549 cells

In the chronic-LPS^{lo} group cells were exposed to low-dose LPS (1 ng/mL) every other day for 4 weeks by adding low-dose LPS to the culture the day after each passage, the control group cells exposed with PBS. After four weeks, cells in both groups were treated with media, H1N1, and high-dose (1μg/mL) LPS. A549 was inoculated with 10^2 $TCID_{50}$/mL H1N1 for 2h, after which the inoculum was removed and fresh serum-free media was added and incubated at 37°C/5% CO_2 for 24h.

Sample preparation and analysis of tandem mass tags labeled quantitative proteomics

A549 cells in control+H1N1 group, chronic-LPS^{lo}+H1N1 group, control+acute-LPS^{hi} and chronic-LPS^{lo}+acute-LPS^{hi} group were harvested for LC-MS analyses. Proteins were precipitated with 25mM DL-dithiothreitol, iodoacetamide, precooled acetone. After pellets we collected by centrifugation, the protein pellets were redissolved with enzymolysis diluent, followed by lyophilization and TMT labeling. Proteomic analysis was performed using a Q-Exactive mass spectrometer (Thermo, USA) after reversed-phase (RP) separation. Proteome Discover 2.4 (Thermo, USA) was used to process LC-MS/MS data, and credible proteins were screened using Score Sequest HT > 0 and unique peptide ≥ 1. Significant differences in proteins between the two groups were determined by performing Student's t-test. Fold changes less than 0.67 or more than 1.5 and p-values less than 0.05 were considered significant. Annotation information of each identified protein was extracted using Uniprot database. Pathway enrichment analysis of differential proteins was performed based on the Kyoto Encyclopedia of Genes and Genomes (KEGG) database.

Generation of A20 KO cells by CRISPR-Cas9

CRISPR–Cas9 system was used to knock out A20 expression in A549 cells. Briefly, two synthetic guide RNA (sgRNA) sequence targeting exon 3 of the A20 gene were designed online (https://www.benchling.com/crispr/) and then cloned into the CRISPR/Cas9 48138-puro vector. The sgRNA sequences were: sgRNA#1: AGGGGTACCCTATGCCCACC; sgRNA#2: CAGCCCTACTGCTATTCTAG. A20 cell clones were selected using green fluorescent protein (GFP) expression and restriction fragment length polymorphism.

Cytokine analysis

TNF-α, IL-6, IL-1β in the supernatant and mouse serum and IFN-α, IFN-β, IFN-γ and IL-18 in mouse alveolar lavage fluid were measured using ELISA kits (Lianke, Hangzhou, China), according to the manufacturer's protocol.

Western blotting

Cells and lung tissues were lysed in RIPA buffer, and protein concentration determined by BCA protein assay kit (Beyotime, Shanghai, China). Denatured protein samples (20μg) were separated by 8% or 15% SDS-PAGE and transferred onto PVDF membranes. The membranes were blocked in 5% nonfat milk for 3 h at room temperature, and probed with specific primary antibodies (1:1000) against p65 (ab16502), p-p65 (ab76302), A20 (ab92324), NLRP3 (ab214185), pro-caspase-1 (ab179515), caspase-1 (ab179515), PPAR-α (ab61182), PPAR-γ (ab209350) and β-actin (ab8227) (Abcam, Cambridge, UK) overnight at 4°C. Goat-derived anti-rabbit HRP conjugated antibody (1:2000) were used as secondary antibody for 1 h. Membranes were developed and analyzed using the Super Signal Chemiluminescent Substrate kit (Thermo Scientific, Rockford, USA) and ImageJ software.

mRNA analysis

Total RNAs from A549 cells and lung tissues were extracted using Trizol (Thermo Scientific, Rockford, USA). RNA was reverse-transcribed to cDNA using first strand cDNA synthesis kit (Thermo Scientific, Rockford, USA). qPCR assays were performed with SYBR Green PCR Master Mix (TaKaRa, Japan) and a Fast qPCR System (Applied Biosystems, USA). GAPDH was used as the internal reference. The relative mRNA level was calculated by $2^{-\Delta\Delta Ct}$ method. The primers used were GAPDH (human), F; TCTTCTTTTGCGTCGCCAG, R; AGCCCCAGCCTTCTCCA, IL-1β (human), F; CTGTCCT GCGTGTTGAAAGA, R; TTGGGTAATTTTTGGGATCTACA, IL-6 (human), F; CACTGGTCTTTTGGAGTTTGAG, R; GGACTTT TGTACTCATCTGCAC, TNF-α (human), F; AGCCC TGGTATGAGCCCATCTATC, R; TCCCAAAGTAGACCTG CCCAGAC, TNFAIP3 (human), F; TGCACACTGTGTTTCATCGAG, R; ACGCTGTGGGACTGACTTTC, GAPDH (mouse), F; AGGTCGGTGTGAACGGATTTG, R; TGTAGACCATGTAGTTGA GGTCA, IL-1β (mouse), F; CACTACAGGCTCCGAGATGAACAAC, R; TGTCGTTGCTTGGTTCTCCTTGTAC, IL-6 (mouse), F; CTTCT TGGGACTGATGCTGGTGAC, R; TCTGTTGGGAGTGGTATC CTCTGTG, TNF-α (mouse), F; CGCTCTTCTGTCTA CTGAACTTCGG, R; GTGGTTTGTGAGTGTGAGGGTCTG, TNF AIP3, F; TCCTCAGGCTTTGTATTTGAGC, R; TGTG TATCGGTGCATGGTTTTA.

Immunofluorescence

A549 cells were cultured in 24 well plate. The cells were fixed in 4% paraformaldehyde for 10 min and then permeabilized with 0.02% Triton X for 5 min. The cells were blocked with goat serum for 60 min. The cells were incubated with primary antibodies against p65 overnight at 4°C. The cells were incubated with the secondary antibodies for 60 min and then stained by DAPI. Fluorescent images were captured with an immunofluorescence microscope (IX71, Olympus, Japan).

Statistical analysis

Statistical analysis was performed using Prism software (GraphPad). Student's t test or One-way analysis of variance (ANOVA), followed by Tukey's *post hoc* analysis was used for calculation of statistical differences. p values <0.05 were considered statistically significant.

Results

Chronic low-dose LPS stimulation ameliorates symptoms and prolongs survival in H1N1-infected mice

Chronic-LPS^{lo} stimulation has been well studied in childhood asthma and farm environments protect children from asthma through exposure to house dust mites and LPS (4, 5). To explore whether chronic-LPS^{lo} stimulation is protective against H1N1 or

high-dose LPS stimulation *in vivo*, we exposed mice to low-dose LPS or control PBS every other day for two weeks prior to H1N1 infection and high-dose LPS stimulation. We examined the lung histological changes of mice in each group, both H1N1 and acute-LPS^{hi} resulted in severe lung injury, diffuse swelling, alveolar cavity collapse, alveolar thickening, and severe infiltration of inflammatory cells (Figure 1A). Chronic-LPS^{lo} stimulation significantly improved lung injury as assessed by pathology scores compared with control+H1N1 and control+acute-LPS^{hi} groups (Figure 1B).

We recorded symptoms and body weight changes in H1N1-infected mice daily. The results showed that on day 2 after intranasal administration of H1N1, the mice began to show signs of decreased activity, loss of appetite, hunched back and ruffled fur. By day 5, mice may experience dyspnea and respiratory distress. Mice in the control group started dying on day 6 post-infection and all died within 10 days post-infection (Figure 1C). The mice gradually lost weight starting on the third day after infection until death (Figure 1D).

Chronic-LPS^{lo} stimulation did not induce significant pathological changes in the lungs of mice, nor cause weight loss in mice, and ameliorated the aforementioned disease symptoms and delayed weight loss and prolonged survival.

Chronic low-dose LPS stimulation inhibits the activation of NF-κB signaling pathway and NLRP3 inflammasome

The activation of NF-κB pathway and NLRP3 inflammasome during infection leads to upregulation of pro-inflammatory cytokines expression. To assess whether severe cytokine storms were generated during H1N1 infection or high-dose LPS stimulation and further clarify the mechanism by which chronic-LPS^{lo} stimulation inhibits inflammation, we analyzed the effects of chronic-LPS^{lo} stimulation on the regulation of NF-κB pathway and NLRP3 inflammasome. In H1N1-infected or high-dose LPS-stimulated mice, chronic-LPS^{lo} stimulation significantly decreased p65 phosphorylation (Figures 2A, B). We examined the production of TNF-α and IL-6 downstream of the NF-κB pathway in mice lung tissues and sera. Compared with the control+AF group, H1N1 infection significantly increased the mRNA and protein levels of TNF-α and IL-6 (Figures 2C, S1 A, B).

Both H1N1 infection and acute-LPS^{hi} stimulation independently induced NLRP3 inflammasome activation, including increased NLRP3 and pro-caspase-1 protein expression and activated caspase-1 production. Chronic-LPS^{lo} stimulation decreased NLRP3, pro-caspase-1 and caspase-1 at protein levels (Figures 2D, E). We examined the production of IL-1β downstream of the NLRP3 inflammasome in mice lung tissues and sera. Chronic-LPS^{lo} stimulation significantly reduced the increase in the expression of IL-1β (Figures 2F, S1 C).

We also examined IFN-α, IFN-β, IFN-γ and IL-18 production in mouse alveolar lavage fluid. Chronic-LPS^{lo} stimulation significantly reduced the increase in IFN-α and IFN-β expression, but had no significant effect on IFN-γ and IL-18 (Figure S2).

Our results showed that chronic-LPS^{lo} stimulation inhibited H1N1 or acute LPS^{hi} induced activation of NLRP3 inflammasome and NF-κB and production of pro-inflammatory cytokines.

Chronic low-dose LPS stimulation upregulates A20 expression

A20 as a key protein in the protection mediated by chronic exposure to low-dose LPS environment is also a major determinant of progression and prognosis in several other inflammatory diseases (6–9). To observe the effects of chronic-LPS^{lo} stimulation on human airway epithelial cells, we exposed A549 cells for 4 weeks to a low-dose of LPS (1ng/mL) or to control PBS before acute H1N1 infection or acute high-dose LPS stimulation. We next assessed the expression of A20 and showed that the mRNA and protein levels of A20 were significantly increased in the chronic-LPS^{lo} group than in the control group *in vivo* (Figures 3A, B) and *in vitro* (Figures 3C, D).

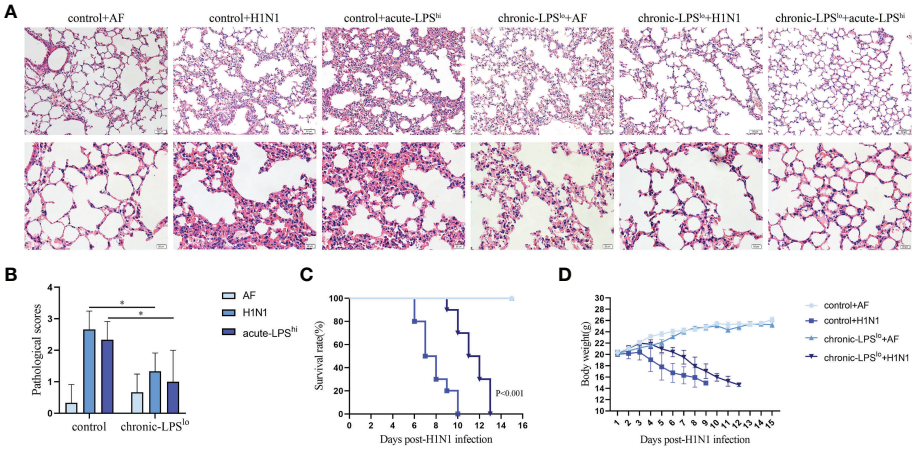

FIGURE 1
The effect of chronic low-dose LPS stimulation on lethal IAV infected mice. **(A)** Female BALB/c mice (n = 3 mice/group) were intranasally infected with 10 LD_{50} H1N1 influenza virus or an equivalent dilution of non-infectious allantoicfluid (AF). The lungs were isolated and sectioned for hematoxylin & eosin staining. **(B)** Pathological scores of the stained sections. **(C)** Survival data of female BALB/c mice (n = 10 mice/group) after intranasal infection with 10 LD_{50} H1N1. **(D)** Body weights of female BALB/c mice (n = 10 mice/group) after intranasal infection with 10 LD_{50} H1N1. *p< 0.05.

10.3389/fimmu.2023.1119473

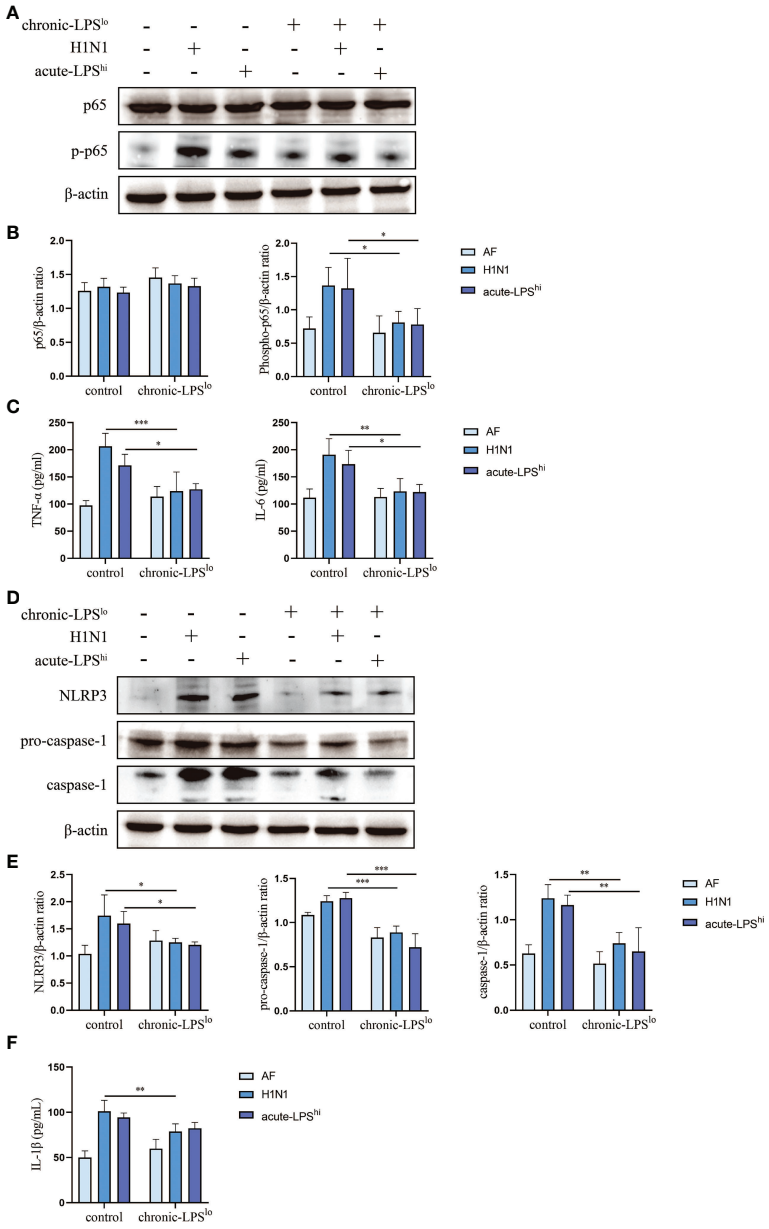

FIGURE 2
Effect of chronic low-dose LPS stimulation on NF-κB signaling pathway and NLRP3 inflammasome in high dose LPS-stimulated or H1N1-infected mice. **(A, B)** Relative protein levels of p65 and p-p65 in lung tissues were detected by western blot. **(C)** TNF-α and IL-6 in mice sera were measured by ELISA. **(D, E)** Relative protein levels of NLRP3, pro-caspase-1 and caspase-1 in lung tissues were detected by western blot. **(F)** IL-1β in mice sera were detected by ELISA. Data are mean ± SD, n = 3. *p< 0.05, **p< 0.01, ***p< 0.001.

A20 knockout abolishes the anti-inflammatory effects by chronic low-dose LPS stimulation

To further assess the roles of A20 in dampening H1N1 and acute-LPS^{hi}-mediated inflammatory responses, we generated A20-deficient A549 cells (A549$^{A20\text{-}KO}$) using CRISPR-Cas9 gene editing, and showed a complete lack of A20 protein expression (Figure 4A). A549$^{A20\text{-}KO}$ cells proliferated at similar rate as wild-type cells (A549^{WT}) and did not show significant morphological differences.

We measured the levels of activity NF-κB by assessing the levels of phosphorylated p65 (p-p65). H1N1 infection or LPS stimulation significantly increased the activation of p-p65 in both control H1N1 and control acute-LPS^{hi} groups. The inhibition of chronic LPS^{lo} stimulation to nuclear translocation of p65 in H1N1-infected and high-dose LPS-stimulated A549$^{A20\text{-}KO}$ cells was lost (Figures 4B–D). There was also no significant difference in the production of TNF-α and IL-6 between the control group and the chronic-LPS^{lo} group (Figures 4E, S3 A, B). These results indicated that the inhibitions of chronic-LPS^{lo} stimulation on NF-κB signaling pathway in H1N1-infected and high-dose LPS-stimulated A549 cells were A20 dependent.

Next, we detected the effect of chronic-LPS^{lo} stimulation on NLRP3 inflammasome after knockout of A20. Knockout of A20 made the inhibition of NLRP3 signaling pathway by chronic low-dose LPS stimulation lost (Figures 4F, G). The inhibitory effect of

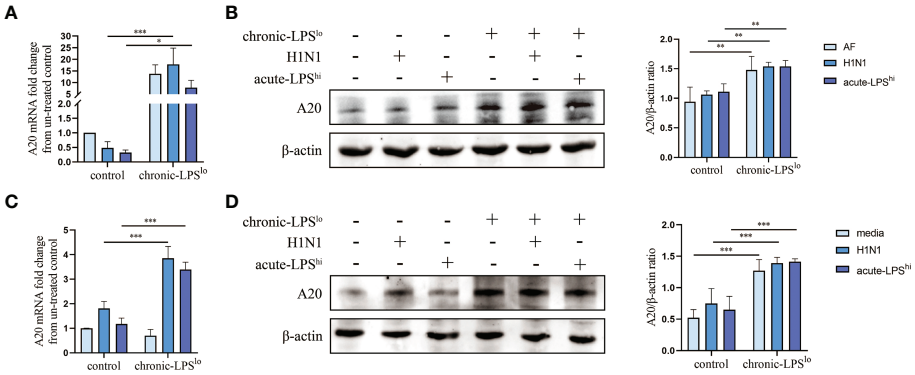

FIGURE 3
Effect of chronic low-dose LPS stimulation on A20. **(A)** A20 mRNA in lung tissues was detected by qPCR. **(B)** Relative protein levels of A20 in lung tissues were detected by western blot. **(C)** A20 mRNA in A549 cells was detected by qPCR. **(D)** Relative protein levels of A20 in A549 cells were detected by western blot. Data are mean ± SD, n = 3. *p< 0.05, **p< 0.01, ***p< 0.001.

chronic-LPS^{lo} stimulation on the production of IL-1β also disappeared (Figures 4H, S3 C). These results indicated that the inhibitions of chronic-LPS^{lo} stimulation on NLRP3 inflammasome in H1N1-infected and high-dose LPS-stimulated A549 cells were A20 dependent.

Chronic low-dose LPS stimulation inhibits H1N1-infected or high-dose LPS-stimulated inflammation *via* PPAR

To assess the global changes induced by chronic-LPS^{lo} stimulation at the protein level, we subjected the cells from control +H1N1 group, chronic-LPS^{lo}+H1N1 group, control+acute-LPS^{hi} and chronic-LPS^{lo}+acute-LPS^{hi} group to TMT-labeled quantitative proteomics. We identified 6,178 quantitative proteins in the control +H1N1 group and chronic-LPS^{lo}+H1N1 group, of which 136 proteins had significantly increased or decreased expression. We identified 6,228 quantified proteins in control+acute-LPS^{hi} and chronic-LPS^{lo} +acute-LPS^{hi} group, of which 86 proteins had significantly increased or decreased expression. Cluster analysis and heat map showed differentially expressed proteins control+H1N1 group compared with chronic-LPS^{lo}+H1N1 group (Figure 5A) and control+acute-LPS^{hi} group compared with chronic-LPS^{lo}+acute-LPS^{hi} group (Figure 5B).

The volcano plot showed that 123 proteins that were increased and 13 proteins that were decreased in the 136 differential proteins in chronic-LPS^{lo}+H1N1 group compared with control+H1N1 group (Figure 5C). 62 proteins were increased and 24 proteins were decreased in the 86 differential proteins in chronic-LPS^{lo}+acute-LPS^{hi} group compared with control+acute-LPS^{hi} group (Figure 5D).

KEGG pathway analysis showed the top 20 pathways that are well characterized in both H1N1 infection and LPS stimulation, including the PPAR, NOD-like receptor, NF-κB, TNF and chemokine signaling pathways. Interestingly we found that PPAR was highly enriched in chronic-LPS^{lo}+H1N1 group (Figure 5E) and chronic-LPS^{lo}+acute-LPS^{hi} group (Figure 5F).

The increase of PPAR expression induced by chronic low-dose LPS stimulation is regulated by A20

Both PPAR-α and PPAR-γ inhibit NF-κB activation like A20 and PPAR-α has been reported to be positively regulated by A20 (10–12). In addition, PPAR-α/γ also exerts anti-inflammatory effects during influenza infection (13, 14). Despite the inflammatory signaling pathway is well characterized, whether PPAR-α/γ is involved in the mechanism by which A20 suppresses the excessive inflammatory response of IAV remains unclear.

To explore whether PPAR plays a key role in the inhibitory effect of chronic-LPS^{lo} stimulation on inflammation, we measured the protein levels of PPAR-α and -γ in A549^{WT} cells and A549$^{A20\text{-}KO}$ cells. Consistent with the proteomics, western blot analysis confirmed the increased expression of PPAR-α and -γ in chronic-LPS^{lo} groups. Furthermore, this elevated PPAR-α and -γ expression induced in chronic low-dose LPS stimulation was abolished in A549$^{A20\text{-}KO}$ cells (Figures 6A, B), indicating that PPAR-α and -γ expression was regulated by A20, and loss of which resulted in exaggerated inflammatory responses by H1N1 or high-dose LPS.

Discussion

Here, we demonstrate that H1N1 infection and high-dose LPS stimulation induce inflammation; however, the inflammatory response, NF-κB and NLRP3 activation were inhibited in chronic low-dose LPS environment. We show that A20 is a negative regulator of NF-κB and NLRP3-mediated inflammation and that A20 gene and protein levels are upregulated in a chronic low-dose LPS environment. Impaired inflammatory response in the chronic low-dose LPS environment was attributed to increased A20 and PPAR-α and -γ expression. Elevated A20 levels increased PPAR expression, leading to dampen of NF-κB and NLRP3 activity and inflammation. A20 knockout resulted in loss of chronic low-dose LPS-mediated suppression of inflammation. Thus, chronic low-dose LPS

10.3389/fimmu.2023.1119473

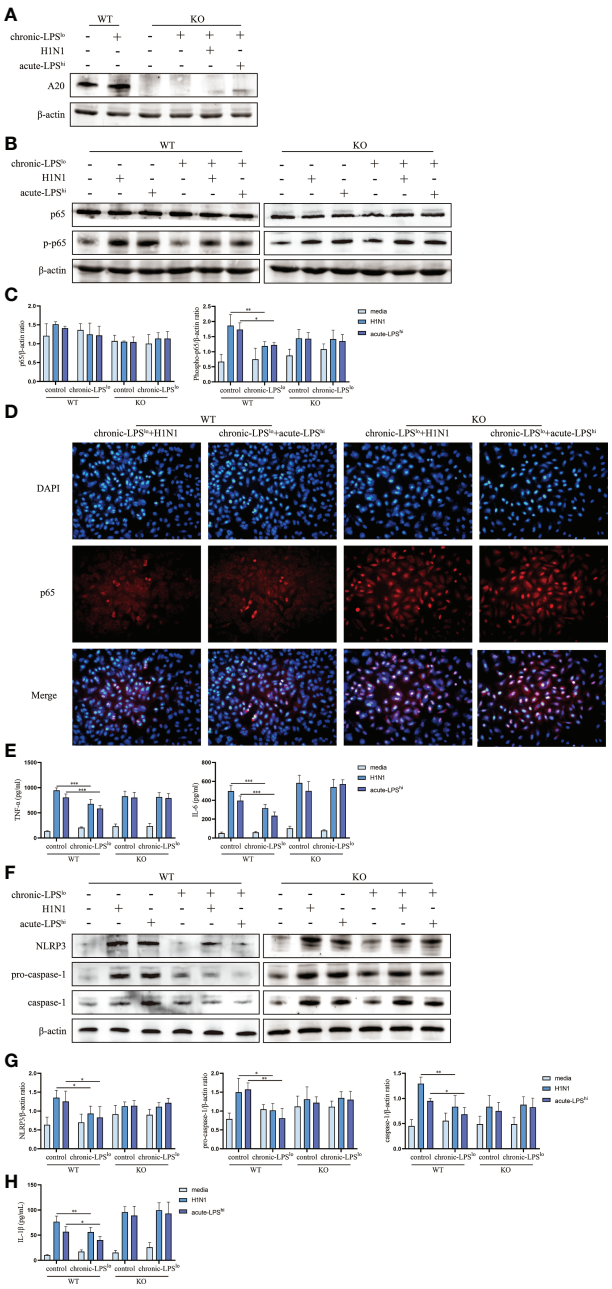

FIGURE 4
Effect of chronic low-dose LPS stimulation on NF-κB signaling pathway and NLRP3 inflammasome in high dose LPS-stimulated or H1N1-infected A549^{WT} and A549$^{A20\text{-}KO}$ cells. **(A)** Relative protein levels of A20 in A549$^{A20\text{-}KO}$ cells were detected by western blot. **(B, C)** Relative protein levels of p65 and p-p65 in A549^{WT} cells and A549$^{A20\text{-}KO}$ cells were detected by western blot. **(D)** Immunofluorescent images of the localization of p65 in A549^{WT} and A549$^{A20\text{-}KO}$ cells. **(E)** TNF-α and IL-6 in A549^{WT} and A549$^{A20\text{-}KO}$ cells culture supernatants were measured by ELISA. **(F, G)** Relative protein levels of NLRP3, pro-caspase-1 and caspase-1 in A549^{WT} and A549$^{A20\text{-}KO}$ cells were detected by western blot. **(H)** IL-1β in A549^{WT} and A549$^{A20\text{-}KO}$ cells culture supernatants were measured by ELISA. Data are mean ± SD, n = 3. *p< 0.05, **p< 0.01.

environment increases A20 and PPAR-α and -γ expression, in turn inhibits NF-κB and NLRP3 induced inflammation following IAV infection or high-dose LPS stimulation (Figure 7).

H1N1 causes serious health problems worldwide as a major infectious pathogen (15, 16). IAV infections cause severe airway inflammation and cytokine storms that lead to high morbidity and mortality (17, 18). Despite recent progress in the fight against IAV, control of inflammation remains a major challenge for severely ill patients (19–21). There are no effective treatments for the excessive inflammation and severe consequences in IAV, and the mechanisms of these events are poorly understood. Significant differences in influenza prevalence between metropolitan and rural areas suggest that environmental exposures may impact influenza severity (22). Possibly metropolitan cities have high hygiene standards, whereas people from small towns are protected because of continuous exposure to LPS or other microbial components (23, 24). Modulators targeting autoimmunity as preventive strategies such as chronic exposure to low-dose LPS environment is emerging as a promising strategy for a variety of inflammatory diseases, including IAV (4, 5).

A20 as a key protein in the protection mediated by chronic exposure to low-dose LPS environment is also a major determinant of progression and prognosis in several other inflammatory diseases (6–9). Environmental protection and A20 are well studied in childhood asthma, and farm environments protect children from asthma by increasing A20 expression (4, 5). Interestingly, A20 has been shown to inhibit NF-κB signaling pathway and NLRP3 inflammasome activation as well as autophagy, thereby preventing pulmonary fibrosis and arthritis (25–29). Here, we show that environment-mediated protection of A20 suppresses IAV or LPS induced inflammation and report new evidence for the molecular mechanisms that may be involved.

Here, we found that chronic-LPS^{lo} environment-mediated increases in A20 expression in cells significantly suppressed NF-κB signaling pathway activity and pro-inflammatory cytokine production to suppress IAV-induced hyper inflammation. Similar findings were reported in myeloid cells and lung epithelial cells (30, 31). Worth mentioning as the first line of defense against IAV infection, cytokines are a double-edged sword. Hyper induction of pro-inflammatory cytokine production also known as 'cytokine storm', it correlated directly with magnified inflammation and an unfavorable prognosis of IAV (18, 32, 33). Although cytokines play an important role in the antiviral response, if cytokines form a cytokine storm will hinder anti-virus immunity (34–36). Therefore, the exact role of A20 during viral infection requires further study. We could not rule out that other factors may also influence the relationship between A20 expression and IAV prognosis.

In addition to its key role in regulating NF-κB, several lines of evidence suggest that A20 regulates NLRP3 activation (37–39). For example, excessive Nlrp3 inflammasome activation drives arthritis pathogenesis in A20 knockout mice due to A20 putting a brake on Nlrp3 inflammasome activation by reducing LPS-induced Nlrp3 expression levels (29). Here, we consistently demonstrate that environment-mediated increases in A20 expression exhibit NLRP3 inflammasome suppression and IL-1beta expression downregulation upon infection with IAV or LPS stimulation, which is consistent with previous reports. Yet, we also explicitly show that A20 knockout cells no longer have the protection mediated by the chronic low-dose LPS environment. Our results combined with previous studies highlight the importance of increased A20 expression through the environment as a potential new therapeutic option for reducing IAV-mediated inflammation and cytokine storm.

10.3389/fimmu.2023.1119473

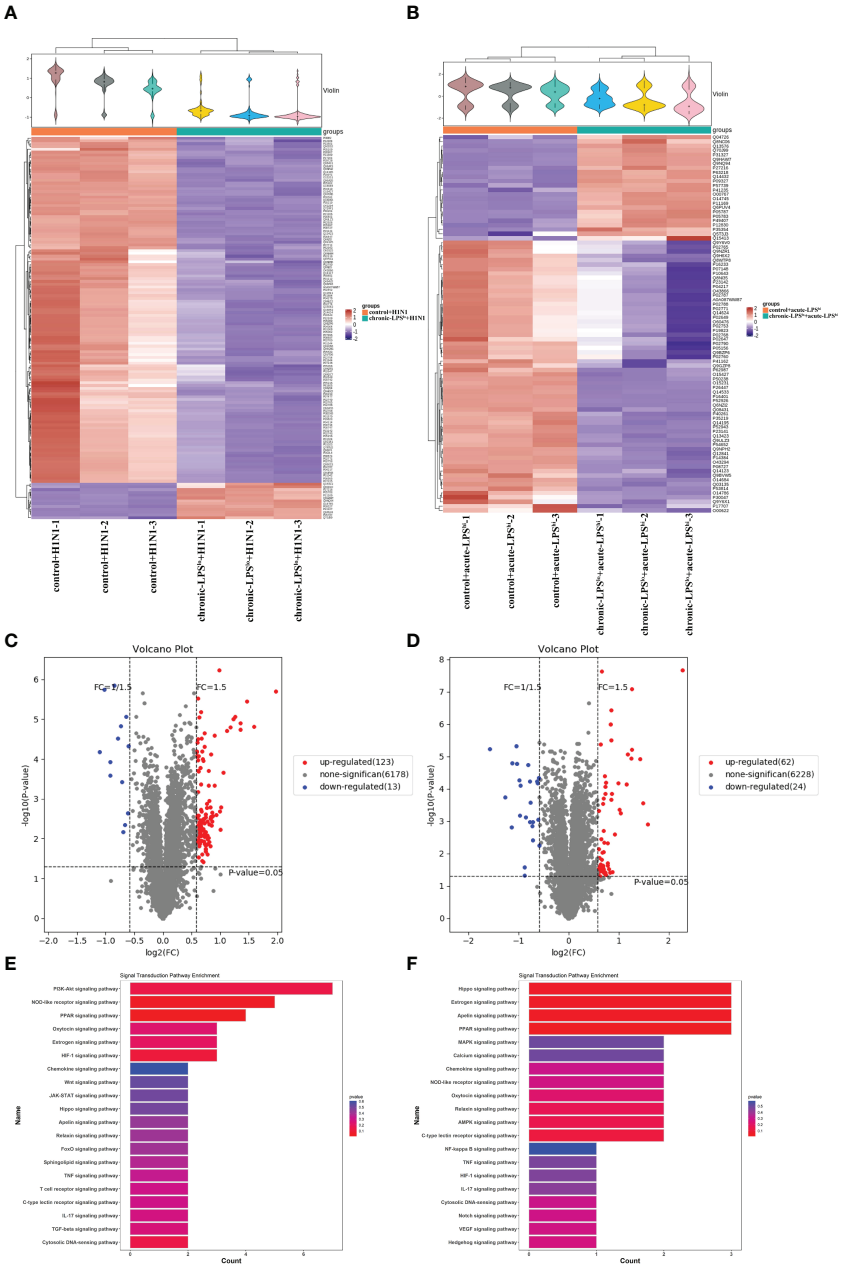

FIGURE 5
Inhibition of inflammation by chronic low-dose LPS stimulation is related to PPAR. **(A)** Hierarchical clustering analysis heat map in control+H1N1 group compared with chronic-LPS^{lo}+H1N1 group. **(B)** Hierarchical clustering analysis heat map in control+acute-LPS^{hi} group compared with chronic-LPS^{lo} +acute-LPS^{hi} group. **(C)** The differentially expressed proteins analyzed by volcano plots in control+H1N1 group compared with chronic-LPS^{lo}+H1N1 group (vertical dotted lines, fold change > 1.5-fold; horizontal dotted line, $p < 0.05$). **(D)** The differentially expressed proteins analyzed by volcano plots in control+acute-LPS^{hi} group compared with chronic-LPS^{lo}+acute-LPS^{hi} group (vertical dotted lines, fold change > 1.5-fold; horizontal dotted line, $p < 0.05$). **(E)** Top 20 of signaling transduction of KEGG pathway enrichment analysis in control+H1N1 group compared with chronic-LPS^{lo}+H1N1 group. **(F)** Top 20 of signaling transduction of KEGG pathway enrichment analysis in control+acute-LPS^{hi} group compared with chronic-LPS^{lo}+acute-LPS^{hi} group.

We also found that PPAR-α and -γ plays an essential role in the protection of environment-mediated A20 elevation against inflammation, and PPAR-α and -γ are positively regulated by A20 and exert a similar inhibitory effect on inflammation as A20. Studies have shown that A20 protects against restenosis after carotid artery injury in rats through PPAR-α inhibition of NF-κB pathway activation (10). In addition, A20 can protect mice from lethal hepatic ischemia-reperfusion injury by increasing PPAR-α expression and inhibiting NF-κB activation (40). Unlike the tight link between PPAR-alpha and NF-κB, PPAR-gamma mainly inhibits NLRP3 inflammasome (41–44). Considering excessive inflammation is tied to IAV related mortality, PPAR-α/γ has been considered as a therapeutic target to limit such harmful inflammation. In a recent study, IAV infection was shown to reduce PPAR-γ mRNA levels in mouse alveolar macrophages (45). In addition, significant activation of PPAR-α and -γ by drugs can protect mice from IAV infection and pneumonia (14). It is crucial that cytokine production is finely tuned during anti-viral responses, in which it provides optimal protection

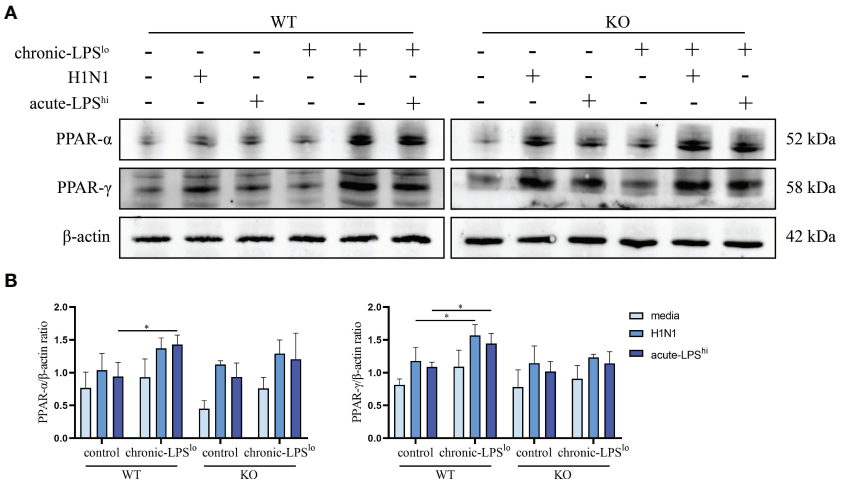

FIGURE 6
Effect of chronic low-dose LPS stimulation on PPAR-α and -γ. **(A, B)** Relative protein levels of PPAR-α and -γ in A549^{WT} and A549$^{A20\text{-}KO}$ cells were detected by western blot. Data are mean ± SD, n = 3. *p< 0.05.

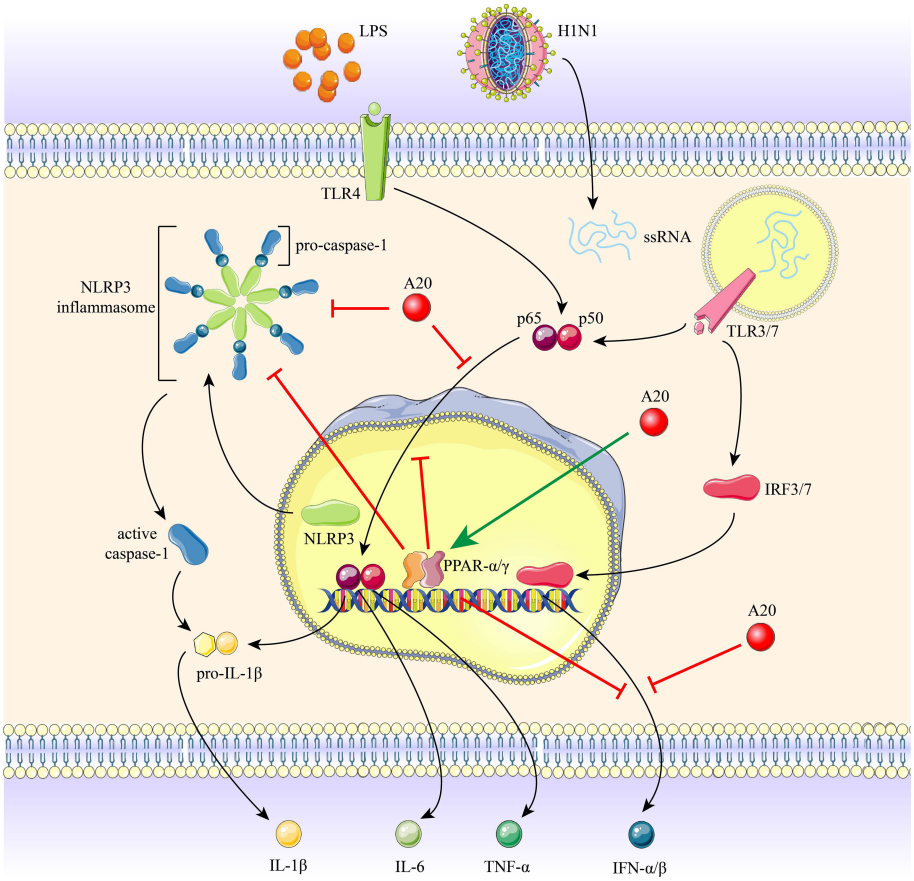

FIGURE 7
The role of A20 and PPAR-α and -γ in H1N1 infection and LPS stimulation induced inflammation. Recognition of H1N1 ssRNA or LPS by TLRs initiates the activation of NF-κB and NLRP3 inflammasome, promoting the production of downstream pro-inflammatory cytokines. Chronic low-dose LPS environment induced a marked increase in A20 expression, resulting in the restriction of NLRP3 inflammasome, caspase-1 cleavage, nuclear translocation of p65 subunit and IFNs expression. A20 increases PPAR-α and -γ expression, and PPAR-α and -γ also inhibit the above-mentioned inflammatory pathway.

while avoiding unwanted inflammation and tissue damage (46, 47). In this study the role of PPAR-α and -γ in environmental-mediated protection of chronic low-dose LPS the positive regulation of PPAR-gamma by A20 were explored for the first time. Whether the balance between A20 and inflammation is dependent on PPAR-α/γ, or whether there is crosstalk between A20 and PPAR-α/γ remains unclear; additional studies are required to resolve these points.

Collectively, our results suggest that inflammatory responses stimulated by H1N1 infection or high-dose LPS *in vitro* and *in vivo* were ameliorated in a chronic low-dose LPS environment. Increased levels of PPAR-α and -γ by A20 inhibits NF-κB and NLRP3 inflammasome activation and subsequently downregulate inflammatory cytokine production. A20 is increasingly recognized as a therapeutic target for a variety of diseases, therefore, long-term exposure to low-dose LPS environmental may help promote the resolution of IAV or LPS induced inflammation, thereby improving adverse clinical outcomes both in lung tissues.

Data availability statement

The original contributions presented in the study are included in the article/Supplementary Material. Further inquiries can be directed to the corresponding authors. The datasets presented in this study can be found in online repositories. The names of the repository/repositories and accession number(s) can be found at: http://proteomecentral.proteomexchange.org; PXD035611.

Ethics statement

The animal study was reviewed and approved by the ethics committee of The College of Basic Medical Sciences of Jilin University.

Author contributions

A-YH and FW designed and supervised the study. YG reviewed the literature and wrote the manuscript. YG, XZ, XG and ZZ performed experiments and analyzed data. SJ and ZO performed statistical analysis. A-YH revised the manuscript. FW obtained funding. All authors contributed to the article and approved the submitted version.

Funding

This work was supported by Key Laboratory of Precision Infectious Diseases of Jilin Province (Grant no.20200601011JC), Jilin Provincial Key Laboratory of Pathogen Biology (Grant no.3D5200117426), Jilin Provincial Development and Reform Commission Common Disease Precision Prevention and Control Engineering Laboratory, Jilin Provincial Science and Technology Innovation Center of Secondary Development of Chinese Traditional Patent Medicine (Grant no.20210502005ZP).

Conflict of interest

The authors declare that the research was conducted in the absence of any commercial or financial relationships that could be construed as a potential conflict of interest.

Publisher's note

Supplementary material

The Supplementary Material for this article can be found online at: https://www.frontiersin.org/articles/10.3389/fimmu.2023.1119473/full#supplementary-material

References

1. Oshansky CM, Gartland AJ, Wong SS, Jeevan T, Wang D, Roddam PL, et al. Mucosal immune responses predict clinical outcomes during influenza infection independently of age and viral load. *Am J Respir Crit Care Med* (2014) 189(4):449–62. doi: 10.1164/rccm.201309-1616OC

2. Herold S, Steinmueller M, von Wulffen W, Cakarova L, Pinto R, Pleschka S, et al. Lung epithelial apoptosis in influenza virus pneumonia: The role of macrophage-expressed tnf-related apoptosis-inducing ligand. *J Exp Med* (2008) 205(13):3065–77. doi: 10.1084/jem.20080201

3. Warnatsch A, Ioannou M, Wang Q, Papayannopoulos V. Inflammation. neutrophil extracellular traps license macrophages for cytokine production in atherosclerosis. *Sci (New York NY)* (2015) 349(6245):316–20. doi: 10.1126/science.aaa8064

4. Schuijs MJ, Willart MA, Vergote K, Gras D, Deswarte K, Ege MJ, et al. Farm dust and endotoxin protect against allergy through A20 induction in lung epithelial cells. *Sci (New York NY)* (2015) 349(6252):1106–10. doi: 10.1126/science.aac6623

5. Krusche J, Twardziok M, Rehbach K, Böck A, Tsang MS, Schröder PC, et al. Tnf-α-Induced protein 3 is a key player in childhood asthma development and environment-mediated protection. *J Allergy Clin Immunol* (2019) 144(6):1684–96.e12. doi: 10.1016/j.jaci.2019.07.029

6. Ma A, Malynn BA. A20: Linking a complex regulator of ubiquitylation to immunity and human disease. *Nat Rev Immunol* (2012) 12(11):774–85. doi: 10.1038/nri3313

7. Priem D, van Loo G, Bertrand MJM. A20 and cell death-driven inflammation. *Trends Immunol* (2020) 41(5):421–35. doi: 10.1016/j.it.2020.03.001

8. Guo W, Ma J, Guo S, Wang H, Wang S, Shi Q, et al. A20 regulates the therapeutic effect of anti-Pd-1 immunotherapy in melanoma. *J immunother Cancer* (2020) 8(2). doi: 10.1136/jitc-2020-001866

9. Martens A, van Loo G. A20 at the crossroads of cell death, inflammation, and autoimmunity. *Cold Spring Harbor Perspect Biol* (2020) 12(1). doi: 10.1101/cshperspect.a036418

10. Meng Z, Gao P, Chen L, Peng J, Huang J, Wu M, et al. Artificial zinc-finger transcription factor of A20 suppresses restenosis in sprague dawley rats after carotid injury *Via* the pparα pathway. *Mol Ther Nucleic Acids* (2017) 8:123–31. doi: 10.1016/j.omtn.2017.06.010

11. Toobian D, Ghosh P, Katkar GD. Parsing the role of ppars in macrophage processes. *Front Immunol* (2021) 12:783780. doi: 10.3389/fimmu.2021.783780

12. Ju Z, Su M, Li D, Hong J, Im DS, Kim S, et al. An algal metabolite-based ppar-Γ agonist displayed anti-inflammatory effect *Via* inhibition of the nf-κb pathway. *Mar Drugs* (2019) 17(6). doi: 10.3390/md17060321

13. Gopal R, Mendy A, Marinelli MA, Richwalls LJ, Seger PJ, Patel S, et al. Peroxisome proliferator-activated receptor gamma (Pparγ) suppresses inflammation and bacterial clearance during influenza-bacterial super-infection. *Viruses* (2019) 11(6). doi: 10.3390/v11060505

14. Bei Y, Tia B, Li Y, Guo Y, Deng S, Huang R, et al. Anti-influenza a virus effects and mechanisms of emodin and its analogs *Via* regulating Pparα/Γ-Ampk-Sirt1 pathway and fatty acid metabolism. *BioMed Res Int* (2021) 2021:9066938. doi: 10.1155/2021/9066938

15. Brody H. Influenza. *Nature* (2011) 480(7376):S1. doi: 10.1038/480S1a

16. Enserink M, Cohen J. Virus of the year. The novel H1n1 influenza. *Sci (New York NY)* (2009) 326(5960):1607. doi: 10.1126/science.326.5960.1607

17. Mudd PA, Crawford JC, Turner JS, Souquette A, Reynolds D, Bender D, et al. Distinct inflammatory profiles distinguish covid-19 from influenza with limited contributions from cytokine storm. *Sci Adv* (2020) 6(50). doi: 10.1126/sciadv.abe3024

18. Liu Q, Zhou YH, Yang ZQ. The cytokine storm of severe influenza and development of immunomodulatory therapy. *Cell Mol Immunol* (2016) 13(1):3–10. doi: 10.1038/cmi.2015.74

19. Ramiro S, Mostard RLM, Magro-Checa C, van Dongen CMP, Dormans T, Buijs J, et al. Historically controlled comparison of glucocorticoids with or without tocilizumab versus supportive care only in patients with covid-19-Associated cytokine storm syndrome: Results of the chic study. *Ann rheumatic Dis* (2020) 79(9):1143–51. doi: 10.1136/annrheumdis-2020-218479

20. Wang Q, Fang P, He R, Li M, Yu H, Zhou L, et al. O-Glcnac transferase promotes influenza a virus-induced cytokine storm by targeting interferon regulatory factor-5. *Sci Adv* (2020) 6(16):eaaz7086. doi: 10.1126/sciadv.aaz7086

21. Guo XJ, Thomas PG. New fronts emerge in the influenza cytokine storm. *Semin immunopathol* (2017) 39(5):541–50. doi: 10.1007/s00281-017-0636-y

22. Dalziel BA-O, Kissler S, Gog JA-O, Viboud CA-O, Bjørnstad OA-O, Metcalf CA-O, et al. Urbanization and humidity shape the intensity of influenza epidemics in U.S. cities. *Science* (2018) 362(6410):1095–9203. doi: 10.1126/science.aat6030

23. Bach JF. The hygiene hypothesis in autoimmunity: The role of pathogens and commensals. *Nat Rev Immunol* (2018) 18(2):105–20. doi: 10.1038/nri.2017.111

24. Lambrecht BN, Hammad H. The immunology of the allergy epidemic and the hygiene hypothesis. *Nat Immunol* (2017) 18(10):1076–83. doi: 10.1038/ni.3829

25. Ventura S, Cano F, Kannan Y, Breyer F, Pattison MJ, Wilson MS, et al. A20-binding inhibitor of nf-κb (Abin) 2 negatively regulates allergic airway inflammation. *J Exp Med* (2018) 215(11):2737–47. doi: 10.1084/jem.20170852

26. Liu SS, Lv XX, Liu C, Qi J, Li YX, Wei XP, et al. Targeting degradation of the transcription factor C/Ebpβ reduces lung fibrosis by restoring activity of the ubiquitin-editing enzyme A20 in macrophages. *Immunity* (2019) 51(3):522–34.e7. doi: 10.1016/j.immuni.2019.06.014

27. Municio C, Dominguez-Soto Á, Fuentelsaz-Romero S, Lamana A, Montes N, Cuevas VD, et al. Methotrexate limits inflammation through an A20-dependent cross-tolerance mechanism. *Ann rheumatic Dis* (2018) 77(5):752–9. doi: 10.1136/annrheumdis-2017-212537

28. Razani B, Whang MI, Kim FS, Nakamura MC, Sun X, Advincula R, et al. Non-catalytic ubiquitin binding by A20 prevents psoriatic arthritis-like disease and inflammation. *Nat Immunol* (2020) 21(4):422–33. doi: 10.1038/s41590-020-0634-4

29. Vande Walle L, Van Opdenbosch N, Jacques P, Fossoul A, Verheugen E, Vogel P, et al. Negative regulation of the Nlrp3 inflammasome by A20 protects against arthritis. *Nature* (2014) 512(7512):69–73. doi: 10.1038/nature13322

30. Maelfait J, Roose K, Bogaert P, Sze M, Saelens X, Pasparakis M, et al. A20 (Tnfaip3) deficiency in myeloid cells protects against influenza a virus infection. *PloS Pathog* (2012) 8(3):e1002570. doi: 10.1371/journal.ppat.1002570

31. Maelfait J, Roose K, Vereecke L, Mc Guire C, Sze M, Schuijs MJ, et al. A20 deficiency in lung epithelial cells protects against influenza a virus infection. *PloS Pathog* (2016) 12(1):e1005410. doi: 10.1371/journal.ppat.1005410

32. Fajgenbaum DC, June CH. Cytokine storm. *New Engl J Med* (2020) 383(23):2255–73. doi: 10.1056/NEJMra2026131

33. Tisoncik JR, Korth MJ, Simmons CP, Farrar J, Martin TR, Katze MG. Into the eye of the cytokine storm. *Microbiol Mol Biol reviews: MMBR* (2012) 76(1):16–32. doi: 10.1128/mmbr.05015-11

34. McNab F, Mayer-Barber K, Sher A, Wack A, O'Garra A. Type I interferons in infectious disease. *Nat Rev Immunol* (2015) 15(2):87–103. doi: 10.1038/nri3787

35. Biron CA. Interferons alpha and beta as immune regulators–a new look. *Immunity* (2001) 14(6):661–4. doi: 10.1016/s1074-7613(01)00154-6

36. Davidson S, Crotta S, McCabe TM, Wack A. Pathogenic potential of interferon αβ in acute influenza infection. *Nat Commun* (2014) 5:3864. doi: 10.1038/ncomms4864

37. Huang X, Feng Z, Jiang Y, Li J, Xiang Q, Guo S, et al. Vsig4 mediates transcriptional inhibition of Nlrp3 and il-1β in macrophages. *Sci Adv* (2019) 5(1):eaau7426. doi: 10.1126/sciadv.aau7426

38. Xue Z, Xi Q, Liu H, Guo X, Zhang J, Zhang Z, et al. Mir-21 promotes Nlrp3 inflammasome activation to mediate pyroptosis and endotoxic shock. *Cell Death Dis* (2019) 10(6):461. doi: 10.1038/s41419-019-1713-z

39. Mouton-Liger F, Rosazza T, Sepulveda-Diaz J, Ieang A, Hassoun SM, Claire E, et al. Parkin deficiency modulates Nlrp3 inflammasome activation by attenuating an A20-dependent negative feedback loop. *Glia* (2018) 66(8):1736–51. doi: 10.1002/glia.23337

40. Ramsey HE, Da Silva CG, Longo CR, Csizmadia E, Studer P, Patel VI, et al. A20 protects mice from lethal liver Ischemia/Reperfusion injury by increasing peroxisome proliferator-activated receptor-alpha expression. *Liver Transplant* (2009) 15(11):1613–21. doi: 10.1002/lt.21879

41. Yang CC, Wu CH, Lin TC, Cheng YN, Chang CS, Lee KT, et al. Inhibitory effect of pparγ on Nlrp3 inflammasome activation. *Theranostics* (2021) 11(5):2424–41. doi: 10.7150/thno.46873

42. Liu Y, Bi X, Zhang Y, Wang Y, Ding W. Mitochondrial Dysfunction/Nlrp3 inflammasome axis contributes to angiotensin ii-induced skeletal muscle wasting *Via* ppar-Γ. *Lab investigation; J Tech Methods Pathol* (2020) 100(5):712–26. doi: 10.1038/s41374-019-0355-1

43. Fu J, Zhao B, Ni C, Ni H, Xu L, He Q, et al. Rosiglitazone alleviates mechanical allodynia of rats with bone cancer pain through the activation of ppar-Γ to inhibit the nf-κb/Nlrp3 inflammatory axis in spinal cord neurons. *PPAR Res* (2021) 2021:6086265. doi: 10.1155/2021/6086265

44. Meng QQ, Feng ZC, Zhang XL, Hu LQ, Wang M, Zhang HF, et al. Ppar-Γ activation exerts an anti-inflammatory effect by suppressing the Nlrp3 inflammasome in spinal cord-derived neurons. *Mediators Inflammation* (2019) 2019:6386729. doi: 10.1155/2019/6386729

45. Huang S, Zhu B, Cheon IS, Goplen NP, Jiang L, Zhang R, et al. Ppar-Γ in macrophages limits pulmonary inflammation and promotes host recovery following respiratory viral infection. *J Virol* (2019) 93(9). doi: 10.1128/jvi.00030-19

46. Xing J, Weng L, Yuan B, Wang Z, Jia L, Jin R, et al. Identification of a role for Trim29 in the control of innate immunity in the respiratory tract. *Nat Immunol* (2016) 17(12):1373–80. doi: 10.1038/ni.3580

47. Dou Y, Xing J, Kong G, Wang G, Lou X, Xiao X, et al. Identification of the E3 ligase Trim29 as a critical checkpoint regulator of nk cell functions. *J Immunol (Baltimore Md: 1950)* (2019) 203(4):873–80. doi: 10.4049/jimmunol.1900171

frontiers | Frontiers in Immunology

TYPE Review
PUBLISHED 20 January 2023
DOI 10.3389/fimmu.2023.1118236

OPEN ACCESS

EDITED BY
Chenhe Su,
Wistar Institute, United States

REVIEWED BY
Yuelong Yan,
University of Texas MD Anderson Cancer Center, United States
Longhuan Ma,
University of Florida, United States

*CORRESPONDENCE
Jinmei Tuo
tjmtjm1227@163.com
Changyin Yu
yuchangyin68@163.com
Zucai Xu
docxzc@126.com

SPECIALTY SECTION
This article was submitted to Viral Immunology, a section of the journal Frontiers in Immunology

RECEIVED 07 December 2022
ACCEPTED 06 January 2023
PUBLISHED 20 January 2023

CITATION
Zhang L, Zhang L, Li F, Liu W, Tai Z, Yang J, Zhang H, Tuo J, Yu C and Xu Z (2023) When herpes simplex virus encephalitis meets antiviral innate immunity. *Front. Immunol.* 14:1118236. doi: 10.3389/fimmu.2023.1118236

When herpes simplex virus encephalitis meets antiviral innate immunity

Linhai Zhang[1,2], Lijia Zhang[1], Fangjing Li[1], Wanyu Liu[1], Zhenzhen Tai[1], Juan Yang[1], Haiqing Zhang[1], Jinmei Tuo[1,2*], Changyin Yu[1,2*] and Zucai Xu[1,2*]

[1]Department of Neurology, Affiliated Hospital of Zunyi Medical University, Zunyi, China, [2]The Collaborative Innovation Center of Tissue Damage Repair and Regeneration Medicine of Zunyi Medical University, Zunyi, China

Herpes simplex virus (HSV) is the most common pathogen of infectious encephalitis, accounting for nearly half of the confirmed cases of encephalitis. Its clinical symptoms are often atypical. HSV PCR in cerebrospinal fluid is helpful for diagnosis, and the prognosis is usually satisfactory after regular antiviral treatment. Interestingly, some patients with recurrent encephalitis have little antiviral effect. HSV PCR in cerebrospinal fluid is negative, but glucocorticoid has a significant effect after treatment. Specific antibodies, such as the NMDA receptor antibody, the GABA receptor antibody, and even some unknown antibodies, can be isolated from cerebrospinal fluid, proving that the immune system contributes to recurrent encephalitis, but the specific mechanism is still unclear. Based on recent studies, we attempt to summarize the relationship between herpes simplex encephalitis and innate immunity, providing more clues for researchers to explore this field further.

KEYWORDS

herpes simplex virus, autoimmune encephalitis, innate immune, NMDAR encephalitis, immunotherapy

1 Introduction

Viral infection causes encephalitis, an inflammation of the brain parenchyma accompanied by neurological dysfunction (1). Symptoms include headache, altered consciousness, seizures, focal dysfunction, papilledema, fever, myalgia, and respiratory or digestive symptoms (2). In general, the prognosis of viral encephalitis is determined by the pathogen and host immune status, but in a small number of cases, viral infection can lead to antibody-mediated autoimmune encephalitis (AE) (3, 4). Several neurological autoimmune diseases can be induced by HSV infection in individuals with selective innate immunodeficiency (5). Unlike adaptive immunity, innate immunity cannot establish and maintain immune memory against reinfection. To restrict viral infections, antiviral innate immunity acts in a non-specific manner when the body is exposed to pathogens (6), which has recently been challenged (7). There is extensive literature claiming that the innate

immune system can create memory after infection and therefore be able to respond rapidly in the event of a second infection (8, 9), while pattern recognition receptors (PRRs) are a prerequisite for this ability, PRRs may also be key signals in the induction of autoimmune encephalitis (10). The purpose of this review was to identify the possible relationship between innate immunity and herpes simplex viral encephalitis (HSVE) and to offer new insight for clinical investigation.

2 Viral replication

An HSV-1 virus consists of a capsid, tegument, and envelope in a spherical shape (11). In addition to gD, gH, gL, and gB, the envelope contains 11 viral glycoproteins, among which the gB function as a fusogen to allow HSV to enter cells. It combined with heparan sulfate, herpesvirus entry mediator, and nectin on the surface of the host cell when cells are infected with HSV using the fusion mechanism involving gB, gD, gH/gL as the core (12, 13). The tegument and capsid enter the host cell after fusion, and the tegument recruits tubulin and dynein to transport the capsid to the nucleus (14, 15). Researchers have shown that the tegument proteins UL36 and UL37 trigger movement to the nucleus (16), releasing the genome into the nucleus (17). In addition, vp16 separates from the capsid and enters the nucleus to form a complex with host cell factor 1 (HCF-1) and octamer binding protein-1 (Oct-1), and finally, it binds to the promoter of the Immediate early (IE) gene, which drives gene expression (IE, E and L genes) (18, 19). HSV codes ICP0, ICP4, ICP22, ICP27, and ICP47 (20) genes can be activated or inhibited by them, thereby promoting or delaying a process. Ultimately, the IE gene produces proteins that regulate viral replication and cellular antigen presentation, and the E gene synthesizes viral DNA and packages proteins, the L gene produces proteins for virion assembly, and mature viruses exit the cell by exocytosis (21) (Figure 1).

Through reverse axoplasmic transport, the virus in the exposed area enters nerve endings and reaches the neuronal cell body after lytic infection (22). Although it has been reported in the vagus nerve and superior cervical ganglion, it is also usually latent in the trigeminal ganglion (23). IE, E, and L genes start to express approximately 24-72 h after infection. IE and E transcription decreases while latency-associated transcript (LAT) gradually increases, thus forming latent infection (21). The mechanism may be related to promoting viral genome silencing by LAT (24). Local latent viruses can be reactivated and replicated by fever, emotional or hormonal imbalance, trauma, or immunosuppression and locally produce blisters, sores, or ulcers (25, 26).

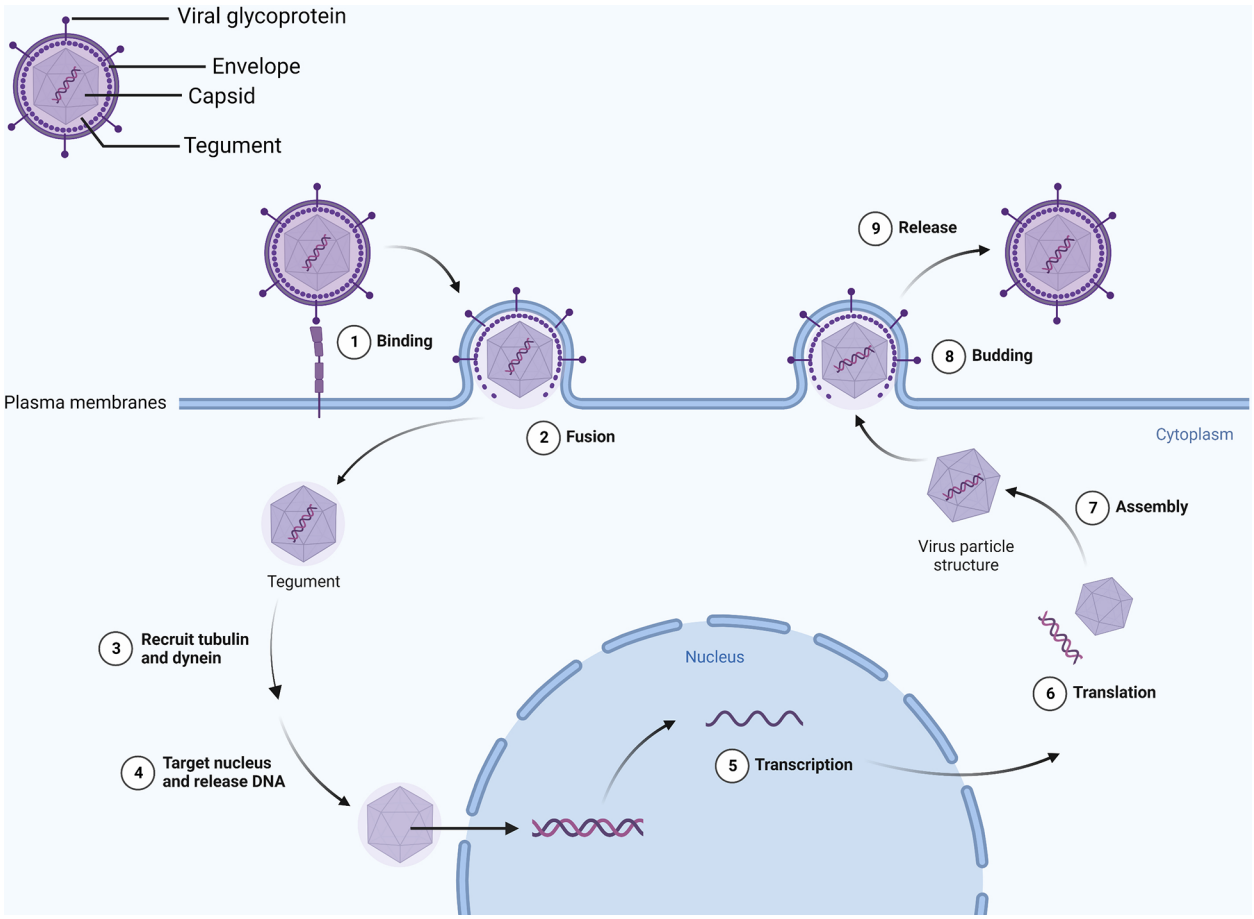

FIGURE 1
Viral envelope glycoproteins mediate binding with the cell membrane. Viral DNA enters the nucleus and transcribes and translates viral particle accessories as the envelope merges with the cell membrane. Eventually, intact virions leave the cell by exocytosis.

3 Immune responses

3.1 Primary immune response in HSVE

For a virus to enter the brain, it must cross the blood-brain barrier, which is different from a peripheral infection. Transcellular transport is severely limited by the tight junctions between cells within the blood-brain barrier, which separates the central nervous system from peripheral blood circulation (27). However, HSV can be transported reversely along the nerve, bypassing the blood-brain barrier and entering the central nervous system, activating innate immune cells and generating an innate immune response (28), Its viral genomic DNA and some RNA intermediates become the true pathogen-related molecular patterns (PAMPs) of pattern recognition receptors (PRRs).

After the virus enters the brain, nucleic acid sensing is important to detect the virus. Microglia express cyclic-GMP-AMP synthase (cGAS), a nucleotidyl transferase and an important cytoplasmic sensor that recognizes DNA ligands in different cell types (29, 30).

Compared to wild-type mice, cGAS- and STING-deficient mice had significantly higher viral loads in brain tissue, according to Reinert et al. (29). cGAS is activated after binding to viral double-stranded DNA (dsDNA) and utilizes ATP and GTP to form cyclic GMP-AMP (cGAMP). CGAMP further activates the stimulator of interferon gene (STING), which is transported to the Golgi by COPII (31), activation of TRAF family member-associated NF-κB activator (TANK)-binding kinase 1 (TBK1) after palmitoylation, leading to the activation of interferon regulatory factor 3 (IRF3) and interferon production (32, 33). A zebrafish model of HSV-1 infection induces robust interferon production and depends on STING expression, but cGAS seems dispensable for the STING signaling, whereas DDX41 and DHX9 were found to be more closely related to interferon production in zebrafish (34).

An immune response is triggered by the DNA-dependent activator of IFN-regulatory factors (DAI), a recently discovered DNA sensor that detects nucleic acids exposed during cell damage or infection. Using artificially induced DAI and B-DNA stimulation of L929 cells, IFN was found to be expressed earlier and at higher levels than controls, which was associated with the synergy of IRF3 and TBK1 and independent of TLR9 (35). Thanh et al. demonstrated that in DAI knockdown HepG2 cells, HSV-1 viral gene and ICP0 expression were increased, but DAI knockdown did not affect cytoplasmic DNA stimulation-mediated interferon release, suggesting that there may be other pathways that can promote interferon expression (36). The receptor-interacting protein 1 (RIP1) and the receptor-interacting protein 3 (RIP3) can also be recruited by DAI through its receptor-interacting protein homotypic interaction motifs (RHIMs), then activating NF-κB (37). A new DNA sensor, IFI16, has been discovered in the cytoplasm, similar to DAI. It is a member of the PYHIN protein family with two DNA-binding domains that can directly bind to viral DNA and recruit STING (38). A nuclear localization signal allows IFI16 to recognize HSV DNA and acetylate itself, which recruits STING and induces the production of IFN (39, 40).

A cytoplasmic-localized RNA sensor, Retinoic acid-inducible gene (RIG)-I-like receptor (RLR) includes RIG-I, MDA5, and LGP2, whose enhanced expression is induced by viral infections and interferon stimulation, which leads to antiviral effects (41–43). HSV replication in mutated human hepatoma cells inactivated by RIG-I demonstrates their relationship (44). According to Emma et al., RIG-I expression is parallel with intracellular DNA load, and RIG-I cooperates with DAI to exert an antiviral effect on HSV through RNA polymerase 3 (45), it is unclear, however, whether RIG-I recognizes RNA transcribed by HSV.

Also, Toll-like receptors (TLRs) play a crucial role in recognition of viruses by the host. HSVE pathogenesis is linked to TLR3 deficiency (46). In the TLR3 molecule, an ectodomain (ECD) is present inside the endosome, and an extracellular Toll/interleukin-1 receptor domain (TIR) is present outside the endosome. The ligand-binding ECD domain promotes the phosphorylation of TLR3, and the TIR domain recruits adaptor proteins, which are important for downstream signaling (47). Multiple cells express TLR3, which recognizes double-stranded RNA (dsRNA), an intermediate in viral replication (48). When TLR3 binds to its ligand, it recruits its only adaptor-TRIF (or TICAM1)-triggering downstream signaling that activates TBK1, an inhibitor of κB (IκB) kinase-related kinase-ϵ (IKK-ϵ), and phosphorylates IRF- 3, while phosphorylated IRF-3 is translocated to the nucleus to induce interferon gene transcription (49–52). TLR2, 7, 9, and other subtypes also contribute to viral recognition (53, 54) (Figure 2). UNC93B1 is a multi-transmembrane protein that plays a crucial role in necleic-acid-sensing TLR signaling (55). Studies have shown that the UNC93B1 regulates the TLR7/9 signaling pathway by transferring TLR7 and 9 to endolysosomes (56). UNC93B1 prevents the STING from hyperactivation, thus inhibiting the cGAS-STING pathway and its subsequent interferon production, this was shown in UNC93B1-deficient mice that UNC93B1 deficiency strengthens the host immune responses to the cytosolic DNA stimulation and UNC93B1-deficient mice are more resistant to HSV-1 infection (57).

3.2 Immune evasion

Even though the host has many antiviral mechanisms, the virus has developed a powerful immune evasion mechanism (58). The enzymatic activity of cGAS is crucial to antiviral effects by triggering downstream interferon signaling by binding to dsDNA. Interferon mRNA was significantly higher in VP22 knockout HSV-infected cells than in wild-type HSV-infected cells, and ectopic expression of viral proteins VP22 are shown to inhibit cGAS/STING-mediated interferon production (59). VP24 can inhibit cGAS and STING-induced promoter activation and interferon production (60).

Many studies have revealed that the tegument proteins are important in viral gene replication and assembly (61). Among them, UL36 ubiquitin-specific protease (UL36USP) acts as a deubiquitinase that inhibits promoter activation of interferon and NF-κB induced by cGAS and STING, which allows the virus to evade host DNA sensing immune responses (62). Furthermore, UL36USP inhibits the degradation of capsids due to its deubiquitylase activity and prevents the viral genome from entering the cytoplasm, thus preventing DNA sensing-induced antiviral immunity (63). UL24 is a conserved protein among the herpes family but essential for viral

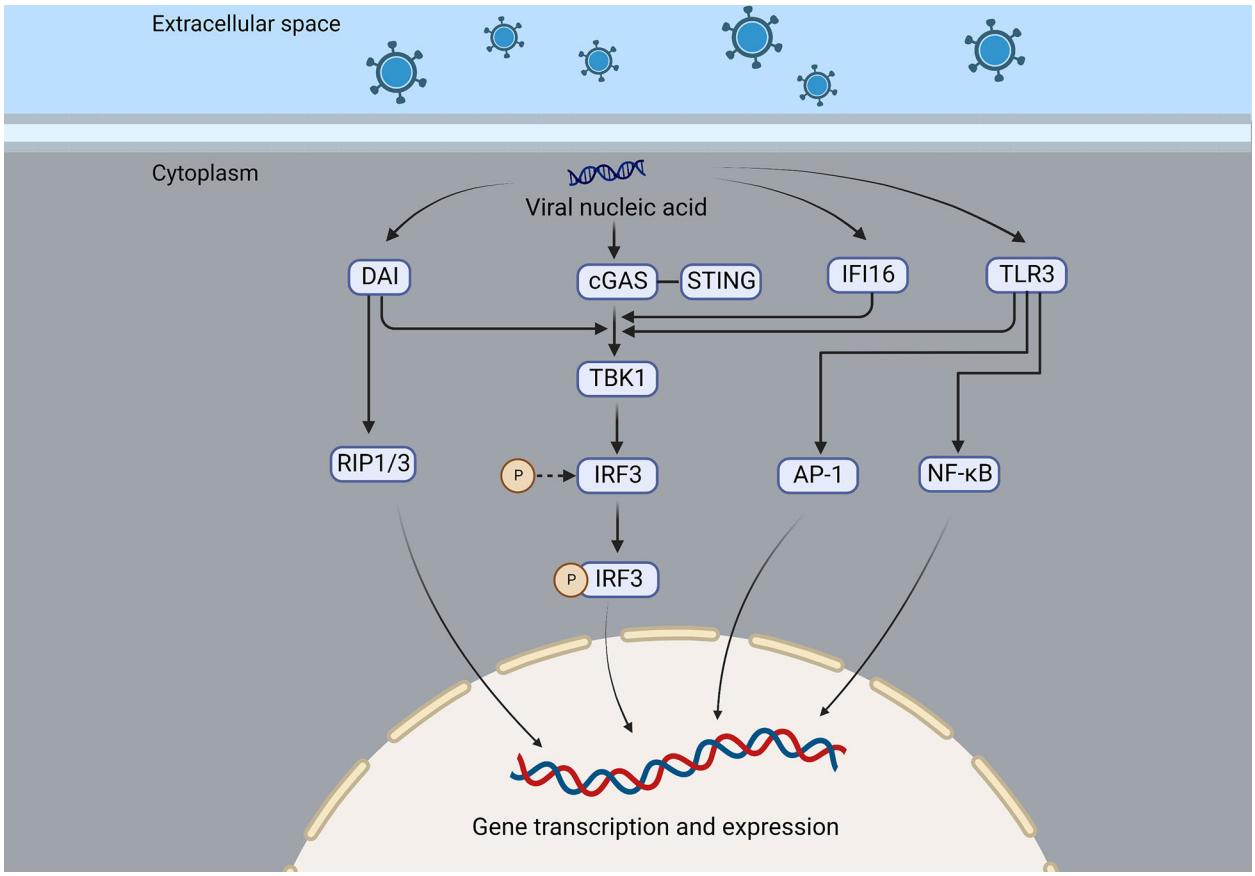

FIGURE 2
DAI, cGAS, IFI16, and TLR3 are nucleic acid sensing mechanisms of the virus that recruit and activate TBK1, which in turn activates IRF3, resulting in the expression of interferon or cytokines. In addition, DAI can also recruit RIP1/3 to promote gene transcription and expression, and TLR3 can activate NF-κB and AP-1 and induce the production of interferon and inflammatory factors.

replication, it can inhibit interferon and interleukin-6 (IL-6) expression mediated by cGAS-STING, and UL24 is also found to block NF-κB promoter activation. All these lead to viral immune evasion (64). A deamidation of the viral tegument protein UL37 inhibits the synthesis of cGAMP catalyzed by cGAS, interrupts downstream signal transduction, reduces interferon production, and promotes viral survival (65). Even though the cGAS-STING pathway is essential for the host against the virus, HSV-1 has evolved to evade host immune responses. Compared to the UL41-null mutant virus, wild-type HSV-1 infection could inhibit activation of the interferon signaling pathway, and UL41 expression inhibits interferon promoter activation and decreases production (66).

ICP34.5 is the virulence factor of HSV, encoded by a leaky-late gene, which can dephosphorylate eIF2α under the action of protein phosphatase 1-α, thereby allowing the continuous synthesis of viral proteins (67). ICP34.5 inhibits downstream antiviral signaling by preventing STING's translocation to the Golgi apparatus (68). IFI16 can induce interferon production early in infection and exert antiviral effects (69), whereas later in infection, ICP0 targets IFI16 for degradation through its E3 ubiquitin ligase activity and promote virus replication (70). β-catenin is crucial for regulating the transcription of target genes. However, HSV-1 US3 protein inhibits interferon production by phosphorylating β-catenin in the Wnt signaling pathway and further restricting β-catenin nuclear translocation, thus antagonizing the interferon production and destroying the host antiviral immune response (71).

3.3 Immune response in HSVE relapse

Infectious, autoimmune, and postinfectious encephalitis is the most common causes of encephalitis, characterized by inflammation of the brain parenchyma with neurological deficits (1), with viral encephalitis accounting for 60% of infectious cases (72). HSVE is one of the most common causes of encephalitis, and although the virus is cleared after regular treatment, patients still experience relapses in neurological symptoms. In some patients, viral DNA was detected in their cerebrospinal fluid, indicating persistent infection or viral reactivation, which signified a true relapse of HSVE.

In some patients, however, the virus was not detected by cerebrospinal fluid PCR after relapse, and the condition improved after Immunotherapy (73), suggesting that the immune mechanism lies at the heart of many of these complications. The authors reviewed a total of 43 patients with herpes simplex encephalitis and anti-N-methyl-D-aspartate receptor (NMDAR) antibody encephalitis, most of whom were children with a biphasic course (74), and anti-NMDAR antibody encephalitis is the most common immune encephalitis after

HSVE (75). Additionally, anti-GABAR antibodies, anti-CASPR2 antibodies, and some unknown antibodies will be produced after HSVE (76–79). 27% (14 of 51) of HSVE patients had autoimmune encephalitis (AEs), and all 14 had neuronal antibodies, while 11 of 37 patients without AEs also had neuronal antibodies (80). It was assumed that the viral infection triggered the immune response because none of the patients had these antibodies before developing HSVE. When mice were intranasally injected with HSV-1, Linnoila et al. found that serum NMDAR antibodies were positive, hippocampal NMDAR decreased, and also produced unknown antibodies (81), which had been observed in patients with autoimmune brains after HSVE.

When combined with anti-NMDAR encephalitis (following a non-HSV infection), patients are more likely to develop HSV antibodies than controls (compared with Cytomegalovirus and Epstein-Barr virus), and there are no neuronal or glial markers in the CSF, it is considered that HSV and NMDAR might be connected (82). A molecular mimicry best demonstrates the link between Campylobacter jejuni and Guillain-Barré syndrome (83). Zhao et al. found that, compared with wild-type HSV-1, the virus with protein UL6 gene knockout could not induce autoimmune diseases and that wild-type autoimmune diseases were triggered by autoreactive T cells (84), suggesting that molecular mimicry may contribute to autoimmune disease development following viral infections.

Despite this, molecular modeling alone may not be sufficient to explain immune encephalitis since HSVE is often associated with extensive neuronal damage, leading to the release of antigens from neurons (73, 74, 85), the presence of unknown antibodies could also explain symptoms other than typical NMDAR encephalitis (86, 87). Previously, 33% of patients with anti-NMDAR encephalitis had abnormal brain MRIs, but few had contrast enhancement (88), while most patients with autoimmune encephalitis after herpes simplex encephalitis had contrast enhancement, suggesting disruption of the blood-brain barrier (89) or inflammation (80, 90).

According to Omae et al., the cerebrospinal fluid cytokines or chemokines in patients with NMDAR encephalitis after HSVE increased in the early stage, suggesting immune infiltration into the central nervous system and damage to blood-brain barrier integrity. After treatment, these cytokines or chemokines gradually decreased; then, in the middle stage, they increased again, but NMDAR antibodies were absent; finally, in the late stage, NMDAR antibodies reached their peak, and the cytokines and chemokines gradually decreased (91). In an evaluation of this case, Wesselingh et al. proposed a hypothesis of the pathogenesis of autoimmune brain following herpes simplex encephalitis: HSV infection results in a breach of the blood-brain barrier that allows innate/adaptive immune cells to infiltrate and cause neuroinflammation. Eventually, B cells and T cells are recruited and produce antibodies against neuronal antigens (90, 92, 93) (Figure 3).

4 The efficacy and prognosis of standardized Immunotherapy

Patients with herpes simplex encephalitis experience a variety of clinical symptoms. The most common symptoms are headache, fever, and focal neurological symptoms. In severe cases, there may be unconsciousness (94). Early identification and targeted treatment are of great significance to the prognosis of patients.

Aciclovir is a nucleoside analog with potent antiviral properties against herpesviruses. As the first-choice treatment for HSVE,

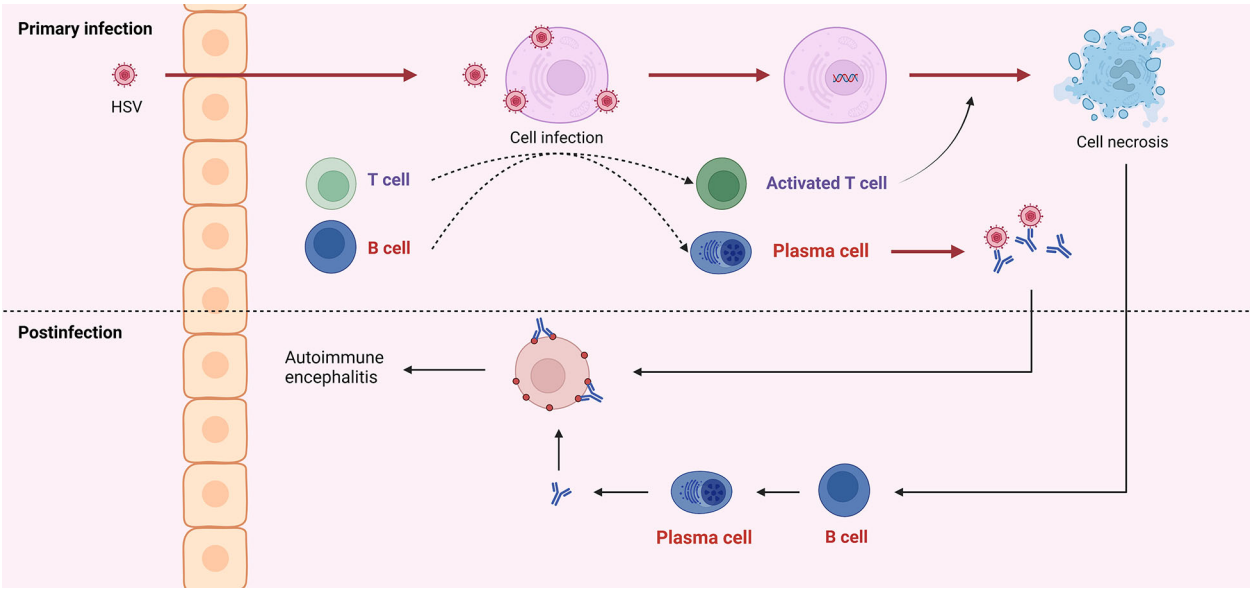

FIGURE 3
HSV into the central nervous system can cause infection of neurons, which is referred to as primary infection. Both viral particles and infected cells can recruit B and T cells. Antibodies produced by B cells can neutralize virus particles, and T cells can exert cytotoxicity to kill infected cells. Due to the similar structure of viral surface antigens to self-tissue, antibodies derived from the primary infection may attack healthy neurons. And cell disintegration leads to self-antigen exposure, induces B cells to produce antibodies, and further attacks self-cells, which is called post-infectious encephalitis or autoimmune encephalitis.

acyclovir has been proven in two previous randomized controlled trials (95, 96). Infectious Diseases Society of America, clinical practice guidelines, recommend treating patients with suspected encephalitis empirically with acyclovir before diagnosis, and for the specific treatment of HSV, acyclovir is also a class III recommendation (97). The British Association of Neurologists and the British Association of Infectious Diseases recommend that if there are no clinical contraindications, cerebrospinal fluid pressure, white blood cell count and classification, protein, and sugar be collected as soon as possible after admission. If there are contraindications, a head CT scan should be performed as soon as possible. When cerebrospinal fluid or imaging suggests viral encephalitis, acyclovir antiviral therapy should be started (10 mg/kg, tid, 14-21 d) (98).

The role of corticosteroids in HSVE is not yet clear, but the treatment is expected to improve cerebral edema, high intracranial pressure, and structural displacements of the brain empirically. In theory, corticosteroids could exacerbate the illness by promoting viral replication. In studies of mice treated with acyclovir combined with corticosteroids, however, the viral load in the brains of mice treated with acyclovir alone did not change significantly, and brain MRI abnormalities in mice treated with corticosteroids decreased significantly (99), demonstrating that corticosteroids can benefit brain injury without affecting viral loads. Acyclovir plus dexamethasone or dexamethasone alone reduced viral load compared to controls (100). A retrospective study describes the benefits of concomitant corticosteroids in patients with HSVE (101). However, British guidelines advise against routinely using corticosteroids for treatment, possibly due to their side effects (98). Corticosteroids have not yet been determined to be the most effective treatment for HSVE. However, if there is obvious edema or mass effect, it is recommended to continue corticosteroids (102). However, animal studies have shown that delayed corticosteroid addition suppresses inflammation and viral genes (103).

In addition to seizures, movement disorders, psychosis, and cognitive changes, NMDAR encephalitis may occur sometime after HSVE (104). The study by Nosadini et al. found that dyskinesia is one of the key symptoms to distinguish HSVE-induced AEs from pure recurrence of HSVE (74). A comprehensive etiology and imaging examination should be performed if symptoms recur and it is impossible to differentiate between virus reactivation and immune induction. New hemorrhage or necrosis on brain MRI often indicates viral replication (74). It is important to consider autoimmune encephalitis if viral testing is negative and to initiate Immunotherapy as soon as possible (105). Immunotherapy is effective in several studies (90, 106–108). AE after HSVE is treated similarly to NMDAR encephalitis, with plasma exchange, corticosteroids, immunoglobulin as first-line treatments, and immunosuppressants, including rituximab, as second-line treatments (109). According to a study, half of the patients with NMDAR encephalitis gradually improved after receiving first-line treatment within 4 weeks. The remaining patients who did not respond well to first-line treatment received a second-line treatment, which was more effective than no treatment (88).

5 Conclusion

It is a common infectious encephalitis caused by HSV. Although many studies have revealed its etiological mechanism, and many targeted treatment options have been developed, the prognosis is still unsatisfactory, especially for HSVE. The immune system plays an important role in the pathogenesis of herpes simplex virus encephalitis, which is also why corticosteroids play an important role in treating autoimmune encephalitis. Whether it is a molecular simulation or neuron damage, the speculation about the pathogenesis of immune encephalitis is constantly being confirmed. Immunotherapy can have certain curative effects, but the timing of initiation of Immunotherapy is still uncertain, and further research is necessary. In this article, we reviewed the general disease characteristics of herpes simplex virus encephalitis, summarized potential immune mechanisms, and discussed its important complication, autoimmune encephalitis, in the hopes of providing further insight for future research.

Author contributions

LinZ, LijZ, LF, LW, JY and HZ designed and wrote the manuscript. JT, CY and ZX helped with proofreading and revision. All authors contributed to the article and approved the final version.

Funding

This work was supported by grants from the Guizhou epilepsy basic and clinical research scientific and technological innovation talent team project (No: CXTD[2022]013), the Collaborative Innovation Center of Chinese Ministry of Education (No: 2020-39), the Guizhou provincial "hundred" level innovative talents funds (No: GCC-2022-038-1), the Guizhou Provincial Science and Technology Foundation (No: ZK2022-656), and the Zunyi City Science and Technology Foundation (No: 2019-71 and 2021-30).

Conflict of interest

The authors declare that the research was conducted in the absence of any commercial or financial relationships that could be construed as a potential conflict of interest.

Publisher's note

References

1. Venkatesan A, Murphy OC. Viral encephalitis. *Neurol Clin* (2018) 36:705–24. doi: 10.1016/j.ncl.2018.07.001

2. Costa B, Sato DK. Viral encephalitis: a practical review on diagnostic approach and treatment. *J Pediatr (Rio J)* (2020) 96 Suppl 1:12–9. doi: 10.1016/j.jped.2019.07.006

3. Stahl JP, Mailles A. Herpes simplex virus encephalitis update. *Curr Opin Infect Dis* (2019) 32:239–43. doi: 10.1097/QCO.0000000000000554

4. Chuquisana O, Strippel C, Gross CC, Melzer N, Kühn J, Kovac S, et al. Antibody response to herpes simplex virus-1 is increased in autoimmune encephalitis. *Eur J Immunol* (2022) 52:1198–200. doi: 10.1002/eji.202249854

5. Vogrig A, Muñiz-Castrillo S, Desestret V, Joubert B, Honnorat J. Pathophysiology of paraneoplastic and autoimmune encephalitis: genes, infections, and checkpoint inhibitors. *Ther Adv Neurol Disord* (2020) 13:1756286420932797. doi: 10.1177/1756286420932797

6. Arneth B. Trained innate immunity. *Immunol Res* (2021) 69:1–7. doi: 10.1007/s12026-021-09170-y

7. Netea MG, Joosten LAB, Latz E, Mills KHG, Natoli G, Stunnenberg HG, et al. Trained immunity: A program of innate immune memory in health and disease. *Sci (New York N.Y.)* (2016) 352:aaf1098. doi: 10.1126/science.aaf1098

8. Kurtz J. Specific memory within innate immune systems. *Trends Immunol* (2005) 26:186–92. doi: 10.1016/j.it.2005.02.001

9. Quintin J, Cheng S-C, van der Meer JWM, Netea MG. Innate immune memory: towards a better understanding of host defense mechanisms. *Curr Opin Immunol* (2014) 29:1–7. doi: 10.1016/j.coi.2014.02.006

10. Li M, Zhou Y, Feng G, Su SB. The critical role of toll-like receptor signaling pathways in the induction and progression of autoimmune diseases. *Curr Mol Med* (2009) 9:365–74. doi: 10.2174/156652409787847137

11. Grünewald K, Desai P, Winkler DC, Heymann JB, Belnap DM, Baumeister W, et al. Three-dimensional structure of herpes simplex virus from cryo-electron tomography. *Sci (New York N.Y.)* (2003) 302:1396–8.

12. Madavaraju K, Koganti R, Volety I, Yadavalli T, Shukla D. Herpes simplex virus cell entry mechanisms: An update. *Front Cell Infect Microbiol* (2020) 10:617578. doi: 10.3389/fcimb.2020.617578

13. Spear PG. Herpes simplex virus: receptors and ligands for cell entry. *Cell Microbiol* (2004) 6:401–10. doi: 10.1111/j.1462-5822.2004.00389.x

14. Radtke K, Kieneke D, Wolfstein A, Michael K, Steffen W, Scholz T, et al. Plus- and minus-end directed microtubule motors bind simultaneously to herpes simplex virus capsids using different inner tegument structures. *PloS Pathog* (2010) 6:e1000991. doi: 10.1371/journal.ppat.1000991

15. Sodeik B, Ebersold MW, Helenius A. Microtubule-mediated transport of incoming herpes simplex virus 1 capsids to the nucleus. *J Cell Biol* (1997) 136:1007–21. doi: 10.1083/jcb.136.5.1007

16. Richards AL, Sollars PJ, Pitts JD, Stults AM, Heldwein EE, Pickard GE, et al. The pUL37 tegument protein guides alpha-herpesvirus retrograde axonal transport to promote neuroinvasion. *PloS Pathog* (2017) 13:e1006741. doi: 10.1371/journal.ppat.1006741

17. Zhu S, Viejo-Borbolla A. Pathogenesis and virulence of herpes simplex virus. *Virulence* (2021) 12:2670–702. doi: 10.1080/21505594.2021.1982373

18. Wysocka J, Herr W. The herpes simplex virus VP16-induced complex: the makings of a regulatory switch. *Trends Biochem Sci* (2003) 28:294–304. doi: 10.1016/S0968-0004(03)00088-4

19. Hancock MH, Corcoran JA, Smiley JR. Herpes simplex virus regulatory proteins VP16 and ICP0 counteract an innate intranuclear barrier to viral gene expression. *Virology* (2006) 352:237–52. doi: 10.1016/j.virol.2006.04.021

20. Jones C. Herpes simplex virus type 1 and bovine herpesvirus 1 latency. *Clin Microbiol Rev* (2003) 16:79–95. doi: 10.1128/CMR.16.1.79-95.2003

21. Pires de Mello CP, Bloom DC, Paixão IC. Herpes simplex virus type-1: replication, latency, reactivation and its antiviral targets. *Antivir Ther* (2016) 21:277–86. doi: 10.3851/IMP3018

22. Antinone SE, Smith GA. Retrograde axon transport of herpes simplex virus and pseudorabies virus: a live-cell comparative analysis. *J Virol* (2010) 84:1504–12. doi: 10.1128/JVI.02029-09

23. Warren KG, Brown SM, Wroblewska Z, Gilden D, Koprowski H, Subak-Sharpe J. Isolation of latent herpes simplex virus from the superior cervical and vagus ganglions of human beings. *N Engl J Med* (1978) 298:1068–9. doi: 10.1056/NEJM197805112981907

24. Nicoll MP, Hann W, Shivkumar M, Harman LER, Connor V, Coleman HM, et al. The HSV-1 latency-associated transcript functions to repress latent phase lytic gene expression and suppress virus reactivation from latently infected neurons. *PloS Pathog* (2016) 12:e1005539. doi: 10.1371/journal.ppat.1005539

25. Marcocci ME, Napoletani G, Protto V, Kolesova O, Piacentini R, Li Puma DD, et al. Herpes simplex virus-1 in the brain: The dark side of a sneaky infection. *Trends Microbiol* (2020) 28:808–20. doi: 10.1016/j.tim.2020.03.003

26. Whitley RJ, Roizman B. Herpes simplex virus infections. *Lancet* (2001) 357:1513–8. doi: 10.1016/S0140-6736(00)04638-9

27. Obermeier B, Daneman R, Ransohoff RM. Development, maintenance and disruption of the blood-brain barrier. *Nat Med* (2013) 19:1584–96. doi: 10.1038/nm.3407

28. Feige L, Zaeck LM, Sehl-Ewert J, Finke S, Bourhy H. Innate immune signaling and role of glial cells in herpes simplex virus- and rabies virus-induced encephalitis. *Viruses 13* (2021). doi: 10.3390/v13122364

29. Reinert LS, Lopušná K, Winther H, Sun C, Thomsen MK, Nandakumar R, et al. Sensing of HSV-1 by the cGAS-STING pathway in microglia orchestrates antiviral defence in the CNS. *Nat Commun* (2016) 7:13348. doi: 10.1038/ncomms13348

30. Sun L, Wu J, Du F, Chen X, Chen ZJ. Cyclic GMP-AMP synthase is a cytosolic DNA sensor that activates the type i interferon pathway. *Sci (New York N.Y.)* (2013) 339:786–91.

31. Zhang C, Shang G, Gui X, Zhang X, Bai X-C, Chen ZJ. Structural basis of STING binding with and phosphorylation by TBK1. *Nature* (2019) 567:394–8. doi: 10.1038/s41586-019-1000-2

32. Zhang X, Shi H, Wu J, Zhang X, Sun L, Chen C, et al. Cyclic GMP-AMP containing mixed phosphodiester linkages is an endogenous high-affinity ligand for STING. *Mol Cell* (2013) 51:226–35. doi: 10.1016/j.molcel.2013.05.022

33. Ishikawa H, Barber GN. The STING pathway and regulation of innate immune signaling in response to DNA pathogens. *Cell Mol Life Sci* (2011) 68:1157–65. doi: 10.1007/s00018-010-0605-2

34. Ge R, Zhou Y, Peng R, Wang R, Li M, Zhang Y, et al. Conservation of the STING-mediated cytosolic DNA sensing pathway in zebrafish. *J Virol* (2015) 89:7696–706. doi: 10.1128/JVI.01049-15

35. Takaoka A, Wang Z, Choi MK, Yanai H, Negishi H, Ban T, et al. DAI (DLM-1/ZBP1) is a cytosolic DNA sensor and an activator of innate immune response. *Nature* (2007) 448:501–5. doi: 10.1038/nature06013

36. Pham TH, Kwon KM, Kim Y-E, Kim KK, Ahn J-H. DNA sensing-independent inhibition of herpes simplex virus 1 replication by DAI/ZBP1. *J Virol* (2013) 87:3076–86. doi: 10.1128/JVI.02860-12

37. Rebsamen M, Heinz LX, Meylan E, Michallet M-C, Schroder K, Hofmann K, et al. DAI/ZBP1 recruits RIP1 and RIP3 through RIP homotypic interaction motifs to activate NF-kappaB. *EMBO Rep* (2009) 10:916–22. doi: 10.1038/embor.2009.109

38. Unterholzner L, Keating SE, Baran M, Horan KA, Jensen SB, Sharma S, et al. IFI16 is an innate immune sensor for intracellular DNA. *Nat Immunol 11* (2010). doi: 10.1038/ni.1932

39. Li T, Diner BA, Chen J, Cristea IM. Acetylation modulates cellular distribution and DNA sensing ability of interferon-inducible protein IFI16. *Proc Natl Acad Sci U S A* (2012) 109:10558–63. doi: 10.1073/pnas.1203447109

40. Ansari MA, Dutta S, Veettil MV, Dutta D, Iqbal J, Kumar B, et al. Herpesvirus genome recognition induced acetylation of nuclear IFI16 is essential for its cytoplasmic translocation, inflammasome and IFN-β responses. *PloS Pathog* (2015) 11:e1005019. doi: 10.1371/journal.ppat.1005019

41. Takeuchi O, Akira S. Pattern recognition receptors and inflammation. *Cell* (2010) 140:805–20. doi: 10.1016/j.cell.2010.01.022

42. Ma Y, He B. Recognition of herpes simplex viruses: toll-like receptors and beyond. *J Mol Biol* (2014) 426:1133–47. doi: 10.1016/j.jmb.2013.11.012

43. Liu Y, Goulet M-L, Sze A, Hadj SB, Belgnaoui SM, Lababidi RR, et al. RIG-I-Mediated STING upregulation restricts herpes simplex virus 1 infection. *J Virol* (2016) 90:9406–19. doi: 10.1128/JVI.00748-16

44. Cheng G, Zhong J, Chung J, Chisari FV, Double-stranded DNA. And double-stranded RNA induce a common antiviral signaling pathway in human cells. *Proc Natl Acad Sci U S A* (2007) 104:9035–40. doi: 10.1073/pnas.0703285104

45. Crill EK, Furr-Rogers SR, Marriott I. RIG-i is required for VSV-induced cytokine production by murine glia and acts in combination with DAI to initiate responses to HSV-1. *Glia* (2015) 63:2168–80. doi: 10.1002/glia.22883

46. Zhang S-Y, Jouanguy E, Ugolini S, Smahi A, Elain G, Romero P, et al. TLR3 deficiency in patients with herpes simplex encephalitis. *Sci (New York N.Y.)* (2007) 317:1522–7.

47. Mielcarska MB, Bossowska-Nowicka M, Toka FN. Functional failure of TLR3 and its signaling components contribute to herpes simplex encephalitis. *J Neuroimmunol* (2018) 316:65–73. doi: 10.1016/j.jneuroim.2017.12.011

48. Chen Y, Lin J, Zhao Y, Ma X, Yi H. Toll-like receptor 3 (TLR3) regulation mechanisms and roles in antiviral innate immune responses. *J Zhejiang Univ Sci B* (2021) 22:609–32. doi: 10.1631/jzus.B2000808

49. Oshiumi H, Matsumoto M, Funami K, Akazawa T, Seya T. TICAM-1, an adaptor molecule that participates in toll-like receptor 3-mediated interferon-beta induction. *Nat Immunol* (2003) 4:161–7. doi: 10.1038/ni886

50. Fitzgerald KA, McWhirter SM, Faia KL, Rowe DC, Latz E, Golenbock DT, et al. IKKepsilon and TBK1 are essential components of the IRF3 signaling pathway. *Nat Immunol* (2003) 4:491–6. doi: 10.1038/ni921

51. Sato M, Suemori H, Hata N, Asagiri M, Ogasawara K, Nakao K, et al. Distinct and essential roles of transcription factors IRF-3 and IRF-7 in response to viruses for IFN-alpha/beta gene induction. *Immunity* (2000) 13:539–48. doi: 10.1016/S1074-7613(00)00053-4

52. Sharma S, tenOever BR, Grandvaux N, Zhou G-P, Lin R, Hiscott J. Triggering the interferon antiviral response through an IKK-related pathway. *Sci (New York N.Y.)* (2003) 300:1148–51.

53. Paludan SR, Bowie AG, Horan KA, Fitzgerald KA. Recognition of herpesviruses by the innate immune system. *Nat Rev Immunol* (2011) 11:143–54. doi: 10.1038/nri2937

54. Hochrein H, Schlatter B, O'Keeffe M, Wagner C, Schmitz F, Schiemann M, et al. Herpes simplex virus type-1 induces IFN-alpha production *via* toll-like receptor 9-dependent and -independent pathways. *Proc Natl Acad Sci U S A* (2004) 101:11416–21. doi: 10.1073/pnas.0403555101

55. He Z, Ye S, Xing Y, Jiu Y, Zhong J. UNC93B1 curbs cytosolic DNA signaling by promoting STING degradation. *Eur J Immunol* (2021) 51:1672–85. doi: 10.1002/eji.202048901

56. Kim Y-M, Brinkmann MM, Paquet M-E, Ploegh HL. UNC93B1 delivers nucleotide-sensing toll-like receptors to endolysosomes. *Nature* (2008) 452:234–8. doi: 10.1038/nature06726

57. Zhu H, Zhang R, Yi L, Tang Y-D, Zheng C. UNC93B1 attenuates the cGAS-STING signaling pathway by targeting STING for autophagy-lysosome degradation. *J Med Virol* (2022) 94:4490–501. doi: 10.1002/jmv.27860

58. Zhu H, Zheng C. The race between host antiviral innate immunity and the immune evasion strategies of herpes simplex virus 1. *Microbiol Mol Biol Rev* (2020) 84. doi: 10.1128/MMBR.00099-20

59. Huang J, You H, Su C, Li Y, Chen S, Zheng C. Herpes simplex virus 1 tegument protein VP22 abrogates cGAS/STING-mediated antiviral innate immunity. *J Virol* (2018) 92. doi: 10.1128/JVI.00841-18

60. Zhang D, Su C, Zheng C. Herpes simplex virus 1 serine protease VP24 blocks the DNA-sensing signal pathway by abrogating activation of interferon regulatory factor 3. *J Virol* (2016) 90:5824–9. doi: 10.1128/JVI.00186-16

61. Xu X, Che Y, Li Q. HSV-1 tegument protein and the development of its genome editing technology. *Virol J* (2016) 13:108. doi: 10.1186/s12985-016-0563-x

62. Ye R, Su C, Xu H, Zheng C. Herpes simplex virus 1 ubiquitin-specific protease UL36 abrogates NF-κB activation in DNA sensing signal pathway. *J Virol* (2017) 91.

63. Zheng C. Evasion of cytosolic DNA-stimulated innate immune responses by herpes simplex virus 1. *J Virol* (2018) 92. doi: 10.1128/JVI.00099-17

64. Xu H, Su C, Pearson A, Mody CH, Zheng C. Herpes simplex virus 1 UL24 abrogates the DNA sensing signal pathway by inhibiting NF-κB activation. *J Virol* (2017) 91.

65. Zhang J, Zhao J, Xu S, Li J, He S, Zeng Y, et al. Species-specific deamidation of cGAS by herpes simplex virus UL37 protein facilitates viral replication. *Cell Host Microbe* (2018) 24. doi: 10.1016/j.chom.2018.07.004

66. Su C, Zheng C. Herpes simplex virus 1 abrogates the cGAS/STING-mediated cytosolic DNA-sensing pathway *via* its virion host shutoff protein, UL41. *J Virol* (2017) 91. doi: 10.1128/JVI.02414-16

67. Manivanh R, Mehrbach J, Charron AJ, Grassetti A, Cerón S, Taylor SA, et al. Herpes simplex virus 1 ICP34.5 alters mitochondrial dynamics in neurons. *J Virol* (2020) 94.

68. Pan S, Liu X, Ma Y, Cao Y, He B. Herpes simplex virus 1 γ34.5 protein inhibits STING activation that restricts viral replication. *J Virol* (2018) 92.

69. Johnson KE, Chikoti L, Chandran B. Herpes simplex virus 1 infection induces activation and subsequent inhibition of the IFI16 and NLRP3 inflammasomes. *J Virol* (2013) 87:5005–18. doi: 10.1128/JVI.00082-13

70. Orzalli MH, DeLuca NA, Knipe DM. Nuclear IFI16 induction of IRF-3 signaling during herpesviral infection and degradation of IFI16 by the viral ICP0 protein. *Proc Natl Acad Sci U S A* (2012) 109:E3008–17. doi: 10.1073/pnas.1211302109

71. You H, Lin Y, Lin F, Yang M, Li J, Zhang R, et al. β-catenin is required for the cGAS/STING signaling pathway but antagonized by the herpes simplex virus 1 US3 protein. *J Virol* (2020) 94. doi: 10.1128/JVI.01847-19

72. Dubey D, Pittock SJ, Kelly CR, McKeon A, Lopez-Chiriboga AS, Lennon VA, et al. Autoimmune encephalitis epidemiology and a comparison to infectious encephalitis. *Ann Neurol* (2018) 83:166–77. doi: 10.1002/ana.25131

73. Gelfand JM. Autoimmune encephalitis after herpes simplex encephalitis: insights into pathogenesis. *Lancet Neurol* (2018) 17:733–5. doi: 10.1016/S1474-4422(18)30279-5

74. Nosadini M, Mohammad SS, Corazza F, Ruga EM, Kothur K, Perilongo G, et al. Herpes simplex virus-induced anti-n-methyl-d-aspartate receptor encephalitis: a systematic literature review with analysis of 43 cases. *Dev Med Child Neurol* (2017) 59:796–805. doi: 10.1111/dmcn.13448

75. Hara M, Nakajima H. [Autoimmune encephalitis triggered by herpes simplex encephalitis: Main syndrome, diagnosis, and treatment]. *Brain Nerve* (2022) 74:1163–70.

76. Alexopoulos H, Akrivou S, Mastroyanni S, Antonopoulou M, Dinopoulos A, Giorgi M, et al. Postherpes simplex encephalitis: a case series of viral-triggered autoimmunity, synaptic autoantibodies and response to therapy. *Ther Adv Neurol Disord* (2018) 11:1756286418768778. doi: 10.1177/1756286418768778

77. Spatola M, Petit-Pedrol M, Simabukuro MM, Armangue T, Castro FJ, Barcelo Artigues MI, et al. Investigations in GABA receptor antibody-associated encephalitis. *Neurology* (2017) 88:1012–20. doi: 10.1212/WNL.0000000000003713

78. Berek K, Beer R, Grams A, Helbok R, Lindner A, Pfausler B, et al. Caspr2 antibodies in herpes simplex encephalitis: an extension of the spectrum of virus induced autoimmunity? - a case report. *BMC Neurol* (2022) 22:131. doi: 10.1186/s12883-022-02637-x

79. Armangue T, Moris G, Cantarín-Extremera V, Conde CE, Rostasy K, Erro ME, et al. Autoimmune post-herpes simplex encephalitis of adults and teenagers. *Neurology* (2015) 85:1736–43. doi: 10.1212/WNL.0000000000002125

80. Armangue T, Spatola M, Vlagea A, Mattozzi S, Cárceles-Cordon M, Martinez-Heras E, et al. Frequency, symptoms, risk factors, and outcomes of autoimmune encephalitis after herpes simplex encephalitis: a prospective observational study and retrospective analysis. *Lancet Neurol* (2018) 17:760–72. doi: 10.1016/S1474-4422(18)30244-8

81. Linnoila J, Pulli B, Armangué T, Planagumà J, Narsimhan R, Schob S, et al. Mouse model of anti-NMDA receptor post-herpes simplex encephalitis. *Neurol Neuroimmunol Neuroinflamm* (2019) 6:e529. doi: 10.1212/NXI.0000000000000529

82. Salovin A, Glanzman J, Roslin K, Armangue T, Lynch DR, Panzer JA. Anti-NMDA receptor encephalitis and nonencephalitic HSV-1 infection. *Neurol Neuroimmunol Neuroinflamm* (2018) 5:e458. doi: 10.1212/NXI.0000000000000458

83. Moran AP, Prendergast MM. Molecular mimicry in campylobacter jejuni and helicobacter pylori lipopolysaccharides: contribution of gastrointestinal infections to autoimmunity. *J Autoimmun* (2001) 16:241–56. doi: 10.1006/jaut.2000.0490

84. Zhao ZS, Granucci F, Yeh L, Schaffer PA, Cantor H. Molecular mimicry by herpes simplex virus-type 1: autoimmune disease after viral infection. *Sci (New York N.Y.)* (1998) 279:1344–7.

85. Höftberger R, Armangue T, Leypoldt F, Graus F, Dalmau J. Clinical neuropathology practice guide 4-2013: post-herpes simplex encephalitis: N-methyl-Daspartate receptor antibodies are part of the problem. *Clin Neuropathol* (2013) 32:251–4. doi: 10.5414/NP300666

86. De Tiège X, De Laet C, Mazoin N, Christophe C, Mewasingh LD, Wetzburger C, et al. Postinfectious immune-mediated encephalitis after pediatric herpes simplex encephalitis. *Brain Dev* (2005) 27:304–7. doi: 10.1016/j.braindev.2004.07.007

87. Galli J, Clardy SL, Piquet AL. NMDAR encephalitis following herpes simplex virus encephalitis. *Curr Infect Dis Rep* (2017) 19:1. doi: 10.1007/s11908-017-0556-y

88. Titulaer MJ, McCracken L, Gabilondo I, Armangué T, Glaser C, Iizuka T, et al. Treatment and prognostic factors for long-term outcome in patients with anti-NMDA receptor encephalitis: an observational cohort study. *Lancet Neurol* (2013) 12:157–65. doi: 10.1016/S1474-4422(12)70310-1

89. Al-Obaidi MMJ, Bahadoran A, Wang SM, Manikam R, Raju CS, Sekaran SD. Disruption of the blood brain barrier is vital property of neurotropic viral infection of the central nervous system. *Acta Virol* (2018) 62:16–27. doi: 10.4149/av_2018_102

90. Morris NA, Kaplan TB, Linnoila J, Cho T. HSV encephalitis-induced anti-NMDAR encephalitis in a 67-year-old woman: report of a case and review of the literature. *J Neurovirol* (2016) 22:33–7. doi: 10.1007/s13365-015-0364-9

91. Omae T, Saito Y, Tsuchie H, Ohno K, Maegaki Y, Sakuma H. Cytokine/chemokine elevation during the transition phase from HSV encephalitis to autoimmune anti-NMDA receptor encephalitis. *Brain Dev* (2018) 40:361–5.

92. Wesselingh R, Butzkueven H, Buzzard K, Tarlinton D, O'Brien TJ, Monif M. Innate immunity in the central nervous system: A missing piece of the autoimmune encephalitis puzzle? *Front Immunol* (2019) 10:2066.

93. Kothur K, Gill D, Wong M, Mohammad SS, Bandodkar S, Arbunckle S, et al. Cerebrospinal fluid cyto-/chemokine profile during acute herpes simplex virus induced anti-n-methyl-d-aspartate receptor encephalitis and in chronic neurological sequelae. *Dev Med Child Neurol* (2017) 59:806–14.

94. Gnann JW, Whitley RJ. Herpes simplex encephalitis: an update. *Curr Infect Dis Rep* (2017) 19:13.

95. Whitley RJ, Alford CA, Hirsch MS, Schooley RT, Luby JP, Aoki FY, et al. Vidarabine versus acyclovir therapy in herpes simplex encephalitis. *New Engl J Med* (1986) 314:144–9.

96. Sköldenberg B, Forsgren M, Alestig K, Bergström T, Burman L, Dahlqvist E, et al. Acyclovir versus vidarabine in herpes simplex encephalitis. randomised multicentre study in consecutive swedish patients. *Lancet* (1984) 2:707–11. doi: 10.1016/S0140-6736(84)92623-0

97. Tunkel AR, Glaser CA, Bloch KC, Sejvar JJ, Marra CM, Roos KL, et al. The management of encephalitis: clinical practice guidelines by the infectious diseases society of america. *Clin Infect Dis* (2008) 47:303–27. doi: 10.1086/589747

98. Solomon T, Michael BD, Smith PE, Sanderson F, Davies NWS, Hart IJ, et al. Management of suspected viral encephalitis in adults–association of british neurologists and british infection association national guidelines. *J Infect* (2012) 64:347–73. doi: 10.1016/j.jinf.2011.11.014

99. Meyding-Lamadé UK, Oberlinner C, Rau PR, Seyfer S, Heiland S, Sellner J, et al. Experimental herpes simplex virus encephalitis: a combination therapy of acyclovir and

glucocorticoids reduces long-term magnetic resonance imaging abnormalities. *J Neurovirol* (2003) 9:118–25. doi: 10.1080/13550280390173373

100. Thompson KA, Blessing WW, Wesselingh SL. Herpes simplex replication and dissemination is not increased by corticosteroid treatment in a rat model of focal herpes encephalitis. *J Neurovirol* (2000) 6:25–32. doi: 10.3109/13550280009006379

101. Kamei S, Sekizawa T, Shiota H, Mizutani T, Itoyama Y, Takasu T, et al. Evaluation of combination therapy using aciclovir and corticosteroid in adult patients with herpes simplex virus encephalitis. *J Neurol Neurosurg Psychiatry* (2005) 76:1544–9. doi: 10.1136/jnnp.2004.049676

102. Bradshaw MJ, Venkatesan A. Herpes simplex virus-1 encephalitis in adults: Pathophysiology, diagnosis, and management. *Neurotherapeutics* (2016) 13:493–508. doi: 10.1007/s13311-016-0433-7

103. Sergerie Y, Boivin G, Gosselin D, Rivest S. Delayed but not early glucocorticoid treatment protects the host during experimental herpes simplex virus encephalitis in mice. *J Infect Dis* (2007) 195:817–25. doi: 10.1086/511987

104. Esposito S, Autore G, Argentiero A, Ramundo G, Principi N. Autoimmune encephalitis after herpes simplex encephalitis: A still undefined condition. *Autoimmun Rev* (2022) 21:103187. doi: 10.1016/j.autrev.2022.103187

105. Abboud H, Probasco JC, Irani S, Ances B, Benavides DR, Bradshaw M, et al. Autoimmune encephalitis: proposed best practice recommendations for diagnosis and acute management. *J Neurol Neurosurg Psychiatry* (2021) 92:757–68. doi: 10.1136/jnnp-2020-325300

106. Dorcet G, Benaiteau M, Bost C, Mengelle C, Bonneville F, Martin-Blondel G, et al. Two cases of late-onset anti-NMDAr auto-immune encephalitis after herpes simplex virus 1 encephalitis. *Front Neurol* (2020) 11:38. doi: 10.3389/fneur.2020.00038

107. Armangue T, Titulaer MJ, Málaga I, Bataller L, Gabilondo I, Graus F, et al. Pediatric anti-N-methyl-D-aspartate receptor encephalitis-clinical analysis and novel findings in a series of 20 patients. *J Pediatr 162* (2013). doi: 10.1016/j.jpeds.2012.10.011

108. Schein F, Gagneux-Brunon A, Antoine J-C, Lavernhe S, Pillet S, Paul S, et al. Anti-N-methyl-D-aspartate receptor encephalitis after herpes simplex virus-associated encephalitis: an emerging disease with diagnosis and therapeutic challenges. *Infection* (2017) 45:545–9. doi: 10.1007/s15010-016-0959-y

109. Prüss H. Postviral autoimmune encephalitis: manifestations in children and adults. *Curr Opin Neurol* (2017) 30:327–33. doi: 10.1097/WCO.0000000000000445

frontiers | Frontiers in Immunology

TYPE Original Research
PUBLISHED 03 February 2023
DOI 10.3389/fimmu.2023.1135625

OPEN ACCESS

EDITED BY
Junji Xing,
Houston Methodist Research Institute,
United States

REVIEWED BY
Jules Hoffmann,
Université de Strasbourg, France
Xiaochuan Liu,
University of California, Riverside,
United States

*CORRESPONDENCE
Jiyong Liu
mangriver@hotmail.com
Renjie Jiao
rjiao@gzhmu.edu.cn
Jianming Chen
chenjm@mju.edu.cn

†These authors have contributed equally to this work and share first authorship

SPECIALTY SECTION
This article was submitted to Viral Immunology, a section of the journal Frontiers in Immunology

RECEIVED 01 January 2023
ACCEPTED 23 January 2023
PUBLISHED 03 February 2023

CITATION
Huang Z, Wang W, Xu P, Gong S, Hu Y, Liu Y, Su F, Anjum KM, Deng W-M, Yang S, Liu J, Jiao R and Chen J (2023) *Drosophila Ectoderm-expressed 4* modulates JAK/STAT pathway and protects flies against *Drosophila* C virus infection. *Front. Immunol.* 14:1135625. doi: 10.3389/fimmu.2023.1135625

Drosophila Ectoderm-expressed 4 modulates JAK/STAT pathway and protects flies against *Drosophila* C virus infection

Zongliang Huang[1,2†], Wei Wang[1,3†], Pengpeng Xu[2†], Shangyu Gong[2], Yingshan Hu[2], Yan Liu[2], Fang Su[2], Khalid Mahmood Anjum[4], Wu-Min Deng[5], Suping Yang[3], Jiyong Liu[2*], Renjie Jiao[2*] and Jianming Chen[1,2*]

[1]Fujian Key Laboratory on Conservation and Sustainable Utilization of Marine Biodiversity, Fuzhou Institute of Oceanography, Minjiang University, Fuzhou, Fujian, China, [2]Sino-French Hoffmann Institute, School of Basic Sciences, Guangzhou Medical University, Guangzhou, Guangdong, China, [3]Department of Bioengineering and Biotechnology, College of Chemical Engineering, Huaqiao University, Xiamen, Fujian, China, [4]Department of Wildlife and Ecology, University of Veterinary and Animal Sciences, Lahore, Punjab, Pakistan, [5]Department of Biological Science, Florida State University, Tallahassee, FL, United States

Sterile alpha and HEAT/Armadillo motif-containing protein (SARM) is conserved in evolution and negatively regulates TRIF-dependent Toll signaling in mammals. The SARM protein from *Litopenaeus vannamei* and its *Drosophila* orthologue Ectoderm-expressed (Ect4) are also involved in immune defense against pathogen infection. However, the functional mechanism of the protective effect remains unclear. In this study, we show that Ect4 is essential for the viral load in flies after a *Drosophila* C virus (DCV) infection. Viral load is increased in *Ect4* mutants resulting in higher mortality rates than wild-type. Overexpression of *Ect4* leads to a suppression of virus replication and thus improves the survival rate of the animals. Ect4 is required for the viral induction of STAT-responsive genes, *TotA* and *TotM*. Furthermore, Ect4 interacts with Stat92E, affecting the tyrosine phosphorylation and nuclear translocation of Stat92E in S2 cells. Altogether, our study identifies the adaptor protein Ect4 of the Toll pathway contributes to resistance to viral infection and regulates JAK/STAT signaling pathway.

KEYWORDS

Ect4, Drosophila C virus, tyrosine phosphorylation, JAK/STAT pathway, innate immunity

1 Introduction

Viral infections seriously threaten human health and majorly cause mortality worldwide. The fruit fly *Drosophila melanogaster* has been proven to be a powerful model for deciphering antiviral immune responses (1). To defend against viruses, *Drosophila* relies on antiviral immunity, including RNA interference (RNAi) and inducible responses (2). Studies have shown RNAi to play a major role in defense against viruses in *Drosophila*. After detecting

viral RNAs, Dicer-2 processes them into small interfering RNAs (siRNAs), which are loaded onto the RISC (RNA-induced silencing complex) complex that contains Argonaute-2 (AGO2) to target the complementary viral sequences for silencing (3). Two cellular processes, autophagy and phagocytosis are involved in antiviral defense. Autophagy plays a relatively minor role in antiviral defenses, whereas phagocytosis only contributes to virus-specific immune responses (4). Genetic studies suggest an involvement of the evolutionarily conserved innate immune pathways in controlling viral infections. The cytosolic DNA sensor cyclic GMP-AMP (cGAMP) synthase (CGAS) catalyzes 2' 3'-cGAMP and activates Sting-dependent antiviral responses in mammals. Recently a class of cGAS-like receptors (cGLRs) was identified in *Drosophila* playing key roles in defense against viral infections (5, 6). Inactivation of the Toll pathway results in increased susceptibility to *Drosophila* X virus (DXV) infection, and the Imd pathway is required for an effective antiviral immune response against Cricket Paralysis Virus (CrPV) (7, 8). Another pathway contributing to *Drosophila* antiviral immunity involves Janus Kinase/Signal Transducer and Activator of Transcription (JAK/STAT) signaling (9). Deficiency in JAK/STAT pathway leads to increased DCV viral loads and higher mortality. In contrast to the Toll and Imd pathways, the JAK/STAT pathway is often activated by different types of stresses, such as mechanical pressure, heat shock, septic wounds, UV irradiation, and damage-associated molecular patterns (DAMPs) released from dead cells, instead of sensing microorganisms (10).

The evolutionarily conserved JAK/STAT pathway plays roles in various biological processes, including hematopoiesis, stress responses, and innate immunity (11–13). Dysregulation of the JAK/STAT pathway has been associated with several human diseases, such as autoimmune disease, allergy, and cancer (14–16). In *Drosophila*, JAK/STAT signaling is initiated by three cytokines of the Unpaired (Upd) family (Upd1, Upd2, and Upd3). The binding of Upd induces Domeless (Dome) dimerization and activation of the receptor-associated JAK molecules (termed Hopscotch). Activated Hopscotch then phosphorylates Dome, creating a docking site for the single *Drosophila* STAT family transcription factor, Stat92E. Phosphorylated Stat92E migrates into the nucleus in dimers, promoting target genes transcription (17). Infection with DCV has been shown to trigger the expression of JAK/STAT-dependent genes, including *virus-induced RNA 1* (*vir-1*) and stress response genes *Turandot A* and *M* (*TotA* and *TotM*) (18). Although the function of these JAK/STAT-dependent genes in *Drosophila* remains unknown, JAK/STAT signaling has been proposed to be involved in host resistance and tolerance to viral or parasitoid challenges (10, 19).

The Ectoderm-expressed 4 (Ect4) protein is evolutionarily conserved from arthropods to mammals (20). The mammalian Ect4 orthologue, Sterile-alpha and Armadillo motif-containing protein (SARM) has been identified as a negative regulator of TLR-mediated NF-κB activation and to mediate axonal death (21, 22). In *Drosophila* and Pacific white shrimp (*Litopenaeus vannamei*), the production of antimicrobial peptides (AMPs) was downregulated by Ect4 and LvSarm (23, 24), suggesting the involvement of Ect4 homologs in Toll pathway suppression is conserved in crustaceans and mammals. Interestingly, in invertebrate species including *C. elegans*, *Drosophila*, and *L. vannamei*, Ect4 homologs were demonstrated to play a positive role in host defense against pathogen infections (24–26). The positive and negative contributions to innate immunity suggested that the invertebrate Ect4 homologs are also involved in immune defense independent of the Toll pathway. This study investigated the role of Ect4 in antiviral defense against DCV infection. As a result, *Ect4* mutant flies exhibit increased susceptibility to infection by DCV, whereas overexpression of *Ect4* confers resistance against DCV infection; *Ect4* regulates the expression of JAK/STAT pathway target genes *TotA* and *TotM*; Ect4 interacts with Stat92E to alter the tyrosine phosphorylation status of Stat92E.

2 Materials and methods

2.1 Fly strains and mutant generation

w^{1118} flies were used as wild-type control. The w^{IR}; $dcr\text{-}2^{L811fsX}$ mutant flies have been previously described (27). *ubi-Gal4,tub-Gal80^{ts}* was a gift from Dr. D. Ferrandon. $hop^{Tum\text{-}l}$, *ppl-Gal4*, *da-Gal4*, *hs-Gal4* were obtained from Bloomington Stock center. The generation of transgenic *UAS-Ect4* and *U6:3-gRNA-Ect4* lines was performed as previously described (28). *Ect4-IR* was obtained from NIG-FLY stocks (HMJ30091). For the generation of Ect4 mutant lines, transgenic *U6:3-gRNA-Ect4* flies were crossed with the *nos-Cas9* flies to get male F_0 (*nos-Cas9*/+; *U6:3-gRNA-Ect4*/+) that were crossed with w^{1118}; *TM3*, *Sb/TM6B*, *Tb* to obtain F_1 progenies. Singular F_1 flies were crossed with w^{1118}; *TM3*, *Sb/TM6B*, *Tb*. PCR products amplified from F_1 flies before being cloned into the *pMD19-T* vector according to the manufacturer's instructions (TAKARA) for mutation identification.

2.2 Plasmid construction

pAC5.1-Ect4-Flag was made by cloning Ect4 cDNA into *pAC5.1-Flag* vectors. For *pAC5.1-Ect4-GFP* constructs, the EGFP fragment was amplified from *pEGFP-C1* and assembled with the *Ect4* fragment into *pAC5.1-V5* vectors using ClonExpress MultiS One Step Cloning Kit (Vazyme). *Stat92E* cDNA was inserted in pAC5.1-HA to generate *pAC5.1-Stat92E-HA*. The hop (or *Dome*) cDNA was inserted in *pAC5.1-V5* to generate *pAC5.1-hop-V5* (or *pAC5.1-Dome-V5*). For the truncated *Ect4* constructs, ARM domain (aa 318-701), SAM domain (aa 680-826), and TIR domain (aa 829-1360) were amplified from *pAC5.1-Ect4-Flag* before assembled into *pAC5.1-Flag* empty vector, respectively.

2.3 Cell transfection, co-immuno-precipitation, and Western blot

S2 cells were cultured at 25°C in Sf-900^{TM} III SFM (Gibco). All S2 cell transfection experiments were carried out with the Effectene Transfection Reagent (QIAGEN). For a co-immunoprecipitation assay, S2 cells were transfected with different plasmids. After 48h, cells were collected and lysed in lysis buffer (150 mM NaCl, 25mM Tris-HCL, pH 7.4, 5% glycerol, 1% NP-40, 1mM EDTA, complete protease inhibitor cocktail tablets [Roche] and phosphatase inhibitor cocktail tablets [Roche]). Lysates were incubated overnight at 4°C with Anti-Flag M2 affinity gel (Sigma) or EZview Red Anti-HA

Affinity Gel (Sigma). After centrifugation, pellets were washed with 1ml lysis buffer three times before resuspension in 2X Laemmli SDS-PAGE buffer and detection by Western blot. Western blot was performed according to standard procedures.

Primary antibodies: Mouse anti-V5 (1:8000, Proteintech 66007-1-Ig); mouse anti-HA (1:8000, Milipore 05-904); mouse anti-α-Tubulin (1:20,000 Sigma T8203); goat anti-Stat (1:5000, Santa Cruz Biotechnology dN-17); mouse anti-FLAG (1:8000, Sigma F3165); rabbit anti-DCV (1:5000, Abcam ab92954); mouse anti-PY20 (1:2000, Abcam ab10321). Secondary antibodies: HRP-linked anti-mouse IgG (1:8000, Cell Signaling Technology 7076P2); HRP-linked anti-rabbit IgG (1:5000, Cell Signaling Technology 7074P2); HRP-linked anti-goat IgG (1:5000 Millipore AP106P); Alexa Fluor 555 goat anti-mouse IgG (1:500, life technologies A21422).

2.4 RNA analysis

According to the manufacturer's instructions, total RNA was extracted from infected flies using RNAiso Plus (TAKARA), and cDNA was synthesized with the HiScript II Q RT SuperMix (Vazyme). The ChamQ SYBR qPCR Master Mix (Vazyme) was used for quantitative. Expression of the gene of interest was normalized to the Rpl32 RNA level. The following primers were used for qPCR: *RpL32* (forward 5'-GACGCTTCAAGGGACAGTATCTG-3'; reverse 5'-AAACGCGGTTCTGCATGAG-3'), *vir-1* (forward 5'-GATCCCAATTTTCCCATCAA-3'; reverse 5'-GATTACAGCTGGGTGCACAA-3'), DCV (forward 5'-TCATCGGTATGCACATTGCT-3'; reverse 5'-CGCATAACCATGCTCTTCTG-3'), *TotA* (forward 5'-CCCTGAGGAACGGGAGAGTA-3'; reverse 5'-CTTTCCAACGATCCTCGCCT-3'), *TotM* (forward 5'-ACCGGAACATCGACAGCC-3'; reverse 5'-CCAGAATCCGCCTTGTGC-3'), *Ect4* (forward 5'-GCCTCCAGTATTACGGT-3'; reverse 5'-ATGTTTCTCCTGACTGATGA-3'), *Vago* (forward 5'-TGCAACTCTGGGAGGATAGC-3'; reverse 5'-AATTGCCCTGCGTCAGTTT-3').

2.5 Virus infection

Virus stocks were prepared as described previously (29). All fly lines confirmed the absence of Wolbachia by PCR and were cured whenever necessary. For infection, 3-6 d old flies were anesthetized with CO_2 and injected with PBS (Gibco) or virus suspension intra-thoracically using the Nanoject II injector (Drummond). Infected flies were monitored daily for survival rate or frozen for RNA analysis at the indicated time points.

2.6 Cell immunofluorescence and eye-pigmentation measurement

S2 cells were transfected with *pAC5.1-Ect4-GFP* and pAC5.1-Stat92E-HA plasmids, and approximately 1×10^6 cells were transferred to 24 well plates containing coverslips 48 h after transfection. Twelve h later, cells were washed in 0.5ml PBS and fixed with 4% formaldehyde in PBS for 15 min, then washed twice in 0.5 PBT (PBS containing 0.1% Tween-20) before blocking with 5% BSA in TBST for 1 h. Cells were then incubated with primary antibody (anti-HA 1:1000) overnight at 4°C before 2×5 min TBST washes. The secondary antibody was incubated for 4 h at room temperature. Nuclei were stained with PBS with 10 μg/ml DAPI for 5 min. Immunostaining samples were photographed with a Zeiss confocal microscope.

For eye pigment assay, the heads of 50 female flies (2-3 **d** old, raised at 25°C) of each indicated genotype were homogenized in methanol (1 **ml**, acidified with 0.1% HCl). After centrifugation, the supernatants were measured for absorbance at 480 nm.

2.7 RNAi knockdown in S2 cells and drug treatment

dsRNA targeting *Ect4* and *GFP* were synthesized according to standard protocol. S2 cells were treated with a culture medium containing 10 μg/ml dsRNA for 3 d. After dsRNA treatment, a solution containing 2 mM H_2O_2 and 1 mM sodium vanadate (final concentrations; Sigma) pre-incubated for 15 min was added to S2 cells to induce tyrosine phosphorylated Stat92E for 30 min. Cell lysates were prepared with the lysis buffer before immune precipitation with an anti-Stat92E antibody at 4°C and incubated with Pierce Protein A/G Plus Agarose (Thermo Scientific) beads. Co-immuno-precipitated proteins were detected with an anti-Stat92E antibody or anti-PY20 antibody.

2.8 Statistical analysis

Survival data were analyzed by the Kaplan-Meier method using GraphPad Prism. Quantification of immunoblots was performed with ImageJ 1.51p. Altered protein levels were presented as normalized fold change compared to the control value. Statistical analysis was performed using the Student's *t*-test. Grey value analysis was performed by the ZEN 2012 (blue edition) system. *P*-values below 0.05 were considered significantly different.

3 Results

3.1 Reduced resistance of Ect4 mutants to DCV infection

To investigate the role of *Ect4* in *Drosophila* antiviral defense, an *Ect4* mutant line was generated with the CRISPR/Cas9 system. The mutation, $Ect4^{17}$, covers a genomic deletion of 17 bp in the coding region of *Ect4* (Figure 1A). $Ect4^{17}$ homozygous mutants are lethal at the second instar larval stage as judged by examining the development of both homo- and heterozygous animals distinguished by a GFP marker (Figure S1A), and heterozygous mutants were used for further experiments.

Variation in the pastrel gene is associated with natural resistance to DCV infection in *D. melanogaster*. The non-synonymous single nucleotide polymorphism (SNP) position 598, located in the last exon, has the strongest effect on DCV susceptibility (30). Sequencing

10.3389/fimmu.2023.1135625

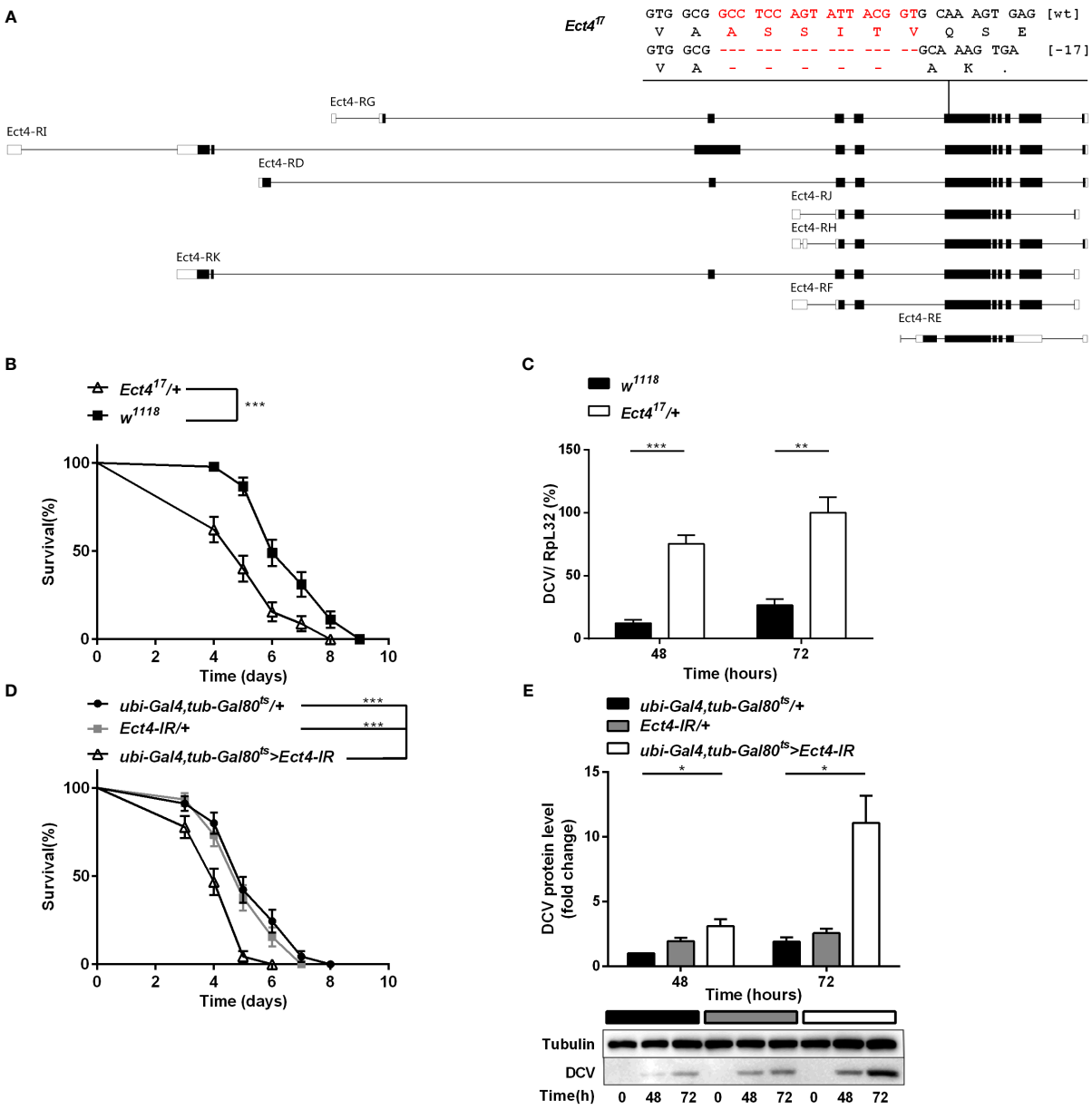

FIGURE 1
Depletion of *Ect4* in adult flies leads to a reduction in viral resistance upon DCV infection. **(A)** Schematic representation of deletions at exon of *Ect4* gene induced by CRISPR/Cas9. The deletion of 17 nucleotides (marked in red) caused a frameshift and created an early stop codons in the $Ect4^{17}$ mutant. Exons are represented by boxes, and introns by lines. UTRs are shown in white, and coding sequences are shown as black blocks. **(B)** Survival of *Ect4* mutants and wild-type flies was monitored daily at 25°C. **(C)** Quantitative RT-PCR analysis of the accumulation of viral RNA at 48 and 72 h post-infection in wild-type and *Ect4* mutant flies. **(D)** Survival of flies carrying the temperature-dependent *Ect4* knockdown system and genetic control flies upon DCV infection at 29°C. **(E)** Immunoblot of the accumulation of DCV capsid polyprotein in *Ect4*-RNAi or control flies, color blocks represented the genotype as indicated. Data represent the means ± standard errors of 3 independent pools of 15 male flies **(B, D)** or 10 male flies **(C, E)** for each genotype. Log-rank test **(B, D)** and *t*-test **(C, E)**: **P*< 0.05, ***P*< 0.01, ****P*< 0.001.

of the pastrel locus revealed that all the strains of *D. melanogaster* tested contained the susceptible allele (data not shown), thus limiting the effect of discordance in the SNP profile between different fly lines to the difference in DCV resistance.

Ect4 transcription in $Ect4^{17}$/+ heterozygotes was reduced by 45% compared with the wild-type flies (Figure S1B). Wild-type and Ect4 mutant files were challenged with DCV by intra-thoraxic injection. *Ect4* mutants were more sensitive to infection than wild-type flies, with a significantly different mean survival of 5 and 6 d for $Ect4^{17}$/+ and w^{1118} male flies, respectively (Figure 1B). Notably, a significant increase in the DCV viral loading was observed in $Ect4^{17}$/+ flies at 48 and 72 h post-infection (Figure 1C), indicating that *Ect4* mutants are more sensitive to DCV infection.

To consolidate the DCV sensitivity phenotype observed with heterozygous *Ect4* individuals, the temperature-sensitive Gal80ts allele (31) was used to knockdown Ect4 expression in adult flies by shifting the culture temperature from 18-20°C to 29°C before and during the infection of DCV. RT-qPCR shows that *Ect4* expression decreased after the temperature shift to 29°C (Figure S3A). As expected, flies with knockdown of *Ect4* succumbed earlier to DCV

10.3389/fimmu.2023.1135625

infection than the control flies (Figure 1D). Consistently, the down-regulation of *Ect4* increased viral proteins (Figure 1E). Since DCV replicates mainly in fat bodies (32), we employed a fat body-specific driver, ppl-Gal4, to knock down Ect4 expression in the fat body. Specific depletion of *Ect4* in the fat body under the control of *ppl-Gal4* also affected the survival rate and viral load upon DCV infection (Figures S2A, B). The decreased survival rate was correlated with the increased viral burden in Ect4-RNAi flies.

3.2 Ect4 protects flies from DCV infection

To verify the specificity of the function of *Ect4* in DCV infection, *UAS-Ect4* transgenic flies were crossed with a ubiquitous *Gal4* driver, *da-Gal4*, to express the *Ect4* transgene ectopically. Remarkably, ubiquitous overexpression of *Ect4* promoted survival after the viral challenge (Figure 2A). Further, the increased dose of *Ect4* led to decreased viral burden in infected flies (Figure 2B). Interestingly, as shown in Figures 2C, D, flies overexpressing *Ect4*, specifically in the fat body using the *ppl-Gal4* driver, showed significantly more resistance to DCV infection than control flies and significantly decreased DCV replication levels. More importantly, rescue experiments by the expression of *Ect4* in $Ect4^{17}$/+ flies under the control of *da-Gal4* were performed to prove the specific role of *Ect4* in protecting flies from viral infections. The decreased survival rate of *Ect4* mutants after DCV infection, as well as increased viral load, was rescued to similar levels of the control flies following transgenic expression of *Ect4* in heterozygous *Ect4* mutants (Figures 2E, F). Similar results were obtained when a *hs-Gal4* driver was used for the rescue experiment. *Ect4* heterozygous mutant flies expressing *Ect4* under the control of *hs-Gal4* exhibited a decreased viral replication at 48 h post-infection. (Figure S2C). These results indicate that *Ect4*

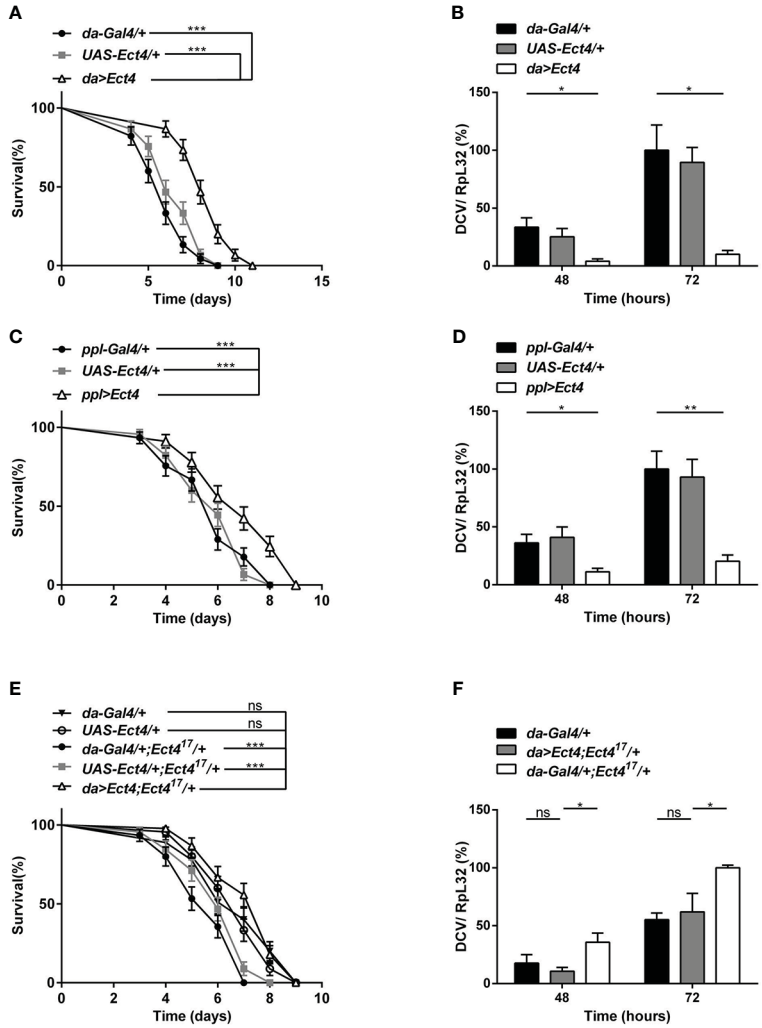

FIGURE 2
Overexpression of *Ect4* provides strong protection against DCV. **(A)** Survival of flies expressing *Ect4* transgene in whole flies by *da-Gal4* driver and control flies following DCV infection. **(B)** Quantitative RT-PCR analysis of the accumulation of viral RNA at 48 and 72 h post-infection in *Ect4* overexpression and control flies. **(C)** Survival of flies expressing *Ect4* transgene specifically in the fat body by the *ppl-Gal4* driver and control flies following DCV infection. **(D)** Quantitative RT-PCR analysis of the accumulation of viral RNA at 48 and 72 h post-infection in *Ect4* overexpression and control flies, specifically in the fat body. **(E)** Survival of *Ect4* mutant flies expressing *Ect4* transgene under the control of *da-Gal4* and control flies post-DCV infection. **(F)** Quantitative RT-PCR analysis of the accumulation of viral RNA at 48 and 72 h post-infection in control or *Ect4* mutant flies expressing *Ect4* transgene. Data represent the means ± standard errors of 3 independent pools of 15 male flies **(A, C, E)** or 10 male flies **(B, D, F)** for each genotype. Log-rank test **(A, C, E)** and *t*-test **(B, D, F)**: **P*< 0.05, ***P*< 0.01, ****P*< 0.001, ns, not significant.

confers resistance against DCV infection and is required to control the accumulation of viruses.

3.3 Deficiency in Ect4 does not alter the activity of the siRNA pathway

RNA interference (RNAi) acts as the first line of defense against viruses in *Drosophila* (33). There was strong genetic evidence that one RNAi-related pathway, the siRNA pathway, plays a major role in antiviral immunity in *Drosophila* (7, 34). Since heterozygous *Ect4* mutant flies are hypersensitive to DCV infection, we asked whether the down-regulation of *Ect4* affects the function of the siRNA pathway. To address this question, siRNA pathway activity was monitored using an *in vivo* sensor assay, wherein the endogenous *white* gene is silenced by the expression of a hairpin dsRNA corresponding to an exon of *white*. Expression of *UAS-wIR* using the eye-specific driver *GMR-Gal4* alters eye pigmentation to a white color or pale orange if the silencing is incomplete. Studies have shown that the siRNA pathway is inactivated without *Dicer-2* (*Dcr-2*). Therefore eye pigmentation of a *Dcr-2* null mutant ($dcr\text{-}2^{L811fsX}$/$dcr\text{-}2^{L811fsX}$) in *GMR>UAS-wIR* background is red, whereas *Dcr-2* heterozygous mutants ($dcr\text{-}2^{L811fsX/+}$) display pale orange (27). Our results show that mutation in *Ect4* did not lead to any changes in the eye pigmentation in w^{IR}; $dcr\text{-}2^{L811fsX}$/+ (Figures 3A, B). Moreover, the expression of *Vago*, induced in DCV infection dependent on *Dicer-2* (33), did not differ between wild-type and *Ect4* mutant flies at 48 and 72 hpi (Figure 3C). These results suggest that *Ect4* does not directly affect the antiviral siRNA pathway.

3.4 Ect4 regulates the expression of JAK/STAT-dependent genes, *TotA*, and *TotM*

The JAK/STAT pathway was shown to contribute to the antiviral response in *Drosophila* (9), where several genes are induced following viral infection *via* the JAK/STAT pathway including *virus-induced RNA-1* (*vir-1*), the stress-induced genes *Turandot A* and *M* (*TotA* and *TotM*) (18). To examine whether the downregulation of *Ect4* affected JAK/STAT pathway activation, we examined the expression of *vir-1*, *TotA*, and *TotM* by RT-qPCR at 48 and 72 h after DCV infection (hpi). As previously reported, DCV infection induced a strong up-regulation of *vir-1*, *TotA*, and *TotM* in wild-type flies (18). However, *vir-1* induction in response to DCV infection in *Ect4* mutant flies was indistinguishable from the control (Figure 4C). Similar results were observed using a ubiquitous temperature-sensitive Gal4 driver, *ubi-Gal4* (Figures S3B, C). A genetic interaction experiment was performed to assess further the relationship between Ect4 and the JAK/STAT pathway. *TotA* and *TotM* were expressed in flies carrying a JAK gain-of-function allele *Tum-l* ($hop^{Tum\text{-}l}$), which encodes a hyperactive JAK kinase due to a G341E substitution (35). Reducing the dosage of *Ect4* by half resulted in a large reduction of the RNA levels of *TotA* and *TotM* in $hop^{Tum\text{-}l}$ flies (Figure 4D). The *TotA* and *TotM* response was also attenuated in the fat body of flies where *Ect4* was downregulated by expressing the *Ect4-IR* transgene using a *ppl-Gal4* driver (Figures S3D, E). This TotA and TotM expression reduction was rescued by ubiquitously expressed *Ect4* (Figures 4E, F). Together, these results suggest that *Ect4* genetically interacts with the JAK/STAT pathway to regulate the expression of *TotA* and *TotM* in response to DCV infection.

3.5 Ect4 physically interacts with Stat92E

To unravel the molecular mechanism underlying the relationship between *Ect4* and JAK/STAT pathway, we examined whether Ect4 interacted with any known components of the JAK/STAT pathway. Differentially tagged forms of JAK/STAT pathway components and Ect4 were expressed in S2 cells, and co-immunoprecipitation studies were performed. As shown in Figure 5A, Ect4 is associated with the transcription factor Stat92E but not other key components (Hop or Dome) of the JAK/STAT pathway. Consistent with previous findings (36), Stat92E protein was located both in the cytoplasm and nucleus as visualized by immunofluorescence staining. Since the green fluorescent protein (GFP)-Ect4 fusion protein was localized in the cytoplasm, the interaction between the two proteins occurs in the cytoplasm (Figure 5B).

Ect4 protein harbor three different domains: ARM (Armadillo motif) domains followed by two SAM (Sterile Alpha motif) domains and TIR (Toll -Interleukin-1 receptor) domain (Figure 5C). To further investigate the molecular basis of the interaction between Ect4 and Stat92E, a series of truncated forms of Ect4 were generated. Co-immuno-precipitation studies showed that ARM and SAM domains were likely not required for Ect4 to interact with Stat92E, whereas the TIR domain was essential since only the TIR domain co-immuno-precipitated with Stat92E (Figure 5D). Together, these results suggest that Ect4 may regulate the JAK/STAT signaling activity by interacting with Stat92E.

3.6 Ect4 is required for phosphorylation and nuclear translocation of Stat92E

As described thus far, we show that *Ect4* regulates the expression of JAK/STAT-dependent genes *TotA* and *TotM* and is associated with Stat92E. It is intriguing to predict that Ect4 may affect Stat92E phosphorylation. To test this hypothesis, we employed an RNAi approach to knock down *Ect4* in S2 cells (Figure 6A). Previous studies have shown that tyrosine residues of Stat92E are phosphorylated after treatment of S2 cells with pervanadate, which activates Stat92E in a ligand-independent manner, while activation is not present in untreated cells (36, 37). As shown in Figure 6, treatment with dsRNA targeting *Ect4* mRNA resulted in a significant reduction of tyrosine phosphorylated Stat92E upon pervanadate treatment, as compared with the control using dsRNA targeting GFP. It was noted that upon DCV infection of S2 cells, phosphorylated Stat92E (p-Stat92E) was not detected by immunostaining, likely due to the transient activity of p-Stat92E dimers. Therefore, is Ect4 required for the nuclear translocation of Stat92E? As expected, reduced nuclear translocation of Stat92E in response to the pervanadate stimulus was detected in cells treated with *Ect4* RNAi (Figures 6C, D).

10.3389/fimmu.2023.1135625

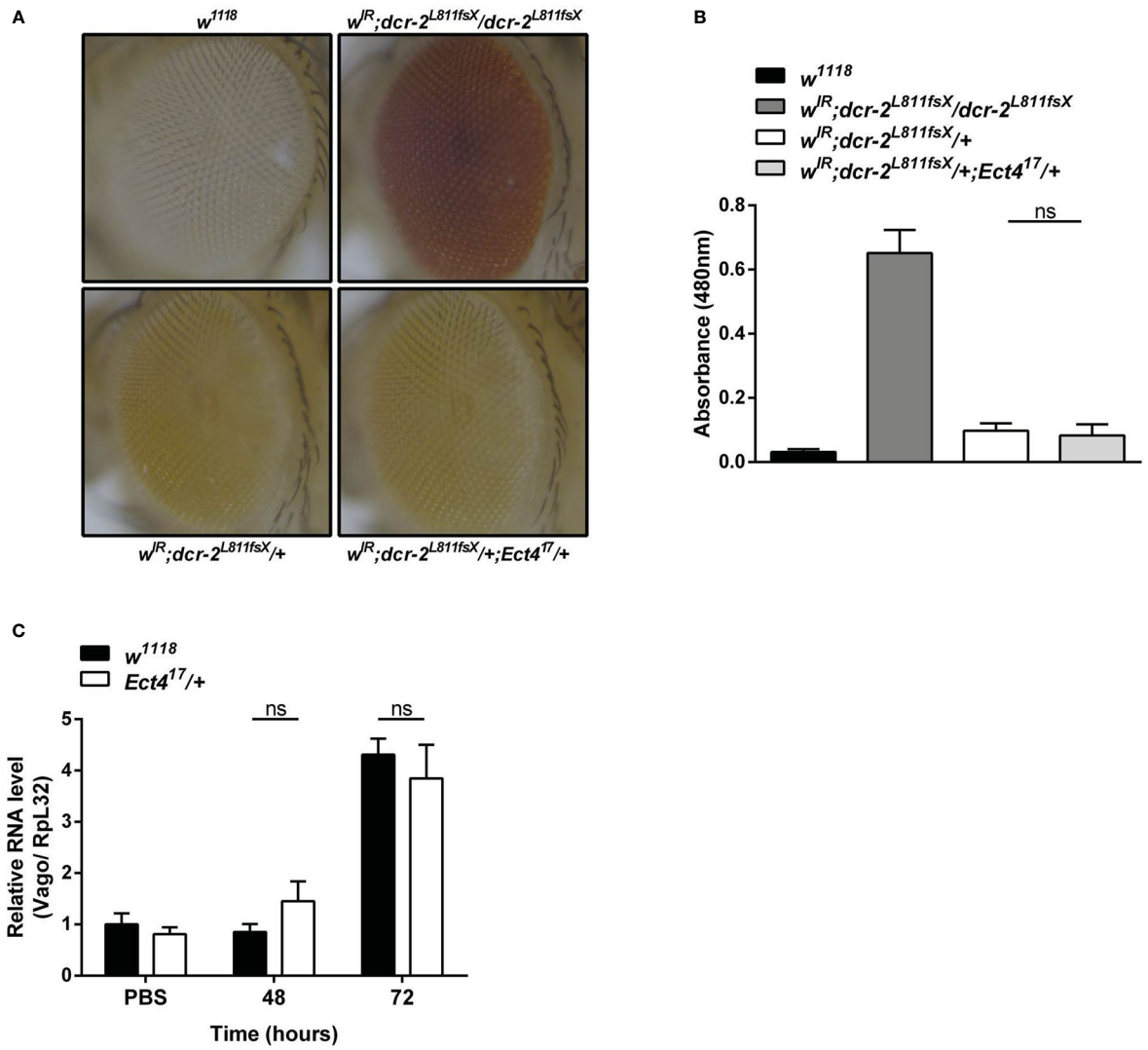

FIGURE 3
Ect4 deficiency did not affect siRNA-mediated gene silencing. **(A)** Effects of altering dosages of *Ect4* in w^{IR}; $dcr\text{-}2^{L811fsX}$ background. The eye color of a *white* null mutant fly (upper left panel) and a $white^{+}$ fly carrying *GMR>UAS-wIR* transgene and homozygous mutant for $dcr\text{-}2^{L811fsX}$ (upper right panel). The eye color of a fly carrying heterozygous $dcr\text{-}2^{L811fsX}$ mutation with (bottom right panel) or without (bottom left panel) one *Ect4* mutant allele. **(B)** Red-eye pigment levels of the indicated phenotype were determined by measuring absorbance at a wavelength of 480 nm (n = 50 for each group). **(C)** Expression levels of *Vago* at 48 and 72 h post-infection in wild-type or *Ect4* mutant flies challenged with DCV. Data represent the means ± standard errors of 3 independent pools of 50 female flies **(B)** or 10 male flies **(C)** for each genotype. The *t*-test **(B, C)**: ns, not significant.

4 Discussion

The innate immune system processes pathogen-induced pathways that detect the pathogen and induce the expression of antiviral effectors that control its proliferation (38). Consequently, it is expected that insufficient resistance mechanisms will lead to an increase in viral load, increased morbidity, and reduced survival. An in-depth understanding of antiviral resistance is important for developing novel methods for treating viral infections and other diseases. Nevertheless, mechanisms of resistance still need to be clearly understood.

Invertebrate *Ect4* orthologues play a positive role in innate immunity. The Ect4 orthologue in *C. elegans* (*TIR-1*) and *L. vannamei* (*LvSarm*) were required to express antimicrobial peptides. Depletion of both led to decreased survival of the animals upon bacterial infections (24, 26, 39). Kemp et al. (40) reported that Ect4 is responsive to DCV infection. And about a 2-fold increase of Ect4 transcription at 72 hpi was observed in this study (data not shown), indicating that Ect4 participated in the immune response upon DCV infection. Furthermore, our study showed that Ect4 contributes to resistance and regulates JAK/STAT signaling in *Drosophila*. Flies with down-regulated *Ect4* showed significantly elevated viral replication and earlier mortality after the DCV challenge, and a high level of *Ect4* expression was associated with increased resistance to DCV.

Compared with invertebrate Ect4 orthologues, the mammalian orthologue SARM acts as a negative regulator of TLR signaling and is not directly antiviral, as mice lacking SARM show enhanced survival after Bunyavirus infection (41) because *SARM* family members have acquired diverse biological functions during evolution. For example, while *Ect4* is essential for development in *Drosophila*, *SARM1* is redundant for viability in mice (21). A previous study revealed that

10.3389/fimmu.2023.1135625

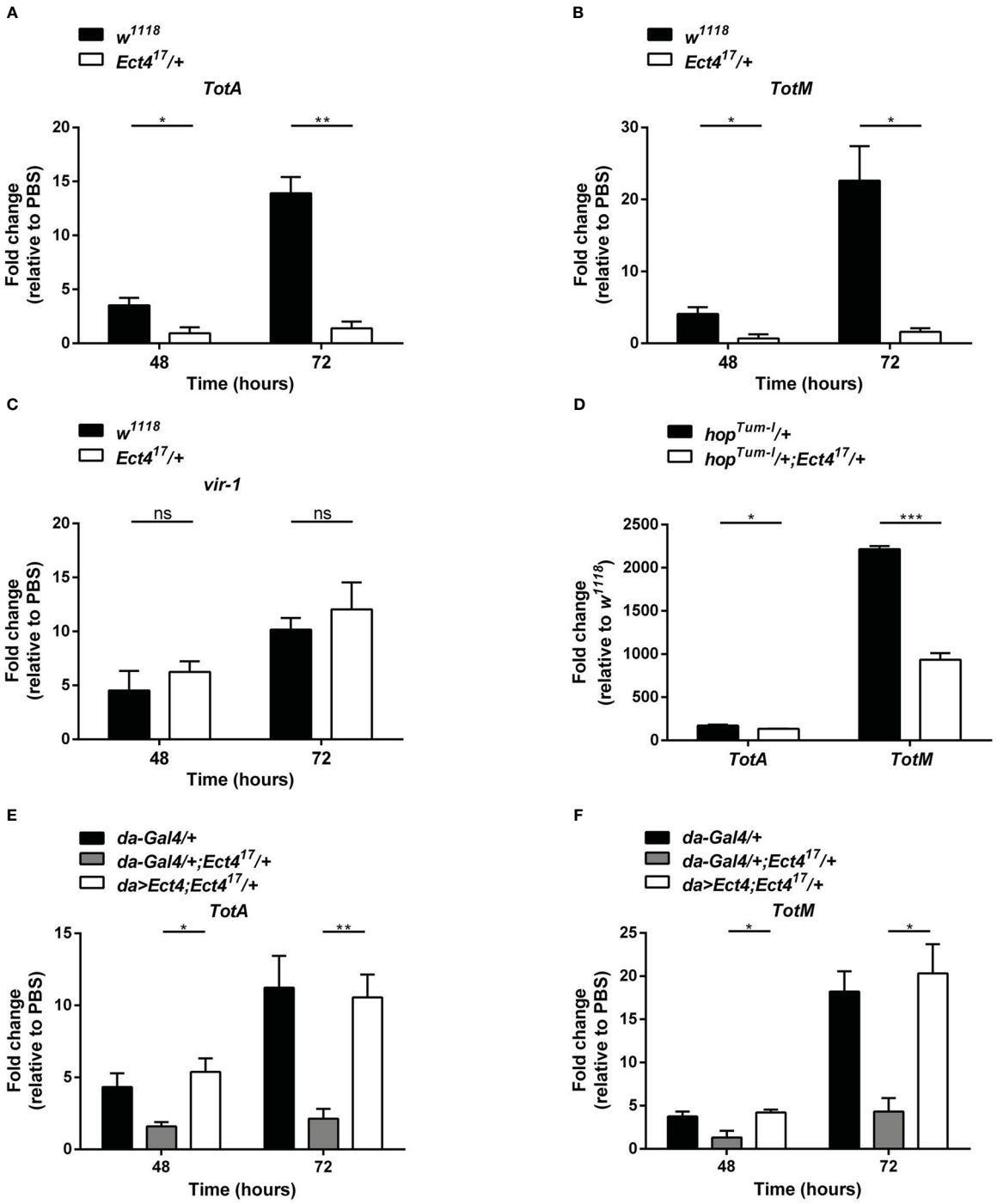

FIGURE 4
Ect4 is required for *TotA* and *TotM* induction in response to DCV infection. **(A–C)** Expression of JAK/STAT-dependent gene *TotA*, *TotM*, and *vir-1* at 48 and 72 h after DCV infection determined by RT-qPCR in whole flies. Expression of the gene of interest was normalized to transcript levels of the housekeeping gene *Rpl32* and expressed as fold change relative to mock infection (PBS). **(D)** Expression levels of *TotA* and *TotM* on 3-5 d-old unchallenged flies carrying one copy of $hop^{Tum\text{-}l}$ allele with or without the *Ect4* mutant allele. Expression of *TotA* and *TotM* was normalized to transcript levels of the housekeeping gene *Rpl32* and expressed as fold change relative to wild-type (w^{1118}) flies. **(E, F)** Expression levels of *TotA* and *TotM* at 48 and 72 h in control flies or *Ect4* mutant flies overexpressing *Ect4* transgene under a ubiquitous *da-Gal4* driver upon DCV infection. Data represent the means ± standard errors of 3 independent pools of 10 male flies **(A–F)** for each genotype. *T*-test **(A–F)**: **P*< 0.05, ***P*< 0.01, ****P*< 0.001, ns, not significant.

SARM is expressed mainly in the mouse brain, whereas its expression in other tissues, such as the spleen and the lymph node, was low (42). However, due to the lack of suitable anti-Ect4 antibodies, detecting Ect4 protein expression in *Drosophila* tissue sections was unsuccessful in the present study. Our results show that ectopic overexpression or knockdown of Ect4 in the fat body has a positive or negative effect on immune resistance upon DCV infection, suggesting that *Ect4* may regulate antiviral immune system function mainly in the fat body.

Our study demonstrated that down-regulation in Ect4 does not directly interfere with the siRNA pathway. Instead, Ect4 regulates

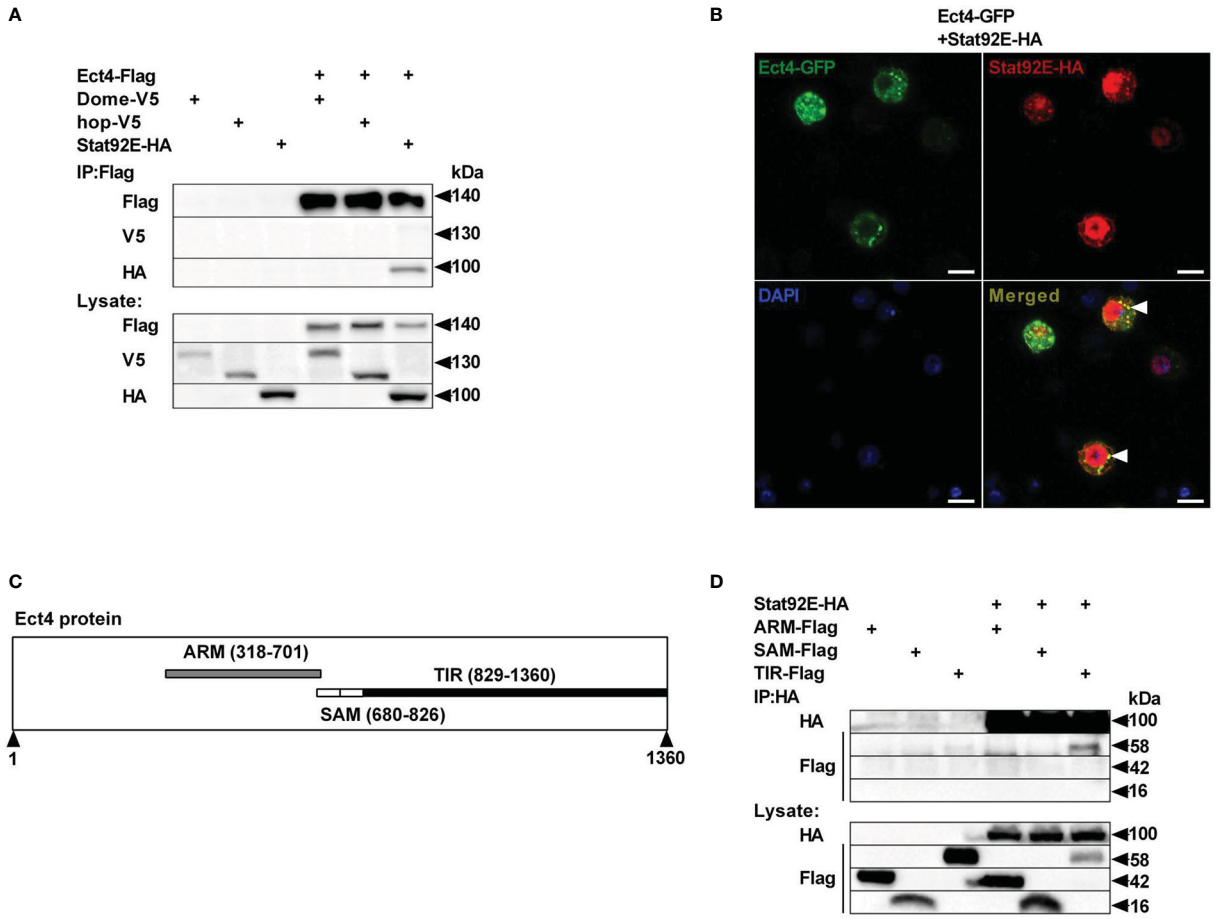

FIGURE 5
Ect4 co-localizes and physically associates with Stat92E. **(A)** S2 cells were transfected with combinations of expression plasmids as indicated. Cell lysates were immunoprecipitated with anti-Flag beads, followed by immunoblot analysis with the indicated antibodies. **(B)** S2 cells were transfected with Ect4-GFP in combination with Stat92E-HA, stained with DAPI (blue) and anti-HA antibody (Red), and imaged by confocal microscopy. Ect4 was co-localized with Stat92E in the cytoplasm (white arrow). **(C)** Ect4 protein includes ARM (gray), SAM (white), and TIR (black) domain. **(D)** S2 cells were cotransfected with Stat92E-HA and domains of Ect4. Cell lysates were immunoprecipitated with anti-HA beads and immunoblot analysis with the indicated antibodies. Scale bar: 10 μm.

JAK/STAT dependent gene expression, *TotA*, and *TotM*, in response to DCV infection. A previous study revealed that the proper level of JAK/STAT signaling activation is required for normal immune response: hyper-activation of JAK/STAT triggered early mortality and loss of function mutations of *hop* in flies causing reduced JAK/STAT activation in flies, also decreasing resistance upon a challenge with DCV (18, 43). Despite being elicited by DCV and commonly used as a read-out of JAK/STAT activation, the function of *TotA* and *TotM* in *Drosophila* remains unclear. The protein products encoded by the Turandot gene family are protein chaperones or signaling molecules, which are produced in the fat body and secreted into the hemolymph (44, 45). This inflammatory response is reminiscent of the acute phase response in mammals, which can be activated by infection and produce acute phase protein. These proteins are involved in the immune responses, including host defense, vascular permeability, and coagulation.

Furthermore, TotM enhanced tolerance against fungal sexually transmitted infections (STIs), and *TotA* confers resistance to heat stress (45, 46). The *Tot* gene family regulates diverse fly physiology aspects that coordinate resistance or tolerance to immune challenges. Indeed, the present study showed that *Ect4* is required for virus-induced expression of *TotA* and *TotM* genes. However, *Ect4* is dispensable for *vir-1* induction in response to DCV infection. It is likely that different factors are involved in the regulation of JAK/STAT downstream genes and that less p-Stat92E in *Ect4* RNAi flies sufficient for inducing *vir-1* expression, which requires a lower threshold of STAT activity.

Ect4 interacts with Stat92E in S2 cells through the highly conserved TIR domain of SARM family origin, which have roles in cell death and neuronal destruction in mammals (47). As an adaptor, SARM has been reported that interact with the mitochondrial antiviral-signaling protein MAVS in the mitochondria to mediate cell death during virus infection (41). Mitochondrial localization of tyrosine-phosphorylated STAT5, a homolog of Stat92E in mammalian, has been supposed to modulate cellular metabolism in cytokine-stimulated cells (48, 49). We show that down-regulation of *Ect4* reduced phosphorylated Stat92E upon pervanadate treatment in S2 cells, which suggests a role of Ect4 in regulating cell death through the modulation of JAK/STAT *via* the interaction with Stat92E.

In addition to antiviral immune defense, apoptosis is a conserved mechanism of programmed cell death that can prevent the infection before viral replication is completed (50, 51). Our *in vivo* study

10.3389/fimmu.2023.1135625

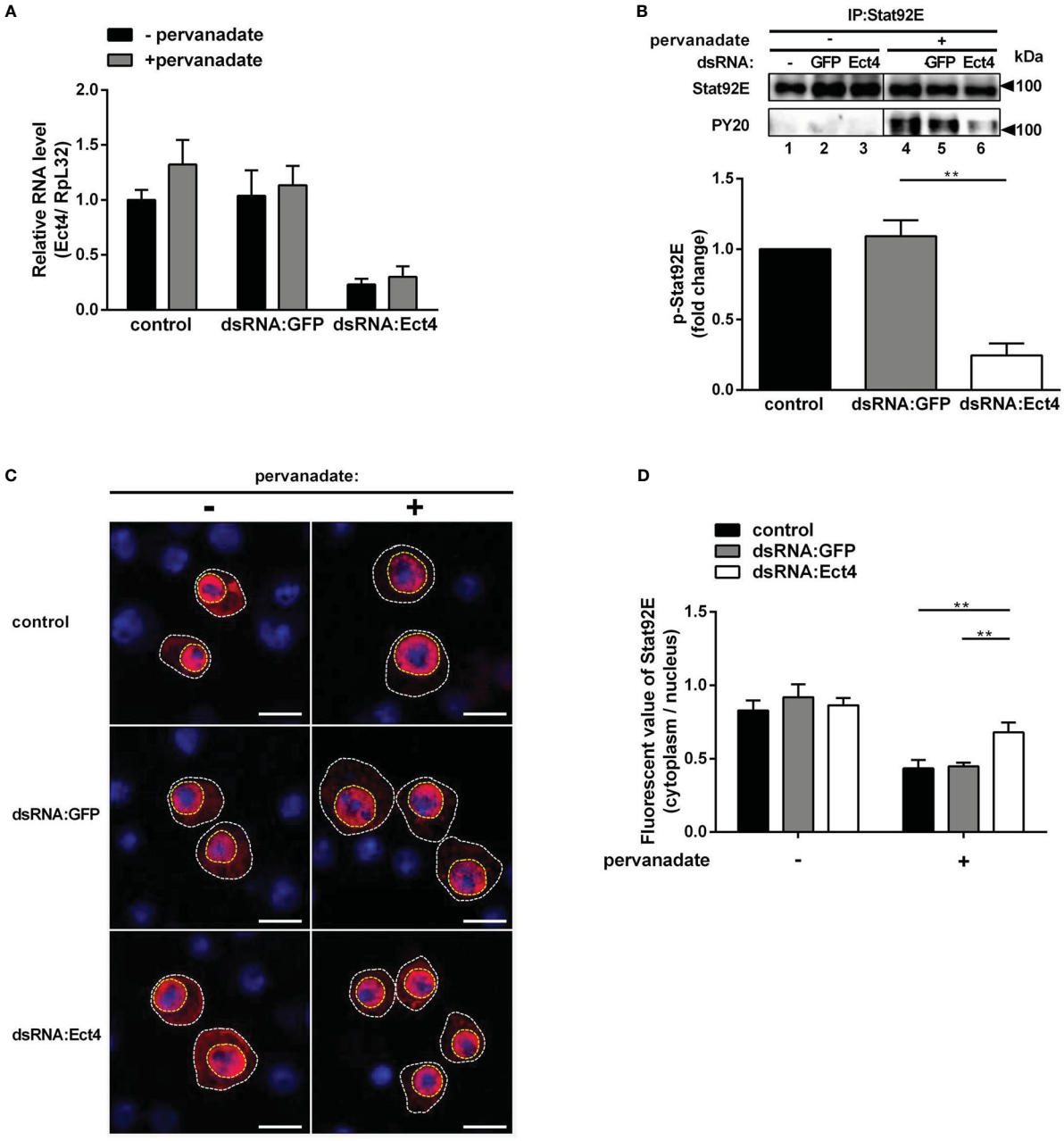

FIGURE 6
Knockdown of *Ect4* mRNA decreased the phosphorylation of Stat92E. **(A)** S2 cells were pretreated with or without dsRNA targeting GFP or Ect4 transcripts for 72 h, and measurement of *Ect4* mRNA by RT-qPCR to confirm RNAi efficiency. **(B)** After dsRNA treatment, S2 cells were either unstimulated or treated with pervanadate. Stat92E proteins were immunoprecipitated with Stat92E antibody, followed by immunoblot analysis with the Stat92E or PY20 antibodies. In the absence of pervanadate, phosphorylated-tyrosine Stat92E (p-Stat92E) was undetectable (lane 1-3). In contrast, after pervanadate treatment, p-Stat92E increased to levels detectable by western blot (lanes 4-6). The phosphorylated Stat92E was quantified from n = 3 independent experiments. **(C)** After transfection with Stat92E-HA, S2 cells were treated with or without dsRNA targeting GFP or Ect4 for 72 h and then left unstimulated or treated with pervanadate. Cells were stained with anti-HA antibody (red) and DAPI (blue) and imaged by confocal microscopy. **(D)** Quantification assays of the ratio between the fluorescent signal intensity of Stat92E in the nucleus (surrounded by a yellow dashed line) and in the cytoplasm (the area in the white dotted line subtracts the area from the yellow dashed line). Cell samples collected from **(C)**, n=15. Scale bar: 10 μm. Data represent the means ± standard errors. The *t*-test **(B, D)**: $^{**}P < 0.01$.

revealed that Ect4 mutants showed enhanced mortality and increased viral load upon DCV challenge. We seek to further elucidate the unknown mechanisms of antiviral response in *Drosophila* by assessing whether *Ect4* affects host resistance to viral infection by regulating cell death.

Our results demonstrate the novel roles for *Drosophila* Ect4 in regulation of JAK/STAT signaling pathway and protection against DCV infection. It is still unclear if Ect4 also participated in the control of other virus infection. The contribution of JAK/STAT signaling to *Drosophila* antiviral protection is virus-specific. Although JAK/STAT pathway can be activated by RNA viruses, including DCV, CrPV, FHV, and DXV, it is only required for resistance against two *Dicistroviridae* family members, DCV and CrPV (18). Our data suggest that Ect4 is required for phosphorylation and nuclear

translocation of Stat92E. Future studies should investigate if the involvement of *Ect4* in activating the JAK/STAT pathway impart resistance in *Drosophila* to other virus infection.

The tight regulation of immune-related signal transduction cascades is essential for the defense against a wide range of pathogens. However, although the key components of the JAK/STAT pathway have been identified, the 'non-core' pathway activity regulators are less known. In mammals, poly (ADP-ribose) polymerase PARP9 was recently reported as a noncanonical sensor for RNA viruses that depends on the PI3K/AKT3 pathway to produce antiviral type I interferon (52). PARP9 interacted with the E3 ubiquitin ligase DTX3L and STAT1 functioned as a chaperone to enhance levels of the PARP9-DTX3L protein complex and STAT1-mediated interferon-stimulated gene expression (53). Another E3 ubiquitin ligase TRIM18 recruited protein phosphatase 1A (PPM1A), a negative regulator of STAT1, to dampen type I interferon-mediated antiviral innate immunity for promoting virus infection (54, 55). Given the conserved nature of the JAK/STAT pathway, *Drosophila* homologs of PARP9 and TRIM18 are potential candidates for JAK/STAT pathway regulators. It will be intriguing to investigate whether other factors or pathways are involved in *Ect4*-mediated JAK/STAT pathway modulation and defense against viral infection. Further exploration will yield more insights into the current understanding of the JAK/STAT pathway immune regulatory mechanism and contributes to establishing an immune signaling network.

Data availability statement

The raw data supporting the conclusions of this article will be made available by the authors, without undue reservation.

Author contributions

ZH and PX carried out experiments. SG contributed to data collection. YH analyzed confocal images. YL, SY, and FS conducted statistical analysis. KA and W-MD revised the manuscript. JL and RJ contributed to the conception and design of the experiments. WW wrote the first draft of the manuscript. JC directed the studies. All authors contributed to the article and approved the submitted version.

Funding

This work was supported by the Natural Science Foundation of Fujian Province of China (2020J01856), Fuzhou Science and Technology Planning Project of (2022-P-008), Research Program of Minjiang University (MYK21004), and Special Projects for Local Science and Technology Development Guided by the Central Government of Fujian Province (2021L3020022).

Conflict of interest

The authors declare that the research was conducted in the absence of any commercial or financial relationships that could be construed as a potential conflict of interest.

Publisher's note

All claims expressed in this article are solely those of the authors and do not necessarily represent those of their affiliated organizations, or those of the publisher, the editors and the reviewers. Any product that may be evaluated in this article, or claim that may be made by its manufacturer, is not guaranteed or endorsed by the publisher.

Supplementary material

The Supplementary Material for this article can be found online at: https://www.frontiersin.org/articles/10.3389/fimmu.2023.1135625/full#supplementary-material

References

1. Younes S, Al-Sulaiti A, Nasser EAA, Najjar H, Kamareddine L. *Drosophila* as a model organism in host–pathogen interaction studies. *Front Cell Infect Mi* (2020) 10:214. doi: 10.3389/fcimb.2020.00214

2. Swevers L, Liu J, Smagghe G. Defense mechanisms against viral infection in *Drosophila*: RNAi and non-RNAi. *Viruses-Basel* (2018) 10(5):230. doi: 10.3390/v10050230

3. Leggewie M, Schnettler E. RNAi-mediated antiviral immunity in insects and their possible application. *Curr Opin Virol* (2018) 32:108–14. doi: 10.1016/j.coviro.2018.10.004

4. Lamiable O, Arnold J, de Faria IJ, Olmo RP, Bergami F, Meignin C, et al. Analysis of the contribution of hemocytes and autophagy to *Drosophila* antiviral immunity. *J Virol* (2016) 90:5415–26. doi: 10.1128/JVI.00238-16

5. Holleufer A, Winther KG, Gad HH, Ai X, Chen Y, Li L, et al. Two cGAS-like receptors induce antiviral immunity in *Drosophila*. *Nat* (2021) 597:114–8. doi: 10.1038/s41586-021-03800-z

6. Slavik KM, Morehouse BR, Ragucci AE, Zhou W, Ai X, Chen Y, et al. cGAS-like receptors sense RNA and control 3'2'-cGAMP signalling in drosophila. *Nature* (2021) 597:109–13. doi: 10.1038/s41586-021-03743-5

7. Machado SR, van der Most T, Miesen P. Genetic determinants of antiviral immunity in dipteran insects–compiling the experimental evidence. *Dev Comp Immunol* (2021) 119:104010. doi: 10.1016/j.dci.2021.104010

8. Schneider J, Imler JL. Sensing and signalling viral infection in *Drosophila*. *Dev Comp Immunol* (2021) 117:103985. doi: 10.1016/j.dci.2020.103985

9. Tafesh-Edwards G, Eleftherianos I. *Drosophila* immunity against natural and nonnatural viral pathogens. *Virol* (2020) 540:165–71. doi: 10.1016/j.virol.2019.12.001

10. Myllymäki H, Rämet M. JAK/STAT pathway in *Drosophila* immunity. *Scand J Immunol* (2014) 79(6):377–85. doi: 10.1111/sji.12170

11. Tokusumi Y, Tokusumi T, Schulz RA. Mechanical stress to *Drosophila* larvae stimulates a cellular immune response through the JAK/STAT signaling pathway. *Biochem Biophys Res Co* (2018) 502(3):415–21. doi: 10.1016/j.bbrc.2018.05.192

12. Zhang Z, Zhang Y, Gao M, Cui X, Yang Y, Van Duijn B, et al. Steamed *Panax notoginseng* attenuates anemia in mice with blood deficiency syndrome *via* regulating hematopoietic factors and JAK-STAT pathway. *Front Pharmacol* (2020) 10:1578. doi: 10.3389/fphar.2019.01578

13. Bang IS. JAK/STAT signaling in insect innate immunity. *Entomol Res* (2019) 49(8):339–53. doi: 10.1111/1748-5967.12384

14. Su Y, Tao T, Liu X, Su W. JAK-STAT signaling pathway in non-infectious uveitis. *Biochem Pharmacol* (2022) 204:115236. doi: 10.1016/j.bcp.2022.115236

15. Hu X, Fu M, Zhao X, Wang W. The JAK/STAT signaling pathway: From bench to clinic. *Signal Transduct Tar* (2021) 6(1):1–33. doi: 10.1038/s41392-021-00791-1

16. Tzeng HT, Chyuan IT, Lai JH. Targeting the JAK-STAT pathway in autoimmune diseases and cancers: a focus on molecular mechanisms and therapeutic potential. *Biochem Pharmacol* (2021) 193:114760. doi: 10.1016/j.bcp.2021.114760

17. Trivedi S, Starz-Gaiano M. *Drosophila* Jak/STAT signaling: regulation and relevance in human cancer and metastasis. *Int J Mol Sci* (2018) 19(12):4056. doi: 10.3390/ijms19124056

18. Merkling SH, Bronkhorst AW, Kramer JM, Overheul GJ, Schenck A, Van Rij RP. The epigenetic regulator G9a mediates tolerance to RNA virus infection in *Drosophila*. *PloS Pathog* (2015) 11:e1004692. doi: 10.1371/journal.ppat.1004692

19. Yang L, Qiu LM, Fang Q, Stanley DW, Ye GY. Cellular and humoral immune interactions between *Drosophila* and its parasitoids. *Insect Sci* (2021) 28(5):1208–27. doi: 10.1111/1744-7917.12863

20. Carty M, Bowie AG. SARM: From immune regulator to cell executioner. *Biochem Pharmacol* (2019) 161:52–62. doi: 10.1016/j.bcp.2019.01.005

21. Panneerselvam P, Ding JL. Beyond TLR signaling–the role of SARM in antiviral immune defense, apoptosis development. *Int Rev Immunol* (2015) 34(5):432–44. doi: 10.3109/08830185.2015.1065826

22. Balaji SP, Chand CV, Justin A, Ramanathan M. Telmisartan mediates anti-inflammatory and not cognitive function through PPAR-γ agonism *via* SARM and MyD88 signaling. *Pharmacol Biochem Be* (2015) 137:60–8. doi: 10.1016/j.pbb.2015.08.007

23. Akhouayri I, Turc C, Royet J, Charroux B. Toll-8/Tollo negatively regulates antimicrobial response in the *Drosophila* respiratory epithelium. *PloS Pathog* (2011) 7 (10):e1002319. doi: 10.1371/journal.ppat.1002319

24. Wang PH, Gu ZH, Wan DH, Zhu WB, Qiu W, Weng SP, et al. *Litopenaeus vannamei* sterile-alpha and armadillo motif containing protein (LvSARM) is involved in regulation of penaeidins and antilipopolysaccharide factors. *PloS One* (2013) 8(2):e52088. doi: 10.1371/journal.pone.0052088

25. Monsanto-Hearne V, Tham AL, Wong ZS, Asgari S, Johnson KN. *Drosophila* miR-956 suppression modulates ectoderm-expressed 4 and inhibits viral replication. *Virol* (2017) 502:20–7. doi: 10.1016/j.virol.2016.12.009

26. Couillault C, Pujol N, Reboul J, Sabatier L, Guichou JF, Kohara Y, et al. TLR-independent control of innate immunity in *Caenorhabditis elegans* by the TIR domain adaptor protein TIR-1, an ortholog of human SARM. *Nat Immunol* (2004) 5(5):488–94. doi: 10.1038/ni1060

27. Lee YS, Nakahara K, Pham JW, Kim K, He Z, Sontheimer EJ, et al. Distinct roles for drosophila dicer-1 and dicer-2 in the siRNA/miRNA silencing pathways. *Cell* (2004) 117:69–81. doi: 10.1016/S0092-8674(04)00261-2

28. Bischof J, Sheils EM, Bjorklund M, Basler K. Generation of a transgenic ORFeome library in *Drosophila.* nat. *Protoc* (2014) 9:1607–20. doi: 10.1038/nprot.2014.105

29. Mukherjee P, Winkler CW, Taylor KG, Woods TA, Nair V, Khan BA, et al. SARM1, not MyD88, mediates TLR7/TLR9-induced apoptosis in neurons. *J Immunol* (2015) 195:4913–21. doi: 10.4049/jimmunol.1500953

30. Magwire MM, Fabian DK, Schweyen H, Cao C, Longdon B, Bayer F, et al. Genome-wide association studies reveal a simple genetic basis of resistance to naturally coevolving viruses in *Drosophila melanogaster*. *PloS Genet* (2012) 8(11):e1003057. doi: 10.1371/journal.pgen.1003057

31. Mondal K, Dastidar AG, Singh G, Madhusudhanan S, Gande SL, VijayRaghavan K, et al. Design and isolation of temperature-sensitive mutants of Gal4 in yeast and *Drosophila*. J. *Mol Biol* (2007) 370(5):939–50. doi: 10.1016/j.jmb.2007.05.035

32. Kemp C, Imler JL. Antiviral immunity in drosophila. *Curr Opin Immunol* (2009) 21:3–9. doi: 10.1016/j.coi.2009.01.007

33. Deddouche S, Matt N, Budd A, Mueller S, Kemp C, Galiana-Arnoux D, et al. The DExD/H-box helicase dicer-2 mediates the induction of antiviral activity in drosophila. *Nat Immunol* (2008) 9:1425–32. doi: 10.1038/ni.1664

34. Bronkhorst AW, van Rij RP. The long and short of antiviral defense: small RNA-based immunity in insects. *Curr Opin Virol* (2014) 7:19–28. doi: 10.1016/j.coviro.2014.03.010

35. Luo H, Hanratty WP, Dearolf CR. An amino acid substitution in the *Drosophila* hopTum-l jak kinase causes leukemia-like hematopoietic defects. *EMBO J* (1995) 14:1412–20. doi: 10.1002/j.1460-2075.1995.tb07127.x

36. Ekas LA, Cardozo TJ, Flaherty MS, McMillan EA, Gonsalves FC, Bach EA. Characterization of a dominant-active STAT that promotes tumorigenesis in *Drosophila*. *Dev Biol* (2010) 344:621–36. doi: 10.1016/j.ydbio.2010.05.497

37. Sweitzer SM, Calvo S, Kraus MH, Finbloom DS, Larner AC. Characterization of a stat-like DNA binding activity in *Drosophila melanogaster*. *J Biol Chem* (1995) 270:16510–3. doi: 10.1074/jbc.270.28.16510

38. Mohammadi Pour P, Fakhri S, Asgary S, Farzaei MH, Echeverria J. The signaling pathways, and therapeutic targets of antiviral agents: focusing on the antiviral approaches and clinical perspectives of anthocyanins in the management of viral diseases. *Front Pharmacol* (2019) 10:1207. doi: 10.3389/fphar.2019.01207

39. Kurz CL, Shapira M, Chen K, Baillie DL, Tan MW. *Caenorhabditis elegans* pgp-5 is involved in resistance to bacterial infection and heavy metal and its regulation requires TIR-1 and a p38 map kinase cascade. *Biochem Biophys Res Co* (2007) 363(2):438–43. doi: 10.1016/j.bbrc.2007.08.190

40. Kemp C, Mueller S, Goto A, Barbier V, Paro S, Bonnay F, et al. Broad RNA interference-mediated antiviral immunity and virus-specific inducible responses in *Drosophila*. *J Immunol* (2013) 190:650–8. doi: 10.4049/jimmunol.1102486

41. Mukherjee P, Woods TA, Moore RA, Peterson KE. Activation of the innate signaling molecule MAVS by bunyavirus infection upregulates the adaptor protein SARM1, leading to neuronal death. *Immunity* (2013) 38(4):705–16. doi: 10.1016/j.immuni.2013.02.013

42. Szretter KJ, Samuel MA, Gilfillan S, Fuchs A, Colonna M, Diamond MS. The immune adaptor molecule SARM modulates tumor necrosis factor alpha production and microglia activation in the brainstem and restricts West Nile virus pathogenesis. *J Virol* (2009) 83:9329–38. doi: 10.1128/JVI.00836-09

43. Dostert C, Jouanguy E, Irving P, Troxler L, Galiana-Arnoux D, Hetru C, et al. The jak-STAT signaling pathway is required but not sufficient for the antiviral response of drosophila. *Nat Immunol* (2005) 6:946–53. doi: 10.1038/ni1237

44. Ekengren S, Hultmark D. A family of turandot-related genes in the humoral stress response of *Drosophila*. *Biochem Biophys Res Commun* (2001) 284:998–1003. doi: 10.1006/bbrc.2001.5067

45. Ekengren S, Tryselius Y, Dushay MS, Liu G, Steiner H, Hultmark D. A humoral stress response in *Drosophila*. *Curr Biol* (2001) 11:714–8. doi: 10.1016/S0960-9822(01)00203-2

46. Zhong W, McClure CD, Evans CR, Mlynski DT, Immonen E, Ritchie MG, et al. Immune anticipation of mating in *Drosophila*: Turandot m promotes immunity against sexually transmitted fungal infections. *Proc Biol Sci* (2013) 280:2013–8. doi: 10.1098/rspb.2013.2018

47. Summers DW, Gibson DA, DiAntonio A, Milbrandt J. SARM1-specific motifs in the TIR domain enable NAD^+ loss and regulate injury-induced SARM1 activation. *Proc Natl Acad Sci USA* (2016) 113:E6271–e80. doi: 10.1073/pnas.1601506113

48. Chueh FY, Leong KF, Yu CL. Mitochondrial translocation of signal transducer and activator of transcription 5 (STAT5) in leukemic T cells and cytokine-stimulated cells. *Biochem Biophys Res Commun* (2010) 402:778–83. doi: 10.1016/j.bbrc.2010.10.112

49. Summers DW, DiAntonio A, Milbrandt J. Mitochondrial dysfunction induces Sarm1-dependent cell death in sensory neurons. *J Neurosci* (2014) 34:9338–50. doi: 10.1523/JNEUROSCI.0877-14.2014

50. Settles EW, Friesen PD. Flock house virus induces apoptosis by depletion of *Drosophila* inhibitor-of-apoptosis protein DIAP1. *J Virol* (2008) 82:1378–88. doi: 10.1128/JVI.01941-07

51. Liu B, Behura SK, Clem RJ, Schneemann A, Becnel J, Severson DW, et al. P53-mediated rapid induction of apoptosis conveys resistance to viral infection in *Drosophila melanogaster*. *PloS Pathog* (2013) 9:e1003137. doi: 10.1371/journal.ppat.1003137

52. Xing J, Zhang A, Du Y, Fang M, Minze LJ, Liu YJ, et al. Identification of poly (ADP-ribose) polymerase 9 (PARP9) as a noncanonical sensor for RNA virus in dendritic cells. *Nat Commun* (2021) 12(1):1–17. doi: 10.1038/s41467-021-23003-4

53. Zhang Y, Mao D, Roswit WT, Jin X, Patel AC, Patel DA, et al. PARP9-DTX3L ubiquitin ligase targets host histone H2BJ and viral 3C protease to enhance interferon signaling and control viral infection. *Nat Commun* (2015) 16(12):1215–27. doi: 10.1038/ni.3279

54. Fang M, Zhang A, Du Y, Lu W, Wang J, Minze LJ, et al. TRIM18 is a critical regulator of viral myocarditis and organ inflammation. *J Biomed Sci* (2022) 29(1):1–20. doi: 10.1186/s12929-022-00840-z

55. Smith SR, Schaaf K, Rajabalee N, Wagner F, Duverger A, Kutsch O, et al. The phosphatase PPM1A controls monocyte-to-macrophage differentiation. *Sci Rep* (2018) 8 (1):1–14. doi: 10.1038/s41598-017-18832-7

frontiers | Frontiers in Immunology

TYPE Review
PUBLISHED 05 April 2023
DOI 10.3389/fimmu.2023.1136051

OPEN ACCESS

EDITED BY
Huifang Zhu,
First Affiliated Hospital of Gannan Medical University, China

REVIEWED BY
Sandeep Gupta,
AgResearch Ltd., New Zealand
Harshad Ingle,
Washington University in St. Louis, United States

*CORRESPONDENCE
Jingqiang Ren
rjq207@163.com
Jingbo Zhai
jbzhai@imun.edu.cn
Yang Song
yangyang2130@126.com

SPECIALTY SECTION
This article was submitted to Viral Immunology, a section of the journal Frontiers in Immunology

RECEIVED 02 January 2023
ACCEPTED 27 March 2023
PUBLISHED 05 April 2023

CITATION
Wen S, Li X, Lv X, Liu K, Ren J, Zhai J and Song Y (2023) Current progress on innate immune evasion mediated by N^{pro} protein of pestiviruses. *Front. Immunol.* 14:1136051. doi: 10.3389/fimmu.2023.1136051

Current progress on innate immune evasion mediated by N^{pro} protein of pestiviruses

Shubo Wen[1,2,5], Xintong Li[4], Xiangyu Lv[1,5], Kai Liu[1,5], Jingqiang Ren[3]*, Jingbo Zhai[1,2]* and Yang Song[1,2]*

[1]Preventive Veterinary Laboratory, College of Animal Science and Technology, Inner Mongolia Minzu University, Tongliao, China, [2]Key Laboratory of Zoonose Prevention and Control, Universities of Inner Mongolia Autonomous Region, Tongliao, China, [3]Wenzhou Key Laboratory for Virology and Immunology, Institute of Virology, Wenzhou University, Zhejiang, Wenzhou, China, [4]State Key Laboratory of Membrane Biology, Institute of Zoology, Chinese Academy of Sciences, Beijing, China, [5]Beef Cattle Disease Control and Engineering Technology Research Center, Inner Mongolia Autonomous Region, Tongliao, China

Interferon (IFN), the most effective antiviral cytokine, is involved in innate and adaptive immune responses and is essential to the host defense against virus invasion. Once the host was infected by pathogens, the pathogen-associated molecular patterns (PAMPs) were recognized by the host pattern recognition receptors (PRRs), which activates interferon regulatory transcription factors (IRFs) and nuclear factor-kappa B (NF-κB) signal transduction pathway to induce IFN expression. Pathogens have acquired many strategies to escape the IFN-mediated antiviral immune response. Pestiviruses cause massive economic losses in the livestock industry worldwide every year. The immune escape strategies acquired by pestiviruses during evolution are among the major difficulties in its control. Previous experiments indicated that Erns, as an envelope glycoprotein unique to pestiviruses with RNase activity, could cleave viral ss- and dsRNAs, therefore inhibiting the host IFN production induced by viral ss- and dsRNAs. In contrast, Npro, the other envelope glycoprotein unique to pestiviruses, mainly stimulates the degradation of transcription factor IRF-3 to confront the IFN response. This review mainly summarized the current progress on mechanisms mediated by Npro of pestiviruses to antagonize IFN production.

KEYWORDS

pestivirus, interferon (IFN), immune evasion, viral proteins, innate immunity

Introduction

The genus Pestivirus, belonging to the family Flaviviridae, comprises pathogens responsible for massive economic losses in livestocks, especially pigs and ruminant species (1–3) and often cause clinical manifestations ranging from mild to severe (4–7). Among pestiviruses, classical swine fever virus (CSFV) and bovine viral diarrhea virus 1 and 2 (BVDV-1 and BVDV-2) are the most impactful ones. Notably, the majority of

pestiviruses are non-cytopathogenic (NCP), while both two biological types: NCP and cytopathogenic (CP) viruses have been reported in CSFV and BVDV strains isolated in clinical samples (4). Several other viruses related to pestivirus have been also described in some studies. These viruses isolated from domestic animals (8–17) and wild species (18–21) have great differences in genetics. Recently, the following eleven viruses: BVDV-1, BVDV-2, CSFV, BDV, pronghorn pestivirus, Bungowannah virus, giraffe pestivirus, HoBi-like pestivirus, Aydin-like pestivirus, rat pestivirus, and atypical porcine pestivirus have been appointed to Pestivirus A-K, respectively (3, 15).

Pestiviruses could transmit from one species of ruminants to another frequently. For example, ruminant pestiviruses often infect pigs (22). However, no evidence is available to suggest the replication of CSFV in ruminants. After infection, pestiviruses are excreted through various body secretions and usually transmitted by direct contact with infected animals or indirect contact with infectious secretions, contaminated food, or needles (23). Animals with pestiviruses infection (especially those with persistent infection) excrete lots of viruses from their body secretions for life.

Pestiviruses are single-stranded, positive-sense RNA viruses with an envelope and a genomic size of about 12.3 kb (24). The genomic RNA is translated into a single polyprotein, which is processed subsequently into four structural proteins (SPs): a basic core protein C and three envelope (E) glycoproteins E^{rns}, E1, and E2, as well as eight non-structural proteins. Proteins unique to the Pestivirus genus are the non-structural protease N^{pro} and E^{rns} envelope glycoprotein which has RNase activity. Both proteins are associated with the suppression of the host's innate antiviral immune response (23). This review compiles current progresses on the roles and functions of Pestivirus N^{pro} in the evasion of type I interferon response.

N^{pro} of pestiviruses has antagonistic activity against type-I IFN production

N^{pro} is the first protein encoded by pestivirus, with a molecular weight of 23 KDa, and is unique to the pestivirus genus. N^{pro} protein is a hydrophilic peripheral membrane protein without signal peptide, and the secondary structure mainly contains β-sheet and random curling. Moreover, it has autoprotease activity and can be cleaved in an autocatalytic manner from nascent polyproteins being translated into mature viral proteins. N^{pro} is not necessary for the replication of pestiviruses but plays an important role in the evasion of the antiviral immune response of host cells. It has been shown that Cys69 and His130 are the catalytic residues of protease cleavage and catalyze the cleavage of peptide bonds between Tyr164 and Vail65. To study the biological activity of N^{pro}, Tratschin et al. prepared a CSFV virus strain vA187-Ubi, the N^{pro} protein gene sequence of which was replaced by the mouse ubiquitin protein gene. It has been shown that vA187-Ubi had similar growth characteristics to the parent vA187-1 virus, both of which showed obvious cytopathological effects. *In vivo* assay results showed a complete loss of virulence of vA187-Ubi, indicating the N^{pro} protein is unnecessary for the virus replication but is essential for its virulence (25). In addition, the N^{pro} protein of pestiviruses could block apoptosis and IFN-α/β production induced by double-stranded RNA. NCP-type BVDV-1 infection was found to protect bovine nose osteocytes from poly (I: C) -induced apoptosis. Further studies showed that NCP-type BVDV inhibited the transcription and secretion of type I interferon-induced poly (I: C) (26). In addition, compared with the parent strain, ΔN^{pro} BVDV can effectively induce IFN-β production, indicating that N^{pro} could inhibit the production of type I interferon (27). The N^{pro} protein of BVDV-2 could also significantly down-regulate oligo adenylate synthetase (OAS), ubiquitin-like protein 15 (ISG15), Myxoviral-resistant protein 1 (Mx1), and type I IFN transcription levels (28).

Studies on CSFV have shown similar results. Ruggli et al. reported that after infection with CSFV, the resistance to poly (I: C) -induced apoptosis by porcine renal cell line SK-6 increased nearly 100 times. ΔN^{pro} CSFV was found to have a similar growth profile to wild-type virus, but with no protection for SK-6 cells against apoptosis induced by poly (I: C) (29). Therefore, it was suggested that N^{pro} could counteract dsRNA-induced apoptosis and IFN-α/β production independently of other CSFV proteins. After treated with poly (I: C), drastically more SK6-EGFP-N^{pro} cells and CSFV-infected SK-6 cells survived compared with the parental SK-6 cells. Luciferase reporter gene experiments showed that N^{pro} also inhibits the expression of luciferase derived by IFN-α/β promoter in human cells, meanwhile, it can also inhibit the production of Newcastle disease virus-induced IFN-α/β (30). Moreover, in dendritic cells (DC), ΔN^{pro} CSFV can promote the expression of IFNα/β, and also up-regulate the expression of CD80/86 and MHC II to promote the maturation of DCs (31).

Bungowannah virus is genetically the most divergent pestivirus with all of the genomic and structural elements of classical pestiviruses. Compared with other pestivirus, they also have many differences in antigenic cross-reaction. To test the influence of N^{pro} of Bungowannah virus on the type I interferon signaling pathway, a chimeric BVDV/Bungowannah virus (vCP7_N^{pro}-Bungo) was rescued by Richter et al. (32). In the virus, the N^{pro} gene of Bungowannah virus replaced that of CP7—a cytopathic BVDV strain. After infected with CP7, Bungowannah virus, and virus vCP7_Npro-Bungo, similar IFN suppression was observed in cells. However, the Npro-deleted mutant had an impaired replication and induced increased type-I IFN response in bovine cells (32). Collectively, these studies indicated that the N^{pro} of pestiviruses had antagonistic protease activity of IFN-α/β production.

Furthermore, it has been shown that the replacement of amino acids Glu22 and His49 of pestiviruses could abolish the ability of N^{pro} to inhibit IFN production, while the replacement of Cys69 had no such effect. There was no antagonistic IFN-α/β activity in the conserved N^{pro} region (L8P) mutant near the N-terminal of the two BVDV biotypes, demonstrating the integrality of the N^{pro} N-terminal structure is essential in the catalytic activity of IFN-α/β inhibition (33).

N^{pro} induces proteasome degradation of IRF3

Overview of IRF3

The IRF family has been reported to have 10 members, namely IRF1-IRF9 and virus IRF (v-IRF). IRF3, a principal transcription factor, is significant in the antiviral immune response (34). IRF3 is highly homologous to IRF7. Both of them regulate the type I IFN synthesis, but play different roles in the innate immune response. IRF3 is critical for early induction of IFN expression in most cells post-viral infection; IRF7, which induces both IFNα and IFNβ expression, has functions in the antiviral activity of IFN in a later stage. In contrast, IRF3 can induce IFNβ gene expression, but not other IFNα expression except IFNα4 (35). Upon viral infection, a series of cellular pathways are activated subsequently to promote the translocation of phosphorylated IRF3 or IRF7 into the nucleus and initiate the transcription of type I interferon genes by attaching to IFN-α/β promoters (36).

N^{pro} mediates ubiquitination and proteasomal degradation of IRF3

By luciferase reporter gene experiment, La Rocca et al. found that CSFV-infected cells could inhibit IRF3 gene transcription. The use of cell lines expressing CSFV N^{pro} confirmed that the N^{pro} protein reduced the expression of IRF3, suggesting that this single viral protein specific to the pestiviruses can inhibit interferon production in the innate immune response to the virus (37) (Figure 1). Hilton et al. reported that NCP-BVDV (pe515) infection could induce the translocation of a small amount of IRF-3 from the cytoplasm to the nucleus at the early stage of infection. In addition, most IRF3 in the cytoplasm was degraded by the ubiquitination-proteasome pathway mediated by the N^{pro} protein (27). Similar to the NCP-BVDV virus, CP-BVDV (NADL strain) does not induce interferon response after infection and blocks interferon-stimulating genes induced by paramyxovirus infection, resulting in a significant decrease in IRF3 expression. However, the IRF3 repression activity is considered independent of the protease activity of N^{pro}. Further studies revealed that N^{pro} could interact with IRF3 before its phosphorylation-induced activation, leading to the ubiquitination and proteasomal degradation of IRF3 (38).

The N^{pro} protein of CSFV can also mediate the degradation of IRF3 after interaction with it. However, different from the research results of La Rocca et al., There are other studies reported that CSFV infection does not inhibit a cytomegalovirus (CMV) promoter-driven IRF3 expression. Furthermore, CSFV neither reduces the transcriptional activity of the IRF3 promoter nor affects the stability of IRF3 mRNA (39, 40).

Ubiquitin contains 76 amino acid residues and is highly conserved in all eukaryotes (41). Selective binding of linear ubiquitin to a protein is the initial signal for target protein degradation. Ubiquitin chains can be conjugated to the specific

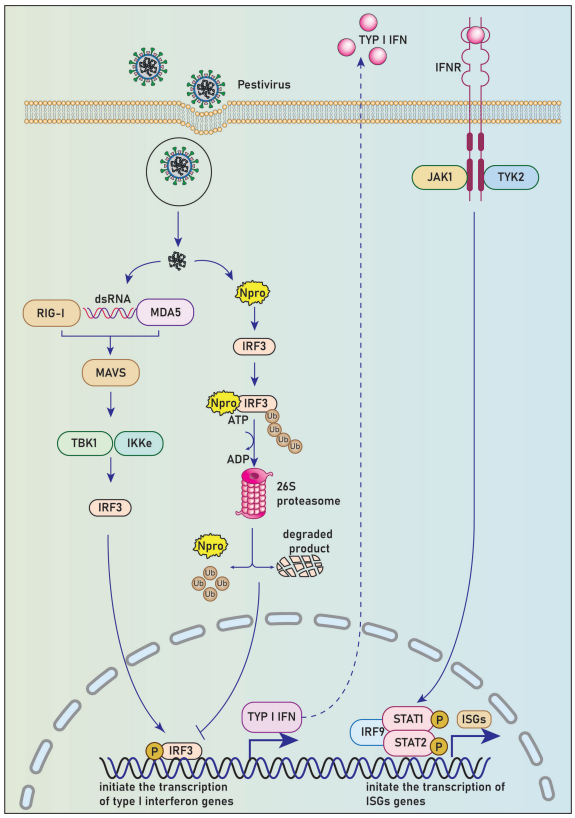

FIGURE 1
N^{pro} blocks the host's IFN-activated immune response by degradation of IRF3. Upon viral infection, pathogenic associated molecular patterns (PAMPs) are recognized by cellular pattern recognition receptors (PRRs). A series of cellular pathways were activated subsequently to promote the translocation of phosphorylated IRF3 into the nucleus and initiate the transcription of type I interferon genes by binding to IFN-α/β promoters. N^{pro} could interact with IRF3 before it's phosphorylation-induced activation, leading to the ubiquitination and proteasomal degradation of IRF-3 and subsequent inhibition of the type I interferon response.

protein substrate through an isopeptide bond between the ubiquitin C-terminal glycine residues and the lysine residues in the substrate. Proteasome-dependent degradation of proteins mediated by ubiquitination regulates a variety of biological reactions in the body, including cell cycle, signaling, DNA repair, and apoptosis (42, 43).

The ubiquitin modification process requires successive events associated with three enzymes: an E1 ubiquitin-activating enzyme, an E2 ubiquitin-conjugating enzyme, and an E3 ubiquitin ligase. Ubiquitin is first connected to the catalytic cysteine residues of endogenous E1 protein by an intermediate thioester bond. It is then conveyed to an E2 conjugating enzyme through a trans-esterification reaction. Subsequently, E3 ubiquitin ligase transfers the activated ubiquitin from an E2 to substrates. Finally, the substrate labeled with ubiquitin is delivered to the 26S proteasome for degradation (44). Once the E1 ubiquitin-activating enzyme was thermal inactivated, the degradation activity of IRF3 mediated by the N^{pro} protein of CP-BVDV was lost (39), indicating that the E1 ubiquitin-activating enzyme is

involved in the N^{pro} protein-mediated ubiquitin modification and degradation of IRF3.

Besides contributing to the antiviral immune response, IRF3 participates in the control of the cell cycle, apoptosis, and tumor suppression as well (45). When cells are infected with Sendai virus or stimulated by double-stranded RNA, IRF3 can bind to cytoplasmic Bax *via* its BH3 region and transfer Bax to mitochondria to activate apoptosis. It has been shown that wild-type N^{pro} could restrain apoptosis signals induced by astrosporin, interferon, double-stranded RNA, sodium arsenate, and hydrogen peroxide, which was mainly achieved by the degradation of IRF3 protein. In addition, the N^{pro} protein can inhibit the Bax-dependent apoptosis pathway by inhibiting mitochondrial lysis and Bax redistribution through interaction with the mitochondrial lumen. Moreover, the N^{pro} protein could rapidly localize to ubiquitin-containing peroxisome. Thus, the N^{pro} protein may bind to IRF3 and degrade it by transporting it to ubiquitin-containing peroxisome (46).

Peptide-prolyl isomerase (Pin1), Ro52 (TRIM21), RBCC protein interacting with PKC1 (RBCK1), RTA-associated ubiquitin ligase (RAUL), Tripartite motif 21 (TRIM21), Forkhead transcription factors of the O class (FOXO1), Casitas B-lineage lymphoma (c-Cbl) have been suggested as E3 ligases to invoke ubiquitination and subsequent degradation of IRF3 in the cytoplasm, thus inhibiting the production of type I IFN (47–51). However, it is unclear which E3 ubiquitin ligase contributes to the ubiquitination degradation of IRF3 mediated by the N^{pro} protein. It is worthy of further exploration whether N^{pro} has crosstalk with these E3 ligases or molecules to regulate the ubiquitination and subsequent degradation of IRF3.

Currently, the N^{pro} binding site on IRF3 is unclear. It has been revealed that N^{pro} can interact with IRF3 directly and forms a soluble 1:1 complex by utilizing recombinant N^{pro} and IRF3 proteins. This interaction requires the complete IRF3 protein rather than any of the single domains, the DBD in N-terminal or the IAD in C-terminal (52). It has been also shown in a previous mammalian two-hybrid analysis that the association of N^{pro} with IRF3 needs both the DBD and the IAD of IRF3 (53). However, the exact arrangement of DBD and the IAD in the IRF3 monomer and dimer is still unknown (35, 54, 55). As the ~60-amino-acid linker region between the two domains is somewhat helical but not structured in the absence of either DBD or IAD (56). The intact linker is thus suggested to be involved in N^{pro} binding (52). N^{pro} has been shown to interact with the IRF3 monomer and phosphomimetic dimer, indicating that the N^{pro} binding site on IRF3 contains areas not affected by the phosphorylation and subsequent activation status of IRF3 (52). N^{pro} can also interact with IRF3 in the complex with its transcriptional cofactor, the CREB-binding protein (CBP). Therefore, the contact surface in the IRF3 dimer and CBP binding site is not required for N^{pro} binding (52).

BVDV N^{pro} protein has been shown to degrade IRF3 in the cytoplasm, whereas IRF3 in the nucleus is resistant to this degradation (26). The influence of cellular localization of N^{pro} on IRF3 degradation is unclear. A recombinant virus vSMS-IRF3 was constructed by inserting the IRF3 gene sequence between the 13th and 14th amino acid sites of the N^{pro} protein of the highly virulent CSFV Shimen strain by Li et, al (57). The fusion protein of IRF3-N^{pro} expressed by the recombinant virus only located in the cytoplasm and vSMS-IRF3 was significantly attenuated. Pigs inoculated with the recombinant virus were all resistant to the lethal CSFV challenge, but the parent virus showed a typical virulent phenotype (57). Therefore, it was suggested that the nuclear localization of N^{pro} is essential to the replication and virulence of CSFV (57).

However, a previous study showed that any mutants of L8P, E22L, and H49V in N^{pro} could abolish its IFN-α/β antagonistic activity, revealing that the 49 amino acids in the N-terminal of N^{pro} protein are necessary to type-I IFN suppression (33). Based on this, we speculate that the insertion of the IRF3 gene into the N^{pro} gene may eliminate its function of IRF3 degradation. Thus, the attenuation of vSM-IRF3 may be caused by the loss of the IFN-α/β antagonistic activity of IRF3-N^{pro} rather than its cytoplasmic localization. Moreover, N^{pro} was observed in the nucleus in a diffuse manner (58, 59), and could bind to IRF3 dimer or the IRF3 dimer in the complex with CBP (52). Therefore, the insertion of IRF3 into N^{pro} could also affect the cellular diffusion of the IRF3-N^{pro} fusion protein, leading to its accumulation in the cytoplasm. The effects of cellular localization of N^{pro} protein on CSFV virulence need further study.

Whether N^{pro} protein is the main determinant of the virulence of pestiviruses is still a controversial topic. Continuous passage of CSFV attenuated vaccine strain GPE- in pigs restored its virulence, but did not regain the ability of its N^{pro} to degrade IRF3 (60). However, strains containing the N136D mutation in N^{pro} restored the IRF3 degradation activity and IFN-α/β antagonistic ability *in vitro* as well as pathogenicity *in vivo*. These results demonstrate that the N^{pro} protein makes a decisive contribution to the virulence of pestiviruses, but there are other factors that can regulate the virulence of pestiviruses.

The N^{pro} protein of CSFV can also interact with IRF7 in plasmacytoid dendritic cells, down-regulating the expression level of IRF7 protein and further inhibiting the IFN-α expression. Whereas, the molecular mechanism of N^{pro} inhibiting the expression of IRF7 protein is still unclear. It is certain, however, that this antagonism does not involve either polyubiquitination or protease degradation pathways (53).

The zinc atom binding motif of N^{pro} is critical for the degradation of IRF3

Analysis by sequence alignment revealed that the C-terminal half of the N^{pro} protein contains a conserved metal binding TRASH motif composed of Cys-X21-Cys-X3-Cys (where X is any amino acid). TRASH motif commonly exists in proteins associated with heavy metal recognizing, resistance, transcription regulation, cation transportation, and hydrogenase. Inductively coupled plasma–mass spectrometry (ICP-MS) assay indicated that each N^{pro} protein molecule could coordinate a single zinc atom. Site-directed mutagenesis studies revealed that the zinc-binding sites of N^{pro} protein include Cys112, Cys134, Cys138, and probably Asp136.

These zinc-binding site mutations lead to the deficit of N^{pro} protein-mediated IRF3 degradation in cells inoculated with CSFV, suggesting that the zinc-binding capacity of N^{pro} protein is critical for virus-mediated IRF3 degradation (61). In addition, the zinc-binding domain of N^{pro} is critical for its protein stability and its interaction with IRF7 (62).

N^{pro} interacts extensively with host proteins

Proteins in cytoplasmic ribonucleoprotein particles

Recently, pull-down combined mass spectrometry showed that N^{pro} binds to more than 55 kinds of proteins, mainly RNA helicase A (DHX9), Y-box binding protein (YBX1), DDX3, DDX5, IGF2BP1, eIF3, and other ribosomal proteins, multiple myeloma tumor protein 2, interleukin enhancer binding factor 3 (IEBP3) guanine nucleotide-binding protein 3, and polyadenylate-binding protein 1 (PABP-1). Many of the interacting proteins are components in cytoplasmic ribonucleoprotein particles (RNPs). They play roles in regulating the translation of mRNA and could be recruited into stress granules to regulate the translational initiation rate or mRNA degradation (63). The assembled stress granules might control the proliferation of viruses and some viruses could in turn hinder their formation or even disassemble them (64). It has been suggested that N^{pro} could redistribute to stress granules after interaction with YBX1 through its TRASH domain. When exposed to oxidative stress, cells expressing N^{pro} alone assembled stress granules and N^{pro} colocalized with stress granule proteins. In contrast, the formation of stress granules in NCP-BVDV-infected cells was inhibited, indicating that this inhibition was not caused by N^{pro} binding to ribonucleoproteins (63). Thereby, N^{pro} may not influence the function and location of ribonucleoproteins although it could be localized to stress granules by interacting with these host proteins. As some interacting proteins of N^{pro} are also involved in RISC function during RNA silencing, further studies were conducted to determine whether N^{pro} affected RNA interference (RNAi). However, the outcomes suggested the expression of N^{pro} had no influence on RNAi silencing activity (65).

S100A9

S100A9, one of the danger-associated molecular patterns (DAMPs) proteins, is vital in the innate immune system and always accumulates in large amounts in ectocytic space during inflammation responses (66). Additionally, the S100A9 could effectively trigger inflammatory responses through Toll-like receptor 4 (TLR4) as a homodimer (67–73). In the heterodimer with S100A8, the S100A9 exerts antimicrobial activity by inhibiting microbes from acquiring nutrients (74–79). Yet, the function of S100A9 in virus infection is unclear. It has been shown that the amount of S100A9 was increased after treatment with poly (I: C), which is an analog of viral dsRNA (80). The expression of S100A9 is also highly enhanced in human papillomavirus-associated dysplastic tissues (81) and BKV-infected recipients post-kidney transplantation (82). Likewise, high levels of S100A9 expression were observed in lungs and livers in autopsied subjects with COVID-19 and pre-existing chronic liver disease (83). Darweesh et al. reported that NCP-BVDV2a 1373 N^{pro} protein has a strong interaction with cellular S100A9 protein. Furthermore, the N^{pro} protein enhances the replication of BVDV in infected cells by inhibiting S100A9 activity in epidermal cells (84).

TRIM56

Currently, the TRIM family consists of more than 60 members and could be divided into 11 subfamilies (85). Although their exact functions are still unclear, the TRIM proteins contribute to a large variety of biological activities, such as cell proliferation, development, differentiation, immunity, apoptosis, and innate immune response to pathogens (86–90). As a protein of the fifth subfamily of TRIM, TRIM56 is expressed in the cytoplasm after type I interferon stimulation (91, 92). A previous study has identified TRIM56 as a cellular protein that associates with BVDV N^{pro} through its C-terminal portion. Although TRIM56 has RING-dependent E3 ubiquitin ligase function, it is not involved in N^{pro}-mediated IRF3 degradation nor degrade N^{pro}. Furthermore, it was suggested that both ectopically and endogenously expressed TRIM56 contribute to impaired replication of BVDV due to its E3 ligase activity. In contrast, the downregulation of TRIM56 expression largely improved BVDV proliferation. Moreover, it is the integrity of the TRIM56 C-terminal, rather than the TRIM56-N^{pro} association that contributes to TRIM56's antiviral activity (91).

pIκBα

To discover host proteins that could bind to N^{pro} of CSFV, Doceul, et al. (58) conducted a yeast two-hybrid assay of a human library. It was revealed that N^{pro} had a direct association with IκBα, which is responsible for apoptosis regulation, the immune reaction, and IFN expression. As an inhibitor of NF-κB, IκBα is also a prime target for immune evasion strategies developed by many viruses (93–95). Further studies suggested the interaction of N^{pro} with aa 213-317 of the C-terminus of pIκBα (pig IκBα) (58), which also contact with NF-κB through the domain between aa214-280 (96, 97). This suggests that N^{pro} competes with NF-κB for unbound pIκBα (58).

Before stimulation, NF-κB remains in an inactive state in the cytoplasm due to its interaction with IκBα, which covers the nuclear localization signals of NF-κB. It has been reported that NF-κB/IκBα complex could be triggered by phosphorylation upon various stimulation, such as viruses and bacteria (98–101). In this case, IκBα is phosphorylated at Ser32 and Ser36 by the IKKβ subunit following the activation of the IKK complex (IKKα/IKKβ/IKKγ). Then, the E3 ubiquitin ligase complex, SCFβ–TRCP, ubiquitinates IκBα and targets it for degradation by the 26S proteasome, resulting in the release of NF-κB for nuclear

translocation (102–105). However, the activated NF-κB initiates regeneration of IκBα, which detaches NF-κB from DNA after its translocation to the nucleus, and conveys NF-κB to the cytoplasm in a nuclear export sequence-dependent process (106–108). Tumor necrosis factor-alpha receptor (TNFR) activated by binding with TNF-α is one of the principal receptors that mediate NF-κB activation (109).

It's reasonable to speculate that under stimulation of TNF-α, new synthesized cytoplasmic IκBα induced by NF-κB activation could bind to N^{pro} in cells expressing N^{pro} proteins. Therefore, limited unbound IκBα translocate into the nucleus, and thus the suppression of NF-κB DNA-binding activity by IκBα should be restricted (Figure 2). It has been suggested that HIV-1 tat transactivator could activate NF-κB by interacting with IκBα and by inhibiting the repressor from binding to the NF-κB complex (110). However, the ability of the p65 subunit of NF-κB to bind the promoter sequence in CSFV-infected PK15 cells was not affected by functional analysis (111). Furthermore, after TNF-α stimulation of N^{pro} stable expression PK15 cells, a high concentration of pIκBα was observed in the nucleus, but the function and expression of NF-κB did not change significantly (58). Therefore, TNF-α may stimulate the rapid resynthesis and massive nuclear translocation of pIκBα, many of which are bound to N^{pro} and does not affect the action of NF-κB thus resulting in the accumulation of a large amount of pIκBα in the nucleus. However, the effect of N^{pro} binding to pIκBα on the activity of NF-κB in the nucleus and cytoplasm is worth further investigation.

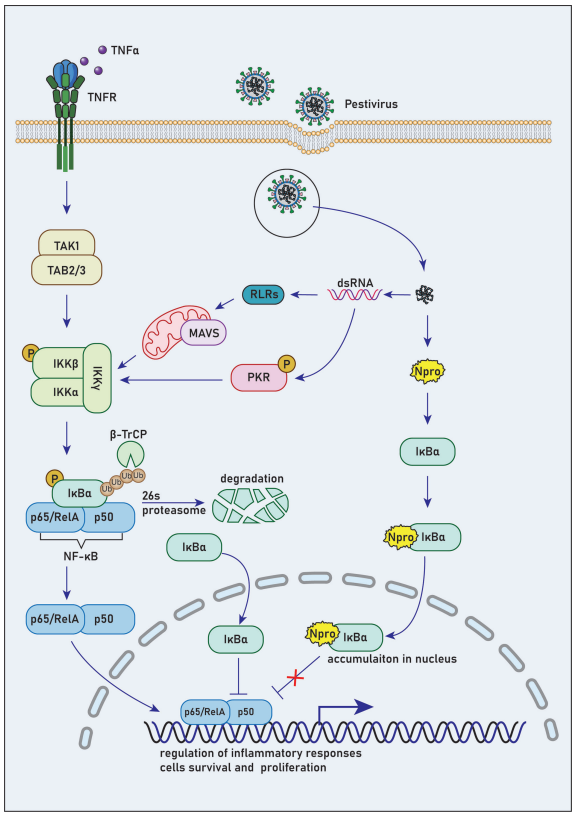

FIGURE 2
N competes with NF-κB to bind with IκBα. Prior to stimulation, NF-κB remains an inactive state in the cytoplasm due to its interaction with IκBα, which masks the unclear localization signals of NF-κB. NF-κB/IκBα complex is activated by phosphorylation in response to various stimuli, such as viral and bacterial pathogens. In this case, IκBα is phosphorylated at Ser32 and Ser36 by the IKKβ subunit following the activation of IKK complex. Then, the E3 ubiquitin ligase complex, SCFβ–TRCP, ubiquitinates IκBα and targets it for degradation by the 26S proteasome, leading to the release of NF-κB for nuclear translocation. However, NF-κB activation induces rapid resynthesis of IκBα, which translocates to the nucleus, dissociates NF-κB from DNA and transports NF-κB to the cytoplasm in a nuclear export sequence-dependent process.

HAX-1

HS-1-associated protein X-1 (HAX-1), a protein of approximately 35-kDa, is universally synthesized in murine and human tissues (112, 113), especially in the mitochondria (114). Primarily, it was shown to play a role in the control of apoptosis or programmed cell death (114). A recent study has indicated that HAX-1 may also contribute to the control of calcium homeostasis and cell survival in cardiac tissue (115). It was found that the protein could bind to the N^{pro} protein of CSFV by yeast two-hybrid, and the interaction between the two proteins was further confirmed by co-immunoprecipitation assay (116). During CSFV infection, the expression level of HAX-1 did not change significantly, indicating that N^{pro} interacting with HAX-1 could not degrade it. However, in the cells co-transfected with HAX-1 and N^{pro}, the two proteins were significantly transported to the endoplasmic reticulum, and the N^{pro} protein in the nucleus was significantly reduced (116). Significantly, the relocation of HAX-1 to the ER in the presence of phospholamban (PLN), a crucial regulator of Ca^{2+} homeostasis and contractility in the heart, correlated with stronger resistance to apoptosis (117). Therefore, it could be hypothesized that during CSFV infection, N^{pro} protein may bind to HAX-1 in the cytoplasm and transport it to ER to enhance the tolerance of infected cells to apoptosis. Thus, less N^{pro} protein synthesized in the cytoplasm diffuses into the nucleus. However, further research is needed to confirm this hypothesis.

PCBPs

As members of the K homology (KH) domain superfamily, Poly (C)-binding proteins (PCBPs) are known for their interaction with both RNA and DNA specifically. It has been suggested that the KH domain superfamily proteins associate with the stability of cellular mRNAs (118–120), regulate their translation (121–125), and also involve in the host antiviral reaction (126, 127). Among the PCBPs, PCBP1 is an ssDNA-binding protein that contributes to the transcription of the neuronal μ-opioid receptor gene (122). Cytoplasmic and nuclear expression of CBP1 been demonstrated (128). Li et al. found that PCBP1 protein could interact with N^{pro} protein. Knocking down the expression of PCBP1 could inhibit the replication of CSFV, while overexpression of PCBP1 could promote the reproduction of CSFV. PCBP1 inhibits the IFN signaling pathway by degrading MAVS and enhances the replication of CSFV genomic RNA, thus promoting the proliferation of CSFV

(129). However, whether the interaction between PCBP1 and N^{pro} has any effect on their cellular localization or CSFV replication needs further exploration.

Response of N^{pro} protein to type-3 interferon

N^{pro} has also been suggested to inhibit the innate immune reaction by restricting type III IFNs (IFN-λs). Although many similarities exist between types I and III IFNs in the signaling networks and expression processes (130, 131), a host of distinctions are evident. Different from type I IFNs induction which needs all IFN enhanceosome elements, type III IFNs are induced independent of IRFs or NF-κB (132). Besides, unlike the ubiquitous receptors for type I IFNs, type III IFN receptors are mainly expressed in mucosal epithelia (133). Thus, type III IFNs are considered to be crucial for immune responses in the respiratory and gastrointestinal tracts (134). As IRFs and NF-κB are important regulators for type III IFNs, IRF1 may have a specific function in this process (135). N^{pro}-deficient CSFV has been shown to significantly enhance the transcription level of IFN-λs 24h post-infection. In contrast, overexpression of N^{pro} significantly reduced the IFN-λs transcription and IFN-λ3 promoter activity. Moreover, in poly (I: C)-treated IPEC-J2 cells, overexpression of N^{pro} or infection with wtCSFV not only down-regulated the production and the promoter activity of IRF1 significantly but also inhibited IRF1 nuclear translocation. This suggests that N^{pro} could restrict type III IFNs response by preventing the production and nuclear translocation of IRF1 (134).

Conclusion

Pestiviruses are counted among the highly destructive and economically important pathogens, which have evolved many strategies to evade elimination by the host antiviral immune response. Studies emphasizing various molecular techniques undertaken during the last two decades have elucidated at least two viral proteins (N^{pro} and E^{rns} RNase) as IFN antagonists of pestiviruses. Unlike repression of the interferon response *via* the effect of N^{pro} on IRF3, the secreted E^{rns} protein distributed by the bloodstream could be taken up by cells, specifically PDCs, and degrade pestiviral RNA. Therefore, E^{rns} hinders IFN production induced by the extracellular synthetic or viral ss- or dsRNAs (136–138). Thus, we conclude that pestiviruses evade the host's IFN-activated innate antiviral immune response in a complex way to establish and maintain a persistent infection status. This article mainly reviewed the progress of innate immune evasion mediated by N^{pro} of pestiviruses. while its detailed process concerning blocking the IFN-1 response remains obscure. Further understanding of the approaches employed by viruses of this genus to control immune response to escape the innate immune system is in need, which will eventually contribute to developing effective strategies to prevent and control pestivirus infection.

Author contributions

Writing-original draft preparation: SW and XLi. Writing review: YS, XLv, and KL. Figures: SW. Supervision: JZ. Funding acquisition: SW, YS, JR, and JZ. All authors contributed to the article and approved the submitted version.

Funding

This work was financially supported by the Young Scientific and Technological Talents in Inner Mongolia (No. NJYT23095, NJYT22053). The Natural Science Foundation of Inner Mongolia (No. 2022LHQN03009). Doctoral Funding of Inner Mongolia Minzu University (No. BS584, BS583), Key Research and Development Program in Inner Mongolia Autonomous Region (No. 2021ZD001301, 2019ZD006). Open Funding Project of Brucellosis Prevention and Treatment Engineering Research Center of Inner Mongolia Autonomous Region (No. MDK2021078).

Conflict of interest

The authors declare that the research was conducted in the absence of any commercial or financial relationships that could be construed as a potential conflict of interest.

Publisher's note

References

1. Houe H. Economic impact of BVDV infection in dairies. *Biologicals* (2003) 31:137–43. doi: 10.1016/s1045-1056(03)00030-7

2. Moennig V, Becher P. Pestivirus control programs: How far have we come and where are we going? *Anim Health Res Rev* (2015) 16:83–7. doi: 10.1017/s1466252315000092

3. Smith DB, Meyers G, Bukh J, Gould EA, Monath T, Scott Muerhoff A, et al. Proposed revision to the taxonomy of the genus pestivirus, family flaviviridae. *J Gen Virol* (2017) 98:2106–12. doi: 10.1099/jgv.0.000873

4. Schweizer M, Peterhans E. Pestiviruses. *Annu Rev Anim Biosci* (2014) 2:141–63. doi: 10.1146/annurev-animal-022513-114209

5. Nettleton PF, Gilray JA, Russo P, Dlissi E. Border disease of sheep and goats. *Vet Res* (1998) 29:327–40.

6. Potgieter LN. Bovine respiratory tract disease caused by bovine viral diarrhea virus. *Vet Clin North Am Food Anim Pract* (1997) 13:471–81. doi: 10.1016/s0749-0720(15)30309-1

7. Lanyon SR, Hill FI, Reichel MP, Brownlie J. Bovine viral diarrhoea: Pathogenesis and diagnosis. *Vet J* (2014) 199:201–9. doi: 10.1016/j.tvjl.2013.07.024

8. Postel A, Hansmann F, Baechlein C, Fischer N, Alawi M, Grundhoff A, et al. Presence of atypical porcine pestivirus (APPV) genomes in newborn piglets correlates with congenital tremor. *Sci Rep* (2016) 6:27735. doi: 10.1038/srep27735

9. Postel A, Schmeiser S, Oguzoglu TC, Indenbirken D, Alawi M, Fischer N, et al. Close relationship of ruminant pestiviruses and classical swine fever virus. *Emerg Infect Dis* (2015) 21:668–72. doi: 10.3201/eid2104.141441

10. Hause BM, Collin EA, Peddireddi L, Yuan F, Chen Z, Hesse RA, et al. Discovery of a novel putative atypical porcine pestivirus in pigs in the USA. *J Gen Virol* (2015) 96:2994–8. doi: 10.1099/jgv.0.000251

11. Kirkland PD, Frost MJ, Finlaison DS, King KR, Ridpath JF, Gu X. Identification of a novel virus in pigs–bungowannah virus: A possible new species of pestivirus. *Virus Res* (2007) 129:26–34. doi: 10.1016/j.virusres.2007.05.002

12. Liu L, Kampa J, Belák S, Baule C. Virus recovery and full-length sequence analysis of atypical bovine pestivirus Th/04_KhonKaen. *Vet Microbiol* (2009) 138:62–8. doi: 10.1016/j.vetmic.2009.03.006

13. Schirrmeier H, Strebelow G, Depner K, Hoffmann B, Beer M. Genetic and antigenic characterization of an atypical pestivirus isolate, a putative member of a novel pestivirus species. *J Gen Virol* (2004) 85:3647–52. doi: 10.1099/vir.0.80238-0

14. Shi K, Xie S, Sun W, Liu H, Zhao J, Yin Y, et al. Evolution and genetic diversity of atypical porcine pestivirus (APPV) from piglets with congenital tremor in guangxi province, southern China. *Vet Med Sci* (2021) 7:714–23. doi: 10.1002/vms3.407

15. Şevik M. Genomic characterization of pestiviruses isolated from bovine, ovine and caprine foetuses in Turkey: A potentially new genotype of pestivirus I species. *Transbound Emerg Dis* (2021) 68:417–26. doi: 10.1111/tbed.13691

16. Chen M, Liu M, Liu S, Shang Y. HoBi-like pestivirus infection leads to bovine death and severe respiratory disease in China. *Transbound Emerg Dis* (2021) 68:1069–74. doi: 10.1111/tbed.13832

17. Pan S, Yan Y, Shi K, Wang M, Mou C, Chen Z. Molecular characterization of two novel atypical porcine pestivirus (APPV) strains from piglets with congenital tremor in China. *Transbound Emerg Dis* (2019) 66:35–42. doi: 10.1111/tbed.13029

18. Becher P, Orlich M, Shannon AD, Horner G, König M, Thiel HJ. Phylogenetic analysis of pestiviruses from domestic and wild ruminants. *J Gen Virol* (1997) 78(Pt 6):1357–66. doi: 10.1099/0022-1317-78-6-1357

19. Avalos-Ramirez R, Orlich M, Thiel HJ, Becher P. Evidence for the presence of two novel pestivirus species. *Virology* (2001) 286:456–65. doi: 10.1006/viro.2001.1001

20. Vilcek S, Ridpath JF, Van Campen H, Cavender JL, Warg J. Characterization of a novel pestivirus originating from a pronghorn antelope. *Virus Res* (2005) 108:187–93. doi: 10.1016/j.virusres.2004.09.010

21. Neill JD, Ridpath JF, Fischer N, Grundhoff A, Postel A, Becher P. Complete genome sequence of pronghorn virus, a pestivirus. *Genome Announc* (2014) 2(3):e00575-14. doi: 10.1128/genomeA.00575-14

22. Tao J, Liao J, Wang Y, Zhang X, Wang J, Zhu G. Bovine viral diarrhea virus (BVDV) infections in pigs. *Vet Microbiol* (2013) 165:185–9. doi: 10.1016/j.vetmic.2013.03.010

23. Tautz N, Tews BA, Meyers G. The molecular biology of pestiviruses. *Adv Virus Res* (2015) 93:47–160. doi: 10.1016/bs.aivir.2015.03.002

24. Tratschin JD, Moser C, Ruggli N, Hofmann MA. Classical swine fever virus leader proteinase npro is not required for viral replication in cell culture. *J Virol* (1998) 72:7681–4. doi: 10.1128/jvi.72.9.7681-7684.1998

25. Schweizer M, Peterhans E. Noncytopathic bovine viral diarrhea virus inhibits double-stranded RNA-induced apoptosis and interferon synthesis. *J Virol* (2001) 75:4692–8. doi: 10.1128/jvi.75.10.4692-4698.2001

26. Hilton L, Moganeradj K, Zhang G, Chen YH, Randall RE, McCauley JW, et al. The NPro product of bovine viral diarrhea virus inhibits DNA binding by interferon regulatory factor 3 and targets it for proteasomal degradation. *J Virol* (2006) 80:11723–32. doi: 10.1128/jvi.01145-06

27. Tao J, Liao J, Wang J, Zhang X, Zhang Q, Zhu L, et al. Pig BVDV-2 non-structural protein (N(pro)) links to cellular antiviral response *in vitro*. *Virus Genes* (2017) 53:233–9. doi: 10.1007/s11262-016-1410-2

28. Ruggli N, Tratschin JD, Schweizer M, McCullough KC, Hofmann MA, Summerfield A. Classical swine fever virus interferes with cellular antiviral defense: Evidence for a novel function of n(pro). *J Virol* (2003) 77:7645–54. doi: 10.1128/jvi.77.13.7645-7654.2003

29. Ruggli N, Bird BH, Liu L, Bauhofer O, Tratschin JD, Hofmann MA. N(pro) of classical swine fever virus is an antagonist of double-stranded RNA-mediated apoptosis and IFN-alpha/beta induction. *Virology* (2005) 340:265–76. doi: 10.1016/j.virol.2005.06.033

30. Bauhofer O, Summerfield A, McCullough KC, Ruggli N. Role of double-stranded RNA and npro of classical swine fever virus in the activation of monocyte-derived dendritic cells. *Virology* (2005) 343:93–105. doi: 10.1016/j.virol.2005.08.016

31. Mou C, Pan S, Wu H, Chen Z. Disruption of interferon-β production by the n (pro) of atypical porcine pestivirus. *Virulence* (2021) 12:654–65. doi: 10.1080/21505594.2021.1880773

32. Richter M, König P, Reimann I, Beer M. N pro of bungowannah virus exhibits the same antagonistic function in the IFN induction pathway than that of other classical pestiviruses. *Vet Microbiol* (2014) 168:340–7. doi: 10.1016/j.vetmic.2013.11.038

33. Gil LH, Ansari IH, Vassilev V, Liang D, Lai VC, Zhong W, et al. The amino-terminal domain of bovine viral diarrhea virus npro protein is necessary for alpha/beta interferon antagonism. *J Virol* (2006) 80:900–11. doi: 10.1128/jvi.80.2.900-911.2006

34. Hiscott J. Triggering the innate antiviral response through IRF-3 activation. *J Biol Chem* (2007) 282:15325–9. doi: 10.1074/jbc.R700002200

35. Qin BY, Liu C, Lam SS, Srinath H, Delston R, Correia JJ, et al. Crystal structure of IRF-3 reveals mechanism of autoinhibition and virus-induced phosphoactivation. *Nat Struct Biol* (2003) 10:913–21. doi: 10.1038/nsb1002

36. Honda K, Taniguchi T. IRFs: Master regulators of signalling by toll-like receptors and cytosolic pattern-recognition receptors. *Nat Rev Immunol* (2006) 6:644–58. doi: 10.1038/nri1900

37. Baigent SJ, Goodbourn S, McCauley JW. Differential activation of interferon regulatory factors-3 and -7 by non-cytopathogenic and cytopathogenic bovine viral diarrhoea virus. *Vet Immunol Immunopathol* (2004) 100:135–44. doi: 10.1016/j.vetimm.2004.04.003

38. La Rocca SA, Herbert RJ, Crooke H, Drew TW, Wileman TE, Powell PP. Loss of interferon regulatory factor 3 in cells infected with classical swine fever virus involves the n-terminal protease, npro. *J Virol* (2005) 79:7239–47. doi: 10.1128/jvi.79.11.7239-7247.2005

39. Chen Z, Rijnbrand R, Jangra RK, Devaraj SG, Qu L, Ma Y, et al. Ubiquitination and proteasomal degradation of interferon regulatory factor-3 induced by npro from a cytopathic bovine viral diarrhea virus. *Virology* (2007) 366:277–92. doi: 10.1016/j.virol.2007.04.023

40. Bauhofer O, Summerfield A, Sakoda Y, Tratschin JD, Hofmann MA, Ruggli N. Classical swine fever virus npro interacts with interferon regulatory factor 3 and induces its proteasomal degradation. *J Virol* (2007) 81:3087–96. doi: 10.1128/jvi.02032-06

41. Seago J, Hilton L, Reid E, Doceul V, Jeyatheesan J, Moganeradj K, et al. The npro product of classical swine fever virus and bovine viral diarrhea virus uses a conserved mechanism to target interferon regulatory factor-3. *J Gen Virol* (2007) 88:3002–6. doi: 10.1099/vir.0.82934-0

42. Nandi D, Tahiliani P, Kumar A, Chandu D. The ubiquitin-proteasome system. *J Biosci* (2006) 31:137–55. doi: 10.1007/bf02705243

43. Wang J, Maldonado MA. The ubiquitin-proteasome system and its role in inflammatory and autoimmune diseases. *Cell Mol Immunol* (2006) 3:255–61.

44. Liu YC. Ubiquitin ligases and the immune response. *Annu Rev Immunol* (2004) 22:81–127. doi: 10.1146/annurev.immunol.22.012703.104813

45. Honda K, Takaoka A, Taniguchi T. Type I interferon [corrected] gene induction by the interferon regulatory factor family of transcription factors. *Immunity* (2006) 25:349–60. doi: 10.1016/j.immuni.2006.08.009

46. Jefferson M, Whelband M, Mohorianu I, Powell PP. The pestivirus n terminal protease n(pro) redistributes to mitochondria and peroxisomes suggesting new sites for regulation of IRF3 by n(pro.). *PloS One* (2014) 9:e88838. doi: 10.1371/journal.pone.0088838

47. Yu Y, Hayward GS. The ubiquitin E3 ligase RAUL negatively regulates type i interferon through ubiquitination of the transcription factors IRF7 and IRF3. *Immunity* (2010) 33:863–77. doi: 10.1016/j.immuni.2010.11.027

48. Lei CQ, Zhang Y, Xia T, Jiang LQ, Zhong B, Shu HB. FoxO1 negatively regulates cellular antiviral response by promoting degradation of IRF3. *J Biol Chem* (2013) 288:12596–604. doi: 10.1074/jbc.M112.444794

49. Zhao X, Zhu H, Yu J, Li H, Ge J, Chen W. C-cbl-mediated ubiquitination of IRF3 negatively regulates IFN-β production and cellular antiviral response. *Cell Signal* (2016) 28:1683–93. doi: 10.1016/j.cellsig.2016.08.002

50. Higgs R, NG J, Ben Larbi N, Breen EP, Fitzgerald KA, Jefferies CA. The E3 ubiquitin ligase Ro52 negatively regulates IFN-beta production post-pathogen recognition by polyubiquitin-mediated degradation of IRF3. *J Immunol* (2008) 181:1780–6. doi: 10.4049/jimmunol.181.3.1780

51. Saitoh T, Tun-Kyi A, Ryo A, Yamamoto M, Finn G, Fujita T, et al. Negative regulation of interferon-regulatory factor 3-dependent innate antiviral response by the prolyl isomerase Pin1. *Nat Immunol* (2006) 7:598–605. doi: 10.1038/ni1347

52. Gottipati K, Holthauzen LM, Ruggli N, Choi KH. Pestivirus npro directly interacts with interferon regulatory factor 3 monomer and dimer. *J Virol* (2016) 90:7740–7. doi: 10.1128/jvi.00318-16

53. Fiebach AR, Guzylack-Piriou L, Python S, Summerfield A, Ruggli N. Classical swine fever virus n(pro) limits type I interferon induction in plasmacytoid dendritic cells by interacting with interferon regulatory factor 7. *J Virol* (2011) 85:8002–11. doi: 10.1128/jvi.00330-11

54. Takahasi K, Suzuki NN, Horiuchi M, Mori M, Suhara W, Okabe Y, et al. X-Ray crystal structure of IRF-3 and its functional implications. *Nat Struct Biol* (2003) 10:922–7. doi: 10.1038/nsb1001

55. Fujii Y, Shimizu T, Kusumoto M, Kyogoku Y, Taniguchi T, Hakoshima T. Crystal structure of an IRF-DNA complex reveals novel DNA recognition and cooperative binding to a tandem repeat of core sequences. *EMBO J* (1999) 18:5028–41. doi: 10.1093/emboj/18.18.5028

56. Shukla H, Vaitiekunas P, Majumdar AK, Dragan AI, Dimitriadis EK, Kotova S, et al. The linker of the interferon response factor 3 transcription factor is not unfolded. *Biochemistry* (2012) 51:6320–7. doi: 10.1021/bi300260s

57. Li Y, Shen L, Sun Y, Wang X, Li C, Huang J, et al. Effects of the nuclear localization of the n(pro) protein of classical swine fever virus on its virulence in pigs. *Vet Microbiol* (2014) 174:391–8. doi: 10.1016/j.vetmic.2014.09.027

58. Doceul V, Charleston B, Crooke H, Reid E, Powell PP, Seago J. The npro product of classical swine fever virus interacts with IkappaBalpha, the NF-kappaB inhibitor. *J Gen Virol* (2008) 89:1881–9. doi: 10.1099/vir.0.83643-0

59. Li Y, Shen L, Li C, Huang J, Zhao B, Sun Y, et al. Visualization of the npro protein in living cells using biarsenically labeling tetracysteine-tagged classical swine fever virus. *Virus Res* (2014) 189:67–74. doi: 10.1016/j.virusres.2014.04.018

60. Tamura T, Nagashima N, Ruggli N, Summerfield A, Kida H, Sakoda Y. Npro of classical swine fever virus contributes to pathogenicity in pigs by preventing type I interferon induction at local replication sites. *Vet Res* (2014) 45:47. doi: 10.1186/1297-9716-45-47

61. Szymanski MR, Fiebach AR, Tratschin JD, Gut M, Ramanujam VM, Gottipati K, et al. Zinc binding in pestivirus n(pro) is required for interferon regulatory factor 3 interaction and degradation. *J Mol Biol* (2009) 391:438–49. doi: 10.1016/j.jmb.2009.06.040

62. Zögg T, Sponring M, Schindler S, Koll M, Schneider R, Brandstetter H, et al. Crystal structures of the viral protease npro imply distinct roles for the catalytic water in catalysis. *Structure* (2013) 21:929–38. doi: 10.1016/j.str.2013.04.003

63. Anderson P, Kedersha N. RNA Granules: Post-transcriptional and epigenetic modulators of gene expression. *Nat Rev Mol Cell Biol* (2009) 10:430–6. doi: 10.1038/nrm2694

64. Lloyd RE. How do viruses interact with stress-associated RNA granules? *PloS Pathog* (2012) 8:e1002741. doi: 10.1371/journal.ppat.1002741

65. Jefferson M, Donaszi-Ivanov A, Pollen S, Dalmay T, Saalbach G, Powell PP. Host factors that interact with the pestivirus n-terminal protease, npro, are components of the ribonucleoprotein complex. *J Virol* (2014) 88:10340–53. doi: 10.1128/jvi.00984-14

66. Harman JL, Loes AN, Warren GD, Heaphy MC, Lampi KJ, Harms MJ. Evolution of multifunctionality through a pleiotropic substitution in the innate immune protein S100A9. *Elife* (2020) 9:e54100. doi: 10.7554/eLife.54100

67. Vogl T, Gharibyan AL, Morozova-Roche LA. Pro-inflammatory S100A8 and S100A9 proteins: self-assembly into multifunctional native and amyloid complexes. *Int J Mol Sci* (2012) 13:2893–917. doi: 10.3390/ijms13032893

68. Källberg E, Vogl T, Liberg D, Olsson A, Björk P, Wikström P, et al. S100A9 interaction with TLR4 promotes tumor growth. *PloS One* (2012) 7:e34207. doi: 10.1371/journal.pone.0034207

69. Duan L, Wu R, Zhang X, Wang D, You Y, Zhang Y, et al. HBx-induced S100A9 in NF-κB dependent manner promotes growth and metastasis of hepatocellular carcinoma cells. *Cell Death Dis* (2018) 9:629. doi: 10.1038/s41419-018-0512-2

70. Schiopu A, Cotoi OS. S100A8 and S100A9: DAMPs at the crossroads between innate immunity, traditional risk factors, and cardiovascular disease. *Mediators Inflammation* (2013) 2013:828354. doi: 10.1155/2013/828354

71. Laouedj M, Tardif MR, Gil L, Raquil MA, Lachhab A, Pelletier M, et al. S100A9 induces differentiation of acute myeloid leukemia cells through TLR4. *Blood* (2017) 129:1980–90. doi: 10.1182/blood-2016-09-738005

72. He Z, Riva M, Björk P, Swärd K, Mörgelin M, Leanderson T, et al. CD14 is a Co-receptor for TLR4 in the S100A9-induced pro-inflammatory response in monocytes. *PloS One* (2016) 11:e0156377. doi: 10.1371/journal.pone.0156377

73. Lee NR, Park BS, Kim SY, Gu A, Kim DH, Lee JS, et al. Cytokine secreted by S100A9 *via* TLR4 in monocytes delays neutrophil apoptosis by inhibition of caspase 9/3 pathway. *Cytokine* (2016) 86:53–63. doi: 10.1016/j.cyto.2016.07.005

74. Hadley RC, Gu Y, Nolan EM. Initial biochemical and functional evaluation of murine calprotectin reveals Ca(II)-dependence and its ability to chelate multiple nutrient transition metal ions. *Biochemistry* (2018) 57:2846–56. doi: 10.1021/acs.biochem.8b00309

75. Damo SM, Kehl-Fie TE, Sugitani N, Holt ME, Rathi S, Murphy WJ, et al. Molecular basis for manganese sequestration by calprotectin and roles in the innate immune response to invading bacterial pathogens. *Proc Natl Acad Sci U.S.A.* (2013) 110:3841–6. doi: 10.1073/pnas.1220341110

76. Clark HL, Jhingran A, Sun Y, Vareechon C, de Jesus Carrion S, Skaar EP, et al. Zinc and manganese chelation by neutrophil S100A8/A9 (Calprotectin) limits extracellular aspergillus fumigatus hyphal growth and corneal infection. *J Immunol* (2016) 196:336–44. doi: 10.4049/jimmunol.1502037

77. Nakashige TG, Stephan JR, Cunden LS, Brophy MB, Wommack AJ, Keegan BC, et al. The hexahistidine motif of host-defense protein human calprotectin contributes to zinc withholding and its functional versatility. *J Am Chem Soc* (2016) 138:12243–51. doi: 10.1021/jacs.6b06845

78. Nakashige TG, Zhang B, Krebs C, Nolan EM. Human calprotectin is an iron-sequestering host-defense protein. *Nat Chem Biol* (2015) 11:765–71. doi: 10.1038/nchembio.1891

79. Hayden JA, Brophy MB, Cunden LS, Nolan EM. High-affinity manganese coordination by human calprotectin is calcium-dependent and requires the histidine-rich site formed at the dimer interface. *J Am Chem Soc* (2013) 135:775–87. doi: 10.1021/ja3096416

80. Voss A, Gescher K, Hensel A, Nacken W, Zänker KS, Kerkhoff C. Double-stranded RNA induces S100 gene expression by a cycloheximide-sensitive factor. *FEBS Lett* (2012) 586:196–203. doi: 10.1016/j.febslet.2011.12.022

81. Tugizov S, Berline J, Herrera R, Penaranda ME, Nakagawa M, Palefsky J. Inhibition of human papillomavirus type 16 E7 phosphorylation by the S100 MRP-8/14 protein complex. *J Virol* (2005) 79:1099–112. doi: 10.1128/jvi.79.2.1099-1112.2005

82. Wang S, Su M, Lin J, Zhang L, Li J, Tian Y, et al. S100A8/A9, an upregulated host factor in BK virus infection after kidney transplantation, is associated with allograft function impairment. *J Proteome Res* (2022) 21:2356–66. doi: 10.1021/acs.jproteome.2c00219

83. Undi RB, Larabee JL, Filiberti A, Ulahannan S, Aravindan S, Stroberg E, et al. Targeting doublecortin-like kinase 1 (DCLK1)-regulated SARS-CoV-2 pathogenesis in COVID-19. *J Virol* (2022) 96:e0096722. doi: 10.1128/jvi.00967-22

84. Darweesh MF, Rajput MKS, Braun LJ, Rohila JS, Chase CCL. BVDV npro protein mediates the BVDV induced immunosuppression through interaction with cellular S100A9 protein. *Microb Pathog* (2018) 121:341–9. doi: 10.1016/j.micpath.2018.05.047

85. Short KM, Cox TC. Subclassification of the RBCC/TRIM superfamily reveals a novel motif necessary for microtubule binding. *J Biol Chem* (2006) 281:8970–80. doi: 10.1074/jbc.M512755200

86. Munir M. TRIM proteins: Another class of viral victims. *Sci Signal* (2010) 3:jc2. doi: 10.1126/scisignal.3118jc2

87. Ozato K, Shin DM, Chang TH, Morse HC3rd. TRIM family proteins and their emerging roles in innate immunity. *Nat Rev Immunol* (2008) 8:849–60. doi: 10.1038/nri2413

88. Meroni G, Diez-Roux G. TRIM/RBCC, a novel class of 'single protein RING finger' E3 ubiquitin ligases. *Bioessays* (2005) 27:1147–57. doi: 10.1002/bies.20304

89. Uchil PD, Quinlan BD, Chan WT, Luna JM, Mothes W. TRIM E3 ligases interfere with early and late stages of the retroviral life cycle. *PloS Pathog* (2008) 4:e16. doi: 10.1371/journal.ppat.0040016

90. Gack MU, Shin YC, Joo CH, Urano T, Liang C, Sun L, et al. TRIM25 RING-finger E3 ubiquitin ligase is essential for RIG-i-mediated antiviral activity. *Nature* (2007) 446:916–20. doi: 10.1038/nature05732

91. Wang J, Liu B, Wang N, Lee YM, Liu C, Li K. TRIM56 is a virus- and interferon-inducible E3 ubiquitin ligase that restricts pestivirus infection. *J Virol* (2011) 85:3733–45. doi: 10.1128/jvi.02546-10

92. Heidary F, Gharebaghi R. Systematic review of the antiviral properties of TRIM56: A potential therapeutic intervention for COVID-19. *Expert Rev Clin Immunol* (2020) 16:973–84. doi: 10.1080/1744666X.2020.1822168

93. Hiscott J, Kwon H, Génin P. Hostile takeovers: Viral appropriation of the NF-kappaB pathway. *J Clin Invest* (2001) 107:143–51. doi: 10.1172/jci11918

94. Hiscott J, Nguyen TL, Arguello M, Nakhaei P, Paz S. Manipulation of the nuclear factor-kappaB pathway and the innate immune response by viruses. *Oncogene* (2006) 25:6844–67. doi: 10.1038/sj.onc.1209941

95. Santoro MG, Rossi A, Amici C. NF-kappaB and virus infection: Who controls whom. *EMBO J* (2003) 22:2552–60. doi: 10.1093/emboj/cdg267

96. Huxford T, Huang DB, Malek S, Ghosh G. The crystal structure of the IkappaBalpha/NF-kappaB complex reveals mechanisms of NF-kappaB inactivation. *Cell* (1998) 95:759–70. doi: 10.1016/s0092-8674(00)81699-2

97. Jacobs MD, Harrison SC. Structure of an IkappaBalpha/NF-kappaB complex. *Cell* (1998) 95:749–58. doi: 10.1016/s0092-8674(00)81698-0

98. Pahl HL. Activators and target genes of Rel/NF-kappaB transcription factors. *Oncogene* (1999) 18:6853–66. doi: 10.1038/sj.onc.1203239

99. Silverman N, Maniatis T. NF-kappaB signaling pathways in mammalian and insect innate immunity. *Genes Dev* (2001) 15:2321–42. doi: 10.1101/gad.909001

100. DiDonato JA, Hayakawa M, Rothwarf DM, Zandi E, Karin M. A cytokine-responsive IkappaB kinase that activates the transcription factor NF-kappaB. *Nature* (1997) 388:548–54. doi: 10.1038/41493

101. Sakurai H, Chiba H, Miyoshi H, Sugita T, Toriumi W. IkappaB kinases phosphorylate NF-kappaB p65 subunit on serine 536 in the transactivation domain. *J Biol Chem* (1999) 274:30353–6. doi: 10.1074/jbc.274.43.30353

102. Beg AA, Ruben SM, Scheinman RI, Haskill S, Rosen CA, Baldwin ASJr. I Kappa b interacts with the nuclear localization sequences of the subunits of NF-kappa b: a mechanism for cytoplasmic retention. *Genes Dev* (1992) 6:1899–913. doi: 10.1101/gad.6.10.1899

103. Winston JT, Strack P, Beer-Romero P, Chu CY, Elledge SJ, Harper JW. The SCFbeta-TRCP-ubiquitin ligase complex associates specifically with phosphorylated destruction motifs in IkappaBalpha and beta-catenin and stimulates IkappaBalpha ubiquitination *in vitro*. *Genes Dev* (1999) 13:270–83. doi: 10.1101/gad.13.3.270

104. Zamanian-Daryoush M, Mogensen TH, DiDonato JA, Williams BR. NF-kappaB activation by double-stranded-RNA-activated protein kinase (PKR) is mediated through NF-kappaB-inducing kinase and IkappaB kinase. *Mol Cell Biol* (2000) 20:1278–90. doi: 10.1128/mcb.20.4.1278-1290.2000

105. Yoneyama M, Fujita T. RNA Recognition and signal transduction by RIG-i-like receptors. *Immunol Rev* (2009) 227:54–65. doi: 10.1111/j.1600-065X.2008.00727.x

106. Arenzana-Seisdedos F, Turpin P, Rodriguez M, Thomas D, Hay RT, Virelizier JL, et al. Nuclear localization of I kappa b alpha promotes active transport of NF-kappa b from the nucleus to the cytoplasm. *J Cell Sci* (1997) 110(Pt 3):369–78. doi: 10.1242/jcs.110.3.369

107. Rodriguez MS, Thompson J, Hay RT, Dargemont C. Nuclear retention of IkappaBalpha protects it from signal-induced degradation and inhibits nuclear factor kappaB transcriptional activation. *J Biol Chem* (1999) 274:9108–15. doi: 10.1074/jbc.274.13.9108

108. Sachdev S, Hoffmann A, Hannink M. Nuclear localization of IkappaB alpha is mediated by the second ankyrin repeat: The IkappaB alpha ankyrin repeats define a novel class of cis-acting nuclear import sequences. *Mol Cell Biol* (1998) 18:2524–34. doi: 10.1128/mcb.18.5.2524

109. Ting AT, Bertrand MJM. More to life than NF-κB in TNFR1 signaling. *Trends Immunol* (2016) 37:535–45. doi: 10.1016/j.it.2016.06.002

110. Fiume G, Vecchio E, De Laurentiis A, Trimboli F, Palmieri C, Pisano A, et al. Human immunodeficiency virus-1 tat activates NF-κB *via* physical interaction with IκB-α and p65. *Nucleic Acids Res* (2012) 40:3548–62. doi: 10.1093/nar/gkr1224

111. Chen LJ, Dong XY, Zhao MQ, Shen HY, Wang JY, Pei JJ, et al. Classical swine fever virus failed to activate nuclear factor-kappa b signaling pathway both. *Vitro vivo. Virol J* (2012) 9:293. doi: 10.1186/1743-422x-9-293

112. Lees DM, Hart IR, Marshall JF. Existence of multiple isoforms of HS1-associated protein X-1 in murine and human tissues. *J Mol Biol* (2008) 379:645–55. doi: 10.1016/j.jmb.2008.04.020

113. Carlsson G, van't Hooft I, Melin M, Entesarian M, Laurencikas E, Nennesmo I, et al. Central nervous system involvement in severe congenital neutropenia: Neurological and neuropsychological abnormalities associated with specific HAX1 mutations. *J Intern Med* (2008) 264:388–400. doi: 10.1111/j.1365-2796.2008.01982.x

114. Suzuki Y, Demoliere C, Kitamura D, Takeshita H, Deuschle U, Watanabe T. HAX-1, a novel intracellular protein, localized on mitochondria, directly associates with HS1, a substrate of src family tyrosine kinases. *J Immunol* (1997) 158:2736–44.

115. Vafiadaki E, Arvanitis DA, Pagakis SN, Papalouka V, Sanoudou D, Kontrogianni-Konstantopoulos A, et al. The anti-apoptotic protein HAX-1 interacts with SERCA2 and regulates its protein levels to promote cell survival. *Mol Biol Cell* (2009) 20:306–18. doi: 10.1091/mbc.e08-06-0587

116. Johns HL, Doceul V, Everett H, Crooke H, Charleston B, Seago J. The classical swine fever virus n-terminal protease n(pro) binds to cellular HAX-1. *J Gen Virol* (2010) 91:2677–86. doi: 10.1099/vir.0.022897-0

117. Vafiadaki E, Sanoudou D, Arvanitis DA, Catino DH, Kranias EG, Kontrogianni-Konstantopoulos A. Phospholamban interacts with HAX-1, a mitochondrial protein with anti-apoptotic function. *J Mol Biol* (2007) 367:65–79. doi: 10.1016/j.jmb.2006.10.057

118. Chkheidze AN, Lyakhov DL, Makeyev AV, Morales J, Kong J, Liebhaber SA. Assembly of the alpha-globin mRNA stability complex reflects binary interaction between the pyrimidine-rich 3' untranslated region determinant and poly(C) binding protein alphaCP. *Mol Cell Biol* (1999) 19:4572–81. doi: 10.1128/mcb.19.7.4572

119. Holcik M, Liebhaber SA. Four highly stable eukaryotic mRNAs assemble 3' untranslated region RNA-protein complexes sharing cis and trans components. *Proc Natl Acad Sci U.S.A.* (1997) 94:2410–4. doi: 10.1073/pnas.94.6.2410

120. Wang X, Kiledjian M, Weiss IM, Liebhaber SA. Detection and characterization of a 3' untranslated region ribonucleoprotein complex associated with human alpha-globin mRNA stability. *Mol Cell Biol* (1995) 15:1769–77. doi: 10.1128/mcb.15.3.1769

121. Kim SS, Pandey KK, Choi HS, Kim SY, Law PY, Wei LN, et al. Poly(C) binding protein family is a transcription factor in mu-opioid receptor gene expression. *Mol Pharmacol* (2005) 68:729–36. doi: 10.1124/mol.105.012245

122. Ko JL, Loh HH. Poly c binding protein, a single-stranded DNA binding protein, regulates mouse mu-opioid receptor gene expression. *J Neurochem* (2005) 93:749–61. doi: 10.1111/j.1471-4159.2005.03089.x

123. Meng Q, Rayala SK, Gururaj AE, Talukder AH, O'Malley BW, Kumar R. Signaling-dependent and coordinated regulation of transcription, splicing, and translation resides in a single coregulator, PCBP1. *Proc Natl Acad Sci U.S.A.* (2007) 104:5866–71. doi: 10.1073/pnas.0701065104

124. Blyn LB, Towner JS, Semler BL, Ehrenfeld E. Requirement of poly(rC) binding protein 2 for translation of poliovirus RNA. *J Virol* (1997) 71:6243–6. doi: 10.1128/jvi.71.8.6243-6246.1997

125. Gamarnik AV, Andino R. Two functional complexes formed by KH domain containing proteins with the 5' noncoding region of poliovirus RNA. *Rna* (1997) 3:882–92.

126. Makeyev AV, Liebhaber SA. The poly(C)-binding proteins: A multiplicity of functions and a search for mechanisms. *Rna* (2002) 8:265–78. doi: 10.1017/s1355838202024627

127. Huang C, Jiang T, Xue M, Li Y, Feng T, Pan W, et al. Poly(C)-binding protein 2 positively regulates interferon downstream signaling. *Acta Biochim Biophys Sin (Shanghai)* (2022) 54:748–51. doi: 10.3724/abbs.2022032

128. Michael WM, Eder PS, Dreyfuss G. The K nuclear shuttling domain: A novel signal for nuclear import and nuclear export in the hnRNP K protein. *EMBO J* (1997) 16:3587–98. doi: 10.1093/emboj/16.12.3587

129. Li D, Dong H, Li S, Munir M, Chen J, Luo Y, et al. Hemoglobin subunit beta interacts with the capsid protein and antagonizes the growth of classical swine fever virus. *J Virol* (2013) 87:5707–17. doi: 10.1128/jvi.03130-12

130. Mordstein M, Neugebauer E, Ditt V, Jessen B, Rieger T, Falcone V, et al. Lambda interferon renders epithelial cells of the respiratory and gastrointestinal tracts resistant to viral infections. *J Virol* (2010) 84:5670–7. doi: 10.1128/jvi.00272-10

131. Onoguchi K, Yoneyama M, Takemura A, Akira S, Taniguchi T, Namiki H, et al. Viral infections activate types I and III interferon genes through a common mechanism. *J Biol Chem* (2007) 282:7576–81. doi: 10.1074/jbc.M608618200

132. Thomson SJ, Goh FG, Banks H, Krausgruber T, Kotenko SV, Foxwell BM, et al. The role of transposable elements in the regulation of IFN-lambda1 gene expression. *Proc Natl Acad Sci U.S.A.* (2009) 106:11564–9. doi: 10.1073/pnas.0904477106

133. Sommereyns C, Paul S, Staeheli P, Michiels T. IFN-lambda (IFN-lambda) is expressed in a tissue-dependent fashion and primarily acts on epithelial cells *in vivo*. *PloS Pathog* (2008) 4:e1000017. doi: 10.1371/journal.ppat.1000017

134. Cao T, Li X, Xu Y, Zhang S, Wang Z, Shan Y, et al. Npro of classical swine fever virus suppresses type III interferon production by inhibiting IRF1 expression and its nuclear translocation. *Viruses* (2019) 11(11):998. doi: 10.3390/v11110998

135. Odendall C, Dixit E, Stavru F, Bierne H, Franz KM, Durbin AF, et al. Diverse intracellular pathogens activate type III interferon expression from peroxisomes. *Nat Immunol* (2014) 15:717–26. doi: 10.1038/ni.2915

136. Mätzener P, Magkouras I, Rümenapf T, Peterhans E, Schweizer M. The viral RNase e(rns) prevents IFN type-I triggering by pestiviral single- and double-stranded RNAs. *Virus Res* (2009) 140:15–23. doi: 10.1016/j.virusres.2008.10.015

137. Lussi C, Schweizer M. What can pestiviral endonucleases teach us about innate immunotolerance? *Cytokine Growth Factor Rev* (2016) 29:53–62. doi: 10.1016/j.cytogfr.2016.03.003

138. Tews BA, Klingebeil A, Kühn J, Franzke K, Rümenapf T, Meyers G. The e(rns) carboxyterminus: Much more than a membrane anchor. *Viruses* (2021) 13(7):1203. doi: 10.3390/v13071203

frontiers | Frontiers in Immunology

TYPE Original Research
PUBLISHED 11 April 2023
DOI 10.3389/fimmu.2023.1162208

OPEN ACCESS

EDITED BY
Huifang Zhu,
First Affiliated Hospital of Gannan Medical University, China

REVIEWED BY
Yuchen Xia,
Wuhan University, China
Yong Lin,
Chongqing Medical University, China

*CORRESPONDENCE
Jianbo Xia
xjb915@126.com

SPECIALTY SECTION
This article was submitted to Viral Immunology, a section of the journal Frontiers in Immunology

RECEIVED 09 February 2023
ACCEPTED 21 March 2023
PUBLISHED 11 April 2023

CITATION
Wu C, Zeng L, Yi W, Miao Y, Liu Y, Wang Q, Liu S, Peng G, Zheng Z and Xia J (2023) Echovirus induces autophagy to promote viral replication *via* regulating mTOR/ULK1 signaling pathway.
Front. Immunol. 14:1162208.
doi: 10.3389/fimmu.2023.1162208

Echovirus induces autophagy to promote viral replication *via* regulating mTOR/ULK1 signaling pathway

Chunchen Wu[1], Luzhi Zeng[1,2], Wenfu Yi[3], Yuanjiu Miao[3], Yihan Liu[1,2], Qiming Wang[2], Shi Liu[4], Guoping Peng[2], Zhenhua Zheng[3] and Jianbo Xia[1]*

[1]Department of Laboratory Medicine, Maternal and Child Health Hospital of Hubei Province, Tongji Medical College, Huazhong University of Science and Technology, Wuhan, China, [2]College of Bioscience and Biotechnology, Hunan Agricultural University, Changsha, China, [3]CAS Key Laboratory of Special Pathogens and Biosafety, Center for Emerging Infectious Diseases, Wuhan Institute of Virology, Chinese Academy of Sciences, Wuhan, China, [4]State Key Laboratory of Virology, Modern Virology Research Center, College of Life Sciences, Wuhan University, Wuhan, China

Among enteroviruses, echovirus can cause severe illnesses in neonates or infants, with high morbidity and mortality. Autophagy, a central component of host defense mechanisms, can function against diverse infections. In the present study, we investigated the interplay between echovirus and autophagy. We demonstrated that echovirus infection increases LC3-II expression dose-dependently, accompanied by an increased intracellular LC3 puncta level. In addition, echovirus infection induces the formation of autophagosome. These results suggest that echovirus infection induces autophagy machinery. Furthermore, phosphorylated mTOR and ULK1 were both decreased upon echovirus infection. In contrast, both levels of the vacuolar protein sorting 34 (VPS34) and Beclin-1, the downstream molecules which play essential roles in promoting the formation of autophagic vesicles, increased upon virus infection. These results imply that the signaling pathways involved in autophagosome formation were activated by echovirus infection. Moreover, induction of autophagy promotes echovirus replication and viral protein VP1 expression, while inhibition of autophagy impairs VP1 expression. Our findings suggest that autophagy can be induced by echovirus infection *via* regulating mTOR/ULK1 signaling pathway and exhibits a proviral function, revealing the potential role of autophagy in echovirus infection.

KEYWORDS

enterovirus, echovirus, autophagy, viral replication, virus-host interaction

Introduction

Human enteroviruses (HEVs) are small, nonenveloped, positive single-strand RNA viruses belonging to the genus *Enterovirus* within the family *Picornaviridae*. More than 100 enterovirus types have been identified and classified into four species, A to D, according to molecular and antigenic properties (1). Echovirus was discovered when the first tissue-culture techniques were introduced into laboratories (2). Currently, echovirus has been classified within the B species, the largest group of the *Enterovirus* genus, together with coxsackievirus group B, coxsackie A9, and several novel enteroviruses. Like other enteroviruses, echovirus infections are associated with a broad spectrum of illnesses, ranging from minor symptoms (e.g., febrile rash, mild hand, foot, and mouth diseases (HFMD)) to severe, potentially fatal conditions (e.g., aseptic meningitis, encephalitis and acute flaccid paralysis (AFP)) (3). Among 30 serotypes, echovirus 11 was one of the most commonly identified serotypes that cause severe illnesses in neonates or infants, with high morbidity and mortality (4–8). In addition, echovirus 11 has frequently been found to be associated with outbreaks in neonatal intensive units (NICUs) or postpartum care centers, causing public health threats globally (9–12). However, the pathogenic mechanisms of echovirus are poorly understood, limiting the development of antiviral strategies against echovirus.

Autophagy is an evolutionarily conserved intracellular degradation process by which misfolded proteins, damaged organelles, and various invading pathogens are sequestered in the cytoplasm and removed to maintain cellular homeostasis (13). A key initial event in autophagy is the formation of the autophagosome, a unique double-membrane organelle that engulfs the cytosolic cargo destined for degradation. A series of autophagy-related genes (ATG) has been identified to participate in these processes (14). As a part of autonomous innate immunity, autophagy functions to defend individual cells against invading pathogens such as bacteria, fungi, parasites, and viruses (15, 16). For example, autophagy can exert antiviral functions during Sindbis virus or tobacco mosaic virus infection by selectively targeting viral particles or components to the lysosomes for degradatio (17). However, many viruses, for example, poliovirus, coxsackievirus, and hepatitis C virus, have evolved various strategies to hijack and subvert host autophagy for their life cycles and pathogenesis (18–20). Although previous studies suggested a potential role for autophagy in echovirus 7 entry (21), the interplay between echovirus and autophagy remains unclear.

In the present study, we explored the induction of autophagy machinery during EchoV infection by monitoring the activation of LC3 and the presence of autophagosome-like structures. Also, we checked the effects of inducing or perturbing the autophagy pathway, using pharmacological inducers or inhibitors, respectively, on viral replication. Our data revealed that autophagy is induced during echovirus infection and is involved in echovirus replication.

Materials and methods

Cell culture and virus infection

Human rhabdomyosarcoma (RD; CCL-136; ATCC) cells were maintained in Dulbecco's modified Eagle Medium (DMEM) containing 10% fetal bovine serum (FBS; Life Technologies) at 37°C in a 5% CO2 incubator. Echovirus 11 strain (NCBI Accession No. OP764694) was isolated from a feces sample of a 24-day-old female neonate with enterovirus infection after passaging in the RD cells. RD cells were infected with echovirus at various multiplicity of infection (MOI) for 1.5 h in serum-free DMEM. The cells were washed with phosphate-buffered saline (PBS) and cultured in a completely fresh medium for various times as indicated until they were harvested. For autophagy induction experiments, cells were infected or mock-infected with echovirus for 1.5 h, then cultured in a complete medium containing rapamycin (Selleck, AY-22989) at indicated concentrations for the indicated times. For autophagy inhibition experiments, cells were cultured in DMEM containing indicated concentrations of 3-methyladenine (3-MA) (Selleck, S2767) for 2 h, followed by echovirus infection for 1.5 h, and then incubated with fresh DMEM for 16 h. Cell counting kit-8 (CCK8) (Vazyme, A311-01) assay was performed to examine the cytotoxicity of rapamycin or 3-MA to RD cells.

Western blotting

Western blotting was performed as described previously (22). The used antibodies were as follows: anti-LC3 (Cell Signaling Technology, 3868), anti-p62 (Proteintech, 18420-1-AP), anti-mTOR (Cell Signaling Technology, 2972), anti-phospho-mTOR (Cell Signaling Technology, 2971), anti-ULK1 (Cell Signaling Technology, 8054), anti-phospho-ULK1 (Ser757) (Cell Signaling Technology, 6888), anti-VPS34 (Proteintech, 12452-1-AP), anti-Beclin-1 (Proteintech, 11306-1-AP) and anti-β-actin (Santa Cruz Biotechnology, sc-47778). Anti-VP1, a rabbit polyclonal antibody, was produced by Wuhan Abclonal Biotechnology. The relative band intensities of the proteins were quantified using the NIH ImageJ software.

Immunofluorescence microscopy

RD cells were transiently transfected with a GFP-tagged LC3 expression vector (GFP-LC3) as described previously (23) using Lipofectamine (Invitrogen). At 24 h post-transfection, cells were infected with echovirus for 1.5 h, then cultured in a complete medium in the presence or absence of rapamycin for 16 h. The fluorescence of GFP-LC3 was observed under a Nikon A1 confocal fluorescence microscope. The nuclei were stained with Hoechst 33258.

Transmission electron microscopy

Echovirus-infected cells were fixed with 0.5% glutaraldehyde at 4°C for 10 min and then fixed with 2.5% glutaraldehyde at 4°C for 1 h. After that, cells were further fixed with 0.1% osmium tetroxide. The cells were then dehydrated in a gradient series of ethanol and embedded with LR White (Agar Shin sections were cut on a Leica EM FC7 UC7 ultramicrotome and viewed under an FEI Tecani G20 TWIN transmission electron microscope.

Real-time PCR

Total RNA was extracted from cells using TRIzol (Invitrogen) and then reverse transcribed into cDNA using FastKing gDNA Dispelling RT SuperMix (TIANGEN, KR118-02). Quantitative reverse transcription-polymerase chain reaction (qRT-PCR) was performed to detect viral RNA using Taq Pro Universal SYBR qPCR Master Mix (Vazyme, Q712-02). The following primers were used: EchoV-F: 5'-AAAGTGG CCAAAGGCAAGTC-3'; EchoV-R: 5'-GGTCAGGATCACACCCAACC-3'; GAPDH-F: 5'-TGGTAT CGTGGAAGGACTCA-3'; GAPDH-R: 5'-CCAGTAGAGG CAGGGATGAT-3'. The relative levels of EV-D68 RNA in different samples were determined using a comparative $2^{-\Delta\Delta CT}$ method and normalized to the GAPDH gene.

Statistical analyses

Statistical analysis was conducted using GraphPad Prism 5.0 software (GraphPad Software). A one-way ANOVA was used to determine statistically significant differences in multiple comparisons. $P<0.05$ was considered statistically significant. The results are presented as the mean ± standard deviations (n≥3).

Results

Echovirus infection induces autophagy

A hallmark of autophagy induction is that the LC3-I protein undergoes a lipidation modification, and phosphatidylethanolamine (PE) is conjugated to LC3-I to generate LC3-II, which becomes membrane-associated and participates in autophagosome formation (24). To determine whether echovirus infection regulates autophagy, we examined the conversion of endogenous LC3-I to LC3-II. Echovirus-infected cells exhibited an increase in LC3-II and viral VP1 protein when compared with uninfected Mock cells (Figure 1A). The densitometry ratio of LC3-II to β-actin showed an increase (Figure 1B). In contrast, the autophagic receptor p62 level correspondingly decreased (Figures 1A, C). These results suggested that echovirus infection may induce autophagy.

Echovirus infection induced-autophagy is positively correlated with viral load

To explore the relationship between viral concentration and the degree of autophagy, RD cells were infected with echovirus at indicated MOIs, and the expression of LC3-II was determined by Western blotting. As the viral MOIs increased, the level of viral capsid protein (VP1) gradually increased. Meanwhile, the level of LC3-II expression gradually increased in echovirus-infected cells. In contrast, the level of p62 expression decreased (Figure 2A). The densitometry ratio of LC3-II to LC3-I showed an increase. In contrast, the densitometry ratio of p62 showed a decrease, especially under virus infection at 1 MOI (Figures 2B, C). These results indicated that echovirus infection induced-autophagy was positively correlated with viral load.

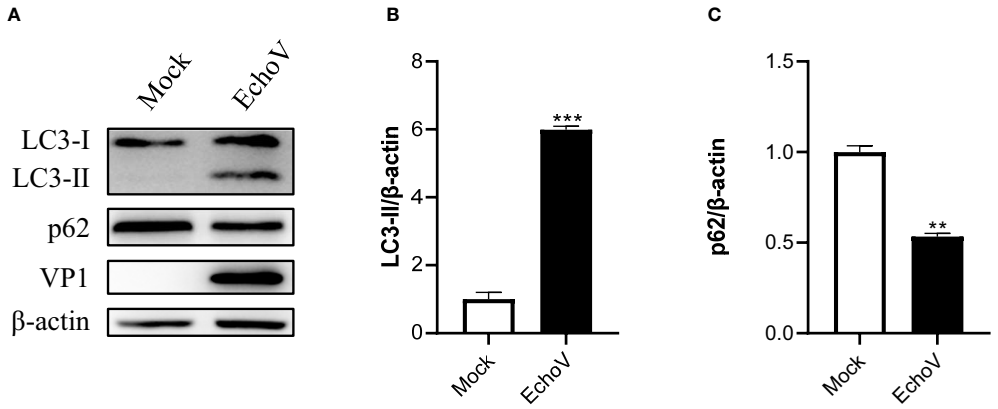

FIGURE 1
Echovirus infection induces autophagy. RD cells were infected or not (Mock) with echovirus 11 at 1 MOI for 1.5 h. At 16 h post-infection, cells were then harvested. **(A)** Intracellular LC3 and p62 proteins were detected *via* western blotting. β-actin served as a loading control. This result is representative of three independent experiments. The relative band intensities of detected proteins were calculated using ImageJ from NIH, and the result was represented as the ratio of LC3-II to β-actin **(B)** or p62 to β-actin **(C)**. A one-way ANOVA was used to determine statistically significant differences in multiple comparisons. **p<0.01, ***$P<0.001$.

10.3389/fimmu.2023.1162208

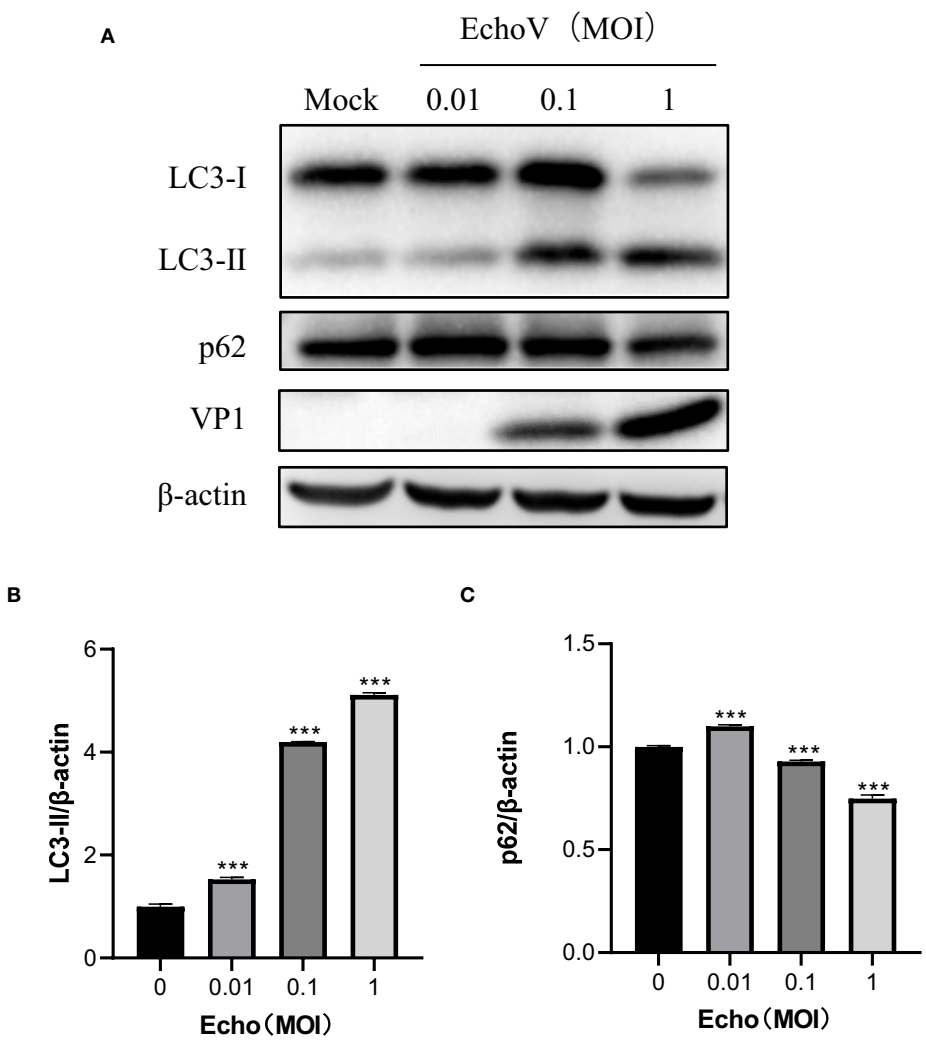

FIGURE 2
Echovirus infection induced-autophagy is positively correlated with viral load. RD cells were infected or not (Mock) with echovirus 11 at different MOI for 1.5 h. At 16 h post-infection, cells were then harvested. **(A)** Intracellular LC3 and p62 proteins were detected *via* western blotting. β-actin served as a loading control. This result is representative of three independent experiments. The relative band intensities of detected proteins were calculated using ImageJ from NIH, and the result was represented as the ratio of LC3-II to β-actin **(B)** or p62 to β-actin **(C)**. A one-way ANOVA was used to determine statistically significant differences in multiple comparisons. ***$P<0.001$.

Echovirus infection increases the level of LC3 puncta formation

The redistribution of LC3 from a diffuse cytoplasmic localization to a characteristic punctate cytoplasmic pattern, which reflects the recruitment of LC3 to autophagic vesicles, is another hallmark of autophagy (25). Therefore, a GFP-tagged LC3 expression vector (GFP-LC3), as described previously (23), was used to assess other autophagy induced by echovirus infection. In cells transfected with GFP-LC3, the level of LC3 puncta formation was increased by echovirus infection (Figures 3A, B). These findings further confirmed that autophagy was induced by echovirus infection.

Echovirus infection induces autophagosome formation

A key initial event in autophagy is the formation of the autophagosome, a unique double-membrane organelle that engulfs the cytosolic cargo destined for degradation. Therefore, ultrastructural analysis was performed with RD cells with or without echovirus infection. Double-membrane vesicles engulfing cytosolic materials were observed in the cytoplasm of infected cells but not in uninfected cells under transmission electron microscopy (Figure 4). The data revealed that echovirus infection induced autophagosome formation.

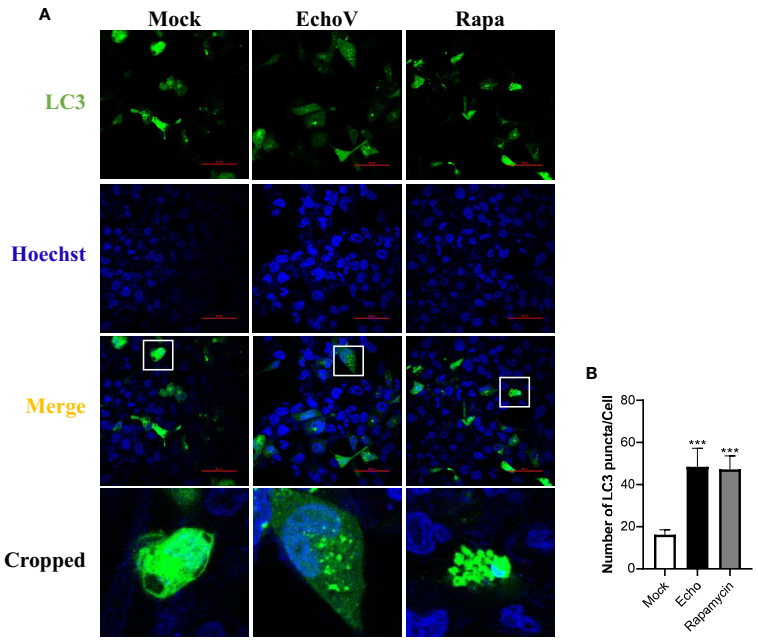

FIGURE 3
Echovirus infection increases the level of LC3 puncta formation. RD cells were transfected with GFP-LC3 plasmid for 24 h, followed by infected or not (Mock) with echovirus 11 at 1 MOI for 1.5 h. **(A)** At 16 h post-infection, cells were fixed and analyzed by confocal fluorescence microscopy. RD cells were treated with rapamycin (500 nM) (Rapa) for 16 h as a positive control. **(B)** Quantitation of the numbers of LC3 puncta in RD cells. Data shown represent the number of LC3 puncta per cell under each condition. A one-way ANOVA was used to determine statistically significant differences in multiple comparisons. ***$P<0.001$.

Echovirus infection induces the activation of signaling pathways involved in autophagosome formation

The mTOR/ULK1 signaling pathway plays a key role in mediating the initiation and formation of an autophagosome (26). The phosphorylation levels of mTOR were decreased in echovirus-infected cells (Figure 5A). Both levels of ULK1 and phosphorylated ULK1 protein on S757 were also decreased in virus-infected cells (Figure 5A). Upon autophagy induction, the ULK1 complex translocates to autophagy initiation sites and regulates the recruitment of a second kinase complex, the vacuolar protein

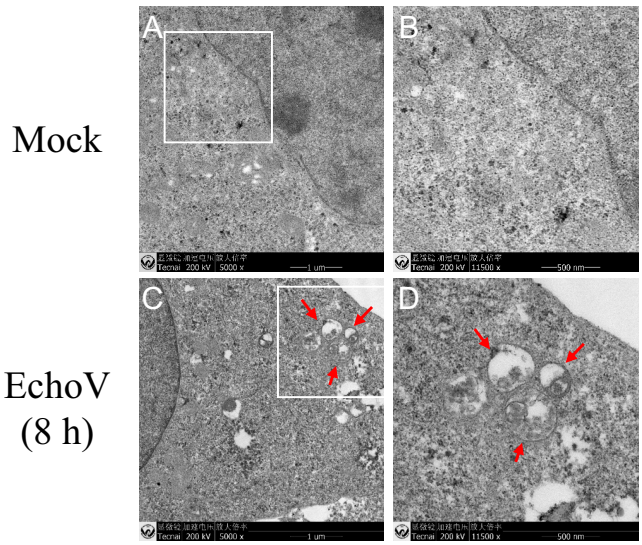

FIGURE 4
Echovirus infection induces autophagosome formation. RD cells were infected or not (Mock) with echovirus 11 at 1 MOI for 1.5 h. At 8 h post-infection, cells were then fixed and subjected to transmission electron microscopy analysis. Lower magnification of Mock **(A)** and EchoV-infected **(C)** cells. **(B)** Higher magnification of the area in white square of **(A)**; **(D)** Higher magnification of the area in white square of **(C)**. Scale bar in A and C, 1 μm; Scale bar in B and D, 500 nm. The autophagosomes are denoted by red arrows.

10.3389/fimmu.2023.1162208

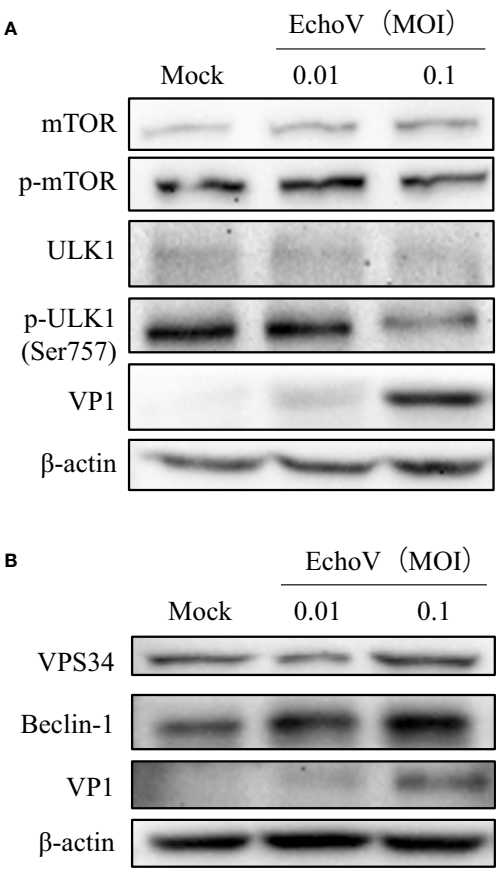

FIGURE 5
Echovirus infection induces the activation of signaling pathways involved in autophagosome formation. RD cells were infected or not (Mock) with echovirus 11 at different MOI for 1.5 h. At 16 h post-infection, cells were then harvested. **(A)** Intracellular mTOR, phosphorylated mTOR (p-mTOR), ULK1, phosphorylated ULK1 (p-ULK1), and viral VP1 proteins were detected *via* western blotting. **(B)** Intracellular VPS34, Beclin-1, and viral VP1 proteins were detected *via* western blotting. β-actin served as a loading control. This result is representative of three independent experiments.

sorting 34 (VPS34) complex consisting of VPS34, as well as Beclin-1, VPS15, and ATG14L, which promotes the formation of autophagic vesicles (26, 27). Therefore, we further checked the levels of VPS34 and Beclin-1. As shown in Figure 5B, both VPS34 and Beclin-1 protein levels increased in echovirus-infected cells in a dose-dependent manner. The results indicated that echovirus infection induced the activation of signaling pathways involved in autophagosome formation.

Induction of autophagy promotes echovirus replication

Previous studies have demonstrated that autophagy may serve an antiviral or proviral function during diverse viral infections (14). Therefore, to investigate the impact of autophagy induction on echovirus infection, we monitored virus expression and replication under autophagy inducer rapamycin treatment. Rapamycin at indicated concentrations showed no toxicity to RD cells (Figure 6A). Induction of autophagy through rapamycin treatment significantly increased viral protein VP1 expression in a dose-dependent manner (Figures 6B–C). Moreover, the levels of viral RNA were also increased under rapamycin treatment in a dose-dependent manner (Figure 6D). These results suggested that induction of autophagy promoted echovirus replication.

Inhibition of autophagy impairs viral protein VP1 expression

To further validate the effect of autophagy on echovirus replication, 3-MA, a widely used selective autophagy inhibitor, was used. As shown in Figure 7, 3-MA at indicated concentrations showed no toxicity to RD cells (Figure 7A). Treatment with 3-MA impaired the level of LC3-II expression, suggesting the inhibition of autophagy (Figure 7B). Correspondingly, viral VP1 protein expression reduction was observed (Figures 7C). This finding confirmed that autophagy might serve a proviral function during echovirus infection.

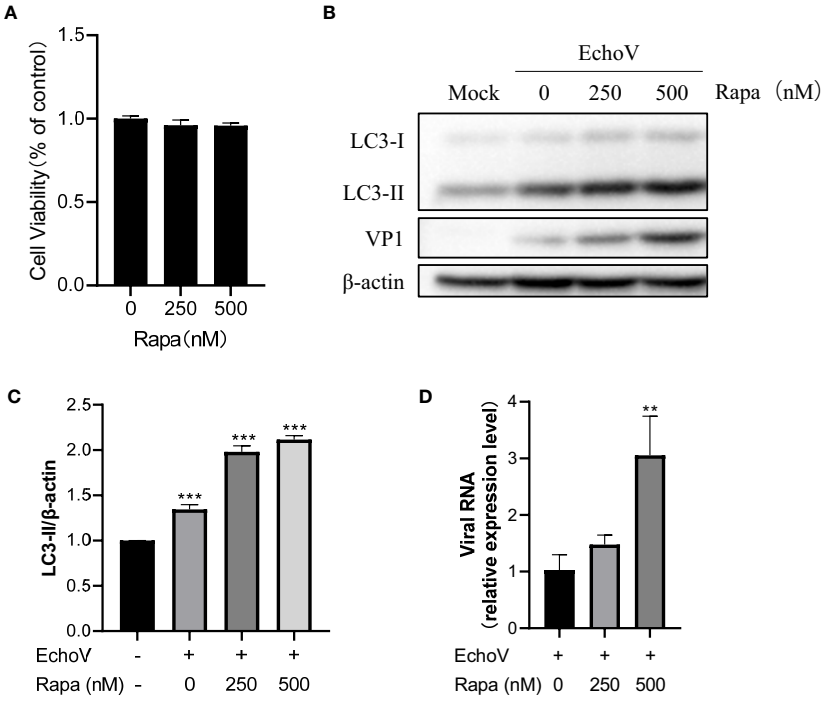

FIGURE 6
Induction of autophagy promotes Echovirus replication. RD cells were infected or not (Mock) with echovirus 11 at 0.1 MOI for 1.5 h and then untreated (Echo) or treated with rapamycin (Rapa) at indicated concentrations for 16 h. Cells were then harvested. **(A)** Cell counting kit-8 (CCK8) assay was performed to examine the cytotoxicity of rapamycin to RD cells. **(B)** Intracellular LC3 and viral VP1 proteins were detected *via* western blotting. β-actin served as a loading control. This result is representative of three independent experiments. The relative band intensities of detected proteins were calculated using ImageJ from NIH, and the result was represented as the ratio of LC3-II to β-actin **(C)**. **(D)** Total RNA was extracted from cells and subjected to a quantitative reverse transcription-polymerase chain reaction (qRT-PCR) to detect viral RNA. A one-way ANOVA was used to determine statistically significant differences in multiple comparisons. $^{**}P<0.01$; $^{***}P<0.001$.

Discussion

Autophagy is an evolutionarily conserved cellular process through which the lysosome could degrade long-lived proteins, damaged organelles, or invading pathogens to maintain cellular homeostasis and host health (13, 17). However, viruses have evolved strategies during a long evolutionary process by which they can hijack and subvert host autophagy to favor their benefits (14). Echovirus is one of the most common worldwide causes of severe illnesses in neonates or infants. The interplay between echovirus and autophagy needs to be better understood. Here, we demonstrated that echovirus 11 induced autophagy to promote its replication *via* regulating mTOR/ULK1 signaling pathway (Figure 8).

Previous studies have indicated that several core components of the autophagy machinery, including Beclin-1, Atg12, Atg14, Atg16L1, and LC3, are important for echovirus 7 entry into polarized Caco-2 cells (21). However, the impact of autophagy on echovirus replication after virus entry was not discussed in that paper. Here, our data provided experimental evidence that autophagy also participates in echovirus replication. Replication of positive-stranded RNA viruses requires intracellular membrane surfaces on which they assemble their replication complexes (28). Double-membrane compartments formed during autophagy can provide a physical platform for the viral replication machinery. For example, the influenza A virus triggers the accumulation of autophagosomes for viral replication (29). Zika virus infection results in membrane rearrangements and induction of autophagy, which are considered to be the sites of viral RNA replication and virion assembly (30). CVB3, another important enterovirus classified within the B species, also uses autophagy for replication (31). Similar to these results, echovirus infection can also induce autophagy. In virus-infected RD cells, autophagosome can be observed. Presumably, echovirus exploited the autophagic membrane to support its replication.

Mechanically, membrane compartments formed during autophagy can locally concentrate essential intermediates and protect viral RNAs from detection by innate immune sensors and degradation (14). For example, HCV induces autophagosome formation but blocks lysosomal fusion, resulting in the

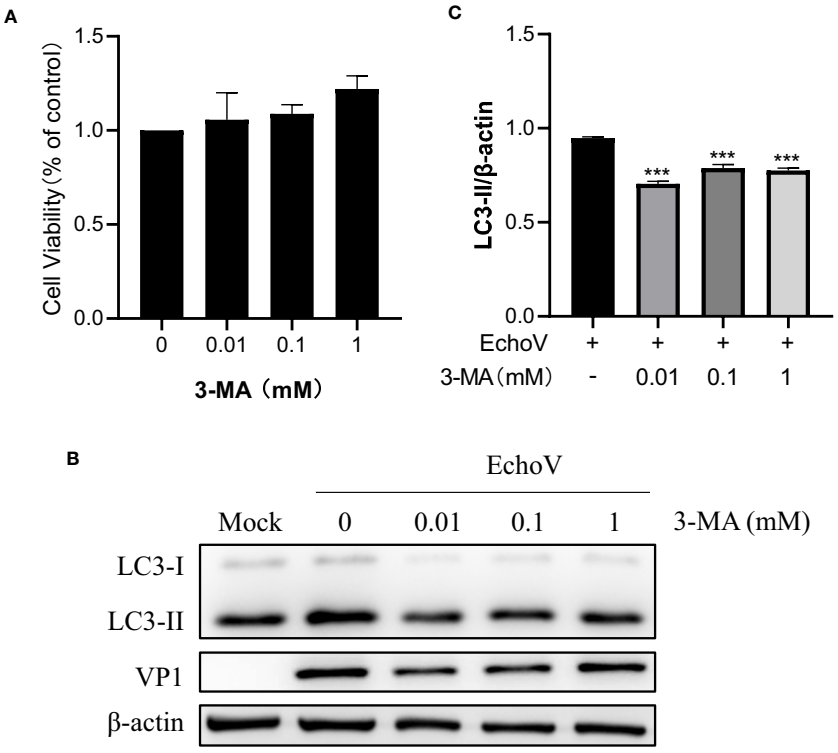

FIGURE 7
Inhibition of Autophagy inhibits EchoV replication. RD cells were pre-untreated or pre-treated with 3-MA at indicated concentrations for 2 h, followed by infected (EchoV) or not (Mock) with echovirus 11 at 0.1 MOI for 1.5 h. At 16 h post-infection, cells were then harvested. **(A)** Cell counting kit-8 (CCK8) assay was performed to examine the cytotoxicity of 3-MA to RD cells. **(B)** Intracellular LC3 and viral VP1 proteins were detected *via* western blotting. β-actin served as a loading control. This result is representative of three independent experiments. The relative band intensities of detected proteins were calculated using ImageJ from NIH, and the result was represented as the ratio of LC3-II to β-actin **(C)**. A one-way ANOVA was used to determine statistically significant differences in multiple comparisons. ***P<0.001.

accumulation of autophagosomes in support of HCV replication (32). CVB3-induced accumulation of autophagosomes *via* blockage of autophagosome-lysosome fusion (33). However, in this study, p62, a marker of autophagy-mediated protein degradation or autophagic flux, decreased during echovirus infection, indicating that echovirus infection may not interfere with the fusion of autophagosomes with lysosomes. Therefore, further studies may be needed to elucidate the mechanism by which echovirus-induced autophagy promotes viral replication. Notably, the expression level of viral VP1 protein increased upon autophagy induction and decreased upon autophagy inhibition. This result suggested that autophagy may play a role in viral protein synthesis.

The process of autophagosome formation is tightly controlled. The serine/threonine protein kinase mTOR is one of the key regulators and negatively controls autophagosome formation (34). We consistently showed that mTOR phosphorylation levels decreased after echovirus infection, suggesting that echovirus-induced autophagy is triggered by mTOR dephosphorylation. Furthermore, we observed that the level of phosphorylated ULK1 on S757 decreased. As phosphorylation of the major autophagy activator ULK1 on S757 by mTORC1 inhibits ULK1 activity and represses autophagy (35), our findings thus suggested that mTOR/ULK1 axis participates in echovirus-induced autophagy. Subsequently, Beclin-1 (a homolog of yeast ATG6) is the first identified mammalian autophagy protein critical for the signaling pathways involved in autophagosome formation (27). Some viral proteins, like hepatitis B virus X protein, can sensitize cells to starvation-induced autophagy *via* up-regulation of Beclin-1 expression. In the present study, we also observed the up-regulation of Beclin-1 during echovirus infection. In addition, Beclin-1 forms the class III PI3K complex with VPS34, which promotes autophagosome formation (36). Our data also showed that the levels of VPS34 increased upon echovirus infection. These results further demonstrated that echovirus could induce autophagy *via* activating autophagy signaling. Our preliminary data showed that VP1, a capsid protein of echovirus, did not participate in echovirus-induced autophagy. Therefore, further studies may be needed to elucidate the mechanism by which echovirus infection regulates mTOR/ULK1 signaling pathway.

In conclusion, our study demonstrates that autophagy can be induced by echovirus infection and exhibits a proviral function, revealing the potential role of autophagy in echovirus infection.

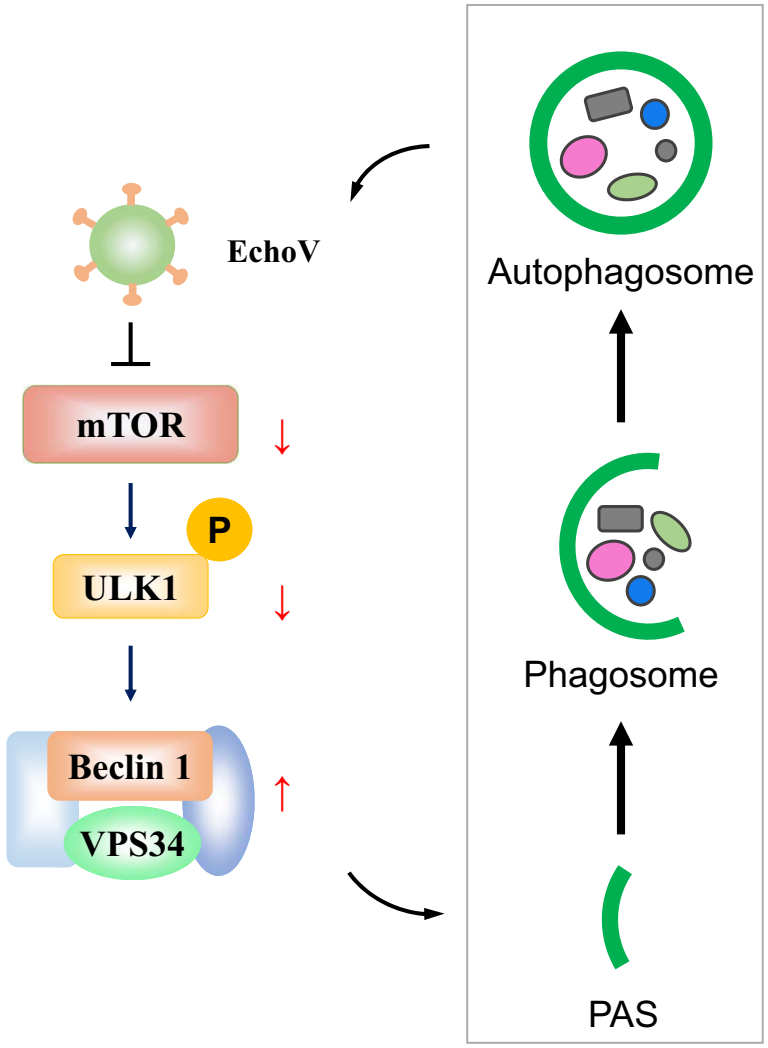

FIGURE 8
A proposed model depicting the interplay between echovirus infection and autophagy *via* regulating mTOR/ULK1 signaling pathway. Upon echovirus infection, the levels of phosphorylated mTOR and phosphorylated ULK1 protein on S757 decreased. Furthermore, both VPS34 and Beclin-1 protein levels increased, which promotes the formation of autophagic vesicles. Echovirus-induced autophagy promoted viral replication.

These findings not only shed light on the molecular mechanisms underlying how echovirus hijacks cellular components and pathways for its benefits but also provide therapeutic options against echovirus infection.

Data availability statement

The original contributions presented in the study are included in the article/supplementary materials. Further inquiries can be directed to the corresponding author.

Author contributions

CW and JX designed the research, wrote and revised the paper. LZ, WY, YM and YL performed the experiments. QW, SL, GP and ZZ analyzed the data. All authors contributed to the article and approved the submitted version.

Funding

This study was supported by grants from the Natural Science Foundation of Hubei Province of China (2022CFB564), the Health Commission Foundation of Hubei Province of China (WJ2023M108), the Open project of National Virus Resource Center (NVRC-PY-03), Sino-German mobility programme (M-0060), Traditional Chinese Medicine Administration Foundation of Hubei Province of China (ZY2023F027) and the Young and Middle-aged Medical Professionals in Wuhan (grant number 1030000301). This work was also supported by the International Cooperation Base of Hubei Province for Infection and Immunity.

Conflict of interest

The authors declare that the research was conducted in the absence of any commercial or financial relationships that could be construed as a potential conflict of interest.

The reviewer YX declared a shared parent affiliation with the author SL at the time of review.

Publisher's note

References

1. Pons-Salort M, Parker EP, Grassly NC. The epidemiology of non-polio enteroviruses: Recent advances and outstanding questions. *Curr Opin Infect Dis* (2015) 28(5):479–87. doi: 10.1097/QCO.0000000000000187

2. Committee ON the Echo Viruses. ENTERIC cytopathogenic human orphan (ECHO) viruses. *Science* (1955) 122(3181):1187–8. doi: 10.1126/science.122.3181.1187

3. Rotbart HA. Enteroviral infections of the central nervous system. *Clin Infect Dis* (1995) 20(4):971–81. doi: 10.1093/clinids/20.4.971

4. Nagington J. Echovirus 11 infection and prophylactic antiserum. *Lancet* (1982) 1 (8269):446. doi: 10.1016/S0140-6736(82)91642-7

5. Nagington J, Wreghittt TG, Gandy G, Roberton NR, Berry PJ. Fatal echovirus 11 infections in outbreak in special-care baby unit. *Lancet* (1978) 2(8092 Pt 1):725–8. doi: 10.1016/S0140-6736(78)92714-9

6. Nagington J, Gandy G, Walker J, Gray JJ. Use of normal immunoglobulin in an echovirus 11 outbreak in a special-care baby unit. *Lancet* (1983) 2(8347):443–6. doi: 10.1016/S0140-6736(83)90402-6

7. Rabkin CS, Telzak EE, Ho MS, Goldstein J, Bolton Y, Pallansch M, et al. Outbreak of echovirus 11 infection in hospitalized neonates. *Pediatr Infect Dis J* (1988) 7(3):186–90.

8. Chevaliez S, Szendroi A, Caro V, Balanant J, Guillot S, Berencsi G, et al. Molecular comparison of echovirus 11 strains circulating in Europe during an epidemic of multisystem hemorrhagic disease of infants indicates that evolution generally occurs by recombination. *Virology* (2004) 325(1):56–70. doi: 10.1016/j.virol.2004.04.026

9. Khetsuriani N, Lamonte A, Oberste MS, Pallansch M. Neonatal enterovirus infections reported to the national enterovirus surveillance system in the united states, 1983-2003. *Pediatr Infect Dis J* (2006) 25(10):889–93. doi: 10.1097/01.inf.0000237798.07462.32

10. Chuang YY, Huang YC. Enteroviral infection in neonates. *J Microbiol Immunol Infect* (2019) 52(6):851–7. doi: 10.1016/j.jmii.2019.08.018

11. Li J, Yan D, Chen L, Zhang Y, Song Y, Zhu S, et al. Multiple genotypes of echovirus 11 circulated in mainland China between 1994 and 2017. *Sci Rep* (2019) 9 (1):10583. doi: 10.1038/s41598-019-46870-w

12. Lu J, Kang M, Zeng H, Zhong Y, Fang L, Zheng X, et al. Tracking echovirus eleven outbreaks in guangdong, China: A metatranscriptomic, phylogenetic, and epidemiological study. *Virus Evol* (2020) 6(1):veaa029. doi: 10.1093/ve/veaa029

13. Mizushima N, Komatsu M. Autophagy: Renovation of cells and tissues. *Cell* (2011) 147(4):728–41. doi: 10.1016/j.cell.2011.10.026

14. Choi Y, Bowman JW, Jung JU. Autophagy during viral infection - a double-edged sword. *Nat Rev Microbiol* (2018) 16(6):341–54. doi: 10.1038/s41579-018-0003-6

15. Deretic V, Levine B. Autophagy balances inflammation in innate immunity. *Autophagy* (2018) 14(2):243–51. doi: 10.1080/15548627.2017.1402992

16. Deretic V, Saitoh T, Akira S. Autophagy in infection, inflammation and immunity. *Nat Rev Immunol* (2013) 13(10):722–37. doi: 10.1038/nri3532

17. Liang S, Wu YS, Li DY, Tang JX, Liu HF. Autophagy in viral infection and pathogenesis. *Front Cell Dev Biol* (2021) 9:766142. doi: 10.3389/fcell.2021.766142

18. Wong J, Zhang J, Si X, Gao G, Mao I, McManus BM, et al. Autophagosome supports coxsackievirus B3 replication in host cells. *J Virol* (2008) 82(18):9143–53. doi: 10.1128/JVI.00641-08

19. Dreux M, Gastaminza P, Wieland SF, Chisari FV. The autophagy machinery is required to initiate hepatitis c virus replication. *Proc Natl Acad Sci USA* (2009) 106 (33):14046–51. doi: 10.1073/pnas.0907344106

20. Taylor MP, Kirkegaard K. Potential subversion of autophagosomal pathway by picornaviruses. *Autophagy* (2008) 4(3):286–9. doi: 10.4161/auto.5377

21. Kim C, Bergelson JM. Echovirus 7 entry into polarized caco-2 intestinal epithelial cells involves core components of the autophagy machinery. *J Virol* (2014) 88(1):434–43. doi: 10.1128/JVI.02706-13

22. Yuan Y, Zhao K, Yao Y, Liu C, Chen Y, Li J, et al. HDAC11 restricts HBV replication through epigenetic repression of cccDNA transcription. *Antiviral Res* (2019) 172:104619. doi: 10.1016/j.antiviral.2019.104619

23. Xia J, Cao L, Zhao Z, Deng Y, Lu M, Wu C, et al. HBV sL13H mutation impairs its surface antigen expression and ability to induce autophagy. *Genes Dis* (2022) 9 (6):1401–4. doi: 10.1016/j.gendis.2022.01.004

24. Klionsky DJ, Abeliovich H, Agostinis P, Agrawal DK, Aliev G, Askew DS, et al. Guidelines for the use and interpretation of assays for monitoring autophagy in higher eukaryotes. *Autophagy* (2008) 4(2):151–75. doi: 10.4161/auto.5338

25. Kabeya Y, Mizushima N, Ueno T, Yamamoto A, Kirisako T, Noda T, et al. LC3, a mammalian homologue of yeast Apg8p, is localized in autophagosome membranes after processing. *EMBO J* (2000) 19(21):5720–8. doi: 10.1093/emboj/19.21.5720

26. Zachari M, Ganley IG. The mammalian ULK1 complex and autophagy initiation. *Ess. Biochem* (2017) 61(6):585–96. doi: 10.1042/EBC20170021

27. Cao Y, Klionsky DJ. Physiological functions of Atg6/Beclin 1: A unique autophagy-related protein. *Cell Res* (2007) 17(10):839–49. doi: 10.1038/cr.2007.78

28. Wileman T. Aggresomes and autophagy generate sites for virus replication. *Science* (2006) 312(5775):875–8. doi: 10.1126/science.1126766

29. Zhou Z, Jiang X, Liu D, Fan Z, Hu X, Yan J, et al. Autophagy is involved in influenza a virus replication. *Autophagy* (2009) 5(3):321–8. doi: 10.4161/auto.5.3.7406

30. Chiramel AI, Best SM. Role of autophagy in zika virus infection and pathogenesis. *Virus Res* (2018) 254:34–40. doi: 10.1016/j.virusres.2017.09.006

31. Robinson SM, Tsueng G, Sin J, Mangale V, Rahawi S, McIntyre LL, et al. Coxsackievirus b exits the host cell in shed microvesicles displaying autophagosomal markers. *PloS Pathogens* (2014) 10(4):e1004045. doi: 10.1371/journal.ppat.1004045

32. Wang L, Tian Y, Ou JH. HCV induces the expression of Rubicon and UVRAG to temporally regulate the maturation of autophagosomes and viral replication. *PloS Pathogens* (2015) 11(3):e1004764. doi: 10.1371/journal.ppat.1004764

33. Tian L, Yang Y, Li C, Chen J, Li Z, Li X, et al. The cytotoxicity of coxsackievirus B3 is associated with a blockage of autophagic flux mediated by reduced syntaxin 17 expression. *Cell Death Dis* (2018) 9(2):242. doi: 10.1038/s41419-018-0271-0

34. Kim YC, Guan KL. mTOR: a pharmacologic target for autophagy regulation. *J Clin Invest* (2015) 125(1):25–32. doi: 10.1172/JCI73939

35. Kim J, Kundu M, Viollet B, Guan KL. AMPK and mTOR regulate autophagy through direct phosphorylation of Ulk1. *Nat Cell Biol* (2011) 13(2):132–41. doi: 10.1038/ncb2152

36. Liang XH, Jackson S, Seaman M, Brown K, Kempkes B, Hibshoosh H, et al. Induction of autophagy and inhibition of tumorigenesis by beclin 1. *Nature* (1999) 402 (6762):672–6. doi: 10.1038/45257

frontiers | Frontiers in Immunology

TYPE Original Research
PUBLISHED 20 April 2023
DOI 10.3389/fimmu.2023.1139808

OPEN ACCESS

EDITED BY
Rongtuan Lin,
McGill University, Canada

REVIEWED BY
David Marchant,
University of Alberta, Canada
Marceline Côté,
University of Ottawa, Canada
Robert E. Cone,
University of Connecticut Health Center, United States

*CORRESPONDENCE
Subhasis Chattopadhyay
subho@niser.ac.in
Soma Chattopadhyay
sochat.ils@gmail.com

SPECIALTY SECTION
This article was submitted to Viral Immunology, a section of the journal Frontiers in Immunology

RECEIVED 07 January 2023
ACCEPTED 29 March 2023
PUBLISHED 20 April 2023

CITATION
Mahish C, De S, Chatterjee S, Ghosh S, Keshry SS, Mukherjee T, Khamaru S, Tung KS, Subudhi BB, Chattopadhyay S and Chattopadhyay S (2023) TLR4 is one of the receptors for Chikungunya virus envelope protein E2 and regulates virus induced pro-inflammatory responses in host macrophages.
Front. Immunol. 14:1139808.
doi: 10.3389/fimmu.2023.1139808

TLR4 is one of the receptors for Chikungunya virus envelope protein E2 and regulates virus induced pro-inflammatory responses in host macrophages

Chandan Mahish[1,2], Saikat De[3,4], Sanchari Chatterjee[3,4], Soumyajit Ghosh[3,4], Supriya Suman Keshry[3,5], Tathagata Mukherjee[1,2], Somlata Khamaru[1,2], Kshyama Subhadarsini Tung[1,2], Bharat Bhusan Subudhi[6], Soma Chattopadhyay[3]* and Subhasis Chattopadhyay[1,2]*

[1]School of Biological Sciences, National Institute of Science Education and Research Bhubaneswar, Jatni, Odisha, India, [2]Homi Bhabha National Institute, Training School Complex, Anushaktinagar, Mumbai, Maharashtra, India, [3]Institute of Life Sciences, Bhubaneswar, India, [4]Regional Centre for Biotechnology, Faridabad, India, [5]School of Biotechnology, Kalinga Institute of Industrial Technology (KIIT) University, Bhubaneswar, India, [6]School of Pharmaceutical Sciences, Siksha O Anusandhan Deemed to be University, Bhubaneswar, Odisha, India

Toll like receptor 4 (TLR4), a pathogen-associated molecular pattern (PAMP) receptor, is known to exert inflammation in various cases of microbial infection, cancer and autoimmune disorders. However, any such involvement of TLR4 in Chikungunya virus (CHIKV) infection is yet to be explored. Accordingly, the role of TLR4 was investigated towards CHIKV infection and modulation of host immune responses in the current study using mice macrophage cell line RAW264.7, primary macrophage cells of different origins and *in vivo* mice model. The findings suggest that TLR4 inhibition using TAK-242 (a specific pharmacological inhibitor) reduces viral copy number as well as reduces the CHIKV-E2 protein level significantly using p38 and JNK-MAPK pathways. Moreover, this led to reduced expression of macrophage activation markers like CD14, CD86, MHC-II and pro-inflammatory cytokines (TNF, IL-6, MCP-1) significantly in both the mouse primary macrophages and RAW264.7 cell line, *in vitro*. Additionally, TAK-242-directed TLR4 inhibition demonstrated a significant reduction of percent E2-positive cells, viral titre and TNF expression in hPBMC-derived macrophages, *in vitro*. These observations were further validated in TLR4-knockout (KO) RAW cells. Furthermore, the interaction between CHIKV-E2 and TLR4 was demonstrated by immuno-precipitation studies, *in vitro* and supported by molecular docking analysis, *in silico*. TLR4-dependent viral entry was further validated by an anti-TLR4 antibody-mediated blocking experiment. It was noticed that TLR4 is necessary for the early events of viral infection, especially during the attachment and entry stages. Interestingly, it was also observed that TLR4 is not involved in the post-entry stages of CHIKV infection in host macrophages. The administration of TAK-242 decreased CHIKV infection significantly by reducing disease manifestations, improving survivability (around

75%) and reducing inflammation in mice model. Collectively, for the first time, this study reports TLR4 as one of the novel receptors to facilitate the attachment and entry of CHIKV in host macrophages, the TLR4-CHIKV-E2 interactions are essential for efficient viral entry and modulation of infection-induced pro-inflammatory responses in host macrophages, which might have translational implication for designing future therapeutics to regulate the CHIKV infection.

KEYWORDS

Chikungunya virus (CHIKV), toll-like receptor 4 (TLR4), CHIKV-E2, pro-inflammatory cytokines, inflammation

1 Introduction

Since the first report in 1952, the Chikungunya virus (CHIKV) (Family: Togaviridae; Genus: Alphavirus) has been considered a global public threat over the years. Two massive outbreaks in the last two decades (2004 and 2013) across different regions of the globe emphasize the severity and re-emerging nature of Chikungunya. One of the major governing factors for these repeated outbreaks are mainly unhygienic densely populated habitat with ineffective mosquito control capacity as Chikungunya in mosquito-borne (*Aedes* sp.) disease. Other associated factors are favorable climate for mosquito breeding, lack of available vaccines and proper medications (1, 2).

The pathophysiological manifestations of Chikungunya can be classified into three stages, namely, acute, sub-acute and chronic. The major symptoms of the acute stage are mainly high fever, polyarthralgia, headache, loss of appetite and rashes. The symptoms may last up to 3 months for the sub-acute stage. Although the acute stage has less severity, it may bring severe complications in neonates, pregnant women, patients suffering from comorbidities and aged people (over 65 years). The reported complications are failure of either neuronal, cardiovascular, renal, or respiratory systems. The chronic stage of infection may affect around 40% of the patients and the major symptoms are chronic arthralgia, myalgia, long term fatigue which might lead to permanent physical disability (1, 3, 4).

The mechanistic view on CHIKV entry in the host is not well understood till date. However, several entry pathways, for example, the clathrin-mediated pathway, epidermal growth factor receptor substrate 15 (Eps15)-dependent pathway and macropinocytosis have been experimentally demonstrated to be associated with CHIKV attachment and entry in the host (5–7). For CHIKV attachment, cell surface glycosaminoglycans (GAG), glycoprotein T-cell immunoglobulin and mucin 1 (TIM-1), TIM-4, Axl, C-type calcium-dependent lectin DC-SIGN (DC-specific intercellular adhesion molecule-3-grabbing non-integrin) and prohibitin (PHB) 1 and 2 were found as interaction and attachment factors in the host (8–17). Recently, a cell adhesion molecule, Mxra8 has been found to block CHIKV infection in presence of an anti-Mxra8 monoclonal antibody, although the absence of functional Mxra8 could not completely block CHIKV infection *in vitro* and *in vivo* (18). Therefore, Mxra8 acts as one of the enhancers for CHIKV attachment and internalization process into the host cell.

Several clinical and experimental studies have revealed that the Chikungunya virus (CHIKV) infection leads to the profound production of pro-inflammatory cytokines and chemokines such as tumor necrosis factor (TNF), interleukin (IL)-6, 4, 1β and 12 in human as well as in mouse macrophages *via* p38 and Jun N-terminal protein kinase (JNK)-mitogen-activated protein kinase (MAPK) mediated pathway, which may aggravate host immune system towards CHIKV infection mediated fever (CHIKF) and polyarthralgia (19–22). However, the initial pathways behind CHIKV-driven pro-inflammatory responses are still unexplored. Interestingly, the role of toll like receptor 4 (TLR4) has been critically investigated for mediating inflammatory responses in various cases of microbial infections, immune regulation in cancer and autoimmunity (23–25). TLR4 has also been well reported to induce massive pro-inflammatory responses upon binding of lipid A region of lipopolysaccharide (LPS), a cell wall component of Gram-negative bacteria (26). Moreover, the functional association of TLR4 is well established for other pro-inflammatory clinical abnormalities such as inflammatory bowel disease (IBD) and necrotizing enterocolitis (NEC) (27, 28). To establish the role of TLR4 in various *in vivo* inflammatory conditions such as mice sepsis model or LPS-induced lung injury model, a cyclohexene derivative molecule, TAK-242, has been used as a specific blocker of TLR4-dependent inflammation (24, 29). Furthermore, TLR4-dependent viral entry and infection progression of respiratory syncytial virus (RSV) has been described in mice model (30). Recently, several viral structural proteins are proposed to act as potential ligands for TLR4 activation (31, 32).

CHIKV-induced host cell activation and a rise in associated pro-inflammatory responses are already reported by us and others (19, 22, 33). Earlier studies have revealed that the pro-inflammatory cytokines along with MAPKs are induced during CHIKV infection in the host macrophages (19, 22). Since TLR4 activation could be connected with TNF response and MAPK activation (34, 35), the possible interaction of TLR4 with CHIKV infection along with subsequent regulation of host immune responses, if any, needs to be explored. Hence, it has been hypothesized that TLR4 might be pivotal to regulate CHIKV infection and associated host immune

responses. Accordingly, in the current study, the probable role of TLR4 has been investigated in CHIKV infection, inflammation and modulation of host immune responses using different *in vitro* models, *in silico* studies and *in vivo* mice model.

2 Materials and methods

2.1 Cells, virus and reagents

The RAW264.7 (ATCC® TIB-71™), BALB/c and C57BL/6 mice-derived peritoneal monocyte-macrophage cells were maintained in complete RPMI media consisting RPMI-1640 (Gibco, USA), supplemented with antibiotic-antimycotic solution, L-glutamine (HiMedia Laboratories Pvt. Ltd, MH, India) and 10% heat-inactivated Fetal bovine serum (Gibco, USA) at 37°C in a humidified incubator with 5% CO_2. The TLR4KO RAW (RAW-Dual KO™-TLR4; catalog number: rawd-kotlr4, Invivogen, USA) (36) and the Vero Cells were maintained in DMEM (catalog number: 11965-092; Gibco, USA) supplemented with 10% FBS, L-glutamine and antibiotic-antimycotic solution. The CHIKV-Indian Strain (IS) (accession no- EF210157.2), anti-CHIKV-E2 antibody and Vero cells were kind gifts from Dr. M.M. Parida, DRDE, Gwalior, India. The anti-CHIKV-E1 antibody was a kind from Dr. T.K. Chowdary, NISER, Bhubaneswar, India. TAK-242 (catalog no: 614316-5MG), a well-cited TLR4 inhibitor was purchased from Merck Millipore, USA (24, 34, 37). The antibodies against CD86 (Fluorochrome: APC; Catalogue number: 17-0862-82) and MHC-II (Fluorochrome: PE; Catalogue number: 12-5321-82) were purchased from eBiosciences, USA. PerCP-Cy5.5 conjugated CD14 antibody (catalog number: 560638) was purchased from BD Biosciences, USA. The unconjugated antibodies against p-NF-κB p65 (Catalogue number: 3031), total p38 (catalog number: 9212), phosphorylated p38 (catalog number:9211), total SAPK-JNK (catalog number:9252) and phosphorylated SAPK-JNK (catalog number: 4668) proteins were bought from Cell Signaling Technology (Denver, USA). Alexa fluor (AF)-647 conjugated TLR4-MD2 monoclonal antibody (clone Number: MTS510, catalog number: NBP2-24865AF647), used in flow cytometry, was purchased from Novus Biologicals (Littleton, Colorado, USA). The TLR4 polyclonal antibody (catalog number: 48-2300), used in co-immunoprecipitation and Western Blot, was purchased from Invitrogen (Carlsbad, USA). Fluorochrome (AF488/AF647) conjugated anti-mouse and rabbit secondary antibodies (used for flow cytometry) and HRP-conjugated anti-mouse and rabbit secondary antibodies (used in Western Blot and co-immunoprecipitation analysis) were purchased from Invitrogen, USA. The GAPDH (catalog number: 10-10011) and β-actin (catalog number: 11-13012) antibodies were bought from Abgenex India Pvt. Ltd, Bhubaneswar, India.

2.2 hPBMC isolation

Human blood was drawn from healthy donors following the guidelines of the Institutional Ethics Committee, NISER, Bhubaneswar (NISER/IEC/2022-04). The procedure for generating myeloid adherent cells from human peripheral blood mononuclear cells (hPBMC) was followed as described elsewhere with little modifications (38–41). Briefly, circulating monocytes were enriched by 2 h adherence after Hi-Sep LSM (catalog number: HiSep LSM™ 1077- LS001; HiMedia Laboratories Pvt Ltd, India) based density gradient-centrifugation according to the manufacturer's instructions. The adherent cells were cultured in RPMI-1640 supplemented with 10% FBS, antibiotic-antimycotic solution and L-glutamine for 3–5 days. The adherent cells obtained after 96 h were of monocyte-macrophage lineages (more than 97%) as found enriched with $CD14^+CD11b^+$ population (42, 43). The monocyte-macrophage cells derived from hPBMC were seeded in 12 well plates (Thermo Fischer, USA) at a density of $0.8x10^6$ cells/well. After 24 h of seeding, pre-incubation was carried out for 3 h with 1 μM of TAK-242, followed by CHIKV infection with MOI 5 for 2 h (19). The infected cells were harvested at 8 hours post-infection (hpi) and downstream experiments were conducted.

2.3 Cell viability assay

The working concentrations of TAK-242 in different host macrophage systems were determined using either the AnnexinV-7-AAD-based method (Annexin V: PE Apoptosis detection kit I, catalog number: 559763; BD Biosciences, USA) or MTT assay-based method (EZcount™ MTT cell assay kit, catalog number: CCK-003-2500; HiMedia laboratories Pvt. Ltd, India) as per manufacturer's protocol.

2.4 LPS induction in RAW264.7 cells

The RAW264.7 cells were induced with LPS as per earlier reports with required modifications (44). Around $4.5x10^6$ cells were seeded per 90 mm cell culture dishes (Genetix Biotech Asia Pvt Ltd, India) for 16-18 h. The cells were washed with 1X PBS (RT) twice and pre-incubated with either DMSO or 1μM TAK-242 for 3 h. Next, the cells were treated with 500 ng/mL of LPS (catalog number: L5293-2ML, Sigma-Aldrich, Germany) for 6 h. Finally, the cells were scraped using a sterile cell scraper (Genetix, India) with 1X PBS and processed for downstream experiments.

2.5 CHIKV infection

The RAW264.7 cell line, TLR4KO RAW cell line, BALB/c and C57BL/6 mice-derived peritoneal monocyte-macrophages were infected with CHIKV-IS as reported earlier with minute modifications (19, 22, 40, 41, 45, 46). Briefly, $4.5x10^6$ cells were seeded in 90 mm dishes and allowed to grow for 16-18 h. Next, the cells were washed with 1X PBS 2 times and pre-incubated with either TAK-242 or DMSO for 3 h. For TAK-242 treated conditions, the cells were incubated with 0.5 and/or 1 μM concentrations of TAK-242 for 3 h before infection, during infection and post-infection. After pre-incubation, the cells were washed followed by

CHIKV infection at 5 MOI for 2 h. Post-CHIKV infection, the cells were washed and supplemented with complete RPMI media till the harvesting time point (8 hpi).

2.6 Flow cytometry

The expression of intracellular and surface markers was investigated using a flow cytometry-based study as described before (19, 22). Briefly, the cells were scrapped out with a cell scraper at 8 hpi time point and washed with 1X PBS before distribution to microcentrifuge tubes. For surface staining, the washed cells were subjected to Fc blocking using Fc blocking reagent (catalog number: 130-092-575; Miltenyi Biotec, Germany) as per the manufacturer's protocol. Next, the cells were incubated with antibodies against surface markers for 30 minutes at 4°C in dark. Finally, the cells were washed with FACS buffer (1X PBS, 1% BSA, 0.01% NAN_3) and acquired immediately in the flow cytometer. TLR4 and the macrophage activation markers such as CD86, MHC-II and CD14 were tested by surface staining using fluorochrome-conjugated monoclonal antibodies and acquired in the flow cytometer. To study the intracellular markers, such as CHIKV-E2, p-NF-κB or total TLR4, the cells were initially fixed with 4% paraformaldehyde (HiMedia Laboratories Pvt. Ltd., India) for 10 minutes at room temperature and washed with chilled 1X PBS two times to remove any remnant paraformaldehyde. The fixed cells were permeabilized with permeabilization buffer (1X PBS, 0.5% BSA, 0.1% Saponin and 0.01% NaN_3) for 15 minutes at RT followed by blocking with blocking buffer (1X PBS, 1% BSA, 0.1% Saponin and 0.01% NaN_3) for 30 minutes at RT. Next, the cells were further treated with primary (anti-M-CHIKV-E2, anti-R-p-NF-κB antibodies) and their respective fluorochrome-conjugated secondary antibodies sequentially diluted in permeabilization buffer. For TLR4 staining, the cells were incubated with fluorochrome-conjugated antibody (anti-M-TLR4-AF647) diluted in permeabilization buffer. Finally, the cells were washed and re-suspended in FACS buffer and kept at 4°C in dark till acquisition in the flow cytometer. The intracellular cytokine staining starter kit -Mouse (catalog number: 51-2041-AK; BD Biosciences, USA) and BD Golgistop Solution (catalog number-554724, BD Biosciences, USA) were used as per the manufacturer's protocol for dual staining of intracellular cytokine (TNF) and CHIKV-E2 protein together. All samples were acquired using BD LSRFortessa flow cytometer and analyzed by the FlowJo™ software (BD Biosciences, USA). Around ten thousand cells were acquired per sample per experimental set (minimum three biological replicates were performed).

2.7 ELISA

The cell-free culture supernatants from different experimental conditions were subjected to cytokine quantification using the BD OptEIA™ Sandwich ELISA kit (BD biosciences, USA) as per the manufacturer's instructions. Quantification of cytokines was done with respect to the standard curves prepared using the recombinant cytokines with different concentrations at pg/mL, as reported earlier (19, 22, 45).

2.8 qRT-PCR and plaque assay

The viral RNA from cell-free culture supernatants was isolated using the QIAamp Viral RNA mini kit (Qiagen, Germany) as performed earlier (40). Briefly, an equal volume of the viral RNA from all experimental conditions was taken for cDNA synthesis using the Primescript™ 1st strand cDNA synthesis kit (Takara Bio Inc, Japan) obeying the manufacturer's protocol. The E1 gene was amplified using specific primers (CL11F: 5'-TGCCGTCACAGTTAAGGACG-3', CL12R: 5'-CCTCGCATG ACATGTCCG-3') and the PowerUp™ SYBR™ Green Master Mix (Thermo Fisher Scientific, USA) in Applied Biosystems™ QuantStudio™ 7 Flex Real-Time PCR System (Applied Biosystems, USA) as per the manufacturer's instructions. The C_t values were plotted against the standard curve to determine the corresponding viral copy number as mentioned earlier (19, 40). To study the intracellular CHIKV copy numbers, the total RNA isolation kit (Catalogue number: MB602-50PR, HiMedia laboratories Pvt. Ltd., India) was used to isolate RNA from the cells. 1 µg of total RNA was converted to cDNA followed by qRT-PCR analysis using the above-mentioned kits and reagents. The intracellular viral copy numbers were normalized against GAPDH, the housekeeping gene (Forward:5'-CAAGGTCATCCATGACAACTTTG-3', Reverse:5'-GTCCACCACCCTGTTGCTGTAG-3').

The plaque assay was performed using Vero cells to assess the viral titre as per the protocol mentioned earlier (19). In brief, the CHIKV-infected cell-free culture supernatants were used to infect Vero cells. Post-infection, 5% FBS-supplemented DMEM media mixed with 20% methyl-cellulose (catalog number: M0387; Sigma-Aldrich, USA) was laid over the infected cells for 3-4 days. Next, the cells were fixed using 8% formaldehyde (catalog number: M0387; HiMedia Laboratories Pvt. Ltd, India) and stained with crystal violet to determine the plaque forming units (PFU) manually under the white light of trans-illuminator (Vilber Lourmat, France).

2.9 Effect of TAK-242 before, during and after CHIKV infection

To investigate the possible anti-CHIKV effect of TAK-242, in specific stages of viral infection, the following experiment was performed in RAW264.7 cells as per the method described earlier (40, 46). Briefly, the TAK-242 treatment was given at different stages of CHIKV infection namely, before CHIKV infection (only pre-incubation), during CHIKV infection, both before and during CHIKV infection (pre+during incubation), post-infection incubation at 0 hpi (the drug was added at 0 hpi) and 8 hpi (the drug was added at 8 hpi). Besides the drug treatment, the CHIKV infection was given in all of the conditions in a similar way as described above i.e., infection was given with MOI 5 for 2 h. The cell

culture supernatants were collected at 9 hpi and qRT-PCR was carried out to determine the CHIKV copy numbers.

2.10 Viral attachment assay

To investigate whether TAK-242 has any role in CHIKV adsorption during virus infection, a study was performed to quantitate the unbound CHIKV particles as performed earlier (45). Briefly, the RAW264.7 cells were pre-treated with either DMSO or 1μM TAK-242 for 3 h and further subjected to CHIKV infection with MOI 5 for 2 h. After CHIKV infection, the inoculum volume containing unbound virus particles was collected and subjected to plaque assay and/or qRT-PCR to assess the effect of the drug on viral attachment to the cells.

2.11 Time of addition experiment

To study the role of TLR4 in specific stages of the CHIKV life cycle, a time of addition experiment was carried out as described earlier (40, 46). To perform the experiment, no drug treatment was given before or during viral infection. Following the CHIKV infection, TAK-242 was added to the cells at different time points post-infection (0,2,4,8,10,12 and 14 hpi). The cell culture supernatants from all of the time points were collected at 15 hpi for the determination of viral titre using plaque assay.

2.12 Western blot

The differential expression of viral E2, E1, TLR4 and MAPK proteins pathways was investigated using Western blot analysis as described before (22). Briefly, the cells were scraped from different experimental groups and washed with cold 1X PBS two times before preparation of whole cell lysate using Radio Immuno Precipitation Assay (RIPA) lysis buffer (150 mM NaCl, pH-8, 1% NP-40, 0.5% Sodium deoxycholate, 0.1% SDS, 50 mM Tris). After lysis, the solutions were centrifuged at 15000 rpm for 30 minutes at 4°C and the supernatants were collected. The protein lysates were quantified using Bradford reagent (catalog number: B6916-500 ML, Sigma-Aldrich, USA). 2X Sample buffer (pH-8, 130mM Tris-Cl, 20% glycerol (v/v), 4.6% SDS (w/v), 2% DTT, and 0.02% Bromophenol blue) was mixed with samples in a ratio of 1:1 and 30 μg of total protein was loaded in each well of 10% SDS-PAGE gel. Next, the proteins on the gel were transferred to a PVDF membrane (catalog number: IPVH00010; Millipore, USA) followed by blocking with 3% BSA (catalog number: MB083; HiMedia Laboratories Pvt Ltd, India). Then, overnight primary antibody incubation was performed using different antibodies like the total and phospho-p38 and SAPK-JNK (1:1000), GAPDH and Beta-Actin (1:2000) and CHIKV-E2 (1:1000). The blots were thoroughly washed five times with 1X tris buffer with 0.1% Tween-20 (TBST) and corresponding anti-Mouse and Rabbit HRP conjugated secondary antibodies (catalog number: 31430 and 31460 respectively; Invitrogen, USA) were probed for 2 h at RT. The blots were washed three times with 1X TBST and the images were captured using the ChemiDoc XRS$^+$ imaging system and analyzed by the Image Lab software (Bio-Rad, USA).

2.13 *In silico* analysis

The ZDOCK webserver was used to study the protein-protein interaction. The protein-protein docking is based on the Fast Fourier Transform algorithm that utilizes a combination of shape complementarity, electrostatics and statistical potential terms for predicting the interaction complex (47). The MD2-TLR4 activated complex (PDB ID: 2Z64) was used as the receptor. The CHIKV-E2 structure extracted from the mature envelope glycoprotein complex of CHIKV (PDB ID: 3N41) was used as a ligand. The top-ranked output was visualized by the PyMol software.

2.14 Co-immunoprecipitation

For TLR4-E2/E1 interaction study, the cells were lysed with 1X RIPA buffer (the composition is the same as described in the WB section) after viral infection. The lysates were subjected to immunoprecipitation by the Dynabeads® Protein G Immunoprecipitation Kit (Thermo Fisher Scientific, USA) as per the protocol mentioned earlier (22). Briefly, both the mock and CHIKV-infected whole cell lysates were incubated with primary antibody (E2 or E1) and Dynabeads® protein G. The Dynabeads®-Ab-Ag complexes were washed, eluted and processed further for Western blot analysis.

2.15 Anti-TLR4 blocking assay

The anti-TLR4 blocking assay was performed in the RAW264.7 macrophage cells as per the protocol described elsewhere with little modifications (48). Before pre-incubation with DMSO or TAK-242, either anti-TLR4 antibody (Catalogue number: 48-2300, Invitrogen, USA) or anti-rabbit IgG antibody (Catalogue Number: 2729s, Cell signaling technology, USA) was added to the pre-incubation media at 5μg/ml concentration. The cells with different treatments were preincubated for 3 h. Next, the cells were given CHIKV infection at MOI 5 for 2 h. The cells were harvested at 8 hpi and subjected to flow cytometry and Western blot-based analysis. The cell culture supernatants were analyzed for secretory TNF level using ELISA based method. Here anti-rabbit IgG antibody was used as a negative control to conduct the experiment.

2.16 Animal studies

All animal experiments were conducted by following the guidelines of the Committee for the Purpose of Control and Supervision of Experiments on Animals (CPCSEA) of India with

the approval of the Institutional Animal Ethics Committee, NISER (1634/GO/ReBi/S/12/CPSCEA) and Institutional Animal Ethics Committee, ILS Bhubaneswar (76/Go/ReBi/S/1999/CPCSEA).

Six to eight-weeks aged male BALB/c and C57BL/6 mice were used to perform isolation of peritoneal macrophages as mentioned earlier with little modifications (49). In brief, 4-5 mice per set of the experiment were injected with 1 ml of 3.8% Brewer's Thioglycolate solution in the peritoneum cavity. After 3 days of injection, the mice were sacrificed and the peritoneal lavages were collected from the peritoneum cavity using chilled 1X PBS with 2% FBS in a sterile manner. Around $6x10^6$ total cells were plated in each 90 mm cell culture dish. After 24 h of seeding, cells were washed with 1X PBS at RT and further experiments were performed with the adherent monocyte-macrophage population.

In vivo mice model work on CHIKV infection was performed in a similar way as mentioned earlier (40, 46). In brief, 8-9 days old C57BL/6 mice were housed under specific germ-free conditions for 2-3 days before experimentation. For CHIKV infected mice group (n=5), 10-12 days old mice were injected subcutaneously with $1x10^7$ PFU of CHIKV-IS at the flank region of the right hind limb. For the mock mice group (n=5), serum-free medium was injected at the same position. For TAK-242 treated group (n=5), (dose:1 mg/kg body weight of mice) the drug was given orally from a day before CHIKV infection to 6 days after infection at every 24 h intervals. The mock and CHIKV-treated groups received an equal volume of serum-free media with DMSO for the same duration of the study. The dose of TAK-242 used in the current study was determined based on previously published data where 3 mg/kg dose was shown to be non-toxic and effective for similar mouse model experimentation (24, 37). Depending on their symptoms, the mice were sacrificed on the 5^{th} or 6^{th}-day post-infection (dpi) followed by the collection of blood serum, quadriceps muscles and spleens from the mock, CHIKV infected with solvent (DMSO) or TAK-242 treated mice groups. The serum TNF level was quantified by ELISA-based cytokine assay. The quadriceps muscles and spleen samples were snap-frozen followed by lysis with RIPA buffer for Western blot analysis. To quantitate the viral titre, an equal amount of tissues from each group was homogenized in serum-free RPMI media followed by syringe filtration using 0.22 µM filters. The solutions were further centrifuged and the supernatants were collected for plaque assay. For, the survival curve and clinical score analysis, a similar protocol was followed as mentioned above (n=6 for all three groups). The mice were monitored every day for the tabulation of clinical score and final survival curve analysis for up to 8 dpi and scored according to the phenotypic symptom-based disease outcomes [no symptoms-0, fur rise-1, hunchback-2, one hind limb paralysis-3, both hind limb paralysis-4, death-5] (40, 46, 50).

2.17 Statistical analysis

The GraphPad Prism 9 software (GraphPad Software Inc., San Diego, USA) was used for statistical analysis. All comparisons among different groups were performed by either the One-way ANOVA with Tuckey posthoc test or the unpaired t-test. All data were represented as mean ± SEM. All analyzed data are representative of at least 3 independent experiments where $p < 0.05$ was taken as statistically significant (ns: non-significant, $*p < 0.05$; $** p \leq 0.01$; $***p \leq 0.001$; $****p \leq 0.0001$).

3 Results

3.1 TLR4 inhibition abrogates LPS-induced macrophage activation and pro-inflammatory responses in the host macrophages, *in vitro*

The previously published literature already reports that TAK-242-driven TLR4 inhibition abrogates the upregulation of LPS-mediated pro-inflammatory responses in the RAW264.7 macrophages as well as in the BALB/c-derived peritoneal macrophages (34). Therefore, the effect of TAK-242 in LPS induced RAW264.7 cells has been studied as the experimental control for the current investigation.

To determine the working concentration of TAK-242, Annexin V-7-AAD staining was carried out in the RAW264.7 cells and peritoneal macrophages from BALB/c and C57BL/6 mice. For, the hPBMC-derived monocyte-macrophage cells, a MTT assay was carried out. The cells were incubated with different concentrations of TAK-242 for 24 h and more than 95% of the cells were found viable at 2µM concentratio n (Figures S1A–D). According to the previously studied data, TAK-242 effectively inhibits the upregulation of LPS-driven pro-inflammatory responses at 1µM concentration in the RAW264.7 cells (34). To investigate the effect of TAK-242 against LPS-mediated pro-inflammatory responses, the RAW264.7 cells were pre-incubated with either DMSO or 1µM of TAK-242 for 3 h and further treated with 500 ng/mL LPS for 6 h (44). TAK-242 was found not to affect the cell surface as well as total TLR4 expressions significantly in the mock RAW264.7 cells (data not shown).

As previously reported, the reduction in the cell surface TLR4 and increase in the total TLR4 occurs upon LPS or virus-mediated stimulations (32, 51, 52). The flow cytometry dot plot analysis revealed that the percent positive cells for the total TLR4 were increased during LPS and LPS with TAK-242 treated conditions with respect to mock significantly [66.5 ± 2.22% (Mock) to 89.5 ± 1.59% (LPS) and 85.5 ± 1.68% (TAK-242+LPS)] (Figure S2A). However, the percent positive cells for the cell surface TLR4 expression were reduced during LPS or LPS+ TAK-242 treatment [43.4 ± 1.42% (Mock) to 27.6 ± 1.1% (LPS) and 36.1 ± 0.757% (LPS +TAK-242)] (Figure S2B), which coincides with previous reports.

Based on LPS mediated TLR4 signaling mechanism (53, 54), CD14, a macrophage activation marker (43), was investigated as one of the TLR4 signaling molecules for the current study. Moreover, inducible activation markers on macrophages such as CD86 and MHC-II were also studied to demonstrate macrophage activation (19). The flow cytometry dot plot analysis of CD14 showed a significant increment during LPS treatment and further reduction upon TAK-242 treatment [16.233 ± 2.44% (Mock) to 25.2 ± 2.97% (LPS) and 21 ± 3.03% (LPS+TAK-242)] (Figure S2C).

CD86 was found to increase during LPS treatment and reduce further in TAK-242 with LPS treated condition [65.17 ± 1.337% (Mock) to 71.30 ± 1.553% (LPS) and 66.13 ± 1.325% (LPS+TAK-242)] (Figure S2D). MHC-II also showed a similar pattern of expression to CD86 under the same experimental conditions [40.07 ± 1.707% (Mock) to 51.07 ± 1.598% (LPS) and 47.33 ± 1.338% (LPS+TAK-242)] (Figure S2E).

The p-NF-κB activation-driven upregulation of pro-inflammatory cytokines (such as TNF) is already reported upon TLR4 activation (34, 55). The p-NF-κB expression was increased during LPS treatment and decreased further upon TAK-242 treatment in the LPS-induced cells [14.73 ± 2.153% (Mock) to 37.15.6 ± 3.762% (LPS) and 25.23 ± 2.533% (LPS+TAK-242)] (Figure S2F).

Furthermore, the earlier reports have described TLR4-directed upregulation of p38 and JNK-MAPK phosphorylation during LPS-induced pulmonary epithelial hyperpermeability and LPS treatment in human neutrophils respectively in a concentration-dependent manner (56, 57). Western Blot analysis revealed upregulation of TLR4 in both the LPS and LPS with TAK-242 treated conditions with respect to mock [2.328 ± 0.067 fold (LPS) and 2.205 ± 0.25 fold (LPS+TAK-242)] (Figures S2G, H). The assessment of phosphorylation of the SAPK-JNK pathway revealed that the LPS induction upregulates p-SAPK-JNK expression during LPS treatment which gets reduced during TAK-242 treatment in LPS induced cells [9.826 ± 0.62 fold (LPS) and 2.573 ± 0.09 fold (LPS+TAK-242)] (Figures S2G, I). Similarly, p-p38 expression showed a similar pattern in the LPS and LPS with TAK-242 treated conditions [2.373 ± 0.39 fold (LPS) and 1.044 ± 0.2465 fold (LPS+TAK-242)] (Figure S2G, J).

An earlier report has suggested that the upregulation of LPS-mediated pro-inflammatory responses was inhibited in presence of TAK-242 (34). In the current study, ELISA-based quantification of the secretory TNF showed a massive upregulation of TNF due to the LPS treatment and subsequent restoration upon TAK-242 treatment in a significant manner [394.4 ± 17.4 pg/mL (Mock) to 2585 ± 57.69 pg/mL (LPS) and 552.5 ± 13.06 pg/mL (LPS+TAK-242)] (Figure S2K).

Altogether, these results infer that TAK-242-directed TLR4 inhibition significantly inhibits the upregulation of the LPS-induced pro-inflammatory responses where TLR4 internalization might have a possible implication.

3.2 TLR4 antagonism reduces CHIKV infection in the host macrophages of different origins, *in vitro*

3.2.1 Inhibition of TLR4 abrogates CHIKV infection in the RAW264.7 cells, significantly

Based on our previous reports, where it was established that maximum CHIKV infection occurs at 8 hours post-infection (hpi) time point in the RAW264.7 macrophages, 8 hpi was selected for cell harvesting to carry out all the experiments of viral infection (19, 22). E2, an envelope protein of CHIKV, was taken as a marker to assess CHIKV infection in different host systems (19, 40, 41, 45, 46).

To understand the role of TLR4 in CHIKV infection, the TAK-242 treated RAW264.7 cells were infected and harvested at 8 hpi. The cells were subjected to flow cytometry to assess viral infection and macrophage activation. The culture supernatants were used to estimate the viral copy number by qRT-PCR and cytokine levels by ELISA. The reduction of E2 percent positive cells [15.43 ± 0.5175% (CHIKV) to 9.813 ± 0.8411% (TAK-242)] (Figure 1A) and significant decrease of corresponding viral copy number [58%] in presence of TAK-242 (1μM) (Figure 1B) indicated that TLR4 antagonism reduces CHIKV infection.

In addition, the flow cytometry data showed that the surface expression of TLR4 was reduced upon infection in a significant manner [from 45.33 ± 1.805% to 23.03 ± 2.266%] and it was further decreased nonsignificantly [18.2 ± 0.76%] in presence of TAK-242 treatment (Figure 1C). Interestingly, the upregulation of the total TLR4 was observed up on CHIKV infection and in presence of TAK-242 (1μM) [from 56.3 ± 2.066 (mock) to 75.5 ± 3.057 (CHIKV) and 73.2 ± 1.172 (TAK-242)] (Figure 1D).

To determine the differential macrophage activation, the percent expressions of CD86, MHC-II and CD14 were investigated in the RAW264.7 cells. It was observed that the percent expression of CD14 was increased in infection and decreased in the presence of TAK-242 (1μM) [from 5.57 ± 0.13% (mock) to 27.9 ± 2.088% (CHIKV) and 10.24 ± 1.157% (TAK-242)] (Figure 1E). Similarly, the CD86 expression was found to increase during CHIKV infection which was further reduced in presence of TAK-242 (1μM) [from 71.67 ± 0.29% (mock) to 89.03 ± 1.467% (CHIKV) and 77.6 ± 0.7234% (TAK-242)] (Figure 1F). The MHC-II expression was found to be upregulated during CHIKV infection significantly and reduced nonsignificantly during TAK-242 (1μM) treatment [from 42.87 ± 4.889% (mock) to 63.53 ± 1.12% (CHIKV) and 50.07 ± 2.896% (TAK-242)] (Figure 1G). Therefore, the data indicate that TLR4 antagonism might reduce CHIKV-mediated macrophage activation.

The level of p-NF-κB was determined by flow cytometry to assess the effect of TAK-242 in TLR4 signaling during CHIKV infection. It was observed that CHIKV infection resulted in an increase of p-NF-κB which was subsequently decreased upon the TAK-242 (1μM) treatment, significantly [from 19.37 ± 2.87% (mock) to 33.43 ± 3.083% (CHIKV) and 17.03 ± 2.854% (TAK-242)] (Figure 1H). As per reports, p-NF-κB activation is directly associated with inflammation (58, 59) and pro-inflammatory cytokines such as TNF, IL-6 and MCP-1 which are already reported to be involved with CHIKV-induced immune activation by us and others (19, 33). Accordingly, TNF was found to increase during CHIKV infection and decrease further upon TAK-242 (1μM) treatment, significantly [from 161.2 ± 28.34 (Mock) to 1340 ± 79.26 pg/mL (CHIKV) to 681.5± 97.3 pg/mL (TAK-242)] (Figure 1I). Similarly, secretory IL-6 was found to decrease significantly in presence of TAK-242 (1μM) treatment [from 411.1 ± 25.34 pg/mL (CHIKV) to 73.61± 8.047 pg/mL (TAK-242)] (Figure 1J). Additionally, reduced MCP-1 expression was

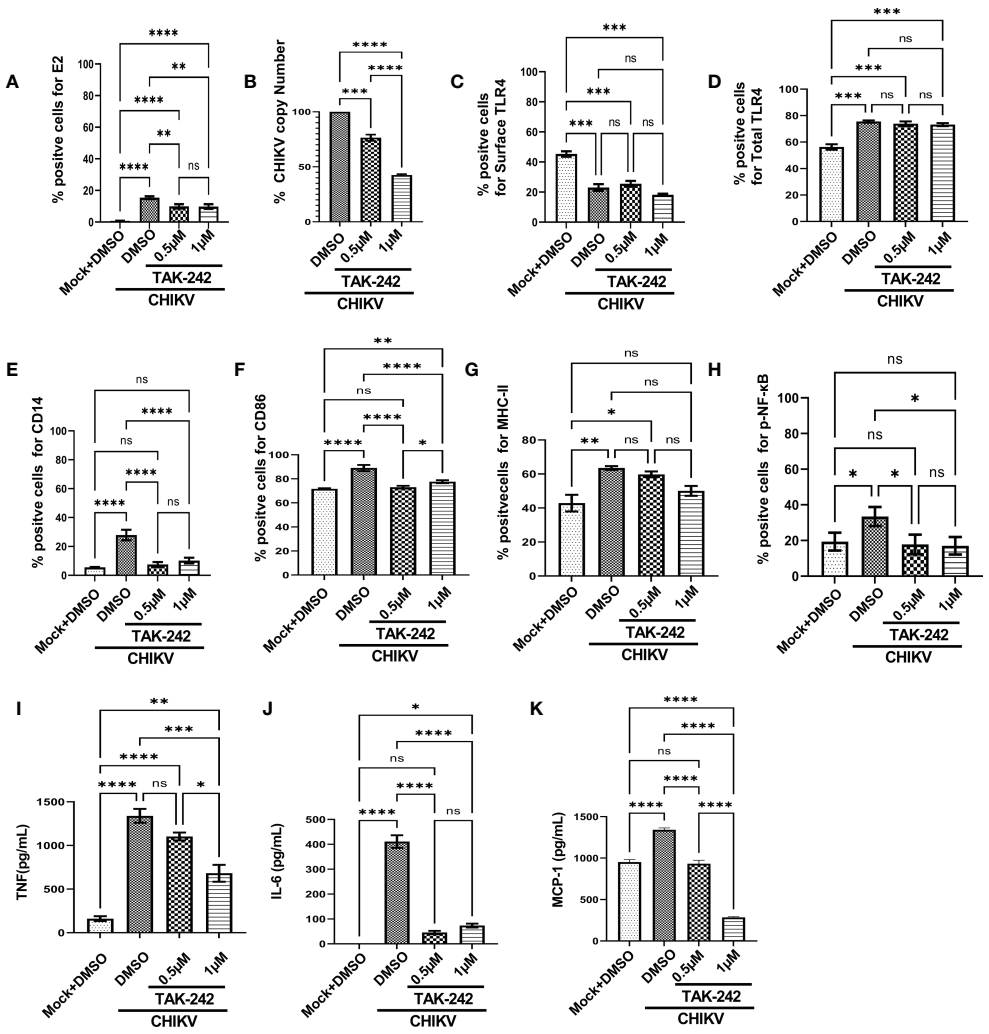

FIGURE 1
TLR4 inhibition decreases CHIKV infection and pro-inflammatory responses in RAW264.7 macrophage cells, *in vitro*. The RAW264.7 cells were either pre-treated with DMSO or TAK-242 for 3 h before CHIKV infection. CHIKV infection was given at 5 MOI for 2 h followed by the cells were harvested at 8 hpi. **(A)** The bar diagram denotes flow cytometry dot plot analysis based on % positive cells for CHIKV-E2, **(B)** q-RT PCR-based analysis showing decreased CHIKV-E1 copy number in presence of TAK-242. The bar diagrams represent percent positive cells obtained by flow cytometry dot plot analysis for **(C)** surface TLR4, **(D)** total TLR4, **(E)** CD14, **(F)** CD86 and **(G)** MHC-II and **(H)** p-NF-κB expression. **(I–K)** ELISA-based cytokine analysis showing differential expression of TNF-α, IL-6 and MCP-1. Data represent the Mean ± SEM of three independent experiments. $p< 0.05$ was considered as a statistically significant difference between the groups (ns: non-significant, *p <0.05; **$p \leq 0.01$; ***$p \leq 0.001$; ****$p \leq 0.0001$).

also found upon TAK-242 (1μM) treatment [from 951.6 ± 17.19 pg/mL (Mock) to 1342± 12.85 pg/mL (CHIKV) and 286.2± 4.242 pg/mL (TAK-242)] (Figure 1K). The representative flow cytometry dot plots of all of the above-mentioned markers were shown in the supplementary section (Figure S3).

Further, the current study aimed to elucidate whether TAK-242-directed TLR4 antagonism promotes reduced activation of macrophages or whether overall macrophage activation is solely dependent on the number/percentage of CHIKV-infected cells. To get a detailed insight, flow cytometry-based ICS cytokine staining analysis of TNF-producing cells was performed in CHIKV-E2 positive cells (Figure S4). The treatment with TAK-242 (1μM) decreased the frequency of the E2 positive RAW264.7 cells in a significant manner [15.67 ± 1.477% (DMSO+CHIKV) and 9.49 ± 0.9% (TAK-242+CHIKV)]. Respective E2 populations from TAK-242 untreated and treated groups were further analyzed to determine the frequency and expression of TNF in the aforementioned population. The frequency (% positive cells) of TNF-positive cells in both TAK-242 treated and untreated cells was found to be comparable under the E2-selected (gated) population. Interestingly, the mean fluorescence intensity (MFI) of TNF in the E2-gated cells was reduced significantly, which complies with the ELISA data mentioned earlier. The expression of TNF is possibly decreased due to lowered frequency of the E2-positive cells upon TAK-242 treatment. Taken together, the results suggest that TAK-242-directed TLR4 inhibition reduces the CHIKV infection (around 58%) and pro-inflammatory responses, significantly, in the RAW264.7 cells.

3.2.2 Inhibition of TLR4 abrogates CHIKV infection in the primary mouse peritoneal macrophages, significantly

The study was further extended to the CHIKV-infected peritoneal macrophages obtained from the BALB/c mice. It was observed that the percent E2 positive cells [from 26.73 ± 0.98 to 13.27 ± 0.5840] (Figure S5A) and the corresponding viral copy number were reduced [60%] significantly in presence of TAK-242 (1μM) (Figure S5B). Flow cytometry-based analysis showed that the surface expression of TLR4 was reduced upon infection and TAK-242 (1μM) treatment, significantly [from 75.87 ± 1.247 to 51.07 ± 0.6360% (CHIKV) and 53.5 ± 0.611% (TAK-242)] (Figure S5C). However, the total expression of TLR4 was found to increase during infection and TAK-242 (1μM) treatment in comparison to mock, significantly [from 81.5 ± 1.592 (Mock) to 90.73 ± 1.874% (CHIKV) and 89.15 ± 1.084% (TAK-242)] (Figure S5D). Moreover, the CD14 expression was found to increase during CHIKV infection and decrease further upon TAK-242 (1μM) treatment, significantly [from 22.53 ± 0.97 (Mock) to 30.73 ± 0.58 (CHIKV) and 26.37 ± 0.44 (TAK-242)] (Figure S5E). The CD86 expression was increased during CHIKV infection and further decreased in the presence of TAK-242 (0.5μM), significantly, although a non-significant reduction was observed in presence of 1μM TAK-242 [from 37.47 ± 0.8 (Mock) to 65.23 ± 1.389 (CHIKV), 55.77 ± 0.67 (0.5μM TAK-242) and 60.93 ± 2.009 (1μM TAK-242)] (Figure S5F). Moreover, the MHC-II expression was also reduced upon TAK-242 (1μM) treatment, significantly [from 58.2 ± 1.25 (Mock) to 77.67 ± 0.09 (CHIKV) and 69.6 ± 1.513 (TAK-242)] (Figure S5G). Next, the p-NF-κB expression was found to increase during CHIKV infection and decrease further upon TAK-242 (1μM) treatment, significantly [from 29.2 ± 3.351 (Mock) to 52.63 ± 3.973 (CHIKV) and 40.87 ± 2.826 (TAK-242)] (Figure S5H). To further validate the total TLR4 level, Western blot analysis revealed a significant increase of TLR4 during CHIKV infection and TAK-242 (1μM) treatment [2.123 ± 0.3 fold (CHIKV) and 2.06 ± 0.16 fold (TAK-242)] (Figures S5I, J). In order to estimate the inflammatory responses, the levels of TNF, IL-6 and MCP-1 were determined. TNF was found to increase during CHIKV infection and decrease further upon TAK-242 (1μM) treatment, significantly [from 773.2 ± 62.88 pg/mL (CHIKV) to 398.6± 27.58 pg/mL (TAK-242)] (Figure S5K). IL-6 was found to increase during CHIKV infection and decrease further upon TAK-242 (1μM) treatment, significantly [from 5.33± 1.294 pg/mL (Mock) to 1078 ± 147.9 pg/mL (CHIKV) and 186.4± 22.98 pg/mL (TAK-242)] (Figure S5L). The MCP-1 expression was found to increase during CHIKV infection and decrease further upon TAK-242 (1μM) treatment, significantly [from 145.4 ± 6.667 pg/mL (Mock) to 2117± 152.8 pg/mL (CHIKV) and 377.5± 76.98 pg/mL (TAK-242)] (Figure S5M). The data indicate that the TLR4 inhibition reduces the CHIKV infection (around 60%) and associated pro-inflammatory responses, significantly in the peritoneal monocyte-macrophages obtained from BALB/c mice.

Furthermore, a similar study was carried out using the C57BL/6 mice-derived peritoneal macrophages. The percent E2 positive cells [from 18.6 ± 0.95 to 6.558 ± 0.89] (Figure S6A) and corresponding viral copy number were significantly reduced [50%] in presence of TAK-242 (Figure S6B). Flow cytometry-based analysis showed a similar kind of change in the surface and total expression of TLR4 upon TAK-242 treatment, significantly (Figures S6C, D). It was further noticed that although the CD14 and MHC-II expressions were significantly modulated in a similar way, the CD86 expression showed a nonsignificant decrease in presence of TAK-242 treatment (1μM) (Figures S6E–G). Accordingly, the p-NF-κB expression was estimated and it was found to increase during CHIKV infection and decrease further upon TAK-242 treatment (1μM), significantly [from 29.6 ± 1.793 (Mock) to 50.7 ± 0.66 (CHIKV) and 35.03 ± 0.5175 (TAK-242)] (Figure S6H). The Western blot analysis revealed significant upregulation of TLR4 upon CHIKV infection and also during TAK-242 treatment (1μM) [1.553 ± 0.08 fold (CHIKV) and 1.489 ± 0.14 fold (TAK-242)] (Figures S6I, J). As observed before, TNF, IL-6 and MCP-1 followed a similar pattern, significantly (Figures S6K–M), indicating that TLR4 inhibition significantly lowers the CHIKV infection (around 50%) and associated pro-inflammatory responses in the peritoneal monocyte-macrophages obtained from C57BL/6 mice as well.

3.2.3 Inhibition of TLR4 abrogates CHIKV infection in the hPBMC-derived macrophages, significantly

To study the effect of TLR4-mediated regulation of CHIKV infection in the higher-order mammalian system, hPBMC derived adherent macrophage population (97% $CD14^{+}CD11b^{+}$ cells) (Figures S7A, B) was subjected to infection in the presence and absence of TAK-242 (1μM). The hPBMC-derived adherent populations collected from 3 healthy donors showed around a 52% decrease in the E2 level with TAK-242 treatment (Figures S7C, D). Similarly, there was a 32.38% reduction in CHIKV infection after TAK-242 treatment as observed by the plaque assay (Figures S7E). To assess the pro-inflammatory responses, secretory TNF level was determined using ELISA, where around 44% reduction was observed in TAK-242 treated condition (Figure S7F). Collectively, these data indicate that TLR4 inhibition in the hPBMC-derived monocyte/macrophages may lead to reduced CHIKV infection (around 33%) and associated inflammatory responses.

3.3 TLR4 inhibition reduces CHIKV infection driven p38 and SAPK-JNK phosphorylation

The role of the p38 and JNK-MAPK pathways towards CHIKV infection and inflammation was recently reported (2). To investigate the possible role of TLR4 in MAPK-mediated CHIKV-induced inflammation, differential induction of p-p38 and p-SAPK-JNK-MAPK was observed by Western blot experiment. Significant upregulations of p-p38 (2.9-fold) and p-JNK (4.03-fold) were observed after CHIKV infection in the RAW264.7 cells (Figures 2A–C). However, phosphorylation of p38 and JNK was reduced by 4.69 and 1.61-fold respectively following TAK-242 treatment (Figures 2A–C). Furthermore, a reduction of the

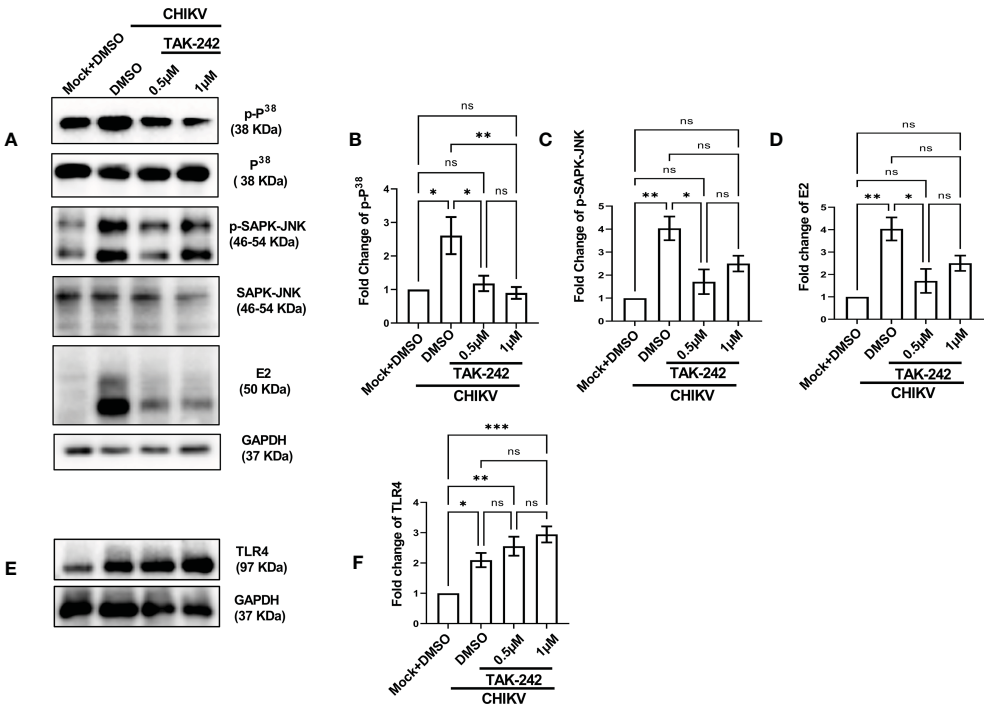

FIGURE 2
TLR4 inhibition lowers p38 and SAPK-JNK phosphorylation in host macrophages, *in vitro*. RAW264.7 cells were either pre-treated with DMSO or TAK-242 for 3 h before CHIKV infection. The CHIKV infection was given at 5 MOI for 2 h followed by the cells were harvested at 8 hpi. **(A–D)** Western blot analysis showing differential expression of p-P^{38}, p-SAPK-JNK, E2 and their quantification normalized against GAPDH, in respective order. (**E, F**) Western blot analysis showing TLR4 expression with the corresponding quantification normalized against GAPDH. Data represent the Mean ± SEM of three independent experiments. $p < 0.05$ was considered as a statistically significant difference between the groups (ns: non-significant, *p <0.05; **$p \leq 0.01$; ***$p \leq 0.001$).

CHIKV-E2 expression (3.27-fold) in presence of TAK-242 (Figures 2A, D) was also observed. In correlation with the total expression of TLR4 measured in flow cytometry-based analysis, an increase in the TLR4 expression was found during CHIKV infection (2.09-fold) and TAK-242 treatment (2.9-fold) (Figures 2E, F). Collectively, these data indicate that the inhibition of TLR4 might lead to reduced viral infection and induction of the p38, and JNK-MAPK pathways.

3.4 CHIKV-E2 and functional TLR4 interaction is necessary for the efficient infection in host macrophages

In order to understand the functional association of TLR4 with CHIKV infection, viral infection was performed in the RAW264.7 and TLR4 functional knockout TLR4KO RAW cells. Interestingly, the TLR4KO RAW cell line was used for the current experiment, which is previously reported to show reduced interferon response against SARS-CoV2 specific protein E antigen (36). Therefore, it seems that the functional presence of TLR4 is necessary to implement the SARS-CoV2-specific antiviral responses. The flow cytometry dot plot analysis suggests that the percent E2 positive population in the RAW264.7 cells was reduced in the case of TLR4KO RAW cells (16.60 ± 0.75% to 3.877 ± 0.43%) during CHIKV infection (Figures 3A, B). Next, Western blot analysis revealed an around 8.651 ± 0.72-fold decrease of the E2 protein level in the CHIKV-infected TLR4KO RAW cells in comparison to RAW264.7 (Figures 3C, D). Assessment of viral titre also showed a 48.11 ± 3.23% reduction in the TLR4KO RAW cells (Figure 3E). The total and surface expressions of TLR4 were found to be non-significantly altered (Figures 3F, G). Moreover, macrophage activation markers like CD14, CD86 and MHC-II were found to increase in a modest yet non-significant manner during CHIKV infection in the TLR4KO RAW cells in comparison to RAW264.7 (Figures 3H–J). However, p-NF-κB was found to increase significantly during CHIKV infection in TLR4KO RAW in comparison to RAW264.7 (Figure 3K). To investigate the differential pro-inflammatory responses during CHIKV infection, comparative levels of TNF, IL-6 and MCP-1 levels were quantified by ELISA. These findings report the elevated expressions of TNF, IL-6 and MCP-1 in RAW264.7 by 2.305 ± 0.2219, 1.702 ± 0.1797 and 1.541 ± 0.05658-fold respectively in comparison with TLR4KO RAW (Figures 3L–N). Hence, the results obtained from functionally knockout TLR4KO RAW delineate that TLR4 is functionally essential for eliciting the CHIKV-induced pro-inflammatory responses.

The RAW264.7 cells were infected with CHIKV with MOI 5 and harvested at 8 hpi for further analysis. Co-immunoprecipitation followed by Western blot analysis demonstrated that TLR4 could be pulled with the CHIKV-E2 protein in host macrophages indicating that CHIKV-E2 interacts

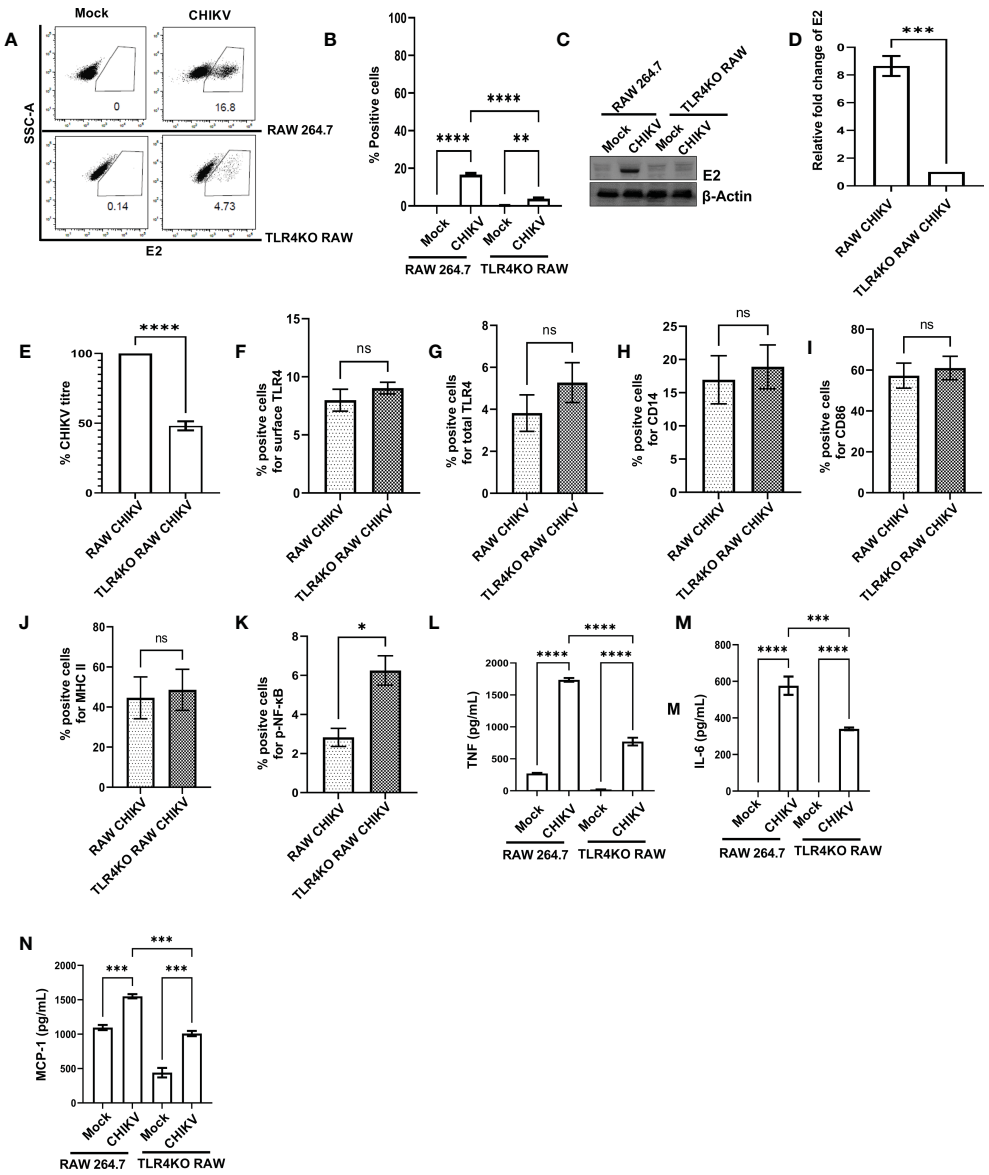

FIGURE 3
The presence of functional TLR4 facilitates CHIKV infection in host macrophages, *in vitro*. RAW264.7 and TLR4KO RAW cells were subjected to CHIKV infection at 5 MOI and harvested at 8 hpi **(A, B)** The flow cytometry dot plot analysis depicts comparative CHIKV-E2 expression. **(C, D)** Western blot analysis showing comparative E2 level. Normalization of E2 expression was done using β-actin as a housekeeping gene. **(E)** The bar diagram showing comparative CHIKV titre obtained from plaque assay **(F–K)** The flow cytometry dot plot-based bar diagram analysis showing percent positive cells expressing surface TLR4, total TLR4, CD14, CD86, MHC-II and p- NF-κB respectively in mock and CHIKV infected TLR4KO RAW cells. **(L–N)** Bar diagrams depicting ELISA-based TNF-α, IL-6 and MCP-1 quantification respectively in RAW 264.7 and TLR4KO RAW cells. Data represent the Mean ± SEM of three independent experiments. $p < 0.05$ was considered as a statistically significant difference between the groups (ns: non-significant, *p <0.05; **$p \leq 0.01$; ***$p \leq 0.001$; ****$p \leq 0.0001$.

with host TLR4 (Figure 4A). To further validate the results, a study on the interaction of E2 and TLR4 was carried out in the TLR4KO RAW cells under similar experimental conditions. However, no detectable interaction between E2 and TLR4 was observed (Figure 4B). To investigate the specificity of the results, the interaction of E1 and TLR4 was studied in the RAW264.7 cells under similar experimental conditions. However, no detectable interaction between E1 and TLR4 was observed (Figure 4C). Moreover, less interaction between CHIKV-E2 and host TLR4 was observed in the presence of TAK-242 (Figure 4D). The interaction of the extracellular domain of TLR4 and CHIKV-E2 was also validated further by *in-silico* analysis using the mouse TLR4-MD2 complex (PDB ID: 2Z64) and CHIKV structural protein E2 (PDB ID: 3N41) (Figure 4E). The analysis showed 12 probable interactions between the amino acid residues of these two structures through molecular docking (Figure 4F) suggesting the possibility of TLR4 activation through the interaction of CHIKV-E2 at the extracellular domain of TLR4 that might be required for the efficient viral infection in host macrophages.

To further validate the positive regulation of TLR4 on CHIKV infection in host macrophages, the anti-TLR4 antibody-mediated blocking experiment was performed. The flow cytometry-based dot

10.3389/fimmu.2023.1139808

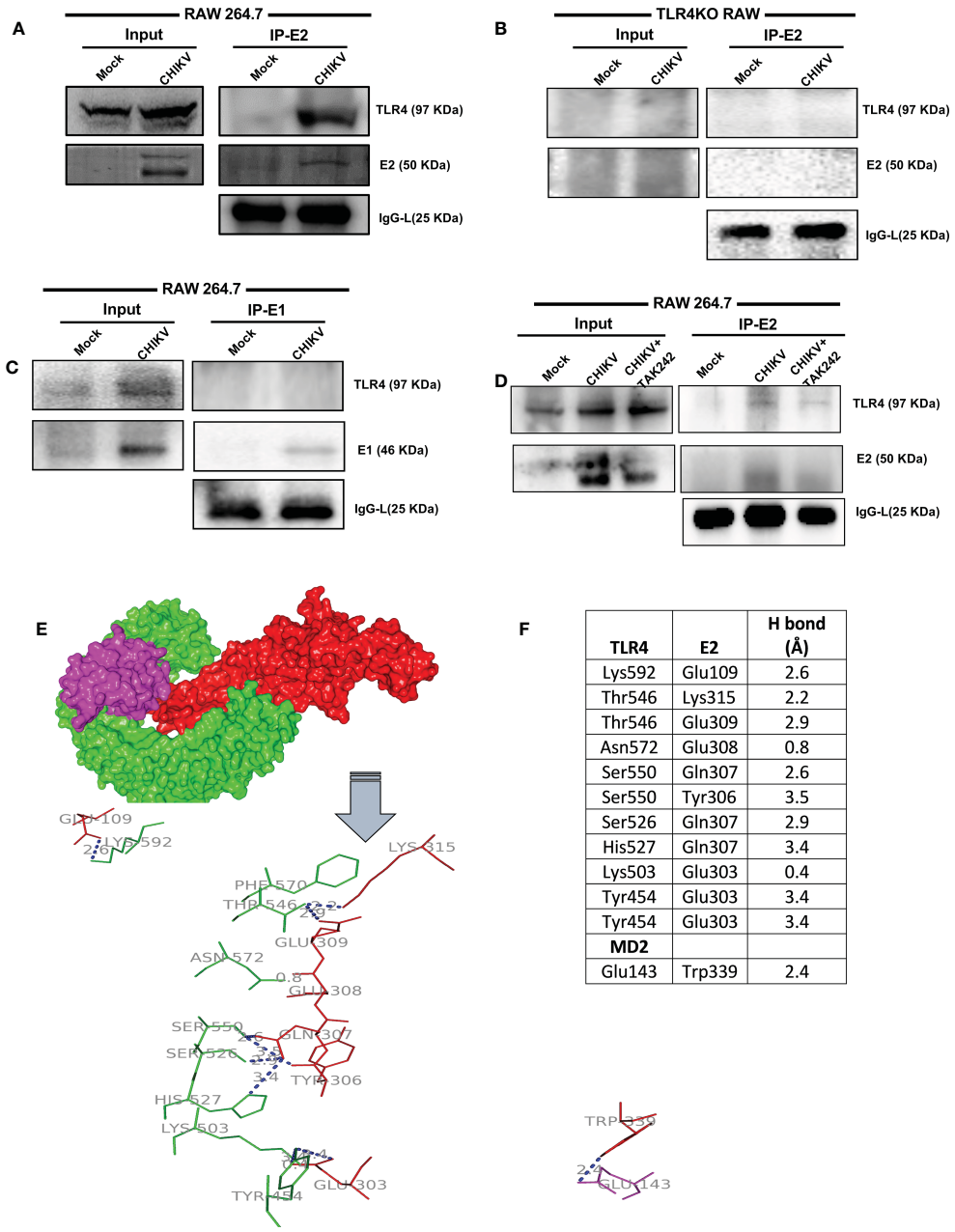

FIGURE 4
TLR4-E2 interaction facilitates CHIKV infection in host macrophages. The RAW264.7 and TLR4KO RAW cells were subjected to study functional TLR4 and E2 interaction. Both mock and CHIKV-infected cells were processed for immunoprecipitation followed by Western blot analysis. **(A)** For RAW264.7 cells, Western blot analysis showing the expressions of E2 and TLR4 in the whole cell lysate (left), co-immunoprecipitation analysis depicting the interaction of CHIKV E2 and TLR4 (right). **(B)** For TLR4KO RAW cells, Western blot analysis showing the levels of E2 and TLR4 in the whole cell lysate (left), co-immunoprecipitation analysis depicting the interaction of CHIKV E2 and TLR4 (right). **(C)** For RAW264.7 cells, Western blot analysis showing the expressions of E1 and TLR4 in the whole cell lysate (left), co-immunoprecipitation analysis depicting the interaction of CHIKV-E1 and TLR4 (right). **(D)** For RAW264.7 cells, Western blot analysis showing the expressions of E2 and TLR4 in the whole cell lysate (left), co-immunoprecipitation analysis depicting the interaction of CHIKV-E2 and TLR4 (right) in the presence/absence of TAK-242. **(E)** Protein–protein docking analysis reveals probable molecular interaction of MD2-TLR4 (PDB ID: 2Z64) with Chikungunya virus (CHIKV) envelope proteins E2 (PDB ID: 3N41). The protein-protein docking was done in the ZDOCK webserver using MD2-TLR4 as receptor and CHIKV-E2 as ligand **(A)** Interaction complex of MD2 (magenta) and TLR4 (green) with E2 (red). The polar interactions are labeled (blue) in the line diagram. **(F)** The residues involved in polar interactions between CHIKV-E2 and TLR4.

plot analysis revealed a significant decrease in CHIKV infection in the RAW264.7 cells in presence of pre-incubation with the anti-TLR4 antibody. However, in presence of both TAK-242 and anti-TLR4 antibody, CHIKV infection didn't show any marked change in comparison to only the anti-TLR4 antibody, which might be indicative towards saturation of TLR4 inhibition [from 19.58 ± 0.375% (CHIKV) to 10.57± 0.8168% (TAK-242), 10.87 ± 1.546% (CHIKV+Antibody) to 11.88± 1.316% (TAK-242+CHIKV +Antibody)] (Figures 5A, B). Moreover, Western blot analysis revealed the decrease in fold change of CHIKV-E2 level in the

10.3389/fimmu.2023.1139808

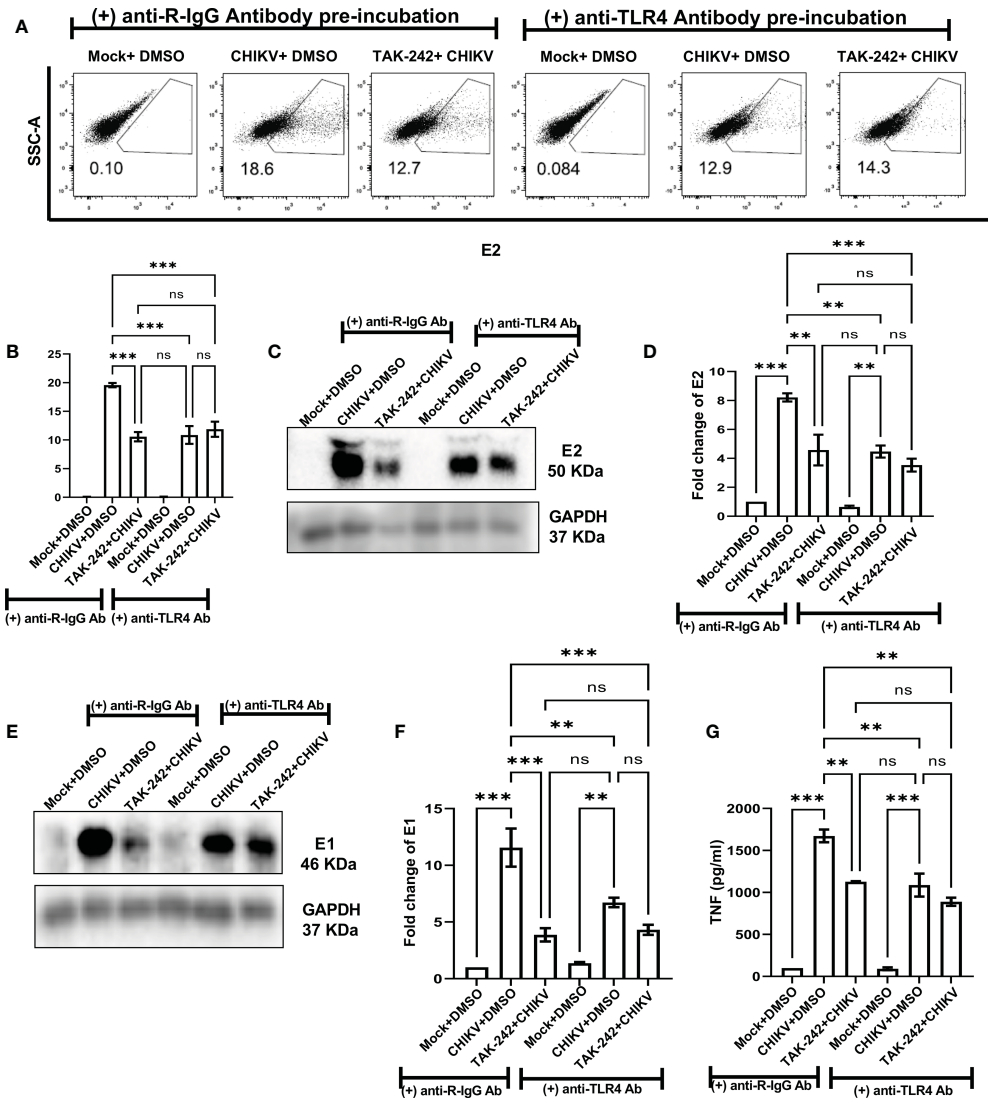

FIGURE 5
Pre-incubation with anti-TLR4 antibody alleviates CHIKV infection in host RAW264.7 macrophages, *in vitro*. Before pre-incubation of the RAW264.7 cells with either DMSO or TAK-242, the anti-TLR4 antibody or anti-R-IgG antibody was added in the pre-incubation volume in respective conditions at 4 µg/ml concentration and the cells from all conditions were preincubated for 3 h. The CHIKV infection was given at 5 MOI for 2 h and the cells were harvested at 8 hpi. **(A, B)** The flow cytometry dot plot analysis shows comparative CHIKV-E2 levels at different conditions. **(C, D)** Western blot analysis shows E2 expression in different experimental conditions. **(E, F)** Western blot analysis shows differential E1 expression. All densitometric quantifications were performed with respect to GAPDH. **(G)** The bar diagram represents ELISA-based cytokine analysis of TNF.

anti-TLR4 antibody preincubated condition [from 8.212 ± 0.29-fold (CHIKV) to 4.577± 1.062-fold (TAK-242), 4.469 ± 0.42-fold (CHIKV+Antibody) to 3.53 ± 0.45-fold (TAK-242+CHIKV +Antibody)] (Figures 5C, D). Furthermore, the CHIKV-E1 level showed a similar trend of expression to CHIKV-E2 [from 11.56 ± 1.6775-fold (CHIKV) to 3.868± 0.59-fold (TAK-242), 6.725 ± 0.42-fold (CHIKV+Antibody) to 4.315 ± 0.44-fold (TAK-242+CHIKV +Antibody)] (Figures 5E, F). Next, ELISA-based cytokine analysis of TNF revealed the reduced level of secretory TNF in presence of the anti-TLR4 antibody-driven pre-incubation, significantly [from 98.84 ± 0.49 pg/ml (Mock) to 1673 ± 75.33 pg/ml (CHIKV), 1127 ± 6.685 pg/ml (TAK-242), 90.68 ± 17.12 pg/ml (Mock+Antibody) 1088 ± 136.6 pg/ml (CHIKV+Antibody) to 889.4 ± 48.26 pg/ml (TAK-242+CHIKV+Antibody)] (Figure 5G). Therefore, the anti-TLR4 antibody-driven blocking study reconfirms the possible engagement of host TLR4 as a potential receptor of CHIKV.

3.5 TLR4 is required to regulate the CHIKV entry in host macrophages

To investigate the possible anti-CHIKV role in specific stages of viral infection, the TAK-242 treatment was given in different stages of the CHIKV life cycle as before CHIKV infection (only pre-incubation), during CHIKV infection, both before and during CHIKV infection (pre+during incubation), only during infection

10.3389/fimmu.2023.1139808

(during incubation), post-infection incubation at 0 hpi (the drug was added at 0 hpi) and post-infection incubation at 8 hpi (the drug was added at 8 hpi). It was noticed that the presence of TAK-242 before CHIKV infection (only pre-incubation) and before as well as during CHIKV infection (pre+ during incubation) is most efficient (62% and 59% decrease of CHIKV-E1 copy number, respectively) to regulate the CHIKV infection. Interestingly, a 45% decrease of CHIKV copy number was observed while TAK-242 was added specifically during CHIKV infection only (during incubation), indicating its anti-CHIKV effect. However, no decrease in the CHIKV copy number was observed during the post-infection incubation condition (Figure 6A). Therefore, the data suggest that the TAK-242-mediated TLR4 inhibition probably plays a pivotal role in the initial phase of CHIKV infection i.e., the entry and/or attachment stage.

To further confirm whether TLR4 is required in the entry and/or attachment phase of viral infection, TAK-242 (1μM) was added to the RAW264.7 cells before infection for 3 h. Once viral adsorption was over at 37°C, the unbound virus particles (CHIKV in SFM) were collected and subjected to plaque assay

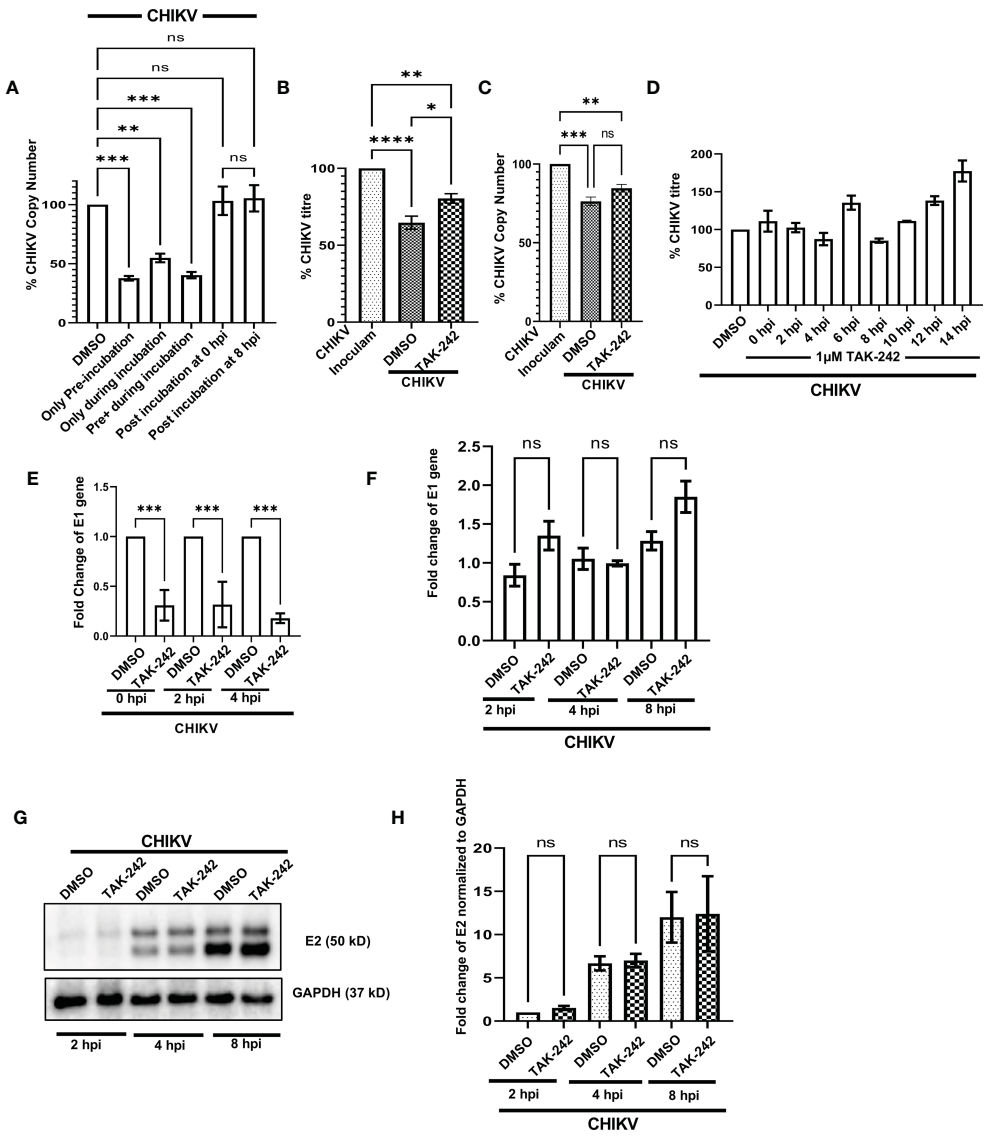

FIGURE 6
TLR4 promotes viral entry at the early stages of CHIKV infection in host macrophages, *in vitro*. **(A)** TLR4 inhibition before CHIKV infection is most effective to regulate viral copy number at 8 hpi **(B, C)** Viral entry assay in RAW 264.7 cells showing the internalization of around 24% and 11% less virus in TAK-242 treated condition using plaque assay-based viral titre determination and q-RT PCR based viral copy number determination respectively. **(D)** Time of addition assay in RAW 264.7 cells showed no significant decrease in viral infection during post-infection treatment. **(E)** TAK-242 pre-treatment decreases CHIKV copy number in different time points inside the RAW264.7 macrophage cells. **(F)** Post-infection TLR4 inhibition (TAK-242 was added at 0 hpi) does not have a role in CHIKV E1 gene transcription in the RAW264.7 cells. **(G, H)** Post-infection TLR4 inhibition (TAK-242 was added at 0 hpi) does not have a role in CHIKV-E2 translation in the RAW264.7 cells. The densitometry was performed with respect to the corresponding GAPDH expression. Data represent the Mean ± SEM of three independent experiments. $p < 0.05$ was considered as a statistically significant difference between the groups (ns: non-significant, *p <0.05; **$p \leq 0.01$; ***$p \leq 0.001$; ****$p \leq 0.0001$).

and qRT-PCR analysis to determine the viral titre and viral copy number, respectively. It was observed that pre-treatment with TAK-242 resulted in the presence of 24.38 ± 2.302% and 10.86% more CHIKV particles in the wash solution containing unbound virus particles as compared to untreated cells by plaque assay and qRT-PCR-based method respectively (Figures 6B, C). Therefore, the data suggest that TLR4 might be required for efficient CHIKV attachment and/or entry in the host macrophages.

In order to confirm whether TAK-242 has any role in a specific phase of the CHIKV life cycle, the "Time of Addition" experiment was carried out as mentioned in the materials and method section. The viral titres were determined for all of the supernatants collected at 15 hpi. The data showed no significant reduction in CHIKV infection at any time point when the drug was added after infection (Figure 6D). Hence, the result suggests that TLR4 might not be required for CHIKV once the virus enters inside the host macrophages.

To understand the role of TLR4 in CHIKV replication, E1 mRNA copy numbers were determined inside the cells at different time points after infection. To perform this experiment, the RAW264.7 cells were pre-incubated with TAK-242 (1μM), followed by CHIKV infection at MOI 5 for 2 h with TAK-242 (1μM) and post-infection incubation with TAK-242 (1μM). Next, the cells were harvested at 0, 2 and 4 hpi and subjected to total RNA isolation, cDNA preparation and qRT -PCR analysis of the E1 gene. It was observed that the copy number of the CHIKV-E1 gene was always lower in TAK-242 treated condition inside the cells (Figure 6E). This result confirms that TLR4 abrogation leads to the reduced CHIKV replication when TAK-242 is added in pre and pre+ during conditions at different time points as it has been already noticed that post-treatment doesn't regulate CHIKV infection.

To investigate whether TLR4 inhibition has any role in the transcription of the CHIKV E1 gene, the CHIKV-infected RAW264.7 cells were subjected to post-infection incubation (0 hpi) with TAK-242 (1μM) or DMSO. The cells were harvested at 2, 4 and 8 hpi and subjected to RNA isolation followed by cDNA synthesis and q-RT PCR analysis of the E1 gene to estimate the CHIKV copy number inside the cells. It was found that there is no marked change of the CHIKV-E1 gene in the TAK-242 treated/untreated group at different time points (Figure 6F) supporting that post-treatment does not affect the CHIKV transcription.

Similarly, to study the effect of TLR4 inhibition on the translation of E2 protein, the CHIKV-infected RAW264.7 cells were subjected to post-infection incubation (0 hpi) with TAK-242 (1μM) or DMSO. The cells were harvested at 2, 4 and 8 hpi and subjected to Western blot analysis of E2 protein (as representative of CHIKV structural proteins) which depicted no significant difference in the E2 protein level in the TAK-242 treated/untreated group at different time points. (Figures 6G, H). These data, therefore, suggest that TLR4 inhibition might not have any role in the viral translation step.

Taken together, all these mechanism-based studies denote that TLR4 might be involved in the CHIKV attachment and entry process in host macrophages and probably doesn't affect post-entry phases of the CHIKV life cycle.

3.6 TLR4 inhibition efficiently reduces the CHIKV infection and inflammation in mice, *in vivo*

The inhibitory role of TAK-242 against CHIKV infection was assessed in 10-12 days old C57BL/6 mice. Interestingly, it was found that TAK-242 treated mice group showed reduced CHIKV-mediated arthritogenic symptoms and impaired limb movements (indicated with an arrow mark in the figure) compared to the only infected group (Figure 7A). Following TAK-242 treatment, the viral titre was found to be reduced to 41.26 ± 2.664% and 47.01 ± 0.4225% in the quadriceps muscle and spleen respectively (Figures 7B, C). In addition, Western blot analysis revealed the reduction of E2 level to 56.08 ± 2.020% and 50.04 ± 0.6860% in muscle and spleen respectively (Figures 7D–F). Moreover, to determine the functional immune response, the serum TNF level was assessed and a reduction of 38.47 ± 2.128% was observed (Figure 7G). The clinical score of the TAK-242 treated group of mice showed significantly reduced arthritogenic symptoms as compared to the only infected mice (Figure 7H). Additionally, to analyze the survival efficiency of mice in presence of TAK-242, the survival curve was determined and it was found that all of the CHIKV-infected mice died on the 8th-day post-infection, while TAK-242 treatment provided 75% better survival during CHIKV infection (Figure 7I). Together, the data suggest that TLR4 antagonism effectively reduces CHIKV infection and inflammation and may ensure better survivability (75%) in mice.

4 Discussion

TLR4, an important member of the innate immune system, acts as one of the earliest determinants of foreign immunogenic components associated with different sets of pathogens. Starting from its discovery, TLR4 has been known to play a critical role to study the functional aspects of host-pathogen interactions and associated pro-inflammatory immune responses, thus it has evolved as a suitable target for modern-age bio-medical research in the field of rheumatoid arthritis, necrotizing enterocolitis, and inflammatory bowel disease (25, 27, 28). Moreover, the prominent regulatory role of TLR4 has also been explored in the LPS-mediated endotoxin shock and sepsis model in mice using TAK-242 as a probable TLR4 antagonist (24, 37). In the case of LPS-driven TLR4 activation, LPS binding protein (LBP), an extracellular protein, first interacts with LPS present over bacterial outer membrane or in micelle form. A single LPS-LBP complex then interacts with either soluble or the membrane-bound CD14 protein, a co-stimulator of the TLR4 signaling pathway. CD14 acts as a carrier to transfer a single molecule of LPS to MD2 which results in the TLR4-MD2 heterodimer formation which represents the functional LPS receptor. The TLR4-MD2 dimerization occurs to initiate a downstream signaling cascade (60). The LPS induction enhances macrophage activation markers like CD14, MHC-II and CD86 expressions and results in the internalization of cell surface TLR4 (51, 52, 61–64). As reported previously, activation of TLR4 leads to

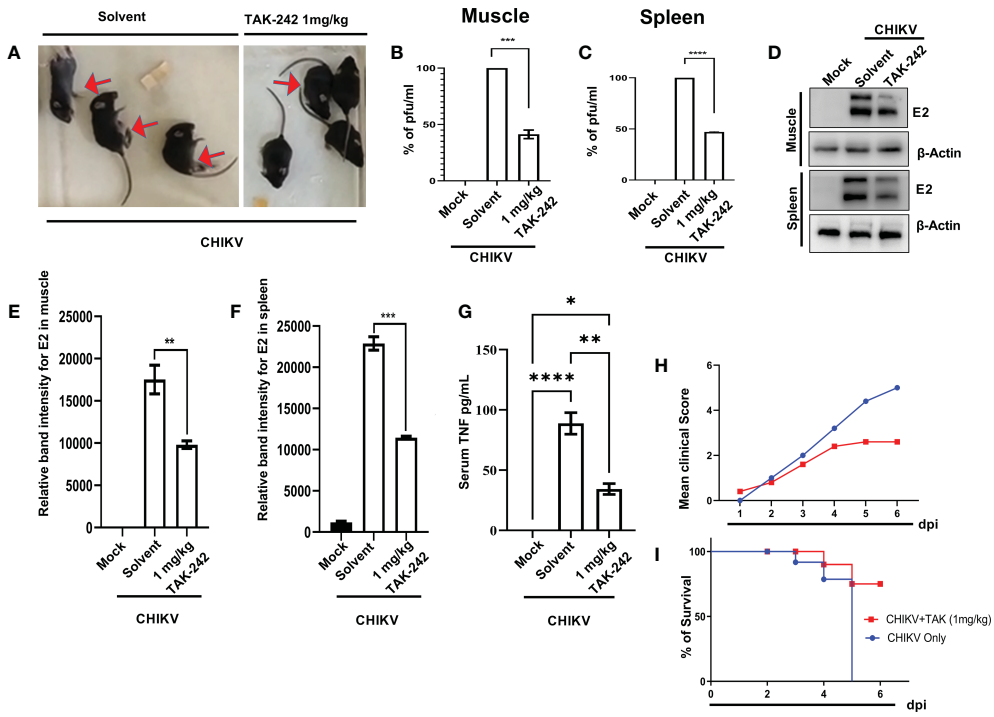

FIGURE 7
TAK-242 protects mice from CHIKV-driven pro-inflammatory responses and increases survival. 10-12 days old C57BL/6 mice (n=5/group) were injected subcutaneously with 10^6 CHIKV-IS and treated with TAK242 (dose:1mg/Kg bodyweight of mice) at every 24h intervals up to 4 dpi. After the mice were sacrificed at 5dpi, serum and different tissues were collected for further downstream experiments. To quantitate viral titre, plaque assay was performed using homogenous and filtered tissues sample. For this, an equal amount of quadriceps muscle and spleen were homogenized and filtrated using 0.22μM membrane filter **(A)** The image showing CHIKV-infected mice in the presence and absence of TAK-242 treatment. The arrows indicate mice with impaired limb movement. **(B, C)** The bar diagram shows % of pfu/mL in infected and TAK-242 treated mice muscle and spleen respectively. **(D)** Western blot showing the CHIKV E2 protein in muscle and spleen. Beta-actin was used as a loading control. **(E, F)** The bar diagram showing the relative band intensities of E2 in muscle and spleen respectively in mock, CHIKV and CHIIKV with TAK-242 treated groups **(G)** The bar diagram depicting serum TNF level in mock, infected and TAK-242 treated mice serum **(H)** The line diagram showing the disease symptoms of CHIKV infection which were monitored from 1dpi to 6dpi. **(I)** The survival curve showing the efficacy of TAK-242 against CHIKV-infected C57BL/6 mice (n=6/group). All bar diagrams were obtained through the GraphPad Prism software. Data represent the Mean ± SEM of three independent experiments. $p < 0.05$ was considered as a statistically significant difference between the groups (ns: non-significant, *p <0.05; **$p \leq 0.01$; ***$p \leq 0.001$; ****$p \leq 0.0001$).

phosphorylation of NF-κB (55) and thus has a direct correlation with inflammation (58, 59). TAK-242, a cyclohexene derivative, has been found to bind selectively to the Cys747 residue of the Toll/interleukin 1 receptor (TIR) domain of TLR4 and inhibits the downstream signaling mechanism (24, 34). According to the previous report, it has been shown that the pre-incubation with 1μM of TAK-242 for 5 minutes can reduce LPS-induced TNF production by 80% in the mouse peritoneal macrophages and the efficacy of the specific anti-inflammatory role of TAK-242 is concentration and time-dependent (34). They have also shown a reduced activation of the NF-κB pathway upon TAK-242-mediated TLR4 inhibition (34). Therefore, the effect of TAK-242-mediated TLR4 inhibition has been simultaneously investigated in the LPS-induced pro-inflammatory model as an experimental control of the current study. Additionally, the re-emergence of CHIKV is considered as one of the global public health threats especially due to the unavailability of possible anti-CHIKV drugs or vaccine to date. The literature on CHIKV infection and pathogenesis report on pro-inflammatory cytokine burst in the host immune system (19). Hence, the current study is intended to explore the involvement of TLR4 during CHIKV infection and associated pro-inflammatory responses.

Earlier studies have already reported that the macrophages could be infected with CHIKV, both *in vivo* as well as *in vitro*, and thus may generate a huge pro-inflammatory cytokine burst (19, 22, 65, 66). The published literature on both mice and macaque models showed that macrophages are one of the immune cells which get recruited at the site of inoculation and generate strong immune responses by pro-inflammatory cytokine release, which might be associated with the CHIKV-induced arthritis, myositis and tenosynovitis (67, 68). CHIKV has already been reported to persist for several months or even years within macrophages and may reappear to cause disease symptoms (65). Therefore, investigating the viral infection-mediated host immune modulation in macrophages might give detailed insight into CHIKV persistence and associated future therapeutic strategies.

TAK-242 (Resatorvid), a well-established TLR4-specific drug has currently been used for clinical trials for several inflammatory diseases, for example, severe sepsis (69) and acute alcoholic hepatitis (ClinicalTrials.gov.Identifier: NCT04620148, https://

clinicaltrials.gov/ct2/show/NCT04620148). Therefore, TAK-242 has been used to explore the regulatory role of TLR4, if any, during CHIKV-induced pro-inflammatory responses. The current findings suggest that TAK-242-mediated TLR4 inhibition may abrogate CHIKV infection, cellular activation and pro-inflammatory responses in mouse and human macrophages, *in vitro*. It also demonstrates that TLR4 inhibition-mediated decrease of CHIKV infection is driven by p38 and SAPK-JNK phosphorylation. Interestingly, it is found that CHIKV-E2 interacts with TLR4 during infection which is essential for efficient viral infection in host macrophages. The interaction of the extracellular domain of TLR4 and CHIKV-E2 has been further validated by *in-silico* analysis using the mouse TLR4-MD2 complex as the ligand and CHIKV structural protein, E2 as the receptor. The analysis demonstrates 12 probable interactions where Thr546, Ser550 and Tyr454 residues of TLR4 are found to be critically essential to interact with CHIKV-E2, *in silico*. Therefore, the study depicts TLR4 as one of the possible receptors of the CHIKV-E2 protein to facilitate viral infection. Moreover, anti-TLR4 antibody-dependent blocking assay strengthens the role of TLR4 as a possible receptor for CHIKV-E2 and thus TLR4-mediated CHIKV entry in the RAW264.7 macrophages. Furthermore, it has also been observed that TLR4 plays a key role in CHIKV attachment process and thus TLR4 inhibition might lead to an overall decrease in viral titre. The study also suggests that TLR4 inhibition has no role in post-entry stages of viral infection i.e. viral transcription, replication and translation inside the host macrophages. Additionally, the TLR4 antagonism effectively reduces CHIKV infection and inflammation, *in vivo* by reducing the disease score, significantly with improved survival of CHIKV-infected mice. Therefore, the positive regulation of TLR4 on CHIKV infection in different host systems could be associated with the inflammation and viral pathogenesis.

An earlier report on the respiratory syncytial virus (RSV) describes that the functional TLR4 is an essential component to promote viral infection and the infection-induced inflammasome activation, vascular damage, T cell activation, B cell maturation and NK cell activation in mice model (30). Recent studies on SARS-CoV2 imply that TAK-242 mediated TLR4 inhibition significantly abolishes viral spike protein-induced pro-inflammatory cytokine responses in association with the p-NF-κB protein in the murine and human macrophages (31, 70). VP3, a structural protein of the foot and mouth disease virus (FMDV) is already reported to interact and induce TLR4 to promote viral infection and associated inflammation (32). Furthermore, previous reports on the reduction in the surface expression of TLR4 and increase in the total TLR4 upon LPS or virus-mediated stimulation are found to be similar to this current investigation (32, 51, 52). Hence, the current study suggests a positive regulation of TLR4 on CHIKV entry, infection and associated inflammation in the host.

Although this study proposes probable TLR4-mediated CHIKV entry, TLR4 inhibition doesn't completely hinder viral entry in the host. Therefore, it seems that the possible involvement of other cellular receptor/s (18) to execute viral entry and pathogenesis might be crucial under the current experimental scenario, which is yet to be explored. Moreover, siRNA-mediated gene silencing could be explored as a suitable tool to investigate the detailed role of TLR4 during viral infection.

The *in-silico* study reveals the association of specific amino acids of TLR4-MD2 complex and CHIKV-E2 proteins in the current investigation. Two amino acid residues, Asn572 and Lys503 of TLR4 (PDB ID: 2Z64) have been found to show high-affinity polar interactions (< 2 Å) with Glu308 and Glu 303 of CHIKV-E2 (PDB ID: 3N41), respectively. Furthermore, Thr546, Ser550 and Tyr454 residues of TLR4 and Gln307 and Glu303 residues of CHIKV-E2 protein have been shown to exhibit multiple polar interactions to emphasize their prominent role in terms of CHIKV-TLR4 association. Further, it will be interesting to investigate the role of these amino acid residues in this interaction through mutational studies in future.

In addition to the mice model, earlier reports are also available on the CHIKV-driven pro-inflammatory cytokine burst and associated symptoms in human patient studies, *in vivo* (20, 21). Accordingly, the effect of TLR4 inhibition could be further explored in experimental *in vitro* or *in vivo* setups with CHIKV-infected patient samples. Therefore, the probable efficacy of TLR4 inhibition against CHIKV infection might be explored in higher-order mammalian systems in future.

In conclusion, the current study reveals the possible regulatory role of TLR4 at the attachment as well as entry stages of viral infection *via* interaction with the CHIKV structural protein E2. Therefore, TLR4 could be considered as a potential receptor of CHIKV and a positive regulator of the virus driven pro-inflammatory host immune responses. Considering this regulatory role of TLR4, this current study might have translational implications for designing future therapeutic strategies against CHIKV infection to modulate the disease pathogenesis.

Data availability statement

The original contributions presented in the study are included in the article/Supplementary Material. Further inquiries can be directed to the corresponding authors.

Ethics statement

The studies involving human participants were reviewed and approved by Institutional Ethics Committee, NISER, Bhubaneswar (NISER/IEC/2022-04). The patients/participants provided their written informed consent to participate in this study. The animal study was reviewed and approved by Institutional Animal Ethics Committee, NISER (1634/GO/ReBi/S/12/CPSCEA) and Institutional Animal Ethics Committee, ILS Bhubaneswar (76/Go/ReBi/S/1999/CPCSEA) under the affiliation of Committee for the Purpose of Control and Supervision of Experiments on Animals (CPCSEA) of India.

Author contributions

SuC, SoC, and CM conceived the idea and designed the experiments. CM, SD, SaC, SG, and SSK did the wet lab experiments. BS performed the *in-silico* experimentation and analysis. SuC and SoC provided the reagents. SuC, SoC, and CM analyzed and interpreted the results. SuC, SoC, CM, TM, SK, and KT wrote the manuscript and prepared the figures. All authors contributed to the article and approved the submitted version.

Funding

The work has been mainly supported by core funding from the Department of Atomic Energy (DAE), Govt. of India and a DST-FIST grant received by the School of Biological Sciences, NISER (Grant No.- SR/FST/LSI-652/2015). The work has been partly supported by the Council of Scientific and Industrial Research (CSIR), India (Grant No.- 37(1542)/12/EMR-II, 37(1675)/16/EMR-II) and Department of Biotechnology, India (Grant No.- BT/NBM0101/02/2018).

Acknowledgments

We are thankful to the central Flow Cytometry facility, Animal House facility and Health Center of NISER, Bhubaneswar for the *in vitro* mouse and human model experiments. We sincerely acknowledge the Animal House facility of ILS, Bhubaneswar for the *in vivo* mouse model experiments.

Conflict of interest

The authors declare that the research was conducted in the absence of any commercial or financial relationships that could be construed as a potential conflict of interest.

Publisher's note

Supplementary material

The Supplementary Material for this article can be found online at: https://www.frontiersin.org/articles/10.3389/fimmu.2023.1139808/full#supplementary-material

References

1. Webb E, Michelen M, Rigby I, Dagens A, Dahmash D, Cheng V, et al. An evaluation of global chikungunya clinical management guidelines: A systematic review. *EClinicalMedicine* (2022) 54:101672. doi: 10.1016/j.eclinm.2022.101672

2. Suhrbier A. Rheumatic manifestations of chikungunya: emerging concepts and interventions. *Nat Rev Rheumatol* (2019) 15:597–611. doi: 10.1038/s41584-019-0276-9

3. Simon F, Javelle E, Cabie A, Bouquillard E, Troisgros O, Gentile G, et al. French Guidelines for the management of chikungunya (acute and persistent presentations). *November 2014 Med Mal Infect* (2015) 45:243–63. doi: 10.1016/j.medmal.2015.05.007

4. Cunha RV, Trinta KS. Chikungunya virus: clinical aspects and treatment - a review. *Mem Inst Oswaldo Cruz* (2017) 112:523–31. doi: 10.1590/0074-02760170044

5. Kielian M, Chanel-Vos C, Liao M. Alphavirus entry and membrane fusion. *Viruses* (2010) 2:796–825. doi: 10.3390/v2040796

6. Bernard E, Solignat M, Gay B, Chazal N, Higgs S, Devaux C, et al. Endocytosis of chikungunya virus into mammalian cells: Role of clathrin and early endosomal compartments. *PloS One* (2010) 5:e11479. doi: 10.1371/journal.pone.0011479

7. Lee CHR, Mohamed Hussain K, Chu JJH. Macropinocytosis dependent entry of chikungunya virus into human muscle cells. *PloS Negl Trop Dis* (2019) 13:e0007610. doi: 10.1371/journal.pntd.0007610

8. Bernard KA, Klimstra WB, Johnston RE. Mutations in the E2 glycoprotein of Venezuelan equine encephalitis virus confer heparan sulfate interaction, low morbidity, and rapid clearance from blood of mice. *Virology* (2000) 276:93–103. doi: 10.1006/viro.2000.0546

9. Gardner CL, Burke CW, Higgs ST, Klimstra WB, Ryman KD. Interferon-alpha/beta deficiency greatly exacerbates arthritogenic disease in mice infected with wild-type chikungunya virus but not with the cell culture-adapted live-attenuated 181/25 vaccine candidate. *Virology* (2012) 425:103–12. doi: 10.1016/j.virol.2011.12.020

10. Gardner CL, Hritz J, Sun C, Vanlandingham DL, Song TY, Ghedin E, et al. Deliberate attenuation of chikungunya virus by adaptation to heparan sulfate-dependent infectivity: A model for rational arboviral vaccine design. *PloS Negl Trop Dis* (2014) 8:e2719. doi: 10.1371/journal.pntd.0002719

11. Klimstra WB, Ryman KD, Johnston RE. Adaptation of sindbis virus to BHK cells selects for use of heparan sulfate as an attachment receptor. *J Virol* (1998) 72:7357–66. doi: 10.1128/JVI.72.9.7357-7366.1998

12. Smit JM, Waarts B-L, Kimata K, Klimstra WB, Bittman R, Wilschut J. Adaptation of alphaviruses to heparan sulfate: Interaction of sindbis and semliki forest viruses with liposomes containing lipid-conjugated heparin. *J Virol* (2002) 76:10128–37. doi: 10.1128/JVI.76.20.10128-10137.2002

13. Weber C, Berberich E, von Rhein C, Henß L, Hildt E, Schnierle BS. Identification of functional determinants in the chikungunya virus E2 protein. *PloS Negl Trop Dis* (2017) 11:e0005318. doi: 10.1371/journal.pntd.0005318

14. Moller-Tank S, Kondratowicz AS, Davey RA, Rennert PD, Maury W. Role of the phosphatidylserine receptor TIM-1 in enveloped-virus entry. *J Virol* (2013) 87:8327–41. doi: 10.1128/JVI.01025-13

15. Jemielity S, Wang JJ, Chan YK, Ahmed AA, Li W, Monahan S, et al. TIM-family proteins promote infection of multiple enveloped viruses through virion-associated phosphatidylserine. *PloS Pathog* (2013) 9:e1003232. doi: 10.1371/journal.ppat.1003232

16. Prado Acosta M, Geoghegan EM, Lepenies B, Ruzal S, Kielian M, Martinez MG. Surface (S) layer proteins of lactobacillus acidophilus block virus infection *via* DC-SIGN interaction. *Front Microbiol* (2019) 10:810. doi: 10.3389/fmicb.2019.00810

17. Wintachai P, Wikan N, Kuadkitkan A, Jaimipuk T, Ubol S, Pulmanausahakul R, et al. Identification of prohibitin as a chikungunya virus receptor protein. *J Med Virol* (2012) 84:1757–70. doi: 10.1002/jmv.23403

18. Zhang R, Kim AS, Fox JM, Nair S, Basore K, Klimstra WB, et al. Mxra8 is a receptor for multiple arthritogenic alphaviruses. *Nature* (2018) 557:570–4. doi: 10.1038/s41586-018-0121-3

19. Nayak T, Mamidi P, Kumar A, Singh L, Sahoo S, Chattopadhyay S, et al. Regulation of viral replication, apoptosis and pro-inflammatory responses by 17-AAG during chikungunya virus infection in macrophages. *Viruses* (2017) 9:3. doi: 10.3390/v9010003

20. Jacob-Nascimento LC, Carvalho CX, Silva MMO, Kikuti M, Anjos RO, Fradico JRB, et al. Acute-phase levels of CXCL8 as risk factor for chronic arthralgia following chikungunya virus infection. *Front Immunol* (2021) 12:744183. doi: 10.3389/fimmu.2021.744183

21. Guerrero-Arguero I, Høj TR, Tass ES, Berges BK, Robison RA. A comparison of chikungunya virus infection, progression, and cytokine profiles in human PMA-

differentiated U937 and murine RAW264.7 monocyte derived macrophages. *PloS One* (2020) 15:e0230328. doi: 10.1371/journal.pone.0230328

22. Nayak TK, Mamidi P, Sahoo SS, Kumar PS, Mahish C, Chatterjee S, et al. P38 and JNK mitogen-activated protein kinases interact with chikungunya virus non-structural protein-2 and regulate TNF induction during viral infection in macrophages. *Front Immunol* (2019) 10:786. doi: 10.3389/fimmu.2019.00786

23. Wu K, Zhang H, Fu Y, Zhu Y, Kong L, Chen L, et al. TLR4/MyD88 signaling determines the metastatic potential of breast cancer cells. *Mol Med Rep* (2018). doi: 10.3892/mmr.2018.9326

24. Takashima K, Matsunaga N, Yoshimatsu M, Hazeki K, Kaisho T, Uekata M, et al. Analysis of binding site for the novel small-molecule TLR4 signal transduction inhibitor TAK-242 and its therapeutic effect on mouse sepsis model. *Br J Pharmacol* (2009) 157:1250–62. doi: 10.1111/j.1476-5381.2009.00297.x

25. Samarpita S, Kim JY, Rasool MK, Kim KS. Investigation of toll-like receptor (TLR) 4 inhibitor TAK-242 as a new potential anti-rheumatoid arthritis drug. *Arthritis Res Ther* (2020) 22:16. doi: 10.1186/s13075-020-2097-2

26. Poltorak A, He X, Smirnova I, Liu M-Y, van HC, Du X, et al. Defective LPS signaling in C3H/HeJ and C57BL/10ScCr mice: Mutations in *Tlr4* gene. *Sci (1979)* (1998) 282:2085–8. doi: 10.1126/science.282.5396.2085

27. Yu R, Jiang S, Tao Y, Li P, Yin J, Zhou Q. Inhibition of HMGB1 improves necrotizing enterocolitis by inhibiting NLRP3 *via* TLR4 and NF-κB signaling pathways. *J Cell Physiol* (2019) 234:13431–8. doi: 10.1002/jcp.28022

28. Han C, Guo L, Sheng Y, Yang Y, Wang J, Gu Y, et al. FoxO1 regulates TLR4/MyD88/MD2-NF-κB inflammatory signalling in mucosal barrier injury of inflammatory bowel disease. *J Cell Mol Med* (2020) 24:3712–23. doi: 10.1111/jcmm.15075

29. Seki H, Tasaka S, Fukunaga K, Shiraishi Y, Moriyama K, Miyamoto K, et al. Effect of toll-like receptor 4 inhibitor on LPS-induced lung injury. *Inflammation Res* (2010) 59:837–45. doi: 10.1007/s00011-010-0195-3

30. Marzec J, Cho H-Y, High M, McCaw ZR, Polack F, Kleeberger SR. Toll-like receptor 4-mediated respiratory syncytial virus disease and lung transcriptomics in differentially susceptible inbred mouse strains. *Physiol Genomics* (2019) 51:630–43. doi: 10.1152/physiolgenomics.00101.2019

31. Zhao Y, Kuang M, Li J, Zhu L, Jia Z, Guo X, et al. SARS-CoV-2 spike protein interacts with and activates TLR41. *Cell Res* (2021) 31:818–20. doi: 10.1038/s41422-021-00495-9

32. Zhang J, Li D, Yang W, Wang Y, Li L, Zheng H. Foot-and-Mouth disease virus VP3 protein acts as a critical proinflammatory factor by promoting toll-like receptor 4-mediated signaling. *J Virol* (2021) 95. doi: 10.1128/JVI.01120-21

33. Felipe VLJ, Paula AV, Silvio U-I. Chikungunya virus infection induces differential inflammatory and antiviral responses in human monocytes and monocyte-derived macrophages. *Acta Trop* (2020) 211:105619. doi: 10.1016/j.actatropica.2020.105619

34. Matsunaga N, Tsuchimori N, Matsumoto T, Ii M. TAK-242 (Resatorvid), a small-molecule inhibitor of toll-like receptor (TLR) 4 signaling, binds selectively to TLR4 and interferes with interactions between TLR4 and its adaptor molecules. *Mol Pharmacol* (2011) 79:34–41. doi: 10.1124/mol.110.068064

35. Lin F-Y, Chen Y-H, Tasi J-S, Chen J-W, Yang T-L, Wang H-J, et al. Endotoxin induces toll-like receptor 4 expression in vascular smooth muscle cells *via* NADPH oxidase activation and mitogen-activated protein kinase signaling pathways. *Arterioscler Thromb Vasc Biol* (2006) 26:2630–7. doi: 10.1161/01.ATV.0000247259.01257.b3

36. Anand G, Perry AM, Cummings CL, Raymond E, Clemens RA, Steed AL. Surface proteins of SARS-CoV-2 drive airway epithelial cells to induce IFN-dependent inflammation. *J Immunol* (2021) 206:3000–9. doi: 10.4049/jimmunol.2001407

37. Sha T, Sunamoto M, Kitazaki T, Sato J, Ii M, Iizawa Y. Therapeutic effects of TAK-242, a novel selective toll-like receptor 4 signal transduction inhibitor, in mouse endotoxin shock model. *Eur J Pharmacol* (2007) 571:231–9. doi: 10.1016/j.ejphar.2007.06.027

38. Chattopadhyay S, Chakraborty NG. Continuous presence of Th1 conditions is necessary for longer lasting tumor-specific CTL activity in stimulation cultures with PBL. *Hum Immunol* (2005) 66:884–91. doi: 10.1016/j.humimm.2005.06.002

39. Chattopadhyay S, Mehrotra S, Chhabra A, Hegde U, Mukherji B, Chakraborty NG. Effect of $CD4^+$ $CD25^+$ and $CD4^+$ $CD25^-$ T regulatory cells on the generation of cytolytic T cell response to a self but human tumor-associated epitope *In vitro*. *J Immunol* (2006) 176:984–90. doi: 10.4049/jimmunol.176.2.984

40. De S, Mamidi P, Ghosh S, Keshry SS, Mahish C, Pani SS, et al. Telmisartan restricts chikungunya virus infection *in vitro* and *in vivo* through the AT1/PPAR-γ/MAPKs pathways. *Antimicrob Agents Chemother* (2021). doi: 10.1128/AAC.01489-21

41. Chatterjee S, Kumar S, Mamidi P, Datey A, Sengupta S, Mahish C, et al. DNA Damage response signaling is crucial for effective chikungunya virus replication. *J Virol* (2022). doi: 10.1128/jvi.01334-22

42. Hogg N, Palmer DG, Revell PA. Mononuclear phagocytes of normal and rheumatoid synovial membrane identified by monoclonal antibodies. *Immunology* (1985) 56:673–81.

43. Ziegler-Heitbrock HWL, Ulevitch RJ. CD14: Cell surface receptor and differentiation marker. *Immunol Today* (1993) 14:121–5. doi: 10.1016/0167-5699(93)90212-4

44. Liu G, Xie J, Shi Y, Chen R, Li L, Wang M, et al. Sec-o-glucosylhamaudol suppressed inflammatory reaction induced by LPS in RAW264.7 cells through inhibition of NF-κB and MAPKs signaling. *Biosci Rep* (2020) 40. doi: 10.1042/BSR20194230

45. Sanjai Kumar P, Nayak TK, Mahish C, Sahoo SS, Radhakrishnan A, De S, et al. Inhibition of transient receptor potential vanilloid 1 (TRPV1) channel regulates chikungunya virus infection in macrophages. *Arch Virol* (2021) 166:139–55. doi: 10.1007/s00705-020-04852-8

46. De S, Ghosh S, Keshry SS, Mahish C, Mohapatra C, Guru A, et al. MBZM-N-IBT, a novel small molecule, restricts chikungunya virus infection by targeting nsP2 protease activity *In vitro* , *In vivo* , and *Ex vivo*. *Antimicrob Agents Chemother* (2022) 66. doi: 10.1128/aac.00463-22

47. Pierce BG, Wiehe K, Hwang H, Kim B-H, Vreven T, Weng Z. ZDOCK server: interactive docking prediction of protein-protein complexes and symmetric multimers. *Bioinformatics* (2014) 30:1771–3. doi: 10.1093/bioinformatics/btu097

48. Yang K, Zhang XJ, Cao LJ, Liu XH, Liu ZH, Wang XQ, et al. Toll-like receptor 4 mediates inflammatory cytokine secretion in smooth muscle cells induced by oxidized low-density lipoprotein. *PloS One* (2014) 9:e95935. doi: 10.1371/journal.pone.0095935

49. Layoun A, Samba M, Santos MM. Isolation of murine peritoneal macrophages to carry out gene expression analysis upon toll-like receptors stimulation. *J Visualized Experiments* (2015). doi: 10.3791/52749

50. Dhanwani R, Khan M, Lomash V, Rao PVL, Ly H, Parida M. Characterization of chikungunya virus induced host response in a mouse model of viral myositis. *PloS One* (2014) 9:e92813. doi: 10.1371/journal.pone.0092813

51. Wang J, Feng X, Zeng Y, Fan J, Wu J, Li Z, et al. Lipopolysaccharide (LPS)-induced autophagy is involved in the restriction of escherichia coliin peritoneal mesothelial cells. *BMC Microbiol* (2013) 13:255. doi: 10.1186/1471-2180-13-255

52. Akashi S, Shimazu R, Ogata H, Nagai Y, Takeda K, Kimoto M, et al. Cutting edge: Cell surface expression and lipopolysaccharide signaling *Via* the toll-like receptor 4-MD-2 complex on mouse peritoneal macrophages. *J Immunol* (2000) 164:3471–5. doi: 10.4049/jimmunol.164.7.3471

53. Gioannini TL, Teghanemt A, Zhang D, Coussens NP, Dockstader W, Ramaswamy S, et al. Isolation of an endotoxin–MD-2 complex that produces toll-like receptor 4-dependent cell activation at picomolar concentrations. *Proc Natl Acad Sci* (2004) 101:4186–91. doi: 10.1073/pnas.0306906101

54. Schromm AB, Lien E, Henneke P, Chow JC, Yoshimura A, Heine H, et al. Molecular genetic analysis of an endotoxin nonresponder mutant cell line. *J Exp Med* (2001) 194:79–88. doi: 10.1084/jem.194.1.79

55. Küper C, Beck F-X, Neuhofer W. Toll-like receptor 4 activates NF-κB and MAP kinase pathways to regulate expression of proinflammatory COX-2 in renal medullary collecting duct cells. *Am J Physiol-Renal Physiol* (2012) 302:F38–46. doi: 10.1152/ajprenal.00590.2010

56. Wang W, Weng J, Yu L, Huang Q, Jiang Y, Guo X. Role of TLR4-p38 MAPK-Hsp27 signal pathway in LPS-induced pulmonary epithelial hyperpermeability. *BMC Pulm Med* (2018) 18:178. doi: 10.1186/s12890-018-0735-0

57. Khan MA, Farahvash A, Douda DN, Licht J-C, Grasemann H, Sweezey N, et al. JNK activation turns on LPS- and gram-negative bacteria-induced NADPH oxidase-dependent suicidal NETosis. *Sci Rep* (2017) 7:3409. doi: 10.1038/s41598-017-03257-z

58. Li C, Zhao B, Lin C, Gong Z, An X. TREM2 inhibits inflammatory responses in mouse microglia by suppressing the PI3K/NF-κB signaling. *Cell Biol Int* (2019) 43:360–72. doi: 10.1002/cbin.10975

59. Hop HT, Reyes AWB, Huy TXN, Arayan LT, Min W, Lee HJ, et al. Activation of NF-kB-Mediated TNF-induced antimicrobial immunity is required for the efficient brucella abortus clearance in RAW 264.7 cells. *Front Cell Infect Microbiol* (2017) 7:437. doi: 10.3389/fcimb.2017.00437

60. Fitzgerald KA, Kagan JC. Toll-like receptors and the control of immunity. *Cell* (2020) 180:1044–66. doi: 10.1016/j.cell.2020.02.041

61. Landmann R, Ludwig C, Obrist R, Obrecht JP. Effect of cytokines and lipopolysaccharide on CD14 antigen expression in human monocytes and macrophages. *J Cell Biochem* (1991) 47:317–29. doi: 10.1002/jcb.240470406

62. Casals C, Barrachina M, Serra M, Lloberas J, Celada A. Lipopolysaccharide up-regulates MHC class II expression on dendritic cells through an AP-1 enhancer without affecting the levels of CIITA. *J Immunol* (2007) 178:6307–15. doi: 10.4049/jimmunol.178.10.6307

63. Tierney JB, Kharkrang M, la Flamme AC. Type II-activated macrophages suppress the development of experimental autoimmune encephalomyelitis. *Immunol Cell Biol* (2009) 87:235–40. doi: 10.1038/icb.2008.99

64. Tsukamoto H, Takeuchi S, Kubota K, Kobayashi Y, Kozakai S, Ukai I, et al. Lipopolysaccharide (LPS)-binding protein stimulates CD14-dependent toll-like receptor 4 internalization and LPS-induced TBK1–IKKε–IRF3 axis activation. *J Biol Chem* (2018) 293:10186–201. doi: 10.1074/jbc.M117.796631

65. Labadie K, Larcher T, Joubert C, Mannioui A, Delache B, Brochard P, et al. Chikungunya disease in nonhuman primates involves long-term viral persistence in macrophages. *J Clin Invest* (2010) 120:894–906. doi: 10.1172/JCI40104

66. Kumar S, Jaffar-Bandjee M-C, Giry C, Connen de Kerillis L, Merits A, Gasque P, et al. Mouse macrophage innate immune response to chikungunya virus infection. *Virol J* (2012) 9:313. doi: 10.1186/1743-422X-9-313

67. Gardner J, Anraku I, Le TT, Larcher T, Major L, Roques P, et al. Chikungunya virus arthritis in adult wild-type mice. *J Virol* (2010) 84:8021–32. doi: 10.1128/JVI.02603-09

68. Hoarau J-J, Jaffar Bandjee M-C, Krejbich Trotot P, Das T, Li-Pat-Yuen G, Dassa B, et al. Persistent chronic inflammation and infection by chikungunya arthritogenic alphavirus in spite of a robust host immune response. *J Immunol* (2010) 184:5914–27. doi: 10.4049/jimmunol.0900255

69. Rice TW, Wheeler AP, Bernard GR, Vincent J-L, Angus DC, Aikawa N, et al. A randomized, double-blind, placebo-controlled trial of TAK-242 for the treatment of severe sepsis*. *Crit Care Med* (2010) 38:1685–94. doi: 10.1097/CCM.0b013e3181e7c5c9

70. Shirato K, Kizaki T. SARS-CoV-2 spike protein S1 subunit induces pro-inflammatory responses *via* toll-like receptor 4 signaling in murine and human macrophages. *Heliyon* (2021) 7:e06187. doi: 10.1016/j.heliyon.2021.e06187

frontiers | Frontiers in Immunology

TYPE Original Research
PUBLISHED 03 May 2023
DOI 10.3389/fimmu.2023.1187035

OPEN ACCESS

EDITED BY
Junji Xing,
Houston Methodist Research Institute, United States

REVIEWED BY
Tian Bin,
Sichuan Agricultural University, China
Yuening Cheng,
Chinese Academy of Agricultural Sciences (CAAS), China

*CORRESPONDENCE
Guang-Cheng Xie
xieguangcheng123@126.com

†These authors have contributed equally to this work

RECEIVED 15 March 2023
ACCEPTED 24 April 2023
PUBLISHED 03 May 2023

CITATION
Sun P-P, Li D, Su M, Ren Q, Guo W-P, Wang J-L, Du L-Y and Xie G-C (2023) Cell membrane-bound toll-like receptor-1/2/4/6 monomers and -2 heterodimer inhibit enterovirus 71 replication by activating the antiviral innate response.
Front. Immunol. 14:1187035.
doi: 10.3389/fimmu.2023.1187035

Cell membrane-bound toll-like receptor-1/2/4/6 monomers and -2 heterodimer inhibit enterovirus 71 replication by activating the antiviral innate response

Ping-Ping Sun[1†], Dan Li[1†], Meng Su[1†], Qing Ren[1], Wen-Ping Guo[1], Jiang-Li Wang[2], Luan-Ying Du[1] and Guang-Cheng Xie[1,3*]

[1]Department of Pathogenic Biology, College of Basic Medicine, Chengde Medical University, Chengde, Hebei, China, [2]Department of Microbiology Laboratory, Chengde Center for Disease Control and Prevention, Chengde, Hebei, China, [3]Institute of Basic Medicine, College of Basic Medicine, Chengde Medical University, Chengde, Hebei, China

Host immune activation is critical for enterovirus 71 (EV71) clearance and immunopathogenesis. However, the mechanism of innate immune activation, especially of cell membrane-bound toll-like receptors (TLRs), against EV71 remains unknown. We previously demonstrated that TLR2 and its heterodimer inhibit EV71 replication. In this study, we systematically investigated the effects of TLR1/2/4/6 monomers and TLR2 heterodimer (TLR2/TLR1, TLR2/TLR6, and TLR2/TLR4) on EV71 replication and innate immune activation. We found that the overexpression of human- or mouse-derived TLR1/2/4/6 monomers and TLR2 heterodimer significantly inhibited EV71 replication and induced the production of interleukin (IL)-8 via activation of the phosphoinositide 3-kinase/protein kinase B (*PI3K/AKT*) and mitogen-activated protein kinase (*MAPK*) pathways. Furthermore,human–mouse chimeric TLR2 heterodimer inhibited EV71 replication and activated innate immunity. Dominant-negative TIR-less (DN)-TLR1/2/4/6 did not exert any inhibitory effects, whereas DN-TLR2 heterodimer inhibited EV71 replication. Prokaryotic expression of purified recombinant EV71 capsid proteins (VP1, VP2, VP3, and VP4) or overexpression of EV71 capsid proteins induced the production of IL-6 and IL-8 via activation of the *PI3K/AKT* and *MAPK* pathways. Notably, two types of EV71 capsid proteins served as pathogen-associated molecular patterns for TLR monomers (TLR2 and TLR4) and TLR2 heterodimer (TLR2/TLR1, TLR2/TLR6, and TLR2/TLR4) and activated innate immunity. Collectively, our results revealed that membrane TLRs inhibited EV71 replication via activation of the antiviral innate response, providing insights into the EV71 innate immune activation mechanism.

KEYWORDS

enterovirus 71, toll-like receptors, capsid proteins, antiviral innate immunity, immune activation

1 Introduction

Enterovirus 71 (EV71) is the major causative agent of hand, foot, and mouth disease (HFMD) that poses a heavy burden on affected infants and children under five years of age. EV71 was first identified in patients with fatal encephalitis in California, USA, in 1969 (1). In 1973, EV71 was recognized as the causative pathogen of HFMD, although it was also observed in patients with aseptic meningitis in Japan (2). Several HFMD outbreaks have occurred worldwide, particularly in Bulgaria in 1975 (3), Malaysia in 1997 (4), and Taiwan in 1998 (5). China also experienced large outbreaks of HFMD in Linyi in 2007 (6), Fuyang in 2008 (7), and Guangdong in 2009 (8). Circulating EV71 has also been reported in Asia-Pacific countries, including Japan, Singapore, Indonesia, Thailand, and the Philippines (9–11). Therefore, HFMD caused by EV71 infection is a serious threat to global public health. EV71 is a single-stranded positive-sense RNA virus belonging to the genus, *Enterovirus*, of the *Picornaviridae* family. The single open reading frame of the EV71 genome encodes only one polyprotein, which is further hydrolyzed and degraded by 2A and 3C proteases to form four structural proteins (VP1, VP2, VP3, and VP4) and seven non-structural proteins (2A, 2B, 2C, 3A, 3B, 3C, and 3D) (12, 13). Four capsid proteins form the icosahedral capsid of EV71. Structural proteins VP1, VP2, and VP3 are located on the surface, whereas VP4 is internalized in the EV71 capsid (11, 12). In the EV71 life cycle, binding of scavenger receptor class B member 2 (SCARB2) or selectin P ligand (SELPLG, also known as PSGL-1) with capsid proteins is a critical step in the EV71 attachment process (14, 15). All four capsid proteins of EV71 play different roles in the infection cycle. VP1 is mainly involved in receptor binding, viral entry, and virion assembly, and mutations at its amino acid residue 145 determine the virulence of EV71 (10, 16). During viral entry, EV71 VP4 protein plays an important role in the formation of pores in the cell membrane to release viral RNA into the host cell cytoplasm via myristoylation of VP4 to interact with the cell membrane (17).

Innate antiviral immunity is the first line of host defense against viral infections. Pattern recognition receptors (PRRs), including toll-like receptors (TLRs), retinoic acid-inducible gene I-like receptors, and nucleotide oligomerization domain-like receptors, recognize conserved viral RNA/DNA or proteins, known as pathogen-associated molecular patterns (PAMPs), to initiate the signaling cascade for the production of effector molecules (18, 19). TLRs are a class of type I transmembrane PRRs. To date, 10 and 12 TLRs have been identified in humans and mice, respectively. Human TLRs are further divided into two groups based on their membrane location: cell membrane-bound TLRs (TLR1, 2, 4, 5, 6, and 10), and endosomal or endolysosomal membrane-bound TLRs (TLR3, 7, 8, and 9) (20–22). Using EV71 viral RNA as a ligand, interferon induced with helicase C domain 1 activates the interferon (IFN) regulatory factor 3 (IRF3) and induces IFN-β expression (23). Transcriptional levels of TLR7 and TLR8 are significantly upregulated in EV71-infected HT29 cells (24) and human primary monocyte-derived macrophages (MDMs) (25).

Clinical samples, such as blood and cerebrospinal fluid samples, of EV71-infected patients exhibit significantly upregulated levels of IFN-γ-induced protein 10 (IP-10), monocyte chemoattractant protein-1 (MCP-1), monokine induced by IFN-γ, and interleukin (IL)-8 (26), and altered levels of proinflammatory cytokines (IL-1β, IL-2, IL-23, IL-33, and tumor necrosis factor [TNF]-α), chemokines (IP-10 and MCP-1), and other cytokines (IL-6, IL-8, IL-10, and IL-18) (27–29), indicating the activation of cellular immune responses and involvement of specific cytokines in the pathogenesis of EV71 infection. Therefore, it is necessary to determine the immune activation mechanism, especially of innate immunity, to understand the antiviral activity of host cells against EV71. Interestingly, EV71 exhibits an immune evasion strategy to avoid innate immunity using its 2A and 3C proteases by cleaving PRRs or adaptors, including TIR-domain-containing adapter-inducing interferon-β, mitochondrial antiviral-signaling protein, and IRF7, to block PRR recognition and inhibit signaling cascade transduction (10, 30). However, the specific innate immune activation mechanism of host cells against EV71 remains unknown. Antiviral innate immunity against EV71 mediated by PRRs sensing viral nucleotides in the cytoplasm is often disrupted. Whether host cells use cell membrane-bound TLRs, such as TLR2 or TLR4, to recognize the viral proteins of EV71 to activate innate immunity remains unclear.

TLR2 and TLR4 mainly recognize bacterial PAMPs, such as lipopolysaccharides and flagellins (31, 32). Various viral proteins, such as dengue virus NS1 protein (33), human immunodeficiency virus (HIV)-1 structural proteins (p17, p24, and pg41) (34), envelope gp120 glycoprotein (35), respiratory syncytial virus (RSV) G protein (36), influenza virus extracellular nucleoprotein (37), and other viral proteins (22, 38), are also recognized by TLR2 and TLR4. TLR2 expression levels are significantly upregulated in human rhinovirus 6 (HRV6)-infected or UV-inactivated HRV6-induced human airway epithelial cells (39). TLR2 expression levels are also significantly increased in EV71-infected or UV-inactivated EV71-induced MDMs (25). We previously reported that the transcriptional levels of TLR2 are upregulated in EV71-infected cells via transcriptomic sequencing (40). Moreover, we previously demonstrated that EV71 replication is significantly inhibited by the transfection of TLR2 or TLR2 heterodimer (TLR2/TLR1 and TLR2/TLR6) plasmids or activation of TLR2 heterodimer by Pam2CSK4 and Pam3CSK4 in HEK293 cells (40). However, the specific effects of TLR2, TLR4, and TLR2 heterodimer on EV71 remain unknown. To determine whether cell membrane-bound TLR1/2/4/6 monomers and TLR2 heterodimer exhibit any antiviral activity

Abbreviations: TLRs, Toll-like receptors; DN, Dominant negative TIR-less; PAMPs, Pathogen-associated molecular patterns; EV71, Enterovirus 71; HFMD, Hand, foot, and mouth disease; SCARB2, Scavenger receptor class B, member 2; PSGL-1, P-selectin glycoprotein ligand-1; PRRs, Pattern recognition receptors; IFN, Interferon; IRF3, Interferon regulatory factor 3; IRF7, Interferon regulatory factor 7; MDMs, Monocyte-derived macrophages; IP-10, IFN-γ-induced protein 10; MCP-1, Monocyte chemoattractant protein-1; IL-8, Interleukin-8; HIV-1, Human immunodeficiency virus type 1; RSV, Respiratory syncytial virus; HRV6, Human rhinovirus 6; VLPs, Virus-like particles; HCV, Hepatitis C virus; PI3K/AKT, phosphoinositide 3-kinase/protein kinase B; MAPK, mitogen-activated protein kinase; PARP9, poly(ADP-ribose) polymerase 9.

against EV71, we systematically investigated the replication of EV71, production of IL-8, and activation of the phosphoinositide 3-kinase/protein kinase B (*PI3K/AKT*) and mitogen-activated protein kinase (*MAPK*) pathways (extracellular signal-regulated kinase [*ERK*], c-Jun N-terminal kinase [*JNK*], and *p38* pathways) in HEK293 cells transfected with different TLR1/2/4/6 monomer and TLR2 heterodimer plasmids. We further evaluated the effects of EV71 capsid proteins on cytokine production and pathway activation using TLR monomers (TLR2 and TLR4) and TLR2 heterodimer (TLR2/TLR1, TLR2/TLR6, and TLR2/TLR4). Our findings revealed that EV71 recognition led to the activation of antiviral innate immunity to inhibit its replication via TLR1/2/4/6 monomers and TLR2 heterodimer. Moreover, we determined the roles of EV71 capsid proteins in the activation of TLR monomer (TLR2 and TLR4) and TLR2 heterodimer (TLR2/TLR1, TLR2/TLR6, and TLR2/TLR4) signaling.

2 Materials and methods

2.1 Cell lines and virus

Human embryonic kidney (HEK293) and rhabdomyosarcoma (RD) cells were cultured in Dulbecco's modified Eagle's medium (Gibco, CA, USA). The human tonsillar epithelial (UT-SCC-60B) cell line was kindly provided by Dr. Reidar Grénman and maintained in the Roswell Park Memorial Institute-1640 medium (Gibco). All media were supplemented with 10% bovine calf serum and 1% 100× penicillin–streptomycin (Biosharp, China). Cells were incubated at 37°C in a 5% CO_2 humidified incubator.

EV71 (Fuyang strain; GenBank: EU703812.1) was used in this study and propagated in RD cells. Propagation and purification methods for EV71 were described in our previous study (40).

2.2 Plasmids

Human TLR plasmids, including pcDNA3-TLR1-YFP (Addgene plasmid #13014), pcDNA3-TLR2-CFP (Addgene plasmid #13015), pcDNA3-TLR4-YFP (Addgene plasmid #13018), and pcDNA3-TLR6-YFP (Addgene plasmid #13020), were gifts from Doug Golenbock. Mouse TLR plasmids, including mTLR1 (Addgene plasmid #13080), mTLR2 (Addgene plasmid #13083), and mTLR4 (Addgene plasmid #13085), were gifts from Ruslan Medzhitov. Point mutation plasmids of TLR4, including pMyc-CMV1-huTLR4mut-C1196T (Addgene plasmid #53526), pMyc-CMV1-huTLR4mut-C2141A (Addgene plasmid #53527), and pMyc-CMV1-huTLR4mut-A896G (Addgene plasmid #53525), were gifts from Linda Yu. All these plasmids were purchased from Addgene (https://www.addgene.org). mTLR6 plasmid pUNO1-mTLR06-HA3x (puno1ha-mtlr6), TLR2 heterodimer plasmids, including pDUO-hTLR6/TLR2 (pduo-htlr6tlr2), pDUO-hTLR1/TLR2 (pduo-htlr1tlr2), and pDUO-hCD14/TLR2 (pduo-hcd14tlr2) plasmids, TLR1/2/4/6 Dominant-negative TIR-less (DN [ΔTIR]) plasmids, pUNO1-hTLR1-DN-HA (puno1ha-htlr1-dn), pUNO1-hTLR2-DN-HA (puno1ha-htlr2-dn), pUNO1-hTLR4-DN-HA (puno1ha-htlr4a-dn), and pUNO1-hTLR6-DN-HA (puno1ha-htlr6-dn), were purchased from InvivoGen (San Diego, CA, USA).

Primers for EV71 structural proteins (VP1, VP2, VP3, and VP4) were designed based on the genome of the EV71 Fuyang strain (GenBank: EU703812.1). HindIII and NotI restriction enzyme sequences were added to forward and reverse primers, respectively. Viral RNA was extracted using the Viral Nucleic Acid Extraction Kit II (Geneaid, Taiwan), and cDNA was synthesized using the First-strand cDNA Synthesis Kit (Beyotime Biotechnology, Shanghai, China). Full-length genes of VP1, VP2, VP3, and VP4 were amplified using Easy-Load PCR Master Mix (Beyotime Biotechnology). Purified genes of VP1, VP2, VP3, VP4, and pcDNA3.1(+)/myc-His A vectors were digested using HindIII and NotI (New England Biolabs, Beijing, China) and ligated using T4 DNA ligase (New England Biolabs, Beijing, China). Recombinant plasmids pcDNA3.1-EV71-VP1, pcDNA3.1-EV71-VP2, pcDNA3.1-EV71-VP3, and pcDNA3.1-EV71-VP4 were confirmed via polymerase chain reaction (PCR) amplification.

2.3 Prokaryotic expression and purification

Full-length VP1, VP2, VP3, and VP4 segments of the EV71 Fuyang strain were codon-optimized and synthesized by Genewiz (Suzhou, China) and cloned into a pGEX4T-1 prokaryotic expression vector. Recombinant pGEX4T-EV71-VP1, pGEX4T-EV71-VP2, pGEX4T-EV71-VP3, and pGEX4T-EV71-VP4 plasmids were transformed into *Escherichia coli* strain BL21(DE3) (TianGen, Beijing, China). Recombinant EV71 VP1, VP2, VP3, and VP4 proteins were expressed with isopropyl-β-D-thiogalactopyranoside at a final concentration of 0.5 mM when the optical density $(OD)_{600}$ of bacterial cultures reached 0.6–0.8. Bacterial sediment was collected and sonicated for 30 min after culture for 16 h at 22°C. The supernatant was centrifuged and filtered by 0.45 and 0.22 μm filter membranes to remove the bacterial debris and mixed with glutathione S-transferase (GST)-tag purification resin (Beyotime Biotechnology) for 2 h at room temperature. GST fusion proteins were collected with an elution buffer (10 mM reduced glutathione, 50 mM Tris-HCl, pH8.0) after washing five times with 30 mL phosphate-buffered saline (PBS; pH7.0). Purified GST fusion proteins were detected using sodium dodecyl sulfate-polyacrylamide gel electrophoresis (SDS-PAGE) and their concentrations were determined using a BCA kit (Beyotime Biotechnology), according to the manufacturer's instructions.

2.4 Transfection and infection

Endotoxin-free TLR-related and EV71 capsid recombinant eukaryotic plasmids were prepared using the E.Z.N.A. Endo-free Plasmid Kit (OMEGA, USA), according to the manufacturer's instructions. HEK293 and RD cells were seeded in a 6-well plate and the TLR-related or EV71 capsid recombinant eukaryotic plasmids were transiently single or co-transfected into host cells at the indicated dose (1 or 2 μg) using the SuperFect Transfection Reagent (Qiagen, Germany), according to the manufacturer's instructions.

After transfecting the plasmids into cells for 24 h, TLR-overexpressing HEK293 and RD cells were infected with EV71 at a multiplicity of infection (MOI) of 0.5 or 1. Then, cytopathic effects (CPEs) on non-transfected and transfected HEK293 and RD cells were observed 24 h after EV71 infection using a microscope (Olympus, Japan).

2.5 Real-time polymerase chain reaction

EV71 viral RNA was extracted from the supernatant using a Viral Nucleic Acid Extraction Kit II (Geneaid) according to the manufacturer's instructions. Reverse transcription was performed using the First-strand cDNA Synthesis Kit (Beyotime Biotechnology) to synthesize cDNA. Real-time polymerase chain reaction (PCR) was performed with the MyiQ2 Real-Time PCR system (Bio-Rad, California, USA) using 2×TransStart Top Green qPCR SuperMix (Trans, Beijing, China) according to manufacturer's instructions. Primers and reaction conditions for real-time PCR were as described in our previous study (40).

2.6 Western blot

Cell lysates were prepared using the radioimmunoprecipitation assay lysis buffer (Beyotime Biotechnology) supplemented with 50× protease and phosphatase inhibitor cocktail (Beyotime Biotechnology). Then, cell lysates were centrifuged to remove the cellular debris and boiled at 100°C for 5 min. All prepared samples were subjected to SDS-PAGE with 12% separating gel, transferred to 0.2-μm PVDF membrane (Merck Millipore, Carrigtwohill, Ireland), and blocked with 5% skim milk in PBST for 1.5 h at room temperature. Primary antibodies were diluted 1:1000 in PBST containing 5% bovine serum albumin. The blocked PVDF membrane was incubated with the diluted primary antibodies at 4°C overnight, followed by incubation with the diluted secondary antibodies for 2 h at room temperature after washing thrice with PBST for 10 min. Finally, the membranes were incubated with an ECL detection kit (Biosharps), and the protein bands were visualized using a Tanon 6100 system (Tanon, Shanghai, China).

The following primary antibodies were used in this study: PI3K p85 (Cell Signaling, Danvers, MA, USA), p-AKT (Ser473; Cell Signaling), p-ERK1/2 (Thr202/Tyr204; Cell Signaling), p-JNK (Thr183/Tyr185; Cell Signaling), p-p38 (Thr180/Tyr182; Cell Signaling), TLR2 (Abcam, Cambridge, MA, USA), TLR1 (Abcam), TLR6 (Cell Signaling), His (Trans), p-PI3K p85α/β/p55γ (Y467/Y464/Y199; Beyotime Biotechnology), and β-actin (Beyotime Biotechnology).

2.7 Enzyme-linked immunosorbent assay

The supernatant was collected from EV71-infected plasmid non-transfected and transfected HEK293 and RD cells. UT-SCC-60B cells were stimulated with recombinant EV71 capsid proteins at a final concentration of 80 μg/mL and single transfected with EV71 capsid recombinant eukaryotic plasmids or co-transfected with TLR-related and EV71 capsid recombinant eukaryotic plasmids. HEK293 cells were transfected with TLR-related plasmids for 24 h and stimulated with recombinant EV71 capsid proteins at a final concentration of 80 μg/mL. Supernatants from the above experiments were collected. Levels of IL-6 and IL-8 in the supernatants were measured using the Human IL-6 and IL-8 ELISA Kits (Beyotime Biotechnology), according to the manufacturer's instructions.

2.8 Statistical analysis

All experiments were conducted in triplicate. Data are represented as the mean ± standard deviation. Statistical analysis was conducted using IBM SPSS Statistics software (version 19.0; IBM Corp., USA). Student's *t*-test was used to determine the statistical differences between the two groups. One-way analysis of variance was used to determine the statistical differences among three or more groups. Differences were considered statistically significant at $p < 0.05$.

3 Results

3.1 Human- or mouse-derived TLR1/2/6 monomers and TLR2 heterodimer inhibit replication of and activate innate immunity against EV71

Previously, we demonstrated that TLR2 and TLR2 heterodimer reduce CPEs and EV71 replication in TLR2 and TLR2 heterodimer-overexpressing cells (40). However, we could not determine the specific mechanism of activation of antiviral innate immunity against EV71 via cell membrane-bound TLRs. To determine the roles of cell membrane-bound TLRs, such as TLR1/2/4/6 monomers and TLR2 heterodimer, in EV71 replication and innate immunity activation, we first transfected human-derived TLR1/2/6 monomers and TLR2 heterodimer (TLR2/TLR1 and TLR2/TLR6) into HEK293 cells and then infected them with EV71 in this study. EV71 replication was significantly and dose-dependently decreased in TLR2 and TLR2 heterodimer (TLR2/TLR1 and TLR2/TLR6)-overexpressing HEK293 cells (Figure 1A). To determine whether mouse-derived TLR2 heterodimer (mTLR2/mTLR1 and mTLR2/mTLR6) inhibit EV71 replication, mouse-derived TLR2 heterodimer (mTLR2/mTLR1 and mTLR2/mTLR6) were overexpressed in HEK293 cells. EV71 replication was inhibited in a dose-dependent manner (Figure 1B). To determine whether TLR1 and TLR6 monomers could inhibit EV71 replication, we transfected human- or mouse-derived TLR1 and TLR6 into HEK293 cells. EV71 replication was significantly decreased in human-derived TLR1- and TLR6-overexpressing HEK293 cells; the TLR2/CD14 heterodimer also decreased EV71 replication (Figure 1C). Similar results were observed in the mTLR1-, mTLR2-, and mTLR6-overexpressing cells (Figure 1D). Levels of the EV71 genome were also significantly decreased in RD cells

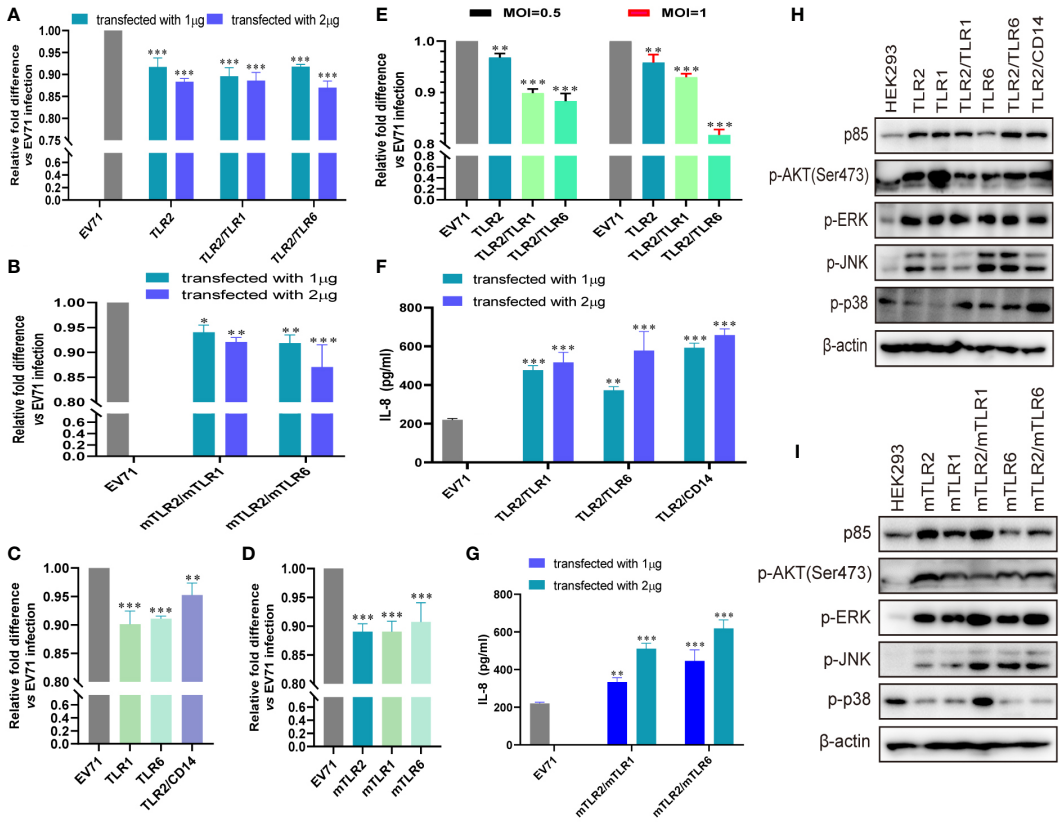

FIGURE 1
EV71 infection activates the antiviral innate immunity via toll-like receptor (TLR) monomers and TLR2 heterodimers to limit its replication. **(A)** Human-derived TLR2 and TLR2 heterodimer (TLR2/TLR1 and TLR2/TLR6) or **(B)** mouse-derived TLR2 heterodimer (mTLR2/mTLR1 and mTLR2/mTLR6) plasmids were transfected into HEK293 cells at a dose of 1 or 2 μg for 24 h, followed by infection with EV71 at a multiplicity of infection (MOI) of 1 for 24 (h) n = 3. **(C)** Human-derived TLR1, TLR6, and TLR2/CD14 or **(D)** mouse-derived mTLR2, mTLR1, and mTLR6 plasmids were transfected into HEK293 cells at a dose of 1 μg for 24 h, followed by infection with EV71 at an MOI of 1 for 24 (h) **(E)** Human-derived TLR2 and TLR2 heterodimer (TLR2/TLR1 and TLR2/TLR6) plasmids were transfected into rhabdomyosarcoma (RD) cells for 24 h and infected with EV71 at an MOI of 0.5 or 1 for 24 (h) Genome copies of EV71 were determined using quantitative polymerase chain reaction (qPCR), and relative fold differences compared with HEK293 cells infected with EV71 for 24 h were calculated. n = 3. **(F)** Human-derived TLR2 heterodimer (TLR2/TLR1, TLR2/TLR6, and TLR2/CD14) or **(G)** mouse-derived TLR2 heterodimer (mTLR2/mTLR1 and mTLR2/mTLR6) plasmids were transfected into HEK293 cells at a dose of 1 or 2 μg for 24 h, followed by infection with EV71 at an MOI of 1 for 24 (h) Supernatants were collected and interleukin (IL)-8 concentrations were determined using an enzyme-linked immunosorbent assay (ELISA) kit. n = 3. **(H)** Human-derived TLR monomer (TLR2, TLR1, and TLR6) and TLR2 heterodimer (TLR2/TLR1, TLR2/TLR6, and TLR2/CD14) plasmids or **(I)** mouse-derived TLR monomer (mTLR2, mTLR1, and mTLR6) and TLR2 heterodimer (mTLR2/mTLR1 and mTLR2/mTLR6) plasmids were transfected into HEK293 cells at a dose of 1 μg for 24 h, followed by infection with EV71 at an MOI of 1 for 24 (h) Total proteins were collected, and activation of the phosphoinositide 3-kinase/protein kinase B (*PI3K/AKT*) and mitogen-activated protein kinase (*MAPK*) pathways was assessed via western blotting. n = 3. *p < 0.05, **p < 0.01, and ***p < 0.001.

overexpressing human-derived TLR2 and TLR2 heterodimer (TLR2/TLR1 and TLR2/TLR6) at different MOI of EV71 infection, especially the TLR2/TLR6 heterodimer (Figure 1E).

EV71 replication is significantly inhibited by cell membrane-bound TLR1/2/6 and TLR2 heterodimer (TLR2/TLR1, TLR2/TLR6, and TLR2/CD14). Given that innate antiviral immunity is the first line of defense against viral infections, we hypothesized that EV71 activates innate immunity via TLR2 heterodimer recognition. First, we confirmed that IL-8 production was significantly upregulated in human TLR2 heterodimer (TLR2/TLR1, TLR2/TLR6, and TLR2/CD14; Figure 1F) or mouse-derived TLR2 heterodimer (mTLR2/mTLR1 and mTLR2/mTLR6; Figure 1G) overexpressing HEK293 cells upon EV71 infection for 24h and appeared in a dose-dependent manner. Second, we investigated whether inflammatory pathways were activated in TLR-overexpressing cells following EV71 infection. Expression of PI3K regulatory subunit p85 was upregulated and phosphorylation levels of AKT, ERK, JNK, and p38 were also increased at different levels in cells overexpressing human-derived TLR monomers (TLR1, TLR2, and TLR6) and TLR2 heterodimer (TLR2/TLR1, TLR2/TLR6, and TLR2/CD14; Figure 1H) or in those overexpressing mouse-derived TLR monomers (mTLR2, mTLR1, and mTLR6) and TLR2 heterodimer (mTLR2/mTLR1, mTLR2/mTLR6; Figure 1I). These results suggest that TLR monomers and TLR2 heterodimer play important roles in inhibiting EV71 replication and activating innate immunity against EV71.

3.2 Conditional changes in TLR2 heterodimer inhibit the replication of and activate innate immunity against EV71

To further determine whether TLR1/2/6 monomers and TLR2 heterodimer play important roles in activating antiviral innate immunity against EV71, we investigated whether conditional changes in TLR2 heterodimer affect the inhibition of EV71 replication and activation of innate immunity. Overexpression of human–mouse chimeric TLR2 heterodimer (mTLR2/TLR1, TLR2/mTLR1, mTLR2/TLR6, and TLR2/mTLR6) significantly inhibited EV71 replication (Figure 2A), and EV71 replication was also inhibited in DN-TLR2 heterodimer (DN-TLR2/TLR1, TLR2/DN-TLR1, DN-TLR2/TLR6, TLR2/DN-TLR6)-overexpressing HEK293 cells (Figure 2B). However, EV71 replication was not inhibited in DN-TLRs (DN-TLR1, DN-TLR2, and DN-TLR6)-overexpressing HEK293 cells (Figure 2C) and UT-SCC-60B cells (Figure 2D). Levels of IL-8 were also significantly upregulated in cells overexpressing human–mouse chimeric TLR2 heterodimer (mTLR2/TLR1, TLR2/mTLR1, mTLR2/TLR6, and TLR2/mTLR6), especially mTLR2/TLR6 heterodimer, in a dose-dependent manner (Figure 2E); however, levels of IL-8 were not upregulated in DN-TLR2 heterodimer (DN-TLR2/TLR1, TLR2/DN-TLR1, DN-TLR2/TLR6, and TLR2/DN-TLR6; Figure 2F) and DN-TLR monomers (DN-TLR1, DN-TLR2, and DN-TLR6; Figure S1A). Expression levels of p85 and phosphorylation levels of AKT, ERK, JNK, and p38 were upregulated in human–mouse chimeric TLR2 heterodimer (mTLR2/TLR1, TLR2/mTLR1, mTLR2/TLR6, and

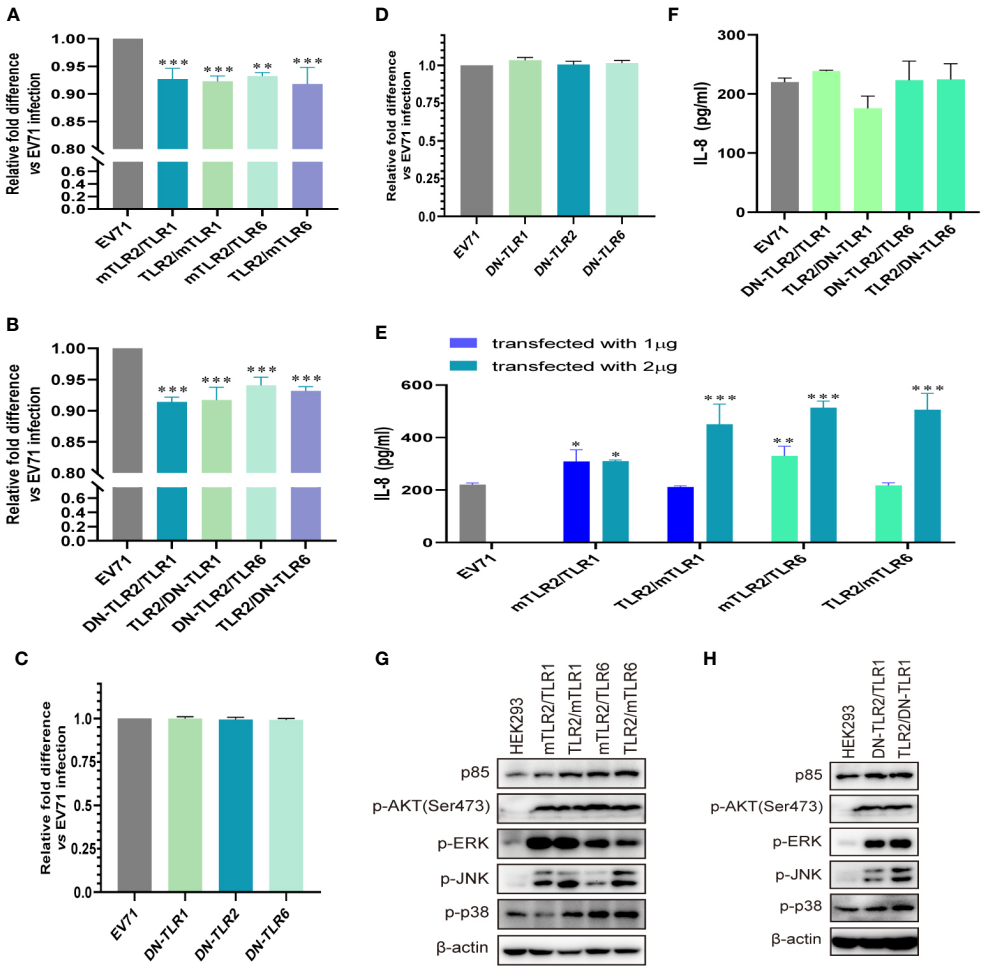

FIGURE 2
EV71 replication is inhibited by conditional changes in TLR2 heterodimers. **(A)** Human–mouse chimeric TLR2 heterodimer (mTLR2/TLR1, TLR2/mTLR1, mTLR2/TLR6, and TLR2/mTLR6) plasmids and **(B)** single dominant-negative TIR-less (DN) TLR2 heterodimer (DN-TLR2/TLR1, TLR2/DN-TLR1, DN-TLR2/TLR6, and TLR2/DN-TLR6) plasmids were transfected into HEK293 cells at a dose of 1 μg for 24 h, followed by infection with EV71 at an MOI of 1 for 24 (h) DN-TLR (DN-TLR1, DN-TLR2, and DN-TLR6) plasmids were transfected into **(C)** HEK293 or **(D)** UT-SCC-60B cells at a dose of 1 μg for 24 h, followed by infection with EV71 at an MOI of 1 for 24 (h) n = 3. Genome copies of EV71 were determined and relative fold differences were calculated. **(E)** Human–mouse chimeric TLR2 heterodimer (mTLR2/TLR1, TLR2/mTLR1, mTLR2/TLR6, and TLR2/mTLR6) plasmids were transfected into HEK293 cells at a dose of 1 or 2 μg for 24 h, followed by infection with EV71 at an MOI of 1 for 24 (h) n = 3. **(F)** Concentrations of IL-8 in the supernatant of group **(B)**. n = 3. **(G)** Human–mouse chimeric TLR2 heterodimer (mTLR2/TLR1, TLR2/mTLR1, mTLR2/TLR6, and TLR2/mTLR6) plasmids or **(H)** single dominant-negative TIR-less TLR2 heterodimer (DN-TLR2/TLR1 and TLR2/DN-TLR1) plasmids were transfected into HEK293 cells at a dose of 1 μg for 24 h, followed by infection with EV71 at an MOI of 1 for 24 (h) Total proteins were collected, and activation of the *PI3K/AKT* and *MAPK* pathways was assessed via western blotting. n = 3. *p < 0.05, **p < 0.01, and ***p < 0.001.

TLR2/mTLR6; Figure 2G) and DN-TLR2 heterodimer (DN-TLR2/TLR1, TLR2/DN-TLR1)-overexpressing HEK293 cells (Figure 2H); however, the opposite results were obtained with DN-TLR monomers (DN-TLR1, DN-TLR2, and DN-TLR6; Figure S1B). These findings confirmed that TLR monomers (TLR1, TLR2, and TLR6) and TLR2 heterodimer (TLR2/TLR1 and TLR2/TLR6) play important roles in inhibiting EV71 replication and activating innate antiviral immunity against EV71.

3.3 Human- and mouse-derived TLR4 and TLR2/TLR4 heterodimer inhibit the replication of and activate innate immunity against EV71

Influenza virus extracellular nucleoprotein and HIV-1 gp120 interact with TLR4 to mediate cytokine induction (35, 37). TLR2 interacts with TLR4 to form a novel TLR2/TLR4 heterodimer via hemoglobin (41). As TLR4 recognizes viral proteins to activate innate immunity, we evaluated the roles of TLR4 and TLR2/TLR4 heterodimer in EV71 infection. EV71 replication was significantly decreased in human-derived (Figure 3A) and mouse-derived (Figure 3B) TLR4 and TLR2/TLR4 heterodimer-overexpressing HEK293 cells. Furthermore, EV71 replication was significantly decreased in human-derived TLR4 and TLR2/TLR4 heterodimer-overexpressing RD cells in an infection-dose-dependent manner (Figure 3C). To assess IL-8 secretion in TLR4-and TLR2/TLR4 heterodimer-overexpressing cells upon EV71 infection, supernatants were collected and IL-8 levels were determined. Upregulation of IL-8 secretion was observed in human-derived TLR4 and TLR2/TLR4 heterodimer-overexpressing cells at a transfection dose of 2 μg (Figure 3D), and induction of IL-8 was also upregulated in mouse-derived TLR4 and TLR2/TLR4 heterodimer-overexpressing cells (Figure 3E). Expression levels of p85 and phosphorylation levels of AKT, ERK, JNK, and p38 were upregulated in human-derived (Figure 3F) and mouse-derived (Figure 3G) TLR2, TLR4, and TLR2/TLR4 heterodimer-overexpressing HEK293 cells. These data indicate that innate immunity is activated via the cell membrane-bound TLR4 monomer and that the TLR2/TLR4 heterodimer recognize EV71 to limit EV71 replication.

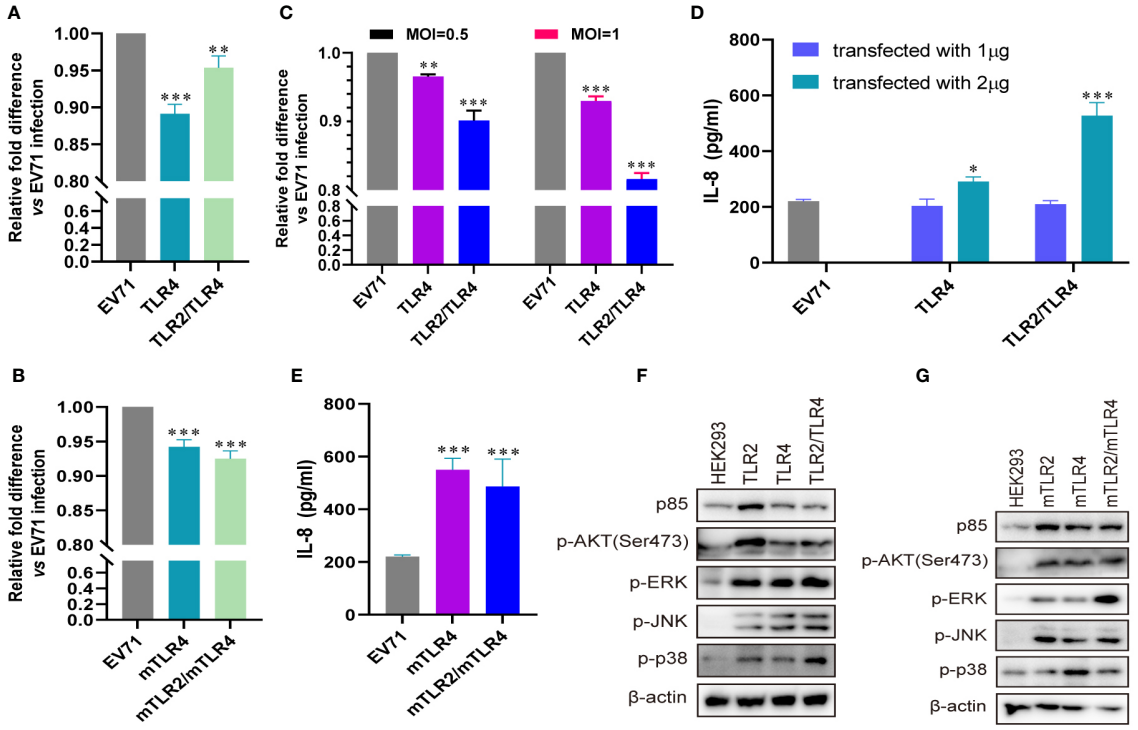

FIGURE 3
EV71 infection activates antiviral innate immunity via TLR4 and TLR2/TLR4 to limit its replication. **(A)** Human-derived TLR4 and TLR2/TLR4 plasmids or **(B)** mouse-derived mTLR4 and mTLR2/mTLR4 plasmids were transfected into HEK293 cells at a dose of 1 μg for 24 h, followed by infection with EV71 at an MOI of 1 for 24 (h) n = 3. **(C)** Human-derived TLR4 and TLR2/TLR4 plasmids were transfected into RD cells at a dose of 1 μg for 24 h, followed by infection with EV71 at an MOI of 0.5 or 1 for 24 (h) n = 3. Genome copies of EV71 were determined and relative fold differences were calculated. **(D)** Human-derived TLR4 and TLR2/TLR4 plasmids were transfected into HEK293 cells at a dose of 1 or 2 μg for 24 h, followed by infection with EV71 at an MOI of 1 for 24 (h) n = 3. **(E)** Concentrations of IL-8 in the supernatant of group **(B)** were determined. **(F)** Human-derived TLR2, TLR4, and TLR2/TLR4 plasmids or **(G)** mouse-derived mTLR2, mTLR4, and mTLR2/mTLR4 plasmids were transfected into HEK293 cells at a dose of 1 μg for 24 h, followed by infection with EV71 at an MOI of 1 for 24 (h) n = 3. Total proteins were collected, and activation of the *PI3K/AKT* and *MAPK* pathways was assessed via western blotting. *p < 0.05, **p < 0.01, and ***p < 0.001.

3.4 Conditional changes in TLR4 and TLR2/TLR4 heterodimer inhibit the replication of and activate innate immunity against EV71

To further confirm the roles of TLR4 and TLR2/TLR4 heterodimer in inhibiting EV71 replication and activating innate immunity, we investigated whether conditional changes in TLR4 and TLR2/TLR4 heterodimer affect EV71 replication and activation of innate immunity. When human–mouse chimeric TLR2/TLR4 heterodimer (mTLR2/TLR4 and TLR2/mTLR4) were overexpressed in HEK293 cells and infected with EV71, the replication of EV71 was significantly decreased in a dose-dependent manner (Figure 4A). We further determined that single dominant-negative TIR-less TLR2/TLR4 heterodimer (DN-TLR2/TLR4, TLR2/DN-TLR4) inhibited EV71 replication (Figure 4B); however, EV71 replication was not affected in DN-TLR4-overexpressing HEK293 (Figure 4C) and UT-SCC-60B (Figure 4D) cells. To identify the nucleotide acting as the major functional site for TLR4, three single nucleotide mutation TLR4 (A896G, C1196T, and C2141A) plasmids were transfected into HEK293 cells to determine their effects on EV71 replication. Mutations in TLR4 at nucleotides A896G, C1196T, and C2141A result in single amino acid mutations in TLR4 (Asp299Gly, Thr399Ile, and Pro714His, respectively) (42). We found that EV71 replication was also inhibited in HEK293 cells

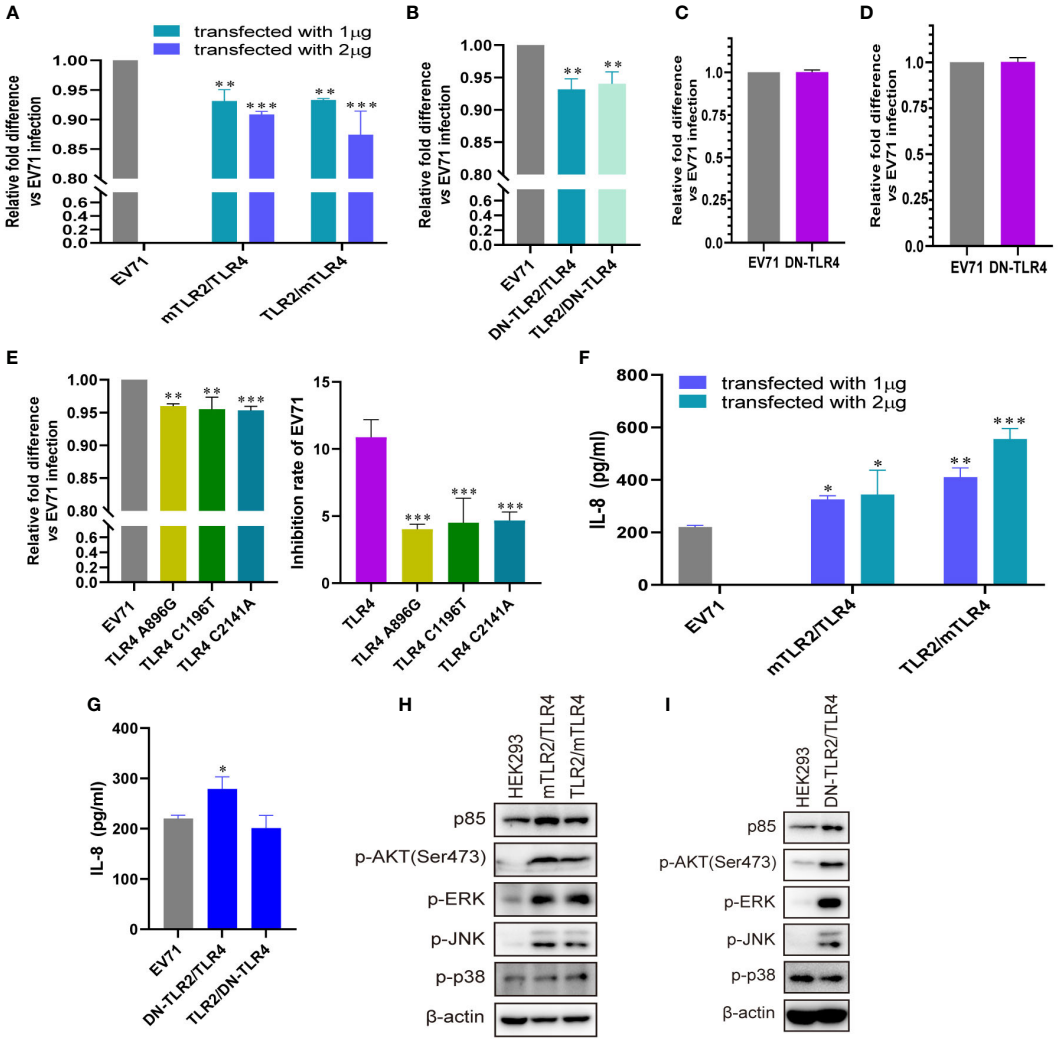

FIGURE 4
Conditional changes in TLR4 and TLR2/TLR4 heterodimers inhibit EV71 replication by activating innate immunity. **(A)** Human–mouse chimeric TLR2 heterodimer (mTLR2/TLR4 and TLR2/mTLR4) plasmids were transfected into HEK293 cells at a dose of 1 or 2 μg for 24 h, followed by infection with EV71 at an MOI of 1 for 24 (h) n = 3. **(B)** Single dominant-negative TIR-less TLR2/TLR4 heterodimer (DN-TLR2/TLR4 and TLR2/DN-TLR4) plasmids were transfected into HEK293 cells at a dose of 1 μg for 24 h, followed by infection with EV71 at an MOI of 1 for 24 **(h)** Single dominant-negative TIR-less TLR4 plasmid was transfected into **(C)** HEK293 or **(D)** UT-SCC-60B cells at a dose of 1 μg for 24 h, followed by infection with EV71 at an MOI of 1 for 24 (h) n = 3. **(E)** TLR4 single nucleotide mutation plasmids (A896G, C1196T, and C2141A) were transfected into HEK293 cells at a dose of 1 μg for 24 h, followed by infection with EV71 at an MOI of 1 for 24 (h) n = 3. Genome copies of EV71 were determined and relative fold differences were calculated. Concentrations of IL-8 in the supernatants of **(F)** human–mouse chimeric TLR2 heterodimer and **(G)** single dominant-negative TIR-less TLR2 heterodimer groups were determined. n = 3. Activation of the *PI3K/AKT* and *MAPK* pathways in **(H)** human–mouse chimeric TLR2 heterodimers and **(I)** DN-TLR2/TLR4 groups was assessed via western blotting. *p < 0.05, **p < 0.01, and ***p < 0.001.

overexpressing TLR4 mutants (A896G, C1196T, and C2141A); however, the inhibition rates of these three TLR4 mutants were significantly lower than those of wild-type TLR4 (Figure 4E). Level of IL-8 secretion was significantly upregulated in HEK293 cells overexpressing human–mouse chimeric TLR2/TLR4 heterodimer (mTLR2/TLR4 and TLR2/mTLR4) in a dose-dependent manner (Figure 4F); however, only DN-TLR2/TLR4, but not TLR2/DN-TLR4 (Figure 4G) and DN-TLR4 (Figure S1A), upregulated IL-8 levels upon EV71 infection. *PI3K/AKT* and *MAPK* (ERK, JNK, and p38) pathways were also activated, with an increase in the phosphorylation levels of AKT, ERK, JNK, and p38 in human–mouse chimeric TLR2/TLR4 heterodimer (mTLR2/TLR4 and TLR2/mTLR4; Figure 4H) and DN-TLR2/TLR4 (Figure 4I). Expression levels of p85 and phosphorylation levels of AKT, ERK, and p38 were decreased in UT-SCC-60B overexpressing DN-TLR4 (Figure S1B). Taken together, these results further support the hypothesis that the TLR4 monomer and TLR2/TLR4 heterodimer inhibit EV71 replication by recognizing EV71 to activate innate immunity against it.

3.5 EV71 capsid proteins activate innate immunity via TLR2 and TLR2 heterodimer

TLR2 expression is upregulated in response to live or UV-inactivated HRV6 and EV71 infection (25, 39, 40), suggesting that the enterovirus capsid may be recognized by TLR2. To determine whether EV71 capsid proteins activate cytokine response, we obtained purified prokaryotic expression recombinant EV71 capsid proteins VP1, VP2, VP3, and VP4 and used them to stimulate UT-SCC-60B cells at a final concentration of 80 μg/mL. IL-6 levels were significantly upregulated by recombinant EV71 VP2, VP3, and VP4, whereas IL-8 levels were significantly upregulated by recombinant EV71 VP1 and VP3 (Figure 5A). We next constructed EV71 capsid recombinant eukaryotic plasmids and transfected them into UT-SCC-60B cells. Levels of IL-6 and IL-8 were significantly upregulated in UT-SCC-60B cells overexpressing EV71 VP1, VP2, VP3, and VP4 (Figure 5B). Expression levels of p85, TLR1, TLR2, and TLR6 were upregulated by the recombinant EV71 capsid proteins VP1 and VP2, and the phosphorylation levels of ERK and p38 were significantly upregulated by recombinant EV71 capsid protein VP4 (Figure 5C). Expression levels of p85, TLR1, TLR2, and TLR6 and the phosphorylation levels of AKT, ERK, and p38 were upregulated in US-SCC-60B cells overexpressing EV71 capsid proteins at different levels (Figure 5D).

To determine whether EV71 capsid proteins activate innate immunity via TLR2 and TLR2 heterodimer (TLR2/TLR1 and TLR2/TLR6), we first transfected TLR2 and TLR2 heterodimer (TLR2/TLR1 and TLR2/TLR6) plasmids into HEK293 cells then stimulated with recombinant EV71 capsid proteins VP1, VP2, VP3, and VP4 at a final concentration of 80 μg/mL. IL-8 levels were significantly upregulated in TLR2 and TLR2 heterodimer (TLR2/TLR1 and TLR2/TLR6)-overexpressing HEK293 in response to stimulation with recombinant EV71 capsid proteins (VP1, VP2, VP3, and VP4), especially for the TLR2/TLR6 heterodimer (Figure 5E). Similar results were observed in TLR2 and TLR2 heterodimer (TLR2/TLR1 and TLR2/TLR6)-overexpressing UT-SCC-60B cells, in which EV71 capsid proteins (VP1, VP2, VP3, and VP4) were also overexpressed, and IL-8 levels were significantly upregulated (Figure 5F). *PI3K/AKT* and *MAPK* (ERK, JNK, and p38) pathways were activated at different levels by the recombinant EV71 capsid proteins via TLR2 and TLR2 heterodimer (TLR2/TLR1 and TLR2/TLR6), particularly EV71 VP1 (Figure 5G). These pathways were also activated in TLR2 heterodimer (TLR2/TLR1 and TLR2/TLR6) and EV71 capsid protein-overexpressing UT-SCC-60B cells (Figure 5H). Altogether, these results indicate that EV71 capsid proteins activate the *PI3K/AKT* and *MAPK* pathways via TLR2 and TLR2 heterodimer (TLR2/TLR1 and TLR2/TLR6), thereby increasing the production of pro-inflammatory cytokines and activating innate immunity.

3.6 EV71 capsid proteins activate innate immunity via TLR4 and TLR2/TLR4 heterodimer

To determine whether the EV71 capsid protein can activate innate immunity via TLR4 and TLR2/TLR4 heterodimer, we first determined the levels of IL-8 in recombinant EV71 capsid protein (VP1, VP2, VP3, and VP4)-stimulated HEK293 cells, in which TLR4 and TLR2/TLR4 heterodimer were overexpressed. IL-8 levels were significantly upregulated in all groups (Figure 6A). TLR4 and TLR2/TLR4 heterodimer were co-transfected with EV71 capsid plasmids into UT-SCC-60B cells, and IL-8 levels were found to be upregulated in all groups, except the TLR2/TLR4-EV71VP3 group (Figure 6B). *PI3K/AKT* and *MAPK* pathways were also activated at different levels in TLR2-, TLR4-, and TLR2/TLR4-overexpressing HEK293 cells stimulated with recombinant EV71 capsid proteins (VP1, VP2, VP3, and VP4; Figure 6C) or in TLR4 and TLR2/TLR4 heterodimer with EV71 capsid protein-overexpressing UT-SCC-60B cells (Figure 6D). These results indicate that EV71 capsid proteins activate innate immunity via TLR4 and TLR2/TLR4 heterodimer.

4 Discussion

Innate antiviral immunity is the first line of defense against viral replication. Determining the EV71-induced activation mechanism of the innate immune system in host cells can provide insights into virus–host interactions and the pathogenesis of EV71 infection. The specific mechanism of activation of the host innate immune response during EV71 infection remains unknown. EV71-infected patients with HFMD, herpangina, severe brainstem encephalitis, and other manifestations associated with the central nervous system exhibit different proinflammatory responses, such as increased levels of IL-6, IL-8, and other cytokines (27, 43–47). Furthermore, EV71-infected host cells exhibit a robust IFN response (24, 48) and excessive pro-inflammatory cytokine responses (24, 25). Neonatal mice infected with EV71 exhibit high levels of IL-6 with severe tissue damage and high mortality (49). These studies indicate that

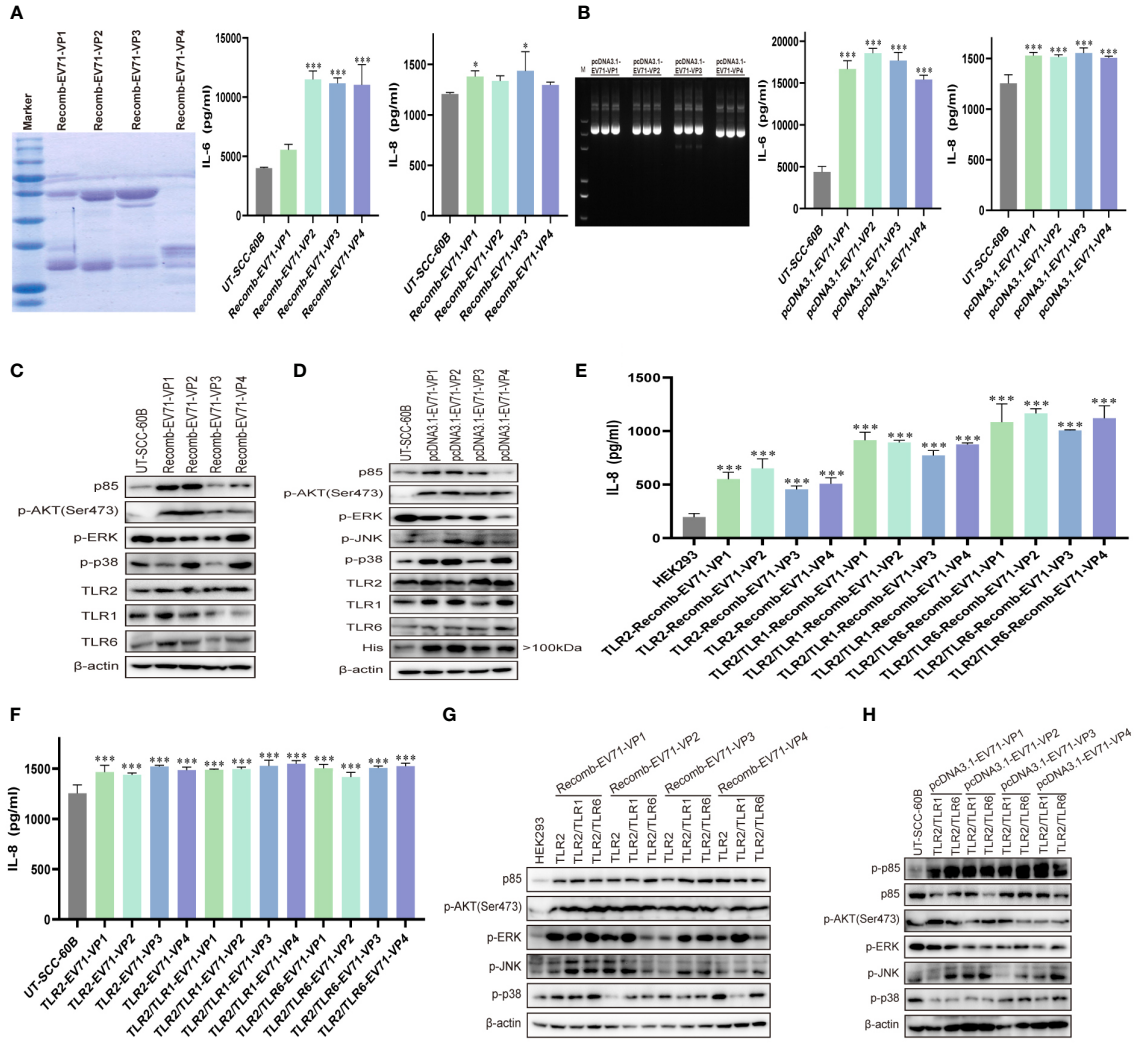

FIGURE 5
EV71 capsid proteins induce cytokine responses via TLR2 and TLR2 heterodimers. UT-SCC-60B cells were stimulated with purified recombinant prokaryotic-expressed EV71 capsid proteins at a final concentration of 80 μg/mL, or EV71 capsid recombinant eukaryotic plasmids were transfected into UT-SCC-60B cells at a dose of 1 μg for 24 (h) n = 3. Concentrations of IL-6 and IL-8 in **(A)** recombinant EV71 capsid protein stimulated and **(B)** EV71 capsid plasmid transfected groups were determined. Activation of the *PI3K/AKT* and *MAPK* pathways in **(C)** recombinant EV71 capsid protein stimulated and **(D)** EV71 capsid plasmid transfected groups were assessed via western blotting. Human-derived TLR2 and TLR2 heterodimer (TLR2/TLR1 and TLR2/TLR6) plasmids were transfected into HEK293 cells at a dose of 1 μg for 24 h and stimulated with recombinant EV71 capsid proteins at a final concentration of 80 μg/mL for 24 (h) n = 3. **(E)** Concentrations of IL-8 and **(G)** activation of the *PI3K/AKT* and *MAPK* pathways were determined. Human-derived TLR2 and TLR2 heterodimer (TLR2/TLR1 and TLR2/TLR6) and EV71 capsid plasmids were co-transfected into UT-SCC-60B cells at a dose of 1 μg for 24 (h) n = 3. **(F)** Concentrations of IL-8 and **(H)** activation of the *PI3K/AKT* and *MAPK* pathways were determined. *p < 0.05, **p < 0.01, and ***p < 0.001.

the host exerts normal immune responses against EV71, which shows immune evasion strategies to increase its replication and spread. Several reviews have summarized the effects of innate immunity on EV71 and the immune evasion process of EV71 (50–53). EV71 mainly depends on its 2A and 3C proteases to cleave PRRs and immune-associated signal molecules to disrupt cellular signal transduction and suppress the production of cytokines and IFN-α/β and IFN-stimulated gene expression. However, the mechanisms involved in the activation of cytokine responses in EV71-infected patients and host cells remain ambiguous. One potential mechanism for activating the innate immunity of host cells against EV71, especially during the early phase of EV71 infection, has been reported but not yet validated.

In this study, we systematically evaluated the roles of cell membrane-bound TLR monomers (TLR1, TLR2, TLR4, and TLR6) and TLR2 heterodimer (TLR2/TLR1, TLR2/TLR6, TLR2/TLR4, and TLR2/CD14) in the inhibition of EV71 replication and activation of innate immunity. We found that EV71 replication was significantly inhibited by TLR monomers and TLR2 heterodimer, and the cellular *PI3K/AKT* and *MAPK* signaling pathways were activated, inducing the production of IL-8. Moreover, EV71 capsid proteins (VP1, VP2, VP3, and VP4) activated TLR monomers (TLR2 and TLR4) and TLR2 heterodimer (TLR2/TLR1, TLR2/TLR6, and TLR2/TLR4), leading to the activation of innate immunity. These results indicate that EV71 and its capsid proteins activate innate immunity, which is necessary for TLR

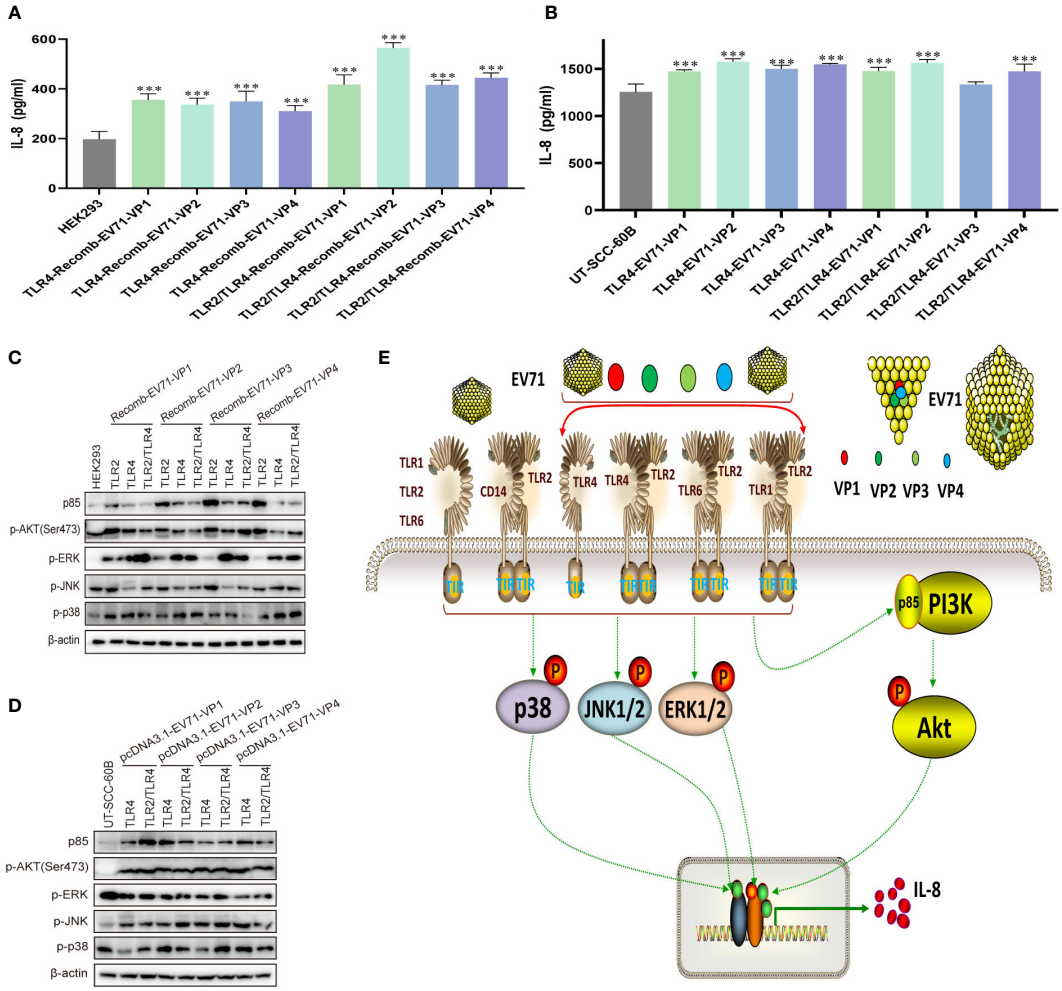

FIGURE 6
EV71 capsid proteins induce cytokine responses via TLR4 and TLR2/TLR4 heterodimer. Human-derived TLR4 and TLR2/TLR4 plasmids were transfected into HEK293 cells at a dose of 1 μg for 24 h, followed by stimulation with recombinant EV71 capsid proteins at a final concentration of 80 μg/mL for 24 (h) n = 3. **(A)** Concentrations of IL-8 and **(C)** activation of the *PI3K/AKT* and *MAPK* pathways were determined. Human-derived TLR4 and TLR2/TLR4 and EV71 capsid plasmids were co-transfected into UT-SCC-60B cells at a dose of 1 μg for 24 (h) n = 3. **(B)** Concentrations of IL-8 and **(D)** activation of the *PI3K/AKT* and *MAPK* pathways were determined. **(E)** Schematic model for the activation of innate immunity by EV71 and capsid proteins via cell membrane-bound TLR1/2/4/6 monomers and TLR2 heterodimers. *p < 0.05, **p < 0.01, and ***p < 0.001.

monomer and TLR2 heterodimer recognition, as well as the innate cytokine signaling cascade during the early phase of EV71 infection (Figure 6E).

To the best of our knowledge, this study is the first to investigate the mechanism of EV71 infection and replication in detail. Specific roles of cell membrane-bound TLR1/2/4/6 monomers and TLR2 heterodimer in recognizing EV71 and activating innate immunity have not yet been fully elucidated. Currently, the roles of TLRs, particularly cell membrane-bound TLRs in activating innate immunity against EV71 remain unclear. Transcriptional levels of TLR7 and TLR8 are upregulated in EV71-infected host cells (24, 25, 54), indicating that the EV71 genome ssRNA is recognized by TLR7 and TLR8. However, TLR3 may recognize the dsRNA produced in the EV71 genome replication process because the level of TLR3 is also upregulated (24, 54). These TLRs mainly recognize viral RNA and are located in intracellular endosomes; however, whether cell membrane-bound TLR1/2/4/6 monomers and TLR2 heterodimer engage in recognizing EV71 requires further investigation. Humans vaccinated with inactivated EV71 showed altered host innate and adaptive response gene expression (55), and EV71 virus-like particles (VLPs) induced the production of IL-12 and IL-10 via TLR4 (56). Additionally, the expression of TLR2 is significantly upregulated by EV71 and UV-inactivated EV71 in the early phase of infection (25). Our previous study also confirmed that the transcriptional level of TLR2 was upregulated using a transcriptomic sequencing method, and that overexpression of TLR2 and TLR2 heterodimer or activation of TLR2 heterodimer by their ligands significantly inhibited EV71 replication (40). These results indicate that cell membrane-bound TLR2, TLR4, and TLR2 heterodimer play a pivotal role in mediating the innate immune response activation induced by EV71 and that EV71 capsid proteins may be recognized by TLR2, TLR4, and TLR2 heterodimer; however, the underlying mechanisms require further investigation.

To determine the roles of cell membrane-bound TLR monomers (TLR1, TLR2, TLR4, and TLR6) and TLR2 heterodimer (TLR2/TLR1, TLR2/TLR6, TLR2/TLR4, and TLR2/CD14) directly sensing EV71 and contributing to activate innate immunity to limit EV71 replication, we set two strategies to determine the roles of these TLR monomers and TLR2 heterodimer. The first strategy was to test whether normal TLR monomers (TLR1, TLR2, and TLR6) and TLR2 heterodimer (TLR2/TLR1 and TLR2/TLR6) derived from humans or mice could inhibit EV71 replication. Our data demonstrated that EV71 replication was significantly inhibited in two types of host cells overexpressing TLR1, TLR2, TLR6, TLR2/TLR1, and TLR2/TLR6, and increased production of IL-8. To ensure the accuracy of the results, we carried out a second strategy using human–mouse chimeric TLR2 heterodimer (mTLR2/TLR1, TLR2/mTLR1, mTLR2/TLR6, and TLR2/mTLR6) or DN-TLR2 heterodimer (DN-TLR2/TLR1, TLR2/DN-TLR1, DN-TLR2/TLR6, and TLR2/DN-TLR6). Furthermore, the roles of DN-TLRs (DN-TLR1, DN-TLR2, and DN-TLR6) were also evaluated. Our data showed that EV71 replication was also inhibited by human–mouse chimeric TLR2 heterodimer and DN-TLR2 heterodimer; however, DN-TLRs lost their inhibitory ability against EV71. These results are in accordance with those of our earlier investigation (40) and support the idea that both human and mouse TLR1/2/6 monomers and TLR2 heterodimer play important roles in the protection of host cells against EV71. Several viral proteins are recognized by TLR2, including RSV G protein recognized by TLR2/TLR6 heterodimer (36), HIV structural protein p17 and gp41 recognized by TLR2/TLR1 heterodimer, HIV p24 recognized by TLR2/TLR6 heterodimer (34), hepatitis C virus (HCV) core and NS3 recognized by TLR2/TLR1 or TLR2/TLR6 heterodimer (57, 58), and rotavirus NSP4-activated proinflammatory cytokine response recognized by TLR2 (59). Taken together, these results suggest that cell-surface TLR2 and TLR2 heterodimer participate in the recognition of viruses, resulting in a decrease in viral replication and activation of antiviral innate immunity. Unlike other TLRs, TLR2 interacts with its co-receptors, such as TLR1 and TLR6, to form TLR2 heterodimer (60, 61). However, the roles of other cell membrane-bound TLR monomers (TLR1 and TLR6) in viral replication remain unknown. In this study, we systematically evaluated human and mouse TLR1, TLR6, DN-TLR2 heterodimer (DN-TLR2/TLR1 and DN-TLR2/TLR6), and DN-TLRs (DN-TLR1 and DN-TLR6) and found that different TLR monomers (TLR1 and TLR6) and DN-TLR2 heterodimer can inhibit EV71 replication, but not DN-TLR1 and DN-TLR6. These results further confirmed that cell surface TLR1 and TLR6 monomers exhibit anti-EV71 effects while facilitating the formation of TLR2 heterodimer.

TLR4 is another cell membrane-bound TLR that recognizes viral proteins to activate innate immunity. RSV activates innate immunity via TLR4, and RSV F protein is recognized by TLR4 (62, 63). Influenza virus hemagglutinin interacts with TLR4 to induce Janus tyrosine kinase-3 activation (64). Extracellular nucleoproteins of the influenza virus interact with TLR2 and TLR4 to induce the production of IL-1β and IL-6 (37). HIV gp120 binds to TLR2 and TLR4 to activate the nuclear factor (*NF*)-*κB* pathway for the production of TNF-α and IL-8 (35). These studies indicate that TLR4 monomers recognize viral proteins to activate innate immunity and also interact with TLR2. Further studies have confirmed that TLR2 interacts with TLR4 to form the TLR2/TLR4 heterodimer (65). Myeloid differentiation primary response gene 88 mediates TLR2/TLR4 heterodimerization (41). Here, we determined the roles of TLR4 and TLR2/TLR4 heterodimer in EV71 infection. Both human and mouse TLR4 and TLR2/TLR4 heterodimer significantly inhibited EV71 replication, and human–mouse chimeric mTLR2/TLR4 and TLR2/mTLR4 also exhibited inhibitory effects on EV71. DN-TLR4 did not show any inhibitory effect, but DN-TLR2/TLR4 and TLR2/DN-TLR4 inhibited EV71 replication. These results indicate that TLR2 and TLR4 monomers limit EV71 replication. Three single nucleotide mutations in TLR4 (A896G, C1196T, and C2141A) also inhibited EV71 replication, but their inhibition rates of EV71 were significantly decreased compared with those of wild-type TLR4. These results suggest these three nucleotides as functional sites of TLR4.

EV71 is a naked virus consisting of four structural proteins (VP1, VP2, VP3, and VP4) forming a promoter. Five promoters are assembled into a pentamer, and 12 pentamers are assembled to form a capsid with an icosahedral structure (12). Unlike enveloped viruses, such as HIV, which use the envelope glycoprotein gp120, a protein attached to its viral receptor CD4 interacts with cell membrane-bound TLR2 and TLR4 (35). In the life cycle of EV71, especially in the attachment and uncoating phases, EV71 capsid is the first to attach to cell surface molecules, such as viral receptors (SCARB2 and PSGL-1) and other receptors (cell membrane-bound TLR1/2/4/6). EV71 capsid proteins VP1, VP2, and VP3 are exposed on the surface of the capsid, whereas VP4 is located in the internal capsid. Whether EV71 capsid proteins are recognized by cell membrane-bound TLR monomers and TLR2 heterodimer remains unknown. In this study, we mainly focused on TLR2 and TLR4 monomers and TLR2 heterodimer (TLR2/TLR1, TLR2/TLR6, and TLR2/TLR4). We first confirm the findings of our previous study that the levels of TLR2 are upregulated in the UT-SCC-60B cell model. Cells were then stimulated with four recombinant or overexpressed EV71 capsid proteins via plasmid transfection. Concentrations of IL-6 and IL-8 were significantly upregulated and the expression levels of TLR1, TLR2, and TLR6 were upregulated in EV71 capsid protein-overexpressing cells. We confirmed that EV71 capsid proteins induce cytokine production and activate the *PI3K/AKT* and *MAPK* pathways. Well-known functions of EV71 include EV71 VP1-mediated receptor-binding (14, 15) and virulence determination (66, 67). Four capsids containing different neutralizing epitopes can be used as candidate EV71 vaccine epitopes (12, 68). Taken together, our results indicate that EV71 capsid proteins play important roles in innate immune activation via cell membrane-bound TLR2, TLR4, and TLR2 heterodimer. Recently study shows interferon-inducible poly(ADP-ribose) polymerase 9 (PARP9) as the host restriction factor to sense viral RNA and employs PI3K/AKT3 pathway to produce type I interferon (69), and our results also find PI3K/AKT pathway is activated by EV71 and its capsid proteins via TLR2, TLR4, and TLR2 heterodimer. Whether TLR2, TLR4, and TLR2 heterodimer could activate PARP9 mediated PI3K/AKT pathway to induce the phosphorylation of IRF3 and IRF7 to induce type I

interferon for inhibiting EV71 replication is still need further investigation.

In summary, our results revealed that cell membrane-bound TLR monomers (TLR1/2/4/6) and TLR2 heterodimer (TLR2/TLR1, TLR2/TLR6, and TLR2/TLR4) recognize EV71, resulting in the activation of innate responses and inhibition of EV71 replication. Moreover, EV71 capsid proteins activated innate immunity via TLR2, TLR4, and TLR2 heterodimer (TLR2/TLR1, TLR2/TLR6, and TLR2/TLR4). Collectively, our results indicated that EV71 capsid proteins, as novel PAMPs, are recognized by membrane-bound TLR monomers and TLR2 heterodimer, improving our understanding of the innate recognition of EV71.

Data availability statement

The original contributions presented in the study are included in the article/Supplementary Material. Further inquiries can be directed to the corresponding author.

Author contributions

G-CX and L-YD conceived and designed this study. P-PS, DL, MS, and QR performed the cell biology experiments. W-PG, L-YD, and J-LW performed the data analysis. G-CX, P-PS, and L-YD were responsible for writing and the critical reading of the manuscript. All authors contributed to the article and approved the submitted version.

Funding

This work was supported by grants from the National Key Research and Development Program of China (2022YFC3500800, 2022YFC3500802), the National Natural Science Foundation of China (81702008); the Natural Science Foundation of Hebei Province (H2018406024); Chengde Medical University (KY2020002, KY202127); Technology Innovation Guidance Project-Science and Technology Work Conference by Hebei Provincial Department of Science and Technology.

Acknowledgments

We thank all members of the Department of Pathogenic Biology, College of Basic Medicine, Chengde Medical University. We also thank the editors for their patience and kindness in helping with this paper. We would like to thank Editage for the English language editing and proofreading of the manuscript.

Conflict of interest

The authors declare that the research was conducted in the absence of any commercial or financial relationships that could be construed as a potential conflict of interest.

Publisher's note

Supplementary material

The Supplementary Material for this article can be found online at: https://www.frontiersin.org/articles/10.3389/fimmu.2023.1187035/full#supplementary-material

References

1. Schmidt NJ, Lennette EH, Ho HH. An apparently new enterovirus isolated from patients with disease of the central nervous system. *J Infect Dis* (1974) 129:304–09. doi: 10.1093/infdis/129.3.304

2. Hagiwara A, Tagaya I, Yoneyama T. Epidemic of hand, foot and mouth disease associated with enterovirus 71 infection. *Intervirology* (1978) 9:60–3. doi: 10.1159/000148922

3. Chumakov M, Voroshilova M, Shindarov L, Lavrova I, Gracheva L, Koroleva G, et al. Enterovirus 71 isolated from cases of epidemic poliomyelitis-like disease in Bulgaria. *Arch Virol* (1979) 60:329–40. doi: 10.1007/BF01317504

4. Chan LG, Parashar UD, Lye MS, Ong FG, Zaki SR, Alexander JP, et al. Deaths of children during an outbreak of hand, foot, and mouth disease in sarawak, malaysia: clinical and pathological characteristics of the disease. for the outbreak study group. *Clin Infect Dis* (2000) 31:678–83. doi: 10.1086/314032

5. Ho M, Chen ER, Hsu KH, Twu SJ, Chen KT, Tsai SF, et al. An epidemic of enterovirus 71 infection in taiwan. Taiwan enterovirus epidemic working group. *N Engl J Med* (1999) 341:929–35. doi: 10.1056/NEJM199909233411301

6. Zhang Y, Tan XJ, Wang HY, Yan DM, Zhu SL, Wang DY, et al. An outbreak of hand, foot, and mouth disease associated with subgenotype C4 of human enterovirus 71 in Shandong, China. *J Clin Virol* (2009) 44:262–67. doi: 10.1016/j.jcv.2009.02.002

7. Zhang Y, Zhu Z, Yang W, Ren J, Tan X, Wang Y, et al. An emerging recombinant human enterovirus 71 responsible for the 2008 outbreak of hand foot and mouth disease in fuyang city of China. *Virol J* (2010) 7:94. doi: 10.1186/1743-422X-7-94

8. De W, Changwen K, Wei L, Monagin C, Jin Y, Cong M, et al. A large outbreak of hand, foot, and mouth disease caused by EV71 and CAV16 in guangdong, China, 2009. *Arch Virol* (2011) 156:945–53. doi: 10.1007/s00705-011-0929-8

9. Huang PN, Shih SR. Update on enterovirus 71 infection. *Curr Opin Virol* (2014) 5:98–104. doi: 10.1016/j.coviro.2014.03.007

10. Kinobe R, Wiyatno A, Artika IM, Safari D. Insight into the enterovirus A71: a review. *Rev Med Virol* (2022) 32:e2361. doi: 10.1002/rmv.2361

11. Solomon T, Lewthwaite P, Perera D, Cardosa MJ, McMinn P, Ooi MH. Virology, epidemiology, pathogenesis, and control of enterovirus 71. *Lancet Infect Dis* (2010) 10:778–90. doi: 10.1016/S1473-3099(10)70194-8

12. Yuan J, Shen L, Wu J, Zou X, Gu J, Chen J, et al. Enterovirus A71 proteins: structure and function. *Front Microbiol* (2018) 9:286. doi: 10.3389/fmicb.2018.00286

13. Wang H, Li Y. Recent progress on functional genomics research of enterovirus 71. *Virol Sin* (2019) 34:9–21. doi: 10.1007/s12250-018-0071-9

14. Nishimura Y, Shimojima M, Tano Y, Miyamura T, Wakita T, Shimizu H. Human p-selectin glycoprotein ligand-1 is a functional receptor for enterovirus 71. *Nat Med* (2009) 15:794–97. doi: 10.1038/nm.1961

15. Yamayoshi S, Yamashita Y, Li J, Hanagata N, Minowa T, Takemura T, et al. Scavenger receptor B2 is a cellular receptor for enterovirus 71. *Nat Med* (2009) 15:798–801. doi: 10.1038/nm.1992

16. Kataoka C, Suzuki T, Kotani O, Iwata-Yoshikawa N, Nagata N, Ami Y, et al. The role of VP1 amino acid residue 145 of enterovirus 71 in viral fitness and pathogenesis in a cynomolgus monkey model. *PLoS Pathog* (2015) 11:e1005033. doi: 10.1371/journal.ppat.1005033

17. Cao J, Qu M, Liu H, Wan X, Li F, Hou A, et al. Myristoylation of EV71 VP4 is essential for infectivity and interaction with membrane structure. *Virol Sin* (2020) 35:599–613. doi: 10.1007/s12250-020-00226-1

18. Kumar H, Kawai T, Akira S. Pathogen recognition by the innate immune system. *Int Rev Immunol* (2011) 30:16–34. doi: 10.3109/08830185.2010.529976

19. Kawai T, Akira S. The roles of TLRs, RLRs and NLRs in pathogen recognition. *Int Immunol* (2009) 21:317–37. doi: 10.1093/intimm/dxp017

20. Kumar H, Kawai T, Akira S. Toll-like receptors and innate immunity. *Biochem Biophys Res Commun* (2009) 388:621–25. doi: 10.1016/j.bbrc.2009.08.062

21. Lester SN, Li K. Toll-like receptors in antiviral innate immunity. *J Mol Biol* (2014) 426:1246–64. doi: 10.1016/j.jmb.2013.11.024

22. Zhou R, Liu L, Wang Y. Viral proteins recognized by different TLRs. *J Med Virol* (2021) 93:6116–23. doi: 10.1002/jmv.27265

23. Kuo R, Kao L, Lin S, Wang RY, Shih S. MDA5 plays a crucial role in enterovirus 71 RNA-mediated IRF3 activation. *PLoS One* (2013) 8:e63431. doi: 10.1371/journal.pone.0063431

24. Chi C, Sun Q, Wang S, Zhang Z, Li X, Cardona CJ, et al. Robust antiviral responses to enterovirus 71 infection in human intestinal epithelial cells. *Virus Res* (2013) 176:53–60. doi: 10.1016/j.virusres.2013.05.002

25. Gong X, Zhou J, Zhu W, Liu N, Li J, Li L, et al. Excessive proinflammatory cytokine and chemokine responses of human monocyte-derived macrophages to enterovirus 71 infection. *BMC Infect Dis* (2012) 12:224. doi: 10.1186/1471-2334-12-224

26. Wang SM, Lei HY, Yu CK, Wang JR, Su IJ, Liu CC. Acute chemokine response in the blood and cerebrospinal fluid of children with enterovirus 71-associated brainstem encephalitis. *J Infect Dis* (2008) 198:1002–06. doi: 10.1086/591462

27. Lin TY, Chang LY, Huang YC, Hsu KH, Chiu CH, Yang KD. Different proinflammatory reactions in fatal and non-fatal enterovirus 71 infections: implications for early recognition and therapy. *Acta Paediatr* (2002) 91:632–35. doi: 10.1080/080352502760069016

28. Zhang Y, Liu H, Wang L, Yang F, Hu Y, Ren X, et al. Comparative study of the cytokine/chemokine response in children with differing disease severity in enterovirus 71-induced hand, foot, and mouth disease. *PLoS One* (2013) 8:e67430. doi: 10.1371/journal.pone.0067430

29. Han J, Wang Y, Gan X, Song J, Sun P, Dong XP. Serum cytokine profiles of children with human enterovirus 71-associated hand, foot, and mouth disease. *J Med Virol* (2014) 86:1377–85. doi: 10.1002/jmv.23929

30. Pathinayake PS, Hsu AC, Wark PA. Innate immunity and immune evasion by enterovirus 71. *Viruses* (2015) 7:6613–30. doi: 10.3390/v7122961

31. Schnare M, Rollinghoff M, Qureshi S. Toll-like receptors: sentinels of host defence against bacterial infection. *Int Arch Allergy Immunol* (2006) 139:75–85. doi: 10.1159/000090001

32. Fitzgerald KA, Kagan JC. Toll-like receptors and the control of immunity. *Cell* (2020) 180:1044–66. doi: 10.1016/j.cell.2020.02.041

33. Chen J, Ng MM, Chu JJ. Activation of TLR2 and TLR6 by dengue NS1 protein and its implications in the immunopathogenesis of dengue virus infection. *PloS Pathog* (2015) 11:e1005053. doi: 10.1371/journal.ppat.1005053

34. Henrick BM, Yao XD, Rosenthal KL. HIV-1 structural proteins serve as PAMPs for TLR2 heterodimer significantly increasing infection and innate immune activation. *Front Immunol* (2015) 6:426. doi: 10.3389/fimmu.2015.00426

35. Nazli A, Kafka JK, Ferreira VH, Anipindi V, Mueller K, Osborne BJ, et al. HIV-1 gp120 induces TLR2- and TLR4-mediated innate immune activation in human female genital epithelium. *J Immunol* (2013) 191:4246–58. doi: 10.4049/jimmunol.1301482

36. Alshaghdali K, Saeed M, Kamal MA, Saeed A. Interaction of ectodomain of respiratory syncytial virus G protein with TLR2/TLR6 heterodimer: an *In vitro* and in silico approach to decipher the role of RSV G protein in pro-inflammatory response against the virus. *Curr Pharm Des* (2021) 27:4464–76. doi: 10.2174/1381612827666210716160030

37. Kim CU, Jeong YJ, Lee P, Lee MS, Park JH, Kim YS, et al. Extracellular nucleoprotein exacerbates influenza virus pathogenesis by activating toll-like receptor 4 and the NLRP3 inflammasome. *Cell Mol Immunol* (2022) 19:715–25. doi: 10.1038/s41423-022-00862-5

38. Khanmohammadi S, Rezaei N. Role of toll-like receptors in the pathogenesis of COVID-19. *J Med Virol* (2021) 93:2735–39. doi: 10.1002/jmv.26826

39. Triantafilou K, Vakakis E, Richer EA, Evans GL, Villiers JP, Triantafilou M. Human rhinovirus recognition in non-immune cells is mediated by toll-like receptors and MDA-5, which trigger a synergetic pro-inflammatory immune response. *Virulence* (2011) 2:22–9. doi: 10.4161/viru.2.1.13807

40. Li D, Su M, Sun PP, Guo WP, Wang CY, Wang JL, et al. Global profiling of the alternative splicing landscape reveals transcriptomic diversity during the early phase of enterovirus 71 infection. *Virology* (2020) 548:213–25. doi: 10.1016/j.virol.2020.06.011

41. Wang YC, Zhou Y, Fang H, Lin S, Wang PF, Xiong RP, et al. Toll-like receptor 2/4 heterodimer mediates inflammatory injury in intracerebral hemorrhage. *Ann Neurol* (2014) 75:876–89. doi: 10.1002/ana.24159

42. Kuo WT, Lee TC, Yang HY, Chen CY, Au YC, Lu YZ, et al. LPS receptor subunits have antagonistic roles in epithelial apoptosis and colonic carcinogenesis. *Cell Death Differ* (2015) 22:1590–604. doi: 10.1038/cdd.2014.240

43. Griffiths MJ, Ooi MH, Wong SC, Mohan A, Podin Y, Perera D, et al. In enterovirus 71 encephalitis with cardio-respiratory compromise, elevated interleukin 1beta, interleukin 1 receptor antagonist, and granulocyte colony-stimulating factor levels are markers of poor prognosis. *J Infect Dis* (2012) 206:881–92. doi: 10.1093/infdis/jis446

44. Lin TY, Hsia SH, Huang YC, Wu CT, Chang LY. Proinflammatory cytokine reactions in enterovirus 71 infections of the central nervous system. *Clin Infect Dis* (2003) 36:269–74. doi: 10.1086/345905

45. Wang SM, Lei HY, Huang KJ, Wu JM, Wang JR, Yu CK, et al. Pathogenesis of enterovirus 71 brainstem encephalitis in pediatric patients: roles of cytokines and cellular immune activation in patients with pulmonary edema. *J Infect Dis* (2003) 188:564–70. doi: 10.1086/376998

46. Wang W, Li W, Yang X, Zhang T, Wang Y, Zhong R, et al. Interleukin-8 is elevated in severe hand, foot, and mouth disease. *J Infect Dev Ctries* (2014) 8:94–100. doi: 10.3855/jidc.3542

47. Chen Z, Li R, Xie Z, Huang G, Yuan Q, Zeng J. IL-6, IL-10 and IL-13 are associated with pathogenesis in children with enterovirus 71 infection. *Int J Clin Exp Med* (2014) 7:2718–23.

48. Lui YL, Tan TL, Timms P, Hafner LM, Tan KH, Tan EL. Elucidating the host-pathogen interaction between human colorectal cells and invading enterovirus 71 using transcriptomics profiling. *FEBS Open Bio* (2014) 4:426–31. doi: 10.1016/j.fob.2014.04.005

49. Khong WX, Foo DG, Trasti SL, Tan EL, Alonso S. Sustained high levels of interleukin-6 contribute to the pathogenesis of enterovirus 71 in a neonate mouse model. *J Virol* (2011) 85:3067–76. doi: 10.1128/JVI.01779-10

50. Jin Y, Zhang R, Wu W, Duan G. Antiviral and inflammatory cellular signaling associated with enterovirus 71 infection. *Viruses* (2018) 10:155. doi: 10.3390/v10040155

51. Rasti M, Khanbabaei H, Teimoori A. An update on enterovirus 71 infection and interferon type I response. *Rev Med Virol* (2019) 29:e2016. doi: 10.1002/rmv.2016

52. Swain SK, Panda S, Sahu BP, Sarangi R. Activation of host cellular signaling and mechanism of enterovirus 71 viral proteins associated with hand, foot and mouth disease. *Viruses* (2022) 14:2190. doi: 10.3390/v14102190

53. Cox JA, Hiscox JA, Solomon T, Ooi MH, Ng L. Immunopathogenesis and virus-host interactions of enterovirus 71 in patients with hand, foot and mouth disease. *Front Microbiol* (2017) 8:2249. doi: 10.3389/fmicb.2017.02249

54. Zhu L, Li W, Qi G, Liu N, Sheng L, Shang L, et al. The immune mechanism of intestinal tract toll-like receptor in mediating EV71 virus type severe hand-foot-and-mouth disease and the MAPK pathway. *Exp Ther Med* (2017) 13:2263–66. doi: 10.3892/etm.2017.4245

55. Liu L, Zhang Y, Wang J, Zhao H, Jiang L, Che Y, et al. Study of the integrated immune response induced by an inactivated EV71 vaccine. *PLoS One* (2013) 8:e54451. doi: 10.1371/journal.pone.0054451

56. Lin YL, Hu YC, Liang CC, Lin SY, Liang YC, Yuan HP, et al. Enterovirus-71 virus-like particles induce the activation and maturation of human monocyte-derived dendritic cells through TLR4 signaling. *PLoS One* (2014) 9:e111496. doi: 10.1371/journal.pone.0111496

57. Chang S, Dolganiuc A, Szabo G. Toll-like receptors 1 and 6 are involved in TLR2-mediated macrophage activation by hepatitis c virus core and NS3 proteins. *J Leukoc Biol* (2007) 82:479–87. doi: 10.1189/jlb.0207128

58. Rajalakshmy AR, Malathi J, Madhavan HN. Hepatitis c virus NS3 mediated microglial inflammation via TLR2/TLR6 MyD88/NF-kappaB pathway and toll like receptor ligand treatment furnished immune tolerance. *PLoS One* (2015) 10:e125419. doi: 10.1371/journal.pone.0125419

59. Ge Y, Mansell A, Ussher JE, Brooks AE, Manning K, Wang CJ, et al. Rotavirus NSP4 triggers secretion of proinflammatory cytokines from macrophages via toll-like receptor 2. *J Virol* (2013) 87:11160–67. doi: 10.1128/JVI.03099-12

60. Kang JY, Nan X, Jin MS, Youn SJ, Ryu YH, Mah S, et al. Recognition of lipopeptide patterns by toll-like receptor 2-toll-like receptor 6 heterodimer. *Immunity* (2009) 31:873–84. doi: 10.1016/j.immuni.2009.09.018

61. Jin MS, Kim SE, Heo JY, Lee ME, Kim HM, Paik SG, et al. Crystal structure of the TLR1-TLR2 heterodimer induced by binding of a tri-acylated lipopeptide. *Cell* (2007) 130:1071–82. doi: 10.1016/j.cell.2007.09.008

62. Haynes LM, Moore DD, Kurt-Jones EA, Finberg RW, Anderson LJ, Tripp RA. Involvement of toll-like receptor 4 in innate immunity to respiratory syncytial virus. *J Virol* (2001) 75:10730–37. doi: 10.1128/JVI.75.22.10730-10737.2001

63. Kurt-Jones EA, Popova L, Kwinn L, Haynes LM, Jones LP, Tripp RA, et al. Pattern recognition receptors TLR4 and CD14 mediate response to respiratory syncytial virus. *Nat Immunol* (2000) 1:398–401. doi: 10.1038/80833

64. Cao K, Chen M, Jie X, Wang Y, Li Q, Xu J. H5N1 virus hemagglutinin inhibition of cAMP-dependent CFTR via TLR4-mediated janus tyrosine kinase 3 activation exacerbates lung inflammation. *Mol Med* (2015) 21:134–42. doi: 10.2119/molmed.2014.00189

65. Fernandez-Lizarbe S, Montesinos J, Guerri C. Ethanol induces TLR4/TLR2 association, triggering an inflammatory response in microglial cells. *J Neurochem* (2013) 126:261–73. doi: 10.1111/jnc.12276

66. Zaini Z, McMinn P. A single mutation in capsid protein VP1 (Q145E) of a genogroup C4 strain of human enterovirus 71 generates a mouse-virulent phenotype. *J Gen Virol* (2012) 93:1935–40. doi: 10.1099/vir.0.043893-0

67. Liu ZW, Zhuang ZC, Chen R, Wang XR, Zhang HL, Li SH, et al. Enterovirus 71 VP1 protein regulates viral replication in SH-SY5Y cells via the mTOR autophagy signaling pathway. *Viruses* (2019) 12:11. doi: 10.3390/v12010011

68. Zhao M, Bai Y, Liu W, Xiao X, Huang Y, Cen S, et al. Immunization of n terminus of enterovirus 71 VP4 elicits cross-protective antibody responses. *BMC Microbiol* (2013) 13:287. doi: 10.1186/1471-2180-13-287

69. Xing J, Zhang A, Du Y, Fang M, Minze LJ, Liu YJ, et al. Identification of poly (ADP-ribose) polymerase 9 (PARP9) as a noncanonical sensor for RNA virus in dendritic cells. *Nat Commun* (2021) 12:2681. doi: 10.1038/s41467-021-23003-4

frontiers | Frontiers in Immunology

TYPE Original Research
PUBLISHED 09 May 2023
DOI 10.3389/fimmu.2023.1186916

OPEN ACCESS

EDITED BY
Chenhe Su,
Wistar Institute, United States

REVIEWED BY
Jie Zhang,
Chinese Academy of Sciences (CAS), China
Daniel Prantner,
University of Maryland, United States

*CORRESPONDENCE
Wen-hai Feng
whfeng@cau.edu.cn

RECEIVED 15 March 2023
ACCEPTED 24 April 2023
PUBLISHED 09 May 2023

CITATION
Hao S, Zheng X, Zhu Y, Yao Y, Li S, Xu Y and Feng W-h (2023) African swine fever virus QP383R dampens type I interferon production by promoting cGAS palmitoylation.
Front. Immunol. 14:1186916.
doi: 10.3389/fimmu.2023.1186916

African swine fever virus QP383R dampens type I interferon production by promoting cGAS palmitoylation

Siyuan Hao[1,2,3,4], Xiaojie Zheng[1,2,3,4], Yingqi Zhu[1,2,3,4], Yao Yao[1,2,3,4], Sihan Li[1,2,3,4], Yangyang Xu[1,2,3,4] and Wen-hai Feng[1,2,3,4]*

[1]State Key Laboratory of Animal Biotech Breeding, College of Biological Sciences, China Agricultural University, Beijing, China, [2]Frontiers Science Center for Molecular Design Breeding, College of Biological Sciences, China Agricultural University, Beijing, China, [3]Ministry of Agriculture Key Laboratory of Soil Microbiology, College of Biological Sciences, China Agricultural University, Beijing, China, [4]Department of Microbiology and Immunology, College of Biological Sciences, China Agricultural University, Beijing, China

Cyclic GMP-AMP synthase (cGAS) recognizes viral DNA and synthesizes cyclic GMP-AMP (cGAMP), which activates stimulator of interferon genes (STING/MITA) and downstream mediators to elicit an innate immune response. African swine fever virus (ASFV) proteins can antagonize host immune responses to promote its infection. Here, we identified ASFV protein QP383R as an inhibitor of cGAS. Specifically, we found that overexpression of QP383R suppressed type I interferons (IFNs) activation stimulated by dsDNA and cGAS/STING, resulting in decreased transcription of IFNβ and downstream proinflammatory cytokines. In addition, we showed that QP383R interacted directly with cGAS and promoted cGAS palmitoylation. Moreover, we demonstrated that QP383R suppressed DNA binding and cGAS dimerization, thus inhibiting cGAS enzymatic functions and reducing cGAMP production. Finally, the truncation mutation analysis indicated that the 284-383aa of QP383R inhibited IFNβ production. Considering these results collectively, we conclude that QP383R can antagonize host innate immune response to ASFV by targeting the core component cGAS in cGAS-STING signaling pathways, an important viral strategy to evade this innate immune sensor.

KEYWORDS

ASFV, QP383R, type I interferons, cGAS, palmitoylation

1 Introduction

African swine fever virus (ASFV) is a large double-stranded, cytoplasmic DNA arbovirus belonging to the genus *Asfivirus* in the family *Asfarviridae* (1, 2). The genomic size of ASFV is approximately 170 to 193 kb, and the genome encodes more than 150 viral proteins that play important roles in viral assembly, viral replication, virus-host interaction,

and immune evasion. However, many viral proteins have unknown functions (3–5). ASFV replicates mainly in the cytoplasm of monocyte- and macrophage-lineage cells (6). As a complex enveloped DNA virus, ASFV is responsible for African swine fever disease (ASF). And this highly contagious hemorrhagic viral disease in domestic pigs (*Sus scrofa domestica*) and wild boars (*Sus scrofa*) has a morbidity and mortality rate of up to 100% and threatens the global pork supply and food security (7). Despite extensive research, there are no effective vaccines or antiviral drugs commercially available for the prevention and control of this deadly disease. Depletion of the virulence factors from field viruses to generate live-attenuated vaccines (LAVs) is the most promising strategy for the development of efficient vaccines so far (8). Therefore, it is critical to identify the virulence and immunosuppressive factors to provide potential targets for vaccine design.

The innate immune system is the first line of host defense against invading pathogens. Upon pathogens infection, cellular pattern recognition receptors (PRRs) recognize pathogen-associated molecular patterns (PAMPs) (9–11), which triggers a series of signaling events that lead to the induction of type I interferons (IFNs) (12), proinflammatory cytokines and other downstream effectors (13, 14). These effectors mediate the inhibition of microbial replication, clearance of infected cells and facilitation of adaptive immune response to eliminate infected pathogens (15, 16).

Among PRRs, cyclic GMP-AMP synthase (cGAS) is a recently identified DNA sensor, which plays a pivotal role in recognizing cytosolic DNA (17). Mechanistically, after binding to dsDNA, cGAS forms a 2:2 complex with DNA, which allows the rearrangement of the cGAS catalytic pocket for the subsequent binding, and then catalyzes its substrates ATP and GTP to produce a cyclic dinucleotide: 2'-3'-cGAMP. As a cytosolic second messenger, cGAMP binds to the adaptor protein STING, and causes a 180° rotation of its carboxyl ligand-binding domain relative to its transmembrane domain, leading to STING activation (18–20). Activated STING serves as the platform for recruitment and activation of TBK1, which in turn phosphorylates STING and IRF3. Phosphorylated IRF3 forms a homo-dimer to enter the nucleus, leading to the transcription of type I IFNs and other antiviral effector genes (21–23). In contrast, STING activation stimulates the inhibitor of nuclear factor-κB (IκB) kinase to release NF-κB, which translocates to the cell nucleus and activates the transcription of type I IFNs and proinflammatory cytokine-related genes (24).

QP383R is classified as an uncharacterized protein, which consists of 383 amino acids. Recently, it has been reported that QP383R represses inflammatory responses by inhibiting AIM2 inflammasome activation (25). In our study, we identified ASFV QP383R as a negative regulator of cGAS-STING mediated innate immunity. We found that overexpression of QP383R reduced dsDNA-triggered and cGAS-STING-mediated innate antiviral response. Furthermore, we found that QP383R interacted with the nucleotidyltransferase (NTase) domain of cGAS through its C-terminal tail (aa284-383). Palmitoylation is an important post-translational modification of cGAS, which restricts its enzymatic activity in the presence of dsDNA. We showed that QP383R promoted cGAS palmitoylation, and also impeded the DNA binding ability and dimerization of cGAS. Importantly, QP383R inhibited cGAS enzymatic functions and reduced cGAMP production, thereby attenuating the downstream innate immune response. Together, our findings reveal a novel immune evasion mechanism of ASFV mediated by the QP383R protein, implying that the QP383R gene could be used as a candidate target gene for the ASFV live-attenuated vaccines.

2 Results

2.1 QP383R inhibits cGAS-STING-mediated signaling

It has been demonstrated that the cGAS-STING axis plays a critical role in the induction of type I IFNs in response to ASFV infection (26). To identify ASFV proteins that target cGAS-STING-mediated signaling, we constructed a series of expression clones each encoding an individual ASFV protein. We performed systematic screens for ASFV proteins that could inhibit cGAS-STING mediated activation of the IFNβ promoter and interferon-stimulated response element (ISRE) by reporter assays in HEK293T cells. These efforts led to the identification of 23 candidate ASFV proteins that could antagonize cGAS-STING mediated signaling (data not shown). Among these candidates, ASFV protein QP383R exhibited a strong ability to inhibit cGAS-STING mediated activation of the IFNβ promoter. HEK293T cells were transfected with porcine IFNβ-Luc expression plasmid and pRL-TK plasmid along with FLAG vector or FLAG-tagged-QP383R (FLAG-QP383R), FLAG-cGAS and FLAG-STING expression plasmids. At 24 h post transfection (hpt), the IFNβ promoter activities were determined by using a Dual-Luciferase assay kit. Overexpression of QP383R inhibited cGAS-STING mediated activation of the IFNβ promoter in HEK293T cells (about 25% decreases). In addition, QP383R also inhibited the activation of interferon-stimulated response elements (ISRE) promoter with a more than 32% decrease (Figure 1A). Since IRF3 and nuclear factor κB (NF-κB) collaborate to induce the transcription of the *IFNB* gene, we further measured the effects of QP383R on the activation of IRF3 and NF-κB. Consistently, QP383R suppressed cGAS-STING mediated activation of IRF3 and NF-κB (ca. 35 and 25% decreases, respectively) (Figure 1B). To investigate whether QP383R affects the expression of IFNβ and IFN-stimulated genes (ISGs), we measured the mRNA expression of antiviral genes in cells that were cotransfected with FLAG-cGAS and FLAG-STING expression plasmids. RT-qPCR experiments indicated that overexpression of QP383R inhibited cGAS-STING-induced transcription of antiviral genes including *IFNB1*, *ISG54*, *ISG15*, and *CXCL10* (Figure 1C). Since phosphorylation of TBK1, IRF3, and IκBα are hallmarks of cGAS-STING mediated signaling, we further examined the effects of QP383R on these events. Consistently, overexpression of QP383R dramatically inhibited phosphorylation of TBK1, IRF3, and IκBα in response to cGAS-STING (Figure 1D). These data suggest that QP383R is an inhibitor of cGAS-STING mediated signaling.

10.3389/fimmu.2023.1186916

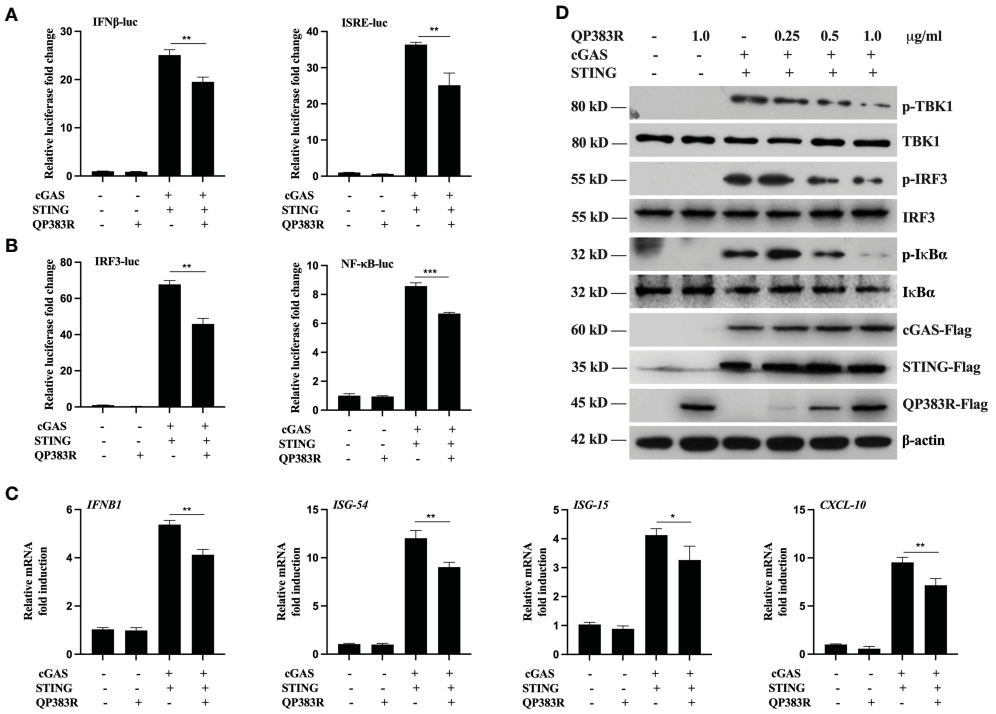

FIGURE 1
QP383R is an inhibitor of cGAS-STING-mediated signaling. **(A, B)** HEK239T cells were co-transfected with cGAS-Flag (40 ng/ml), STING-Flag (160 ng/ml), QP383R-Flag (0.5 μg/ml) or their empty vectors, and the indicated reporters (50 ng/ml) and pRL-TK (8 ng/ml). Twenty-four hours later, the cells were harvested to determine the activities of IFNβ and ISRE promoters **(A)**, and IRF3 and NF-κB promoters **(B)** by luciferase assays. **(C)** HEK239T cells were co-transfected with cGAS-Flag (40 ng/ml), STING-Flag (160 ng/ml), QP383R-Flag plasmid (0.5 μg/ml) or their empty vectors for 24 h. The expression of antiviral genes including *IFNB1*, *ISG54*, *ISG15*, and *CXCL10* were examined by qPCR. **(D)** HEK293T cells were transfected with cGAS-Flag and STING-Flag or an empty vector, and the indicated amounts of QP383R-Flag plasmids for 24 h. Immunoblots were performed with anti-Flag and the other indicated antibodies. The data are representative of three independent experiments (means ± the standard errors of the mean [SEM]). *$P \leq 0.05$; **$P \leq 0.01$; ***$P \leq 0.001$.

2.2 QP383R inhibits dsDNA-triggered induction of downstream antiviral genes

It has been previously reported that porcine macrophages and monocytes are the primary target cells of ASFV (27–29). To further determine the effect of QP383R on IFNβ promoter activation, the primary porcine alveolar macrophage (PAM) cell line 3D4/21 (CRL-2843) cells were cotransfected with FLAG vector or FLAG-QP383R and porcine IFNβ-Luc expression plasmids, as well as pRL-TK plasmid. At 24 hpt, the cells were treated with the synthetic double-stranded DNA (dsDNA)-mimetic poly(dA:dT) for 12 h, and then the activation of the IFNβ promoter was evaluated. The results showed that QP383R inhibited poly(dA:dT)-induced IFNβ promoter activation in a dose-dependent manner (Figure 2A). Overexpression of QP383R also inhibited the activation of the ISRE promoter in a dose-dependent manner in response to transfected poly(dA:dT) (Figure 2A). Consistently, QP383R suppressed poly(dA:dT)-mediated activation of IRF3 and NF-kB in a dose-dependent manner (Figure 2B). The mRNA expression of antiviral genes in 3D4/21 cells treated with poly (dA:dT) were measured. The results showed that the mRNA levels of *IFNB1*, *ISG54*, *CXCL10* and *IL-6* genes induced upon transfection of poly (dA:dT) were impaired with QP383R overexpression in a dose-dependent manner (Figure 2C).

Next, we wanted to verify whether the production of biologically active IFNβ protein and IL-6 protein is decreased by QP383R in poly(dA:dT)-transfected 3D4/21 cells. For this purpose, supernatants from 3D4/21 cells stimulated with poly(dA:dT) were harvested and assessed by enzyme-linked immunosorbent assay (ELISA) for IFNβ and IL-6 production. Consistent with the results obtained with RT-qPCR, when cells were transfected with QP383R and stimulated with poly(dA:dT), the productions of IFNβ and IL-6 proteins were inhibited as compared to empty vector-transduced control cells (ca. 30 and 28% decreases, respectively), confirming that the transduction pathway leading to IFNβ production is impaired in the presence of QP383R (Figure 2D). Taken together, these data indicate that QP383R suppresses the activation of the cGAS/STING pathway stimulated by poly(dA:dT) and blocks type I IFN production in porcine cells.

2.3 QP383R acts at the level of cGAS

The observed inhibition of type I IFN production by the ASFV QP383R protein raises the possibility that QP383R targets one or several components of the cGAS-STING signaling pathway. To identify the potential target regulated by QP383R, the porcine IFNβ-Luc and pRL-TK plasmids were co-transfected with FLAG-

10.3389/fimmu.2023.1186916

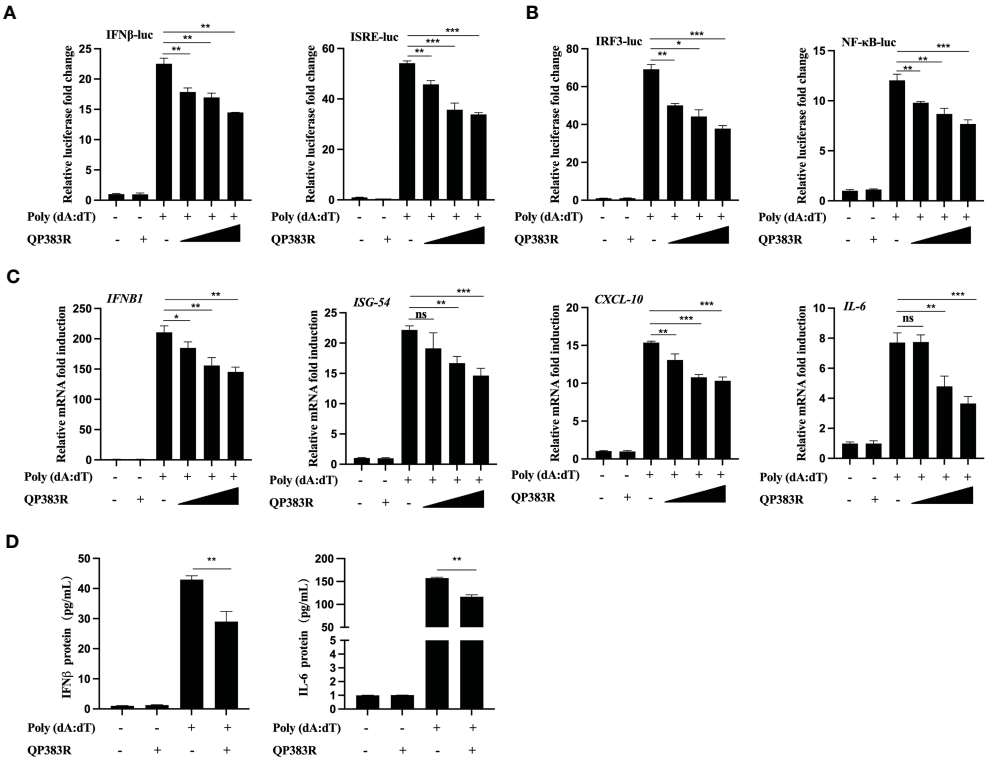

FIGURE 2
QP383R negatively regulates dsDNA-induced antiviral response. **(A, B)** 3D4/21 cells were transfected with the indicated amounts of QP383R plasmids (0.25, 0.5, and 1.0 μg/ml), and the indicated reporters (50 ng/ml) and pRL-TK (8 ng/ml). Twenty-four hours later, the cells were treated with or without poly(dA:dT) for 12 h, and then the activation of the IFNβ and ISRE promoters **(A)** and IRF3 and NF-κB promoters **(B)** were examined by luciferase assays. **(C)** 3D4/21 cells were transfected with different doses of QP383R expression vectors (0.25, 0.5, and 1.0 μg/ml). At 24 h post-transfection, cells were treated with or without poly(dA:dT) for 12 h, and then *IFNB1*, *ISG54*, *CXCL-10* and *IL-6* mRNAs were detected by q-PCR. **(D)** 3D4/21 cells were transfected with QP383R expression vector or an empty vector for 24 h, and supernatants were harvested after stimulated with or without poly(dA:dT) for 12 h to measure IFNβ and IL-6 productions by ELISA. The data are representative of three independent experiments (means ± the standard errors of the mean [SEM]). *$P \leq 0.05$; **$P \leq 0.01$; ***$P \leq 0.001$.

QP383R expression plasmid and plasmid expressing each component of the cGAS-STING signaling pathway (including cGAS, STING, TBK1, IRF3, IRF3/5D, Ikkα, Ikkβ, and p65) into HEK293T cells. The activation of the IFNβ promoter was determined at 24 hpt. Luciferase reporter assays indicated that overexpression of these component molecules activated IFNβ promoter activity, while overexpression of QP383R protein specially inhibited the activation of the IFNβ promoter induced by cGAS-STING but not STING or TBK1 or other molecules (Figure 3A; Supplementary Figures 1A–E). These results suggest that QP383R seems to target steps upstream of STING in the cGAS-cGAMP-STING signal pathway.

To further confirm the specific target of QP383R, we measured the activation of the IFNβ promoter and ISRE in 3D4/21 cells stimulated with poly(dG:dC) (another mimic of double-stranded DNA) and 2'3'-cGAMP (an activator of STING downstream of cGAS). Luciferase reporter assays indicated that overexpression of QP383R inhibited poly(dG:dC)- but not 2'3'-cGAMP-induced activation of the IFNβ promoter and ISRE in a dose-dependent manner (Figure 3B). In addition, transcription of genes including *IFNB1*, *ISG54* and *CXCL10* following transfection of poly(dG:dC) but not 2'3'-cGAMP, was impaired by QP383R as compared to empty vector-transduced control cells (Figure 3C). These results suggest that QP383R seems to regulate the cGAS/STING pathway upstream of cGAMP production. And this conclusion was further confirmed since ectopic expression of QP383R dramatically inhibited the phosphorylation of TBK1, IRF3, and IκBα in response to poly(dG:dC). In contrast, QP383R did not have marked effects on the phosphorylation of TBK1, IRF3, or IκBα induced by 2'3'-cGAMP in 3D4/21 cells (Figure 3D). Thus, these findings imply that QP383R targets cGAS for antagonizing innate antiviral response.

2.4 QP383R interacts with cGAS

Given that cGAS is the potential cellular target of QP383R, we next investigated whether QP383R directly interacted with cGAS under physiological conditions. We conducted coimmunoprecipitation (co-IP) experiments to examine whether QP383R is associated with signaling components in cGAS-STING pathways. HEK293T cells were transfected with HA-QP383R expression plasmid and plasmids expressing each of the components in cGAS-STING signaling pathway (including cGAS, STING, TBK1, IRF3, IRF3/5D, p65, and Ikkβ) for 24 h before coimmunoprecipitation and immunoblotting analysis with the

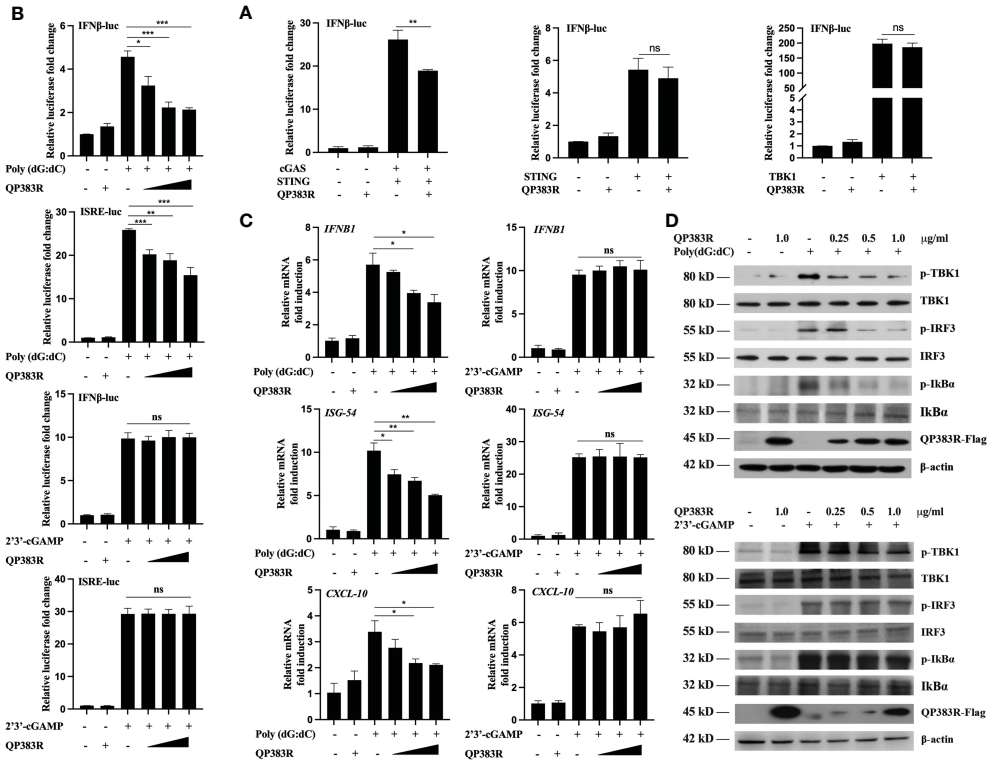

FIGURE 3
QP383R targets cGAS for antagonizing innate antiviral response. **(A)** HEK239T cells were co-transfected with IFN-luc reporter promoter plasmid, pRL-TK, the expression plasmids for cGAS + STING, STING or TBK1 along with QP383R or empty control plasmid. At 24 h post-transfection, cells were analyzed using dual-luciferase reporter assays. **(B)** 3D4/21 cells were co-transfected with different amounts of QP383R plasmids (0.25, 0.5, and 1.0 μg/ml), pRL-TK, and IFN-luc or ISRE-luc reporter plasmid. Twenty-four hours later, the cells were treated with poly(dG:dC) or 2'3'-cGAMP for 12 h, and the activation of the IFNβ or ISRE promoter was examined by luciferase assays. **(C)** 3D4/21 cells were transfected with different doses of QP383R expression vectors (0.25, 0.5, and 1.0 μg/ml). At 24 h post-transfection, cells were treated with poly(dG:dC) or 2'3'-cGAMP for 12 h, and *IFNB1*, *ISG54*, *CXCL-10* mRNA were detected by q-PCR. **(D)** 3D4/21 cells were transfected with the indicated amounts of QP383R-Flag plasmids for 24 h. Cells were then treated with poly(dG:dC) or 2'3'-cGAMP for 12 h before harvest and analyzed by Western blotting. The data are representative of three independent experiments (means ± the standard errors of the mean [SEM]). *$P \leq 0.05$; **$P \leq 0.01$; ***$P \leq 0.001$.

indicated antibodies. The results indicated that QP383R was specifically associated with cGAS but not STING, TBK1, IRF3, IRF3/5D (an active mutant of IRF3), p65 or Ikkβ in overexpression system (Figure 4A). Consistently, a reverse immunoprecipitation experiment was also performed, and the results showed that cGAS reciprocally coimmunoprecipitated with QP383R in transfected HEK293T cells (Figure 4B). Endogenous coimmunoprecipitation experiments further confirmed the association between QP383R and cGAS in PK15 and 3D4/21 cells following poly(dA:dT) transfection (Figure 4C). In line with this result, through immunofluorescence assays, we found that QP383R colocalized with cGAS in 3D4/21 cells (Figure 4D). Moreover, an *in vitro* glutathione S-transferase (GST) pull-down assay further verified their direct association, indicating a direct interaction between cGAS and QP383R (Figure 4E).

Porcine cGAS contains three domains: an RD domain (amino acid residues 1 to 134), a nucleotidyltransferase (NTase) domain (amino acid residues 135 to 305), and a Mab21 domain (amino acid residues 238 to 495) (30, 31). To further study which domain of cGAS is involved in their interaction, we constructed a series of truncation mutants of cGAS. HEK293T cells were cotransfected with HA-QP383R expression plasmid and the indicated truncation mutants of cGAS for 24 h before coimmunoprecipitation and immunoblotting analysis with the indicated antibodies. Coimmunoprecipitation experiments showed that both enzymatically active core (aa135-305) and the deletion of RD domain (aa135-495) of cGAS could interact with QP383R. However, RD domain (aa1-134) or Mab21 domain (aa306-495) of cGAS could not interact with QP383R (Figure 4F). Collectively, these results show the specific interaction between cGAS and QP383R, and the enzymatically active core of cGAS is essential for its binding to QP383R.

2.5 QP383R impairs DNA binding, dimerization, and enzymatic activity of cGAS through palmitoylation

In previous reports, the formation of a 2:2 complex with DNA is shown to be important for cGAS activation (32). Therefore, we next determined whether QP383R affected cGAS binding to dsDNA. Purified proteins Flag-QP383R, Flag-cGAS, and PRK5-Flag were incubated with or without biotinylated HSV120 (Bio-HSV120) for *in vitro* pull-down assays. As shown in Figure 5A, QP383R did not

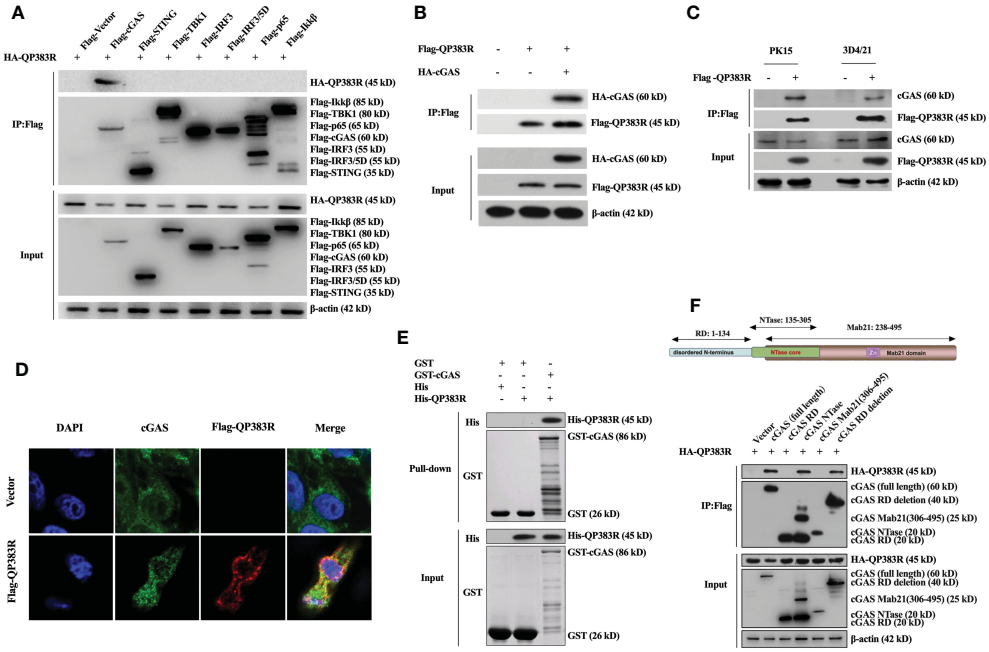

FIGURE 4
QP383R interacts with cGAS. **(A)** HEK293T cells were transfected with HA-tagged QP383R and Flag-tagged cGAS, STING, TBK1, IRF3, IRF3/5D, p65, Ikkβ or an empty vector for 24 h. Coimmunoprecipitations and immunoblots were performed with the indicated antibodies. **(B)** HEK293T cells were co-transfected with HA-cGAS and Flag-QP383R or their empty vectors for 24 h. Coimmunoprecipitations and immunoblots were performed with the indicated antibodies. **(C)** 3D4/21 and PK15 cells were transfected with Flag-QP383R or an empty vector for 24 h. Cells were then stimulated with poly(dA:dT) for 12 h before harvest and endogenous coimmunoprecipitation and immunoblotting analysis with the indicated antibodies. **(D)** 3D4/21 cells were transfected with Flag-QP383R expression vector or an empty vector (1.0 μg/ml) for 24 h. The colocalization of cGAS and QP383R was observed with confocal microscope (cGAS: green; Flag-QP383R: red; nucleus: blue). **(E)** Purified protein GST-cGAS was incubated with glutathione agarose beads and purified His-QP383R before pull-down assays analysis with the indicated antibodies. **(F)** HEK293T cells were co-transfected with HA-QP383R expression plasmid and Flag-cGAS or its truncation mutants for 24 h before coimmunoprecipitation and immunoblotting analysis with the indicated antibodies.

bind to Bio-HSV120 dsDNA in DNA-pull-down assays. However, QP383R dramatically inhibited the binding of cGAS to Bio-HSV120 dsDNA (Figure 5A). The inhibitory effect of QP383R on cGAS binding to dsDNA was in a dose-dependent manner (Figure 5B). These results suggest that QP383R impairs cGAS binding to dsDNA.

Previously, it has been shown that cGAS self-association and oligomerization are important for its activation after binding to dsDNA (33, 34). Since QP383R inhibits cGAS binding to dsDNA, we speculated that QP383R also affected cGAS dimerization. To test this hypothesis, we conducted coimmunoprecipitation experiments to examine whether QP383R inhibits self-association of cGAS. Co-IP experiments indicated that Flag-cGAS interacted with HA-cGAS, while this self-association was inhibited with the overexpression of QP383R (Figure 5C). Consistently, QP383R markedly inhibited cGAS dimerization in a dose-dependent manner in Co-IP assays (Figure 5D). The results reveal that cGAS dimerization is inhibited by QP383R.

As previously described (35, 36), the extracts from DNA-transfected cells contain cGAMPs, which activate the IFNβ and ISRE promoters, trigger the expression of *IFNB1*, *ISG56*, *ISG54* and *CXCL10* genes, and induce TBK1, IRF3, and IκBα phosphorylation. To elucidate the mechanisms on how QP383R antagonizes innate antiviral response, we next assessed whether QP383R affected cGAS enzymatic activity. Using a previously developed bioassay (37), we transfected 3D4/21 cells with or without QP383R for 24 h, then stimulated with HSV60 (another mimic of double-stranded DNA) to stimulate cGAMP production. Cell lysates were digested with DNase and then boiled to remove DNA and proteins, and the supernatant containing cGAMPs were collected by centrifugation and added to 3D4/21 cells with digitonin, followed by measurement of IFNβ expression, which indirectly represents the cGAMP level. As shown in Figure 5E, the activation of IFNβ and ISRE promoter in 3D4/21 cells was dramatically increased with the addition of the supernatant, indicating that cGAS was activated to produce a large amount of cGAMPs. However, QP383R overexpression significantly reduced the activation of IFNβ and ISRE promoters, suggesting that QP383R restricted cGAS activity and cGAMP production (Figure 5E). Consistently, QP383R overexpression inhibited the cGAMP-mediated expression of antiviral genes, including *IFNB1*, *ISG56*, *ISG54* and *CXCL10* (with decreases of ca. 36, 45, 50, and 26%, respectively). (Figure 5F). The same results were obtained when we assessed the phosphorylation level of TBK1, IRF3, and IκBα (Figure 5G). TBK1, IRF3, and IκBα were apparently phosphorylated after transfection of the supernatant, whereas QP383R overexpression markedly inhibited TBK1, IRF3, and IκBα phosphorylation, confirming the negative role of QP383R on the enzymatic activity of cGAS. Taken together, our findings suggest that QP383R impairs the synthesis of cGAMPs by inhibiting DNA binding and dimerization of cGAS.

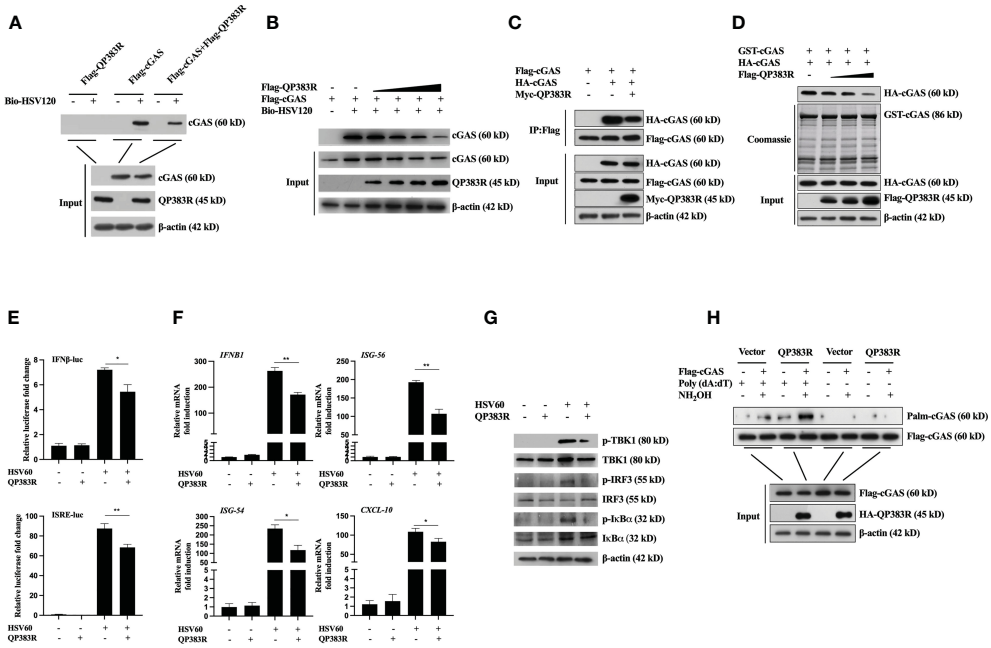

FIGURE 5
QP383R inhibit cGAS activation. **(A, B)** HEK293T cells were transfected with Flag-QP383R, Flag-cGAS and PRK5-Flag plasmids (1.0 μg/ml). Twenty-four hours later, the cell lysates were incubated with anti-FLAG M2 magnetic beads at 4°C for 4 hours, then eluted with 3 × Flag peptide to purify proteins. The purified proteins were incubated with biotinylated HSV120 and streptavidin-Sepharose beads for *in vitro* pull-down assays. The bound proteins were then analyzed by immunoblots with the indicated antibodies. **(C)** HEK293T cells were transfected with the indicated plasmids for 24 h before co-immunoprecipitation and immunoblotting analysis with the indicated antibodies. **(D)** HEK293T cells were transfected with HA-cGAS (1.0 μg/ml) and Flag-QP383R (0.5, 1.0, and 2.0 μg/ml) for 24 h, cell extracts were incubated with purified GST-cGAS and glutathione agarose beads for 3 hours at 4°C before coomassie staining and/or immunoblot analysis. **(E–G)** Effects of QP383R on cGAMP synthesis induced by transfected HSV60. 3D4/21 cells were transfected with QP383R expression vector or an empty vector (1.0 μg/ml). Twenty-four hours later, cells were stimulated with HSV60 (3.0 μg/ml) for 6 h, and then cell extracts containing cGAMP were delivered to digitonin-permeabilized 3D4/21 cells for 4 h before luciferase assays **(E)**, qPCR analysis **(F)** or western blot analysis **(G)**. **(H)** HEK293T cells were co-transfected with Flag-cGAS (0.5 μg/ml) and HA-QP383R (1.0 μg/ml). At 24 h post-transfection, the cells were harvested after stimulated with or without poly(dA:dT) for 12 h to determine cGAS palmitoylation by IP-ABE assay. The data are representative of three independent experiments (means ± the standard errors of the mean [SEM]). *$P \leq 0.05$; **$P \leq 0.01$.

In the cGAS-STING signaling pathway, it has been reported that palmitoylation of cGAS inhibits DNA binding and cGAS dimerization, and also restricts its enzymatic activity (38). Next, we wanted to verify whether QP383R regulates the palmitoylation of cGAS. We detected cGAS palmitoylation using IP-ABE assay. We replaced the palmitoylation modification of cGAS with biotin modification, and analyzed the changes in the palmitoylation levels of cGAS by western blot using the affinity of biotin and streptavidin. As shown in Figure 5H, the protein samples treated with NH_2OH developed a cGAS band, indicating that cGAS was modified by palmitoylation. Interestingly, we found that QP383R promoted elevation of the palmitoylation level of cGAS stimulated with poly(dA:dT) (Figure 5H).

These results suggest that QP383R inhibits DNA binding, cGAS dimerization, and the enzymatic activity of cGAS due to palmitoylation of cGAS promoted by QP383R.

2.6 Amino acids 284-383 in QP383R are responsible for its inhibitory effect on IFN-I production

QP383R is a non-structural protein of ASFV, which is known as an uncharacterized protein. QP383R is highly conserved among virulent and nonvirulent isolates and consists of 383 amino acids, which contains a predicted "aminotransferase class-V" motif (aa32-283). To identify the key domains in QP383R that were essential for its interaction with cGAS, a series of truncated mutants were generated, including FLAG-QP383R 1-31aa, FLAG-QP383R 32-283aa, FLAG-QP383R 284-383aa, FLAG-QP383R 1-283aa and FLAG-QP383R 32-383aa. HEK293T cells were cotransfected with FLAG vector, FLAG-QP383R, or each of the FLAG-QP383R mutant expression plasmids, and HA-cGAS expression plasmid. And then, the cell lysates were immunoprecipitated with anti-FLAG antibody and analyzed by Western blotting. The co-IP result showed that only the amino acids 284-383 in QP383R retained the interaction with cGAS, whereas other QP383R mutant expression plasmids without 284-383aa abolished the binding with cGAS (Figure 6A), suggesting that the region of amino acids 284-383 in QP383R is essential for the interaction between QP383R and cGAS.

Based on this observation, we speculate that the immunosuppressive function of QP383R maybe need its interaction with cGAS. To test this hypothesis, we cotransfected HEK293T cells with HA vector, HA-QP383R, or HA-QP383R-1-283 (deletion of the amino acid 284 to 383 region of QP383R) mutant expression plasmid and stimulated with poly(dA:dT) for 12 h, and IP-ABE assay was used to analyze the changes in the palmitoylation levels of cGAS. As expected, QP383R promoted the palmitoylation of cGAS, while

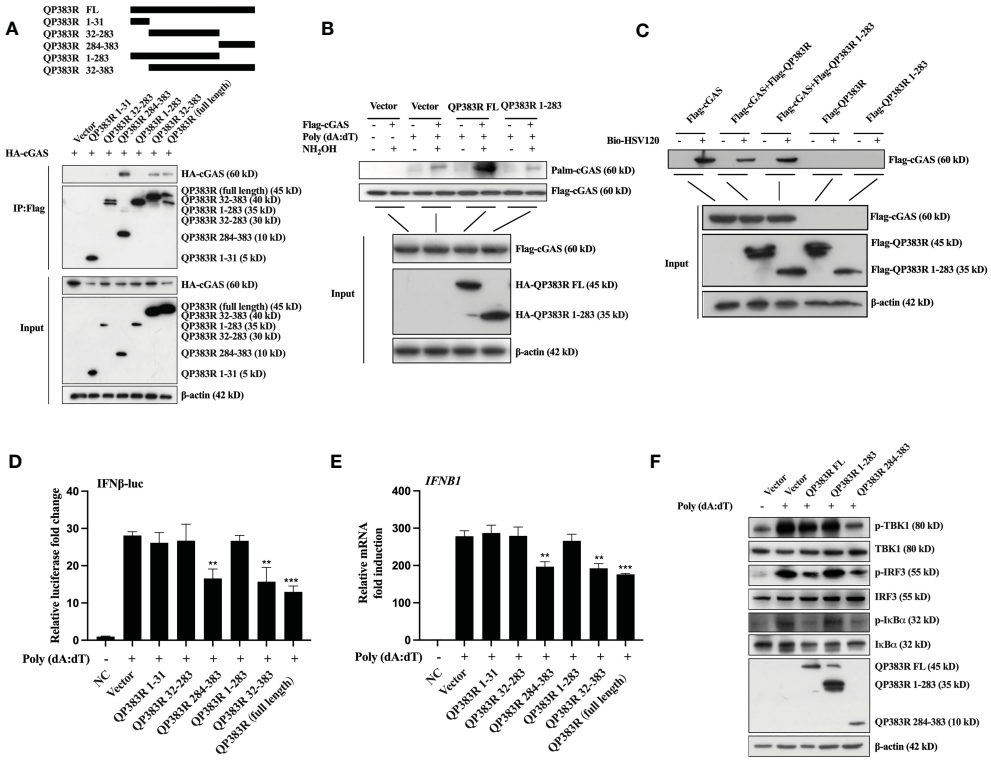

FIGURE 6
284-383aa of QP383R was essential for its inhibitory effect. **(A)** HEK293T cells were co-transfected with HA-cGAS expression plasmid and Flag-QP383R or its truncation mutants for 24 h before coimmunoprecipitation and immunoblotting analysis with the indicated antibodies. **(B)** HEK293T cells were co-transfected with Flag-cGAS (0.5 μg/ml) and HA-QP383R FL (1.0 μg/ml) or HA-QP383R 1-283 (1.0 μg/ml). At 24 h post-transfection, the cells were harvested after stimulated with or without poly(dA:dT) for 12 h to determine cGAS palmitoylation by IP-ABE assay. **(C)** The purified proteins were incubated with the indicated biotinylated HSV120 and streptavidin-Sepharose beads for *in vitro* pull-down assays. The bound proteins were then analyzed by immunoblots with the indicated antibodies. **(D)** 3D4/21 cells were transfected with the indicated plasmids (1.0 μg/ml), IFN-luc reporter promoter plasmid (50 ng/ml), and pRL-TK (8 ng/ml). Twenty-four hours later, the cells were treated with or without poly(dA:dT) for 12 h, and then the activation of the IFNβ promoter was examined by luciferase assays. **(E)** 3D4/21 cells were transfected with the indicated plasmids (1.0 μg/ml). At 24 h post-transfection, cells were treated with or without poly(dA:dT) for 12 h, and IFNB1 mRNA was detected by q-PCR. **(F)** 3D4/21 cells were transfected with the indicated plasmids (1.0 μg/ml). At 24 h later, the cells were stimulated with or without poly(dA:dT) for 12 h. The cells were then harvested and lysed for Western blot analysis to determine the levels of p-TBK1, p-IRF3 and p-IκBα. The data are representative of three independent experiments (means ± the standard errors of the mean [SEM]). $^{**}P \leq 0.01$; $^{***}P \leq 0.001$.

the deletion of the amino acid 284 to 383 region of QP383R completely abrogated the promotion of cGAS palmitoylation (Figure 6B). These results suggest that the amino acid 284 to 383 region in QP383R is essential for QP383R to modulate cGAS palmitoylation, implying that QP383R promotes cGAS palmitoylation needs its amino acid 284-383 region to interact with cGAS first.

To further confirm whether the deletion of the amino acid 284 to 383 region in QP383R loses its inhibitory effect on dsDNA binding to cGAS, HEK293T cells were cotransfected with FLAG-QP383R or FLAG-QP383R-1-283 and HA vector or HA-cGAS. Then cell lysates were incubated with biotinylated HSV120 for 1 hour followed by incubation with streptavidin agarose for 2 h. The agarose beads were analyzed by immunoblotting. As expected, QP383R impaired the interaction between cGAS and HSV-120 (a double-stranded DNA). While, deletion of amino acid 284 to 383 region in QP383R lost its inhibitory activity against dsDNA binding to cGAS (Figure 6C).

The amino acids 284 to 383 region of QP383R was further clarified to be crucial for its immunosuppressive function. 3D4/21 cells were cotransfected with FLAG vector or FLAG-QP383R or FLAG-QP383R mutant expression plasmid along with porcine IFNβ-Luc expression plasmid and pRL-TK plasmid. At 24 hpt, the cells were treated with poly(dA:dT) for 12 h, and the activation of the IFNβ promoter was evaluated. QP383R, QP383R 284-383aa and QP383R 32-383aa but not other QP383R mutant expression plasmids suppressed IFNβ promoter activation (Figure 6D), suggesting that the C-terminal domain of QP383R (aa284-383) is responsible for blocking cGAS-STING signaling pathway activation.

We also measured the mRNA expression of IFNβ in 3D4/21 cells. 3D4/21 cells were cotransfected with FLAG vector or FLAG-QP383R or FLAG-QP383R mutant expression plasmid and stimulated with poly(dA:dT) for 12 h. Consistently, only QP383R, QP383R 284-383aa, and QP383R 32-383aa reduced the transcription of *IFNB1* (Figure 6E). In line with these results, through Western blot, we found that only QP383R and QP383R 284-383aa inhibited the phosphorylation of TBK1, IRF3 and IκBα in response to poly(dA:dT) (Figure 6F).

Taken together, these results indicate that QP383R has an activity to suppress the host antiviral response through blocking

type I IFN production, while the amino acid 284 to 383 region in the C-terminal domain of QP383R is indispensable for its inhibitory function against type I IFN production.

3 Discussion

Type I interferons represent one of the first lines of defense against the invasion of virus. When a virus infects hosts, various pattern recognition receptors recognize pathogen-associated molecular patterns and result in the activation of innate immune signaling pathways to produce IFN-I (39). As an important axis in activating innate immune signaling pathways to produce IFN-I, the cGAS-STING signaling axis could not only detects pathogenic DNA to trigger an innate immune reaction involving a strong type I interferon response against microbial infections, but also can be activated by endogenous DNA, including extranuclear chromatin resulting from genotoxic stress and DNA released from mitochondria (40).

As the cGAS-STING axis plays a crucial role in host antiviral defense (41), many viruses have evolved various mechanisms to antagonize this signaling pathway for efficient infection and replication (42). For example, HCMV tegument protein UL82 contributes to HCMV immune evasion by inhibiting the cellular trafficking and activation of MITA/STING to evade antiviral immunity (35). UL83 inhibits gamma-interferon-inducible protein 16 (IFI16)- and cGAS-mediated DNA sensing for immune evasion (43). PPRV infection impairs the interaction of IRF3 with TBK1 and inhibits IRF3 nuclear translocation, resulting in the suppression of IFN synthesis (44). Virulent poxviruses suppresses host type I IFN production by preventing STING activation (45). Similar to many other DNA viruses, the cGAS-STING axis also plays a crucial role in ASFV-induced host antiviral defense (26, 46). Meanwhile, several proteins encoded by ASFV could antagonize cGAS-STING signaling pathway through different mechanisms for efficient infection and replication (47–49). For example, it has been demonstrated that ASFV protein pA137R negatively regulates the cGAS-STING-mediated IFNβ signaling pathway *via* the autophagy-mediated lysosomal degradation of TBK1 (50). EP364R and C129R of ASFV cleave 2'3'-cGAMP to inhibit the cGAS-STING signaling pathway (51). Moreover, DP96R of ASFV China 2018/1 strain subverts type I IFN production in the cGAS sensing pathway by inhibiting both TBK1 and IKKβ (52). However, whether other ASFV proteins are involved in antagonization of innate antiviral response are largely unclear. Here we identified ASFV protein QP383R as an inhibitor of cGAS-STING-mediated innate antiviral response. Overexpression of QP383R inhibited cGAS-induced activation of the IFNβ promoter and ISRE promoter. Consistently, QP383R inhibited cytosolic dsDNA-induced production of type I IFNs and transcription of downstream antiviral effector genes. These results suggest that ASFV QP383R acts to antagonizing cGAS-STING-mediated innate antiviral immune response, and has the potential to help ASFV achieve immune escape.

As a nonredundant cytosolic DNA sensor, cGAS plays an important role in anti-DNA virus. Therefore, different antagonistic mechanisms targeting cGAS have been identified in various viruses. For example, herpes simplex virus 1 (HSV-1) tegument protein UL37 has been reported to deamidate cGAS, which impairs the ability of cGAS to catalyze cGAMP synthesis (53). HSV-1 protein UL41 has been reported to directly degrade cGAS mRNA to inhibit antiviral signaling (54). ICP27 targets the TBK1-activated MITA/STING signalosome to inhibit antiviral response (55). Kaposi sarcoma herpesvirus (KSHV) protein ORF52 and cytoplasmic isoforms of LANA counteract cGAS-STING pathways through binding to cGAS (56, 57). However, to date, knowledge of the ASFV proteins that regulate cGAS function is limited (58). In this report, several lines of evidence suggest that QP383R directly targets cGAS. Firstly, overexpression of QP383R inhibited cGAS-STING- and dsDNA-, but not cGAMP-induced induction of type I IFNs in 3D4/21 cells and HEK293T cells, suggesting that QP383R targets components upstream of cGAMP. Secondly, co-IP experiments indicated that QP383R was reciprocally associated with cGAS *in vivo* and *in vitro*. Immunofluorescence assays further confirmed the colocalization of QP383R with cGAS in 3D4/21 cells. Thirdly, an *in vitro* GST pull-down assay further verified the direct interaction between cGAS and QP383R.

Extensive studies have revealed the essential roles of cGAS in multiple biological processes, including pathogen invasion and autoimmune diseases. The function of cGAS must be tightly controlled, preventing both over inhibition, which leads to silenced innate immune responses and pathogen invasion, and over activation, which may lead to auto-immune or chronic inflammatory diseases. cGAS activity is reported to be regulated by various PTMs, including ubiquitylation, sumoylation, glutamylation, phosphorylation, acetylation and palmitoylation (59). As a PTM, palmitoylation usually occurs on membrane-associated proteins to regulate their subcellular localization or conformational state. For the first time, cGAS is found to have palmitoylation, but cGAS palmitoylation does not affect its subcellular localization (38). Palmitoylation is a common regulatory mechanism in conformational change. Shi et al. have found that human cGAS palmitoylation alters the interaction between specific amino acid residues and causes conformational changes through MD simulation and biochemical verification. In our study, we found that porcine cGAS also had palmitoylation. Porcine cGAS is not palmitoylated in the resting state, while cGAS palmitoylation appears under stimulation by cytosolic double-stranded DNA. Overexpression of QP383R promoted elevation of the palmitoylation level of cGAS stimulated with poly(dA:dT), which inhibited DNA binding, dimerization, and the enzymatic activity of cGAS. In our study, the palmitoylation modification of porcine cGAS was found for the first time, and cGAS palmitoylation was identified as a novel inhibitory mechanism of the innate immune response to ASFV. Because the structure or function of QP383R is still unknown, whether QP383R has palmitoylase activity, or recruits palmitoyltransferase to interact with cGAS, or inhibits the interaction between depalmitoylase and cGAS to promote cGAS palmitoylation needs further investigation.

Live attenuated vaccines, developed by deleting one or more of their specific virulence-associated and immunosuppressive

genes in the genome of the virulent strains, have been shown to elicit protection against experimental challenge with virulent parental viruses (60–66). These findings suggest that the development of attenuated ASFV recombinant viruses through the genetic manipulation of specific gene(s) could be the most promising strategy for vaccine development so far. As an immunosuppressive factor, QP383R might be a potential target for LAVs design. It has been reported that QP383R is an inhibitor of inflammatory response and deletion of the QP383R genes (ASFV-ΔQP383R) from the highly virulent ASFV CN/GS/2018 strain results in partly viral attenuation in pigs (67). In our study, we found that QP383R is an immunosuppressive factor, inhibited innate antiviral response by reducing the production of type I IFNs. Meanwhile, the amino acid 284 to 383 region of QP383R is indispensable for its inhibitory function against type I IFN production. Therefore, we assume that existing LAVs with the deletion of QP383R gene or deletion/mutation of its key domain (amino acid 284 to 383) at the same time, would dramatically induce the production of type I IFNs, which might play an important role in improving vaccine efficacy.

Interestingly, a recent study shows that the ASFV CN/GS/2018 strain lacking the QP509L and QP383R genes (ASFV-ΔQP509L/QP383R) is completely attenuated *in vivo* in pigs. However, the recombinant ASFV-ΔQP509L/QP383R does not induce protection against lethal ASFV challenge due to its lower levels of type I interferon induction in porcine macrophages (67), which seems to be in contrast to our findings that QP383R inhibits type I interferon production. We speculate that the lower levels of type I interferon induction in porcine macrophages infected with ASFV-ΔQP509L/QP383R is due to its low- or no-replication phenotype. On the other hand, it is reported that the same genes might have different functions in different ASFV strains (8, 61, 63, 64, 66). Therefore, QP383R could play a different function in ASFV CN/GS/2018 strain and ASFV Pig/HLJ/2018 strain.

Based on our results, we propose a working model on QP383R-mediated immune evasion of ASFV (Figure 7). Upon ASFV infection, QP383R is expressed and recruited to cGAS. Subsequently, QP383R uses its amino acid 284-383 to interact with the enzymatically active core of cGAS (aa135-305), and promotes the palmitoylation of cGAS. While, cGAS palmitoylation alters the interactions between specific amino acid residues and causes a conformational change, leading to the inhibition of cGAS DNA binding and dimerization, and the synthesis of cGAMPs. This causes the inhibition of type I IFNs production and innate antiviral response. In summary, these findings expand our knowledge on regulatory mechanisms of the cGAS-STING signal pathway, as well as the strategies of immune evasion by ASFV, which may facilitate the development of the vaccines and therapeutics against ASFV infection.

4 Materials and methods

4.1 Cells

Human embryonic kidney 293T (HEK293T) cells (ATCC CRL-3216^{TM}) and porcine kidney 15 (PK-15) cells (ATCC CCL-33) were cultured in Dulbecco's modified Eagle medium (DMEM; Gibco). A porcine alveolar macrophage cell line 3D4/21 cells (ATCC CRL-2843, which is established by transformation of PAMs with SV40 large T antigen) were maintained in RPMI medium 1640 (Gibco). Cells were supplemented with 10% heat-inactivated fetal bovine serum (FBS; Gibco) and 1% antibiotic/antimycotic (Gibco) and incubated in a humid 5% CO_2 incubator at 37°C.

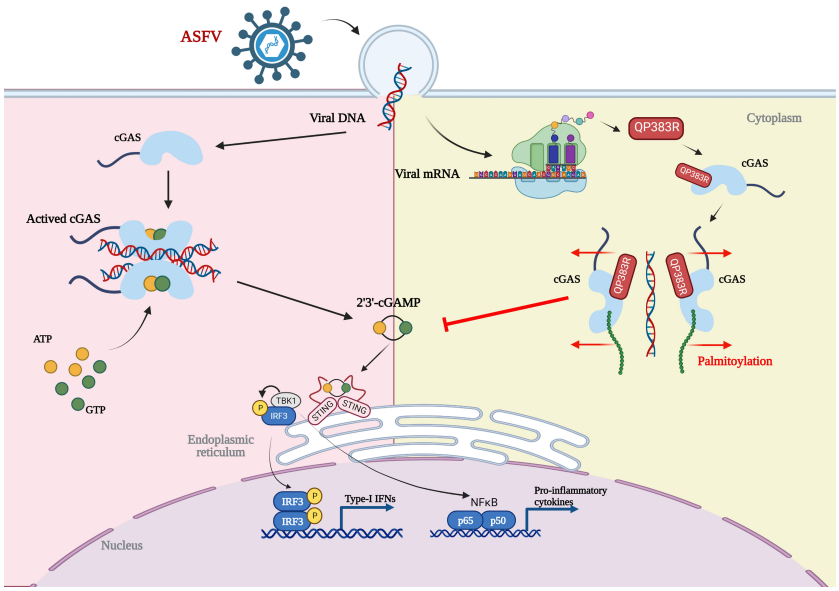

FIGURE 7
Model of the molecular mechanism for QP383R to inhibit IFN-I production. Upon ASFV infection, QP383R is expressed. QP383R interacts with cGAS to inhibit cGAS dimerization, DNA binding, and enzymatic activity *via* promoting its palmitoylation, resulting in the suppression of IFN-I production. Figure was created with BioRender (https://biorender.com).

4.2 Reagents and antibodies

Poly(dA:dT) naked, Poly(dG:dC) naked, 2'3'-cGAMP, and HSV-60 naked were acquired from Invivogen. Lipofectamine 3000 transfection kit (Invitrogen); jetPRIME transfection reagent (Polyplus-transfection); dual-luciferase reporter assay system (Promega); digitonin (Sigma); streptavidin agarose (Solarbio); hydroxylamine solution (HAM, Sigma-Aldrich); EZ-Link BMCC-Biotin (ThermoFisher). The commercial antibodies used in this study included rabbit FLAG mAb (#14793), mouse FLAG mAb (#8146), mouse His mAb (#2366), rabbit TBK1/NAK mAb (#3504), rabbit phosphorylated-TBK1/NAK (p-TBK1) mAb (#3504), mouse IRF3 mAb (#10949), rabbit IRF3 mAb (#4302), rabbit p-IRF3 (Ser 396) mAb (#4947), mouse IκBα mAb (#4814), and rabbit p-IκBα (Ser 32) mAb (#2859). Streptavidin-HRP antibody (#3999) were acquired from Cell Signaling Technology (Boston, MA, USA). The rabbit cGAS pAb (HA500023) was obtained from HuaAn Biotechnology (Hangzhou, Zhejiang, China). The rabbit p-IRF3 (Ser 396) mAb (SAB4504031), rabbit HA mAb (H6908), and mouse β-actin mAb (A1978) were purchased from Sigma-Aldrich (St. Louis, MO, USA).

4.3 RNA extraction and real-time PCR

Total RNAs were extracted from treated cells with TRIzol reagent (CWBIO, China), and 1μg of total RNAs were then reverse transcribed to cDNA using HiFiScript cDNA Synthesis Kit (CWBIO, China) according to the manufacturer's instructions. Real-time PCR analysis was performed by using M5 HiPer Real-time PCR Super Mix (Mei5Bio, China) in a ViiA 7 real-time PCR system (Applied Biosystems). The gene-specific primers for human *IFNB1*, *ISG15*, *ISG54*, and *CXCL10*, and porcine *IFNB1*, *ISG54*, *ISG56*, *IL-6* and *CXCL10* were listed in Supplementary Table 1. The level of gene mRNA was normalized according to the amount of endogenous control glyceraldehyde-3-phosphate dehydrogenase (GAPDH) expression.

4.4 ELISA

The IFNβ and IL-6 protein levels in cell culture supernatants were measured using pig IFNβ ELISA kits (CUSABIO, China) and pig IL-6 ELISA kits (CUSABIO, China) respectively in accordance with the manufacturer's instructions.

4.5 Plasmid construction

The QP383R gene of ASFV Pig/HLJ/2018 (GenBank submission No. MK333180) was synthesized by BGI, and cloned into the pcDNA3.1(+), PRK5-HA, PRK5-Flag, pCMV-Myc or pET-32a vectors by standard molecular biology techniques. ASFV QP383R's truncation mutants including QP383R 1-31aa, QP383R 32-283aa, QP383R 284-383aa, QP383R 1-283aa, and QP383R 32-383aa were cloned into PRK5-Flag, respectively, using seamless assembly cloning kit (cloneamarter, USA). Porcine cGAS, STING, TBK1, IRF3, IRF3/5D, p65, Ikkβ expression plasmids and pGL3-IFNβ-luc, pGL3-ISRE-luc, pGL3-IRF3-luc, pGL3-NFκB-luc reporter vectors were constructed and preserved in our laboratory previously (68, 69). Truncation mutants of porcine cGAS in this article including cGAS RD (1-134aa), cGAS NTase (135-305aa), cGAS Mab21 (306-495aa), and cGAS RD deletion (135–496) were amplified using the cGAS plasmid as a template and cloned into PRK5-Flag respectively, using seamless assembly cloning kit (cloneamarter, USA). The primers for amplification of plasmids were listed in Supplementary Table 2.

4.6 Luciferase reporter assays

HEK293T cells and 3D4/21 cells seeded in 24-well plates were transfected with the constructed plasmids using Lipofectamine 3000 according to the manufacturer's protocol, and pRL-TK reporter plasmid was transfected as an internal control. After 24 h, the cells were treated with or without the synthetic double-stranded DNA-mimetic for 12 h. Cell extracts were prepared and analyzed for firefly and Renilla luciferase activities using a dual-luciferase reporter assay kit (Promega) according to the manufacturer's instructions.

4.7 Western blot

HEK293 cells, or 3D4/21 cells were lysed in radioimmunoprecipitation assay (RIPA) lysis buffer (CWBIO) with 100 U of proteinase inhibitors (CWBIO) and 20 μM NaF on ice for 20 min. Protein levels were quantified using bicinchoninic acid assay. Similar amounts of protein from each extract were separated by SDS-12% PAGE and transferred to polyvinylidene difluoride membranes (Millipore). Membranes were blocked with 5% skim milk in PBS with 0.05% Tween 20, followed by incubation overnight at 4°C with the indicated antibodies. The membranes washed three times with PBST, and then incubated with the appropriate secondary antibody for 1 h at room temperature. Signals were visualized using enhanced chemiluminescence.

4.8 Coimmunoprecipitation

HEK293 cells, or 3D4/21 cells were lysed in l ml NP-40 lysis buffer (50 mM Tris-HCl pH 7.5, 150 mM NaCl, 5 mM EDTA, 1% Nonidet P-40, 10% glycerin) with 100 U of proteinase inhibitors and 20 M NaF for 20 min on ice. Cell lysates were clarified by centrifugation at 12,000 rpm for 10 minutes (4°C). For each immunoprecipitation, the cell lysates was incubated with anti-FLAG M2 magnetic beads at 4°C for 4 hours or overnight. The protein-bound beads were then collected and washed three times with lysis buffer.

4.9 Fluorescent confocal microscopy

3D4/21 cells were transfected with Flag-QP383R or PRK5-Flag for 24 h and fixed in 4% paraformaldehyde for 10-20 min at room

temperature. After being washed three times with PBS, the cells were permeabilized in 0.1% Triton X-100 for 5 min on ice. After being washed three times with PBS, the cells were incubated with 1% BSA for 1 h at room temperature. The cells were incubated with rabbit anti-cGAS MAb (1:500) and mouse anti-Flag MAb (1:1000) overnight at 4°C. Following incubation with Alexa Fluor 555-conjugated goat anti-mouse IgG antibody (1:500) or Alexa Fluor 488-conjugated goat anti-rabbit IgG antibody (1:500) for 1 h at room temperature in the dark, the cells were washed with PBS. Subsequently, the cells' nuclei were stained with 4',6-diamidino-2-phenylindole (DAPI) (1:1,000) and observed by laser confocal microscopy.

4.10 DNA oligonucleotides

HSV120: 5'-AGACGGTATATTTTTGCGTTATCACTGTCCCGGATTGGACACGGTCTTGTGGGATAGGCATGCCCAGAAGGCATATTGGGTTAACCCCTTTTTATTTGTGGCGGGTTTTTTGGAGGACTT-3'.

4.11 DNA pull-down assays

Bio-HSV120 upstream and downstream primers were synthesized by Sangon. HEK293T cells transfected with the indicated plasmids were lysed with lysis buffer (20 mM Tris-HCl pH 7.4, 150 mM NaCl, 5 mM EDTA, 1% Nonidet P-40, 10% glycerin) and cell lysates were incubated with anti-FLAG M2 magnetic beads at 4°C for 4 hours. The protein-bound beads were then collected and eluted with 3×Flag peptide to purify proteins. The purified proteins were incubated with biotinylated HSV120 for 2 hours at 4°C, followed by incubation with streptavidin-Sepharose beads for 3 hours at 4°C. The agarose beads were collected and washed three times with lysis buffer before immunoblotting analysis with the indicated antibodies.

4.12 GST pull-down assay

Purified GST-cGAS were incubated with glutathione agarose beads at 4°C for 1 hour, followed by incubation with purified His-QP383R for 3 hours at 4°C. The beads were washed three times each with lysis buffer (50 mM Tris-HCl pH 7.5, 150 mM NaCl, 5 mM EDTA, 1% Nonidet P-40, 10% glycerin, 100 U proteinase inhibitors, 20 M NaF), and then mixed with an equal volume of 2 × SDS loading buffer and boiled for 10 min. The input/elutes were resolved by SDS-PAGE and analyzed by coomassie staining and/or immunoblot analysis.

4.13 cGAMP activity assays

3D4/21 cells were transfected with FLAG vector or FLAG-QP383R for 24 h, then treated with HSV60 (3 μg/ml) for 6 hours. Cell extracts were then prepared and heated at 95°C for 5 min to denature most proteins, which were removed by centrifugation. The supernatants containing cGAMP were delivered to 3D4/21 cells pretreated with digitonin permeabilization solution (50 mM HEPES pH 7.0, 100 mM KCl, 3 mM $MgCl_2$, 0.1 mM DTT, 85 mM Sucrose, 0.2% BSA, 1 mM ATP, 0.1 mM GTP and 10μg/ml digitonin) at 37° C for 30 min. Four hours later, the cells were collected for Luciferase, qPCR analysis, or western blot.

4.14 IP-ABE assays

The *in vitro* palmitoylation assay was performed as previously described, with minor modifications (70, 71). HEK293T cells transfected with the indicated plasmids were lysed with ABE lysis buffer (50 mM Tris-HCl pH 7.5, 150 mM NaCl, 1% Nonidet P-40, 10% glycerin, 1 mM PMSF, 50 mM NEM, 100 U proteinase inhibitors) for 20 min on ice. The cell lysate was incubated with anti-FLAG M2 magnetic beads at 4°C overnight in dark. The protein-bound beads were then collected and washed three times with ABE lysis buffer (pH 7.2), and were then divided into two equal groups: group added with HAM (+HAM) as experimental group, and group added without HAM (-HAM) as control group. The samples were incubated separately with HAM buffer (50 mM Tris-HCl pH 7.2, 150 mM NaCl, 1% Nonidet P-40, 10% glycerin, 1 mM PMSF, 50 mM NEM, 100 U proteinase inhibitors, 1 M 50% HAM) and ABE lysis buffer (pH 7.2) for 50 min at room temperature. The protein-bound beads were washed with ABE lysis buffer (pH 6.2), following incubation with Biotin-BMCC buffer (50 mM Tris-HCl pH 6.2, 150 mM NaCl, 1% Nonidet P-40, 10% glycerin, 1 mM PMSF, 50 mM NEM, 100 U proteinase inhibitors, 1 μM Biotin-BMCC) for 45 min at 4 °C. After washed by ABE lysis buffer (pH 7.5) for three times, the protein-bound beads were mixed with an equal volume of 2 × SDS loading buffer and incubated for 10 min at 70-85°C, and were then analyzed by immunoblot analysis.

4.15 Statistical analysis

Statistical analysis was performed using GraphPad Prism software, and differences were analyzed using a Student's *t-test*. Significance is denoted in the figures as follows: *, $P < 0.05$; **, $P < 0.01$; ***, $P < 0.001$; and ns, not significant.

Data availability statement

The original contributions presented in the study are included in the article/Supplementary Material. Further inquiries can be directed to the corresponding author.

Author contributions

SH, and W-hF conceived and designed experiments, analyzed data, and wrote the manuscript. XZ, YZ, YY, SL, and YX provided

scientific insights and critical reagents. All authors contributed to the article and approved the submitted version.

Funding

This study was supported by the National Natural Science Foundation of China (Grant No. 32172869), China.

Conflict of interest

The authors declare that the research was conducted in the absence of any commercial or financial relationships that could be construed as a potential conflict of interest.

Publisher's note

Supplementary material

The Supplementary Material for this article can be found online at: https://www.frontiersin.org/articles/10.3389/fimmu.2023.1186916/full#supplementary-material

References

1. Gaudreault NN, Madden DW, Wilson WC, Trujillo JD, Richt JA. African Swine fever virus: an emerging DNA arbovirus. *Front Vet Sci* (2020) 7:215. doi: 10.3389/fvets.2020.00215

2. Alonso C, Borca M, Dixon L, Revilla Y, Rodriguez F, Escribano JM, et al. ICTV virus taxonomy profile: asfarviridae. *J Gen Virol* (2018) 99(5):613–4. doi: 10.1099/jgv.0.001049

3. Xia NW, Wang H, Liu XL, Shao Q, Ao D, Xu YL, et al. African Swine fever virus structural protein p17 inhibits cell proliferation through ER stress-ROS mediated cell cycle arrest. *Viruses* (2021) 13(1):21. doi: 10.3390/v13010021

4. Alejo A, Matamoros T, Guerra M, Andres G. A proteomic atlas of the African swine fever virus particle. *J Virol* (2018) 92(23):e01293–18. doi: 10.1128/JVI.01293-18

5. Karger A, Perez-Nunez D, Urquiza J, Hinojar P, Alonso C, Freitas FB, et al. An update on African swine fever virology. *Viruses* (2019) 11(9):864. doi: 10.3390/v11090864

6. Dixon LK, Chapman DAG, Netherton CL, Upton C. African Swine fever virus replication and genomics. *Virus Res* (2013) 173(1):3–14. doi: 10.1016/j.virusres.2012.10.020

7. He WR, Yuan J, Ma YH, Zhao CY, Yang ZY, Zhang YH, et al. Modulation of host antiviral innate immunity by African swine fever virus: a review. *Animals* (2022) 12(21):2935. doi: 10.3390/ani12212935

8. Bosch-Camos L, Lopez E, Rodriguez F. African Swine fever vaccines: a promising work still in progress. *Porcine Health Manag* (2020) 6:17. doi: 10.1186/s40813-020-00154-2

9. Kawai T, Akira S. Toll-like receptors and their crosstalk with other innate receptors in infection and immunity. *Immunity* (2011) 34(5):637–50. doi: 10.1016/j.immuni.2011.05.006

10. Sun LJ, Wu JX, Du FH, Chen X, Chen ZJJ. Cyclic GMP-AMP synthase is a cytosolic DNA sensor that activates the type I interferon pathway. *Science* (2013) 339(6121):786–91. doi: 10.1126/science.1232458

11. Luecke S, Paludan SR. Molecular requirements for sensing of intracellular microbial nucleic acids by the innate immune system. *Cytokine* (2017) 98:4–14. doi: 10.1016/j.cyto.2016.10.003

12. Dempsey A, Bowie AG. Innate immune recognition of DNA: a recent history. *Virology* (2015) 479-480:146–52. doi: 10.1016/j.virol.2015.03.013

13. Akira S, Uematsu S, Takeuchi O. Pathogen recognition and innate immunity. *Cell* (2006) 124(4):783–801. doi: 10.1016/j.cell.2006.02.015

14. Medzhitov R. Recognition of microorganisms and activation of the immune response. *Nature* (2007) 449(7164):819–26. doi: 10.1038/nature06246

15. Tigano M, Vargas DC, Tremblay-Belzile S, Fu Y, Sfeir A. Nuclear sensing of breaks in mitochondrial DNA enhances immune surveillance. *Nature* (2021) 591(7850):477–81. doi: 10.1038/s41586-021-03269-w

16. Carpenter S, Ricci EP, Mercier BC, Moore MJ, Fitzgerald KA. Post-transcriptional regulation of gene expression in innate immunity. *Nat Rev Immunol* (2014) 14(6):361–76. doi: 10.1038/nri3682

17. Song JX, Villagomes D, Zhao HC, Zhu M. cGAS in nucleus: the link between immune response and DNA damage repair. *Front Immunol* (2022) 13:1076784. doi: 10.3389/fimmu.2022.1076784

18. Chen SL, Rong M, Lv Y, Zhu DY, Xiang Y. Regulation of cGAS activity by RNA-modulated phase separation. *EMBO Rep* (2022) 24(2):e51800. doi: 10.15252/embr.202051800

19. Cao DF, Han XA, Fan XY, Xu RM, Zhang XZ. Structural basis for nucleosome-mediated inhibition of cGAS activity. *Cell Res* (2020) 30(12):1088–97. doi: 10.1038/s41422-020-00422-4

20. Shang GJ, Zhang CG, Chen ZJJ, Bai XC, Zhang XW. Cryo-EM structures of STING reveal its mechanism of activation by cyclic GMP-AMP. *Nature* (2019) 567(7748):389–93. doi: 10.1038/s41586-019-0998-5

21. Zhang CG, Shang GJ, Gui X, Zhang XW, Bai XC, Chen ZJJ. Structural basis of STING binding with and phosphorylation by TBK1. *Nature* (2019) 567(7748):394–8. doi: 10.1038/s41586-019-1000-2

22. Ishikawa H, Ma Z, Barber GN. STING regulates intracellular DNA-mediated, type I interferon-dependent innate immunity. *Nature* (2009) 461(7265):788–92. doi: 10.1038/nature08476

23. Dobbs N, Burnaevskiy N, Chen DD, Gonugunta VK, Alto NM, Yan N. STING activation by translocation from the ER is associated with infection and autoinflammatory disease. *Cell Host Microbe* (2015) 18(2):157–68. doi: 10.1016/j.chom.2015.07.001

24. Sharma S, tenOever BR, Grandvaux N, Zhou GP, Lin RT, Hiscott J. Triggering the interferon antiviral response through an IKK-related pathway. *Science* (2003) 300(5622):1148–51. doi: 10.1126/science.1081315

25. Song J, Li K, Li T, Zhao G, Zhou S, Li H, et al. Screening of PRRSV- and ASFV-encoded proteins involved in the inflammatory response using a porcine iGLuc reporter. *J Virol Methods* (2020) 285:113958. doi: 10.1016/j.jviromet.2020.113958

26. Garcia-Belmonte R, Perez-Nunez D, Pittau M, Richt JA, Revilla Y. African Swine fever virus Armenia/07 virulent strain controls interferon beta production through the cGAS-STING pathway. *J Virol* (2019) 93(12):e02298–18. doi: 10.1128/JVI.02298-18

27. Li TT, Zhao GH, Zhang TQ, Zhang ZX, Chen X, Song J, et al. African Swine fever virus pE199L induces mitochondrial-dependent apoptosis. *Viruses* (2021) 13(11):2240. doi: 10.3390/v13112240

28. Woehnke E, Fuchs W, Hartmann L, Blohm U, Blome S, Mettenleiter TC, et al. Comparison of the proteomes of porcine macrophages and a stable porcine cell line after infection with African swine fever virus. *Viruses* (2021) 13(11):2198. doi: 10.3390/v13112198

29. Jia N, Ou YW, Pejsak Z, Zhang YG, Zhang J. Roles of African swine fever virus structural proteins in viral infection. *J Vet Res* (2017) 61(2):135–43. doi: 10.1515/jvetres-2017-0017

30. Civril F, Deimling T, Mann CCD, Ablasser A, Moldt M, Witte G, et al. Structural mechanism of cytosolic DNA sensing by cGAS. *Nature* (2013) 498(7454):332–7. doi: 10.1038/nature12305

31. Seo GJ, Kim C, Shin WJ, Sklan EH, Eoh H, Jung JU. TRIM56-mediated monoubiquitination of cGAS for cytosolic DNA sensing. *Nat Commun* (2018) 9(1):613. doi: 10.1038/s41467-018-02936-3

32. Zhang X, Wu JX, Du FH, Xu H, Sun LJ, Chen Z, et al. The cytosolic DNA sensor cGAS forms an oligomeric complex with DNA and undergoes switch-like conformational changes in the activation loop. *Cell Rep* (2014) 6(3):421–30. doi: 10.1016/j.celrep.2014.01.003

33. Andreeva L, Hiller B, Kostrewa D, Lassig C, Mann CCD, Drexler DJ, et al. cGAS senses long and HMGB/TFAM-bound U-turn DNA by forming protein-DNA ladders. *Nature* (2017) 549(7672):394–8. doi: 10.1038/nature23890

34. Fu YZ, Guo Y, Zou HM, Su S, Wang SY, Yang Q, et al. Human cytomegalovirus protein UL42 antagonizes cGAS/MITA-mediated innate antiviral response. *PloS Pathog* (2019) 15(5):e1007691. doi: 10.1371/journal.ppat.1007691

35. Fu YZ, Su S, Gao YQ, Wang PP, Huang ZF, Hu MM, et al. Human cytomegalovirus tegument protein UL82 inhibits STING-mediated signaling to evade antiviral immunity. *Cell Host Microbe* (2017) 21(2):231–43. doi: 10.1016/j.chom.2017.01.001

36. Huang ZF, Zou HM, Liao BW, Zhang HY, Yang Y, Fu YZ, et al. Human cytomegalovirus protein UL31 inhibits DNA sensing of cGAS to mediate immune evasion. *Cell Host Microbe* (2018) 24(1):69–80.e4. doi: 10.1016/j.chom.2018.05.007

37. Wu JX, Sun LJ, Chen X, Du FH, Shi HP, Chen C, et al. Cyclic GMP-AMP is an endogenous second messenger in innate immune signaling by cytosolic DNA. *Science* (2013) 339(6121):826–30. doi: 10.1126/science.1229963

38. Shi CR, Yang XK, Liu Y, Li HP, Chu HY, Li GH, et al. ZDHHC18 negatively regulates cGAS-mediated innate immunity through palmitoylation. *EMBO J* (2022) 41 (11):e109272. doi: 10.15252/embj.2021109272

39. Ivashkiv LB, Donlin LT. Regulation of type I interferon responses. *Nat Rev Immunol* (2014) 14(1):36–49. doi: 10.1038/nri3581

40. Hopfner KP, Hornung V. Molecular mechanisms and cellular functions of cGAS-STING signalling. *Nat Rev Mol Cell Biol* (2020) 21(9):501–21. doi: 10.1038/s41580-020-0244-x

41. Kato K, Omura H, Ishitani R, Nureki O. Cyclic GMP-AMP as an endogenous second messenger in innate immune signaling by cytosolic DNA. *Annu Rev Biochem* (2017) 86:541–66. doi: 10.1146/annurev-biochem-061516-044813

42. Ma Z, Damania B. The cGAS-STING defense pathway and its counteraction by viruses. *Cell Host Microbe* (2016) 19(2):150–8. doi: 10.1016/j.chom.2016.01.010

43. Biolatti M, Dell'Oste V, Pautasso S, Gugliesi F, von Einem J, Krapp C, et al. Human cytomegalovirus tegument protein pp65 (pUL83) dampens type I interferon production by inactivating the DNA sensor cGAS without affecting STING. *J Virol* (2018) 92(6):e01774–17. doi: 10.1128/JVI.01774-17

44. Zhu ZX, Li PF, Yang F, Cao WJ, Zhang XL, Dang W, et al. Peste des petits ruminants virus nucleocapsid protein inhibits beta interferon production by interacting with IRF3 to block its activation. *J Virol* (2019) 93(16):e00362–19. doi: 10.1128/JVI.00362-19

45. Georgana I, Sumner RP, Towers GJ, de Motes CM. Virulent poxviruses inhibit DNA sensing by preventing STING activation. *J Virol* (2018) 92(10):e02145–17. doi: 10.1128/JVI.02145-17

46. Razzuoli E, Franzoni G, Carta T, Zinellu S, Amadori M, Modesto P, et al. Modulation of type I interferon system by African swine fever virus. *Pathogens* (2020) 9 (5):361. doi: 10.3390/pathogens9050361

47. Reis AL, Netherton C, Dixon LK. Unraveling the armor of a killer: evasion of host defenses by African swine fever virus. *J Virol* (2017) 91(6):e02338–16. doi: 10.1128/JVI.02338-16

48. Galindo I, Alonso C. African Swine fever virus: a review. *Viruses* (2017) 9(5):103. doi: 10.3390/v9050103

49. Fraczyk M, Wozniakowski G, Kowalczyk A, Bocian L, Kozak E, Niemczuk K, et al. Evolution of African swine fever virus genes related to evasion of host immune response. *Vet Microbiol* (2016) 193:133–44. doi: 10.1016/j.vetmic.2016.08.018

50. Sun MW, Yu SX, Ge HL, Wang T, Li YF, Zhou PP, et al. The A137R protein of African swine fever virus inhibits type I interferon production *via* the autophagy-mediated lysosomal degradation of TBK1. *J Virol* (2022) 96(9):e0195721. doi: 10.1128/jvi.01957-21

51. Dodantenna N, Ranathunga L, Chathuranga WAG, Weerawardhana A, Cha JW, Subasinghe A, et al. African Swine fever virus EP364R and C129R target cyclic GMP-AMP to inhibit the cGAS-STING signaling pathway. *J Virol* (2022) 96(15): e0102222. doi: 10.1128/jvi.01022-22

52. Wang XX, Wu J, Wu YT, Chen HJ, Zhang SF, Li JX, et al. Inhibition of cGAS-STING-TBK1 signaling pathway by DP96R of ASFV China 2018/1. *Biochem Biophys Res Commun* (2018) 506(3):437–43. doi: 10.1016/j.bbrc.2018.10.103

53. Zhang JJ, Zhao J, Xu SM, Li JH, He SP, Zeng Y, et al. Species-specific deamidation of cGAS by herpes simplex virus UL37 protein facilitates viral replication. *Cell Host Microbe* (2018) 24(2):234–48.e5. doi: 10.1016/j.chom.2018.07.004

54. Su CH, Zheng CF. Herpes simplex virus 1 abrogates the cGAS/STING-mediated cytosolic DNA-sensing pathway *via* its virion host shutoff protein, UL41. *J Virol* (2017) 91(6):e02414–16. doi: 10.1128/JVI.02414-16

55. Christensen MH, Jensen SB, Miettinen JJ, Luecke S, Prabakaran T, Reinert LS, et al. HSV-1 ICP27 targets the TBK1-activated STING signalsome to inhibit virus-induced type I IFN expression. *EMBO J* (2016) 35(13):1385–99. doi: 10.15252/embj.201593458

56. Wu JJ, Li WW, Shao YM, Avey D, Fu BS, Gillen J, et al. Inhibition of cGAS DNA sensing by a herpesvirus virion protein. *Cell Host Microbe* (2015) 18(3):333–44. doi: 10.1016/j.chom.2015.07.015

57. Zhang GG, Chan B, Samarina N, Abere B, Weidner-Glunde M, Buch A, et al. Cytoplasmic isoforms of kaposi sarcoma herpesvirus LANA recruit and antagonize the innate immune DNA sensor cGAS. *Proc Natl Acad Sci USA* (2016) 113(8):E1034–43. doi: 10.1073/pnas.1516812113

58. Zheng XJ, Nie SM, Feng WH. Regulation of antiviral immune response by African swine fever virus (ASFV). *Virol Sin* (2022) 37(2):157–67. doi: 10.1016/j.virs.2022.03.006

59. Yu L, Liu PD. Cytosolic DNA sensing by cGAS: regulation, function, and human diseases. *Signal Transduct Target Ther* (2021) 6(1):170. doi: 10.1038/s41392-021-00554-y

60. O'Donnell V, Holinka LG, Krug PW, Gladue DP, Carlson J, Sanford B, et al. African Swine fever virus Georgia 2007 with a deletion of virulence-associated gene 9GL (B119L), when administered at low doses, leads to virus attenuation in swine and induces an effective protection against homologous challenge. *J Virol* (2015) 89 (16):8556–66. doi: 10.1128/JVI.00969-15

61. O'Donnell V, Risatti GR, Holinka LG, Krug PW, Carlson J, Velazquez-Salinas L, et al. Simultaneous deletion of the 9GL and UK genes from the African swine fever virus Georgia 2007 isolate offers increased safety and protection against homologous challenge. *J Virol* (2017) 91(1):e01760–16. doi: 10.1128/JVI.01760-16

62. Borca MV, Ramirez-Medina E, Silva E, Vuono E, Rai A, Pruitt S, et al. Development of a highly effective African swine fever virus vaccine by deletion of the I177L gene results in sterile immunity against the current epidemic Eurasia strain. *J Virol* (2020) 94(7):e02017–19. doi: 10.1128/JVI.02017-19

63. Monteagudo PL, Lacasta A, Lopez E, Bosch L, Collado J, Pina-Pedrero S, et al. BA71DeltaCD2: a new recombinant live attenuated African swine fever virus with cross-protective capabilities. *J Virol* (2017) 91(21):e01058–17. doi: 10.1128/JVI.01058-17

64. Reis AL, Goatley LC, Jabbar T, Sanchez-Cordon PJ, Netherton CL, Chapman DAG, et al. Deletion of the African swine fever virus gene DP148R does not reduce virus replication in culture but reduces virus virulence in pigs and induces high levels of protection against challenge. *J Virol* (2017) 91(24):e01428–17. doi: 10.1128/JVI.01428-17

65. Sanchez-Cordon PJ, Jabbar T, Berrezaie M, Chapman D, Reis A, Sastre P, et al. Evaluation of protection induced by immunisation of domestic pigs with deletion mutant African swine fever virus BeninDeltaMGF by different doses and routes. *Vaccine* (2018) 36(5):707–15. doi: 10.1016/j.vaccine.2017.12.030

66. Chen WY, Zhao DM, He XJ, Liu RQ, Wang ZL, Zhang XF, et al. A seven-gene-deleted African swine fever virus is safe and effective as a live attenuated vaccine in pigs. *Sci China Life Sci* (2020) 63(5):623–34. doi: 10.1007/s11427-020-1657-9

67. Li D, Wu P, Liu H, Feng T, Yang W, Ru Y, et al. A QP509L/QP383R-deleted African swine fever virus is highly attenuated in swine but does not confer protection against parental virus challenge. *J Virol* (2022) 96(1):e0150021. doi: 10.1128/JVI.01500-21

68. Huang C, Zhang Q, Guo XK, Yu ZB, Xu AT, Tang J, et al. Porcine reproductive and respiratory syndrome virus nonstructural protein 4 antagonizes beta interferon expression by targeting the NF-kappa b essential modulator. *J Virol* (2014) 88 (18):10934–45. doi: 10.1128/JVI.01396-14

69. Du L, Liu YH, Du YP, Wang HL, Zhang MJ, Du YJ, et al. Porcine reproductive and respiratory syndrome virus (PRRSV) up-regulates IL-15 through PKC beta 1-TAK1-NF-kappa b signaling pathway. *Virology* (2016) 496:166–74. doi: 10.1016/j.virol.2016.06.007

70. Cao Y, Qiu T, Kathayat RS, Azizi SA, Thorne AK, Ahn D, et al. ABHD10 is an s-depalmitoylase affecting redox homeostasis through peroxiredoxin-5. *Nat Chem Biol* (2019) 15(12):1232–40. doi: 10.1038/s41589-019-0399-y

71. Brigidi GS, Bamji SX. Detection of protein palmitoylation in cultured hippocampal neurons by immunoprecipitation and acyl-biotin exchange (ABE). *J Vis Exp* (2013) 72):50031. doi: 10.3791/50031

frontiers | Frontiers in Immunology

TYPE Original Research
PUBLISHED 14 August 2023
DOI 10.3389/fimmu.2023.1211980

OPEN ACCESS

EDITED BY
Rongtuan Lin,
McGill University, Canada

REVIEWED BY
Juandy Jo,
University of Pelita Harapan, Indonesia
Chuanwu Zhu,
Fifth People's Hospital of Suzhou, China

*CORRESPONDENCE
Jin-li Lou
loujinli@ccmu.edu.cn

†These authors share first authorship

RECEIVED 25 April 2023
ACCEPTED 20 July 2023
PUBLISHED 14 August 2023

CITATION
Liu X, Chen S-x, Liu H and Lou J-l (2023) Host immunity and HBV S gene mutation in HBsAg-negative HBV-infected patients. *Front. Immunol.* 14:1211980. doi: 10.3389/fimmu.2023.1211980

Host immunity and HBV S gene mutation in HBsAg-negative HBV-infected patients

Xin Liu†, Shu-xiang Chen†, Hui Liu and Jin-li Lou*

Department of Clinical Laboratory Center, Beijing Youan Hospital, Capital Medical University, Beijing, China

Background: Clinically, some patients whose HBsAg becomes negative owing to antiviral therapy or spontaneously still show a low level of HBV DNA persistence in serum. T-lymphocyte subsets, cytokine levels and HBV S gene sequences were analyzed in this study.

Methods: A total of 52 HBsAg-negative and HBV DNA-positive patients(HBsAg-/HBV DNA+ patients), 52 persistently HBsAg-positive patients(HBsAg+/HBV DNA+ patients) and 16 healthy people were evaluated. T-lymphocyte subsets of these patients were detected by flow cytometry, serum cytokines and chemokines were detected by the Luminex technique, and the HBV S region was evaluated by Sanger sequencing. T%, T-lymphocyte, CD8+ and CD4+T lymphocyte were lower in the HBsAg-negative group than in the HC group. Compared with the HBsAg-positive group, the HBsAg-negative group had lower levels in T lymphocyte %, CD8+T lymphocyte %, CD8+T lymphocyte and CD4/CD8. These difference were statistically significant ($P<0.05$). Serum IFN-γ, IFN-α and FLT-3L levels were significantly higher in the HBsAg-negative group than in the HBsAg-positive group ($P<0.05$). However, levels of many cytokines related to inflammation (i.e., IL-6, IL-8, IL10, IL-12, IL-17A) were lower in the HBsAg-negative group. Fifty-two HBsAg-negative samples were sequenced, revealing high-frequency amino acid substitution sites in the HBV S protein, including immune escape mutations (i.e., Y100C, S114T, C124Y, P127L, G130R, T131N, M133T, C137S, G145A) and TMD region substitutions (i.e., E2K/R/D, G7D/R, G10D, A17R, F20L/S, L21V, L22V).

Conclusions: According to the results of T-lymphocyte subsets and serum cytokines, it can be deduced that the cellular immune function of HBsAg-negative patients is superior to that of HBsAg-positive patients, with attenuation of liver inflammation. HBsAg-negative patients may show a variety of mutations and amino acid replacement sites at high frequency in the HBV S region, and these mutations may lead to undetectable HBsAg, HBsAg antigenic changes or secretion inhibition.

KEYWORDS

T lymphocyte, cytokine, HBsAg negative, HBV DNA, Occult hepatitis B virus infection

Hepatitis B virus (HBV) infection is a major global health problem. According to the latest data released by the WHO in 2020, there are approximately 257 million cases of chronic HBV infection worldwide. Moreover, approximately 887,000 people die each year due to uncompensated liver cirrhosis, liver failure, primary liver cancer and other end-stage liver diseases caused by HBV infection, indicating that the HBV infection rate has not decreased (1). In hepatitis B virus infection, the most representative serological marker is hepatitis B surface antigen (HBsAg), but some patients infected with hepatitis B virus infection may be negative for HBsAg. Occult HBV infection (OBI) is described as having HBV DNA in the blood, and the current detection methods do not include hepatitis B surface antigen (HBsAg) (2). Loss of HBsAg and anti-HBs seroconversion are considered signs of hepatitis B virus (HBV) elimination. However, serum/intrahepatic HBV DNA can be found in some patients who are negative for serum HBsAg. This status is described as OBI (1, 2). OBI may lead to progression of liver cirrhosis and eventually become an important risk factor for hepatocellular carcinoma (3). Cases of OBI arise from a variety of sources, including patients who are clinically cured of chronic hepatitis B, with HBsAg being serologically cleared but with a small amount of HBV remaining in the liver, or patients infected with mutant HBV (3–5). In addition, it is important to emphasize that the window of acute hepatitis B virus infection is not OBI patients. At present, the mechanism of OBI and how it participates in the occurrence of liver injury remain uncertain, and more studies and long-term clinical follow-up are necessary to better understand the viral and host biological mechanisms and clinical significance of OBI. This study included patients with HBsAg-negative and HBV DNA-positive states in the clinic.

There are several mechanisms that might explain such a state of infection, including the following: mutations in HBV genes, particularly HBsAg escape mutations that are undetectable by commercial HBsAg assays; host mechanisms that lead to strong suppression of HBV replication and transcription; host immune surveillance; coinfection with other viruses, such as hepatitis C virus (HCV); and epigenetic mechanisms (6). The HBV S region can be divided into three sections: N-terminal (aa 1-99), major hydrophilic region (MHR) (aa 100-169) and C-terminal (aa 170-226) regions (7, 8). The 'α' antigen determinant (aa 124-147 or 149) in the major hydrophilic region (MHR) is the primary target by which HBsAg is recognized by anti-HBs and immune cells (9). There are four transmembrane domains of HBsAg (TMDs): TMD1 (aa 4-24), TMD2 (aa 80-98), TMD3 (aa 160-193) and TMD4 (aa 202-222). Amino acid substitution in and around the 'α' antigen determinant may change the conformation of HBsAg and T-cell epitopes, altering immunogenicity (10). HBV S gene mutations are known to influence the occurrence of HBsAg-negative and HBV DNA-positive cases. These mutations are called immune escape-associated mutations, and they are mainly located in the MHR. A variety of mutations associated with HBsAg-negative and HBV DNA-positive cases have been discovered. The most well-known immune escape mutant is G145R, which impairs HBsAg secretion, antigenicity and anti-HBs binding (11).

It is generally believed that HBV infection can cause disruption of the function and proliferation of various immune cells involved in innate and adaptive immune responses. In general, the result of HBV infection is determined by the interaction between the virus and host (12). HBV itself is a noncytopathogenic virus, and liver damage is mainly attributed to the host's immune response. During HBV infection, the host immune response is a double-edged sword that defends against infection by destroying virus-infected cells while inducing liver inflammation and aggravating liver injury (13, 14). Cellular immunity is crucial in the occurrence and progression of hepatitis B disease. T helper cells (Th cells) are classified into Th1 and Th2 subsets according to the different cytokines produced, and the Th1/Th2 balance is critical for maintaining immune function. In chronic HBV infection, Th cells secrete high levels of Th2-type cytokines, inducing the cellular immune balance toward Th2 cells, high expression of HBsAg in serum and liver tissues, a decrease in the number of T lymphocyte subsets, significantly reduced cytokine production ability, and functional exhaustion (15–17).

At present, clinical research on HBsAg-negative and HBV DNA-positive patients is still lacking. Based on a large amount of clinical data, serum HBsAg clearance after nucleotide antiviral treatment or spontaneously may endure for more than 6 months in a small number of HBV-infected patients while serum HBV DNA remains present at a low level in serum. Nevertheless, the majority of HBV-infected patients remain positive for HBsAg after antiviral treatment, and HBV DNA can become negative or be present in serum to varying degrees. The aim of this study was to elucidate the characteristics of T lymphocyte subsets, serum cytokines and HBV S gene status in HBsAg-negative and HBV DNA-positive patients.

Materials and methods

Population studied

This is a cross-sectional study. Between May 2019 and May 2022, 279 patients who were HBsAg negative(<0.05 IU/mL, S/CO<1) and HBV DNA positive(≥10 IU/mL) were screened by hospital data systems. Only 52 of the 279 patients had persistent HBsAg-/HBV DNA+ serological status(>3 months). They had all been diagnosed with chronic hepatitis B in the past. 52 HBsAg+/HBV DNA+ patients who were diagnosed with chronic hepatitis B were matched by sex, age, and disease type. At the same time, clinical residual serum samples from 16 healthy people were collected as the control group. The criteria for healthy subjects were: healthy, no liver disease, no other diseases, and normal laboratory tests. The HBsAg-positive patient samples came from the patient's first blood draw after admission, before antiviral treatment. The diagnostic criteria are based on WHO guidelines for the prevention and treatment of chronic hepatitis B (2019 version) (12). The exclusion criteria were as follows: HBV infection window period; HCV infection not combined with other viral infections; alcoholic liver disease; streptocarpus; drug-induced liver injury; autoimmune diseases, hematological tumors and other serious genetic and metabolic diseases; use of immunosuppressants and hormones within the past three months; and post chemotherapy. The study was approved by the Medical Ethics Committee of Capital Medical University, Beijing Youan Hospital. Because the study used clinical residual serum samples, it was exempt from informed consent.

Laboratory assays

Roche automatic immaterialize was routinely used to detect serum HBsAg, anti-HBs, HBeAg, anti-HBe and anti-HBc at the hospital clinical examination center. HBsAg titer<0.05 IU/mL and anti-HBs<10 IU/L, HBeAg S/CO<1, or anti-HBe and anti-HBc S/CO>1 was considered negative. Quantitative detection of serum HBV DNA was carried out by Abbott Real-Time fluorescence quantitative PCR. The lower limit of quantification was 10 IU/mL (34.1 HBV DNA copies/mL) in the 0.5 mL sample preparation protocol. The results of the assay were expressed as undetected, detectable but below the lower limit of quantification (i.e., HBV DNA detected but not quantifiable), and calculated results in IU/mL within the linear range of the assay. The Siemens Aptio automatic biochemical assembly pipeline was used to detect liver function indexes, such as serum alanine aminotransferase (ALT), aspartate aminotransferase (AST), total bilirubin (TBIL), and direct bilirubin (DBIL).

Detection of peripheral blood T-lymphocyte subsets

Whole-blood samples were analyzed using a BECKMAN flow cytometer (Coulter, USA). Lymphocytes were analyzed using a gate set on a forward scatter vs. side scatter, and three-color flow cytometry was applied to combine CD3, CD4 and CD8. The peripheral blood T-lymphocyte subsets detected in each sample were analyzed using CellQuest software (Coulter, USA).

Cytokine and chemokine profiles

We use MILLIPLEX MAP Human Cytokine/Chemokine/Growth Factor Panel A 48 Plex Premixed Magnetic Bead Panel Kit (Merck, USA) following the manufacturer's recommendations and a Luminex MAGPIX Instrument System, as used for simultaneous quantification of any or all of the following analytes in human tissue/cell lysate and culture supernatant samples and serum or plasma samples: Soluble Cluster of Differentiation 40 Ligand (sCD40L), epidermal growth factor (EGF), Eotaxin, fibroblast growth factor 2 (FGF-2), Fms-related tyrosine kinase 3 ligand (FLT-3L), Fractalkine, granulocyte-stimulating factor(G-CSF), granulocyte macrophage colony-stimulating factor (GM-CSF), growth-regulated oncogene-α (GRO-α), interferon-α2 (IFN-α2), interferon-γ (IFN-γ), IL-1α, IL-1β, interleukin 1 receptor antagonist (IL-1RA), IL-2, IL-3, IL-4, IL-5, IL-6, IL-7, IL-8, IL-9, IL-10, IL-12 (p40), IL-12(p70), IL-13, IL-15, IL-17A, IL-17E/IL-25, IL-17F, IL-18, IL-22, IL-27, interferon gamma-induced protein 10 (IP-10), monocyte chemoattractant protein 1 (MCP-1/CCL2), MCP-3, macrophage-stimulating factor(M-CSF), macrophage-derived chemokine (MDC), monokine induced by IFN-γ (MIG/CXCL9), macrophage inflammatory protein 1α (MIP-1α/CCL3), MIP-1β/CCL4, platelet-derived growth factor AA (PDGF-AA), PDGF-AB/BB, regulated upon activation normal T-Cell expressed and presumably secreted (RANTES/CCL5), TGF-α, tumor necrosis factor α (TNF-α), TNF-β/lymphotoxin alpha (LTA), and vascular endothelial growth factor A (VEGF-A). Serum cytokine profiles were quantitatively measured in 52 HBsAg-negative and HBV DNA-positive patients, 52 HBsAg-positive patients and 16 healthy subjects. MILLIPLEX® products are based on Luminex xMAP technology. Cytokines with more than 50% missing data were not analyzed. Cytokine concentrations have an intra-assay coefficient of variation within 15%. As 4 of the 48 cytokines were not detectable in more than 50% of the samples (GM-CSF, IL-3, IL-7, IL-22), these four cytokines were not analyzed. A variety of cytokine levels are shown in the Supplementary Materials.

Sequencing analysis of the HBV S region

HBV DNA was extracted from 1.0 ml of serum using the silica gel membrane centrifugal column method. First-round and second-round PCR were performed to amplify the HBV S region using PrimeSTAR MAX DNA polymerase. The primers used for both rounds of PCR were PF (5'-TTCCTGC TGGTGGCTCCAGTTC-3', nt54-75) and PR (5'-TTCCGCAGTATGGATCGGCAG-3', nt1258-1278), amplifying a 1224-bp fragment. PCR amplicons were assessed by 1% agarose gel electrophoresis (200 V for 20 min), and positive amplicons were purified. Both strands of purified amplification products were sequenced directly using ABI 3730xl DNA Analyzer. Homology evaluations were performed with the GenBank database using BLAST analysis at https://www.ncbi.nlm.nih.gov. Nucleic and amino acid sequences were analyzed using MEGA 7.0 software. HBV was genotyped based on the full sequence of the S gene using an online prediction tool (https://hbv.geno2pheno.org/index.php). Amino acid substitutions were determined by comparing specimen sequences to the genotype consensus sequence from the alignment of genotype sequences downloaded from https://www.ncbi.nlm.nih.gov. The immune escape mutation of the HBV S protein was determined by the Geno-2-pheno-hbv tool (https://hbv.geno2pheno.org/index.php).

Statistical analysis

Statistical analysis was performed using SPSS 26.0. Single-factor ANOVA was employed for comparison of continuous variables following a normal distribution and the *SNK-q* test for comparisons between groups. A t test was used to compare two groups of continuous variables. The *Kruskal-Wallis H* test was used to compare continuous variables with a nonnormal distribution between groups, and the *Mann-Whitney U* test was used to compare the two groups. Two groups of classifying variables were compared using the X^2 test. Continuous variables are expressed as ($\bar{x}\pm s$) or the median (P25-P75), and a difference was considered to be statistically significant at $P< 0.05$. GraphPad Prism 8 was utilized for the statistical analysis.

Results

Basic clinical data and laboratory test results

The HBsAg-negative patients were mainly male, at 76.92% (40/52), and the mean age was 53 years old. Most of the HBsAg-negative patients had received antiviral therapy with nucleotide analogs and/or interferon according to their clinical history. The positive rates of anti-HBs and anti-HBe in HBsAg-negative patients were significantly higher than those among HBsAg-positive patients [51.92%(27/52) vs. 0.00%(0/52), 80.77% (42/52) vs. 57.69%(30/52)] (P<0.05). A total of 80.77% of HBsAg-negative patients had HBV DNA below 200 IU/mL, and the median value of HBV DNA load was significantly lower than that of HBsAg-positive patients (log, 1.76 vs. 5.77 IU/mL) (P<0.05). Compared with HBsAg-positive patients, median levels of ALT, AST and TBA in HBsAg-negative patients were lower (36 vs. 103 U/L, 38 vs. 92 U/L and 12.40 vs. 120.00 μmol/L), and the differences were significant (P<0.05) (Table 1).

Characteristics of peripheral blood T-lymphocyte subsets

The number of T lymphocytes and CD8+T lymphocytes decreased successively in the healthy control group, HBsAg-negative group and HBsAg-positive group. Each group of data was compared with the mean and median(Table 2). Levels of T lymphocytes and CD8+ T lymphocytes in HBsAg-negative group were higher than HBsAg-positive group, and the difference was statistically significant (P<0.05). The number of T-lymphocyte subsets in the HBsAg negative group and HBsAg positive group was lower than that in the healthy control group. Ratios of T lymphocytes/lymphocytes(T lymphocyte%), T lymphocytes, CD8+T lymphocytes/ lymphocytes (CD8+T lymphocyte%) and CD8+T lymphocytes in the HBsAg-

TABLE 1 General clinical information of HBsAg negative group, HBsAg positive group, and healthy control group.

	HBsAg negative group (N=52)	HBsAg positive group (N=52)	HC (N=16)	P values
Gender				
Female (%)	12 (23.08)	12 (23.08)	5 (31.25)	0.327
Male (%)	40 (76.92)	40 (76.92)	11 (68.75)	0.327
Age (years)	53±12#	51±12	37±4	0.01
HBsAg + (%)	0 (0)*	100 (100.00)	0 (0)	<0.001
Anti-HBs + (%)	27 (51.92)*#	0 (0)	16 (100.00)	<0.001
HBeAg + (%)	1 (1.92)*#	27 (42.31)	0 (0)	<0.001
Anti-HBe + (%)	42 (80.77)*#	30 (57.69)	0 (0)	<0.001
HBV DNA (IU/mL)				
<200 (%)	42 (80.77)*#	6 (11.54)	0 (0)	<0.001
≥200 (%)	10 (19.23)*#	46 (88.46)	0 (0)	<0.001
HBV DNA load (log, IU/mL)	1.76 (1.30-2.20)*#	3.58 (2.67-5.91)	0 (0)	<0.001
ALT (U/L)	36.00 (21.25-84.00)*#	103.00 (53.255-200.00)	15.50 (12.25-21.75)	<0.001
AST (U/L)	38.00 (22.25-102.00)*#	92.00 (44.50-175.00)	22.50 (18.00-24.75)	<0.001
TBIL (μmol/L)	25.60 (16.33-74.75)#	27.5 (17.35-85.73)	16.25 (12.23-17.90)	0.001
DBIL (μmol/L)	10.40 (6.35-52.40)#	12.75 (5.30-104.60)	4.40 (3.73-5.88)	<0.001
TP (g/L)	68.05 (62.15-73.40)	71.60 (62.28-76.65)	67.45 (60.28-77.03)	0.601
TBA (μmol/L)	12.40 (4.23-61.08)	120.00 (78.00-169.00)	19.55 (9.38-53.90)	<0.001
Antivirals-experienced (%)	43 (82.69)*#	0 (0)	0 (0)	<0.001

*, compared with HBsAg positive group, the difference was statistically significant(P<0.05); #, compared with healthy control group(HC), the difference was statistically significant(P<0.05); P values, Compare the three groups; ALT, alanine aminotransferase. AST, aspartate aminotransferase. CHB, Chronic hepatitis B. LC, liver cirrhosis. HCC, Hepatocellular carcinoma. HBsAg-, HBsAg negative and HBV DNA positive. HBsAg+, HBsAg positive. HC, Healthy control. αAntiviral experience means that patients who have been treated with nucleotide analogues and/or peg-interferon-α2b can be found in their medical records (Those patients are still receiving the antivirals treatment).

TABLE 2 Comparison of T lymphocyte subsets among three groups.

Cytokines (pg/mL)	HBsAg- group(N=52)	HBsAg+ group(N=52)	HC(N=16)	*P* values
	Median(P25-P75) $\bar{X}$±SD	Median(P25-P75) $\bar{X}$±SD	Median(P25-P75) $\bar{X}$±SD	
T lymphocyte %	69.02 (62.60-77.08)*#	66.25 (55.88-72.21)	74.45 (69.18-75.85)	<0.001
	68.70±11.79*	63.73±10.81	72.92±4.71	<0.001
T lymphocyte (/μL)	1077 (650-1661)#	1086 (737-1312)	1654 (1289-2406)	<0.001
	1129±610#	1061±376	1889±673	<0.001
CD8 T lymphocyte %	25.31 (19.57-35.29)*	18.86 (16.16-24.07)	26.55 (23.65-30.34)	<0.001
	27.49±10.97*	20.09±6.74	26.20±4.93	<0.001
CD8 T lymphocyte (/μL)	405 (181-710)*#	321 (217-443)	598 (496-882)	<0.001
	459±301*#	332±145	669±242	<0.001
CD4 T lymphocyte %	38.55 (31.14-43.13)	40.03 (28.62-48.18)	39.29 (33.15-45.60)	0.329
	37.86±8.29	39.08±10.26	39.50±6.82	0.575
CD4 T lymphocyte (/μL)	619 (291-826)#	609 (494-874)	994 (712-1159)	<0.001
	607±320#	649±258	1021±412	<0.001
CD4/CD8	1.51 (1.05-2.12)	2.13 (1.37-2.80)*	1.38 (1.04-2.29)#	0.017
	1.68±0.94	2.21±0.98	1.72±1.02	0.005

*, compared with HBsAg positive group, the difference was statistically significant(P<0.05); #, compared with healthy control group(HC), the difference was statistically significant(P<0.05); P values, Compare the three groups; T lymphocyte %, T lymphocyte/lymphocyte; CD8 T lymphocyte %, CD8 T lymphocyte/lymphocyte; CD4 T lymphocyte%, CD4 T lymphocyte/lymphocyte; The data is represented by the median(P25-P75).

negative group were significantly lower than those in the HBsAg-positive group(P<0.05). However, the CD4/CD8 ratio was the highest in HBsAg-positive group, and the difference was statistically significant compared with the other two groups(P<0.05). There was no difference in the CD4/CD8 ratio between HBsAg-negative group and healthy control group (Figure 1).

Levels of serum cytokines and chemokines

By comparing median levels of cytokines and chemokines between the HBsAg-negative group and HBsAg-positive groups, significant differences in IFN-γ, IFN-α, FLT-3L, IP-10, TNF-α, IL-1β, IL-2, IL-4, IL-8, IL-10, IL-12, IL-15 IL-17A and IL-18 were found (P<0.05). Additionally, higher median values of IFN-γ, IFN-α and FLT-3L were detected in the HBsAg-negative group and higher median levels of IL-1β, IL-2, IL-4, IL-8, IL-10, IL-12, IL-15, IL-17A and IL-18 were detected in the HBsAg-positive group (Figure 2, Table 3). Among the 48 cytokines and chemokines detected, 14 each showed significant differences between the two groups, with the other cytokines having no significant difference. Furthermore, median levels of IFN-γ and FLT-3 L in the HBsAg-positive group were lower than those in the HBsAg-negative group and healthy controls, with significant differences (P<0.05); median values of IFN-α were highest in the HBsAg-negative group, with significant differences between groups (P<0.05). Moreover, median levels of IFN-α, IP-10, TNF-α, IL-1β, IL-2, IL-8, IL-10, IL-12, IL-15, IL-17A and IL-18 were higher in the HBsAg-negative and HBsAg-positive groups than in the healthy controls, a statistically significant difference (P<0.05). The median (P25-P75) and differences in cytokines in the three groups are shown in Figure 2 and Table 3.

HBV S region mutation and amino acid substitution in HBsAg-negative and HBV DNA-positive patients

Only 43 of 52 HBsAg-negative samples were successfully sequenced; thus, 43 HBV S gene sequences were analyzed. Genotypes of HBV were determined according to the S gene sequence. Of the 30 HBV S region fragments identified in HBsAg-negative strains, 30 were classified as genotype B (30/43, 69.77%) and 13 strains as genotype C (13/43, 31.23%). DNA sequencing revealed an amino acid substitution in the HBV S protein in 39 of the 43 (90.70%) HBsAg-negative and HBV DNA-positive patients. E kinds of immune escape mutation sites were detected in the genotype B HBV S protein, namely, G119D, T126I, T127P, A128V, G130R, S132F, M133K and C137S, in six HBsAg-negative and HBV DNA-positive patients (6/43, 13.95%). Additionally, 8 kinds of immune escape mutation sites were detected in the genotype C HBV S protein in five HBsAg-negative and HBV DNA-positive patients: Y100C, S114T, C124Y, P127L, G130R, T131N, M133T and G145A (5/43, 11.63%). Amino acid substitution in the transmembrane domain (TMD) region was observed in 31 HBsAg-negative patients (31/43, 72.09%), but only 8 HBsAg-negative samples showed an amino acid substitution in the "α" determinant (amino acids 124-147) of the S protein (Table 4). One female patient's HBV DNA load was as high as

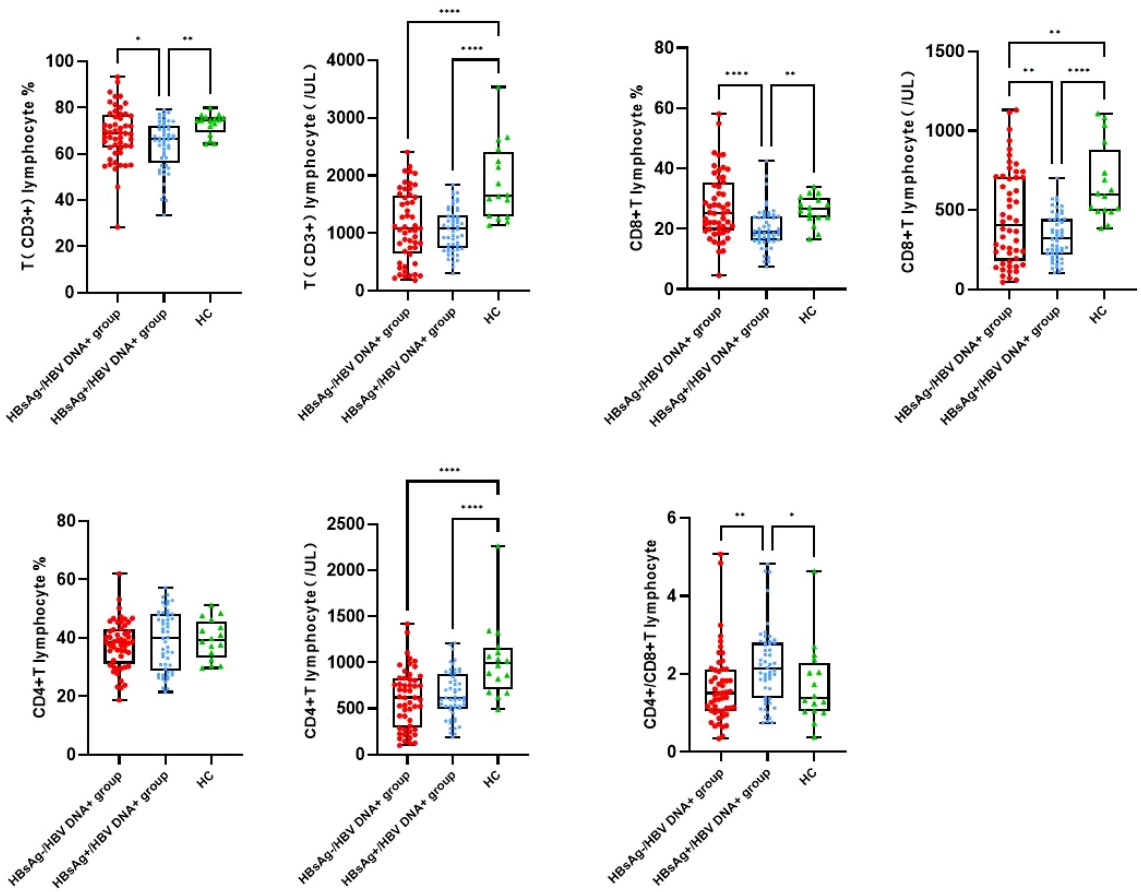

FIGURE 1
Peripheral blood T lymphocyte subsets among the three groups. Comparison of the mean of T lymphocyte, CD4 and CD8 T lymphocyte and CD4/CD8 ratio. HBsAg-, HBsAg negative and HBV DNA positive. HBsAg+, HBsAg positive. *P<0.05, **P<0.01, ****P<0.0001.

7.81×10^5 IU/mL, but HBsAg was negative after antiviral treatment with entecavir. In her sample, we detected many HBV S region mutations resulting in multiple amino acid replacement sites, including immune escape mutations (S114T, C124Y, P127L, G130R, T131N and M133T) and TMD region mutations (L8H, V14A, F19S, V168A, S174N, L175S, Q181R and P203R). There were also three patients with high HBV DNA loads at more than 1×10^4 IU/mL, and they also showed many HBV S region mutations (Table 4).

Amino acid substitution frequency in HBV S protein

A total of 43 samples from HBsAg-negative patients and 49 samples from HBsAg-positive patients were successfully sequenced. Among 43 HBV S-region sequences in HBsAg-negative patients, 30 (30/43, 69.77%) were genotype B and 13 (13/43, 31.23%) genotype C; 34 of 49 (34/49, 69.39%) HBV S-region sequences in HBsAg-positive patients were genotype B and 15 (15/49, 31.23%) genotype C. The mutation rate of the HBV S protein in HBsAg-negative patients was 90.70% (39/43) and that in HBsAg-positive patients was 28.57% (14/49), significantly higher in HBsAg-negative patients. F20L/S (9/30, 30.00%) displayed the highest occurrence frequency in HBsAg-negative patients with genotype B, followed by L22V (5/30, 16.67%) and G10D (5/30, 16.67%). The frequency of multiple immune escape mutations in HBsAg-negative patients with the B and C genotypes was higher than that in HBsAg-positive patients. A variety of amino acid substitution sites also occurred at high frequency in the TMD region of the S protein in HBsAg-negative patients. The details of amino acid substitution frequencies for HBsAg-negative and HBsAg-positive patients are provided in Table 5.

Discussion

In this study, HBsAg-negative patients were treated with antiviral therapy or spontaneously experienced a gradual decrease in HBsAg titer until it disappeared; the HBV DNA load also decreased but remained at a low level in serum. This paper describes T-lymphocyte subsets, various cytokine levels and HBV S gene mutations in HBsAg-negative and HBV DNA-positive patients. The subjects of this study were clinically HBsAg-negative and HBV DNA-positive patients, and their serological characteristics and viral load were the same as those of OBI patients

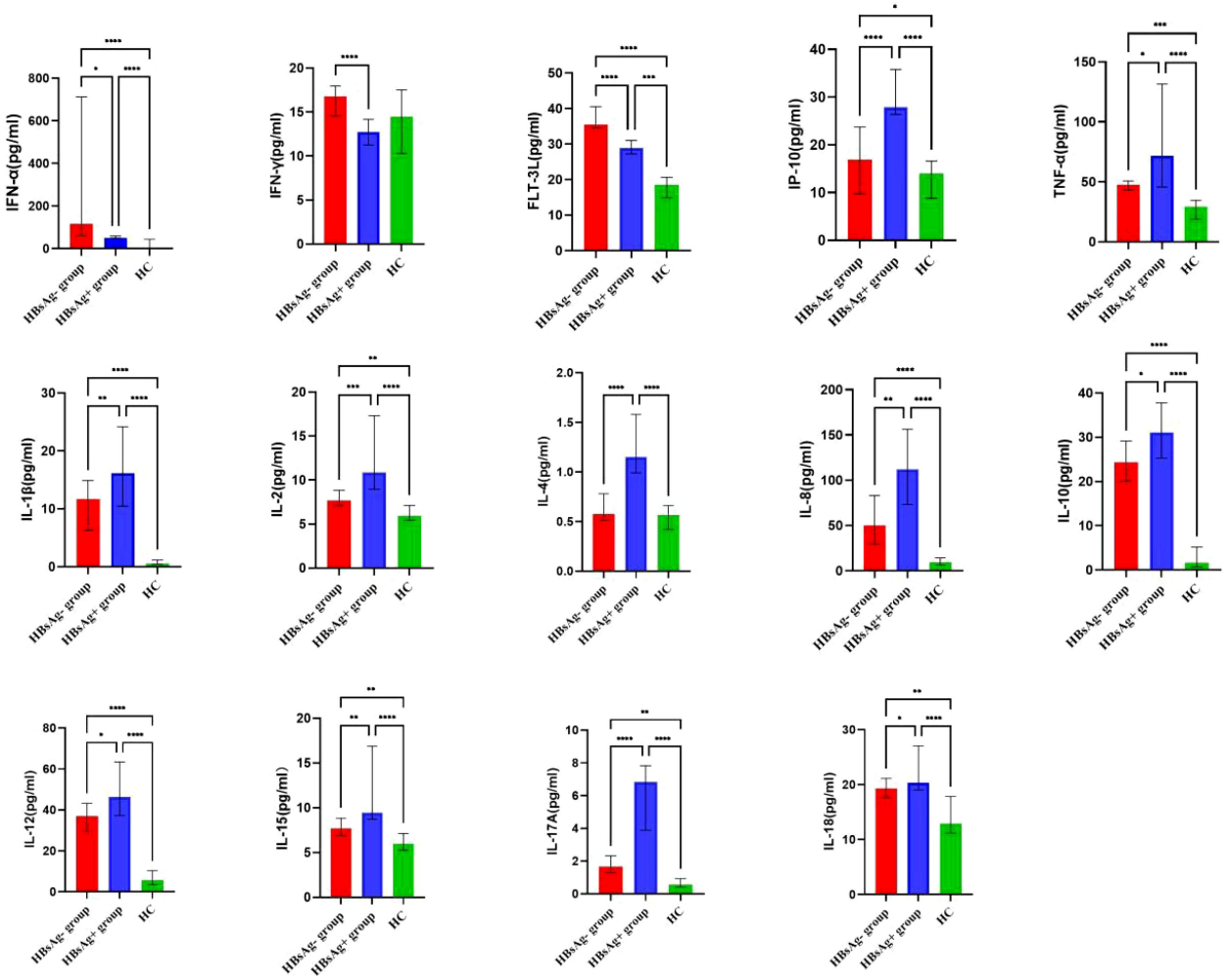

FIGURE 2
Comparison of the median levels of serum cytokine in the HBsAg negative, HBsAg positive and healthy control group. The figure shows the median with 95%CI of cytokines in three groups patients. *Kruskal-Wallis H* test was used for comparison among the three groups, and *Benjamini* test was used for pairwise comparison between groups. HBsAg-, HBsAg negative and HBV DNA positive. HBsAg+, HBsAg positive. *P<0.05. **P<0.01. ***P<0.001, ****P<0.0001.

among blood donors in previous studies (18–20). Hence, regardless of whether HBsAg-negative cases are caused by antiviral therapy or naturally occurring OBI, clinical indicator characteristics are the same.

HBeAg is a marker of active HBV DNA replication in hepatocytes. However, most HBsAg-negative patients are negative for HBeAg, suggesting low viral replication in these patients. The positive rates of anti-HBs and anti-HBe in HBsAg-negative and HBV DNA-positive patients in our study were 51.92% and 80.77%, respectively, significantly higher than those in HBsAg-positive patients. Thus, most HBsAg-negative patients have undergone serological conversion, with low levels of viral replication and protein expression. To explore the host immune function and inflammatory state in HBsAg-negative patients, levels of T lymphocyte subsets and serum cytokines were analyzed in this study; the HBV S gene was also sequenced and analyzed. Despite suppression of HBV DNA replication and protein expression, the virus may not be completely eliminated. In fact, a small amount of HBV cccDNA remains in liver tissue, with the potential to progress to cirrhosis and hepatocellular carcinoma. As it is considered a risk factor for hepatocellular carcinoma, it cannot be ignored (21–23).

Some studies have suggested that HBsAg-negative and HBV DNA-positive cases are related to viral genome mutations, that is, HBsAg antigenicity changes in HBsAg-negative and HBV DNA-positive patients with mutations in the HBV PreS/S region. Mutations located in the immunodominant "α" determinant region (aa124-147 or 149) can impair the efficiency of HBsAg detection reagents by reducing the binding affinity of the HBsAg capture antibody (24). A single mutation in the "α" determinant in the main hydrophilic region (MHR) of the HBV S region can also inhibit HBsAg secretion (25). Additionally, amino acid substitution in the reverse transcriptase (RT) domain may lead to low levels of HBV DNA replication and HBsAg synthesis, resulting in HBsAg-negative and HBV DNA-positive cases (26). The substitutions M133T and T131N generate an extra N-linked glycosylation site that reportedly does not affect HBsAg secretion but may mask

TABLE 3 Circulating cytokine profiles in HBsAg negative, HBsAg positive, and Healthy control group.

Cytokines (pg/mL)	HBsAg- group(N=52)	HBsAg+ group(N=52)	HC(N=16)	*P* values
	Median(P25-P75) $\bar{X}$±SD	Median(P25-P75) $\bar{X}$±SD	Median(P25-P75) $\bar{X}$±SD	
IFN-γ	16.74 (13.01-19.38)*	12.74 (10.45-14.54)	14.46 (10.53-17.40)	<0.001
	19.84±13.31	13.17±3.41	14.40±3.68	
IFN-α	116.90 (40.74-784.2)*#	49.47 (36.56-274.50)	0.94 (0.52-34.01)	<0.001
	419.90±459.90	290.00±497.20	16.65±31.76	
FLT-3L	35.45 (32.67-42.04)*#	29.97 (26.79-40.77)	18.94 (15.99-21.02)	<0.001
	38.00±7.68	36.77±18.42	19.43±8.34	
TNF-α	47.73 (38.88-55.56)*#	71.51 (42.47-160.40)	29.24 (19.31-34.09)	<0.001
	53.11±26.68	136.00±161.90	30.00±11.44	
IP-10	33.30 (19.54-61.67)*#	24.31 (16.23-34.11)	54.06 (40.33-72.08)	<0.001
	49.56±48.54	29.41±21.13	56.51±20.59	
IL-1β	11.66 (2.95-21.61)*#	16.18 (7.71-74.11)	0.58 (0.47-1.11)	<0.001
	16.14±14.77	73.16±121.20	2.05±4.02	
IL-2	7.68 (6.77-9.43)*#	10.85 (8.20-19.21)	5.95 (5.48-6.95)	<0.001
	9.84±6.06	15.37±9.31	6.20±1.01	
IL-4	0.58 (0.49-1.09)*	1.15 (0.81-2.65)	0.57 (0.45-0.66)	<0.001
	0.78±0.41	1.59±1.10	0.57±0.13	
IL-8	49.92 (21.49-126.70)*#	111.80 (55.99-273.60)	9.32 (6.71-13.62)	<0.001
	120.90±193,40	191.70±220.10	11.00±6.04	
IL-10	24.34 (15.77-40.67)*#	31.06 (21.88-66.33)	1.58 (0.70-5.18)	<0.001
	31.93±26.00	53.75±48.69	3.18±3.47	
IL-12 (p40)	36.94 (27.18-52.58)*#	46.36 (31.50-89.73)	5.64 (3.63-9.49)	<0.001
	39.59±19.86	62.70±40.58	6.53±4.28	
IL-15	7.68 (6.52-9.43)*#	9.43 (7.45-18.96)	5.95 (5.38-6.64)	<0.001
	9.79±6.09	14.03±8.72	6.07±0.89	
IL-17A	1.67 (1.23-3.04)*#	6.81 (3.08-10.67)	0.55 (0.42-0.87)	<0.001
	2.71±3.59	8.11±7.00	3.15±9.15	
IL-18	19.31 (16.41-22.19)*#	20.32 (18-28.17)	12.94 (11.35-17.49)	<0.001
	19.94±7.70	25.63±14.16	14.03±4.39	

SD, standard deviation. P25, 25th percentile. P75, 75th percentile. HBsAg-, HBsAg negative and HBV DNA positive. HBsAg+, HBsAg positive. HC, healthy control group. To know the difference between the groups, the Mann–Whitney U nonparametric test was used.: *, compared with HBsAg positive group, the difference was statistically significant(P<0.05); #, compared with healthy control group(HC), the difference was statistically significant(P<0.05); P values, Compare the three groups.

antigenic sites affecting detection (27). Moreover, the mutants Y100C and P127L may affect HBsAg expression and secretion as well as anti-HBs binding (28).

Among the 43 successfully sequenced HBsAg-negative samples, 39 HBV S region fragments showed mutations; among HBsAg-positive samples, 49 samples were sequenced successfully, and 14 HBV S region fragments showed mutations. The mutation rate of the HBV S gene in HBsAg-negative patients (39/43, 90.70%) was significantly higher than that in HBsAg-positive patients (14/49, 28.57%) in our study. Six HBsAg-negative samples showed immune escape mutation sites in the genotype B HBV S region, G119D, T126I, T127P, A128V, G130R, S132F, M133K and C137S (29), with immune escape mutation sites in the genotype C HBV S region in five HBsAg-negative samples, Y100C, S114T, C124Y, P127L, G130R, T131N, M133T and G145A (29). No immune escape mutation was detected in HBsAg-positive patients. These HBsAg immune escape mutants may have arisen as a result of specific selection, such as through the host immune system due to vaccination or antiviral selective pressure attenuating production of HBsAg and resulting in low plasma HBV DNA levels (30). Furthermore, these mutations may be responsible for virus detection

10.3389/fimmu.2023.1211980

TABLE 4 HBsAg negative patients with amino acids substitutions in HBV S protein.

Sample	Sex	HBV DNA oading (IU/mL)	Anti-HBc	Anti-HBs level (IU/L)	HBV genotype	S protein amino acid substitutions	Immune escape mutations	TMD mutations
1	F	73	Pos	34.9	B	N40S, L49H, F200Y, S204N, V224A	N	S204N
2	F	7.81×10^5	Pos	12.6	C	L8H, V14A, F19S, I57T, I68T, S114T, C124Y, P127L, G130R, T131N, M133T, V168A, S174N, L175S, Q181R, P203R, M213I	S114T, C124Y, P127L, G130R, T131N, M133T	L8H, V14A, F19S, V168A, S174N, L175S, Q181R, P203R
3	M	196	Pos	844	B	F219V	N	F219V
4	M	159	Pos	25.4	B	N207H	N	N207H
5	M	117	Pos	61.9	B	E2D	N	N
6	M	136	Pos	neg	C	V18G, Y100C, V159A, I218L	Y100C	V18G, I218L
7	M	62	Pos	neg	B	E2R, L13I, F20L, L22V, T23D, G50A	N	L13I, F20L, L22V
8	M	307	Pos	neg	C	Y100C, I218L	Y100C	I218L
9	F	110	Pos	neg	B	E2K, L22V	N	L22V
10	F	31	Pos	955.2	B	P135S	N	N
11	M	96	Pos	252.8	B	L12C, L13R, A17P, F19L, G50A	N	L12C, L13R, A17P, F19L
12	M	39.9	Pos	184	B	L21C, L22V	N	L21C
13	M	21.7	Pos	neg	B	N40Q, R78G	N	N
14	M	4853	Pos	neg	B	S132F, C137S	S132F, C137S	N
15	F	215	Pos	neg	B	T118P, T125P, T126I, A128V, G130R, S132F, M133K, C137S	T126I, A128V, G130R, S132F, M133K, C137S	
16	M	178	Pos	110.4	B	F20S	N	F20S
17	M	747	Pos	neg	B	F93S, L95W. V96S. V106L C107S. PIOSL, G119D	G119D	F93S, L95W. V96S
18	M	155	Pos	82.61	B	C48S. P66L. P70L F80L I86F. 192N. F93L, L94C. L95G. V96F. C107V. PLOSS	N	I86F. 192N. F93L. L94C, L95G. V96F
19	M	28	Pos	20.20	B	F20L, L2IV, T27P. I28N, P29T	N	F20L. L21V
20	F	73	Pos	19.5	B	N40S. L49H, F200Y, S204N. V224A	N	F200Y, S204N
21	M	<10	Pos	neg	B	F20L, L2IV, L22V	N	F20L. L21V. L22V
22	M	45	Pos	1000	C	L15V. I37S, L39V. N40R F41V. L42P	N	L15V
23	M	20	Pos	neg	C	N	N	N
24	M	48	Pos	neg	C	V14G L15V, P46L. T47K I68T	N	V14G,L15V
25	M	45.3	Pos	neg	C	N31 P49L ISST. L98V. V184A	N	L98V. V184A
26	M	146	Pos	neg	C	GIOR G145A L216F	G145A	N
27	M	814	Pos	1000	B	W35C. L39P. S58C, R79H, T127P. W182*	T127P	W182*
28	F	41.6	Pos	neg	C	C65G. G71C, V184A	N	V184A
29	M	20	Pos	neg	C	N	N	N
30	M	104	Pos	1000	C	F19V. L22V. T23D. S38L	N	F19V. L22V. T23D
31	M	773	Pos	neg	C	GIOR G145A R160G W201G P217Q. D28F	G145A	W201G P217Q. 1218F
32	F	23.8	Pos	neg	C	N	N	N

(Continued)

10.3389/fimmu.2023.1211980

TABLE 4 Continued

Sample	Sex	HBV DNA oading (IU/mL)	Anti-HBc	Anti-HBs level (IU/L)	HBV genotype	S protein amino acid substitutions	Immune escape mutations	TMD mutations
33	M	22	Pos	46.47	B	G7R L9*. GIOD. F20L T27P	N	G7R L9*. G10D. F20L
34	M	100	Pos	neg	B	F20L	N	F20L
35	M	20	Pos	52.48	B	N	N	N
36	M	104	Pos	1000	B	G7R GIOD. A17R GISV. F20L L21V	N	G7R G10D,A17R G18V. F20L, L21V
37	M	595	Pos	187.8	B	G10D. A17R	N	G10D. A17R
38	F	110	Pos	1000	B	G10D. F20S. T27P	N	G10D, F20S
39	F	20	Pos	362.7	B	Q5IK N52L C64L C65S. 168T. C69R G71A FSOL L97F. L98W	N	L97F. L98W
40	M	53	Pos	neg	B	G7D. A17R F20L L21V,L22V	N	G7R, A17R, F20L. L21V. L22V
41	F	1097	Pos	1000	B	M133K C137S	M133K C137S	N
42	M	1.28*10	Pos	neg	B	T125P. A128V, S132E	A128V. S132F	N
43	M	20	Pos	neg	B	G10D. L22* T23Q	N	GIOD. L22*. T23Q

F, Female. M, Male. Pos, positive. neg, negtive. N, none. TMD, transmembrane domain. *, stop codon.

failure in routine screening (25). Indeed, this is common in the clinical setting in which patients may have HBsAg-negative results but classical symptoms and, if tested for HBV DNA, will show high HBV DNA levels. In general, detection of some of these emerging mutants has become a major challenge for commercially available immunoassays. Thirty-one HBsAg-negative samples in the TMD region exhibited multiple amino acid substitution sites, many of which were newly discovered, such as E2K/R/D, G10D, A17R, F20L/S, L21V, L22V, F200Y, and S204N. E2 site mutations in the S protein are confirmed to impair secretion of HBsAg, which significantly affected detection of HBsAg (31). For genotype B, the highest mutation frequency of the S protein in HBsAg-negative patients was sF20L/S; regarding genotype C, sF19V/S had the highest frequency. Both mutations occur in the TMD region of the S protein. sF20L/S and sF19V/S are high-frequency mutations associated with HBsAg negativity, which may be a result of the pressure of antiviral therapy and have certain effects on HBsAg production or secretion. The truncation mutant sW182* was present in one HBsAg-negative patient in the study of Pollicino et al (32). This mutation induces retention of the truncated S protein in the perinuclear endoplasmic reticulum (ER) and is associated with lower HBV transcript levels due to decreased stability (33). Large-scale studies and *in vitro* experiments are needed to determine the significance of newly detected mutations.

Studies have shown that the immune system of HBsAg-negative and HBV DNA-positive patients strongly inhibits viral replication and gene expression (34–37). The ability of CD8 T lymphocytes to proliferate and secrete cytokines (e.g., IFN-γ, IL-2) is weakened in chronic HBV infection (38), and T-lymphocyte subsets can be used to assess the immune function of the host. As cytokines can alter the process of infection and affect the tendency and progression of chronic hepatitis B, they are worthy of study.

In this study, the number of CD4+ T lymphocytes, CD8+ T lymphocytes, CD4+ T lymphocytes/lymphocytes (CD4+ T%) and CD8+ T lymphocytes/lymphocytes (CD8+ T%) was lowest in the HBsAg-positive group, which may be related to the low immune function caused by chronic HBV infection. The numbers of CD4+ T cells and CD8+ T cells in the HBsAg-negative group were higher than those in the HBsAg-positive group. Levels of a variety of cytokines and chemokines (IFN-γ, IFN-α, FLT-3 L) related to immune regulation and virus clearance were also higher in the HBsAg-negative group. Therefore, the immune function of HBsAg-negative patients is enhanced compared with HBsAg-positive patients, which may be related to virus suppression in the former after antiviral treatment. The immune function of HBV-infected patients treated with antiviral interferon may also be enhanced, which can increase the clearance rate of HBsAg. Because this study was a cross-sectional study and we could only determine T lymphocyte subsets and serum cytokine levels after HBsAg clearance, it is unclear whether enhanced host immune function occurred before or after HBsAg clearance. Regardless, it can be confirmed that HBsAg-negative patients have strong host immune function. Although the number of CD4 and CD8 T cells in the HBsAg-negative patients was higher than that in the HBsAg-positive patients, it was lower than that in the healthy controls. Therefore, the immune function of HBsAg-negative patients did not completely recover to the normal level, which corresponds to the low level of serum HBV DNA in HBsAg-negative patients. A high level of HBsAg is associated with impairment of anti-HBV-specific T and B-cell immune function. Reducing the HBsAg level should promote recovery of specific immune function and in turn promote clearance of HBsAg (39, 40). In this study, we only analyzed the increase in overall T-lymphocyte subsets in HBsAg-negative patients and did not detect the immune function of HBV-specific T lymphocytes. Further research is needed.

10.3389/fimmu.2023.1211980

TABLE 5 Frequency of amino acid substitution of HBV S protein in HBsAg negative and HBsAg positive patients.

Amino acid substitution site(%)	Genotype B			Amino acid substitution site(%)	Genotype C		
	HBsAg- group (N=30)	HBsAg+ group (N=34)	*P* values		HBsAg- group (N=13)	HBsAg+ group (N=15)	*P* values
E2K/R/D	3 (10.00)	0 (0.00)*	0.001	N3I	1 (7.69)	0 (0.00)*	0.004
G7D/R	3 (10.00)	0 (0.00)*	0.001	V14G/A	2 (15.38)	0 (0.00)*	<0.001
G10D	5 (16.67)	1 (2.94)*	0.001	G10R	2 (15.38)	1 (6.67)	0.071
A17R	3 (10.00)	0 (0.00)*	0.001	F19V/S	3 (23.08)	0 (0.00)*	<0.001
F20L/S	9 (30.00)	1 (2.94)*	<0.001	L15V	2 (15.38)	0 (0.00)*	<0.001
L21V	4 (13.33)	1 (2.94)*	0.009	L22V	1 (7.69)	0 (0.00)*	0.004
L22V	5 (16.67)	0 (0.00)*	<0.001	T23D	2 (15.38)	0 (0.00)*	<0.001
T27P	3 (10.00)	0 (0.00)*	0.001	I68T	3 (23.08)	2 (13.33)	0.066
G50A	2 (6.67)	0 (0.00)*	0.007	L98V	1 (7.69)	0 (0.00)*	0.004
T125P	2 (4.65)	0 (0.00)*	0.007	Y100C	2 (15.38)	0 (0.00)*	<0.001
T127P	2 (4.65)	0 (0.00)*	0.007	S114T	1 (7.69)	0 (0.00)*	0.004
A128V	2 (4.65)	0 (0.00)*	0.007	C124Y	1 (7.69)	0 (0.00)*	0.004
S132F	3 (6.98)	0 (0.00)*	0.001	P127L	1 (7.69)	0 (0.00)*	0.004
M133K	2 (4.65)	0 (0.00)*	0.007	G130R	1 (7.69)	0 (0.00)*	0.004
C137S	3 (6.98)	0 (0.00)*	0.001	T131N	1 (7.69)	0 (0.00)*	0.004
F200Y	2 (4.65)	0 (0.00)*	0.007	M133T	1 (7.69)	0 (0.00)*	0.004
S204N	2 (4.65)	0 (0.00)*	0.007	G145A	2 (15.38)	0 (0.00)*	<0.001
V224A	2 (4.65)	0 (0.00)*	0.007	V159A	1 (7.69)	0 (0.00)*	0.004
				V184A	2 (15.38)	0 (0.00)*	<0.001
				I218L	2 (15.38)	0 (0.00)*	<0.001

*, compared with HBsAg- group, the difference was statistically significant(P<0.05).

Cytokines represent a large family of molecules, including the following: Th1-associated cytokines [e.g., IL-2 and IFN-γ], which have a functional contribution to cellular immune responses; Th2-associated cytokines (e.g., IL-4, IL-6, and IL-10), which have roles in humoral immune responses; regulatory T-cell (Treg)-associated cytokines [e.g., tumor growth factor-beta (TGF-β) and IL-10], which have been associated with immunomodulation and immunosuppression; and Th17-associated cytokines (e.g., IL-17, IL-22, and IL-23), which play critical roles in mediating inflammation (41). There are few studies on the production profile of cytokines and chemokines in HBsAg-negative and HBV DNA-positive patients, and the mechanism of liver injury is still unclear, but some studies have shown that persistence and transcription of HBV cccDNA in hepatocytes can stimulate production of cytokines, such as TNF-α and IFN-γ, resulting in hepatocyte injury (17). We conclude that levels of TNF-α and IFN-γ in HBsAg-negative patients are significantly higher than those in healthy subjects, which may be related to a small amount of HBV in the body. The persistence and transcription of HBV cccDNA in hepatocytes can lead to the production of cytokines, such as TNF-α and INF-γ (38). Cytokines and chemokines are essential effector molecules in the HBV-related inflammatory response. CD4+ T cells, CD8+ T cells, NK cells, DC cells and their related cytokines participate in the immune injury process of chronic HBV infection (42, 43).

In addition, IFN-γ, IFN-α and FLT-3 L levels in HBsAg-negative patients were significantly higher than those in HBsAg-positive patients in our study. High HBV DNA load and high HBeAg and HBsAg levels may inhibit immune cell function, leading to a reduction in FLT-3L, IFN-γ, and other cytokines with virus clearance effects and to an increase in the level of the most important cytokine for immunosuppression: IL-10 (43–45). HBsAg induces depletion phenotypes and dysfunction of T and B cells, leading to innate and adaptive immune deficiencies, and lowering serum HBsAg contributes to recovery of the host immune response (46). The increase in IFN-γ and FLT-3 L in the HBsAg-negative patients in the present study may be due to the decrease in HBV DNA and clearance of HBsAg after the use of nucleotide analog antiviral drugs. HBV DNA reduction and HBsAg clearance in HBsAg-negative patients after antiviral therapy may promote recovery of cellular immune function, thus leading to increased serum IFN-γ and FLT-3L levels. In general, levels of various proinflammatory cytokines (IL-2, IL-4, IL-8, IL-10, IL-12, IL-15, IL17A, IL-18) in HBsAg-positive patients were higher than those in HBsAg-negative patients and healthy people. Compared with HBsAg-positive patients, the inflammatory reaction of HBsAg-negative

patients was reduced and the immune response function enhanced, but they were still in a state of HBV infection. Overall, a mild inflammatory response compared to healthy people was observed.

Conclusion

High HBsAg serum levels lead to failure of the host immune system, preventing an effective antiviral response. Levels of HBsAg and virus decrease after antiviral treatment, and the inhibitory effect on host cellular immune function is weakened. Cellular immune function is gradually enhanced, which further increases the virus clearance effect. However, HBV S gene mutation may occur in HBsAg-negative patients during antiviral therapy, which leads to amino acid substitutions in the S protein. If the mutation occurs in the main hydrophilic region, the antigenicity of the surface antigen would be changed, rendering commercial detection reagents unable to detect it. If the mutation occurs in the TMD region and changes the S protein conformation, it may affect production and secretion of HBsAg and result in a concentration of serum HBsAg lower than the limit of detection. The decrease in HBsAg secretion is beneficial to host cellular immune function, and antiviral immune responses are continuously stimulated by persistent/intermittent low levels of HBV antigens. This study found a variety of new high-frequency mutation sites in clinically HBsAg-negative and HBV DNA-positive patients.

Data availability statement

The original contributions presented in the study are publicly available. This data can be found here: https://doi.org/10.6084/m9.figshare.23903928.v1.

Ethics statement

The study was approved by the Medical Ethics Committee of Capital Medical University, Beijing Youan Hospital. Because the study used clinical residual serum samples, it was exempt from informed consent.

Author contributions

XL and S-XC are joint first authors(Equal & First authors). XL and S-XC are responsible for designing research plans, collecting clinical data, analyzing data, and writing first drafts of papers. HL participate in the review and editing of the first draft. J-LL participates in the acquisition of research funds and the review and revision of papers. All authors contributed to the article and approved the submitted version.

Funding

This study was supported by the Beijing Outstanding Talents Training fund young backbone individual project (grant no. 2018000021469G287).

Conflict of interest

The authors declare that the research was conducted in the absence of any commercial or financial relationships that could be construed as a potential conflict of interest.

Publisher's note

Supplementary material

The Supplementary Material for this article can be found online at: https://www.frontiersin.org/articles/10.3389/fimmu.2023.1211980/full#supplementary-material

References

1. Stasi C, Silvestri C, Voller F. Hepatitis B vaccination and immunotherapies: an update. *Clin Exp Vaccine Res* (2020) 9(1):1–7. doi: 10.7774/cevr.2020.9.1.1

2. European Association for the Study of the Liver. EASL 2017 Clinical Practice Guidelines on the management of hepatitis B virus infection. *J Hepatol* (2017) 67 (2):370–98. doi: 10.1016/j.jhep.2017.03.021

3. Locarnini S, Raimondo G. How infectious is the hepatitis B virus? Readings from the occult. *Gut* (2019) 68(2):182–3. doi: 10.1136/gutjnl-2018-316900

4. Hoofnagle JH, Seeff LB, Bales ZB, Zimmerman HJ. Type B hepatitis after transfusion with blood containing antibody to hepatitis B core antigen. *N Engl J Med* (1978) 298(25):1379–83. doi: 10.1056/NEJM197806222982502

5. Cho HJ, Cheong JY. Role of immune cells in patients with hepatitis B virus-related hepatocellular carcinoma. *Int J Mol Sci* (2021) 22(15):8011. doi: 10.3390/ijms22158011

6. Bréchot C, Hadchouel M, Scotto J, Fonck M, Potet F, Vyas GN, et al. State of hepatitis B virus DNA in hepatocytes of patients with hepatitis B surface antigen-positive and negative liver diseases. *Proc Natl Acad* (1981) 78:3906–10. doi: 10.1073/pnas.78.6.3906

7. Jiang X, Chang L, Yan Y, Wang L. Paradoxical HBsAg and anti-HBs coexistence among chronic HBV infections:causes and consequences. *Int J Biol Sci* (2021) 17 (4):1125–37. doi: 10.7150/ijbs.55724

8. Wu Y, Zhu Z, Wu J, Bi W, Xu W, Xia X, et al. Evolutionary analysis of pre-S/S mutations in HBeAg-negative chronic hepatitis B with HBsAg< 100 IU/ml. *Front Public Health* (2021) 9:633792. doi: 10.3389/fpubh.2021.633792

9. Yong-Lin Y, Qiang F, Ming-Shun Z, Jie C, Gui-Ming M, Zu-Hu H, et al. Hepatitis B surface antigen variants in voluntary blood donors in Nanjing, China. *Virol J* (2012) 9:82. doi: 10.1186/1743-422X-9-82

10. Zhu HL, Li X, Li J, Zhang ZH. Genetic variation of occult hepatitis B virus infection. *World J Gastroenterol* (2016) 22(13):3531–46. doi: 10.3748/wjg.v22.i13.3531

11. Xue Y, Wang MJ, Yang ZT, Yu DM, Han Y, Huang D, et al. Clinical features and viral quasispecies characteristics associated with infection by the hepatitis B virus G145R immune escape mutant. *Emerg Microbes Infect* (2017) 6(3):e15. doi: 10.1038/emi.2017.2

12. Wu J, Han M, Li J, Yang X, Yang D. Immunopathogenesis of HBV infection. *Adv Exp Med Biol* (2020) 1179:71–107. doi: 10.1007/978-981-13-9151-4_4

13. Khanam A, Chua JV, Kottilil S. Immunopathology of chronic hepatitis B infection: role of innate and adaptive immune response in disease progression. *Int J Mol Sci* (2021) 22(11):5497. doi: 10.3390/ijms22115497

14. Nguyen LN, Nguyen L, Zhao J, Schank M, Dang X, Cao D, et al. Immune activation induces telomeric DNA damage and promotes short-lived effector T cell differentiation in chronic HCV infection. *Hepatology* (2021) 74(5):2380–94. doi: 10.1002/hep.32008

15. Bertoletti A, Ferrari C. Innate and adaptive immune responses in chronic hepatitis B virus infections: towards restoration of immune control of viral infection. *Gut* (2012) 61(12):1754–64. doi: 10.1136/gutjnl-2011-301073

16. Martinot-Peignoux M, Lapalus M, Asselah T, Marcellin P. The role of HBsAg quantification for monitoring natural history and treatment outcome. *Liver Int* (2013) 33(Suppl 1):125–32. doi: 10.1111/liv.12075

17. Ribeiro CR, de Almeida NA, Martinelli KG, Pires MA, Mello CE, Barros JJ, et al. Cytokine profile during occult hepatitis B virus infection in chronic hepatitis C patients. *Virol J* (2021) 18(1):15. doi: 10.1186/s12985-021-01487-2

18. Liu CJ, Chen DS, Chen PJ. Epidemiology of HBV infection in Asian blood donors: emphasis on occult HBV infection and the role of NAT. *J Clin Virol* (2006) 36 (Suppl 1):S33–44. doi: 10.1016/S1386-6532(06)80007-7

19. Ye X, Liu L, Chen L, Nie X, Huang L, Ye D, et al. High-frequency notable HBV mutations identified in blood donors with occult hepatitis B infection from heyuan city of southern China. *Front Immunol* (2022) 13:754383. doi: 10.3389/fimmu.2022.754383

20. Fopa D, Candotti D, Tagny CT, Doux C, Mbanya D, Murphy EL, et al. Occult hepatitis B infection among blood donors from Yaoundé, Cameroon. *Blood Transfus* (2019) 17(6):403–8. doi: 10.2450/2019.0182-19

21. Wang J, Liu Y, Liao H, Liu L, Chen R, Si L, et al. The sK122R mutation of hepatitis B virus (HBV) is associated with occult HBV infection: Analysis of a large cohort of Chinese patients. *J Clin Virol* (2020) 130:104564. doi: 10.1016/j.jcv.2020.104564

22. Simonetti J, Bulkow L, McMahon BJ, HOman C, Snowball M, Negus S, et al. Clearance of hepatitis B surface antigen and risk of hepatocellular carcinoma in a cohort chronically infected with hepatitis B virus. *Hepatology* (2010) 51(5):1531–7. doi: 10.1002/hep.23464

23. Chen L, Zhao H, Yang X, Gao JY, Cheng J. HBsAg-negative hepatitis B virus infection and hepatocellular carcinoma. *Discovery Med* (2014) 18(99):189–93.

24. Cao GW. Clinical relevance and public health significance of hepatitis B virus genomic variations. *World J Gastroenterol* (2009) 15(46):5761–9. doi: 10.3748/wjg.15.5761

25. Salpini R, Colagrossi L, Bellocchi MC, Surdo M, Becker C, Alteri C, et al. Hepatitis B surface antigen genetic elements critical for immune escape correlate with hepatitis B virus reactivation upon immunosuppression. *Hepatology* (2015) 61(3):823–33. doi: 10.1002/hep.27604

26. Li S, Zhao K, Liu S, Wu C, Yao Y, Cao L, et al. HBsAg sT123N mutation induces stronger antibody responses to HBsAg and HBcAg and accelerates in *vivo* HBsAg clearance. *Virus Res* (2015) 210:119–25. doi: 10.1016/j.virusres.2015.08.004

27. Bi X, Tong S. Impact of immune escape mutations and N-linked glycosylation on the secretion of hepatitis B virus virions andsubviral particles: Role of the small envelope protein. *Virology* (2018) 518:358–68. doi: 10.1016/j.virol.2018.03.011

28. Taffon S, Genovese D, Blasi M, Pierotti P, Degli Esposti A, Catone S, et al. HBV whole-genome mutation profile in HIV-1/HBV coinfected patients in a long-term follow-up study. *Infection* (2014) 42(4):675–87. doi: 10.1007/s15010-014-0616-2

29. Kim MH, Kang SY, Lee WI. Occult HBV among anti-HBc alone: mutation analysis of an HBV surface gene and pre-S gene. *Yonsei Med J* (2017) 58(3):557–63. doi: 10.3349/ymj.2017.58.3.557

30. Liu Y, Wang CM, Cheng J, Liang ZL, Zhong YW, Ren XQ, et al. Hepatitis B virus in tenofovir-naive Chinese patients with chronic hepatitis B contains no mutation of rtA194T conferring a reduced tenofovir susceptibility. *Chin Med J (Engl)* (2009) 122:1585–6.

31. Wang H, Liao F, Xie J, Gao W, Wang M, Huang J, et al. E2 site mutations in S protein strongly affect hepatitis B surface antigen detection in the occult hepatitis B virus. *Front Microbiol* (2021) 12:664833. doi: 10.3389/fmicb.2021.664833

32. Pollicino T, Amaddeo G, Restuccia A, Raffa G, Alibrandi A , Cutroneo G, et al. Impact of hepatitis B virus (HBV) preS/S genomic variability on HBV surface antigen and HBV DNA serum levels. *Hepatology* (2012) 56:434–43. doi: 10.1002/hep.25592

33. Xiang KH, Michailidis E, Ding H, Peng YQ, Su MZ , Li Y, et al. Effects of amino acid substitutions in hepatitis B virus surface protein on virion secretion, antigenicity, HBsAg and viral DNA. *J Hepatol* (2017) 66(2):288–96. doi: 10.1016/j.jhep.2016.09.005

34. Pollicino T, Raffa G, Costantino L, Lisa A, Campello C, Squadrito G, et al. Molecular and functional analysis of occult hepatitis B virus isolates from patients with hepatocellular carcinoma. *Hepatology* (2007) 45(2):277–85. doi: 10.1002/hep.21529

35. Pollicino T, Belloni L, Raffa G, Pediconi N, Squadrito G, Raimondo G, et al. Hepatitis B virus replication is regulated by the acetylation status of hepatitis B virus cccDNA-bound H3 and H4 histones. *Gastroenterology* (2006) 130(3):823–37. doi: 10.1053/j.gastro.2006.01.001

36. Toscanini F, De Leo P, Calcagno G, Malfatti F, Grasso A, Anselmo M. Hepatitis B reactivation in a HBsAg-negative, HBcAb-positive patient receiving fludarabine for the treatment of chronic lymphocytic leukaemia. *Case Rep Hepatol* (2011) 2011:258791. doi: 10.1155/2011/258791

37. Hoofnagle JH. Reactivation of hepatitis B. *Hepatology* (2009) 49(5 Suppl):S156–65. doi: 10.1002/hep.22945

38. Xiong S, Zhu D, Liang B, Li M, Pan W, He J, et al. Longitudinal characterization of phenotypic profile of T cells in chronic hepatitis B identifies immune markers associated with HBsAg loss. *EBioMedicine* (2021) 69:103464. doi: 10.1016/j.ebiom.2021.103464

39. Kondo Y, Ninomiya M, Kakazu E, Kimura O, Shimosegawa T. Hepatitis B surface antigen could contribute to the immunopathogenesis of hepatitis B virus infection. *ISRN Gastroenterol* (2013) 2013:935295. doi: 10.1155/2013/935295

40. Tsai KN, Kuo CF, Ou JJ. Mechanisms of hepatitis B virus persistence. *Trends Microbiol* (2018) 26(1):33–42. doi: 10.1016/j.tim.2017.07.006

41. Huang Z, van Velkinburgh JC, Ni B, Wu Y. Pivotal roles of the interleukin-23/T helper 17 cell axis in hepatitis B. *Liver Int* (2012) 32(6):894–901. doi: 10.1111/j.1478-3231.2012.02764.x

42. Oh IS, Park SH. Immune-mediated liver injury in hepatitis B virus infection. *Immune Netw* (2015) 15(4):191–8. doi: 10.4110/in.2015.15.4.191

43. Li M, Zhang L, Xie S, Sun F, Zeng Z, Deng W, et al. Dynamic changes of cytokine profiles and virological markers associated with HBsAg loss during peginterferon alpha-2a treatment in HBeAg-positive chronic hepatitis B patients. *Front Immunol* (2022) 13:892031. doi: 10.3389/fimmu.2022.892031

44. Li MH, Zhang D, Zhang L, Qu XJ, Lu Y , Shen G, et al. Ratios of T-helper 2 cells to T-helper 1 cells and cytokine levels in. *Chin Med J* (2017) 130(15):1810–5. doi: 10.4103/0366-6999.211541

45. Li Y, Fan W, Link F, Wang S, Dooley S. Transforming growth factor β latency: A mechanism of cytokine storage and signalling regulation in liver homeostasis and disease. *JHEP Rep* (2021) 4(2):100397. doi: 10.1016/j.jhepr.2021.100397

46. Wu S, Yi W, Gao Y, Deng W, Bi X, Lin Y, et al. Immune mechanisms underlying hepatitis B surface antigen negative in chronic hepatitis B patients with viral coinfection. *Front Immunol* (2022) 13:893512. doi: 10.3389/fimmu.2022.893512

10.3389/fimmu.2023.1211980

Glossary

HBV	Hepatitis B virus
HBsAg negative and HBV DNA positive patients	Occult HBV infection
HBsAg	Hepatitis B virus surface antigen
anti-HBs	Hepatitis B virus surface antibody
HBeAg	Hepatitis B virus e antigen
anti-HBe	Hepatitis B virus e antibody
anti-HBc	Hepatitis B virus core antibody
ALT	alanine aminotransferase
AST	aspartate aminotransferase
TBIL	total bilirubin
DBIL	Indirect bilirubin
Alb	albumin
Glb	globulin
γ-GT	γ-glutamyl transpeptidase
ALP	alkaline phosphatase
CHB	Chronic hepatitis B
LC	liver cirrhosis
HCC	Hepatocellular carcinoma
PBMCs	peripheral blood mononuclear cells
sCD40L	Soluble Cluster of Differentiation 40 Ligand
EGF	epidermal growth factor
FGF-2	fibroblast growth factor 2
FLT-3L	Fms-related tyrosine kinase 3 ligand
G-CSF	granulocyte-stimulating factor
GM-CSF	granulocyte macrophage colony-stimulating factor
GRO-α	growth-regulated oncogene-α
IFN-α2	interferon-α2
IFN-γ	interferon-γ
IP-10	interferon gamma- induced protein 10
MCP-1/CCL2	monocyte chemoattractant protein 1
M-CSF	macrophage-stimulating factor
MDC	macrophage-derived chemokine
MIG/CXCL9	monokine induced by IFN-γ
MIP-1α/CCL3	macrophage inflammatory protein 1α
PDGF-AA	platelet-derived growth factor AA
RANTES/CCL5	regulated upon activation normal T Cell expressed and presumably secreted
TNF-α	tumoral necrosis factor α
LTA	TNF-β/lymphotoxin alpha
VEGF-A	vascular endothelial growth factor A
NA	Nucleotide analogue.

Frontiers in Immunology

Explores novel approaches and diagnoses to treat immune disorders.

The official journal of the International Union of Immunological Societies (IUIS) and the most cited in its field, leading the way for research across basic, translational and clinical immunology.

Discover the latest Research Topics

See more →

Frontiers

Avenue du Tribunal-Fédéral 34
1005 Lausanne, Switzerland
frontiersin.org

Contact us

+41 (0)21 510 17 00
frontiersin.org/about/contact